

NASA Conference Publication 10087
Part 2

First Annual High-Speed Research Workshop

(NASA-CP-10087-Pt-2) FIRST ANNUAL
HIGH-SPEED RESEARCH WORKSHOP, PART
2 (NASA. Langley Research Center)
521 p

N94-33462
--THRU--
N94-33486
Unclas

G3/02 0011990

Compiled by
Allen H. Whitehead, Jr.
Langley Research Center
Hampton, Virginia

Proceedings of a workshop sponsored by the
National Aeronautics and Space Administration,
Washington, D.C., and held in
Williamsburg, Virginia
May 14-16, 1991

APRIL 1992

Date for general release April 30, 1994

NASA


National Aeronautics and
Space Administration

Langley Research Center
Hampton, Virginia 23665-5225

FOREWORD

The First Annual High-Speed Research (HSR) Workshop was hosted by NASA Langley Research Center and was held May 14-16, 1991, in Williamsburg, Virginia. The purpose of the workshop was to provide a national forum for the government, industry and university participants in the program to present and discuss important technology issues related to the development of a commercially viable, environmentally compatible U.S. High-Speed Civil Transport. The workshop sessions and this publication are organized around the major task elements in NASA's Phase I - High-Speed Research Program which basically addresses the environmental issues of atmospheric emissions, community noise and sonic boom.

The opening Plenary Session provided program overviews and summaries by senior management from NASA and industry. The remaining twelve technical sessions were organized to preview the content of each program element, to discuss planned activities and to highlight recent accomplishments.

Attendance at the workshop was by invitation only and included only industry, academic and government participants who were actively involved in the High-Speed Research Program. The technology presented at the meeting is considered commercially sensitive, and as such, the conference results and this publication are protected by the NASA designation 

THIS PAGE INTENTIONALLY BLANK



TABLE OF CONTENTS

Part I*

FOREWORD	i
TABLE OF CONTENTS	iii
SESSION I. -- Plenary Session	
A. Headquarters Perspective	3
<i>Robert E. Anderson, NASA Headquarters, Code RJ</i>	
B. Boeing HSCT Program Summary	25
<i>Michael L. Henderson, Boeing Commercial Airplane Group</i>	
C. Update on Douglas' High-Speed Civil Transport Studies	93
<i>Bruce L. Bunin, Douglas Aircraft Company</i>	
D. General Electric/Pratt & Whitney Summary Report	135
<i>Samuel C. Gilkey, GE Aircraft Engines</i>	
<i>Richard W. Hines, Pratt & Whitney Aircraft</i>	
E. NASA Headquarter's Summary Reports	197
<i>Howard L. Wesoky, Code RJ, Dr. Michael J. Prather, Code EEU, John R. Facey, Code RP, George F. Unger, Code RF, and Samuel L. Venneri, Code RM</i>	
SESSION II. -- Airframe Systems Studies	
A. NASA High-Speed Civil Transport Studies--Airframe Systems Studies Review	303
<i>Frank D. Neumann, Boeing Commercial Airplane Group</i>	
B. Douglas Aircraft HSCT--Status and Future Research Needs	359
<i>H. Robert Welge, Douglas Aircraft Company</i>	
C. High-Speed Research Program Systems Analysis Activities at Ames Research Center	385
<i>George H. Kidwell, NASA Ames Research Center</i>	
D. Overview of Langley Systems Studies	421
<i>Samuel D. Dollyhigh, NASA Langley Research Center</i>	
SESSION III. -- Atmospheric Effects	
A. Stratospheric Models and Measurements: A Critical Comparison	459
<i>Dr. Ellis E. Remsberg, NASA Langley Research Center</i>	
B. Previous Model Comparisons	465
<i>Charles H. Jackman, NASA Goddard Space Flight Center</i>	
C. Model Capabilities, 3-D	469
<i>Dr. William L. Grose, NASA Langley Research Center</i>	
D. Model Capabilities, 2-D	471
<i>Charles H. Jackman, NASA Goddard Space Flight Center</i>	

*Published under separate cover.

SESSION III. -- Atmospheric Effects (continued)

E. Quality of Existing Data Sets - Total Ozone and Chemical Species	477
<i>Dr. Richard McPeters, NASA Goddard Space Flight Center</i>	
<i>Dr. Stephen R. Kawa, NOAA</i>	
F. Comparison of the Impact of Volcanic Eruptions and Aircraft Emissions on the Aerosol ...	479
Mass Loading and Sulfur Budget in the Stratosphere	
<i>Dr. Glenn K. Yue and Dr. Lamont R. Poole, NASA Langley Research Center</i>	
G. High Resolution Infrared Datasets Useful for Validating Stratospheric Models	497
<i>Curtis P. Rinsland, NASA Langley Research Center</i>	

Part II

SESSION IV. -- Source Noise

A. NASA HSR Phase I Low Noise Nozzle Technology Program Overview	507	-1
<i>Bernard J. Blaha, NASA Lewis Research Center</i>		
B. High-Speed Jet Noise Research at NASA Lewis	517	-2
<i>Eugene A. Krejsa, B. A. Cooper and C. M. Kim, NASA Lewis Research Center</i>		
<i>Abbas Khavaran, Sverdrup Technology, Inc.</i>		
C. HSCT Nozzle Source Noise Programs at Pratt & Whitney	533	-3
<i>Alfred M. Stern, Pratt & Whitney Aircraft</i>		
D. HSCT Noise Reduction Technology Development at General Electric Aircraft Engines	551	-4
<i>Rudramuni K. Majjigi, GE Aircraft Engines</i>		
E. Community Noise Sources and Noise Control Issues	591	-5
<i>Gene L. Nihart, Boeing Commercial Airplane Group</i>		
F. NASA LaRC Jet Plume Research	607	-6
<i>Dr. John M. Seiner, Michael K. Ponton and James C. Manning, NASA Langley Research Center</i>		
G. Theoretical Aspects of Supersonic Jet Noise	645	-7
<i>Dr. Christopher K. W. Tam, Florida State University</i>		

SESSION V. -- Sonic Boom (Aerodynamic Performance)

A. Sonic Boom Program Overview and Sonic Boom Source Design/Prediction/Performance ..	665	on 17
Overview		
<i>Dr. Christine M. Darden, NASA Langley Research Center</i>		
B. Design and Analysis of Low Boom Concepts at Langley Research Center	673	-8
<i>Dr. Christine M. Darden, Robert J. Mack, Kathy E. Needleman, Daniel G. Baize,</i>		
<i>Peter G. Coen, Raymond L. Barger, N. Duane Melson, Mary S. Adams, Elwood W. Shields</i>		
<i>and Marvin E. McGraw, Jr., NASA Langley Research Center</i>		
C. HSCT Design for Reduced Sonic Boom	701	-9
<i>George T. Haglund, Boeing Commercial Airplane Group</i>		

SESSION V. -- Sonic Boom (Aerodynamic Performance)(continued)

D. Sonic Boom Prediction and Minimization Using Computational Fluid Dynamics	721	-10
<i>Dr. Thomas A. Edwards and Raymond Hicks, NASA Ames Research Center</i>		
<i>Samson Cheung, MCAT Institute</i>		
<i>Susan Cliff-Hovey, Mike Madson and Joel Mendoza, NASA Ames Research Center</i>		
E. Sonic Boom Configuration Minimization	739	-11
<i>Robert A. Sohn, Douglas Aircraft Company</i>		
F. Sonic Boom Predictions Using a Modified Euler Code	757	-12
<i>Dr. Michael J. Siclari, Grumman Corporate Research Center</i>		
G. Overview of Feasibility Study on Conducting Overflight Measurements of Shaped	785	-13
Sonic Boom Signatures Using RPV's		
<i>Domenic J. Maglieri, Victor E. Sothcott, Thomas N. Keefer and Percy J. Bobbitt, Eagle Engineering, Inc. - Hampton Division</i>		

SESSION VI. -- Propulsion Systems Studies

A. The NASA Sponsored HSCT Propulsion Studies	811	-14
<i>William C. Strack, NASA Lewis Research Center</i>		
B. A NASA Lewis Comparative Propulsion System Assessment for the High-Speed Civil	829	-15
Transport		
<i>Jeffrey J. Berton, William J. Haller, Jonathon A. Seidel and Paul F. Senick, NASA Lewis Research Center</i>		
C. Pratt & Whitney/General Electric Propulsion Systems Studies Introduction	867	-16
<i>Samuel C. Gilkey, GE Aircraft Engines; and Richard W. Hines, Pratt & Whitney Aircraft</i>		
D. Results of GEAE HSCT Propulsion System Studies	879	-17
<i>Fred H. Krause, GE Aircraft Engines</i>		
E. Pratt & Whitney Propulsion Systems Studies Results/Status	919	-18
<i>Martin G. Smith, Jr. and George A. Champagne, Pratt & Whitney Aircraft</i>		

SESSION VII. -- Emission Reduction

A. Low Emissions Combustor Technology for High-Speed Civil Transport Engines	951	-19
<i>Richard W. Niedzwiecki, NASA Lewis Research Center</i>		
B. Theoretical Study of Thermodynamic Properties and Reaction Rates of Importance	965	-20
in the High-Speed Research Program		
<i>Stephen Langhoff, Dr. Charles W. Bauschlicher, Jr. and Richard Jaffe, NASA Ames Research Center</i>		
C. HSR Combustion Analytical Research	981	-21
<i>Dr. H. Lee Nguyen, NASA Lewis Research Center</i>		
D. LeRC In-House Experimental Research	997	-22
<i>Dr. Valerie J. Lyons, NASA Lewis Research Center</i>		
E. Lean Burn Combustor Technology at GE Aircraft Engines	1025	-23
<i>Willard J. Dodds, GE Aircraft Engines</i>		
F. Rich Burn Combustor Technology at Pratt & Whitney	1043	-24
<i>Robert P. Lohmann, Pratt & Whitney Aircraft</i>		
<i>T. J. Rosfjord, United Technologies Research Center</i>		

SESSION VII. -- Emission Reduction (continued)

G. Low NOx Combustor Design	1057
<i>Dr. Hukam Mongia, Allison</i>	
H. Low NOx Mixing Research	1059
<i>Professor Scott Samuelson, University of California-Irvine</i>	

Part III*

SESSION VIII. -- Aeroacoustic Analysis and Community Noise

A. Aeroacoustics Analysis and Community Noise Overview	1063
<i>Robert A. Golub, NASA Langley Research Center</i>	
<i>Paul T. Soderman, NASA Ames Research Center</i>	
B. New Broadband Shock Noise Model and Computer Code for ANOPP	1073
<i>N. N. Reddy, Lockheed Aeronautical Systems Company</i>	
C. Community Noise Technology Needs - Boeings Perspective	1103
<i>Gene L. Nihart, Boeing Commercial Airplane Group</i>	
D. HSCT Climb to Cruise Noise Assessment	1121
<i>Alan K. Mortlock, Douglas Aircraft Company</i>	
E. ANOPP/VMS HSCT Ground Contour System	1135
<i>John W. Rawls, Jr. and Louis J. Glaab, Lockheed Engineering and Sciences Company</i>	
F. High Performance Jet-Engine Flight Test Data Base for HSR	1159
<i>Jeffrey Kelly, Lockheed Engineering and Sciences Company</i>	
G. Status and Plans for the ANOPP/HSR Prediction System	1179
<i>Sandra K. Nolan, Lockheed Engineering and Sciences Company</i>	

SESSION IX. -- Sonic Boom (Human Response and Atmospheric Effects)

A. Atmospheric Effects on Sonic Boom--A Program Review	1199
<i>Dr. Gerry L. McAninch, NASA Langley Research Center</i>	
B. Relaxation and Turbulence Effects on Sonic Boom Signatures	1209
<i>Dr. Allan D. Pierce and Victor W. Sparrow, Pennsylvania State University</i>	
C. The Effect of Turbulence and Molecular Relaxation on Sonic Boom Signatures	1241
<i>Dr. Kenneth J. Plotkin, Wyle Laboratories</i>	
D. Statistical and Numerical Study of the Relation Between Weather and Sonic Boom	1263
Characteristics	
<i>Lixin Yao, Dr. Henry E. Bass and Richard Raspet, The University of Mississippi</i>	
<i>Walton E. McBride, Planning Systems, Inc.</i>	
E. Overview of NASA Human Response to Sonic Boom Program	1285
<i>Dr. Kevin P. Shepherd, NASA Langley Research Center</i>	
F. Sonic Boom Acceptability Studies	1293
<i>Dr. Kevin P. Shepherd, NASA Langley Research Center</i>	
<i>Brenda M. Sullivan, Lockheed Engineering and Sciences Company</i>	
<i>Dr. Jack E. Leatherwood and David A. McCurdy, NASA Langley Research</i>	

*Published under separate cover.

SESSION IX. -- Sonic Boom (Human Response and Atmospheric Effects)(continued)

G. Georgia Tech Sonic Boom Simulator	1313
<i>Dr. Krish K. Ahuja, Georgia Institute of Technology</i>	
H. Sonic Boom (Human Response and Atmospheric Effects) Outdoor-to-Indoor Response ...	1343
to Minimized Sonic Booms	
<i>David Brown, Wyle Research</i>	
<i>Louis C. Sutherland, Consultant to Wyle</i>	

SESSION X. -- Airframe/Propulsion Integration

A. PAI Session Overview and Review of Lewis PAI Efforts	1367
<i>Peter G. Batterton, NASA Lewis Research Center</i>	
B. Nacelle-Wing Integration	1381
<i>Gelsomina Cappuccio, NASA Ames Research Center</i>	
C. HSCT Inlet Development Issues	1401
<i>Joseph L. Koncsek, Boeing Commercial Airplane Group</i>	
D. Status of an Inlet Configuration Trade Study for the Douglas HSCT	1423
<i>Jay R. Jones and H. Robert Welge, Douglas Aircraft Company</i>	
E. Transonic Airframe Propulsion Integration	1437
<i>Robert E. Coltrin and Bobby W. Sanders, NASA Lewis Research Center</i>	
<i>Daniel P. Bencze, NASA Ames Research Center</i>	
F. Results of a Preliminary Investigation of Inlet Unstart on a High-Speed Civil	1461
Transport Airplane Concept	
<i>Christopher S. Domack, Lockheed Engineering and Sciences Company</i>	
G. Status of the Variable Diameter Centerbody Inlet Program	1481
<i>John E. Saunders and A. A. Linne, NASA Lewis Research Center</i>	
H. HSCT Integrated Propulsion Control Issues	1505
<i>Christopher M. Carlin, Boeing Commercial Airplane Group</i>	

SESSION XI. -- Airframe and Engine Materials

A. Enabling Propulsion Materials for High-Speed Civil Transport Engines	1521
<i>Joseph R. Stephens and Dr. Thomas P. Herbell, NASA Lewis Research Center</i>	
B. Combustor Materials Requirements and Status of Ceramic Matrix Composites	1547
<i>Ralph J. Hecht, Pratt & Whitney Aircraft</i>	
<i>Andrew M. Johnson, GE Aircraft Engines</i>	
C. Nozzle Material Requirements and the Status of Intermetallic Matrix Composites	1565
<i>Andrew M. Johnson, GE Aircraft Engines</i>	
<i>Ralph J. Hecht, Pratt & Whitney Aircraft</i>	
D. Airframe Materials for HSR	1583
<i>Thomas T. Bales, NASA Langley Research Center</i>	
E. HSR Airframe Materials - The Boeing Perspective	1607
<i>Donald L. Grande, Boeing Commercial Airplane Group</i>	
F. HSCT Materials and Structures - An MDC Perspective	1623
<i>Jay O. Sutton, Douglas Aircraft Company</i>	

Part IV*

SESSION XII. -- High Lift

A. Overview of NASA HSR High-Lift Program	1645
<i>William P. Gilbert, NASA Langley Research Center</i>	
B. Status of LaRC HSR High-Lift Research	1661
<i>Dr. Paul L. Coe, Jr., NASA Langley Research Center</i>	
C. Status of CFD for LaRC's HSR High-Lift Program	1693
<i>Edgar G. Waggoner and Jerry C. South, Jr., NASA Langley Research Center</i>	
D. HSR High Lift Research Program--Status and Plans	1719
<i>Jim Rose, NASA Ames Research Center</i>	
E. HSCT High Lift System Aerodynamic Requirements	1739
<i>John A. Paulson, Boeing Commercial Airplane Group</i>	
F. HSCT High-Lift Technology Requirements	1765
<i>D. L. Antani and J. M. Morgenstern, Douglas Aircraft Company</i>	
G. Lift Enhancement by Trapped Vortex	1789
<i>Vernon J. Rossow, NASA Ames Research Center</i>	

SESSION XIII. -- Supersonic Laminar Flow Control

A. NASA F-16XL Supersonic Laminar Flow Control Program Overview	1809
<i>Dr. Michael C. Fischer, NASA Langley Research Center</i>	
B. Supersonic Laminar Flow Control - Challenges and Opportunities	1821
<i>Arthur G. Powell, Douglas Aircraft Company</i>	
C. Status of the F-16XL Supersonic Laminar Flow Control Numerical Design Validation	1841
<i>Mike George, Rockwell International</i>	
<i>Marta Bohn-Meyer and Bianca Anderson, NASA Ames-Dryden Flight Research Facility</i>	
D. Code Validation for the Simulation of Supersonic Viscous Flow About the F-16XL	1891
<i>Jolen Flores, Eugene Tu and Lyndell King, NASA Ames Research Center</i>	
E. Inviscid and Viscous Flow Calculations for the F-16XL Configuration	1909
<i>Dr. Vinket Iyer, Vigyan, Inc.</i>	
F. Linear Stability Theory and Three-Dimensional Boundary Layer Transition	1975
<i>Robert E. Spall and Mujeeb Malik, High Technology Corporation</i>	
G. Supersonic HLFC: Potential Benefits and Technology Development Requirements	2001
<i>Frank Neumann, Boeing Commercial Airplane Group</i>	

*Published under separate cover.

Session IV. Source Noise

THIS PAGE INTENTIONALLY BLANK

omit

Session IV. Source Noise

NASA HSR Phase I Low Noise Nozzle Technology Program Overview
Bernard J. Blaha, NASA Lewis Research Center

PRECEDING PAGE BLANK NOT FILMED

THIS PAGE INTENTIONALLY BLANK

N94-33463

NASA HSR PHASE I LOW NOISE
NOZZLE TECHNOLOGY PROGRAM
OVERVIEW

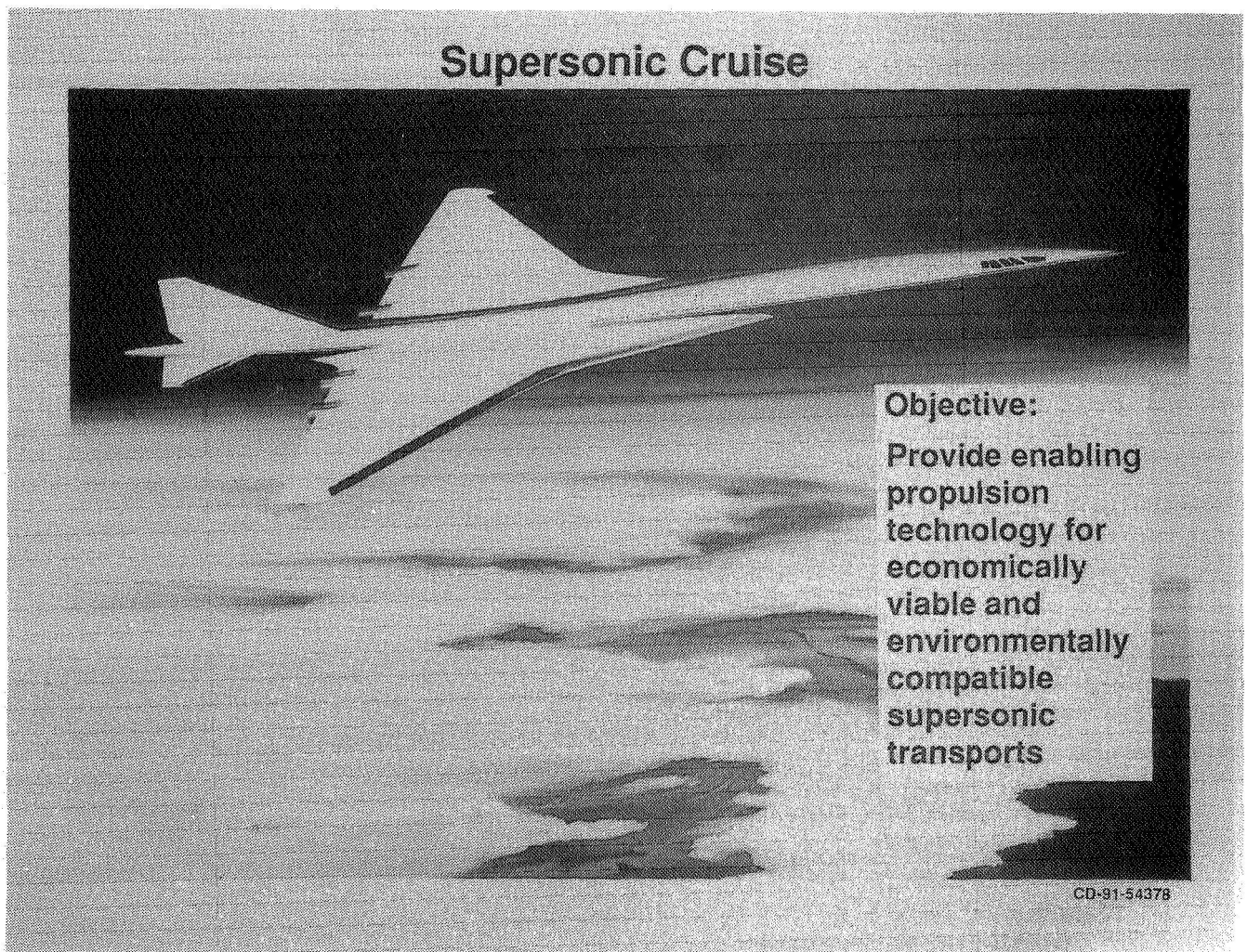
SI-07
11991

Bernard J. Blaha
NASA Lewis Research Center
Cleveland, Ohio

First Annual High Speed Research Workshop
Williamsburg, Virginia
May 15, 1991

SUPERSONIC CRUISE

Significant advances in propulsion performance are required if supersonic transport vehicles are to become an important part of the 21st century international air transportation system. The objective of the NASA Supersonic Cruise propulsion research is to provide the critical propulsion technologies to the industry in a timely fashion to contribute to the design of economically viable and environmentally acceptable high-speed civil transport (HSCT).



HIGH-SPEED RESEARCH PROGRAM

The NASA Phase I High-Speed Research Program (HSRP) emphasizes solutions to the critical environmental barrier issues associated with any future HSCT aircraft. Two of these barrier issues - atmospheric ozone depletion and community noise - are primarily propulsion issues and are addressed in the Lewis portion of HSRP. The critical economical viability issues will be the emphasis of a proposed Phase II HSRP, which could be initiated as early as FY 1992.

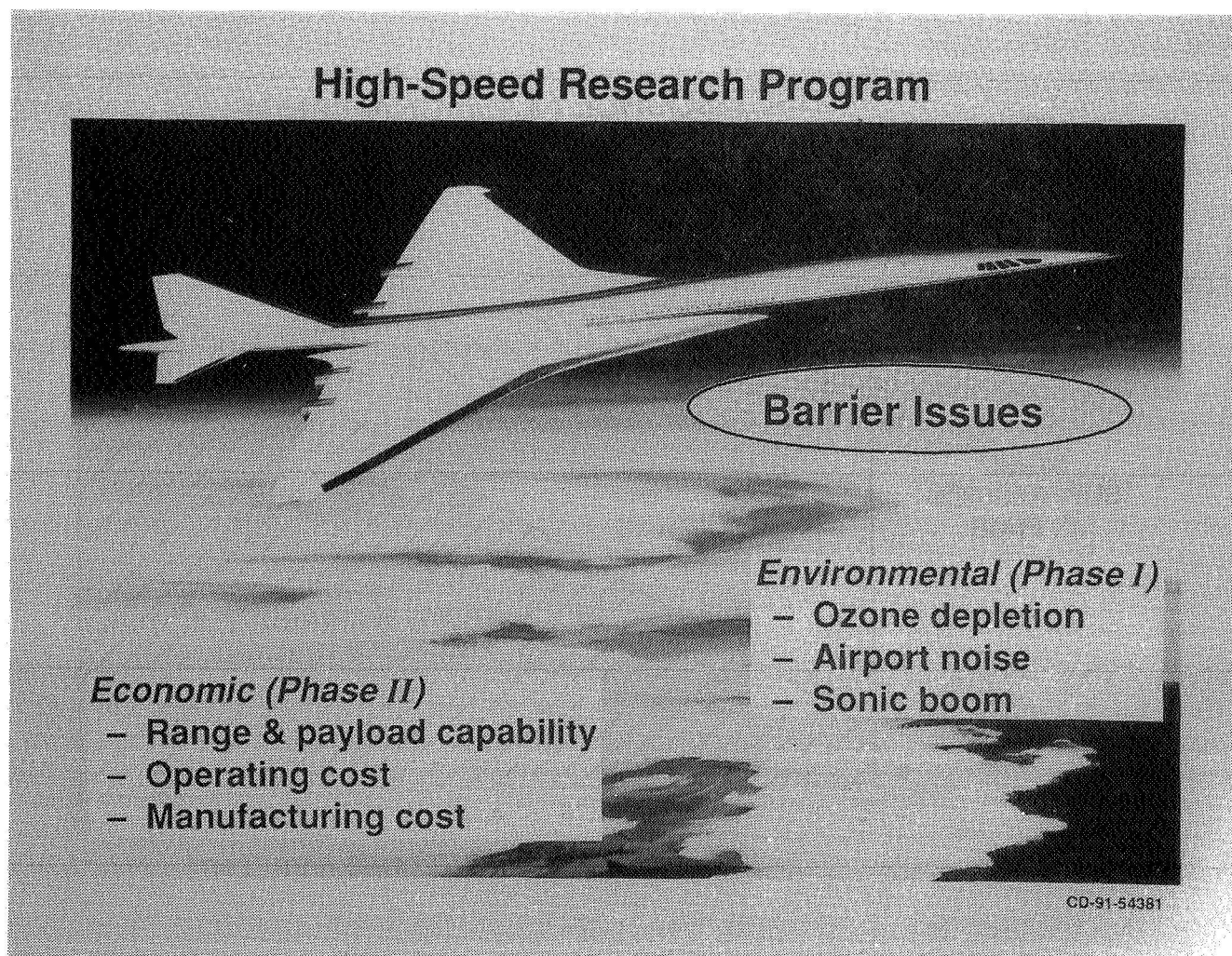
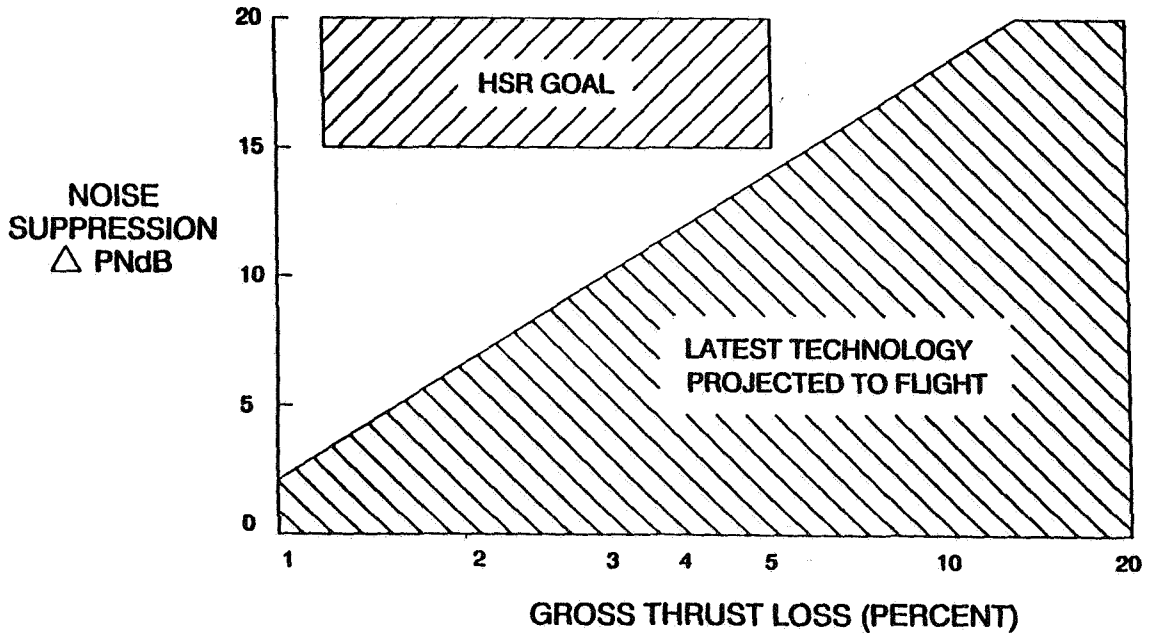


Figure 2

HSCT SOURCE NOISE CHALLENGE

The HSCT source noise challenge is illustrated in this figure. The jet exhaust noise levels at takeoff and landing conditions must be reduced by 15 to 20 db relative to reference conic nozzle levels before any future HSCT can hope to have noise levels below FAA noise regulation limits. At the same time, the nozzle aerodynamic performance levels must be kept high if vehicle overall mission performance goals are to be met. This combined acoustic-aerodynamic challenge is often expressed as a ratio of decibel noise reduction to resultant percent thrust loss. For a viable HSCT design this ratio should be in the neighborhood of 4:1. As this figure shows, current technology would yield a nozzle design with a ratio of no better than 2:1.

HSCT SOURCE NOISE CHALLENGE



LOW-NOISE NOZZLE TECHNOLOGY ELEMENTS

The major elements of the source noise portion of HSRP are shown in this figure. Heavy emphases are being placed in the first years of HSRP on computer code development and validation and on subscale experiments to evaluate potentially attractive nozzle concepts. The emphases regarding the codes is again on applying available solvers for both nozzle aerodynamic flows and for the acoustic signatures of the various configurations. The laboratory experiments and computer code developments and the insights they provide as to the governing fluid physics will be key inputs to the development of advanced nozzle configurations that will meet the HSRP goals, both for aerodynamic performance and acoustic suppression.

Propulsion Noise Reduction—High Speed Research Program Elements

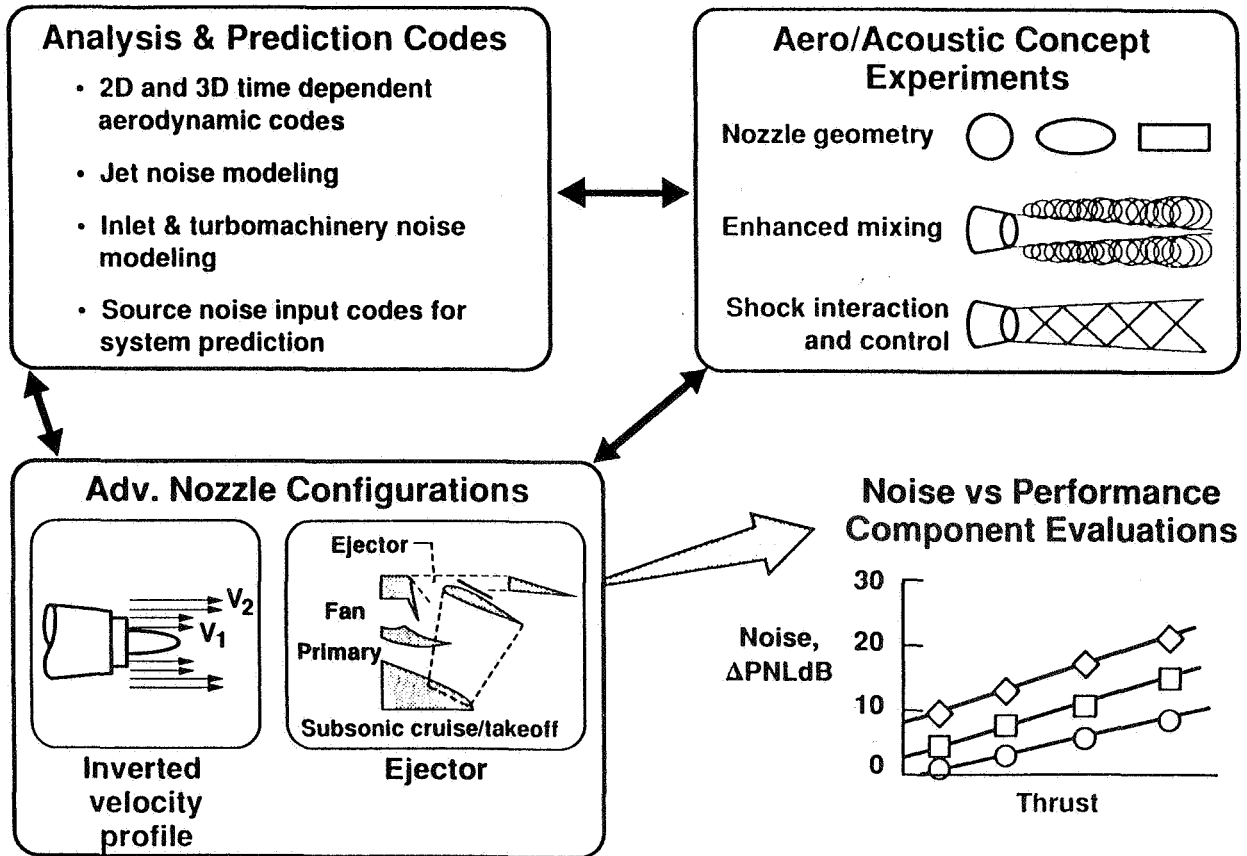
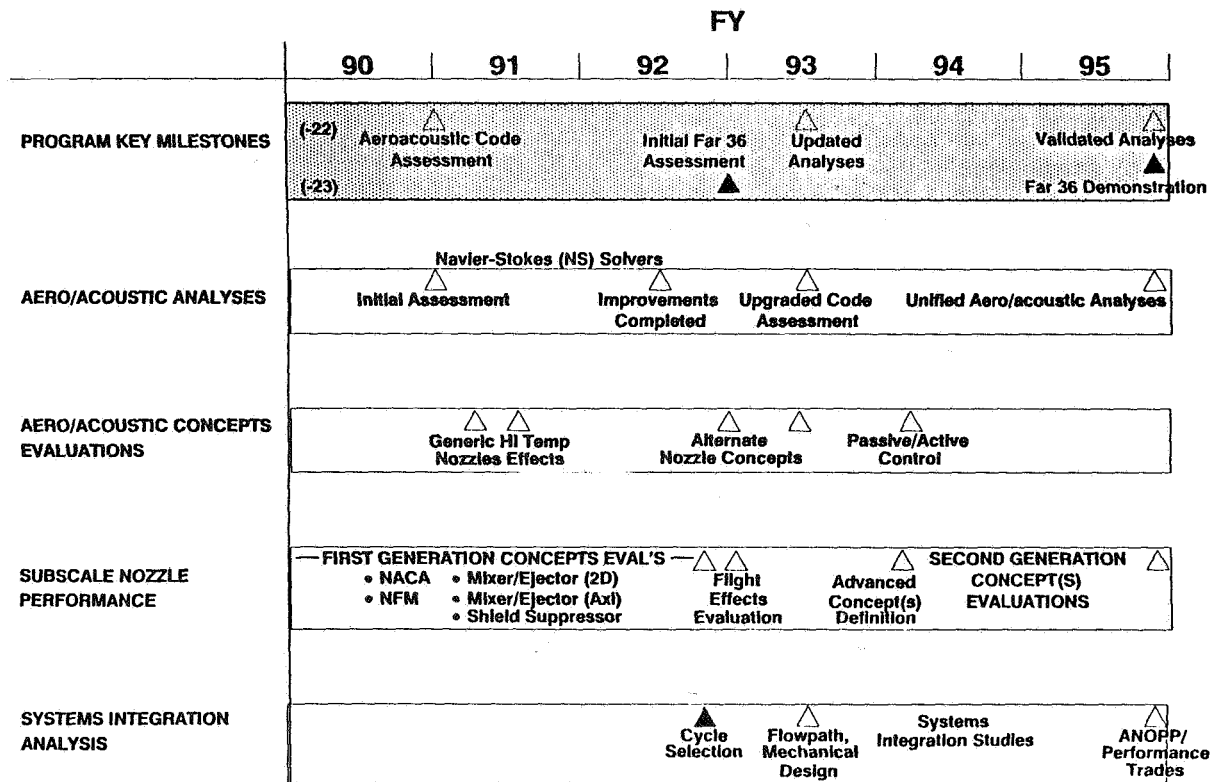


Figure 4

HSR SOURCE NOISE REDUCTION PROGRAM

This figure represents the HSR Source Noise Reduction Program in a slightly different or bar chart form. This represents basically the same information identified in the elements figure but also includes the program major milestones. The first darkened bar represents the whole program with major milestones shown at the halfway point and then at the end. The next three bars represent the previously identified activities including Aero/Acoustic Analyses, Aero/Acoustic Concept Evaluations or Experiments, and then Subscale Nozzle Performance Experiments with Advanced Configurations. Also included here is the activity relative to engine cycle analyses to determine the cycle benefits to be gained and overall aircraft system noise prediction (e.g., ANOPP). The HSR Phase I program indicated here is a six year activity with major milestones again at the halfway point at the end of FY92 and then overall at the end of FY95. The milestones shown at the halfway point represent the completion of a series of initial screening activities of either the advanced codes or the nozzle concepts. The best of these concepts will then be researched in more detail through the rest of program. Details of the activities occurring relative to each of the program bars will be discussed in the various papers presented in this session of the workshop including inputs from NASA, Industry, and an example of support from the Academic Community.

HSR SOURCE NOISE REDUCTION PROGRAM



NASA HIGH-SPEED RESEARCH PLAN PROPULSION ELEMENTS

The roadmap for the propulsion elements of NASA's overall High-Speed Research Program is shown in this figure. HSRP Phase I efforts will result in demonstrations of low-NO_x combustor and low-noise nozzle concepts as well as determination of preferred HSCT propulsion cycles. NASA's HITEMP engine materials program will provide the basis for the development of the advanced composite materials required for the combustor and nozzle components of any future HSCT engine.

The HSRP Phase I and HITEMP research results will be the inputs to the proposed HSRP Phase II Program currently advocated by NASA. The propulsion elements of HSRP II would demonstrate HSCT propulsion technology readiness initially through large-scale testing of the critical components (inlet, fan, combustor, and nozzle); then these components would be combined with an available core engine in propulsion systems technology demonstrations at both low-speed (takeoff) and high-speed (supersonic cruise) conditions.

The Enabling Propulsion Materials of HSRP II would demonstrate the materials technology readiness through tests of an uncooled ceramic matrix composite (CMC) combustor liner and a nozzle substructure element fabricated from an advanced intermetallic matrix composite (IMC) developed in HSRP II.

NASA High-Speed Research Plan Propulsion Elements

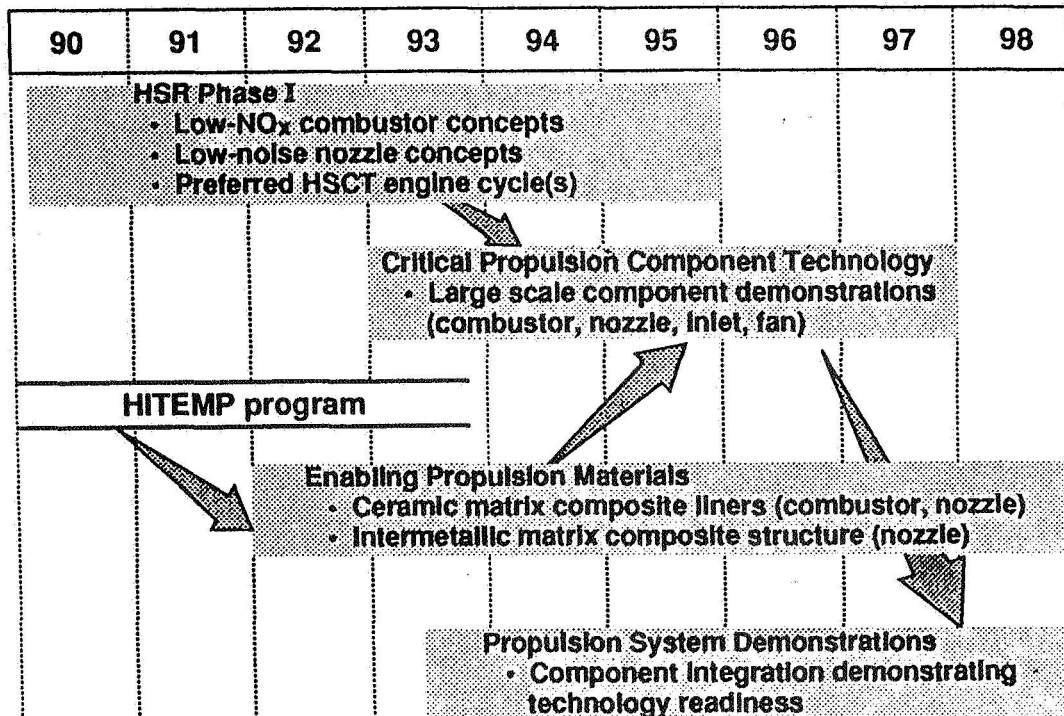


Figure 6

THIS PAGE INTENTIONALLY BLANK

omit

Session IV. Source Noise

High-Speed Jet Noise Research at NASA Lewis

Eugene A. Krejsa, B. A. Cooper and C. M. Kim, NASA Lewis Research Center; and Abbas Khavaran, Sverdrup Technology, Inc.

PRECEDING PAGE BLANK NOT FILMED

THIS PAGE INTENTIONALLY BLANK

N94-33464

52-71
11992

High Speed Jet Noise Research at NASA Lewis

E. A. Krejsa, B. A. Cooper, C. M. Kim
NASA Lewis Research Center
and
A. Khavaran
Sverdrup Technology Inc.

First Annual High-Speed Research Workshop
May 14-16, 1991
Williamsburg, Virginia

HIGH SPEED JET NOISE RESEARCH AT NASA LEWIS
PROGRAM CONTENT

The source noise portion of the High Speed Research Program at NASA Lewis is focused on jet noise reduction. A number of jet noise reduction concepts are being investigated. These include two concepts, the Pratt & Whitney ejector suppressor nozzle and the General Electric 2D-CD mixer ejector nozzle, that rely on ejectors to entrain significant amounts of ambient air to mix with the engine exhaust to reduce the final exhaust velocity. Another concept, the G.E. "Flade Nozzle" uses fan bypass air at takeoff to reduce the mixed exhaust velocity and to create a fluid shield around a mixer suppressor. Additional concepts are being investigated at Georgia Tech Research Institute and at NASA Lewis. These will be discussed in more detail in later figures.

Analytical methods for jet noise prediction are also being developed. Efforts in this area include upgrades to the GE MGB jet mixing noise prediction procedure, evaluation of shock noise prediction procedures, and efforts to predict jet noise directly from the unsteady Navier Stokes equation.

High Speed Jet Noise Research at NASA Lewis

Program Content

Noise reduction concept evaluation

- **P & W ejector suppressor nozzle**
- **GE 2D-CD mixer/ejector nozzle**
- **GE flade nozzle**
- **GTRI novel concepts evaluation**
- **Shear layer modification**

Analytical methods development

- **MGB model upgrade**
- **Shock noise prediction/evaluation**
- **Unsteady Navier stokes solutions**

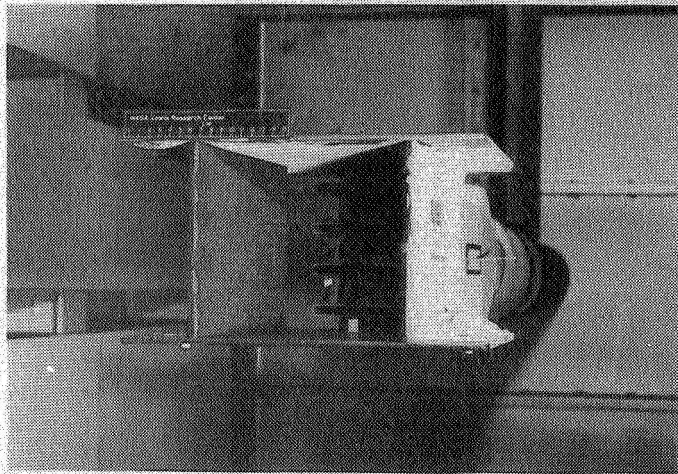
2D P&W MIXER/EJECTOR AEROACOUSTIC NOZZLE TEST IN THE NASA LEWIS 9x15 LSWT

Shown in this figure is an early version of the P&W developed mixer/ejector nozzle. This nozzle was tested in the NASA Lewis 9x15 LSWT as a proof of concept test to evaluate ejector pumping capability and noise reduction potential. Since this was the first jet noise test conducted in the 9x15 wind tunnel, the test also served as a means of evaluating the suitability of this facility for jet noise testing. Results from this test will be presented in the next two figures. Details regarding modification to the design and follow-on testing will be presented in a later paper.

2D P&W Mixer/Ejector Aeroacoustic Nozzle Test in NASA Lewis 9x15 LSWT

Objectives:

- P&W - Conduct simple 2D proof-of-concept test.
- Lewis - Obtain first jet source acoustic data in 9x15.



Results:

- Convergent nozzle noise significantly above background.
- Ejector pumping exceeded predictions ($W_g/W_p > 1.0$).
- Nozzle noise reductions observed (-6 to -8 EPNDB relative to -18 EPNDB goal).
- CFD (PARC/NASTAR) results agree with experiment.

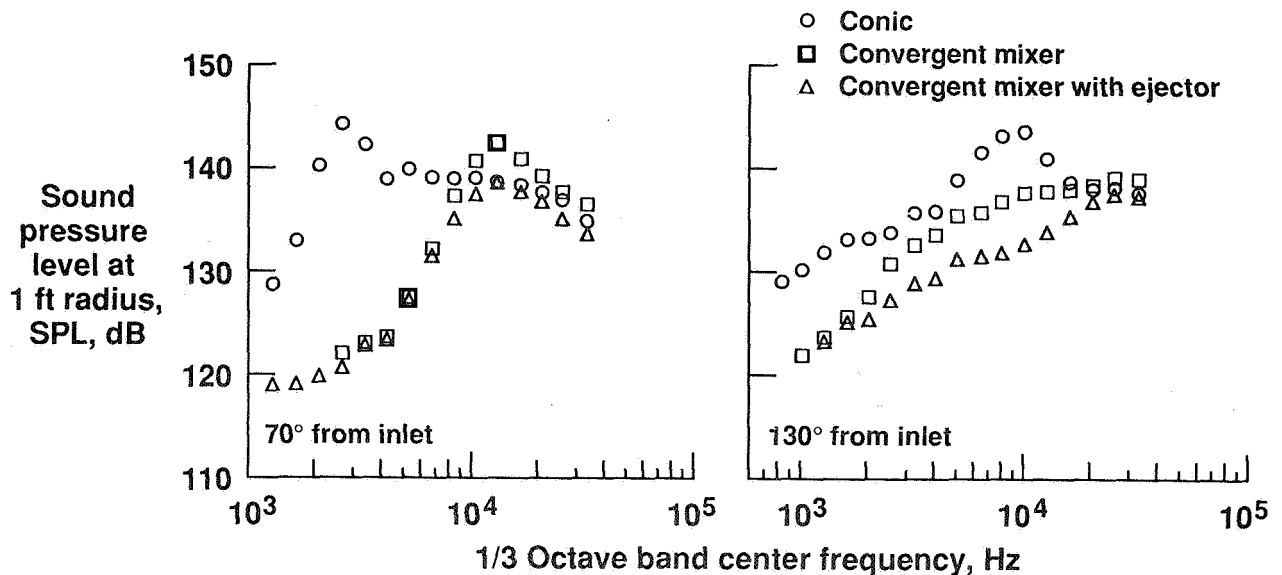
2D P&W MIXER/EJECTOR AEROACOUSTIC NOZZLE TEST
IN THE NASA LEWIS 9x15 LSWT

COMPARISON OF MIXER-EJECTOR, CONVERGENT MIXER
AND CONIC NOZZLE NOISE SPECTRA

Typical acoustic results from the test of the P&W mixer/ejector nozzle are shown in this figure. One-third octave spectra from the mixer ejector nozzle are compared with those from the mixer alone and a round conic nozzle at angles of 70 and 130 degrees from the inlet axis. These data can be used to assess the noise reduction achieved by the mixer alone and from the addition of the hardwall ejector. The addition of acoustic treatment to the ejector wall would result in additional noise reduction by absorbing noise generated within the ejector.

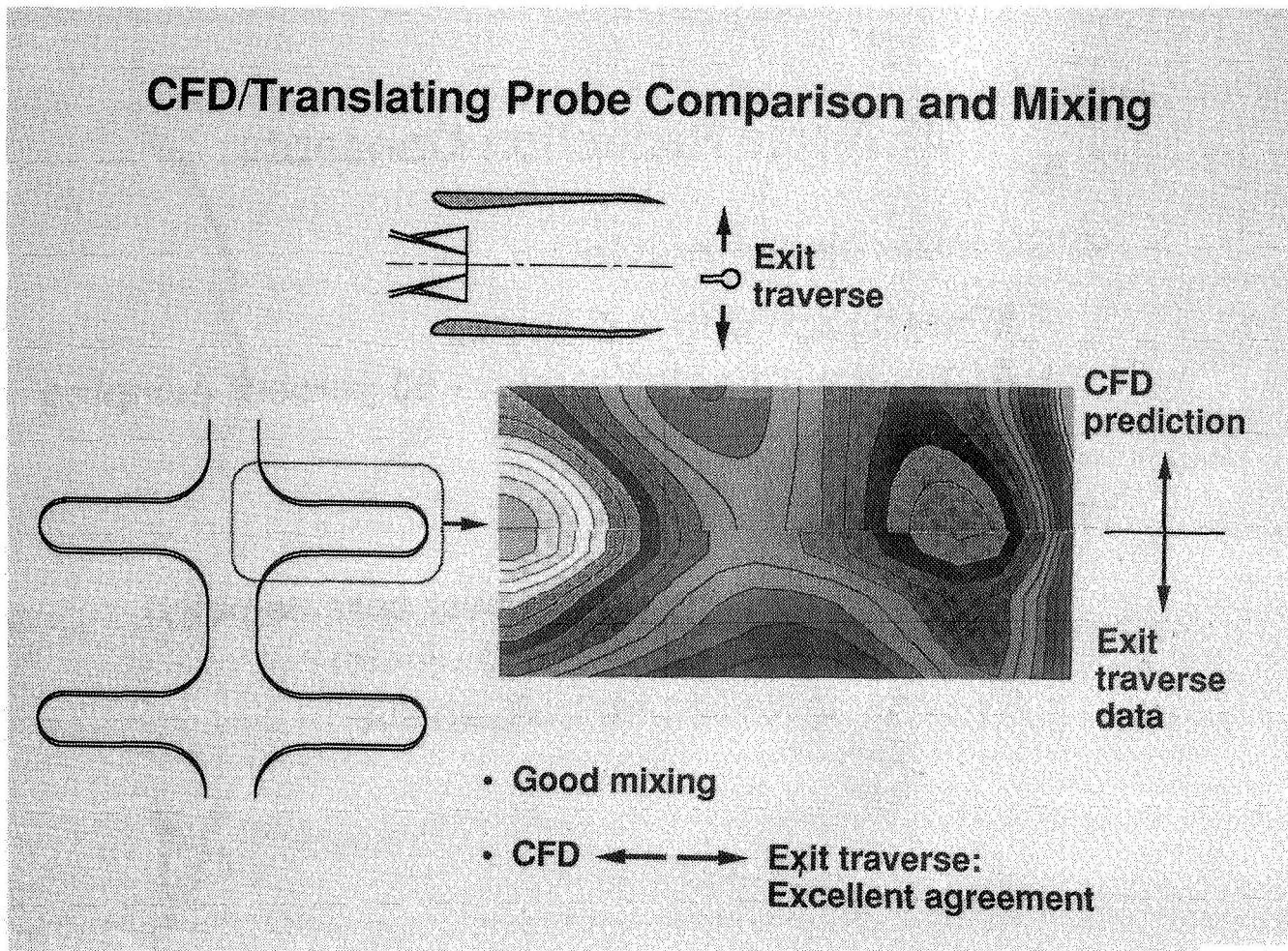
**2D P&W Mixer/ejector Aeroacoustic Nozzle Test in
NASA Lewis 9x15 LSWT**
Comparison of Mixer-ejector, Convergent Mixer and
Conic Nozzle Noise Spectra

Nozzle pressure ratio = 3.5 Nominal jet temperature = 900 °R Tunnel mach number = 0.2



CFD/TRANSLATING PROBE COMPARISON AND MIXING

Shown in this figure are results from a temperature traverse at the ejector exhaust. The results indicate that good mixing between the primary and the induced flows was achieved. Also shown is a corresponding predicted temperature field at the same location. Good agreement between measured and predicted temperatures was achieved.



GE NOISE REDUCTION CONCEPTS

The main characteristics of two noise reductions concepts developed by General Electric are given in this figure. Details regarding these concepts will be given in a later paper. The first concept, like that of Pratt & Whitney, is mixer ejector nozzle. The mixer nozzle is designed with convergent-divergent chutes to minimize shock noise. The ejector, designed to achieve 60% pumping, will be acoustically treated to absorb noise generated within the ejector.

The second GE concept, the Flade Nozzle, is designed for an engine cycle with reduced mixed exhaust velocity. The fan flow from this cycle will be used to produce a fluid shield around a mixer nozzle.

GE Noise Reduction Concepts

2DCD mixer ejector nozzle

- **Mixer nozzle with C-D chutes**
- **Acoustically treated ejector - 60 percent pumping**

Flade nozzle

- **Increased by-pass ratio (lower core velocity)**
- **Mixer on primary nozzle (no ejector)**
- **By-pass flow used for fluid shield**

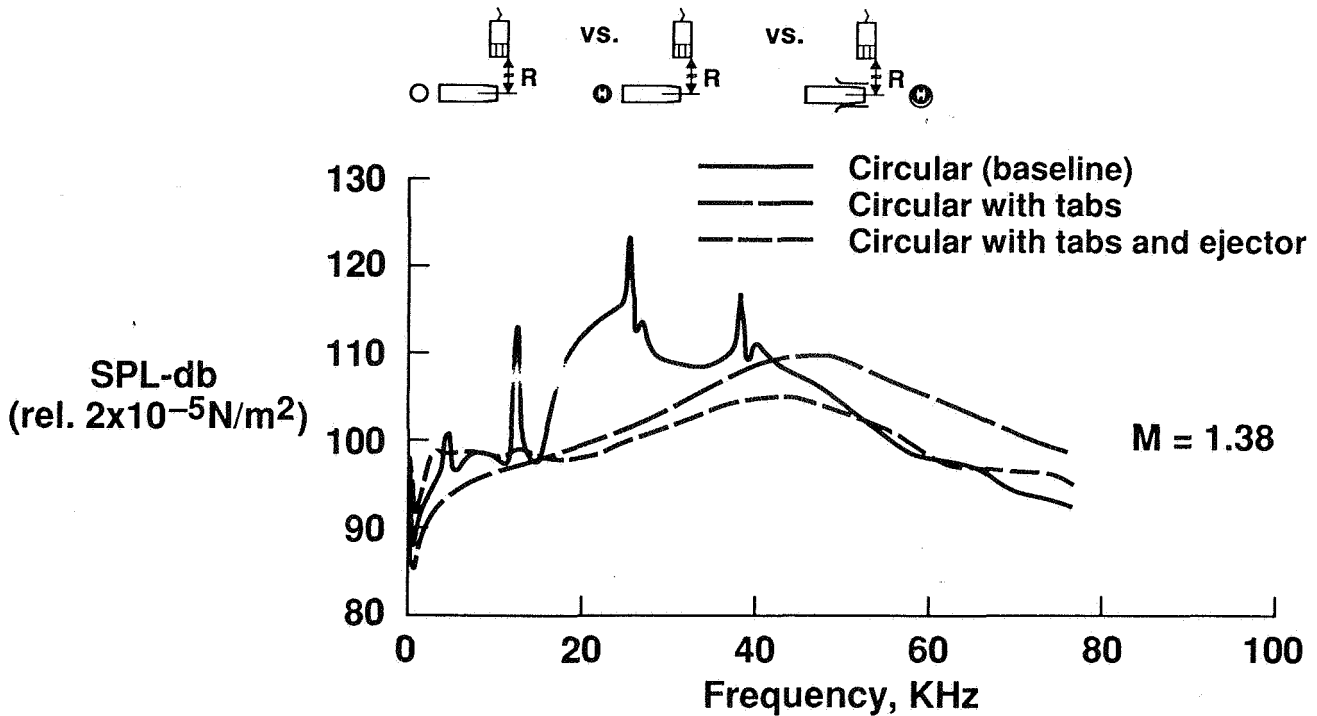
NOVEL JET NOISE REDUCTION CONCEPTS

CIRCULAR NOZZLE WITH TABS AND EJECTOR

In this figure, acoustic results from tests conducted by Georgia Tech Research Institute of a circular nozzle with tabs and an ejector are shown. Previous results with tabs and a circular nozzle have shown that the tabs can significantly enhance the mixing of the nozzle flow with ambient air. By combining the rapid mixing of the tabbed nozzle with the noise suppression potential of a treated ejector, it is hoped that significant jet noise reduction can be achieved with simple nozzle geometries and a short ejectors.

Novel Jet Noise Reduction Concepts Georgia Tech Research Institute

Circular nozzle with tabs and ejector



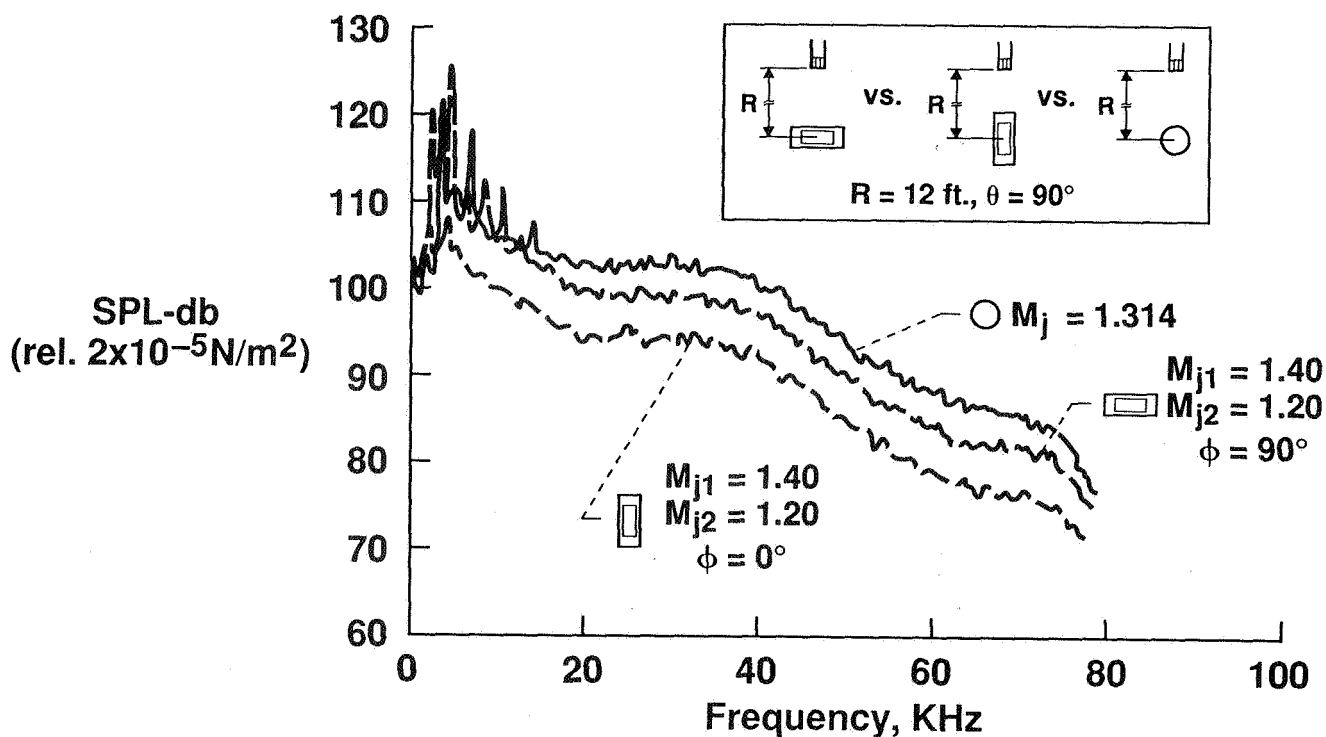
NOVEL JET NOISE REDUCTION CONCEPTS

COAXIAL RECTANGULAR NOZZLE

Another concept being investigated at Georgia Tech Research Institute is the coaxial rectangular nozzle. In this figure, test results show the noise reduction, relative to a conic nozzle, achieved by using a dual flow rectangular nozzle. The concept's success at supersonic flow conditions may indicate that it is most effective in reducing shock noise.

Novel Jet Noise Reduction Concepts Georgia Tech Research Institute

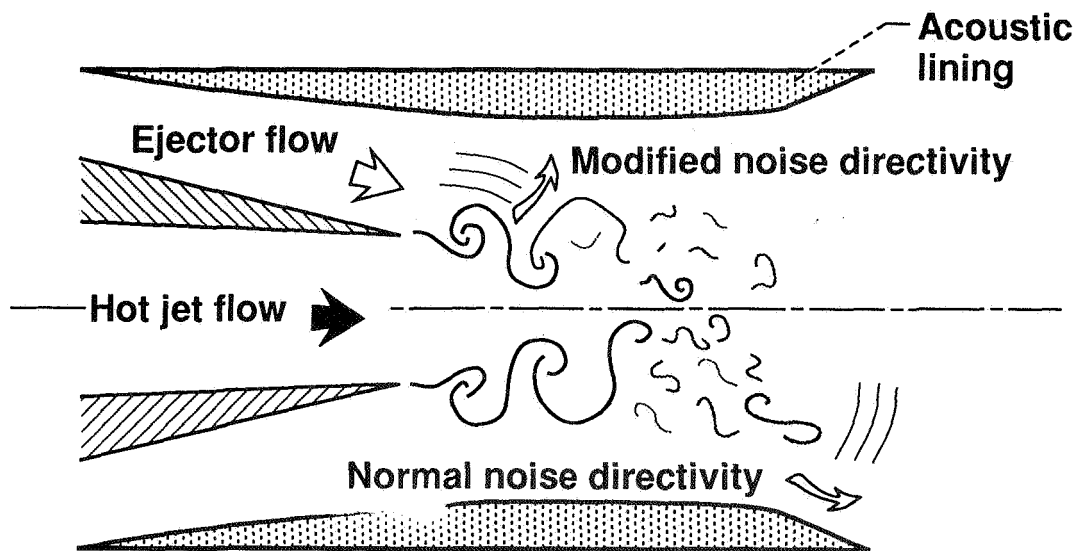
Coaxial rectangular nozzle



NOISE REDUCTION BY SHEAR LAYER MODIFICATION

At Lewis, jet screech is being investigated as a means of exciting the jet shear layer and enhancing the mixing within an ejector. Enhanced mixing can significantly shorten the ejector or provide more treatment length to suppress internally generated noise. The effect of excitation on the directivity of the internally generated noise is also being studied. The effectiveness of wall treatment within an ejector could be enhanced if the internally generated noise can be made to propagate toward the side walls.

Noise Reduction by Shear Layer Modification

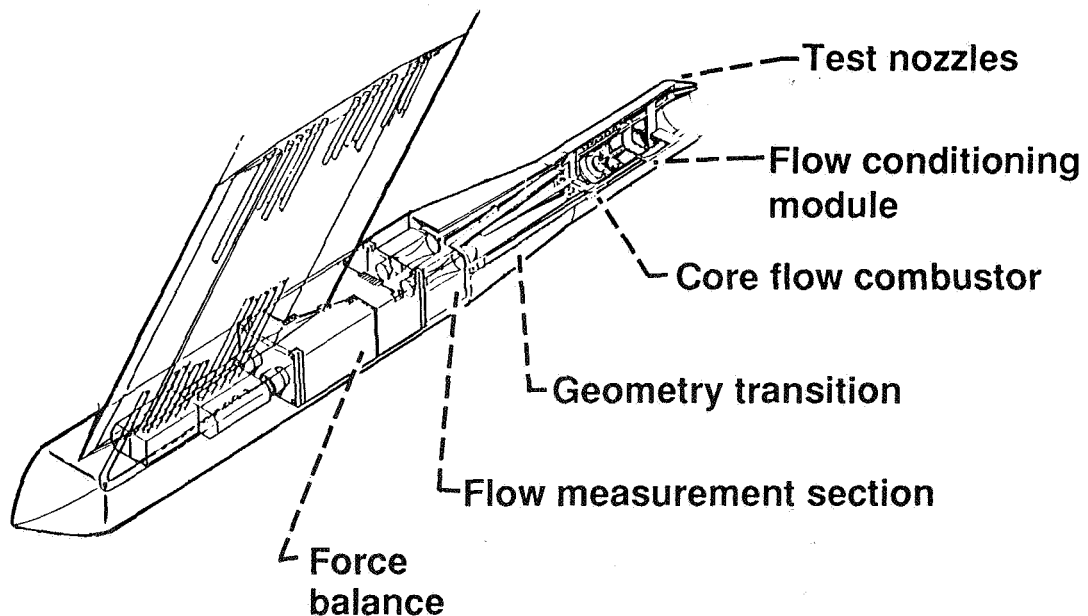


- Apply aerodynamic excitation principles to enhance mixing and minimize performance penalty.
- Apply aerodynamic excitation principles to alter directivity of internal shear layer noise to maximize liner effectiveness.

JET EXIT RIG WITH TRANSITION FOR
AXISYMMETRIC NOZZLES

Shown in this figure is a schematic of the NASA Lewis Research Center jet exit rig. This rig is designed for testing of both NASP and HSR nozzles and is compatible with the NASA Lewis 8x6 and 10x10 supersonic wind tunnels and the 9x15 low speed wind tunnel, the NASA Ames 40x80 wind tunnel, and the new Lewis nozzle acoustic test rig.

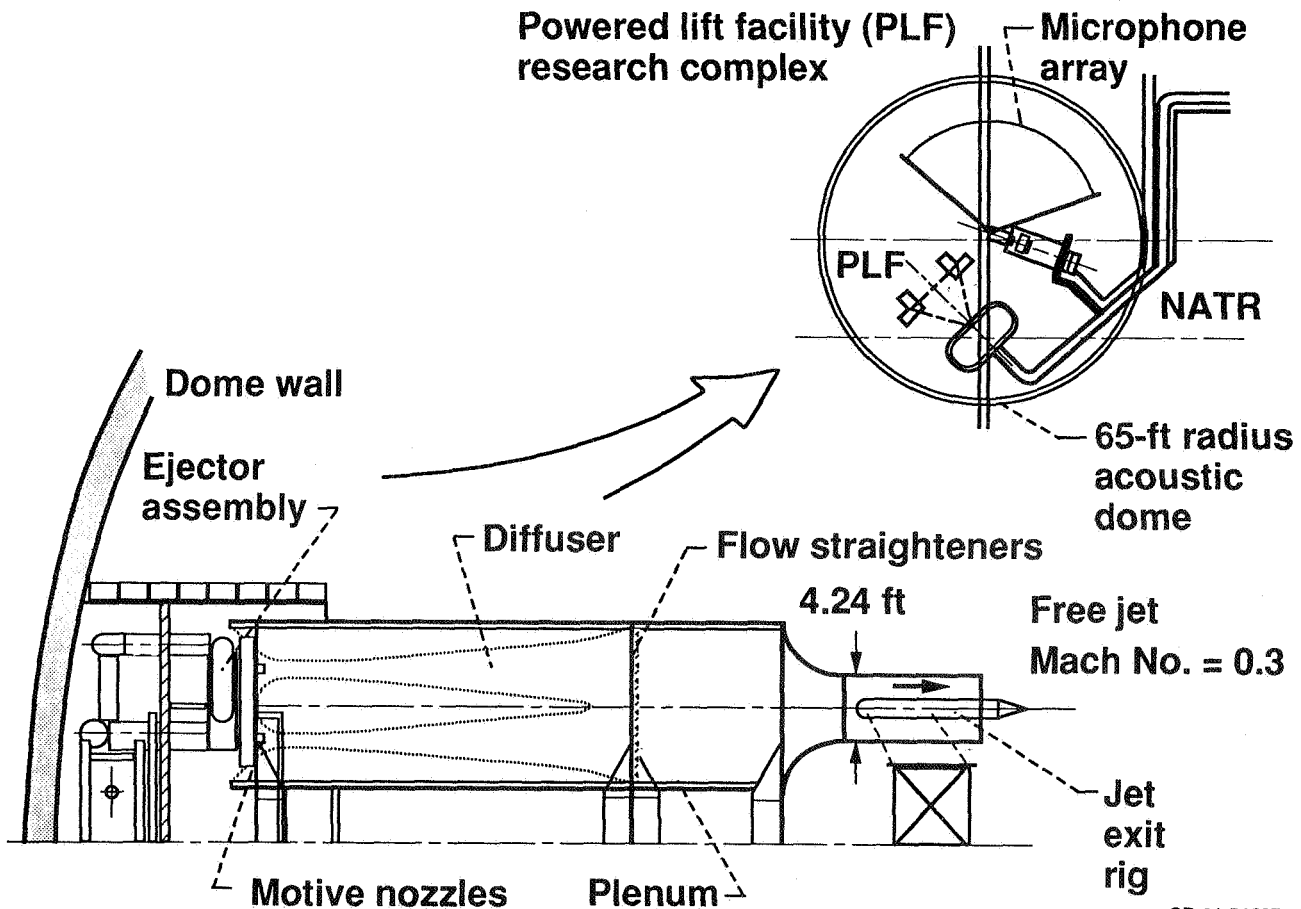
Jet Exit Rig With Transition for Axisymmetric Nozzles



NOZZLE ACOUSTIC TEST RIG (NATR)

A schematic of a new nozzle acoustic test rig is shown in this figure. The rig will be located within a 65 foot radius geodesic dome. The dome is designed to minimize community noise problems from the nozzle acoustic test rig and the adjacent Powered Lift Facility. Acoustic treatment will be installed on the inside of the dome to provide an anechoic environment for acoustic testing. Forward flight effects will be simulated by means of a free jet. Heated air will be provided to test nozzles by the jet exit rig discussed previously.

Nozzle Acoustic Test Rig (NATR)



CD-91-54567

JET NOISE PREDICTION EFFORTS

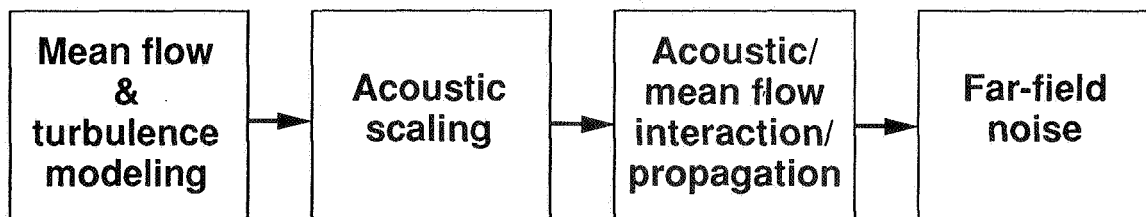
Efforts at Lewis to improve the state-of-the-art of jet noise prediction include the evaluation and improvement of existing jet mixing and shock noise prediction procedures and the development of new prediction procedures. Planned improvements to the existing, GE developed, MGB procedure include replacing Reichardt's mean flow prediction method with the Parc code and adding non-axisymmetric effects to the acoustic/mean flow interaction radiation model. Shock noise prediction methods are currently being evaluated over a range of jet Mach numbers and temperatures both with and without forward flight effects.

In House Jet Noise Prediction Efforts

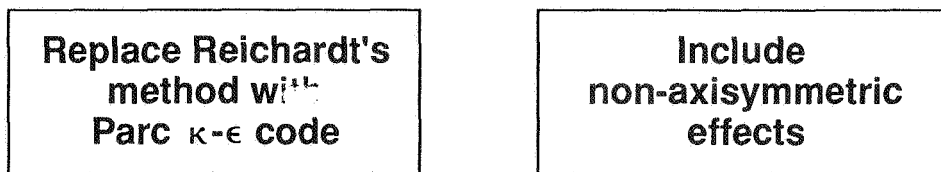
Improve jet mixing noise prediction

- Improve 'MGB' procedure

Prediction Procedure Elements



Planned improvements



Evaluate/improve shock noise prediction

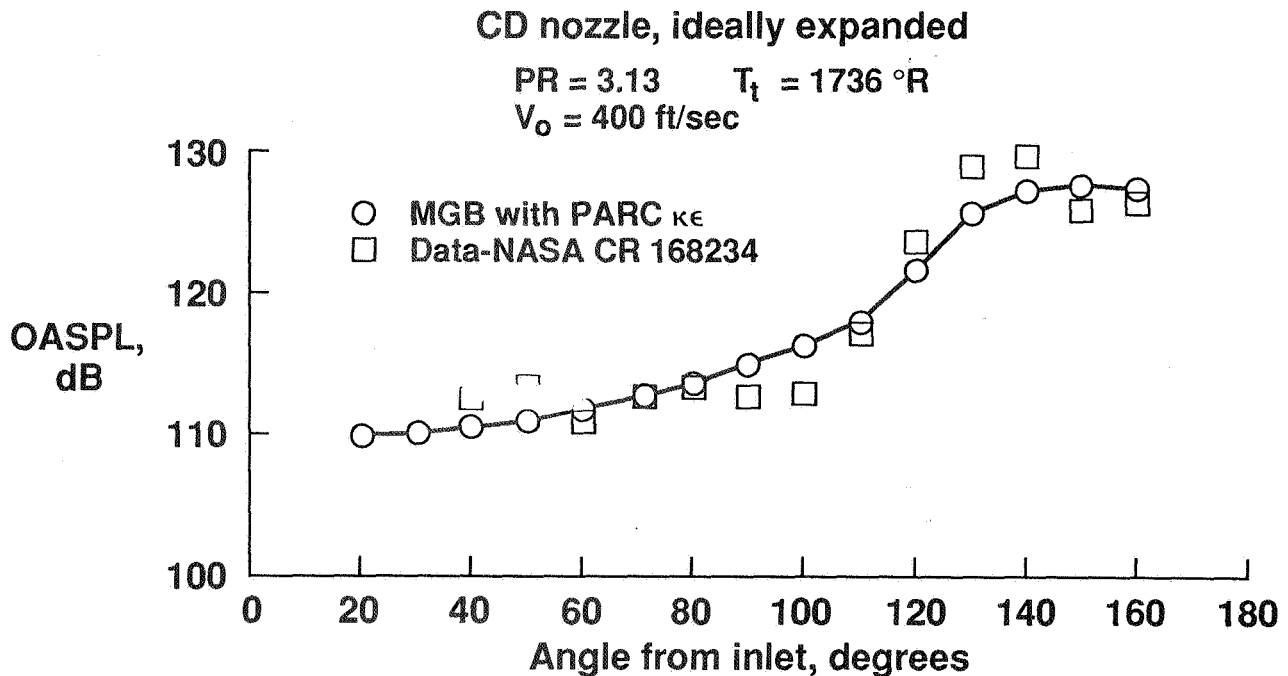
- Evaluate current shock noise prediction procedures
- Incorporate CFD predicted shock characteristics into current shock noise prediction procedures

MGB JET NOISE PREDICTION MODEL
WITH PARC AERO INPUT

Shown in this figure are typical results comparing predicted and measured jet noise directivities for a convergent-divergent nozzle at the nozzle design pressure ratio. The prediction was made using the GE MGB method with aerodynamic inputs from the Parc code.

MGB Jet Noise Prediction Model with PARC- $\kappa\epsilon$ Aero Input

Comparison of Measured and Predicted Jet Noise Directivity



HIGH SPEED JET NOISE RESEARCH
AT NASA LEWIS

SUMMARY

Significant progress has been made. High ejector pumping, necessary for the success of ejector suppressor concepts, has been demonstrated. Detailed designs have been completed for several promising noise reduction concepts that are to be tested this year. Other more novel concepts are being investigated. Initial steps have been taken to upgrade jet noise prediction procedures.

High Speed Jet Noise Research at NASA Lewis

Summary

- High ejector pumping demonstrated
- Two acoustically treated ejector/suppressor designs plus fluid shield/mixer concept to be evaluated this year
- Other novel concepts being investigated
- Aeroacoustic prediction procedures being upgraded

omit

Session IV. Source Noise

HSCT Nozzle Source Noise Programs at Pratt & Whitney
Alfred M. Stern, Pratt & Whitney Aircraft

THIS PAGE INTENTIONALLY BLANK

N94-33465

53-71

11993

**HSCT NOZZLE SOURCE NOISE
PROGRAMS AT PRATT & WHITNEY**

**ALFRED M. STERN
PRATT & WHITNEY**

**NATIONAL AERONAUTICS AND SPACE ADMINISTRATION
FIRST ANNUAL HIGH SPEED RESEARCH WORKSHOP
MAY 14-16, 1991**

PRECEDING PAGE BLANK NOT FILMED

20dB JET NOISE SUPPRESSION NEEDED

Jet noise from the high velocity exhaust flow will dominate takeoff noise spectra of high speed aircraft. Although available noise suppression technologies can be used to quiet other engine noise sources, jet noise requires new, unique developments in noise reduction technology.

With the resurgent interest in the High Speed Civil Transport, successful control of the dominant jet noise (along with emissions and materials) has again been identified as one of the two or three technologies critical to a successful HSCT. Without an economically viable approach to FAR36 Stage 3 noise requirements, there can be no commercial transport. Alternate means of meeting this noise rule (such as engine oversizing) have been shown to adversely impact the system's economics.

Recent low noise nozzle accomplishments at P&W and future plans are discussed in the pages that follow:

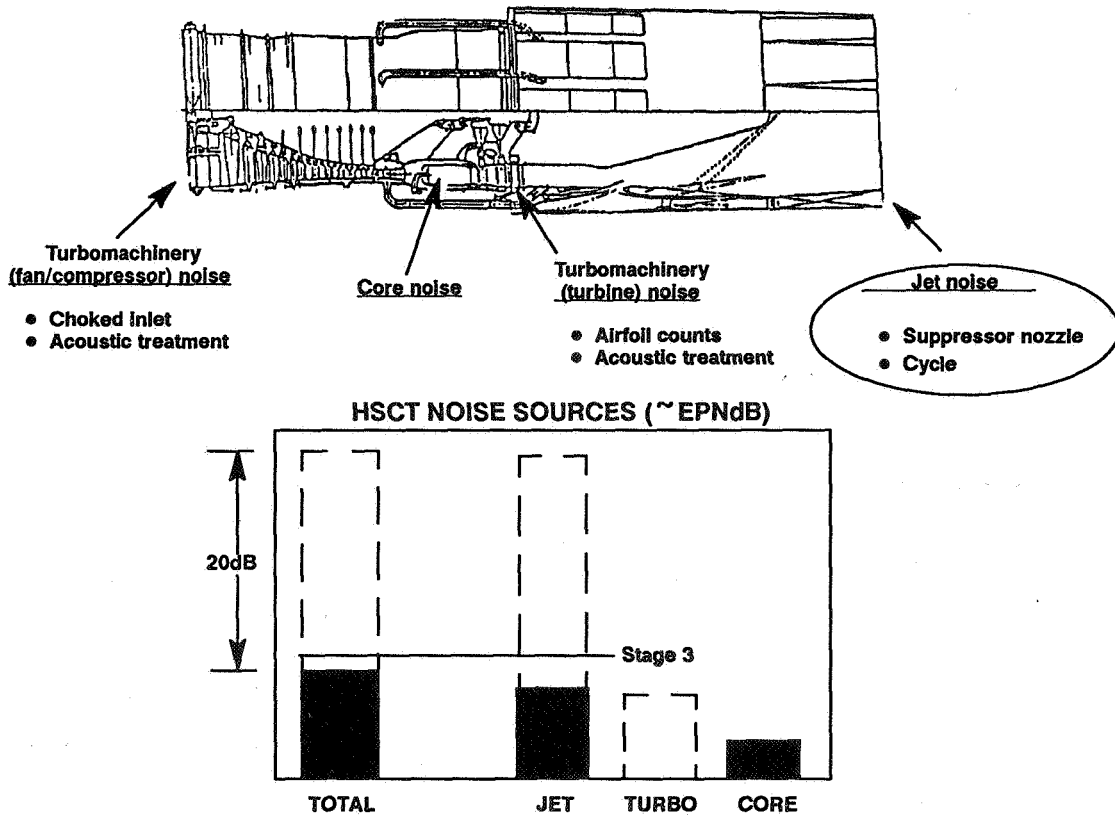


Figure 1

EJECTOR NOZZLE TECHNOLOGY PROGRAM

NOISE REDUCTION VS FLOW AUGMENTATION

Jet noise suppression of magnitude 20 EPNdB will be needed relative to a suppressed exhaust system optimized for performance only. The major low noise exhaust nozzle effort at P&W has focused on high flowing, mixer ejector nozzle systems with secondary airflow entrainment levels as high as 120-140%.

Since the early days of supersonic transports, both Pratt & Whitney and General Electric Aircraft Engines have been key participants in studies and evaluations of candidate HSCT exhaust nozzle concepts. Teaming between P&W and GEAE to develop a HSCT propulsion system is a major milestone in the United States effort toward a successful program.

GEAE have been looking at similar ejector systems, trading reduced pumping levels for smaller diameter and drag. The lower pumping alternative requires some modest engine resigning to meet Stage III. Having two levels of pumping under parallel investigation by GEAE and P&W provides us the opportunity to better understand the range of ejector capabilities and assess them back-to-back in terms of overall installed performance. One of our objectives is a down select decision to one common ejector type by the end of 1992.

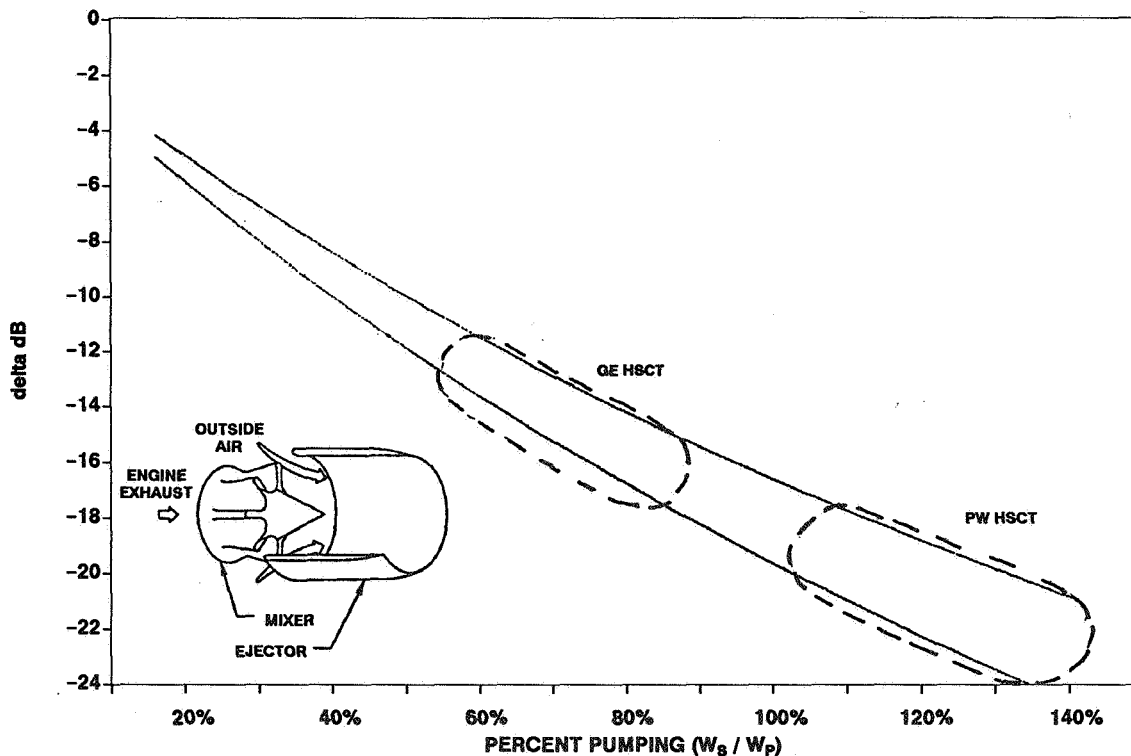


Figure 2

**MIXER EJECTOR NOZZLE
TECHNOLOGY CHALLENGES**

One major noise challenge to a successful mixer ejector nozzle is good aerodynamic design. The major benefit for the ejector comes from reducing overall jet velocity from over 3000 ft/sec to something near 1500 ft/sec, while maintaining thrust. The process of mixing tertiary air with the high velocity primary exhaust flow, however, produces its own noise. This mixing process must be optimized to 1) minimize the internal noise generated and 2) produce this noise in a form more easily attenuated by acoustic liners in the ejector shroud.

Acoustic liner technology capable of effectively attenuating the internally generated noise within the highly turbulent and high velocity and temperature environment of the ejector must also be developed.

Internal expansion ratios can be quite high causing internal shocks with associated shock noise. This also needs to be addressed in the mixer and ejector's aerodynamic design.

Economic viability demands additional considerations such as nozzle performance over the full aircraft operating range and advanced enabling materials.

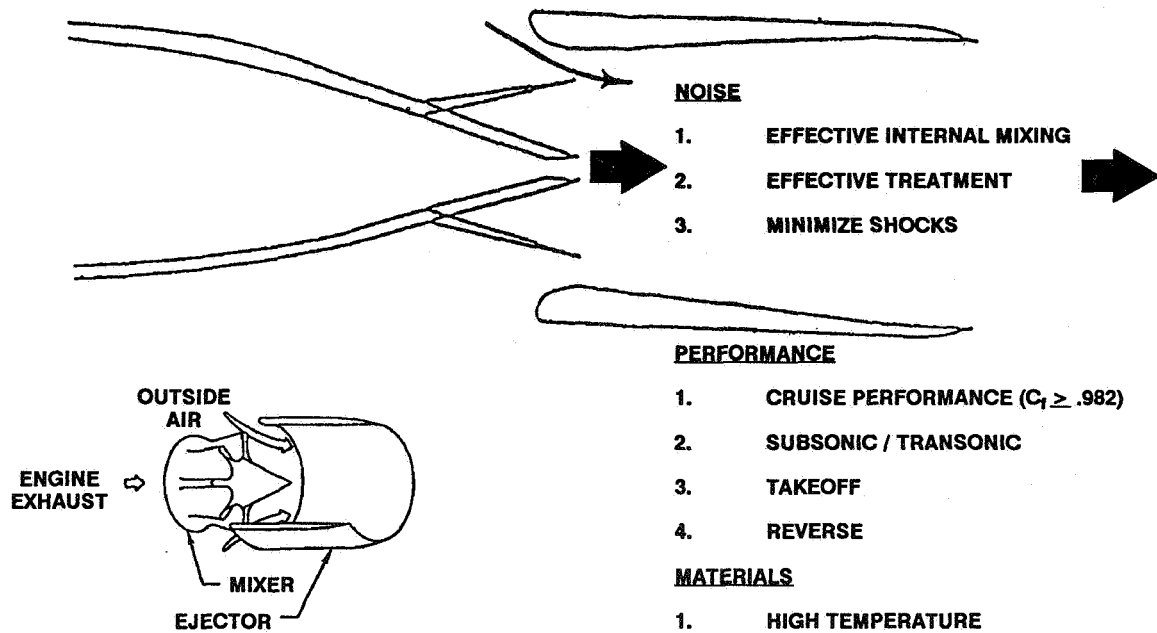


Figure 3

**1989 HSCT 2D EJECTOR MODEL TEST
IN NASA 's 9 x 15 TUNNEL**

Since 1988, Pratt & Whitney has conducted two HSCT model ejector test programs and will soon begin a third. The original HSCT high-flowing ejector designs were based on related programs conducted at United Technologies Research Center (UTRC) during the 1980's.

P&W's first HSCT ejector model program was conducted in NASA Lewis' 9x15 low speed acoustic wind tunnel in mid-1989. The 2D ejector nozzle hardware was jointly provided by P&W, UTRC, and NASA LeRC. Test facility was provided by NASA and the data analyses were shared among NASA and P&W. The 1/10 scale (approximate) model was tested with and without the ejector shroud and over a range of ejector area ratios and nozzle expansion ratios. A reference, conic nozzle was also evaluated to provide a baseline. Facility limitations at that time restricted testing to 450F jet flow. Ejector shroud static pressure taps and an exit pressure and temperature traverse were used to evaluate pumping and mixing.

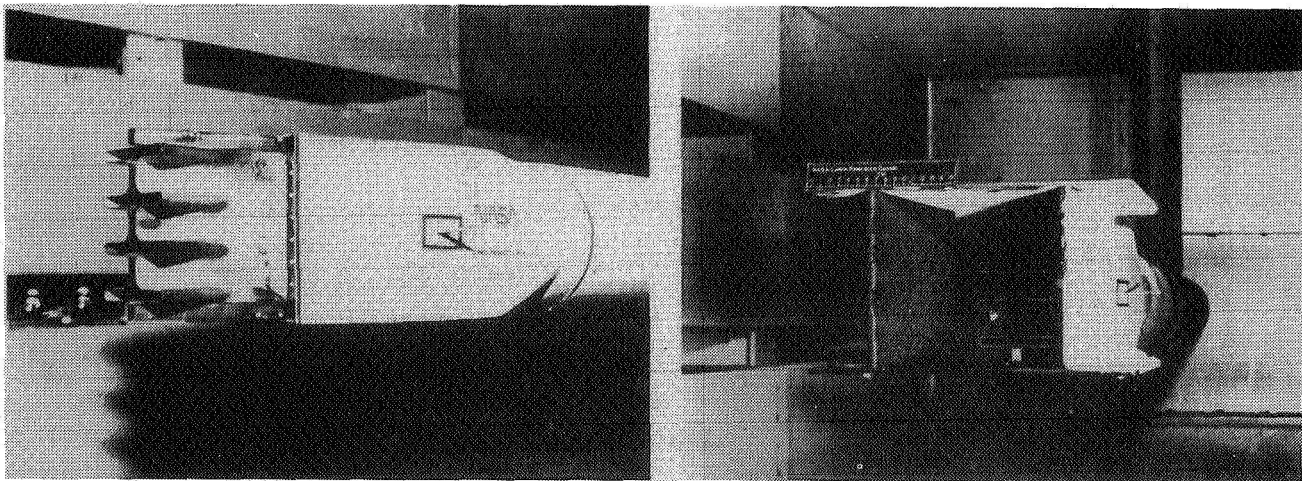


Figure 4

ORIGINAL PAGE
BLACK AND WHITE PHOTOGRAPH

TERTIARY AIRFLOW
1989 2D EJECTOR TEST

Wall static pressure taps in the ejector shroud were initially used to assess secondary airflow levels (pumping). These measured levels were later corroborated and calibrated using exit rake temperature and pressure traverses.

Ejector area ratios ($A_{mix}/A_{primary}$) in the range of 3.77 to 4.7 were tested and goal levels of pumping were shown to be technically feasible. When corrected to the engine temperature conditions of a typical HSCT engine, the goal 0.6 corrected pumping level translates to an absolute pumping level of order 120% at HSCT engine exhaust conditions.

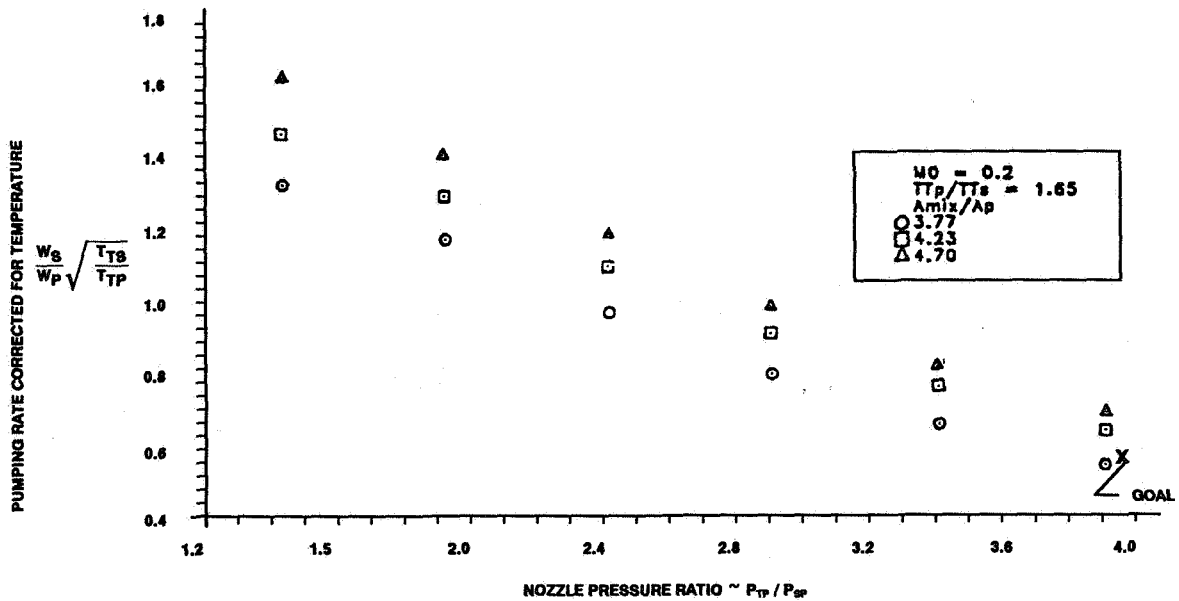


Figure 5

SHOCK NOISE DOMINATES 2D EJECTOR TEST

With the 450F temperature limit, the 2D model noise data from the 1989 program was dominated by shock noise. The measured levels for the reference conic nozzle were as predicted, verifying that the shock noise dominates. Tunnel background noise was measured and did not directly prevent acquisition and credible data. Without the higher nozzle temperatures needed to simulate realistic engine exhaust conditions (i.e.: jet velocity); the key, jet mixing noise source was not directly observable.

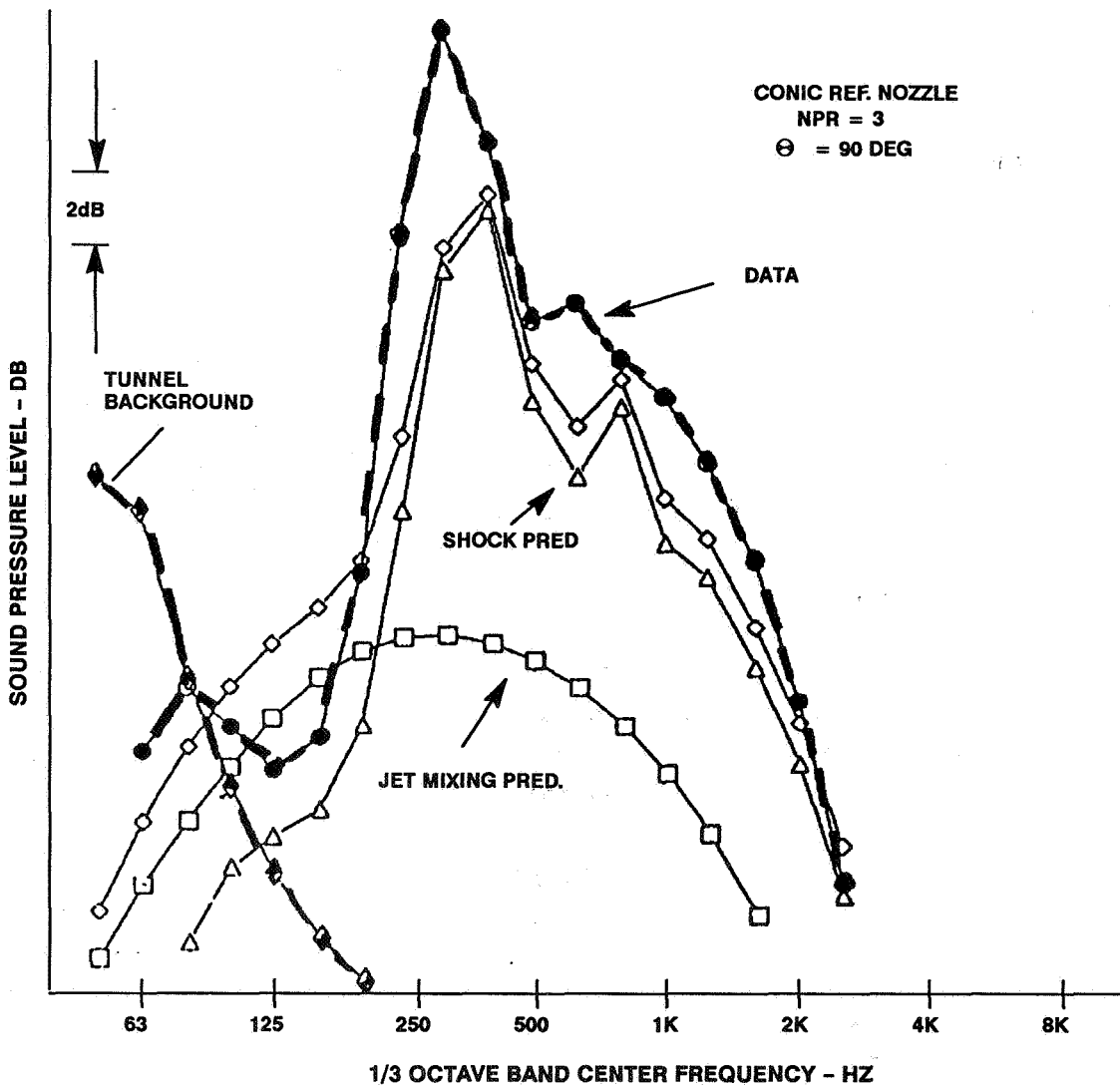


Figure 6

LESSONS LEARNED: 2D MIXER / EJECTOR IN 9' x 15'

Pressure and temperature traverses at the ejector exit indicated good mixing was achieved within the ejector. Subsequent CFD analysis of the mixing region using P&W NASTAR Navier Stokes code showed excellent agreement with the traverses. The predicted internal wall static pressure measurements made along the shroud also showed excellent agreement with the NASTAR code.

In summary, the first HSCT model nozzle test showed that very aggressive pumping levels exceeding 120% (at HSCT engine conditions) can be achieved with good mixing. Also learned was the effectiveness of CFD analysis in assessing the mixing region. More realistic temperatures would be needed in future programs, however, to obtain the proper balance between shock and mixing noise in far field noise measurements.

- NEED HIGHER JET TEMPERATURES FOR ACOUSTIC TESTING
- EXCEEDED AIR ENTRAINMENT GOALS
- GOOD MIXING
- CFD ↔ EXIT TRAVERSE: EXCELLENT AGREEMENT

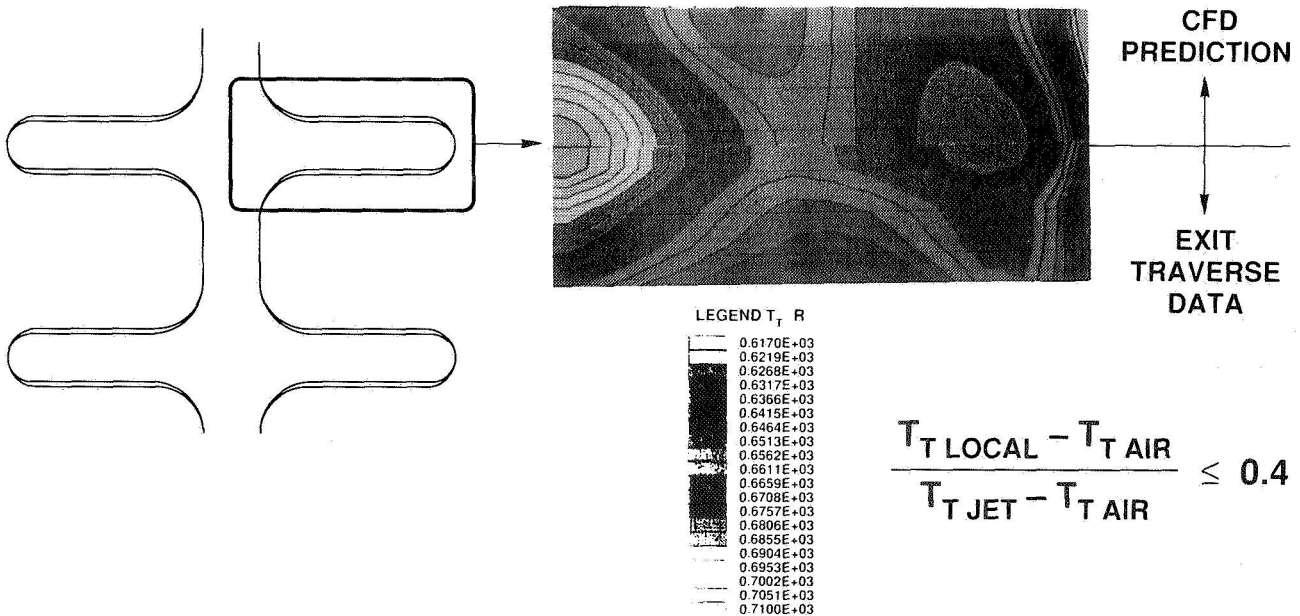


Figure 7

1990 HSCT AXISYMMETRIC EJECTOR MODEL TEST IN BOEING'S LSAF

Based on the encouraging results from the previous year's 2D ejector program at NASA, two axisymmetric ejectors were designed and procured, one with deep penetration and one with shallower lobes. An acoustically treated ejector shroud was also provided to evaluate the ability to attenuate internally generated noise.

The models were tested in Boeing's Low Speed Aeroacoustic Facility (LSAF) in mid 1990 in a joint NASA/Boeing/P&W program with the model hardware provided under NASA LeRC contract and tunnel time provided by Boeing. The models were mounted to Boeing's high temperature jet rig providing primary nozzle flows at temperatures up to 1500F.

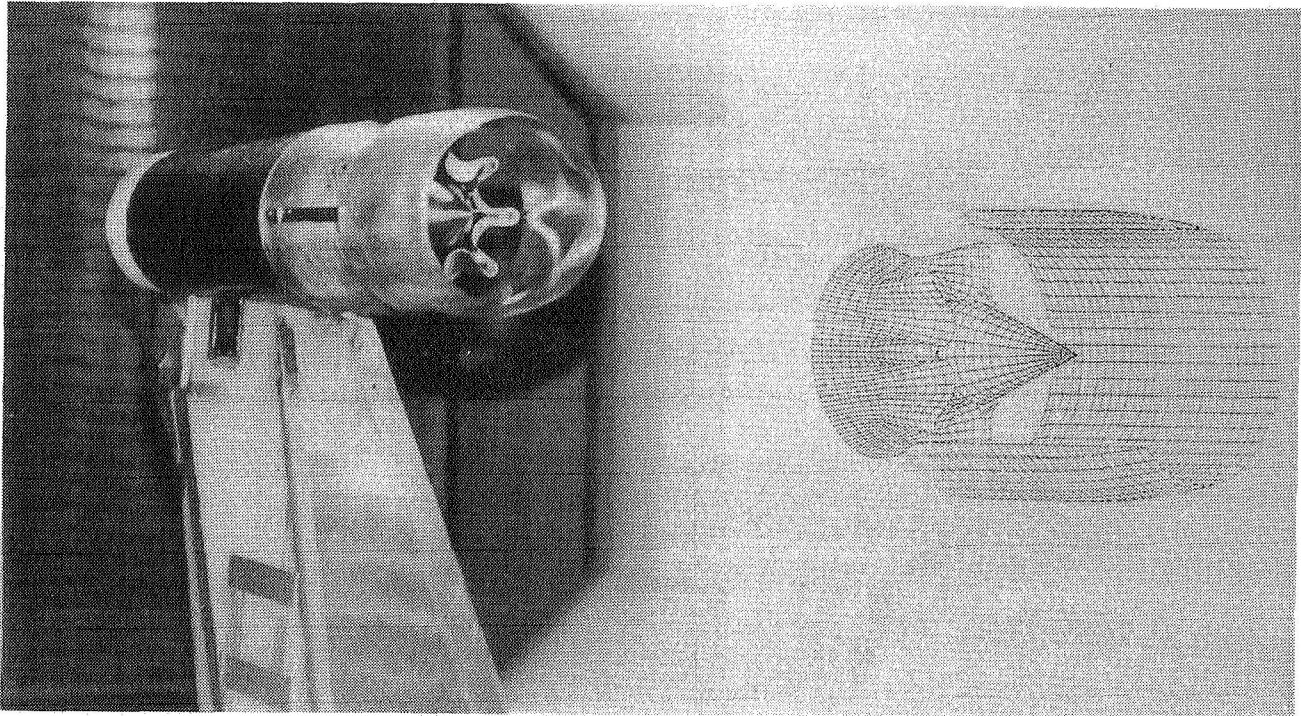


Figure 8

ORIGINAL PAGE
BLACK AND WHITE PHOTOGRAPH

AXISYMMETRIC MIXER / EJECTOR MACH CONTOURS - PEAK AND VALLEY - NASTAR
PRE TEST PREDICTIONS

The ability to successfully use P&W's CFD NASTAR code to match the previous year's model data in both exit profile and internal static instrumentation lent impetus to a pretest evaluation of the axisymmetric model. This analysis indicated two potential problems with the existing axisymmetric mixer hardware. Higher than expected local expansion ratios at the mixer exit indicated the presence of strong shocks. Ejector exit hot streaks were also projected at the core coming off the plug and near the outer wall at each mixer lobe. These hot streaks were subsequently confirmed during the test by Boeing with their IR camera.

If present, the noise associated with these hot streaks external to the ejector would not be attenuatable with ejector acoustic treatment. The test, subsequently did show this ejector acoustic liner to be ineffective with the external hot streak dominating the higher frequencies.

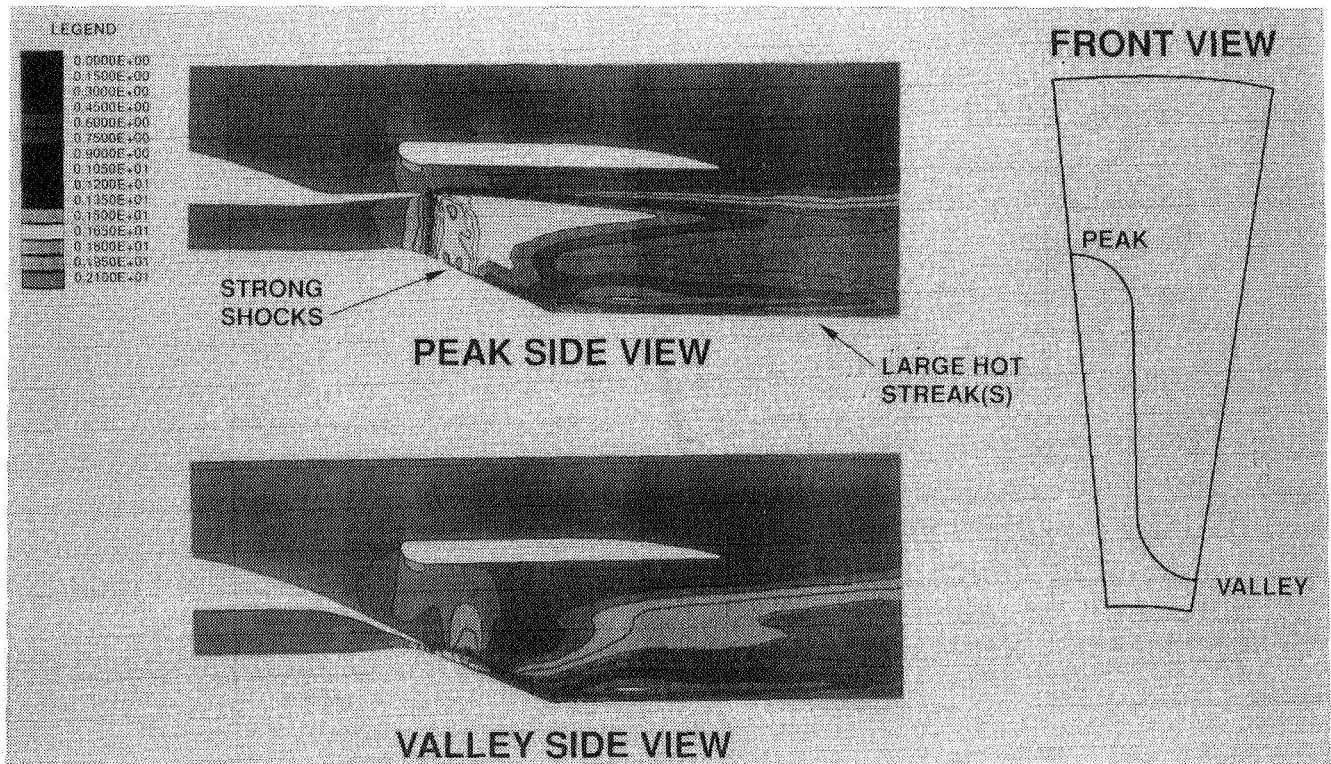


Figure 9

TERTIARY AIRFLOW OBJECTIVES ACCOMPLISHED

1990 AXI MODEL

While indicating mixing levels below target, the pre test NASTAR CFD analysis indicated design pumping levels would be achieved. Similar to the previous year's 2D model in the 9x15, the internal model aero/performance data confirmed excellent agreement with the analysis and with our goals.

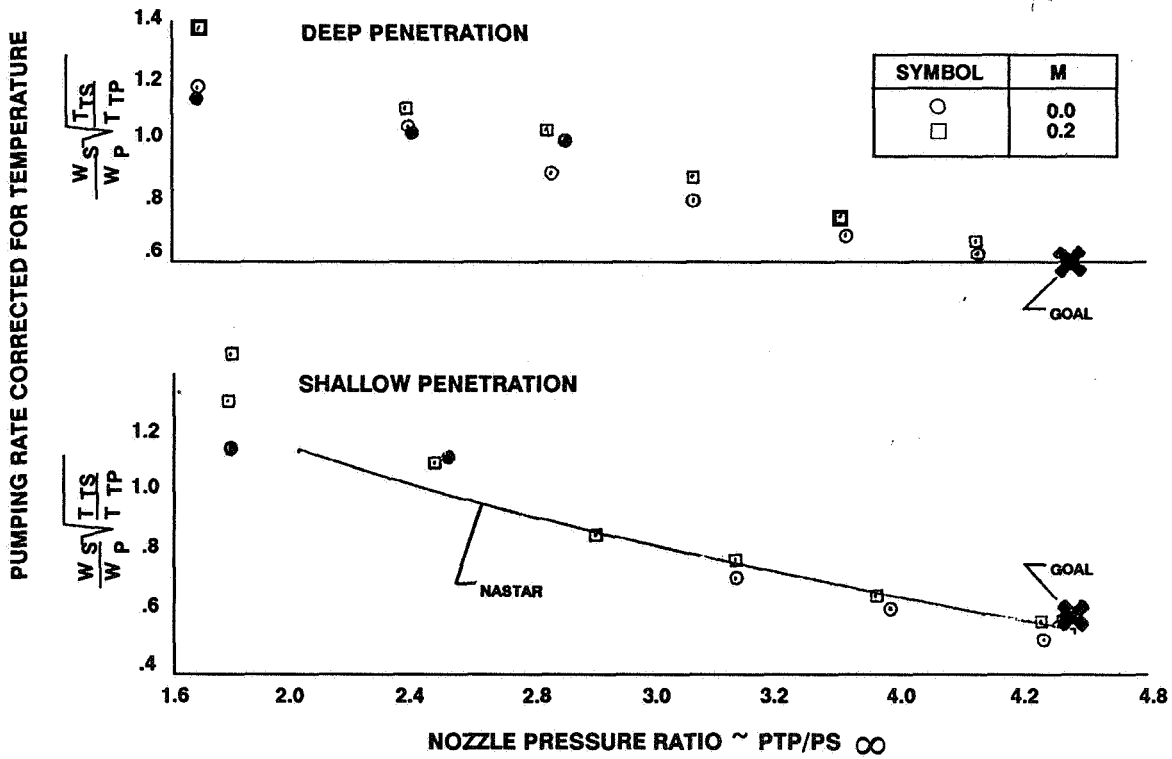


Figure 10

JET NOISE SUPPRESSOR TECHNOLOGY SUPPRESSION VS. NOZZLE PERFORMANCE

In addition to higher temperature capability, the Boeing facility also provided the opportunity to measure nozzle thrust. When compared to the reference conic nozzle, also tested by Boeing, the ejectors showed only minimal thrust decrease at forward flight conditions simulating takeoff. Even with the known aeromixing deficiencies, the ejectors provided significant noise reductions.

Compared to previous generations of jet suppressor nozzles, the ejector concept demonstrated a significant technology leap forward in terms of noise reduction per pound of thrust loss.

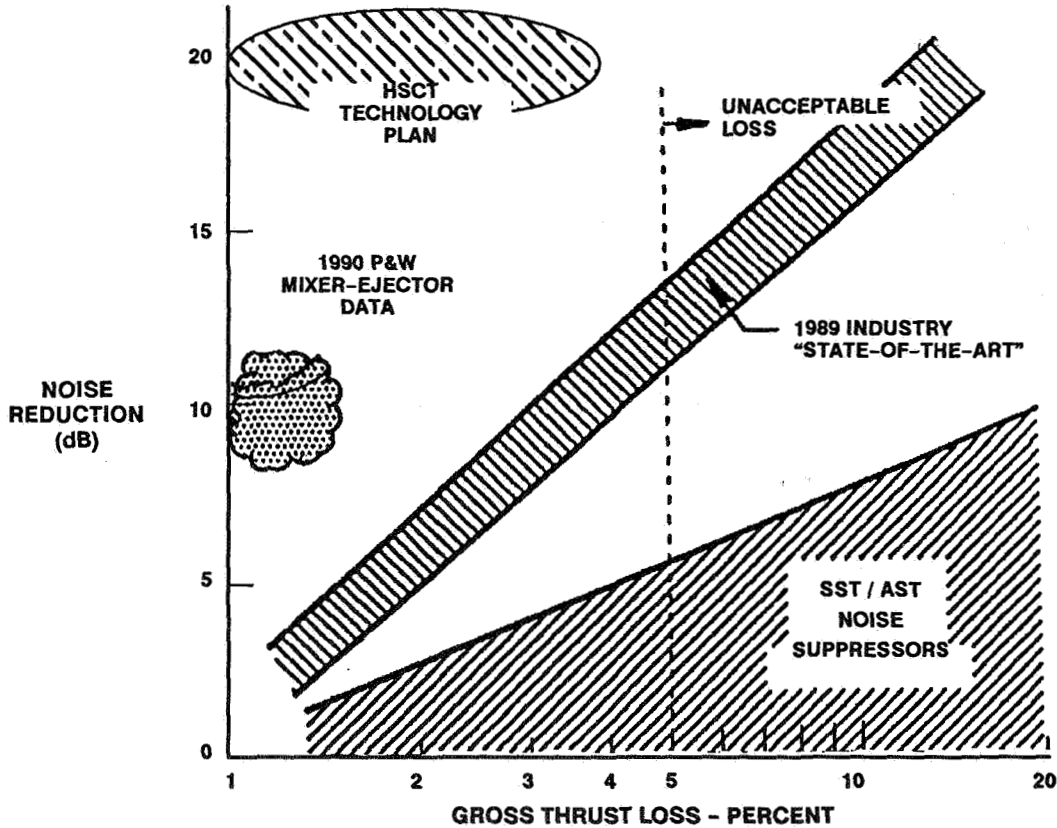


Figure 11

1991 PW / NASA HSCT EJECTOR MODEL NOISE PROGRAM

P&W and NASA are currently preparing to test the next generation 2D HSCT ejector nozzle in Lewis' 9x15 tunnel during the third quarter of 1991. In addition to a new mixer/ejector design based of CFD tools, the use of the NASA jet exit rig will provide both the higher temperature capability (1500F) and thrust measurement capability lacking in the first 9x15 test program.

The current program is a joint, cooperative effort with P&W providing the CFD analysis, hardware being pro-cured under contract to NASA Lewis, and using the NASA 9x15 tunnel and jet exit rig. Further, windows in the ejector sidewalls will also be procured enabling NASA Langley to measure the internal mixing using flow visualization techniques. The program is also being coordinated with GE's 1991 2DCD HSCT ejector model program covering a complimentary range of ejector design parameters.

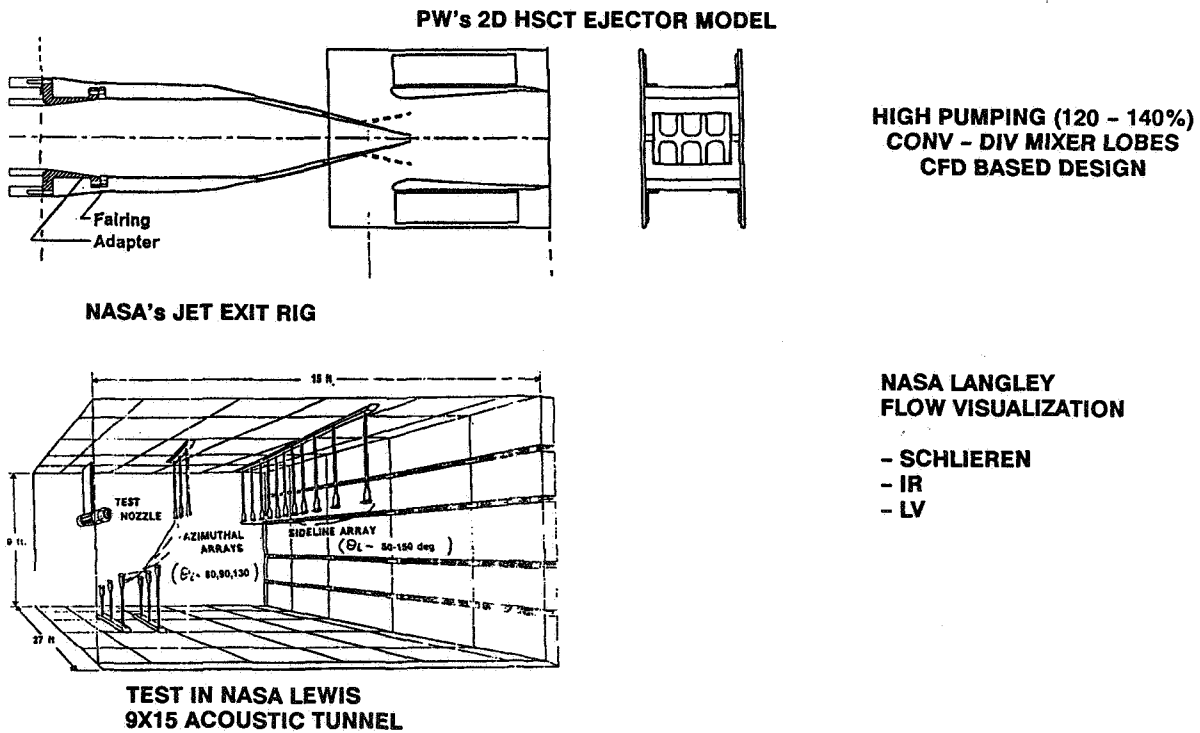


Figure 12

EJECTOR LENGTH STUDIES

An understanding of mixing length and ejector acoustic liner quantity are critical parameters in the design of a effective low noise HSCT exhaust nozzle. The upcoming 2D ejector model program in NASA Lewis' 9x15 Tunnel will specifically address both of these technology issues. A range of mixing lengths will be tested utilizing both hardwall and treated ejector shrouds and sidewalls.

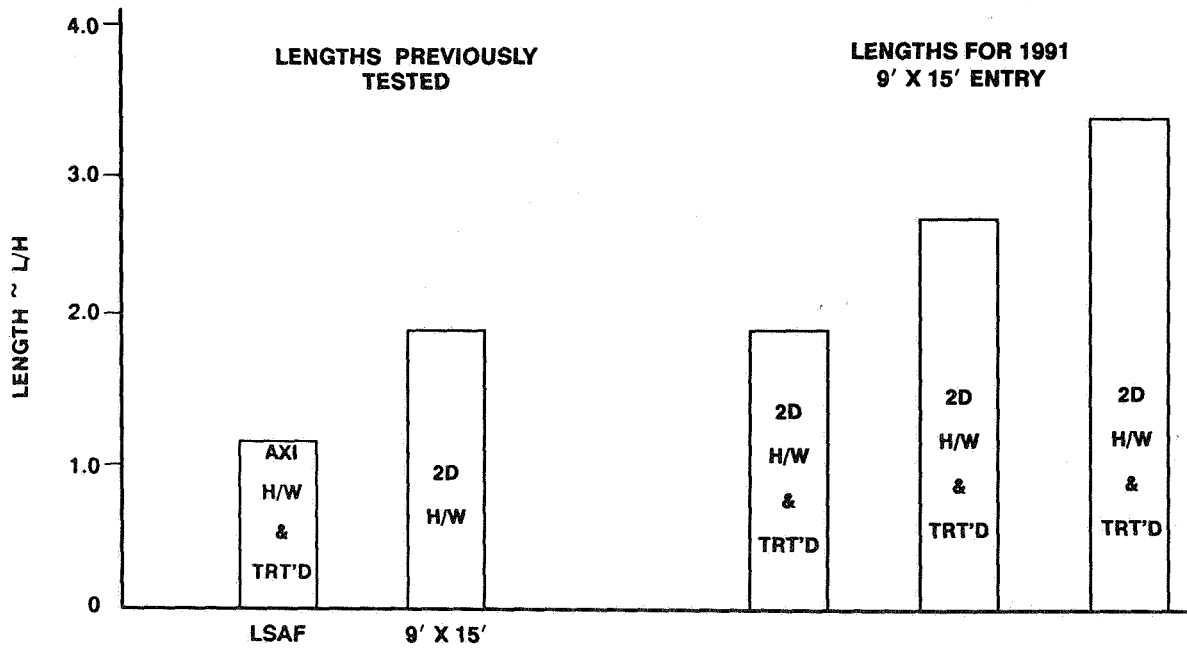
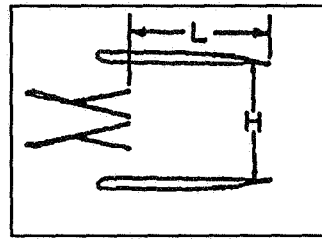


Figure 13

HSCT LOW NOISE EXHAUST TECHNOLOGY PROGRAMS (MAY 1991)

Pratt & Whitney has conducted two HSCT model ejector test programs and will soon begin a third. These current model programs are focused on the issue of ejector acoustic viability and noise reduction potential. Also being studied are needed mixing length and acoustic liner quantity.

The HSR Phase 2 program will carry the results of the model testing into a large scale demo program to verify exhaust nozzle technologies in the more realistic size. A parallel materials program will provide for critical materials enabling a viable commercial nozzle.

One outstanding issue is ejector nozzle acoustic liner technology which is projected to provide almost half the overall noise reduction from the mixer/ejector concept. Locally high temperatures, Mach numbers, and turbulence as well as large spatial gradients present a technology challenge for acoustic liner which will be required in the HSCT ejector. The selection of candidate HSCT liner concepts will also be a key HSR Phase 2 element in directing the nozzle materials effort and in the design of a demo engine nozzle. P&W and GEAE are in process off jointly developing a liner program to address these issues of acoustic liners in the unique environment of the ejector shroud.

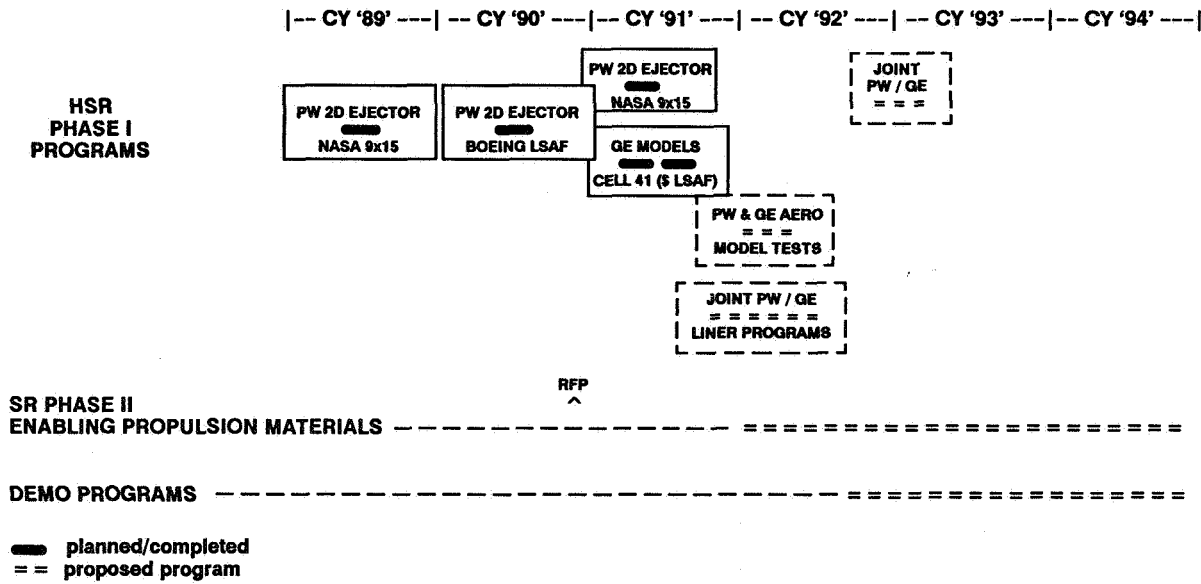


Figure 14

THIS PAGE INTENTIONALLY BLANK

Session IV. Source Noise

omit

HSCT Noise Reduction Technology Development at General Electric Aircraft Engines
Rudramuni K. Majjigi, GE Aircraft Engines

PRECEDING PAGE BLANK NOT FILMED

THIS PAGE INTENTIONALLY BLANK

**FIRST ANNUAL HIGH-SPEED RESEARCH WORKSHOP
WILLIAMSBURG, VIRGINIA**

HSCT NOISE REDUCTION TECHNOLOGY DEVELOPMENT AT GE AIRCRAFT ENGINES

**MUNI MAJJIGI
MAY 15, 1991**

54-71
11994



HSCT EXHAUST NOZZLE DESIGN APPROACHES - GEAE AND P & W

GEAE AND P&W ARE EVALUATING HIGH FLOW EJECTOR-SUPPRESSOR-MIXER NOZZLES

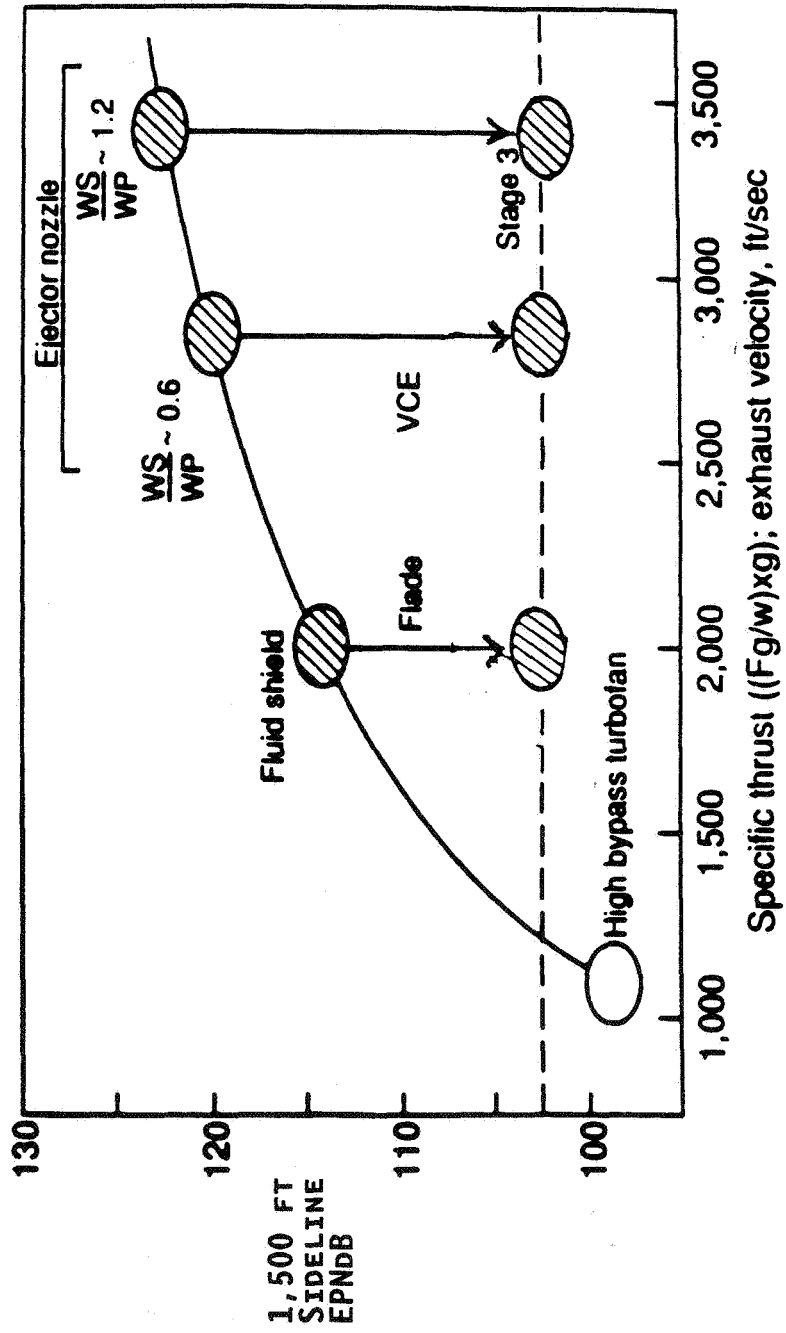
($\frac{WS}{WP} = 0.6$ AND 1.2) AS A MEANS OF OBTAINING 16-20 EPNdB SUPPRESSION

RELATIVE A SIMPLE CONIC NOZZLE TO ACHIEVE FAR 36-STAGE 3 NOISE LEVELS.

GEAE IS ALSO PURSUING A FLUID SHIELD NOZZLE IN CONJUNCTION WITH FLADE CYCLE, WHICH EMPLOYS A MUCH LOWER MASS-AVERAGED SPECIFIC THRUST (~2000 FPS) COMPARED TO EJECTOR NOZZLE. BY VIRTUE OF THE LOWER MASS-AVERAGED SPECIFIC THRUST, FLUID SHIELD NOZZLE NEEDS TO ACHIEVE ONLY 12-13 EPNdB SUPPRESSION. ACOUSTIC SUPPRESSION, NOZZLE PERFORMANCE AND PROPULSION SYSTEM WEIGHT NEED TO BE CONSIDERED IN MAKING A FINAL SELECTION AS ALL THE ABOVE HAVE A SIGNIFICANT IMPACT ON HSCT TOGW AND ECONOMIC VIABILITY.

HSCT EXHAUST NOZZLE DESIGN APPROACHES - GEAE AND P&W

- o HIGH FLOW ENGINE + MODEST NOISE REDUCTION
- o HIGH IMPULSE ENGINE + AGGRESSIVE NOISE REDUCTION



GEAE HSCT ACOUSTICS RESEARCH IS COMPOSED OF TEST, ANALYSES & SYSTEM TRADE STUDIES

THE CHART ENUMERATES THE MAJOR PROJECTS (NASA FUNDED AS WELL AS GEAE'S IR&D) CURRENTLY UNDER PROGRESS AND THEIR PRIMARY FOCUS. THE PROJECTS OFFER A SYNERGISTIC BLEND OF TEST PROGRAMS, ANALYTICAL ACTIVITIES AND HSCT SYSTEM TRADE STUDIES.

GEAE HSCT ACOUSTICS RESEARCH IS COMPOSED OF TEST, ANALYSES & SYSTEM TRADE STUDIES

PROGRAM

FOCUS

- o 2D-CD NOZZLE PROGRAM (NASA)
 - o DEMONSTRATE ~ 16-17 EPNdB SUPPRESSION REL. TO A CONIC NOZZLE @ VJ~2800 FPS
 - o ASSESS IMPACT ON A/C TOGW.
- o FLUID SHIELD PROGRAM (NASA)
 - o DEMONSTRATE FEASIBILITY OF A FLUID SHIELD NOZZLE SYSTEM (~ 12-13 EPNdB @ VMIX ~ 2000 FPS)
 - o ASSESS IMPACT ON A/C TOGW
- o IR&D PROGRAM (GEAE)
 - o GE/BOEING JOINT TEST OF HIGH AREA RATIO NOZZLE SUPPRESSOR/EJECTOR
 - o SYSTEM STUDIES SUPPORT (ANOPP, CYCLES)
 - o M*G*B JET NOISE MODEL UPGRADING
- o UNIQUE PROPULSION SYSTEM ANALYSIS (NASA)
 - o CYCLE/NOZZLE SYSTEM TRADE STUDIES

CONTRACT NAS 3-25415 - 2D-CD NOZZLE PROGRAM

BASE PROGRAM AIMED AT EVOLVING A 'PRELIMINARY DESIGN' OF AN INNOVATIVE 2D-CD SUPPRESSOR-EJECTOR NOZZLE COMBINING THE ACOUSTIC REQUIREMENTS FOR HIGH LEVELS OF AMBIENT AIR ENTRAINMENT ($\frac{M_S}{W_P} = 0.6$), SUPERSONIC CRUISE PERFORMANCE (CFG ~ 0.98) AND ACCEPTABLE NOZZLE WEIGHT (~ 5000 LBS.).

ADVANCED CFD AND ACOUSTIC CODES WERE UTILIZED IN EVOLVING THE PRELIMINARY DESIGN. CURRENT ACTIVITIES ARE AIMED AT PERFORMING SCALE MODEL ACOUSTIC TESTS IN GEAE'S CELL-41, AERO PERFORMANCE TESTS AT TAKEOFF IN A WIND TUNNEL AND AERO-MIXING EXPERIMENTS IN GEAE'S AERO RESEARCH LAB'S FREEJET WIND TUNNEL.

Contact NAS3-25415 - 2D-CD Nozzle Program Program Scope and Schedule

Task	Title	1989	1990	1991	1992
1	<u>Base program</u> Preliminary design	_____	_____▲		
2	Code utilization	_____	_____▲		
3	<u>Option A</u> Scale model tests - Cell 41 acoustic tests - Aero performance tests			_____▲ C-41 test	_____▲ Fluidyne test
4	Data analysis				_____▲
5	<u>Option B</u> Aero mixing experiments			_____▲ ARL test	
7	Program management	_____			_____▲

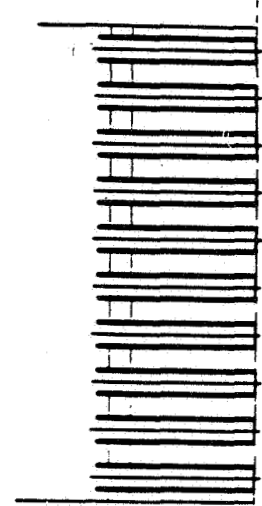
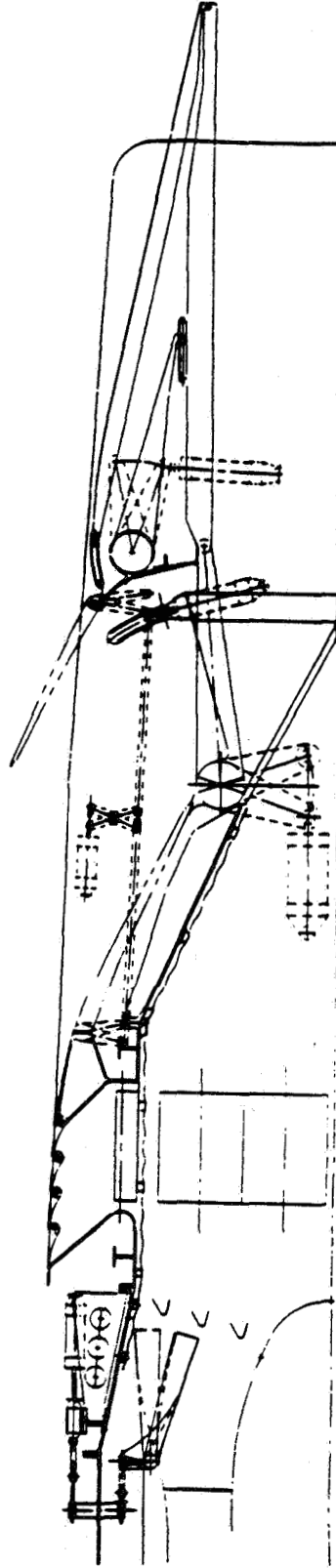
2DCD NON-IVP SUPPRESSOR EJECTOR

THE ACOUSTIC 'PRELIMINARY DESIGN' EVOLVED THRU AN EXTENSIVE REVIEW OF PAST ACOUSTIC DATA, WHICH INDICATED THAT 'INVERTED VELOCITY PROFILE' CONCEPT IN CONJUNCTION WITH SUPPRESSOR DOES NOT YIELD ANY ADDITIONAL ACOUSTIC BENEFIT AND HENCE WAS DELETED. THIS RESULTED IN A SIMPLER WEDGELESS 2D-CD NOZZLE. SIGNIFICANT CARE WAS EXERCISED IN DESIGNING AN EFFICIENT AERODYNAMIC DESIGN FOR THE EJECTOR INLET TO ENSURE THAT AMBIENT AIR ACCELERATED SMOOTHLY WITH MINIMAL INDICATION OF SEPARATION. SINCE IVP IS NOT NEEDED ANYMORE, FAN AND CORE STREAMS OF THE VARIABLE CYCLE ENGINE (VCE) ARE MIXED IN A MIXER. THE AMOUNT OF $\frac{w_s}{w_p} = 0.6$ IS DICTATED BY AS/AP, WHICH IN TURN IS LIMITED BY CRUISE NOZZLE AREA RATIO (A9/A8), AND BOATTAIL CONSIDERATIONS FOR ACCEPTABLE CRUISE PERFORMANCE AND CHUTE STOWABILITY.

2DCD Non-IVP Suppressor Ejector

September 1990 (PDR)

- Key features
 - IVP feature deleted
 - Wedgeless 2DCD nozzle
 - Efficient aerodynamic design for ejector inlet
 - Independent thrust reverser
 - Fan-core stream mixer



KEY SENSITIVITIES FROM REFERENCE AIRCRAFT ARE ESTABLISHED

IMPACT OF NOISE, AERODYNAMIC PERFORMANCE OF NOZZLE AT TAKEOFF AND CRUISE, NOZZLE WEIGHT, TAKEOFF OPERATIONAL PROCEDURES AND LOW SPEED AIRCRAFT PERFORMANCE (SUBSONIC L/D) ON HSCT TOGW ARE ENUMERATED FOR A VCE WITH 2D-CD SUPPRESSOR EJECTOR NOZZLE. CRUISE PERFORMANCE HAS THE LARGEST IMPACT ON HSCT TOGW AND WILL UNDOUBTEDLY IMPACT THE ECONOMIC VIABILITY OF HSCT. THE PAYLOAD FRACTION FOR HSCT IS ~8%.

Key Sensitivities From Reference Aircraft are Established

<u>Parameter varied</u>	<u>% change in TOGW</u>
• Sideline noise higher by 1 EPNdB	+2.4%
• Cruise performance reduced by 0.01	+4.75%
• Takeoff performance reduced by 0.01	+0.8%
• Nozzle weight increased by 2% (100 lb)	+0.35%
• PLR vs. single cutback	-5.1%
• PLR vs. single cutback and increase takeoff (L/D) of aircraft by 10%	-8.3%

Notes:

Reference TOGW, 743,810 lb

Mission, payload are constant

FAR36 Stage III noise rules satisfied

Individual linear sensitivities only

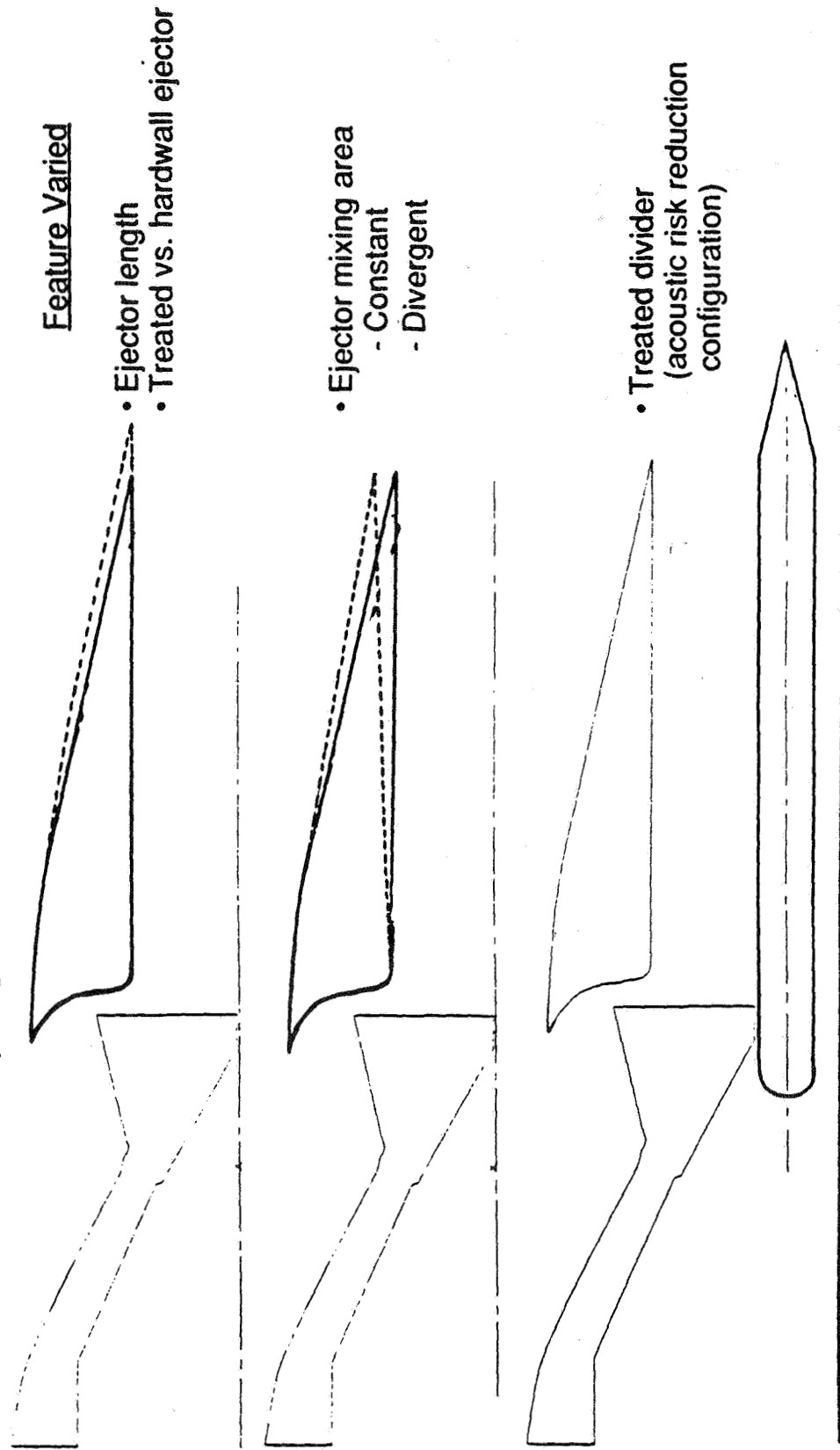
Coupled sensitivities are not necessarily additive

ACOUSTIC EXPERIMENTS

TYPICAL CONFIGURATIONAL VARIATIONS OF THE BASELINE 2D-CD SUPPRESSOR-EJECTOR NOZZLE TO BE EXPLORED IN 1/7TH SCALE ACOUSTIC MODELS IN GEAE'S CELL-41 ANECHOIC FREEJET FACILITY IN LATTER HALF OF 1991 ARE SHOWN. TREATED DIVIDER INCREASES THE ACOUSTICALLY TREATED AREA FOR THE SAME LENGTH OF THE EJECTOR FLAP. IT IS ANTICIPATED THAT THE TREATED DIVIDER WILL INCREASE FRICTIONAL LOSS AND HENCE DEGRADE CRUISE PERFORMANCE. NOISE SUPPRESSION AND CRUISE PERFORMANCE NEED TO BE TRADED.

Acoustic Experiments

Effect of ejector geometry on noise
(length, treatment, mixing area and treated divider)

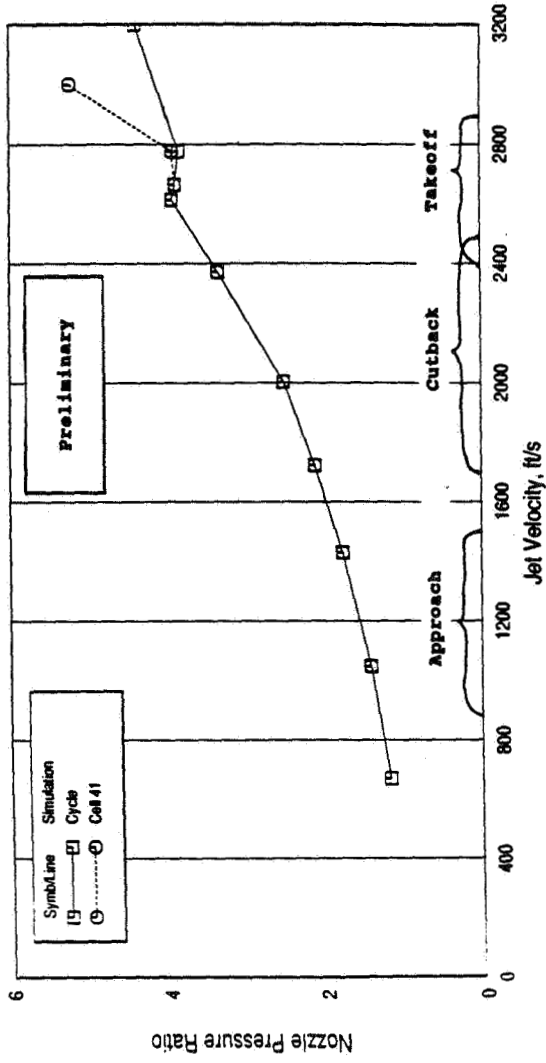


ACOUSTIC EXPERIMENTS

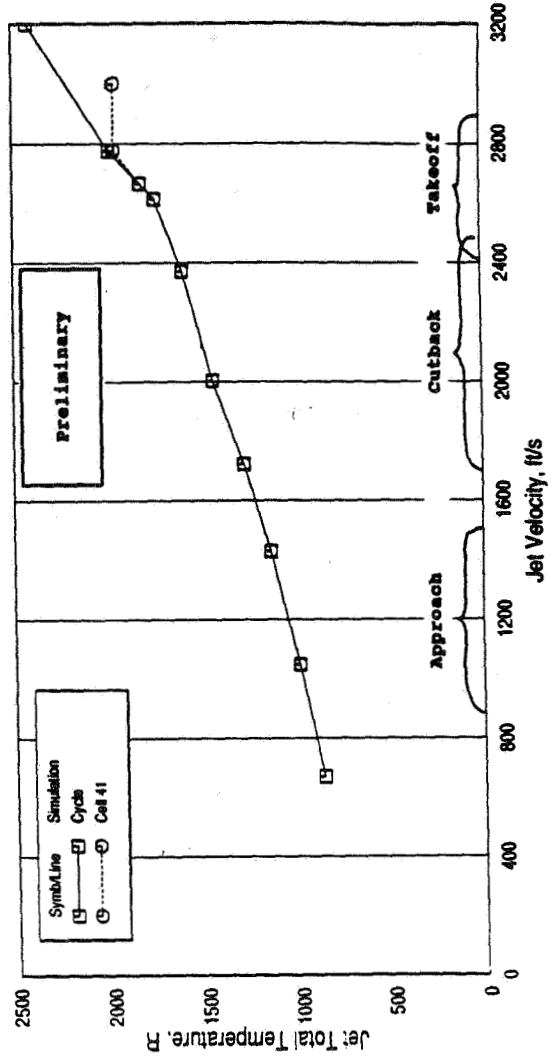
THE CHART SHOWS THE CAPABILITIES OF CELL-41 FACILITY TO SIMULATE THE GE21/F14 LIM VARIABLE CYCLE ENGINE'S EXHAUST NOZZLE AERO THERMODYNAMIC CONDITIONS. FOR $V_{MIX} \leq 2800$ FPS. THE SIMULATION OF TOTAL TEMPERATURE (T_T) AND NOZZLE PRESSURE RATIO (NPR) IS IDENTICAL. VELOCITIES GREATER THAN 2800 FPS ARE OBTAINED IN CELL-41 BY INCREASING NPR WHILE KEEPING $T_T \sim 1960$ R.

ACOUSTIC EXPERIMENTS

GE21/F14 L1M Cycle Simulation in Cell 41 - NPR



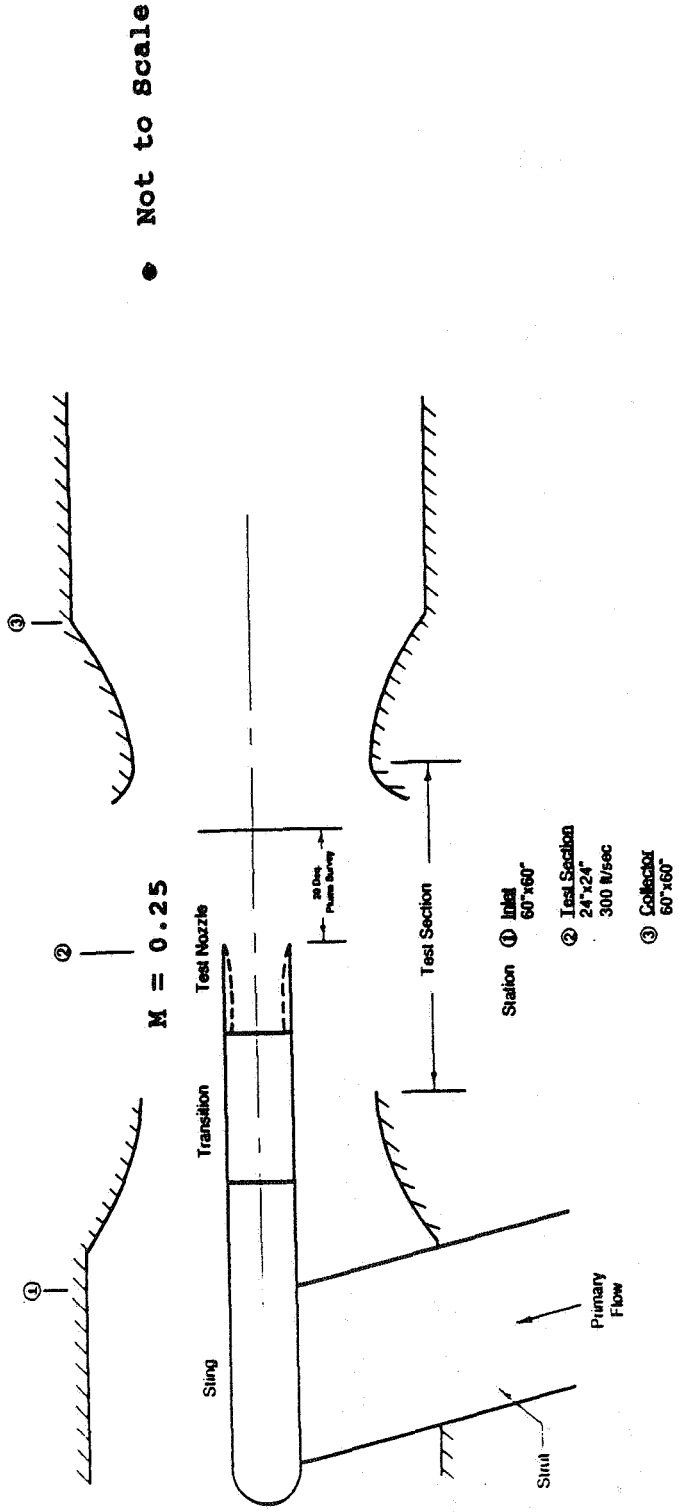
GE21/F14 L1M Cycle Simulation in Cell 41 - Tt



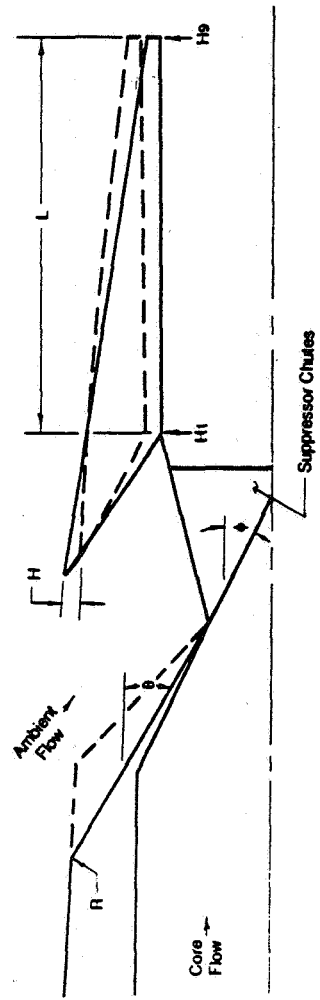
AERO-MIXING EXPERIMENTAL SET-UP AT GEAE'S ARL

THE PRINCIPAL OBJECTIVE IS TO MEASURE AND UNDERSTAND AERODYNAMIC MIXING PHENOMENA BETWEEN AMBIENT AIR AND CORE FLOW IN A FREEJET ENVIRONMENT FOR VARIOUS CHUTE SUPPRESSOR, EJECTOR INLET CONFIGURATIONS. ALSO, THE TESTS WILL BE UTILIZED TO DEVELOP AERO DESIGN DATA BASE AND SCREEN PREFERRED CONCEPTS FOR FUTURE ACOUSTIC TESTING. THE AERODYNAMIC DATA WILL BE UTILIZED FOR THE VALIDATION OF CFD CODES. TYPICAL MODEL CONFIGURATIONAL VARIANTS BEING CONSIDERED AND MEASUREMENT PLANNED ARE ALSO ILLUSTRATED.

AERO-MIXING EXPERIMENTAL SET-UP AT GEAE'S ARL



NOZZLE GEOMETRIC VARIABLES

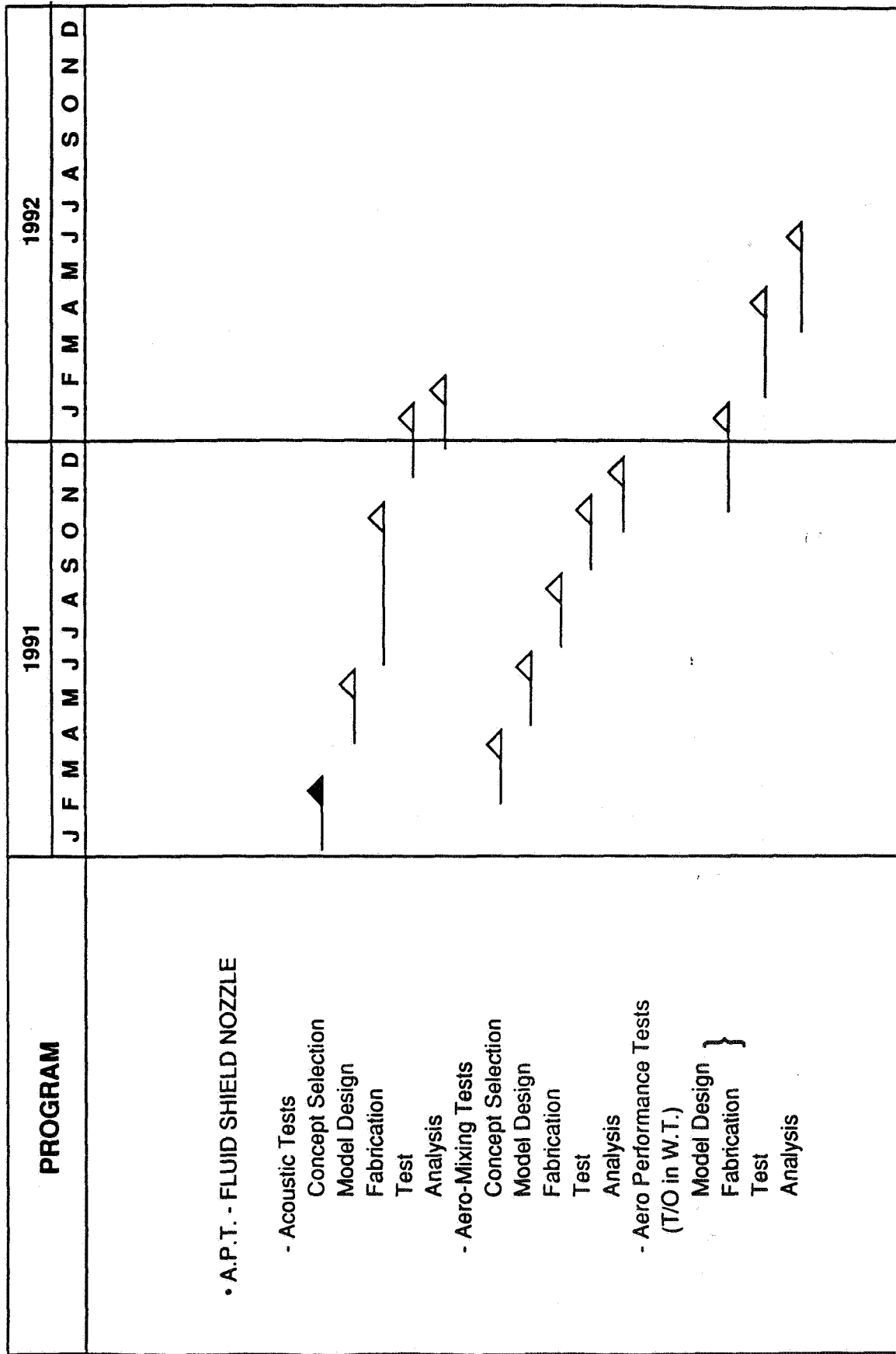


Measurements

- LV
- Kiel Probe
- Wall Static Pressure
- Pt Rakes

A.P.T. - FLUID SHIELD NOZZLE

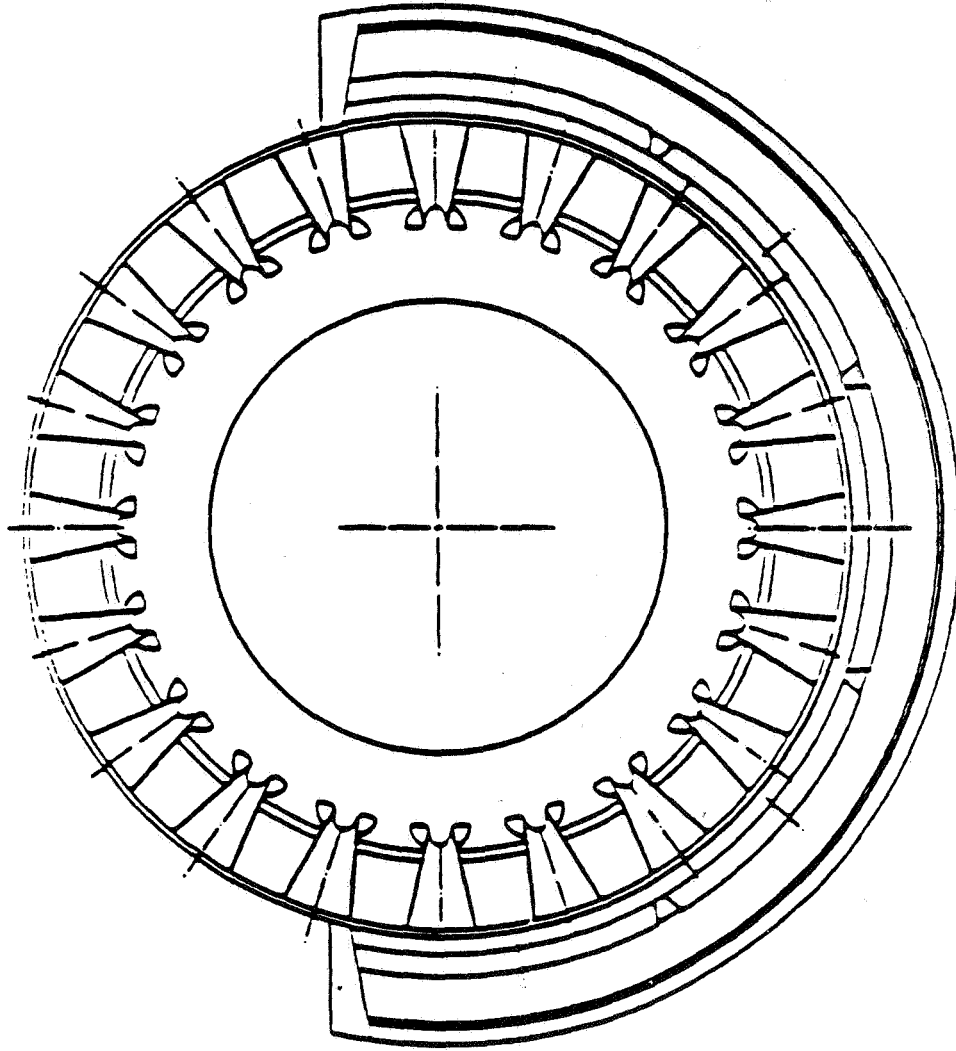
THE FLUID SHIELD NOZZLE PROGRAM CONSISTS OF ACOUSTIC RO-MIXING
AND AERO PERFORMANCE TESTS, PER ATTACHED SCHEDULE.



HSCT MACH 2.4 FLADE NOZZLE

THE CROSS-SECTIONAL VIEW OF M=2.4 FLADE NOZZLE PRELIMINARY DESIGN AT
EXIT SHOWS THE CONFIGURATION DURING TAKE-OFF MODE. THE NOZZLE EMPLOYS
A MECHANICAL SUPPRESSOR WITH 20 CHUTES AND A FLUID SHIELD SURROUNDING
THE LOWER 200 DEGREES SECTOR.

HST Mach 2.4 Flade Nozzle



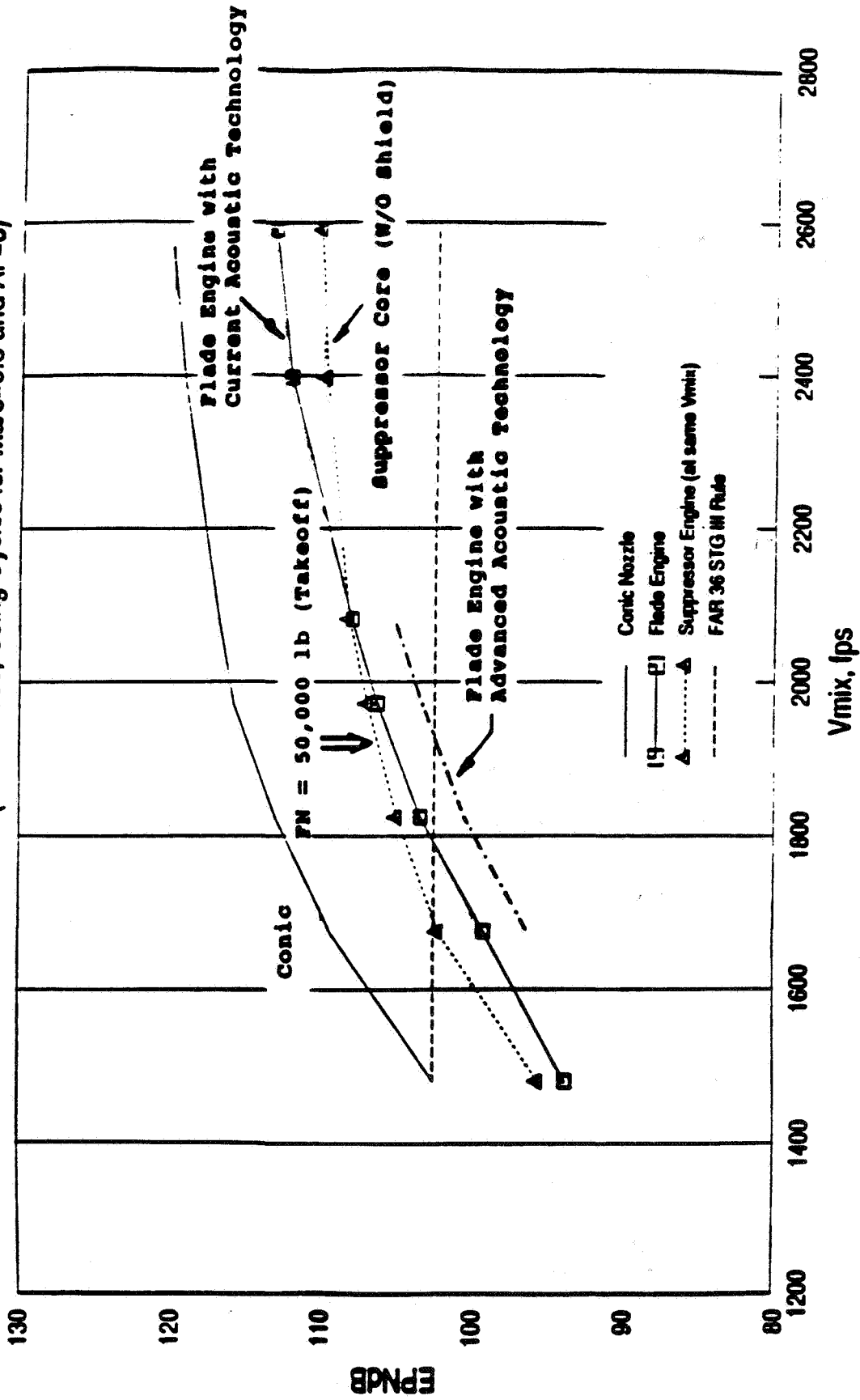
View All Looking Forward

SIDELINE NOISE PREDICTION FOR M2.4 FLADE ENGINE

ACOUSTIC PRELIMINARY DESIGN CODES AND DATABASES WERE UTILIZED IN PREDICTING THE SIDELINE EPNL AS A FUNCTION OF MASS-AVERAGED VELOCITY (V_{MIX}) FOR THE M2.4 FLADE ENGINE EMPLOYING THE FLUID SHIELD CONCEPT. FOR AN ENGINE SIZED TO PROVIDE 50,000 LBS OF NET THRUST DURING TAKEOFF, A FLADE ENGINE EMPLOYING ADVANCED ACOUSTIC TECHNOLOGY FEATURES IS ABLE TO MEET FAR-36 STAGE 3 NOISE LEVELS AT A $V_{MIX} \approx 1900-2000$ FPS

Sideline Noise Prediction for M2.4 Flade Engine

Ma/c = 0.32 and Alt = 689 ft (Shock Free, Using Cycles for Ma/c=0.3 and Al = 0)

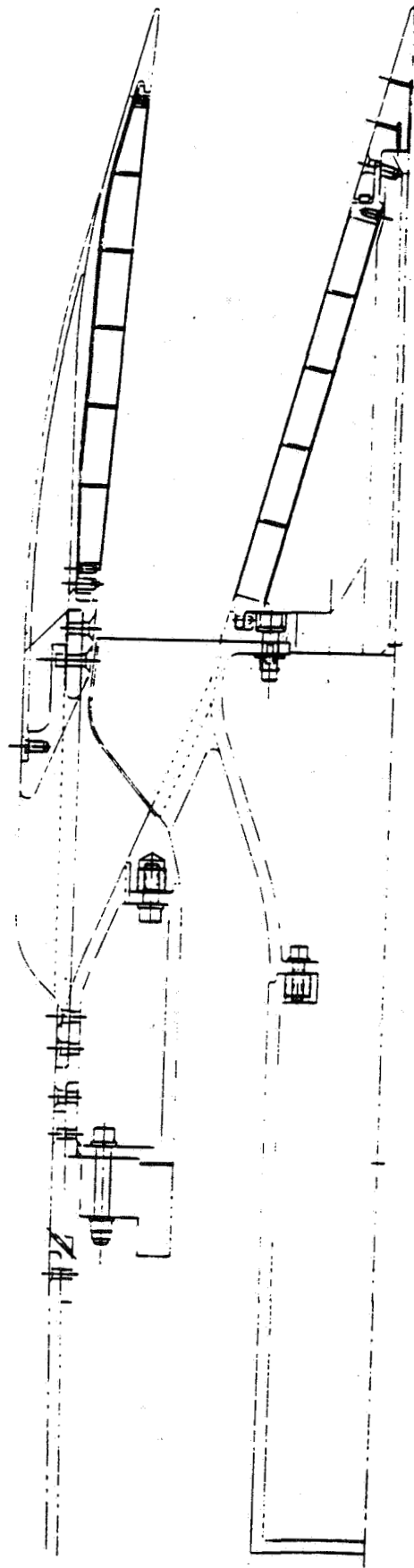


NOZZLE CONCEPT FOR GE/BOEING JOINT TEST

THIS SCALE MODEL OF A HIGH SUPPRESSOR AREA RATIO EJECTOR NOZZLE IS
DESIGNED AND FABRICATED BY GEAE FOR A COOPERATIVE TEST IN BOEING'S
LOW SPEED AEROACOUSTIC FACILITY (LSAF) DURING THE 3RD QUARTER OF 1991.
THE NOZZLE EMPLOYS ACOUSTIC SUPPRESSION FEATURES SUCH AS CONVERGENT-
DIVERGENT CHUTES, POROUS PLUG.

NOZZLE CONCEPT FOR GE/BOEING JOINT TEST

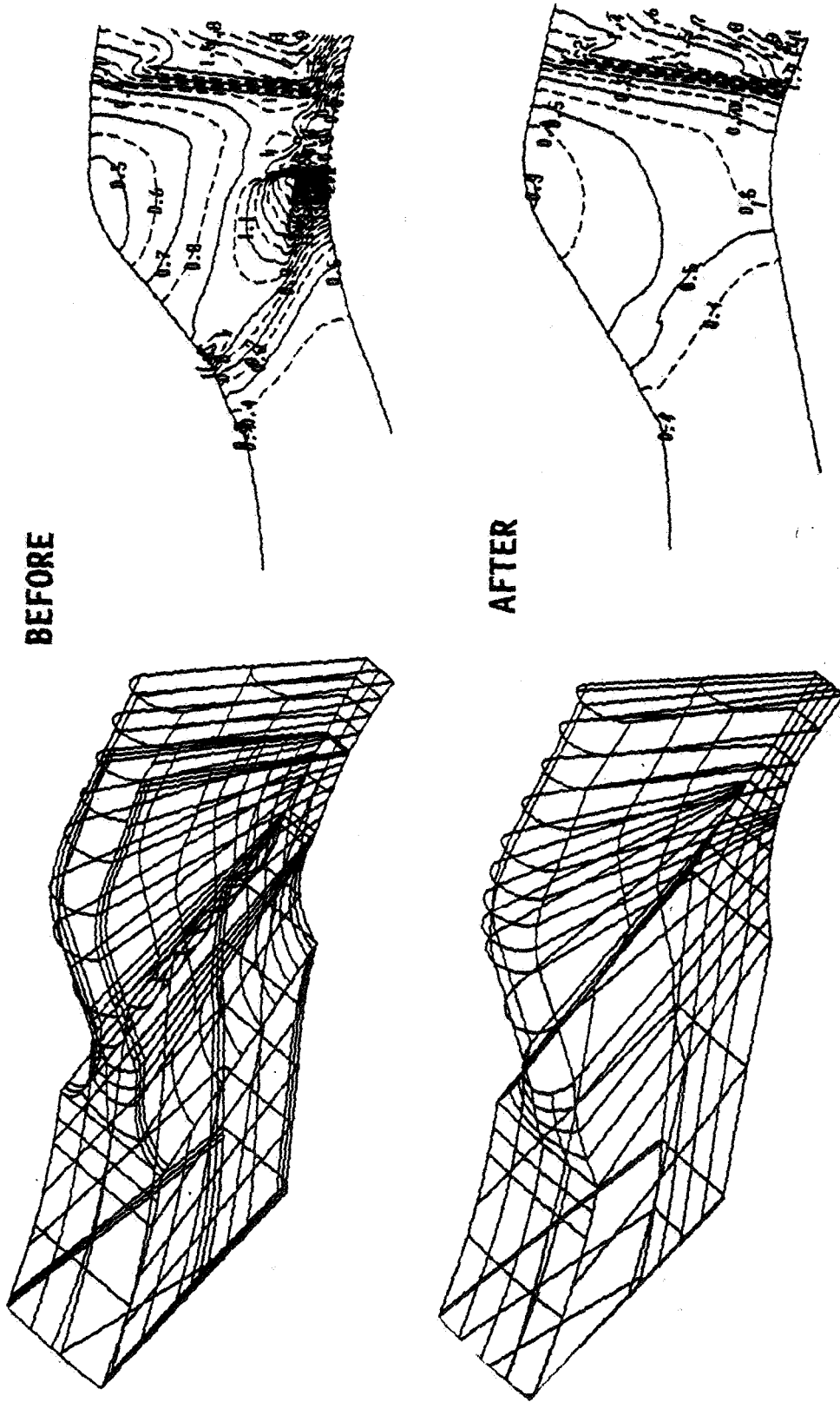
- $A_8 \approx 13 \text{ IN}^2$
- 24 C-D CHUTES
- POROUS PLUG
- SAR ~ 3
- DIVERGENT AREA MIXING



SCALE MODEL HOT CORE FLOW PATH MODIFIED TO PREVENT HUB-CHOKING CFL3D SOLUTION

INVISCID VERSION OF CFL3D CODE WAS UTILIZED IN THE DESIGN OF HOT CORE FLOWPATH. INITIAL DESIGN RESULTED IN A MINIMUM AREA IN THE REGION OF ENTRANCE TO CHUTE DUE TO THE SUPPORT STRUTS. OPENING UP THE HUB AREA PREVENTED HUB-CHOKING AND RESULTED IN A UNIFORM FLOW ACCELERATION TO THE ACTUAL THROAT OF THE C-D CHUTE. CFL3D IS UTILIZED AS A DESIGN TOOL IN THIS ILLUSTRATION.

SCALE MODEL HOT CORE FLOW PATH MODIFIED TO PREVENT HUB-CHOKING - CFL3D SOLUTION



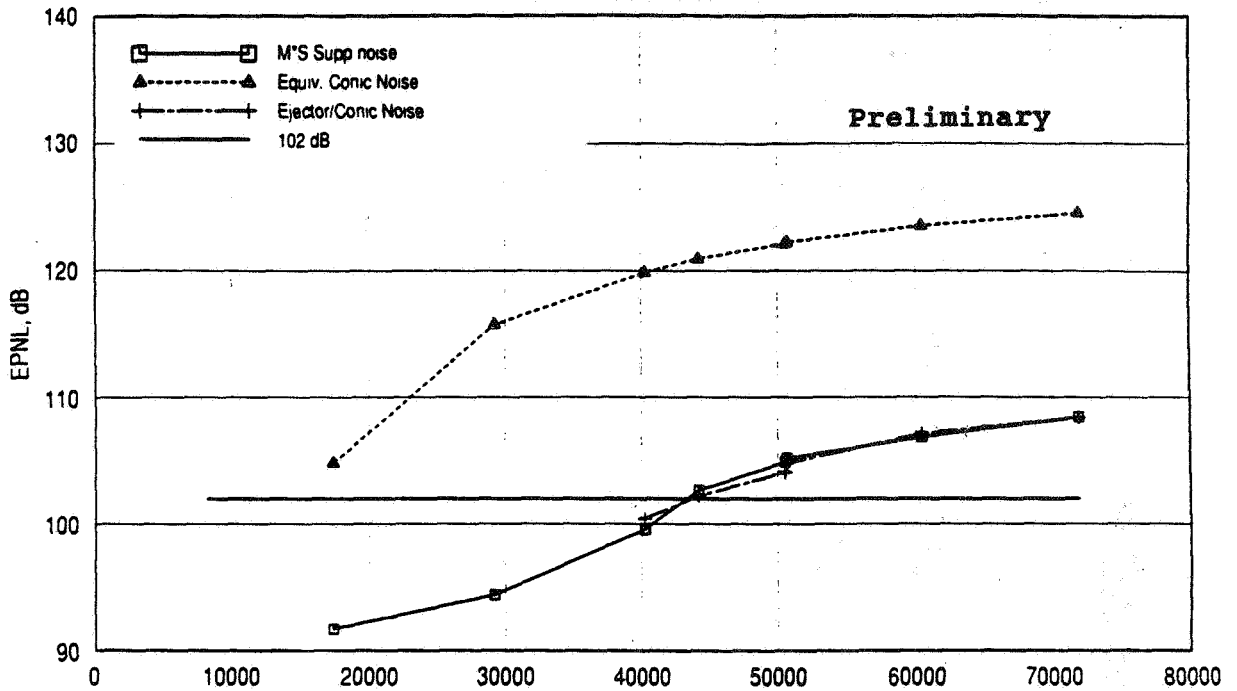
PRE-TEST NOISE PREDICTION

GEAE'S MS EMPIRICAL PREDICTION METHOD WAS UTILIZED TO MAKE THE PRE-TEST PREDICTIONS FOR A TYPICAL VCE CYCLE. FOR A FN = 50,000 LBS. 17-18 EPNdB SUPPRESSION RELATIVE TO CONIC NOZZLE IS BEING PREDICTED FOR SIDELINE (ALT = 689 FT). FOR COMMUNITY NOISE (ALT ~ 1000 FT). SIMILAR LEVELS OF SUPPRESSION ARE PREDICTED AT FN = 42000 LBS.

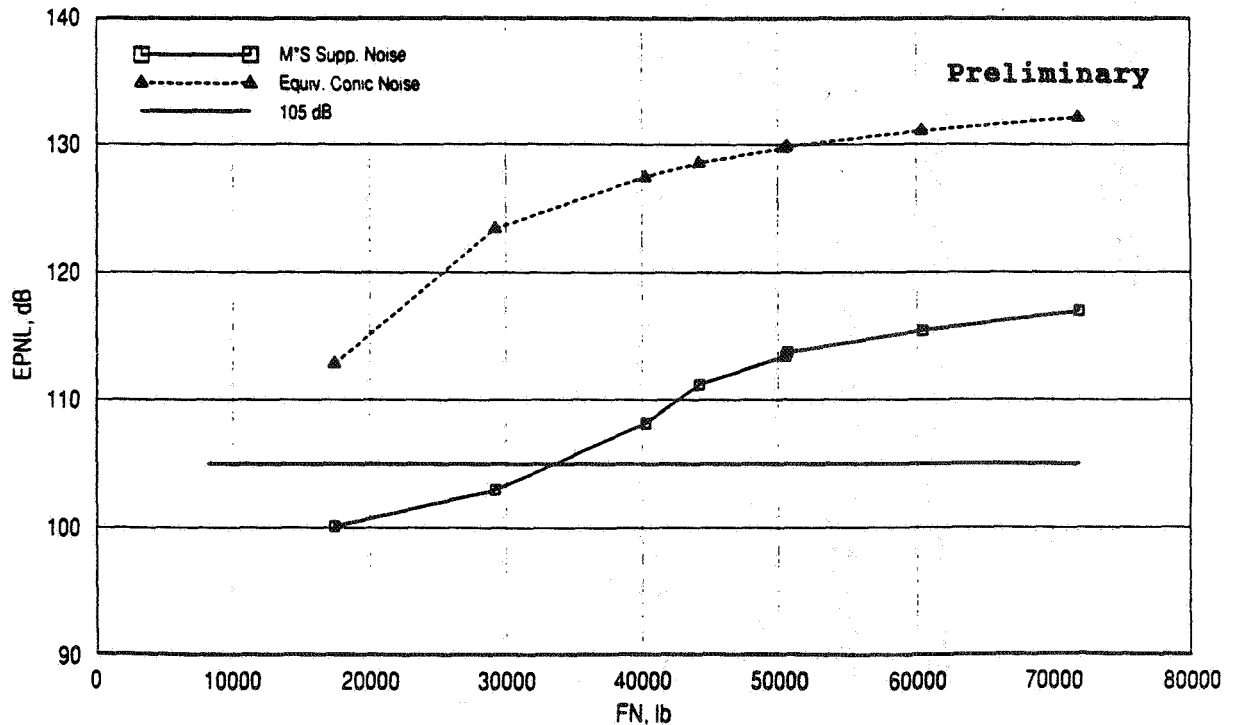
PRE-TEST NOISE PREDICTION

M = 0.23

Sideline Noise. Alt = 689 ft



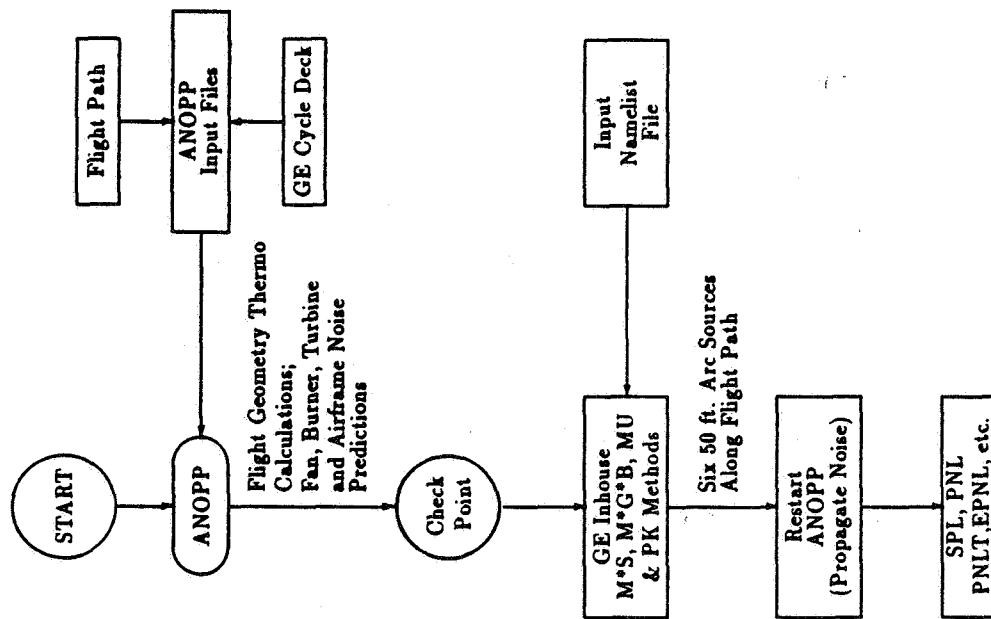
Community Noise. Alt = 1000 ft



FLOW CHART FOR THE GEAE CUSTOMIZED ANOPP

NASA LANGLEY' AIRCRAFT NOISE PREDICTION PROGRAM (ANOPP) HAS BEEN CUSTOMIZED TO UTILIZE GEAE'S CYCLE DECK, TAKEOFF TRAJECTORY AND SOURCE NOISE MODELS (SUCH AS MS, M*G*B, ETC.) FOR ASSESSING IMPACT OF TAKEOFF OPERATIONAL PROCEDURES AND LOW SPEED AIRCRAFT PERFORMANCE ON HSCT FAR 36 STAGE 3 RULE COMPLIANCE. HSCT TOGW INFORMATION COULD BE FURTHER UTILIZED FOR ASSESSING ECONOMIC VIABILITY.

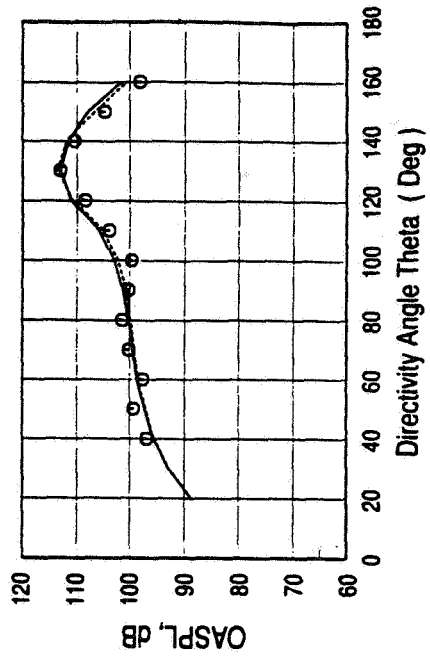
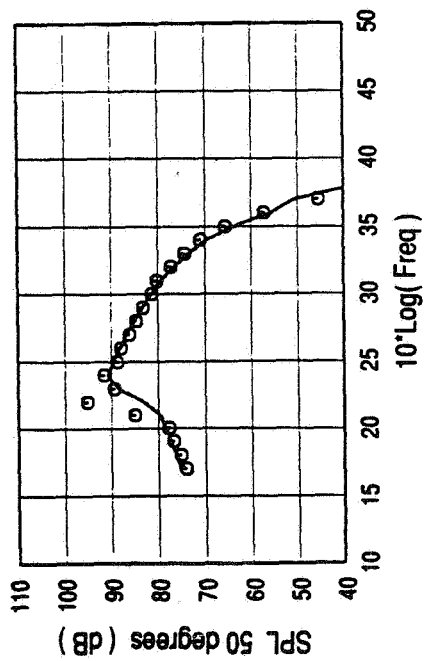
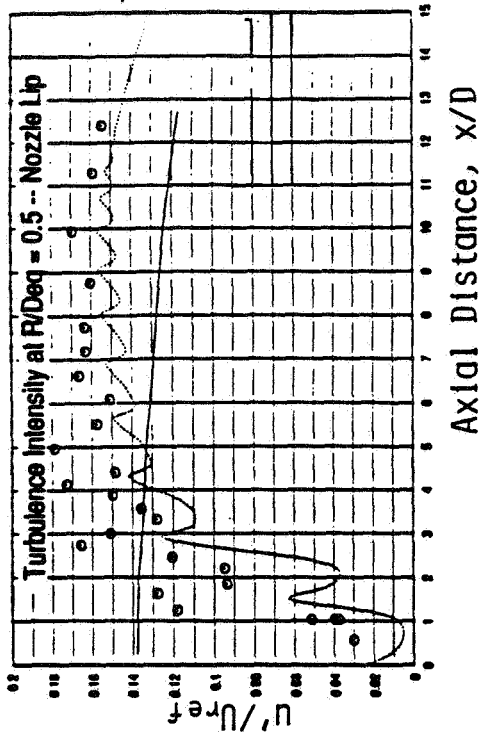
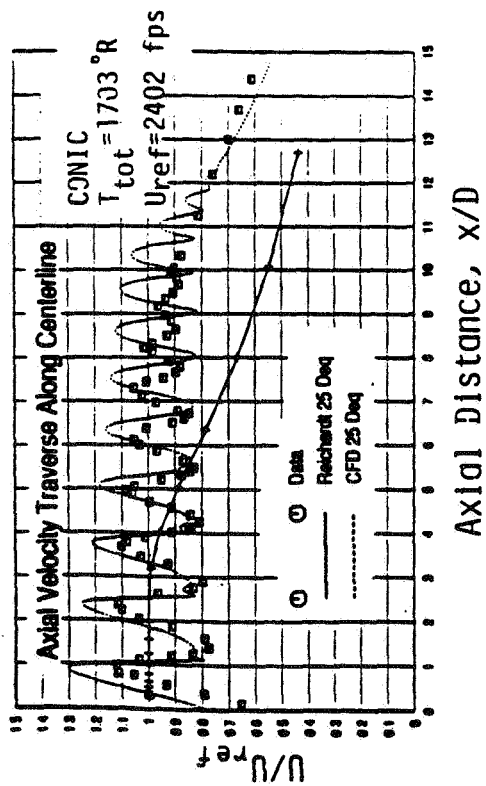
Flow Chart for the GEAE Customized ANOPP



**GEAE'S M*G*B JET NOISE CODE IMPROVEMENTS INCLUDE CFD PLUME FLOW FIELD
AND TAM'S SHOCK NOISE MODEL**

ADVANCED CFD CODES WITH K-E TURBULENCE MODELING PROVIDE MORE ACCURATE
FLOW FIELD INFORMATION FOR NOISE PREDICTIONS UTILIZING GEAE'S M*G*B CODE.
STATE-OF-THE-ART SHOCK NOISE MODEL OF PROF. TAM IS INCLUDED. EXCELLENT
AGREEMENT FOR CONIC NOZZLE (SPECTRAL AND DIRECTIVITY) ARE OBTAINED. MORE
COMPLEX NOZZLE SHAPES ARE PLANNED TO BE ANALYZED.

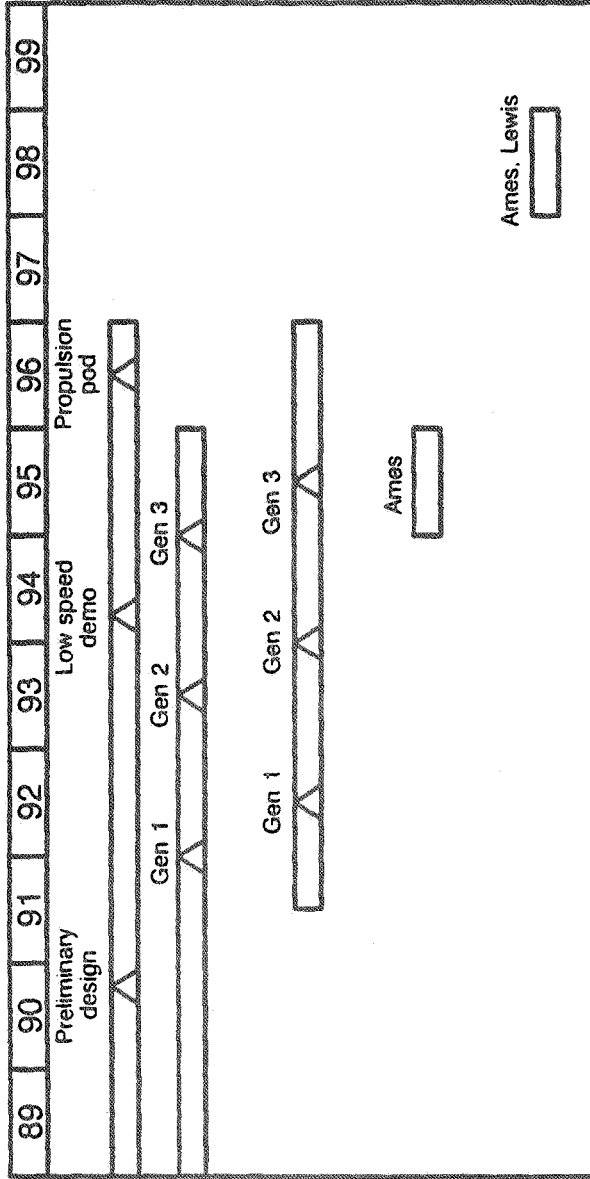
GEAE'S M*G*B JET NOISE CODE IMPROVEMENTS INCLUDE CFD PLUME FLOW FIELD AND TAM'S SHOCK NOISE MODEL



HSCT EXHAUST NOZZLE STATUS

THE HSCT EXHAUST NOZZLE TECHNOLOGY DEVELOPMENT INVOLVES SIGNIFICANT AERODYNAMIC AND ACOUSTIC SCALE MODEL TESTING. INITIAL SCREENING TESTS ARE PLANNED TO BE COMPLETED BY THE END OF 1991 TO EVALUATE THE VARIOUS APPROACHES TO NOISE REDUCTION. ENHANCED COMPUTATIONAL CAPABILITY IS BEING USED IN THE EXHAUST NOZZLE DESIGNS. EXHAUST NOZZLE ACOUSTIC LINING HAS BEEN IDENTIFIED AS A CRITICAL TECHNOLOGY AND PLANS ARE UNDERWAY TO BEGIN TO DEVELOP THIS TECHNOLOGY. THE NEED FOR AN EARLY LARGE SCALE EXHAUST NOZZLE TEST TO VERIFY THE SCALE MODEL RESULTS HAS BEEN IDENTIFIED. TESTING IS PLANNED TO BE CONDUCTED IN THE AMES 40 X 80 WIND TUNNEL. A SECOND LARGE SCALE TEST INCORPORATING A SECOND OR THIRD GENERATION EXHAUST NOZZLE IS PLANNED FOR 1998. THIS NOZZLE WILL BE TESTED IN THE LEWIS 10 X 10 SUPERSONIC TUNNEL, IN ADDITION TO THE AMES FACILITY.

HSCT Exhaust Nozzle Status



Accomplishments

- Preliminary designs of 3 exhaust nozzle systems
- Tested 2 high entrainment ejector concepts
- Initiated 3 additional generation 1 model test programs for 1991
- Assessed/developed analytical tools for nozzle design (aero and acoustics)
- Identified acoustic lining as critical technology
- Utilized ANOPP to evaluate aircraft takeoff noise and impact of operational procedures and aircraft low speed performance

KEY ACOUSTIC TECHNOLOGY ISSUES FOR HSCT

GEAE'S PERSPECTIVE

THIS WORD CHART IS SELF-EXPLANATORY.

KEY ACOUSTIC TECHNOLOGY ISSUES FOR HSCI
GEAE'S PERSPECTIVE

- o **ADVANCED LOW NOISE NOZZLE CONCEPTS MUST BE MECHANICALLY VIABLE WITH DUE CONSIDERATION GIVEN TO MISSION REQUIREMENTS (CRUISE PERFORMANCE, WEIGHT, STOWABILITY, INSTALLATION, ETC.)**
- o **ALTERNATE CYCLES (HIGH FLOW) WHICH SIMPLIFY EXHAUST NOZZLE CONSIDERABLY SHOULD CONTINUE TO BE STUDIED.**
- o **FOR EJECTOR NOZZLE CONCEPT TO SUCCEED, CRITICAL ELEMENTS OF ACOUSTIC LINER TECHNOLOGY (SUPPRESSION POTENTIAL, SCALING, DESIGN CONCEPTS, HIGH MACH AND TEMPERATURE EFFECTS, ETC.) NEED TO BE DEVELOPED AGGRESSIVELY.**
- o **CONTROLLED EXPERIMENTS TO ASSESS BASELINE NOZZLE NOISE LEVELS IN FLIGHT ARE NECESSARY TO QUANTIFY SUPPRESSION NEEDED.**
- o **OTHER NOISE SOURCES (FAN, CORE, TURBINE) MAY NEED TO BE CONSIDERED FOR APPROACH NOISE ASSESSMENT.**

THIS PAGE INTENTIONALLY BLANK

omit

Session IV. Source Noise

Community Noise Sources and Noise Control Issues
Gene L. Nihart, Boeing Commercial Airplane Group

PRECEDING PAGE BLANK NOT FILMED

THIS PAGE INTENTIONALLY BLANK

N94-33467

COMMUNITY NOISE SOURCES
AND NOISE CONTROL ISSUES

55-71
11995

G. L. Nihart

Boeing Commercial Airplane Group

Seattle, Washington

High Speed Research
First Annual Workshop
May 14-16, 1991

PRECEDING PAGE BLANK NOT FILMED

593



COMMUNITY NOISE SOURCES AND NOISE CONTROL ISSUES

- TURBINE BYPASS ENGINE (TBE) NOISE LEVELS FIGURE 1

- JET NOISE CONTROL
 - * ENGINE CYCLE IMPLICATIONS FIGURE 2
 - * NOZZLE DEVELOPMENT SCHEDULE FIGURE 3
 - * NOZZLE TEST RESULTS
 - NACA NOZZLE FIGURES 4, 5
 - NFM NOZZLE FIGURES 6 - 8

- TEST TECHNOLOGY FIGURES 9 - 11

- CONCLUSIONS

NOISE COMPONENTS TBE TURBOJET

Unsuppressed levels for the Turbine Bypass Turbojet Engine (TBE) at each of the certification points indicates the suppression needed to achieve FAR 36 Stage 3. At sideline 20 EPNdB jet noise suppression is needed, at cutback 16 EPNdB jet noise and 2 EPNdB burner noise, at approach 6 EPNdB jet noise, 7 EPNdB burner noise and 10 EPNdB suppression of turbine noise.

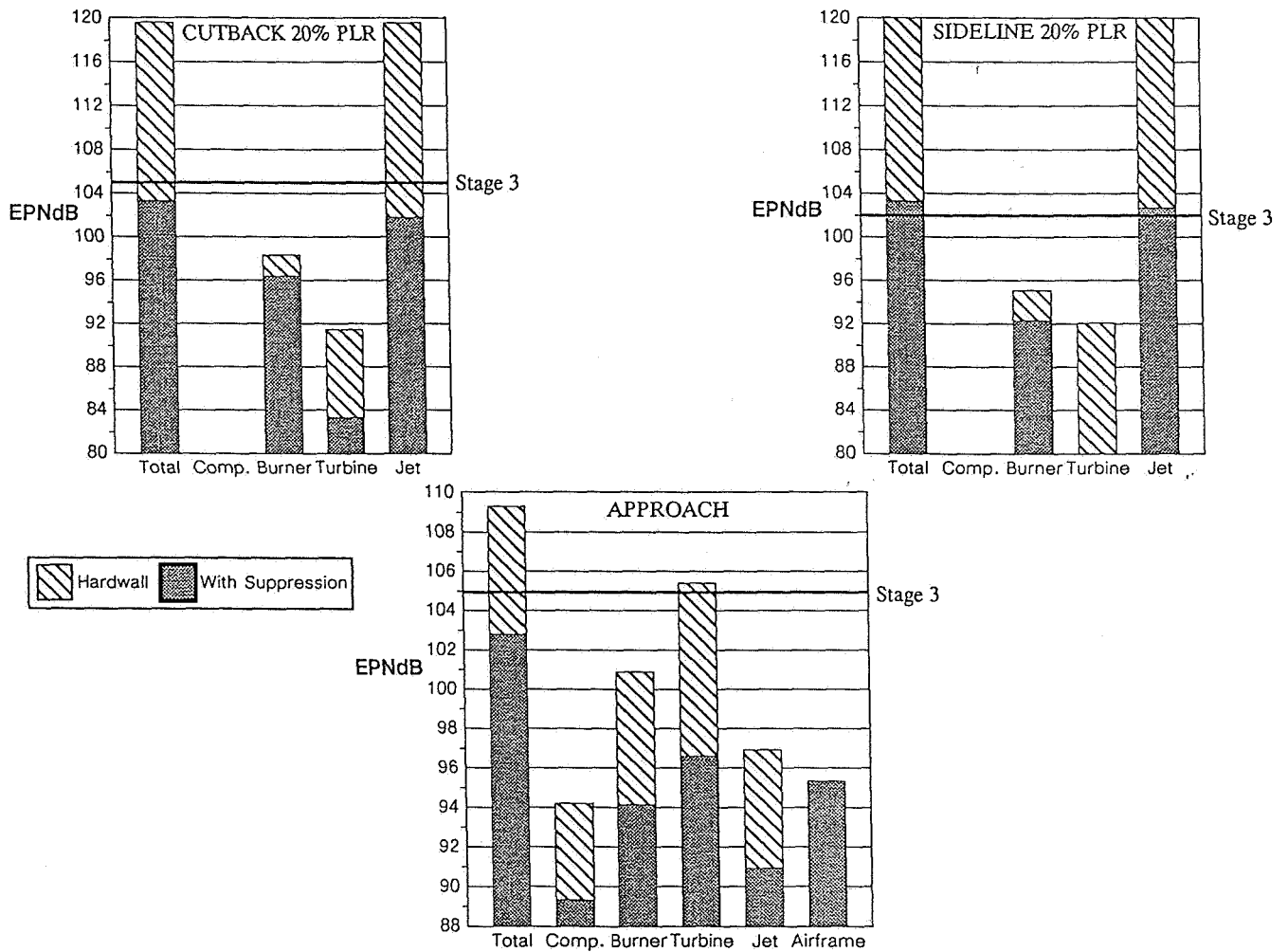


Figure 1 Noise Components Turbine Bypass Turbojet Engine

ENGINE CYCLE SELECTION AND NOISE

The engine cycle selection will determine the jet noise suppression required from 20 EPNdB for the turbojet to less than 10 EPNdB for some of the low specific thrust variable cycle engines. Understanding of nozzle technology to achieve 20 EPNdB suppression is needed to understand the engine cycle / jet suppression trades.

Variable Cycle Engine Developments

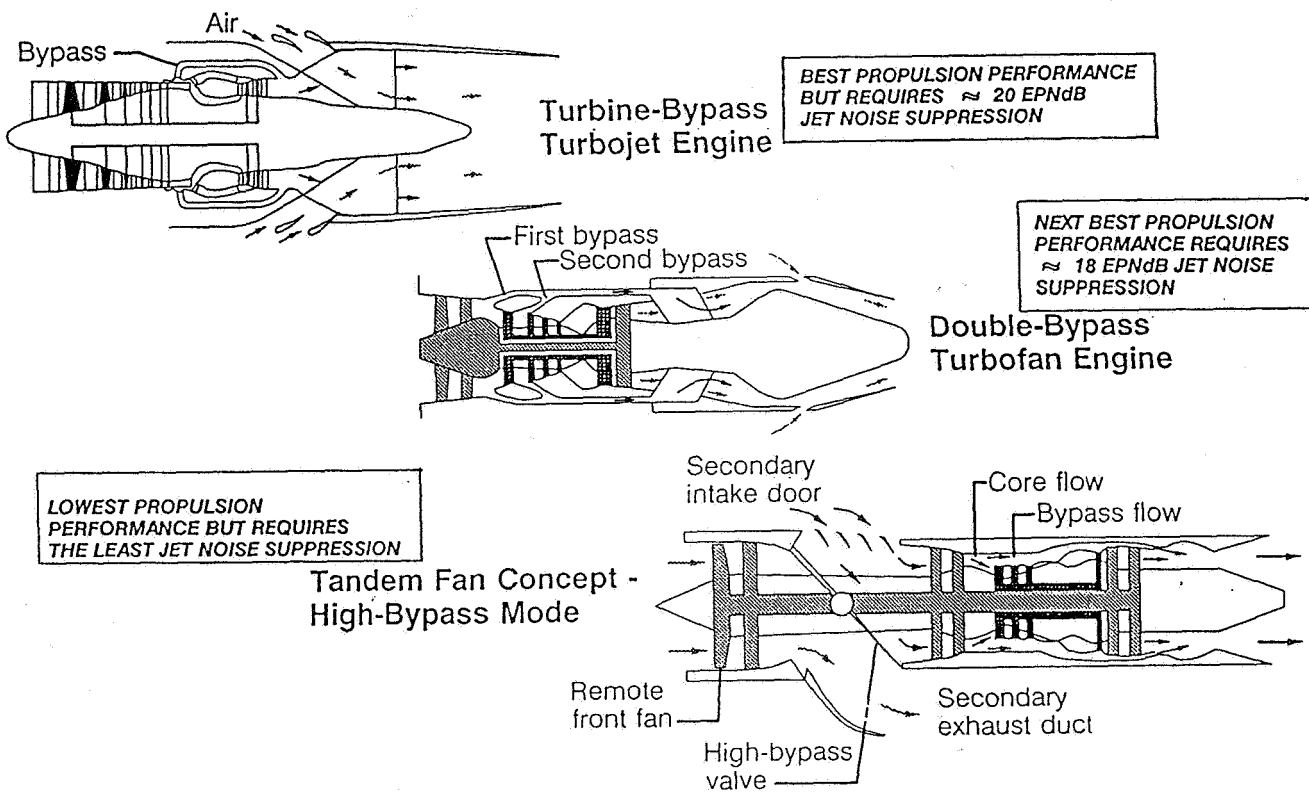


FIGURE 2

~~es~~

NOZZLE DEVELOPMENT SCHEDULE

Model scale nozzle development testing will continue through 1995 followed by verification testing using a large scale demonstrator engine. Tests in 1991 include elements of the nearly fully mixed (NFM) nozzle, a variable geometry version of the NFM nozzle and source diagnostics of the NFM nozzle. Source diagnostics will include cross-correlation of far field noise with internal velocity fluctuations.

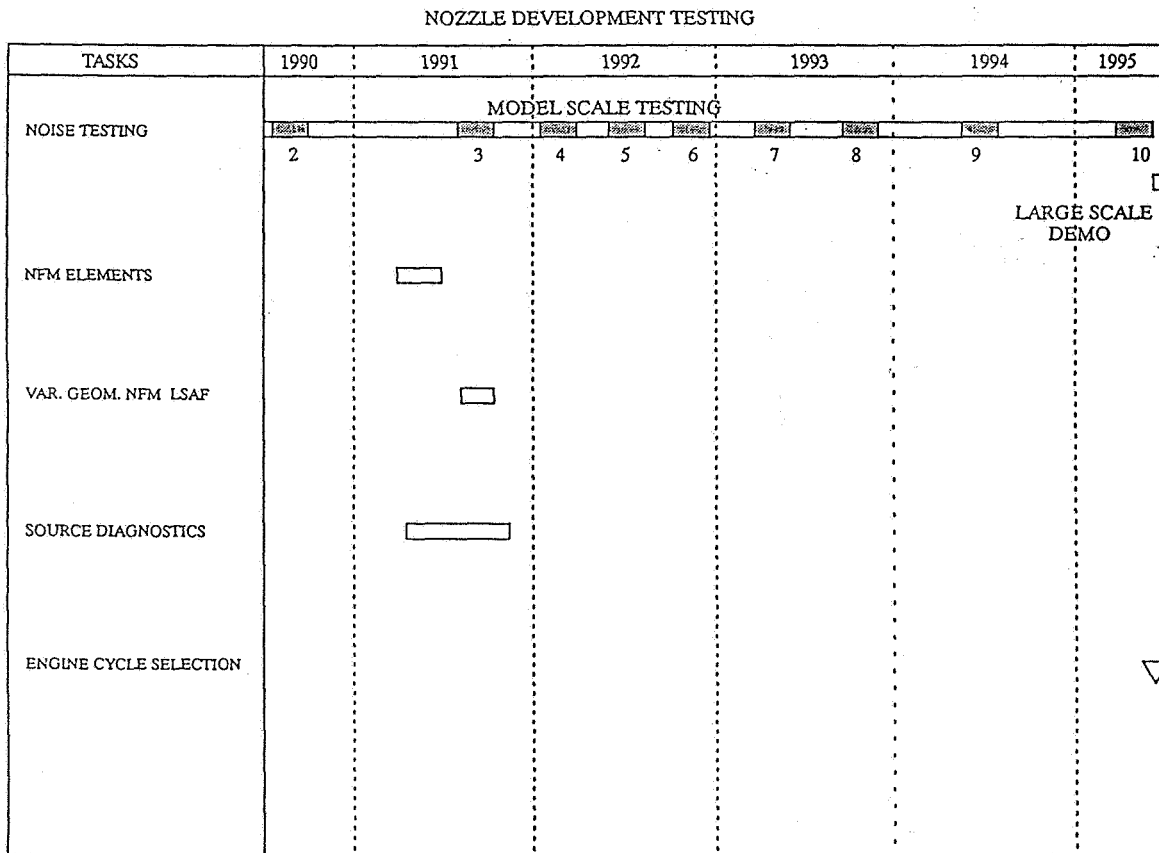
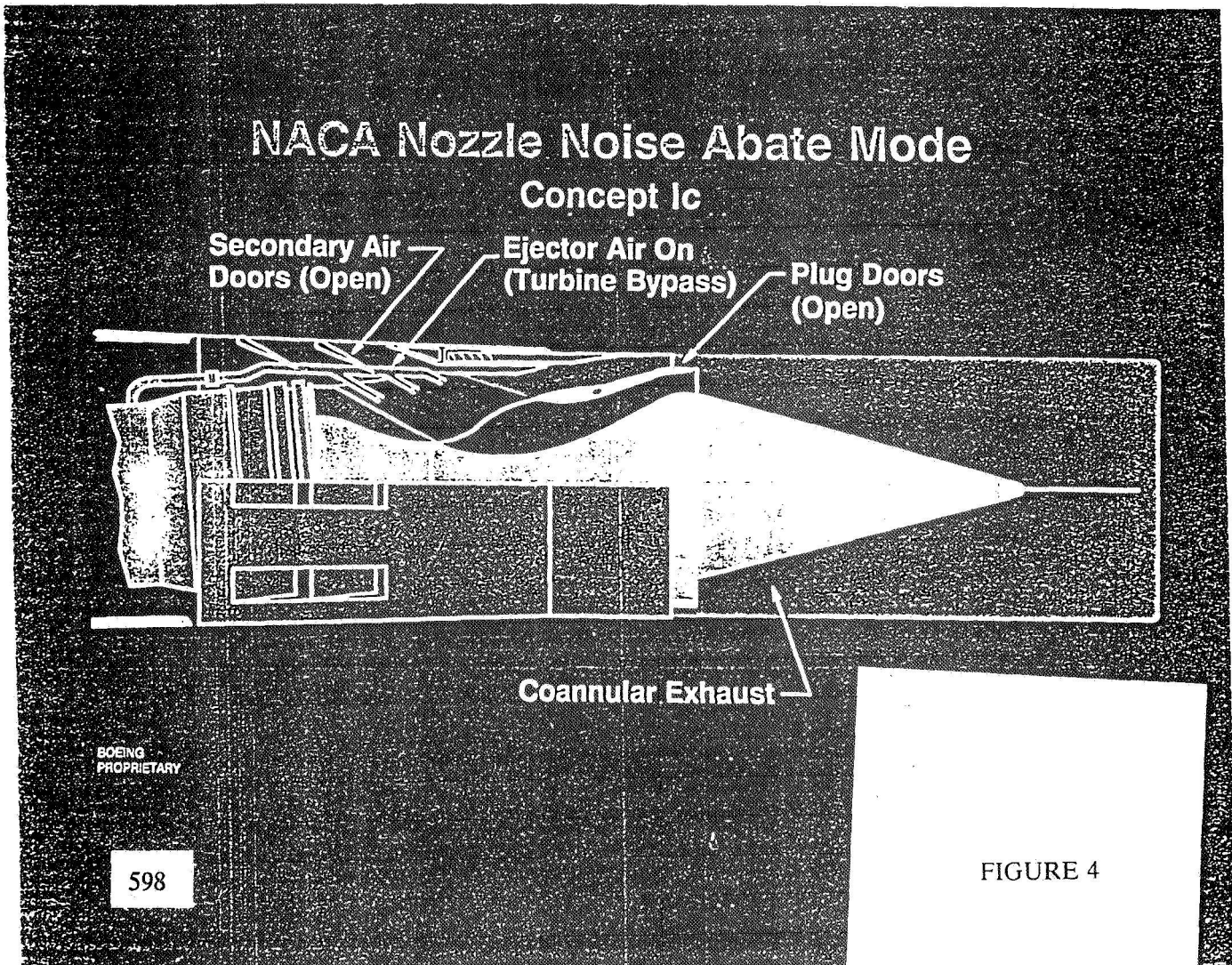


FIGURE 3

NACA NOZZLE DESIGN

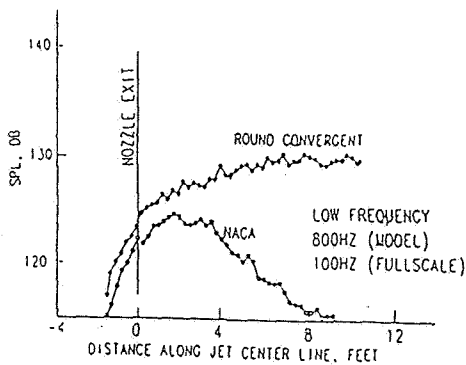
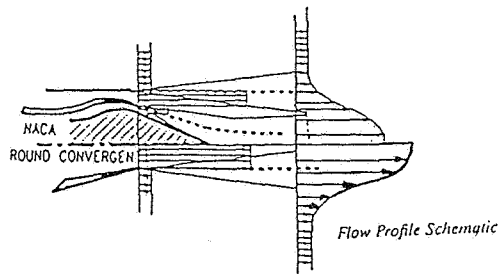
A jet suppression test was completed on the Naturally Aspirated Co-Annular (NACA) nozzle in 1989. The original design NACA nozzle aspirated 40% of the core flow. This was increased to over 60% by using the turbine bypass air as a second ejector. The core flow crosses over the aspirated flow into an annulus. This produces an inverted velocity profile as a noise reduction feature. A large external plug was used in addition.



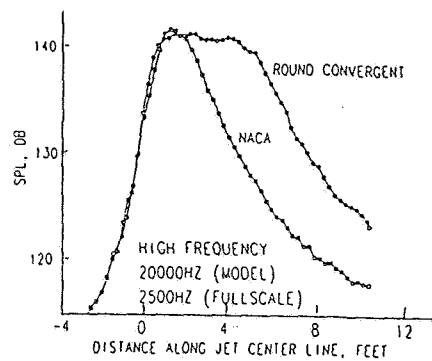
NACA NOZZLE TEST RESULTS

The mixing of the aspirated flow and the primary jet takes place outside of the nozzle so that the primary stream is at full velocity in the initial mixing region. This results in large noise reduction down stream but no reduction of high frequency noise generated in the initial mixing region limiting the suppression to 10 EPNdB.

NATURALLY ASPIRATING CO-ANNULAR, NACA, NOZZLE SOURCE LOCATION



Elliptic Mirror Noise Source Distribution Scan at a Low Frequency



Elliptic Mirror Noise Source Distribution Scan at a High Frequency

FIGURE 5

NFM NOZZLE DESIGN

One solution to the NACA nozzle limitation is to mix the aspirated flow inside a treated ejector and Boeings version of this nozzle is called the Nearly Fully Mixed (NFM) nozzle. This nozzle aspirates 100+ % of the core flow, fully mixes the core and aspirated flows inside the ejector and minimizes internal shock cell noise from the primary nozzle. The internally generated mixing and shock cell noise is reduced with acoustic lining.

Internally Mixed Ejector - Suppressor Nozzle Concept

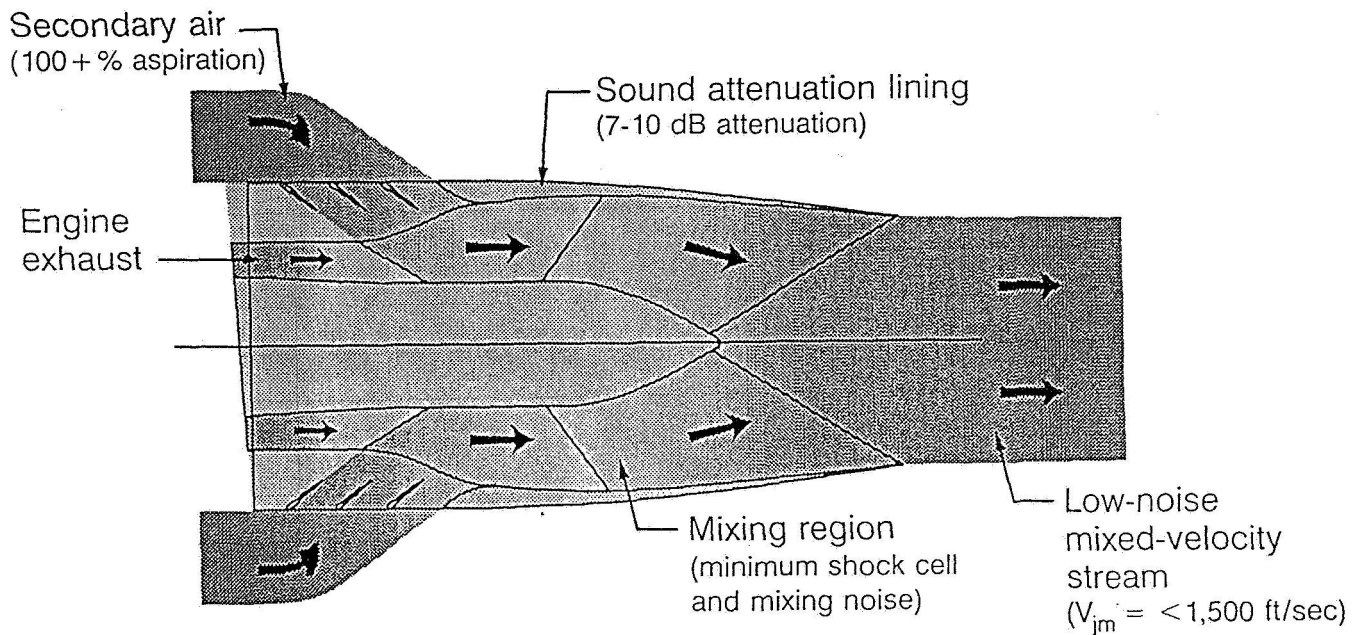


FIGURE 6

NOISE VERSUS ASPIRATION RATE

Noise reduction of an aspirating nozzle has the potential of reducing noise to the level of an equivalent nozzle with the fully mixed stream flow conditions. The noise reduction potential of an aspirating nozzle versus aspiration rate is shown. NACA nozzle and NFM nozzle data are also shown. Neither nozzle reaches its full potential, the NACA nozzle because the streams are mixed outside the nozzle and the NFM nozzle because some internally generated noise is still radiated out.

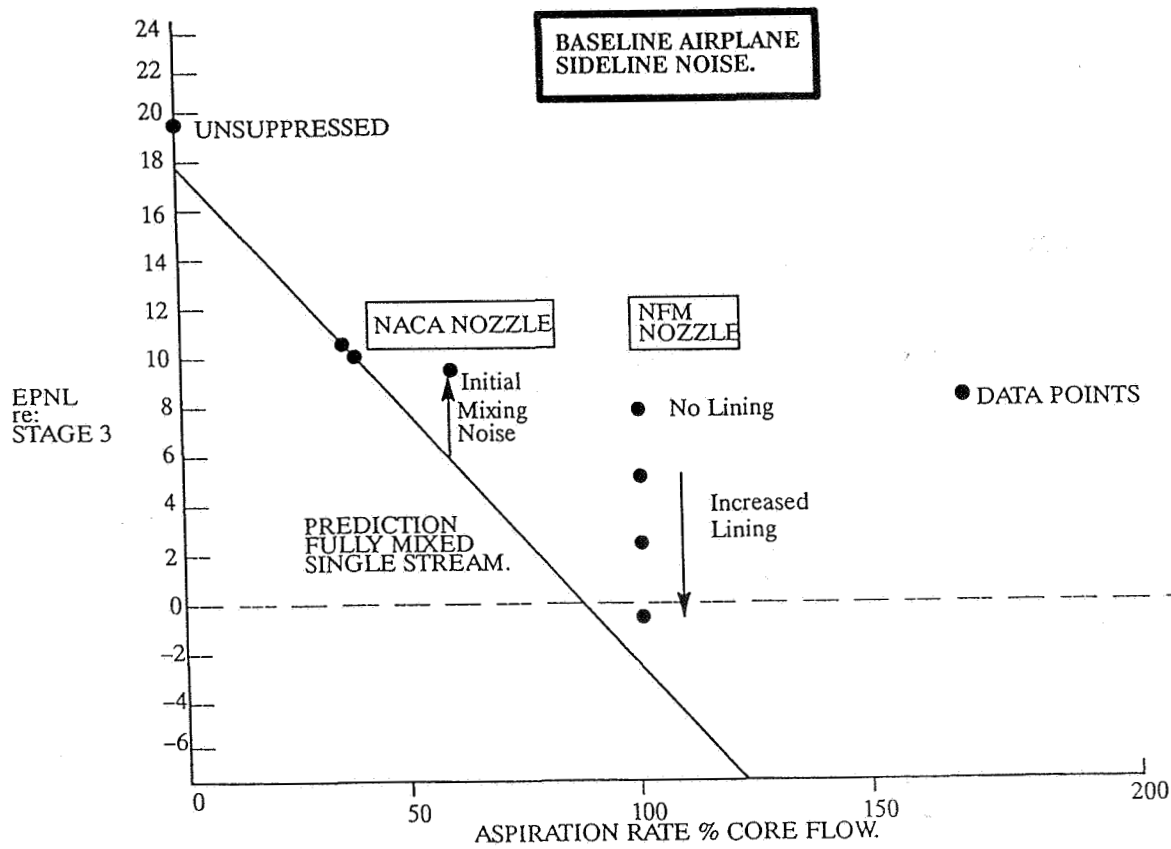


FIGURE 7

PEAK NOISE TEST RESULTS

The reference RC nozzle noise spectrum is shown at its peak radiation angle (140°) compared to the NACA and NFM nozzles at their peak angles (110°). The high frequency noise reduction of the NACA nozzle is limited because the mixing takes place outside the nozzle. The NFM nozzle, with the longest treated ejector, shows large noise reductions at all frequencies.

NFM, NACA, and RC Nozzle Noise Comparison

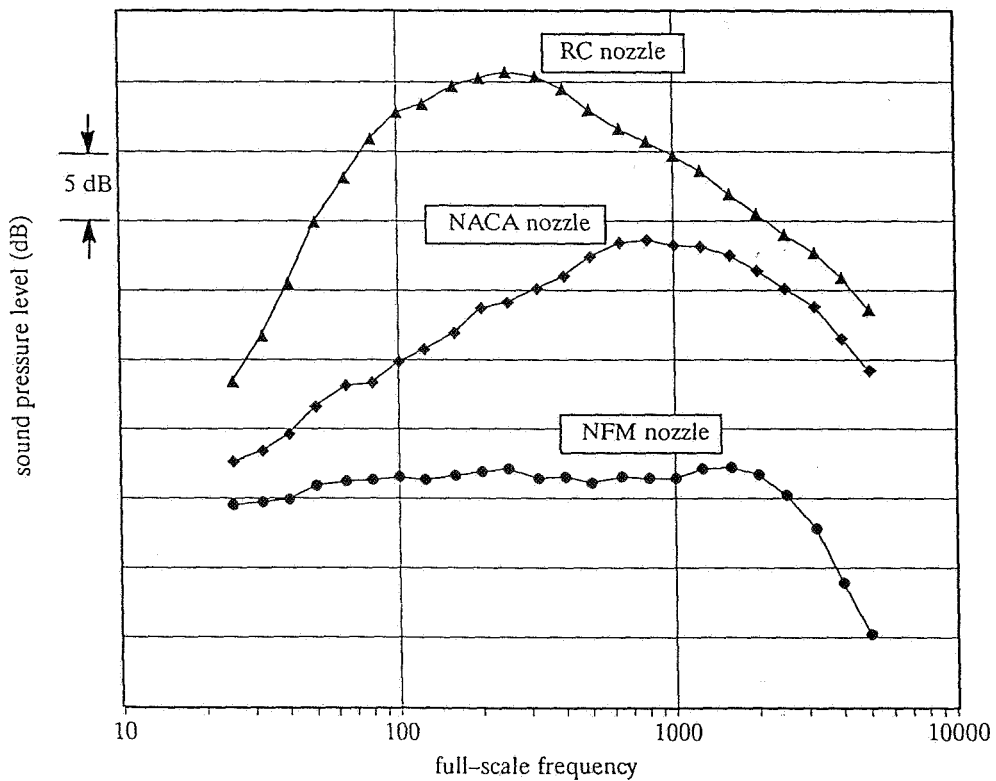


FIGURE 8

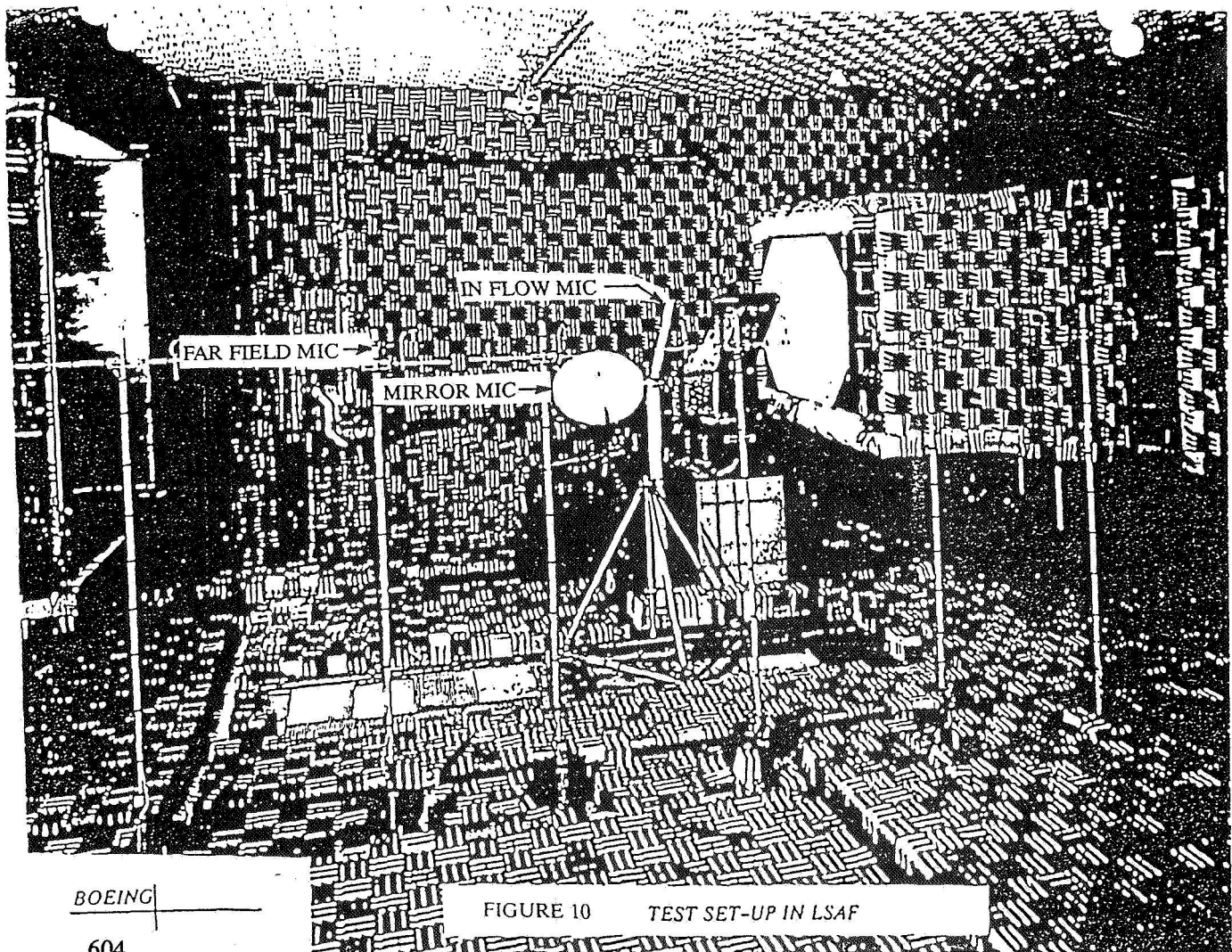
TEST TECHNOLOGY

- ◆ NOISE SOURCE LOCATION TECHNIQUES
- ◆ FLOW PARAMETER MEASUREMENT TECHNIQUES
- ◆ TECHNIQUES FOR CROSS-CORRELATION OF NOISE
WITH FLOW PARAMETERS
- ◆ FLOW VISUALIZATION TECHNIQUES

FIGURE 9

NOZZLE TEST IN LSAF

A nozzle test in progress in the Low Speed Aeroacoustic Facility (LSAF) wind tunnel at Boeing. The 9' X 12' free jet nozzle is shown as well as microphone locations. The translating elliptic mirror microphone is used to determine the noise source location. Far field noise measurements are made at 20 ft. sideline distance with fixed microphones out of the tunnel flow and within the flow with translating microphones at 4.7 ft.



SCHLIEREN PICTURES OF NACA NOZZLE

Flow visualization pictures taken by Jack Seiner's group from NASA Langley are shown. These pictures of the NACA nozzle test show the effect of translating the outer shroud length on shock cell strength. As the shroud was translated the expansion ratio (A/A^*) was changing.

SCHLIEREN RECORDS FOR CONFIGURATIONS 2.3 AND 2.1

(NPR=3.5, $M_T=0.23$, TTPA=1000°F, WBP ON)

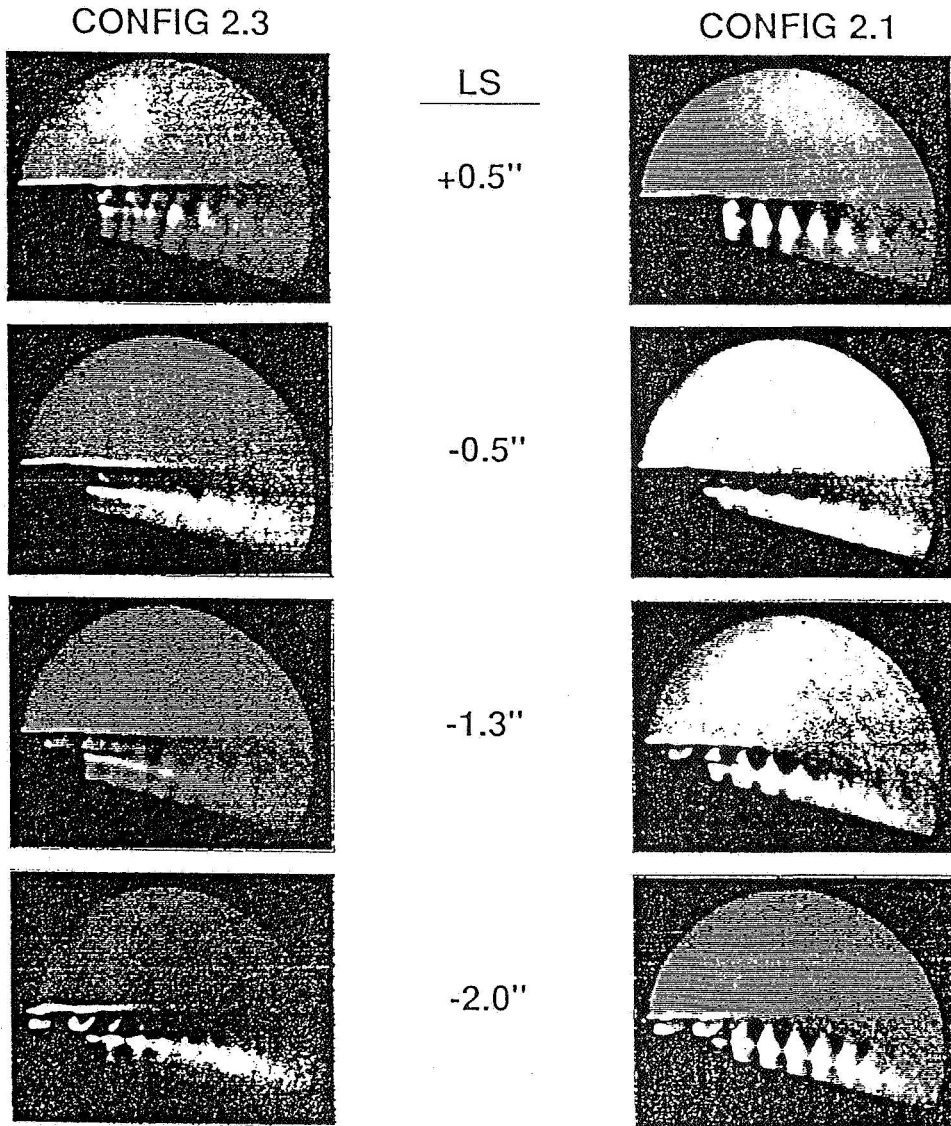


FIGURE 11

CONCLUSIONS

- * AN HSCT WILL REQUIRE NOISE CONTROL OF SEVERAL NOISE SOURCES, IN PARTICULAR JET NOISE, TO GET AIRPORT COMMUNITY ACCEPTANCE

- * ENGINE EXHAUST NOZZLE TECHNOLOGY DEVELOPMENT IS NEEDED TO ESTABLISH THE PENALTIES FOR 20 EPNDB SUPPRESSION SO THAT ENGINE CYCLE AND AIRPLANE TRADE STUDIES CAN BE MADE

- * IMPROVEMENTS IN JET NOISE TEST TECHNOLOGY AND PREDICTION TECHNOLOGY WOULD GREATLY ENHANCE THE NOZZLE DEVELOPMENT EFFORT

Session IV. Source Noise

omit

NASA LaRC Jet Plume Research

Dr. John M. Seiner, Michael K. Ponton and James C. Manning, NASA Langley Research Center

THIS PAGE INTENTIONALLY BLANK

N94-33468

56-07
11996

NASA/LARC JET PLUME RESEARCH

JOHN M. SEINER, MICHAEL K. PONTON, AND JAMES C. MANNING

NASA LANGLEY RESEARCH CENTER

HAMPTON, VA

FIRST ANNUAL

HIGH-SPEED RESEARCH WORKSHOP

MAY 14-16, 1991

SCOPE OF RESEARCH

The following provides a summary for research being conducted by NASA/LaRC and its contractors and grantees to develop jet engine noise suppression technology under the NASA High Speed Research (HSR) program for the High Speed Civil Transport (HSCT). The objective of this effort is to explore new innovative concepts for reducing noise to Federally mandated guidelines with minimum compromise on engine performance both in take-off and cruise. The research program is divided into four major technical areas as outlined below,

OUTLINE

A - JET NOISE RESEARCH ON ADVANCED NOZZLES

- 1 - LANGLEY AXISYMMETRIC MIXED FLOW NOZZLE**
- 2 - PRATT & WHITNEY 2-D HYPERMIX NOZZLE**
- 3 - HIGH TEMPERATURE EJECTOR LINERS**
- 4 - BOEING NACA NOZZLE**
- 5 - LANGLEY FORWARD FLIGHT SIMULATOR**
- 6 - LDV AND WATER COOLED PROBE DEVELOPMENTS**

B - PLUME PREDICTION AND VALIDATION

- 1 - EVALUATION OF RNS TO BASELINE AXISYMMETRIC JETS**
- 2 - AXISYMMETRIC PLUG VALIDATION EXPERIMENT**
- 3 - EVALUATION OF COMPRESSIBLE TURBULENCE MODELS**
- 4 - SHOCK/VORTEX INTERACTION STUDY**

C - PASSIVE AND ACTIVE CONTROL

- 1 - NOZZLE GEOMETRY EFFECTS**
- 2 - MULTIPLE JET INTERACTIONS**
- 3 - CURVED JET MIXING**
- 4 - ACTIVE CONTROL OF INITIAL JET SHEAR LAYER**

D - METHODOLOGY FOR NOISE PREDICTION

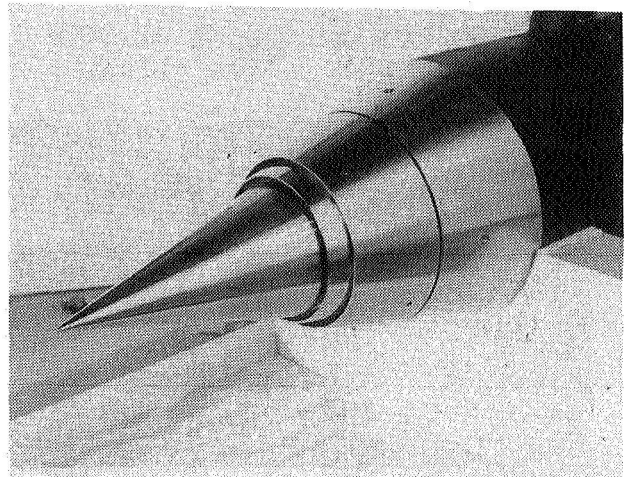
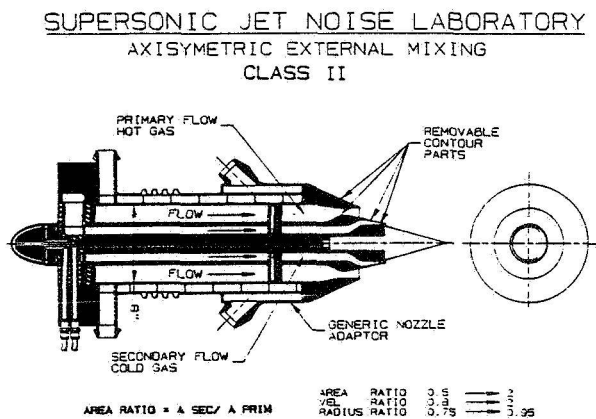
- 1 - SUPERSONIC INSTABILITY WAVES**
- 2 - NON-LINEAR WAVE INTERACTIONS**
- 3 - COMPRESSIBLE RAYLEIGH EQUATION DEVELOPMENT**
- 4 - PREDICTION OF NOISE FOR NON-ROUND JET GEOMETRY**
- 5 - LOW REYNOLDS NUMBER RESEARCH**

AI - LANGLEY AXISYMMETRIC MIXED FLOW NOZZLE

A dual co-annular stream axisymmetric nozzle has been designed (figure 1a) and fabricated (figure 1b) to support HSR. The model was designed with removable contour parts at the nozzle exit to accommodate a wide range of geometries for concept investigations, including conversion to single stream configurations. These removable parts are fabricated from Haynes 230 alloy, which along with water cooling of the non-removable stainless steel nozzle duct, permits testing the model to 2500°R. Depending on the nozzle geometry selected, the mixed flow model scale size to full was designed to be between eight and ten to one.

The Jet Noise Laboratory (JNL) at Langley can supply two independently controlled air streams (25 lbm./sec. each) to power the mixed flow model. The outer stream is supplied by a Marquart sudden expansion propane/air fueled burner, which enables testing to the 2500°R temperature limit of the model at a nozzle pressure ratio of 10.5. Air supplied to the propane burner is pre-heated electrically to improve combustor stability. The inner stream is electrically heated (500 KW), enabling testing to 1460°R with 2 lbm./sec. air to a nozzle pressure ratio of 10.5. Both inner and outer flow stream air, fuel, electrical heat, and water system are remotely controlled using a distributive process system controller.

The design of a two dimensional mixed flow nozzle system, like that shown in figure 1a, is currently in progress.



a - schematic of dual stream nozzle design concept.

b - photograph of high radius ratio mixed flow nozzle.

Figure 1. Langley mixed flow axisymmetric nozzle with removable high temperature alloy nozzle parts.

A2 - PRATT & WHITNEY 2-D HYPERMIX NOZZLE

A sharp focus schlieren apparatus with imaging radiometer is being developed at Langley to provide flow visualization for diagnostic evaluation of individual mixer elements of the Pratt & Whitney 2-D mixer ejector nozzle. This nozzle is scheduled for test later this year in the NASA Lewis 9 X 15 foot wind tunnel.

As shown in figure 2, the model contains four mixer lobes. These lobes were designed as convergent-divergent passages to minimize shock noise. High temperature air (2000°R) is ducted from the NASA/Lewis hydrogen/air fueled propulsion model through these mixer lobes. In addition to the noise reduction produced by mass flow augmentation by the ejector, the model additionally reduces noise through the creation of large scale axial vorticity on the nozzle afterbody. The large scale vorticity accelerates mixing of external air with hot flow from the lobes, thereby reducing flow velocity and noise.

The flow visualization experiments will enable interpretation of noise reduction to the flow physics inside the ejector. Figure 3 provides a schematic for the sharp focus schlieren apparatus being assembled for the NASA/Lewis tunnel. The designed of this apparatus is based on the methods developed by Weinstein (1991). The optical axis is vertical. The ejector's flat sidewalls will be replaced with a set having optical viewports. The optical glass is Infrasil 302, which transmits in the infra-red to 3.2 microns. This glass can be ground to achieve schlieren quality. A double pulsed ND-YAG laser with 35 mJ output in the green (532 nm) is the light source. This laser can be fired as a single shot laser or synchronized externally at 30 Hz. to a video camera. The laser's pulse duration is 7 nsec, thus allowing instantaneous view of flow features.

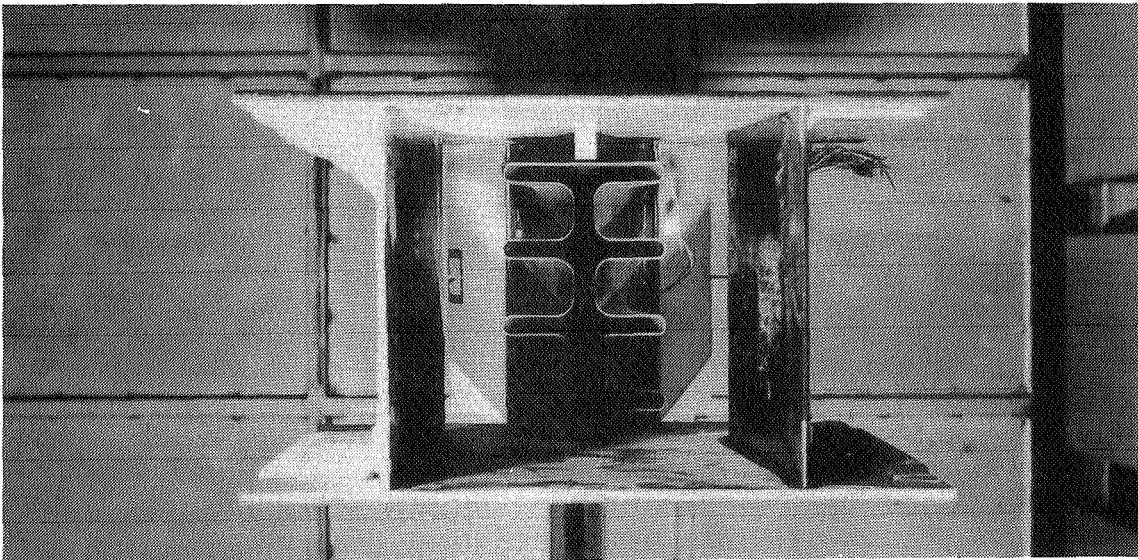


Figure 2. Pratt & Whitney 2-D mixer ejector nozzle in NASA/Lewis 9 X 15

A2 - APPLICATION OF SHARP FOCUSED SCHLIEREN

Flush mounted optical windows are being constructed for both the tunnel floor and ceiling. The 20" X 24" crown glass floor window contains the first schlieren grid and fresnel lens. The ceiling window is Infrasil 302. A f/3.6 lens with 6" clear aperture is mounted behind the ceiling window. Based on the fixed distances of the model in the tunnel and the optical aperture through the model, the f/3.6 lens was selected to produce a sharp focus less than the 0.4 inch mixer lobe thickness. Flow features beyond 1.25 inches cannot be distinguished with this apparatus. This means that the schlieren apparatus will be able to isolate flow details from a single mixer lobe. A rigid support mounted to the tunnel ceiling is used to support the second schlieren grid, image plane viewfinder, 70 mm film and video camera.

Radiometric measurements with a dual imaging radiometer will be conducted using the same optical access ports. The radiometer contains a narrow band filter centered at 2.6 microns to enable imaging of water produced as a by-product of combustion between hydrogen and air. Because the radiometer's depth of focus exceeds that of the model width, it will be necessary to seed a given mixer lobe with CO₂. Since CO₂ emits at 4.2 microns, both the model and ceiling windows will be replaced with sapphire to conduct these tests. The radiometer is equipped with a narrow band filter around 4.2 microns. Using this method, the mixing of a single mixer lobe can be traced.

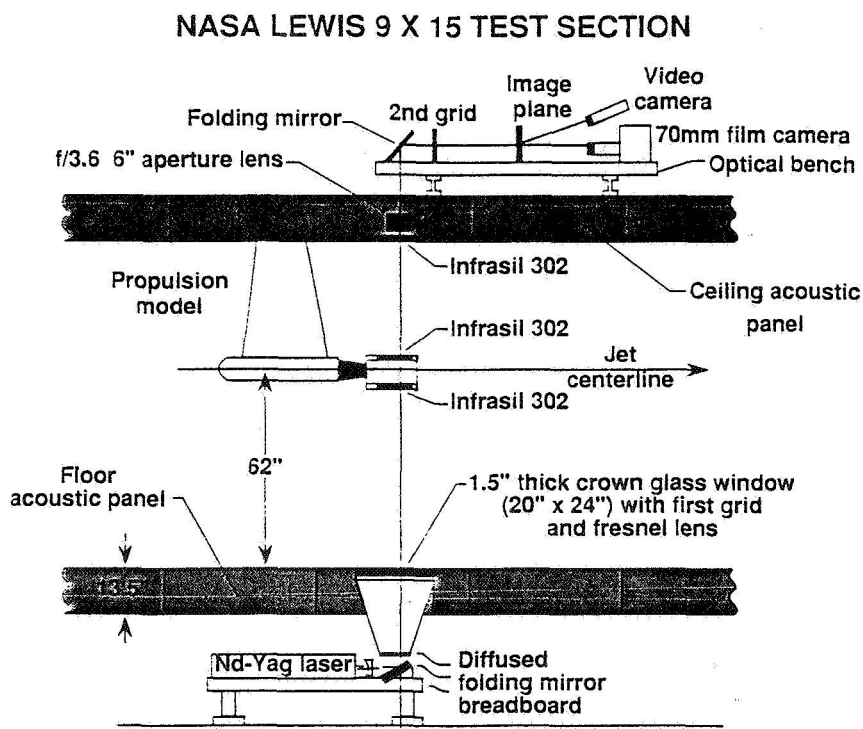


Figure 3. Schematic of sharp focus schlieren apparatus for NASA/Lewis test of P & W nozzle.

A3 - HIGH TEMPERATURE EJECTOR LINERS

Application of acoustic treatment to mixer ejector walls has been proposed as a method to achieve additional noise reduction. Both P & W, GEAE, and Boeing have used ejector liners in previous suppressor nozzle studies, achieving varying degrees of success. These liners have typically been fabricated using a bulk absorber with perforated face sheet. Little is known about the effectiveness of such a concept in the presence of distributed broadband sources, whose locations and frequencies depend on the mixer suppressor geometry. Temperature gradients and high speed grazing flow with shocks provide a formidable challenge to existing liner technology.

NASA Langley has begun an investigation of acoustic liners for the HSCT. The study will use the JNL to study candidate materials in the presence of high speed and high temperature grazing flows. In parallel efforts to this effort, T.L. Parrott, of the Langley Applied Acoustics Branch, will develop candidate materials for these studies using a flow impedance tube, and Gary Settles of Penn State Univ. will evaluate the aerodynamic performance of these candidate materials.

The JNL studies will initially begin by using a small 2-D C-D 1460°R Mach 2 rectangular nozzle with ejector, as shown in figure 4a. The sidewalls of the ejector are adjustable. The construction of this model is complete. The aspect ratio of the nozzle is 7.2 to simulate two dimensional wave emission. The sidewalls of the ejector contain optical viewports to permit flow visualization. For large plume/wall separations, it is possible to identify the emitted Mach wave angle to the impedance boundary, provided no acoustic interaction occurs between the plume and duct modes. This is illustrated in figure 4b, which provides indication that in-situ measurements of material impedance will also be determined. For small plume/wall separations the aerodynamic boundary layer over the liner face sheet can be visualized. Both aerodynamic flow measurements and far field acoustic measurements (ejector treated on four walls) will be conducted to support this research.

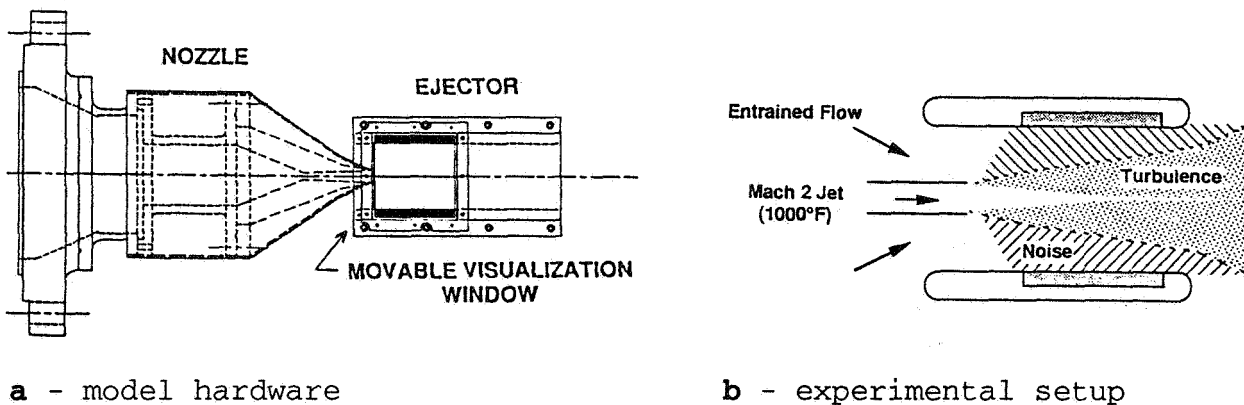


Figure 4. Initial JNL study of acoustic liners for HSCT ejectors.

A3 - HIGH TEMPERATURE EJECTOR LINERS

The upper and lower walls of the ejector will be lined with various length and depth candidate materials being developed in the Flow Impedance Tube Laboratory (FITL). Early concepts to be studied in the JNL include investigation of ceramic honeycomb material with small diameter cells, whose absorption is dominated by viscous dissipation. Such materials are aerodynamically smooth and do not require a face sheet. Such smoothness does, however, bring into question liner absorption capabilities at high angles of grazing incidence. To achieve broadband absorption characteristics using ceramic honeycomb, both stepped and variable depth liners will be investigated. A broadband liner material, Permablique (figure 5), will also be investigated. In addition to the ceramic honeycomb, bulk liners using Kevlar with perforated face sheets will be investigated to provide comparison to industry experience.

In the JNL, in-situ measurements of impedance will be conducted using water cooled pressure transducers. This technology has been successfully developed to enable measurement of dynamic pressure in high temperature environments, as indicated in figure 6. To apply this technology to the liner program will, however, require an investigation of the phase characteristics of piezoresistive transducers. Similar measurements will be performed in FITL, with eventual development of a theoretical model to describe absorption behavior.

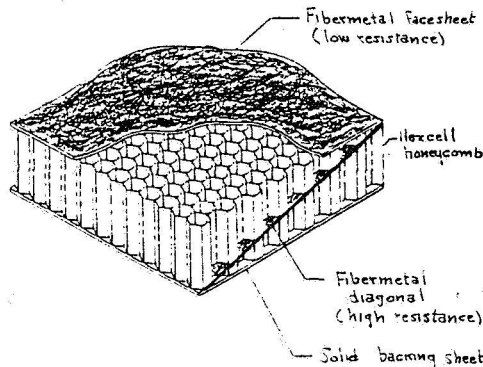


Figure 5. Permablique, a locally reacting acoustic liner with spatially dependent frequency tuning.

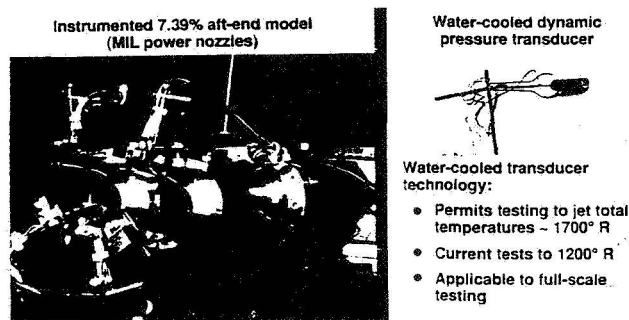


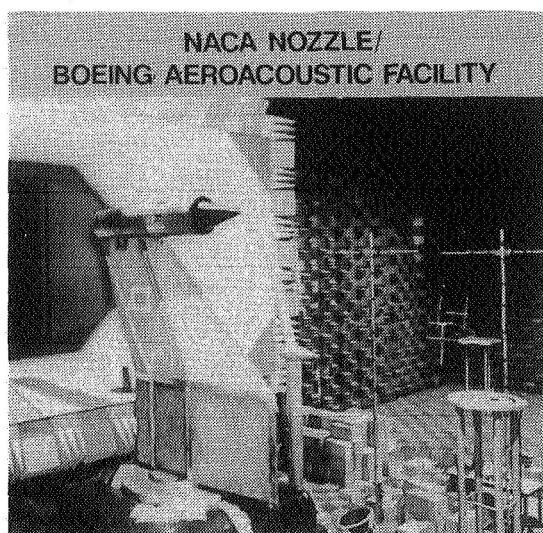
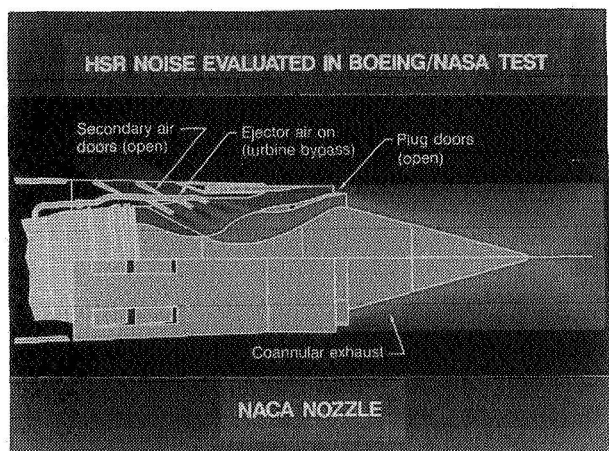
Figure 6. Water cooled piezoresistive transducer for high temperature flow.

A4 - BOEING NACA NOZZLE

In a joint effort with Boeing, a flow visualization investigation of the Boeing NACA nozzle series was conducted in their LSAF by the Langley JNL staff. The objective of the Langley effort was to assist Boeing with analysis of the aeroacoustic data, primarily through acquisition of flowfield data. For these tests both a conventional schlieren system and imaging radiometer were used for flow visualization. Figure 7a shows the NACA nozzle mounted in the Boeing LSAF. Both the imaging radiometer and linear array are visible in this figure.

The naturally aspirated coannular (NACA) nozzle of Boeing is shown schematically in figure 7b. Supersonic hot exhaust air from the turbine is ducted to the outside duct of the nozzle. The outer stream shroud could translate, thus providing an outer stream with adjustable area ratio. Subsonic secondary air is entrained through the ejector and ducted to the inner stream. The secondary air is augmented by air bypassed from the turbine stage, since an HSCT engine should have margin at take-off. The secondary air stream is unheated and subsonic. Acoustically, the scaled NACA nozzle achieved between 9 and 10 EPNdB of suppression with little performance penalty.

The conventional schlieren apparatus utilized a 100 nsec 10 kHz spark source with capability of being fired externally to obtain conditionally sampled data. A video camera was used to record data and post processed using image analysis software. The most difficult part of the set-up involved folding the optical axis with a mirror located in the upper left hand corner of the forward flight nozzle. This requirement arises in LSAF due to the proximity of the nozzle and forward flight nozzle to a wall.



a - schematic of NACA nozzle

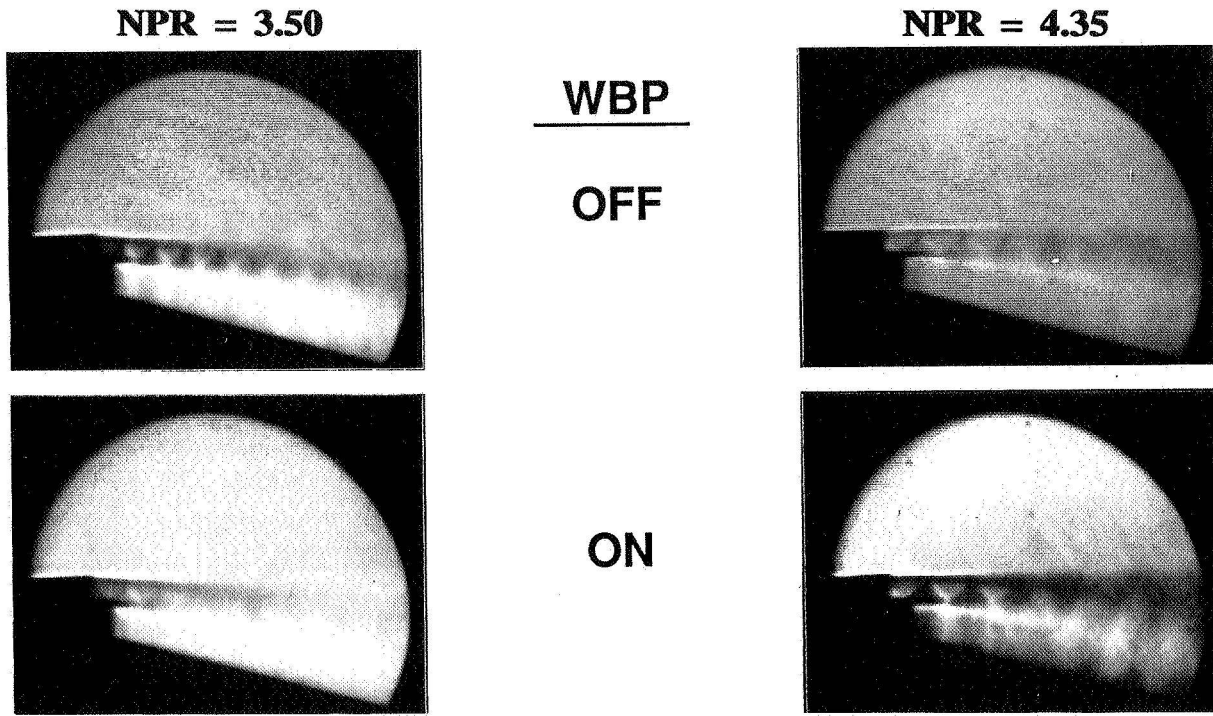
b - NACA nozzle mounted in LSAF

Figure 7. Boeing NACA nozzle flow visualization study.

A4 - NACA NOZZLE SCHLIEREN DATA

With the schlieren data, it was possible to determine the optimum location for shock free flow. This was determined to occur at the translating shroud position $L_s = -0.5"$. The optimum shroud location was found to be dependent on forward flight Mach number and turbine bypass flow. Example schlieren results obtained with NACA 2.3 are shown in figure 8. As can be observed, in addition to changes in shock structure, the shear layer spread rate is very dependent on operational parameters of the nozzle.

($M_t = 0.23$, TTPA = 1460°R, LS = -0.5")



(NPR = 3.5, TTPA = 1460°R, WBP OFF)

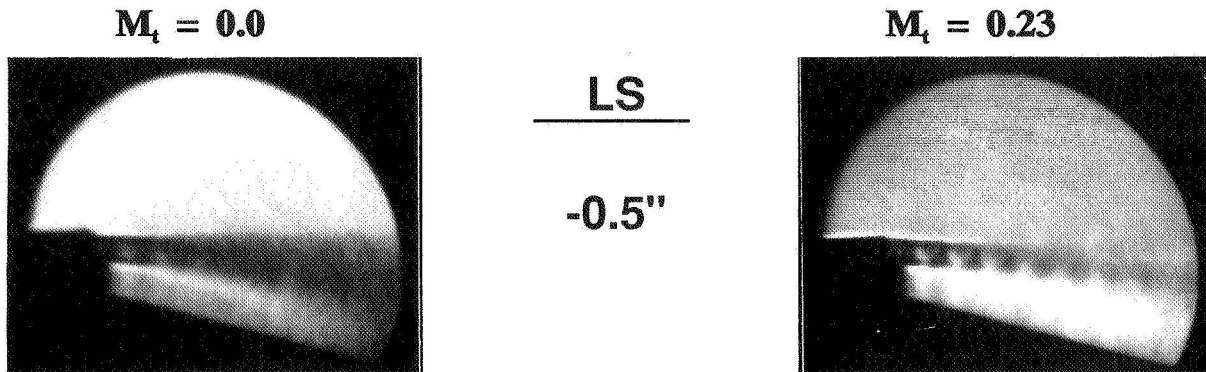


Figure 8. Schlieren data from NACA nozzle study.

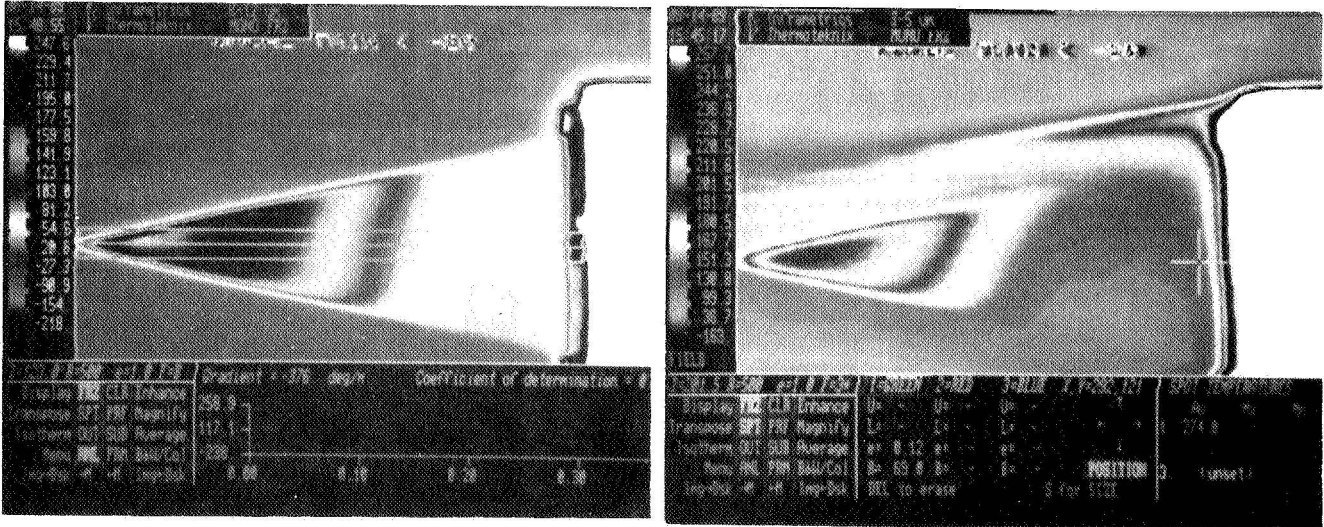
A4 - NACA NOZZLE RADIOMETRIC DATA

The imaging radiometer used in this study proved valuable in providing information on the flow uniformity of the model and post merged regions of the flow. The radiometer was capable of simultaneously imaging radiation between 8 and 12 microns through one channel, and 4.2 microns through a second channel with narrow band filter. The long wavelength channel is used to image metallics associated with the nozzle, while the short wavelength is used to image CO₂, a by-product of the propane air combustion. Figure 9 shows the degree of flow non-uniformity (later traced to unsymmetric flow in combustor) and the enhanced mixing produced by application of the turbine bypass flow. These results, which represent an average of 100 consecutive frames, were obtained for NPR = 3.5, TTPA = 1460°R, and LS = -0.5".

NACA 6 CONFIGURATION 2.3

8-12 MICRON, $\epsilon = 0.95$

4.2 MICRON, $\epsilon = 0.12$



NACA 6 CONFIGURATION 2.1 (4.2 MICRONS)

WBP OFF

WBP ON

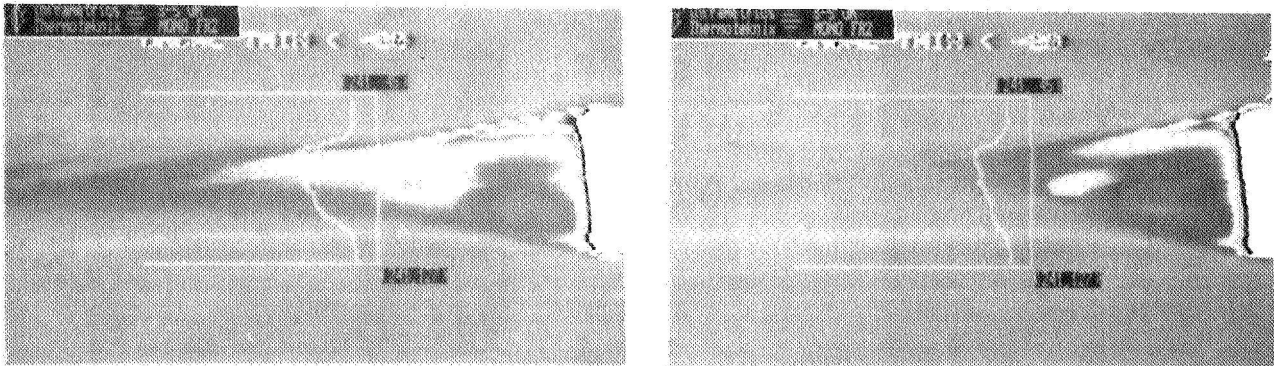


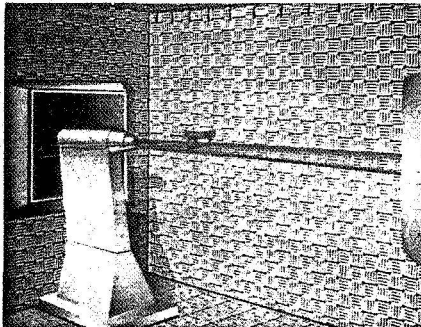
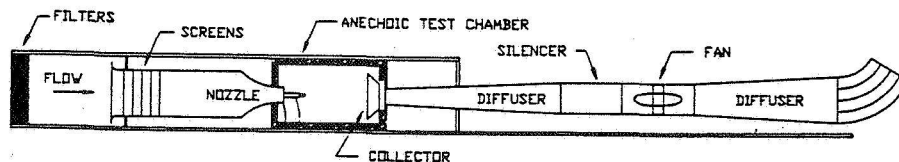
Figure 9. NACA nozzle dual wavelength band radiometric results.

A5 - LANGLEY FORWARD FLIGHT SIMULATOR

A forward flight simulator with propulsion model is currently being designed on a FY-92 CoF for installation in the NASA/LaRC Jet Noise Laboratory. The simulator and propulsion model will complete all facility requirements necessary for HSCT research in the take-off mode. Figure 10 provides a schematic of the proposed forward flight system and propulsion model.

The tunnel is powered by a 10 ft. diameter two stage axial flow fan that is driven by a variable speed drive with a 4000 HP motor. The fan is capable of pulling 50" H₂O at 420,000 CFM. With a 4 X 5 foot nozzle exit, this corresponds to a forward flight simulation velocity of 350 ft./sec. The area contraction ratio of the nozzle is 11.25. The nozzle inlet duct entrance is equipped with a honeycomb flow straightener and six continuously woven wire mesh screens. The anechoic test section is 36 X 18 X 18 ft., wedge tip to wedge tip. The first diffuser utilizes a 2.5 degree half angle with a 5 X 5 ft. throat. A collector is used to help recovery of the free jet static pressure. A second diffuser, of 3° half angle, is used to slow the flow for the final duct silencer.

The propulsion model will have similar features to existing JNL nozzle hardware, allowing existing nozzle parts to be utilized. The model will house a burner capable of heating 10 lbm./sec of air to 2460°R. The primary mode of combustion will be propane/air, with capability of operating from a hydrogen/air supply. A single component balance will be installed for rudimentary performance assessments.



PROPANE/AIR FUELED COMBUSTOR

$$T_{\max} = 2500^{\circ}\text{R}$$

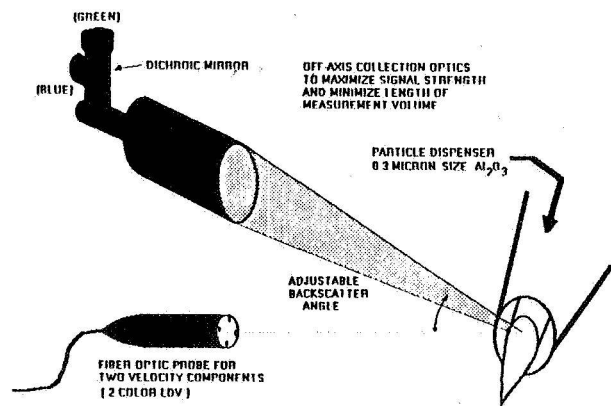
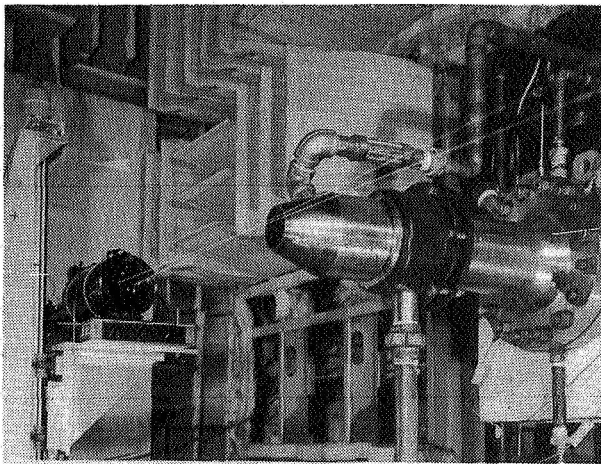
$$Q = 420,000 \text{ CFM @ } 50'' \text{ WATER}$$

$$V_{\max} = 350 \text{ FT./SEC.}$$

Figure 10. NASA/LaRC Jet Noise Laboratory Forward Flight Simulator.

A6 - JNL LASER VELOCIMETER SYSTEM

The JNL laser Doppler velocimeter is capable of measuring 2 velocity components. A schematic of the system is shown in figure 11a. The system is based on a fiber optic LDV probe which allows the 15 watt argon-ion laser to be located remotely (25 meters) from the test chamber so that it is not subject to high intense noise fields. Figure 11b shows the now obsolete single axis fiber optic system mounted in the test chamber. The probe's nominal dimensions of 3" diameter by 18" long. make the probe easily mountable on the Laboratory's 3 axis digital probe traverse mechanism. At the laser end of the probe, there are four fiber ends for laser beam transmission to the jet test cell. Two transmit 514.5 nm and two transmit 488.0 nm. The optical components at the laser site allow for color separation, beam splitting, and frequency shifting before transmission through the optical fibers. In the test chamber, a lens is mounted with a focal length of 600 mm., which will produce a minimum of 20 good fringes. The light scattered by seed particles entering the probe volume are collected in the off-axis backscatter mode. Six inch diameter collection optics are mounted on a movable platform that allows the backscatter angle to be optimized for maximum signal strength. Off-axis backscatter is generally superior for collecting light from small seed particles. The seed particles used in the JNL for hot flows are alumina powders with nominal particle size of 0.3 microns. Particles are injected into the air supply line with a fluidized bed seeder operated from the control room.



a - schematic of JNL 2-color LDV

b - single component LDV in JNTC

Figure 11. Description of JNL laser velocimetry system.

A6 - JNL WATER COOLED PROBE DEVELOPMENTS

Three types of water cooled supersonic probes were developed and tested to study high temperature jet plumes. The probe types include total temperature and total and static pressure. All probes were designed with a diameter of 4.76 mm and a wall thickness of 0.38 mm. An annular coolant system was utilized for all three designs, and proved satisfactory to temperatures of 2460°R in Mach 2 flow. A three dimensional cut-away view of the static pressure probe is shown in figure 12. A single center tube, proceeding up to the backside of the tip, provides coolant water to the probe. The water sprays the back of the tip, and symmetrically immerses the region between the inlet water tube and inner wall of the probe as it proceeds to the probe aft. Four tubes inside the probe serve to read the average static pressure. The shape of the exterior probe geometry matches that previously used with uncooled probes in the JNL. The total pressure probe, not shown, is designed by similar methods. The total temperature probe incorporated the annular cooling up to a region near the thermocouple bead as shown in figure 13. The thermocouple bead is located in a blackbody cavity and samples high temperature air, whose velocity is controlled by the probe inlet and exit ports. The area ratio of inlet to exit ports are selected to produce subsonic flow over the thermocouple bead. A portion of the thermocouple sheath forms a liquid tight seal between the test and coolant chambers.

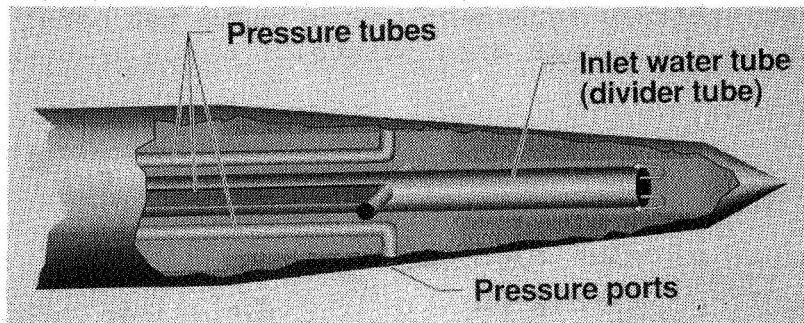


Figure 12. Illustrated cut-away view of cooled static pressure probe.

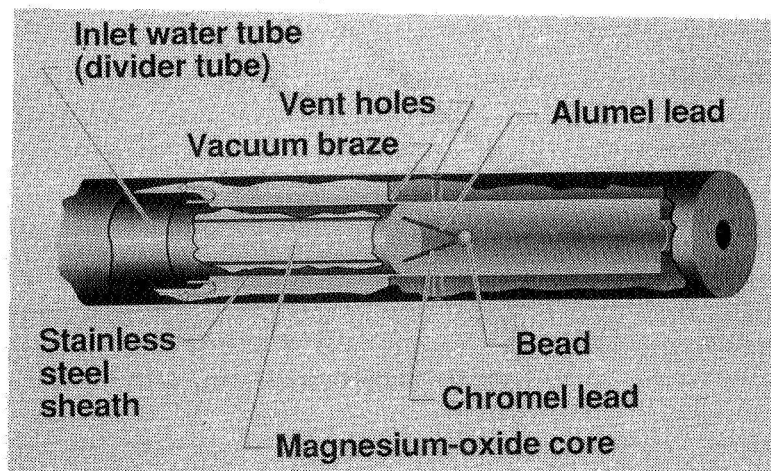


Figure 13. Cut-away view of cooled total temperature probe tip.

A6 - JNL WATER COOLED PROBE DEVELOPMENTS

The data obtained from the total and static pressure probes were found satisfactory to temperatures of 2460°R in Mach 2 flow. The data from the water cooled temperature probe, however, was affected by the water coolant. This required the development of a phenomenological model for heat transfer to the thermocouple bead to account for heat transferred to the coolant. The rate of heat transfer to the TC junction was found, for example, significantly higher with water coolant activated.

The heat transfer analysis developed a relationship between the indicated probe bead temperature and freestream flow total temperature. This analysis solves a heat balance equation involving radiative, convective and conductive modes at the TC junction. The accuracy of this relationship is shown in figure 14, which compares indicated and corrected bead temperatures. The indicated bead temperature is represented by the triangular and circular points. The circular points represent data obtained at jet plume locations with known local total temperature, whereas the triangular points represent data at unknown local jet total temperatures. Comparison of the circular and triangular data points shows the degree of departure from ideal response. The three known data points were used to obtain coefficients for the heat transfer analysis. Application of the model analysis, produces corrected temperatures that appear to be in satisfactory agreement to the known jet total temperature. This is indicated by the square data points.

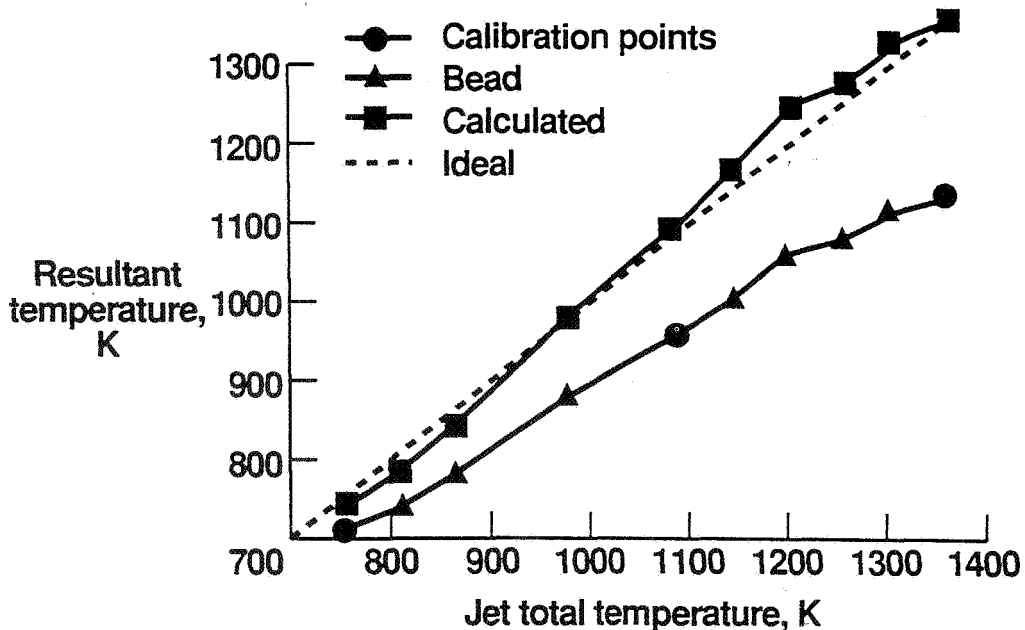


Figure 14. Calculated total temperature compared to indicated bead temperature for various jet centerline temperatures.

B1 - EVALUATION OF RNS TO BASELINE AXISYMMETRIC JETS

Numerical prediction of jet plume structure provides support for theoretical and empirical based jet noise prediction methods. For extremely complex nozzle geometry, like that of an HSCT suppressor nozzle, CFD prediction of flow structure is essential. Prior application of the PNS code SCIPVIS to a Mach 2 underexpanded axisymmetric jet provided satisfactory agreement to measured data as shown in the plume static pressure variations of figure 10. In this example, SCIPVIS is using the kW two equation turbulence model. These results are encouraging, however, several important deficiencies exist in applying PNS to more complex jet flows.

The PNS cannot handle non-uniform subsonic external flow, large Mach discs, multiple jets, or large scale 3D vortical behavior. All these are important in application to HSCT. Even for the simple axisymmetric jet, it is remarkable that the PNS could achieve such good success, since it neglects all streamwise stress/diffusive terms. In a recent study, SAIC finds that neglect of the streamwise terms actually produce errors that are compensated by those introduced by the simplified treatment of the subsonic portion of the shear layer. Their results show that pressure variations in the subsonic layer, which are produced by shock/shear layer interactions, influence the upstream development of the flow.

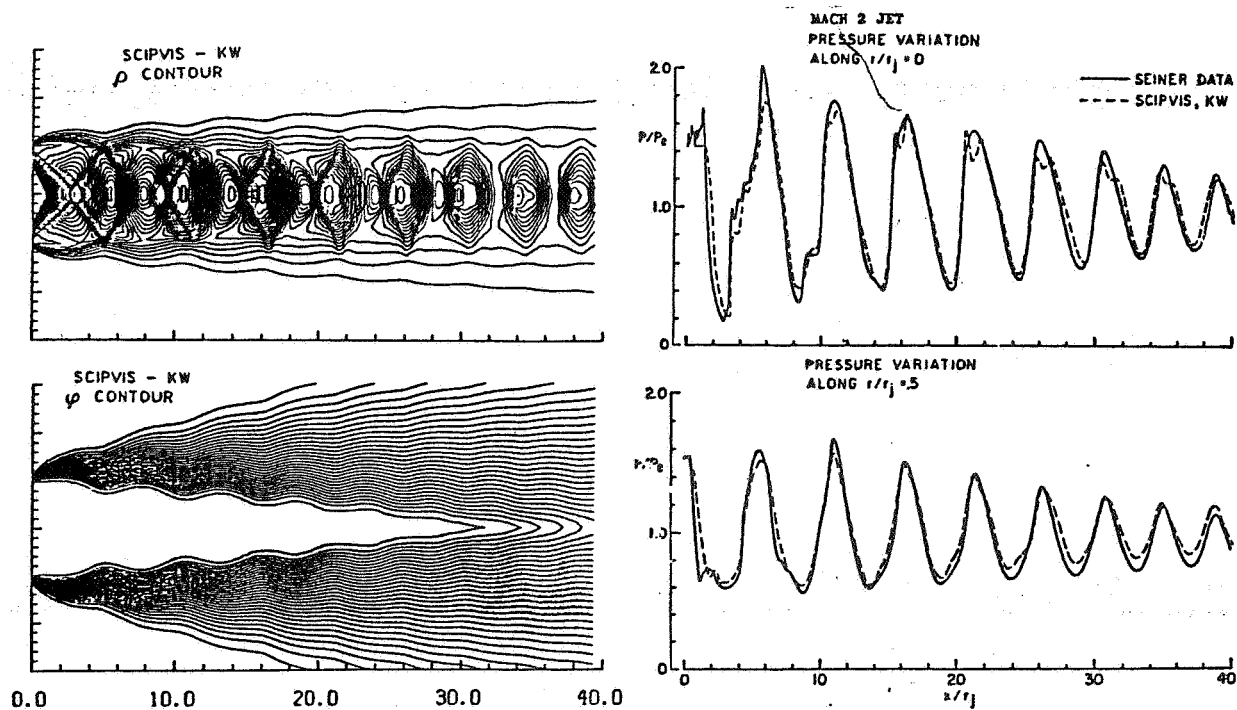


Figure 15. PNS prediction of Mach 2 underexpanded jet with kW model.

B1 - EVALUATION OF RNS TO BASELINE AXISYMMETRIC JETS

In the SAIC investigation of the Mach 2 underexpanded axisymmetric jet, two RNS (Reynolds Averaged Navier-Stokes) codes, PARCH and CRAFT, were studied using the $k\epsilon$ turbulence model. The SCIPVIS code with $k\epsilon$ was used as a benchmark. The PARCH code uses an implicit central-differencing Beam-Warming algorithm to solve the full Navier-Stokes equations. The PARCH code contains blocking and complex gridding schemes that make it attractive for use with complex nozzle geometry. The CRAFT code is finite volume with upwind numerics. Figure 11 shows a comparison between all three codes in their prediction of the jet static pressure and total enthalpy along the centerline of the Mach 2 underexpanded jet plume. As can be observed, even though both RNS and PNS exhibit the same rate of mixing, substantial differences exist between the codes with regard to wave attenuation beyond the second shock cell. The CRAFT code produces less wave attenuation than PARCH, but both RNS codes show significant wave attenuation relative to PNS.

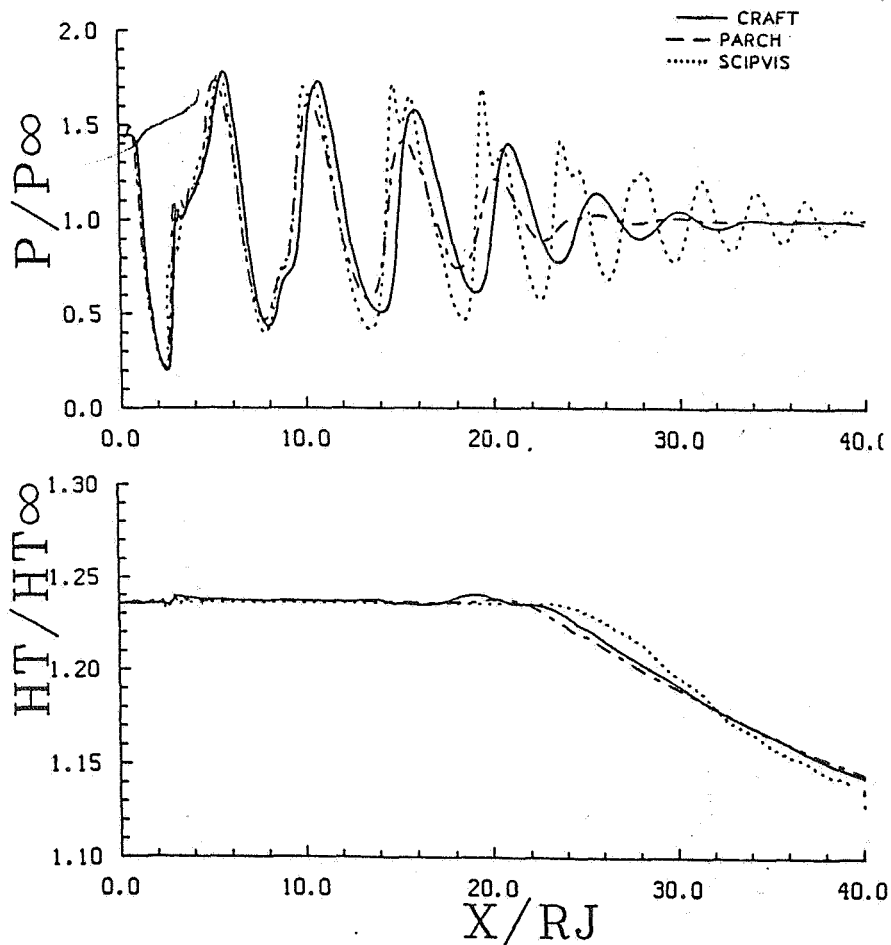


Figure 16. Comparison of PNS and RNS prediction of Mach 2 jet.

B1 - EVALUATION OF RNS TO BASELINE AXISYMMETRIC JETS

In an attempt to understand the mechanism for wave damping, SAIC first compared the performance of all three codes using laminar calculations with thin shear layer. The results showed that all three codes predicted the same overall shock structure, the CRAFT code showing the smallest level of numerical dissipation. As a final step, numerical calculations were made using the PARCH code with the full stress tensor retained and with the streamwise viscous/diffusive terms dropped. As can be observed in figure 12, this has a profound influence on wave damping. Retention of the full stress tensor leads to significant damping of the wave structure beyond the third shock cell. This suggests that the turbulence model used in the calculation is critical to achieving a satisfactory prediction for plume shock structure. Thus at this point more research is required on these 3D RNS codes before they can be reliably used to assist in a shock noise calculation.

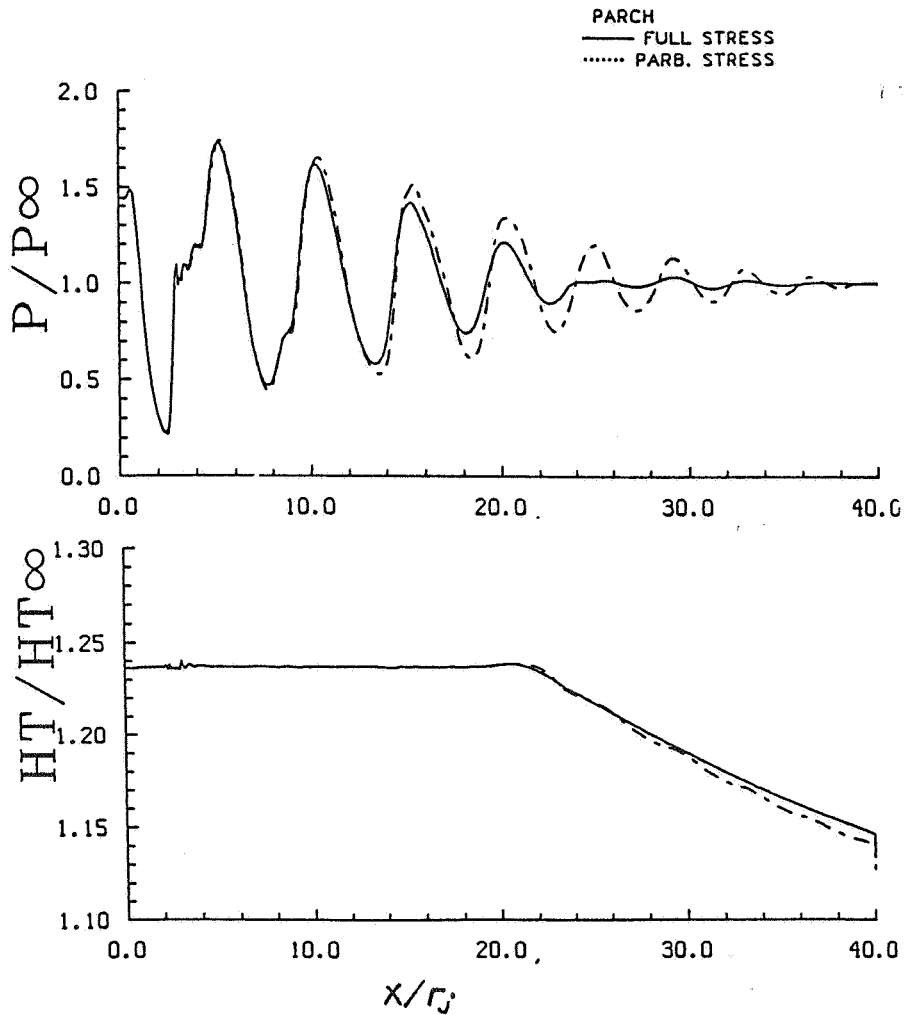


Figure 17. Effect of streamwise viscous/diffusive terms on wave damping.

B2 - AXISYMMETRIC PLUG VALIDATION EXPERIMENT

The axisymmetric plug nozzle represents a good candidate for validation of CFD for HSCT applications. The internal boundary and large wall curvature are all features that can be associated with a complex suppressor nozzle configuration. The nozzle design area ratio is equivalent to Mach 1.5 at 2060°R. For the present numerical/experimental program a plug half angle of 15° is initially being considered. The plug contains ventilation for boundary layer control to prevent separation and for shock management. The geometry of the wall ports are selected to minimize noise. The degree of ventilation can be controlled. Figure 11 illustrates the nozzle geometry. A removable hatch is used to enable installation of various plug surface measuring devices. The plug is being manufactured to include an non-instrumented and non-ventilated plugs. The measurement methodologies to be utilized are as follows:

Plug Body

STATIC WALL PRESSURES
 DYNAMIC WALL PRESSURE
 SURFACE TEMPERATURE
 HEAT TRANSFER MEAS.
 WALL SHEAR STRESS
 PLUG VENTILATION

PLUME

TOTAL & STATIC PRESSURE
 MEAN VELOCITY (LDV)
 REYNOLDS STRESS (LDV)
 TOTAL TEMPERATURE CONTOURS
 STATIC TEMPERATURE MEAS.
 FLOW VISUALIZATION

ACOUSTICS

FAR FIELD LINEAR ARRAY
 NEAR FIELD CONTOURS
 SOURCE LOCATION

AXISYMMETRIC NOZZLE WITH 15° PLUG

**DESIGN POINT:
 MACH = 1.5
 T₀ = 2060° R**

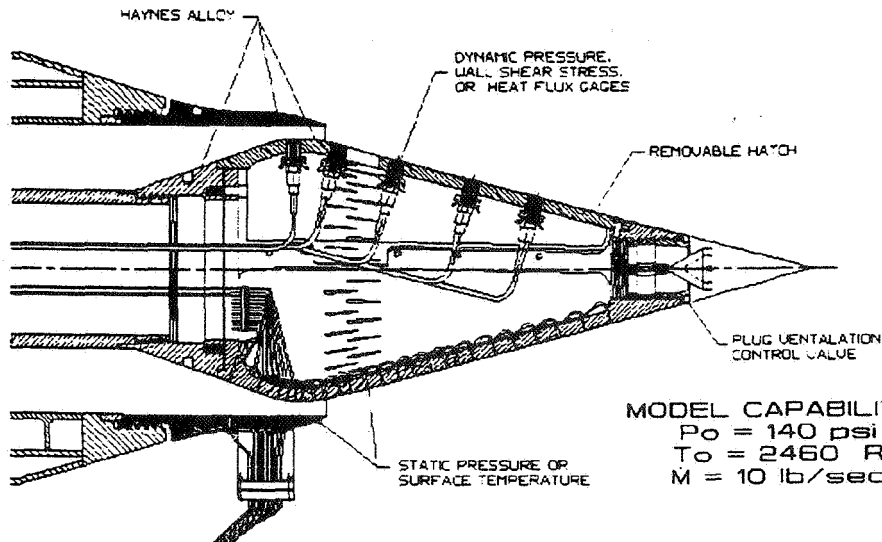


Figure 18. Single stream axisymmetric plug flow nozzle for validation experiment.

B2 - AXISYMMETRIC PLUG PARCH CODE RESULTS

Initial calculations have been performed at SAIC using PARCH for the axisymmetric plug nozzle geometry described above. In a parallel effort, Nick Georgiadis of NASA Lewis has applied the PARC code using the same nozzle geometry. For the work at SAIC, a full Navier-Stokes analysis is applied to determine slip wall versus no slip wall behavior. The flow calculation begins internal to the nozzle, where a 91 X 71 adaptive grid is used to compute internal flow. The Chien low Reynolds number $k\epsilon$ turbulence model is used to enable calculation into the wall region. The PARCH code predicts transition to occur inside the nozzle duct. The plug jet adaptive grid consisted of a 201 streamwise by 101 crossstream mesh. The analysis assumes an adiabatic wall. In the experimental model, heat flux measurements will be conducted using specially designed calorimeters to aid the numerical analysis.

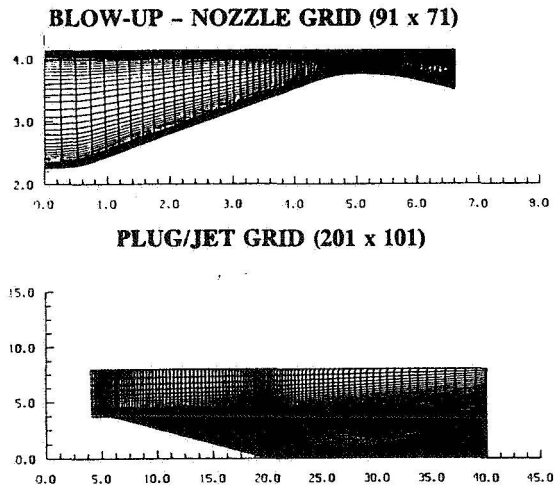
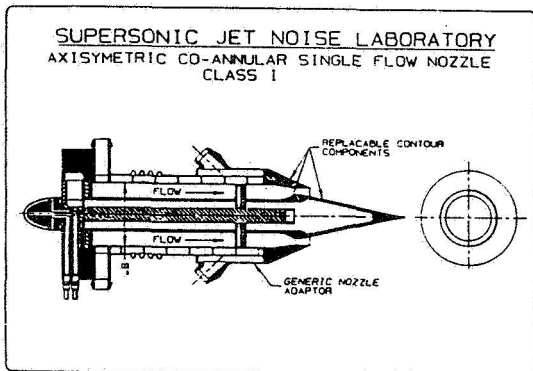
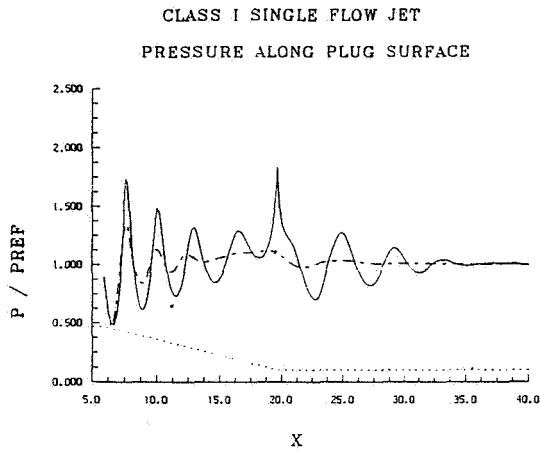


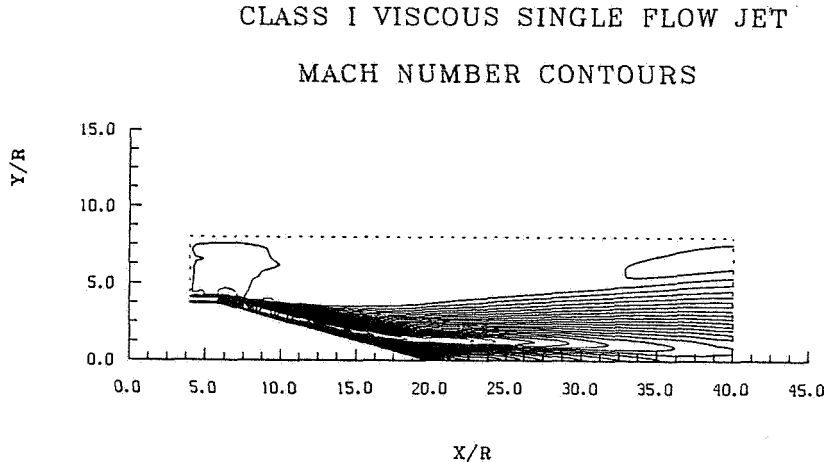
Figure 19. Parch code adaptive grid for axisymmetric plug nozzle.

B2 - AXISYMMETRIC PLUG PARCH CODE RESULTS

Figure 15a compares static pressure results between the slip and non-slip wall. As can be observed significant attenuation of shock/wave structure occurs due to interaction with the turbulent plug boundary layer. The numerical simulation involves operation of the nozzle at its design pressure and temperature ratios. On exiting the nozzle, both the slip and non-slip solutions accelerate the flow beyond the nozzle design point. The nozzle exit is located at $X = 5.8733$ ". Both the inviscid and viscous wall solutions achieve a maximum stream Mach number of 1.9 at the nozzle exit. The inviscid wall solution indicates that in order to turn the flow at the plug tip, a shock is generated. Figure 15b shows corresponding Mach number contours associated with the viscous wall solution. As can be seen supersonic flow extends to a region near $X = 36$.



a - comparison of plug wall and centerline static pressures for slip and non-slip solutions.



b - predicted Mach number contours.

Figure 20. PARCH code analysis of axisymmetric plug nozzle flow.

B3 - EVALUATION OF COMPRESSIBLE TURBULENCE MODELS

As described in section B1, accurate numerical prediction of supersonic shock containing flows is dependent upon the turbulence model installed in the code. Recently Sarkar (1990) has developed a new compressible turbulence model that shows an increase in the compressible turbulent dissipation, ϵ_{ij} , that would lead to a decreased growth rate with Mach number. From his results one sees that ϵ_{ij} only depends on Mach number,

$$\epsilon_{ij} = \frac{2}{3} \bar{\rho} \epsilon_s (1 + \alpha_1 M_t^2) \delta_{ij}$$

$$\bar{\rho} \epsilon_s (\text{Solenoidal Dissipation}) = \bar{\mu} (\omega_i'')^2$$

A preliminary experiment was conducted in the NASA/LaRC JNL to examine the prediction. Using schlieren optical data, LDV and pitot tube measurements, the spread rate in the initial shear layer was measured. The results are shown in Figure 21. Except for the data at 305 K, the results are consistent with the Sarkar model. Future studies will investigate other Mach numbers.

Jet Stagnation Temp (Deg K)	dδ/dx
293 (Pitot)	0.22
305	0.08
810	0.17
925	0.17
1090	0.20
1090 (LDV)	0.19
1255	0.22
1255 (LDV)	0.21
1365	0.21
1430	0.19
1480	0.20
1580	0.22

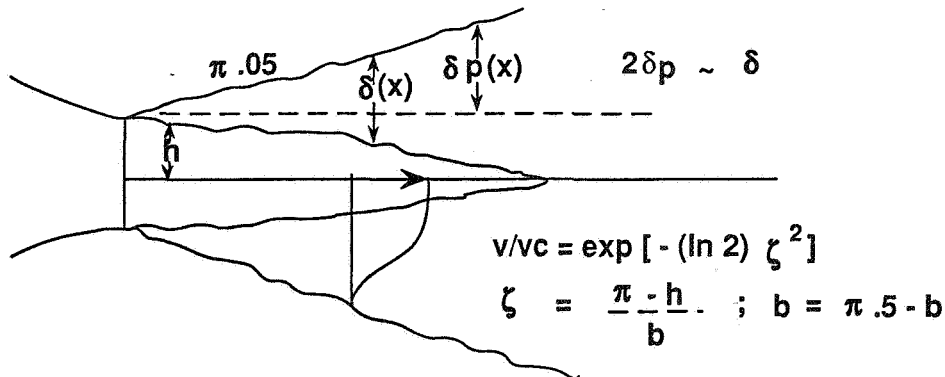


Figure 21. Examination of new compressible turbulent model.

C1 - NOZZLE GEOMETRY EFFECTS, CENTERLINE VELOCITY

For a shock-free supersonic jet, the amplitude of the emitted noise is a high power of the jet exit velocity. Therefore, any technique which rapidly reduces the plume speed without generating any additional noise will exhibit an acoustic benefit. Although round nozzle designs typically are used for turbine engines, a viable passive control of noise may be the use of asymmetric nozzles which promote rapid mixing thus lowering plume velocities and the associated noise. Possible geometries would be those which can be designed shock-free to eliminate the presence of shock-associated noise.

An elliptic nozzle design method which produces a shock-free flow was developed by Seiner, Baty, and Kumar at the NASA-Langley Research Center. Two nozzles were constructed: Mach 2 of aspect ratio 3 and Mach 1.5 of aspect ratio 2. A comparison of the centerline velocity distribution is presented in figure 22 between the elliptic and shock-free axisymmetric nozzles. The axial dimension is normalized by the equivalent diameter of the nozzle. As is evident in the figure, the centerline velocity of the elliptic nozzles decays more rapidly than that of the round nozzles. One may expect a noise reduction through the use of this type of geometry.

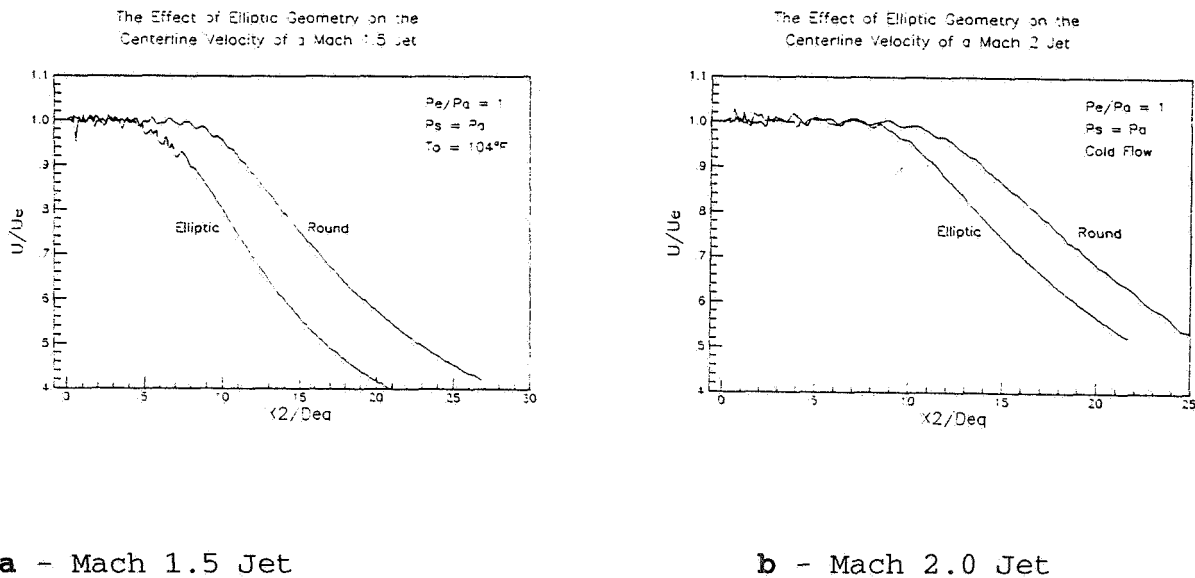
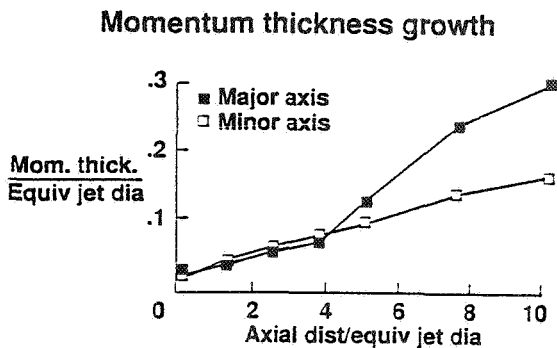


Figure 22. The effect of elliptic geometry on the centerline velocity distribution.

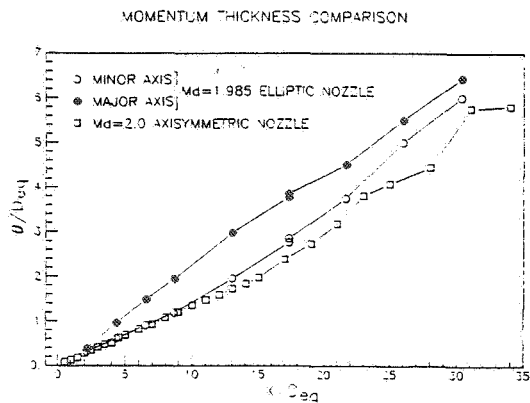
C1 - NOZZLE GEOMETRY EFFECTS, MOMENTUM THICKNESS

The momentum thickness has been used as a length scale of the initial turbulent shear layer (Ho, 1987). The initial azimuthal distribution of the momentum thickness controls the initial roll-up of shed vorticity while the axial distribution provides an indicator of the distortion of the jet column with downstream distance (Baty, 1990). The observed centerline velocity decay due to the elliptic geometry can be related to the asymmetric distortion of the major and minor axes momentum thickness. This distortion leads to enhanced mixing with the surrounding medium.

Figure 23a presents the axial momentum thickness distribution for the Mach 1.5 elliptic nozzle along both major and minor axes. Within the potential core ($X/Deq < 5$), the momentum thickness is essentially independent of major or minor axes and grows linearly, similar to a round jet. This indicates little azimuthal variation in the scales of initially shed vorticity. However, beginning approximately at the end of the potential core, the jet undergoes a large three dimensional distortion. The behavior of the Mach 2 elliptic nozzle is different as seen in figure 23b. The major axis momentum thickness increases at a greater rate with axial distance than does the minor axis momentum thickness. This is in contrast to the behavior of the Mach 1.5 elliptic nozzle. It is not known if this is related to the increased nozzle design Mach number or its increased aspect ratio. The minor axis momentum thickness of the round and elliptic jets are equal in the potential core region. Beyond the core region even the minor axis momentum thickness increases faster than the round nozzle.



a - Mach 1.5 Jet



b - Mach 2.0 Jet

Figure 23. The axial momentum thickness distributions

CI - NOZZLE GEOMETRY EFFECTS, SPECTRAL COMPARISON

The differences in the major and minor axes momentum thickness measurements for the Mach 1.5 elliptic nozzle would indicate the existence of a complex three-dimensional flow structure. This type of flow should have equally complex stability properties which would be manifest in the acoustic emission.

Figure 24 is a spectral comparison between the acoustic radiation of two azimuthal angles of the Mach 1.5 elliptic nozzle operating at a total temperature of 1160 R. Also included is a spectrum of the Mach 1.5 round nozzle corrected to the thrust of the elliptic nozzle. $\phi = 0$ degrees is in a plane which contains the minor axis and the jet axis; $\phi = 90$ degrees represents a plane containing the major axis and jet axis. The ψ angle is referenced to the nozzle inlet axis and a value of 128 degrees is the approximate direction of maximum overall acoustic emission. The data were acquired at approximately 127 equivalent diameters from the nozzle exit.

As is evident in the figure, a strong dependency exists between the spectral partitioning of acoustic energy and the nozzle geometry. Also, the acoustic field of the elliptic nozzle is azimuthally varying similar to the momentum thickness distribution. The overall sound pressure level of the round nozzle is 1 dB greater than the elliptic at $\psi = 0$ degrees and 4 dB greater than the elliptic at $\psi = 90$ degrees. Thus, geometry alone can yield acoustic amplitude benefits and possibly be used in the spectral redistribution of energy.

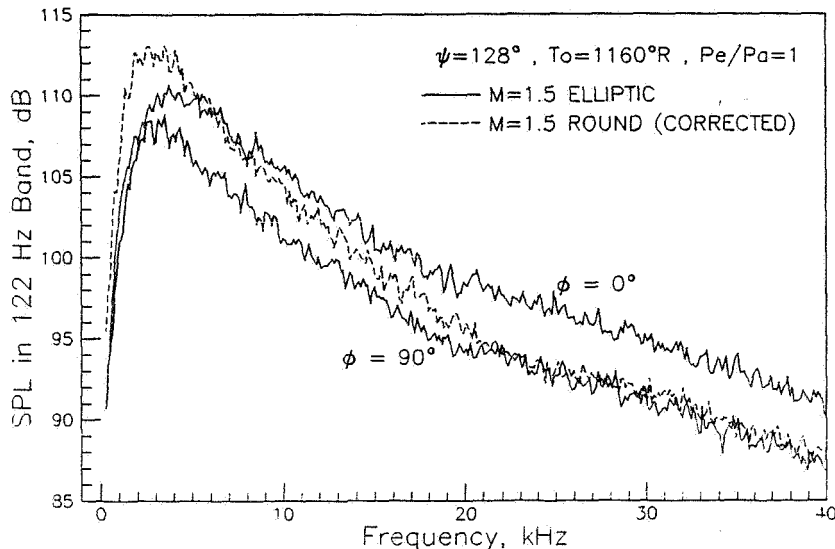


Figure 24. Spectral comparison of the acoustic emission from round and elliptic nozzle geometries.

C1 - NOZZLE GEOMETRY EFFECTS, PERCEIVED NOISE LEVEL

Due to the spectral differences created by nozzle geometry variations, the frequency-weighted perceived noise level would provide an important comparative metric for full scale applications. Acoustic data were acquired via a linear array for not only the Mach 1.5 round and elliptic geometries but also for an augmented deflecting exhaust nozzle (ADEN). The ADEN is a rectangular nozzle with parallel sidewalls and convergent-divergent flaps that differ in length in the nozzle exit plane. The data were scaled to 50000 lb of thrust at a sideline distance of 1476 feet and were propagated through a standard atmosphere using appropriate spectral corrections. These full scale conditions are representative of the requirements of the proposed high speed civil transport. ϕ is referenced as previously for the elliptic nozzle and for the ADEN $\phi = 0$ degrees contains the nozzle's convergent-divergent plane.

Figure 25a indicates that for $\phi = 0$ degrees, the elliptic geometry provides an acoustic reduction at the low ψ angles presented. The ADEN is not a three-dimensional contoured nozzle design and thus should contain shock noise which would increase the lower ψ angle amplitudes. Figure 25b shows an acoustic reduction for the elliptic nozzle as well as the ADEN when compared to the round geometry. Again note the presence of shock noise for the ADEN. This indicates the importance of identifying a passive noise control nozzle geometry which can produce a shock-free flow, similar to the elliptic nozzle tested.

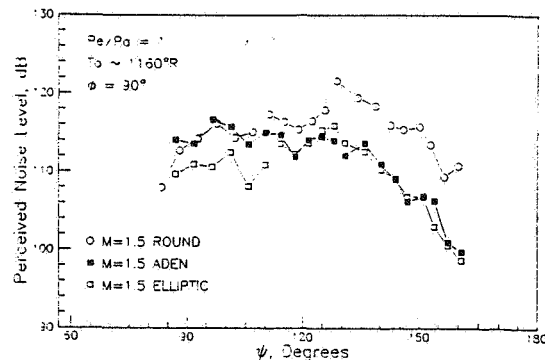
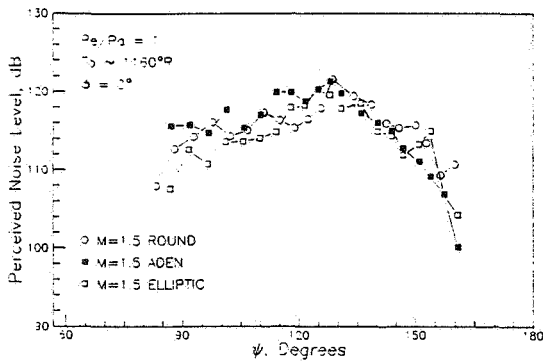


Figure 25. Comparison of the perceived noise level for various nozzle geometries scaled to a full scale application.

C1 - NOZZLE GEOMETRY EFFECTS, DESIGN MACH NUMBER

Figure 26 presents the azimuthal variation of the perceived noise level for both elliptic nozzles tested. The data is scaled similar to figure 25. The ψ angle corresponds to the approximate location of maximum acoustic emission. For flows which are shock-free, the data indicates a strong dependence of noise emitted on the velocity of the plume; i.e., greater exit velocities produce higher acoustic amplitudes. This dependence is evident for all azimuthal angles as indicated by the Mach 1.5 nozzle data for the two temperatures presented and also the Mach 2 data compared to the Mach 1.5 nozzle data.

The data also shows (similar to the previously presented spectra) that the acoustic amplitude is dependent on the azimuthal angle ϕ . In general, the perceived noise level decreases as ϕ approaches 90 degrees. This dependence represents another passive control method by which the nozzle orientation on a full scale engine can be manipulated to radiate the majority of the acoustic energy away from noise sensitive areas. It is important to note that because all nozzles are scaled to constant thrust, the lower temperature nozzle case should appear with smaller scaled noise because it is a higher mass flow nozzle.

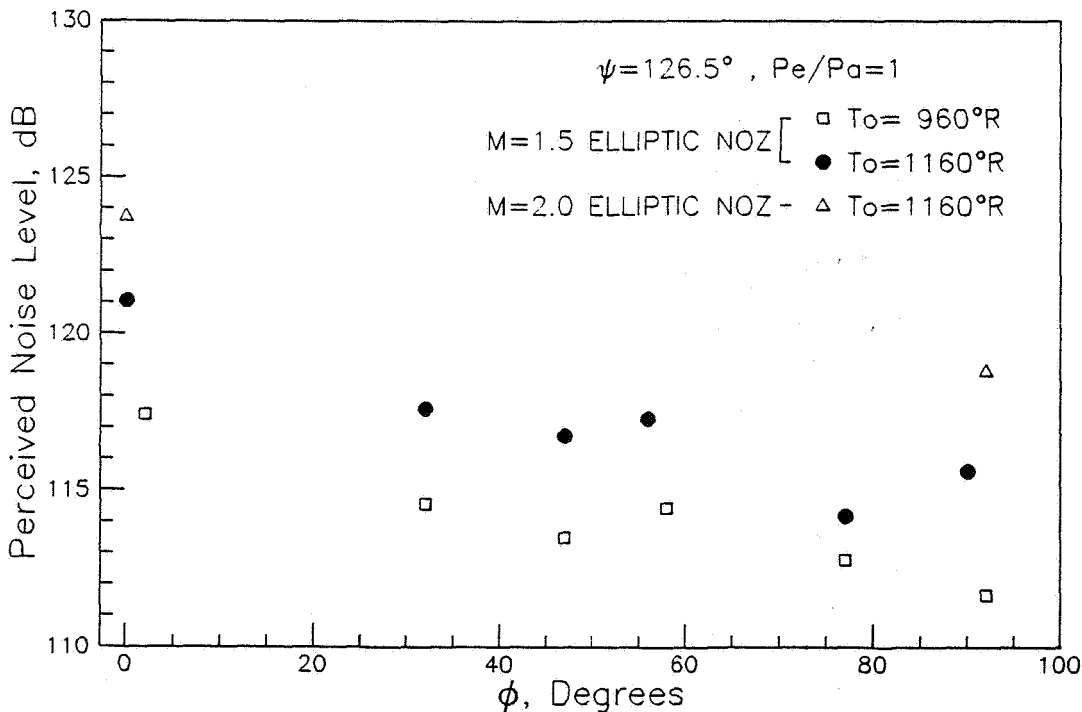


Figure 26. Comparison of the perceived noise level for the two elliptic nozzle geometries tested.

C2 - MULTIPLE JET INTERACTIONS

The HSCT suppressor nozzle, as currently envisioned, utilizes multiple hot high speed jets surrounded by afterbodies that promote rapid mixing with these jets. To show the types of interactions possible with multiple jet configurations, figure 27 presents a phased-averaged Schlieren photograph of unheated twin choked-tube nozzles (the strobe light is locked to the screech frequency for a given phase of the measured acoustic wave).

These nozzles were operated at a fully expanded Mach number of 1.32 where the dominant instability wave in the jet shear layer is a flapping structure (double helix). Generally, this type of large scale structure has no azimuthally preferred orientation. However, due to the mutual excitation of the jets, the flapping motion of both jets is now oriented in a plane containing the axes of both jets. This alters not only the azimuthal directivity of the screech noise but also promotes a more rapid mixing configuration as compared to a single nozzle. The potential thus exists for using the passive control feature of multiple jet interaction for acoustic benefits.

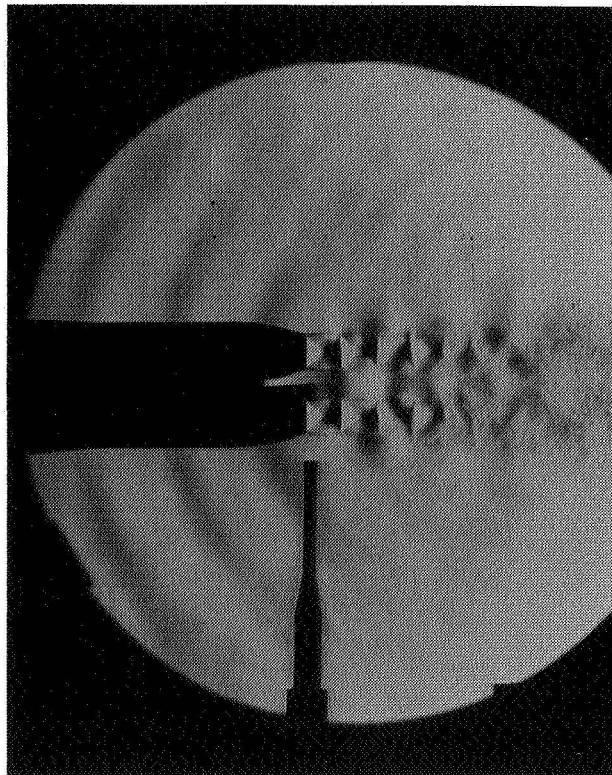
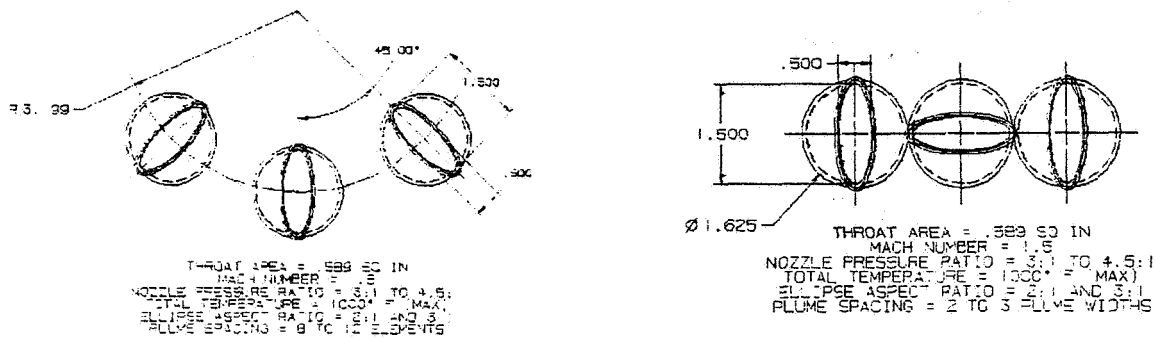


Figure 27. Phased-average Schlieren of twin choked-tube nozzles.

C2 - MULTIPLE JET INTERACTIONS

The envelope geometry for multiple jets in an HSCT application is either round or a low aspect ratio rectangular. The high speed jets emerge from geometries that are complex, but often driven by the geometric constraint of packaging in the envelope shape. The suppressor also makes use of an acoustically treated ejector that provides augmentation to the engine mass flow.

The elliptic jet geometry discussed previously shows that passive methods can be used to reduce noise. The properties of these non-round geometries, as exhibited by the deformation of the jet column (momentum thickness distribution), suggest that the orientation and location of the high speed mixer lobes is not arbitrary. A study of multiple jet interactions from a tri-axial configuration of nozzles (figure 28) is now underway at NASA Langley. The initial system uses a set of elliptic nozzles with varying aspect ratio combinations. The mechanism to support the tri-axial nozzle system permits location of the three nozzles to be arbitrarily rotated and positioned about a central axis. All elliptic nozzles are designed to be shock-free, so that an assessment of 3-D turbulent interaction can be studied without the influence of plume shocks. One cannot differentiate non-symmetric pressure gradients produced by shocks in the flow from that produced by turbulence.



a - Simulated Suppressor Nozzle

b - Interaction Mode

Figure 28. Example of tri-axial elliptic nozzle configuration.

C4 - ACTIVE CONTROL OF INITIAL JET SHEAR LAYER

The primary noise generation mechanisms of supersonic jet flows have been attributed to the presence of large scale structures in the shear layer. These dominant structures develop when small scale disturbances in the initial region of the jet grow in amplitude as they convect downstream. Therefore it may be reasonable to assume that by actively controlling initial shear layer instabilities, which have maximum growth rates, one can also control the noise emission.

C.M. Ho at University of Southern California is investigating practical methods for controlling the most unstable modes and their azimuthal energy distribution. These methods involve the use of sound, temperature, tuned cavities, and piezo-ceramic actuators to control the initial shear layer disturbances of axisymmetric and asymmetric nozzles operating in both the subsonic and supersonic regimes. Acoustic measurements have been made for a circular jet tested from the low subsonic to the transonic range. These measurements span the near field pressure fluctuations to the far field noise. The far field spectra presented in figure 29 indicate that for $M=.2$ to $.35$, the noise generated by large scale coherent structures in the thin shear layer dominates (high frequency peaks), while beginning at $M=.4$, the noise of the preferred mode dominates (broadband peak). The data will be compared to that acquired when various control methodologies are implemented.

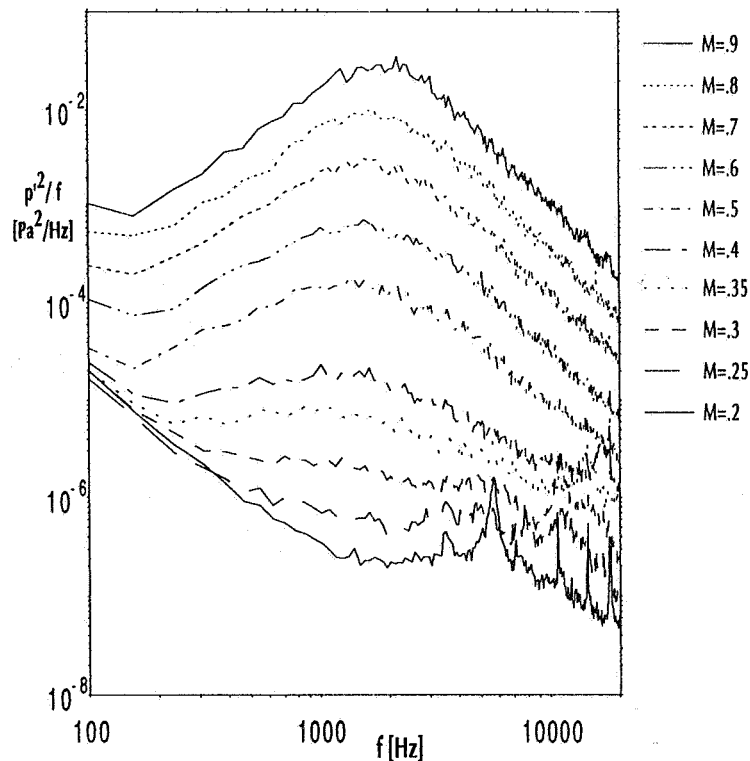


Figure 29. Far field spectra for an unheated circular jet operating subsonically.

DI - SUPERSONIC INSTABILITY WAVES

An experiment is being planned in the NASA/LaRC JNL to verify the theoretical predictions of Tam (1990) on the occurrence of supersonic instability waves in high temperature jets where $T_j/T_a > 2.5$. The predictions of figure 30 show that with increasing jet temperature ratio, the Kelvin-Helmholtz instability wave amplitude decreases, but there is the appearance of a supersonic instability wave. These waves are produced by turbulence structure in the shear layer that convect supersonically relative to the local jet sound speed.

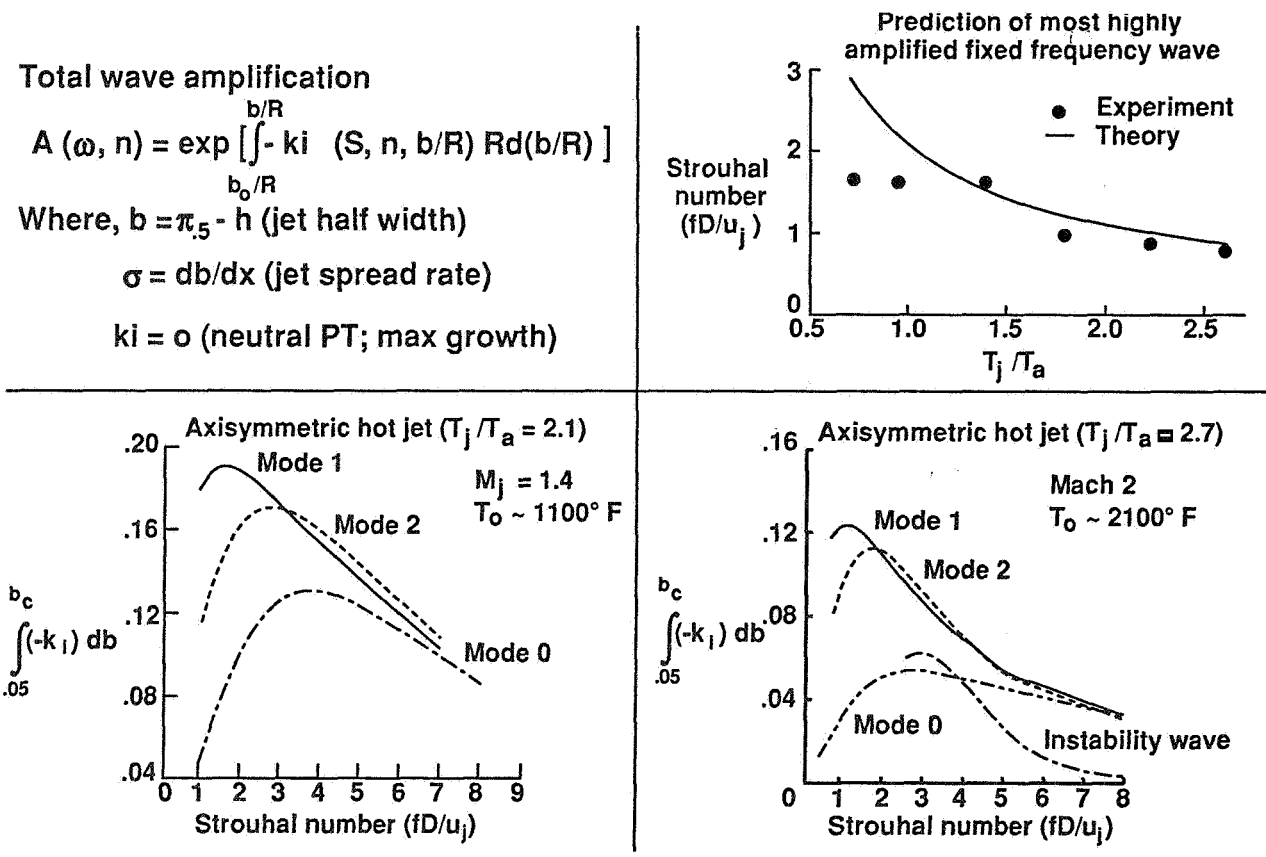


Figure 30. Instability waves in high temperature supersonic jets.

DI - HIGH TEMPERATURE WATER COOLED NOZZLE

As a preliminary investigation into properties of hot supersonic jets and the questions regarding the directivity frequency and amplitude of the supersonic instability wave, Schlieren records were acquired from the hot Mach 2 axisymmetric nozzle shown in figure 31. This nozzle was designed to be shock-free at Mach 2 and a temperature of 2460 R. The nozzle exit diameter is 3.6 inches and is heated by the sudden expansion (SUE) burner in the JNL facility. This nozzle is water cooled and capable of being tested to 3000 R.

**ORIGINAL PAGE
BLACK AND WHITE PHOTOGRAPH**

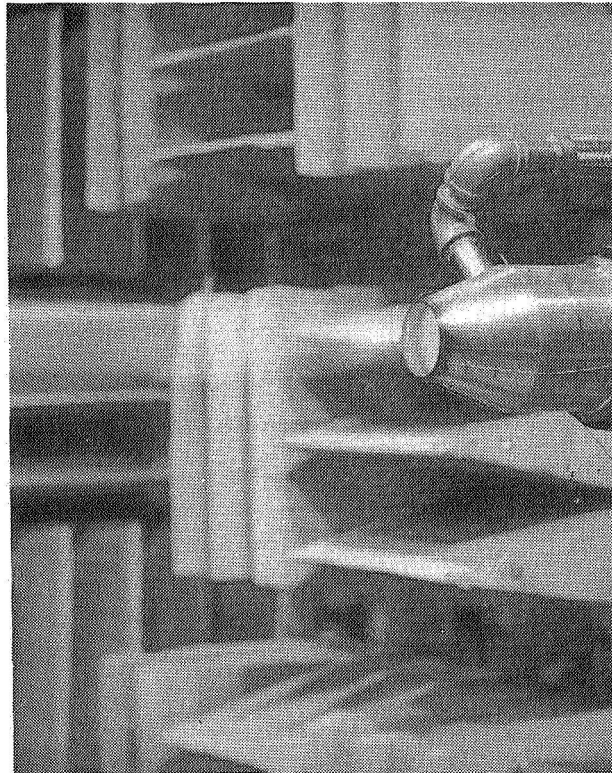
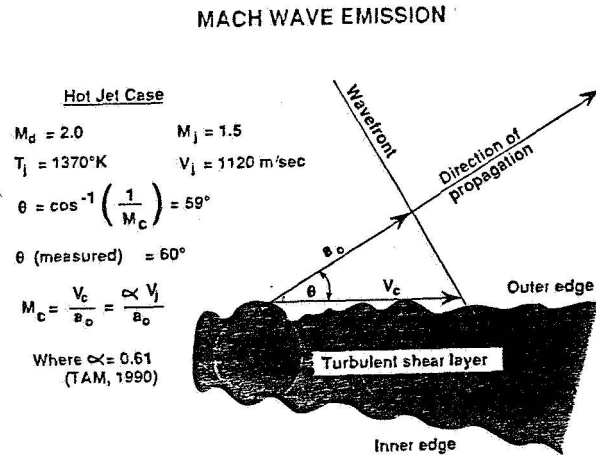
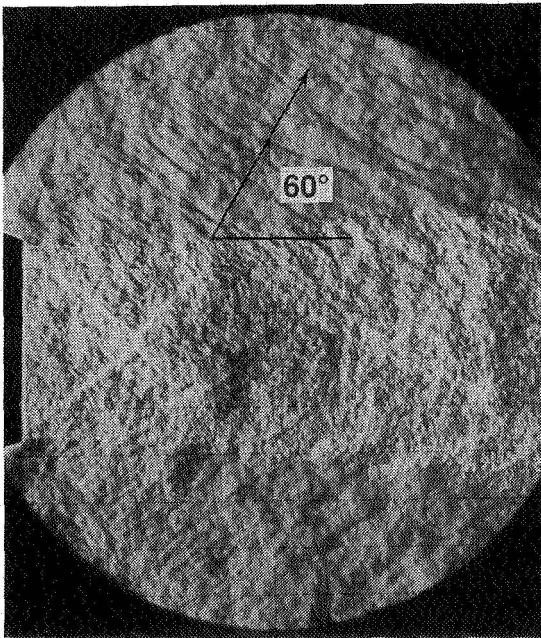


Figure 31. Mach 2 high temperature water cooled axisymmetric nozzle mounted in the JNL.

D1 - MEASURED AND PREDICTED MACH WAVE EMISSION ANGLE

Figure 32 illustrates a specific example between the measured and predicted Mach wave emission angle for a hot supersonic jet. In this example, the Mach 2 jet is being operated overexpanded at $M_j = 1.5$ and a temperature of 2466 R. Figure 32a shows the measured Schlieren data for this example. The Mach waves, which emerge from the edge of the shear layer, have wave normals that appear orientated 60 degrees to the jet axis. Based on Tam's (1990) large scale wave model, instability waves for this example will convect at 61% of the jet exit velocity. Based on this, the predicted wave angle is 59 degrees to the jet axis, as shown in figure 32b.



a - Schlieren of Mach 2 Jet

b - Predicted Mach Wave Angle

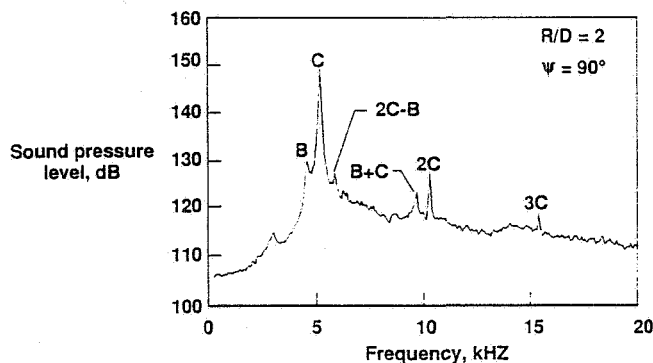
Figure 32. Measured and predicted Mach wave emission for a hot jet.

D2 - NON-LINEAR WAVE INTERACTIONS

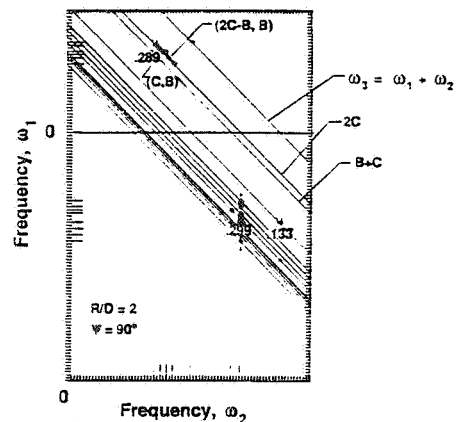
Under certain operating conditions, shock-containing supersonic free jets have been shown to emit high amplitude narrowband acoustic signals referred to as screech tones. It has been suggested that the generation of this noise component is due to the interaction of the dominant large scale coherent structure in the turbulent shear layer with the shock cell system (Tam, 1986). Screech has been observed to be multi-modal, i.e. the jet exhibits different instability characteristics depending on the operating condition of the nozzle (Ponton, 1989). To better understand this noise mechanism, it is important to determine whether different screech modes are independent or interact non-linearly.

Two particular screech modes can be identified in the acoustic spectrum presented in figure 33a. These modes are the B and C modes, and are labelled accordingly. Also identified are the second and third harmonics of the C mode (2C and 3C) as well as narrowband processes occurring at the frequencies B+C and 2C-B. These latter two spectral components provided the impetus to perform a bispectral analysis on the data to determine if non-linear wave-wave interactions are occurring between the fundamental screech modes. This higher-order spectral technique reveals phase coherences between three frequencies satisfying the selection criteria $\omega_3 = \omega_1 + \omega_2$, indicative of a non-linear quadratic interaction (Ritz, 1987).

The bispectral analysis produced the auto-bicoherence contour plot shown in figure 33b. The diagonal lines are constant ω_3 lines and the two additional frequencies satisfying the selection criteria are obtained from the abscissa and the ordinate. As labelled on the plot, phase coherences are seen to exist between the C, B, and B+C frequencies as well as between the 2C-B, B, and 2C frequencies. This indicates that non-linear interactions are occurring and suggests that future acoustic models should encompass the observed source non-linearity.



a - Auto-Spectrum

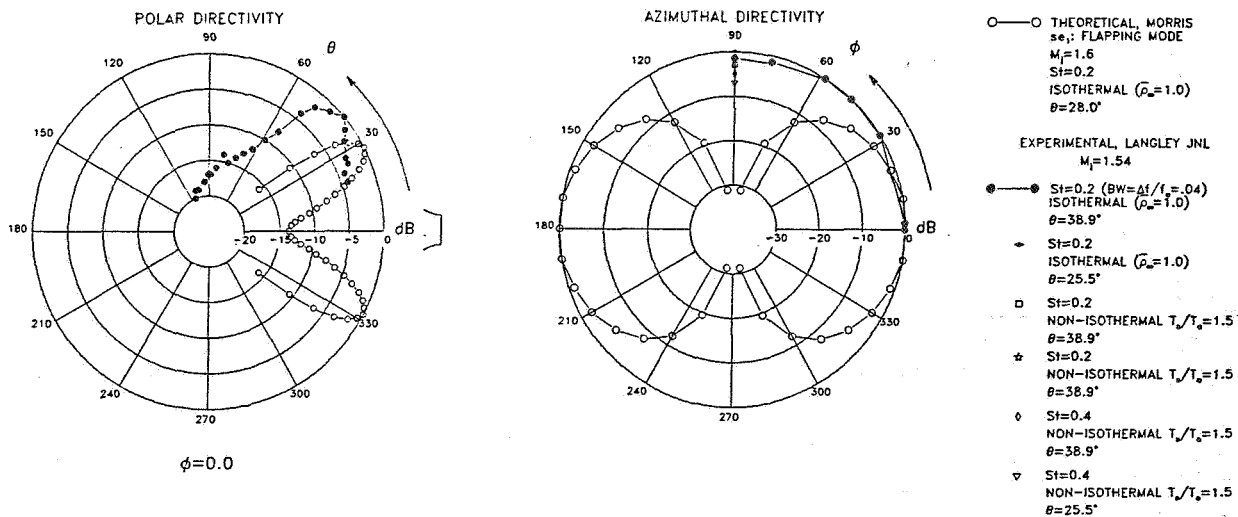


b - Auto-bicoherence Spectrum

Figure 33. Spectral analysis of the acoustic emission from an unheated round conical nozzle operating at $M_j = 1.44$.

D4 - PREDICTION OF NOISE FOR NON-ROUND JET GEOMETRY

The dominant sources of supersonic jet noise may be associated with the coherent structures in the jet mixing region, the jet's shock cell structure, and the interaction between these two phenomena. In this study the changes to the noise radiation associated with a change in the nozzle exit geometry is examined. An elliptic jet of aspect ratio 2 has been considered. The large scale structures in the jet are modelled as instability waves. These structures convect downstream with a velocity on the order of the jet exit velocity. For high Mach number or heated jets there is a direct coupling between the pressure fluctuations in the jet flow field and the acoustic field. This results in intense noise radiation. In the present study the characteristics of the large scale structures or instability waves are obtained from a solution of the compressible Rayleigh equation. In the region just outside the jet flow the pressure fluctuations are described in terms of Mathieu functions and modified Mathieu functions. These fluctuations are matched with the acoustic field using the method of matched asymptotic expansions. Figure 34 shows a typical far field calculation for the se_1 flapping mode. The two sections through the directivity pattern shown in figure 34 show (a) the variation with azimuthal angle ϕ for a polar angle of 30 degrees, and (b) the variation with polar angle θ for an azimuthal angle of 0 degrees. The decibel levels are in arbitrary units. Experimental data acquired at similar operating conditions, indicate the preference for axisymmetric structure and a wave direction at a steeper angle to the jet axis. Future calculations are being made to investigate stability properties of axisymmetric structure.



a - Polar Directivity

b - Azimuthal Directivity

Figure 34. Far field directivity with azimuthal and polar angles.

D5 - LOW REYNOLDS NUMBER RESEARCH

The most promising theoretical developments in the prediction of supersonic jet noise involve the modeling of large scale turbulence structure (that produces a dominant portion of the radiated noise) with instability wave theory. Operation of model jets under low Reynolds numbers are achieved by exhausting the jets at low density (pressure) conditions in the low pressure anechoic chamber jet test facility (figure 35). Standard condenser microphones are used for the acoustic measurements and miniature hot-wire probes measure the turbulence structure in the jets. The unique feature of the latest measurements is that jets with helium/air mixtures are used to simulate heated jet conditions. This approach is a reliable way to evaluate the predictive capability of the analytical model. The first and simplest check is of the most unstable frequency of the primary jet instability (and radiated noise). Initial experiments have been performed with a jet operating at Mach 2, with a helium/air mixture that produces a velocity that is approximately 50% greater than the pure air jet. Shown in figure 36 are the acoustic spectra of air and an air/helium mixture jet. The most unstable frequency is shown to increase as the instability theory predicts it should. Numerous additional measurements are underway to explore these phenomena in more detail.

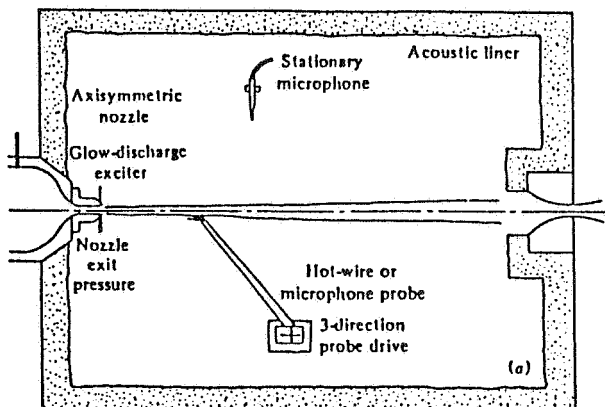


Figure 35. Low pressure anechoic jet test facility.

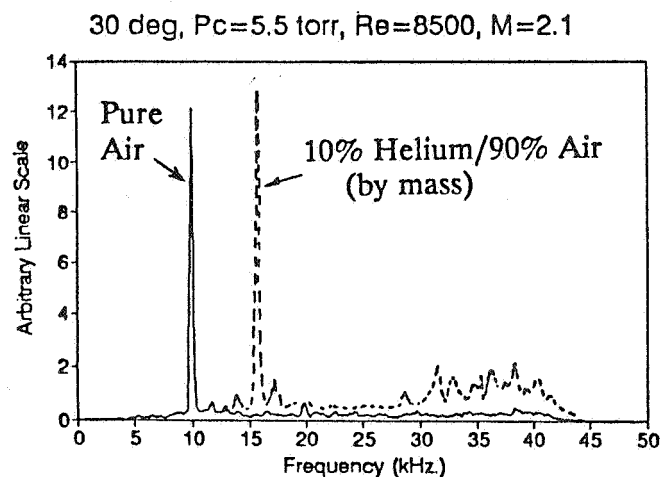


Figure 36. Acoustic spectra; $M=2.1$ air and helium/air jets.

REFERENCES

- Baty, R.S., Seiner, J.M. & Ponton, M.K. 1990** Instability of a supersonic shock-free elliptic jet. AIAA Paper 90-3959.
- Ho, C.M. & Gutmark, E. 1987** Vortex induction and mass entrainment in a small aspect ratio elliptic jet. J. Fluid Mech., 179, 383.
- Ponton, M.K. & Seiner, J.M. 1989** The effects of initial jet exit conditions on plume resonance. AIAA Paper 89-1054.
- Ritz, Ch.P., Powers, E.J. & An, C.K. 1987** Applications of digital bispectral analysis to nonlinear wave phenomena. ISSPA 87 Signal Processing, Theories, Implementations and Applications, 352.
- Tam, C.K.W. 1990** Broadband shock associated noise of moderately expanded supersonic jets. J. Sound and Vib., 140, 55.
- Tam, C.K.W., Seiner, J.M. & Yu, J.C. 1986** Proposed relationship between broadband shock associated noise and screech tones. J. Sound and Vib. 110, 309.
- Weinstein, L.M. 1991** An improved large-field focusing Schlieren system. AIAA Paper 91-0567.

Session IV. Source Noise

omit

Theoretical Aspects of Supersonic Jet Noise
Dr. Christopher K. W. Tam, Florida State University

THIS PAGE INTENTIONALLY BLANK

N94-33469

THEORETICAL ASPECTS OF SUPERSONIC JET NOISE

54-71
11997

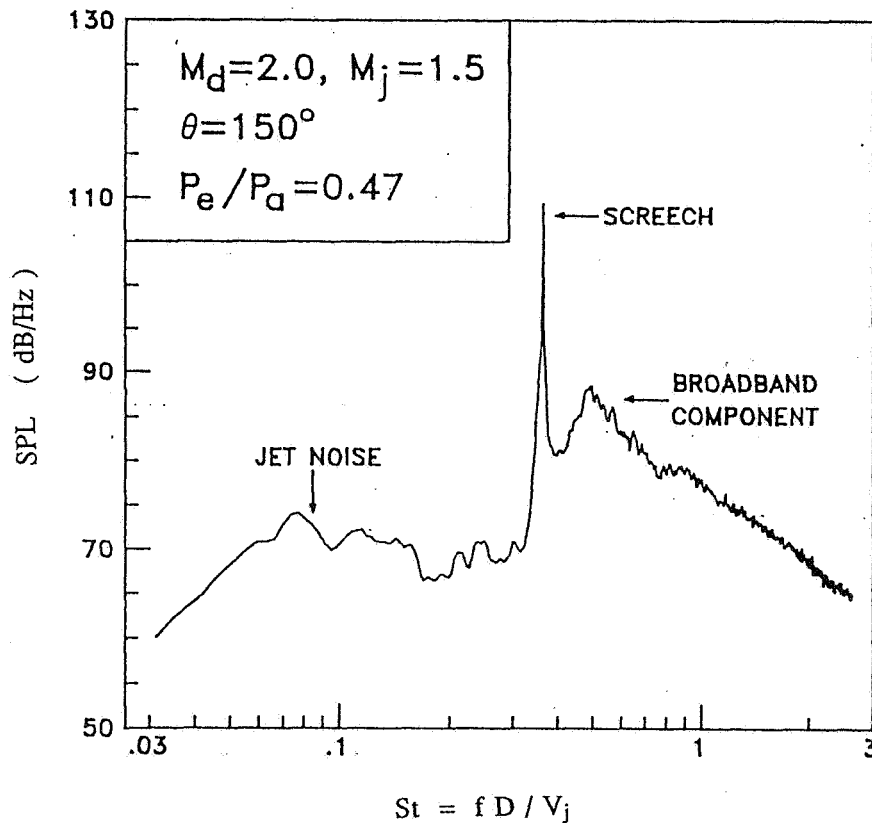
Christopher Tam
Department of Mathematics
Florida State University
Tallahassee, Florida 32306-3027

First Annual High-Speed Research Workshop
May 14-16, 1991

PRECEDING PAGE BLANK NOT FILMED

THE THREE COMPONENTS OF SUPERSONIC JET NOISE

The noise of supersonic jets consists of three principal components. They are the turbulent mixing noise, the screech tones and the broadband shock associated noise. The turbulent mixing noise forms the low frequency peak of a typical supersonic jet noise spectrum. The screech tones are sound waves of discrete frequencies. Broadband shock associated noise is the high frequency component of the jet noise spectrum. It is made up of a main peak and sometimes a few secondary peaks at higher frequencies. Experimental observations and theory indicate that the fundamental screech tone frequency marks the low frequency limit of broadband shock associated noise. Both the screech tones and broadband shock associated noise are generated by the presence of a shock cell structure in the jet. For a perfectly expanded jet the total radiated noise is less and comprises of only turbulent mixing noise.

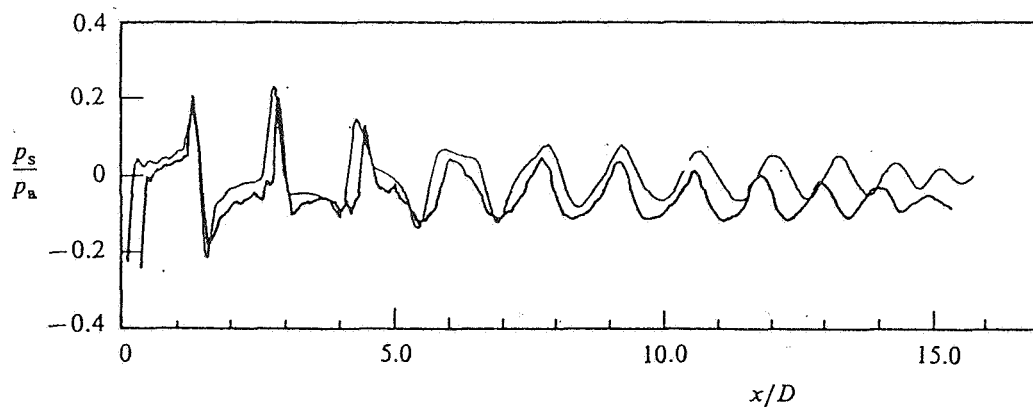
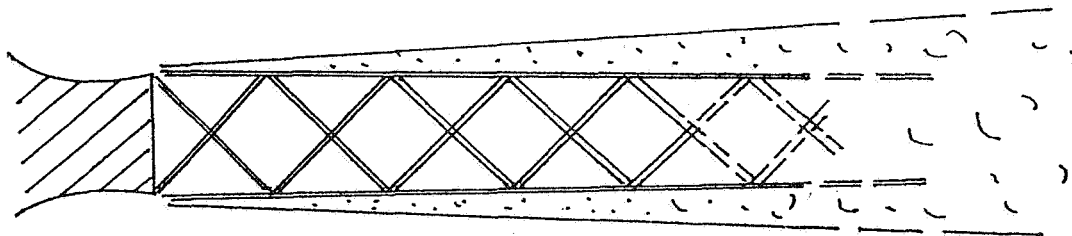


Typical far field supersonic jet noise spectrum

SHOCK CELL STRUCTURE OF IMPERFECTLY EXPANDED JETS

The static pressure at the nozzle exit of an imperfectly expanded jet is not equal to the ambient pressure. To obtain pressure equilibrium at the nozzle lip a shock wave or an expansion fan is formed. The shock or expansion fan allows the gas of the jet to adjust quickly to the ambient pressure. From the nozzle lip the shock or expansion fan propagate across the jet to the mixing layer on the other side. Outside the jet the gas is stationary or in low subsonic motion. Shock or expansion is not allowed. As a result the shock or expansion fan is reflected back at the mixing layer. The reflected expansion fan or shock will continue to propagate downstream bouncing back and forth from one side of the jet to the other. In this way a quasi-periodic shock cell structure is formed. The details of the shock cell structure can be calculated analytically [1] or computationally [2]. Of importance to broadband shock associated noise and screech tone predictions are the gross features of the shock cell structure, namely, the shock cell spacing and pressure amplitude.

QUASI-PERIODIC SHOCK CELL STRUCTURE

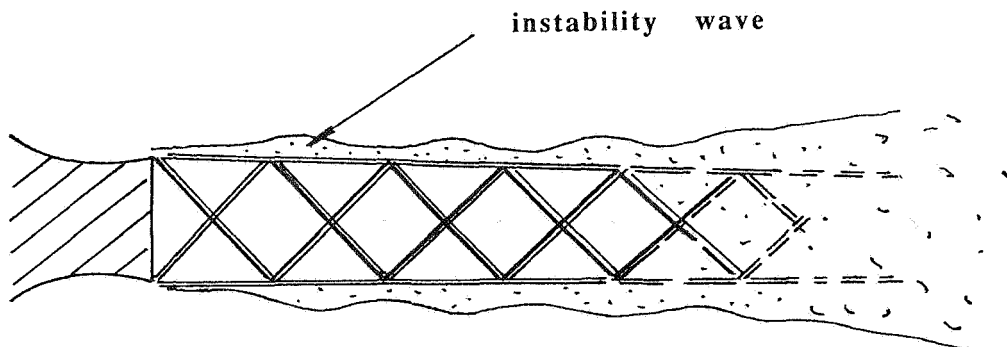


Axial pressure distribution at $r/D = 0.38$, $M_j = 1.82$, $M_d = 2.0$
Measured -- dark line : Calculated -- light line

LARGE TURBULENCE STRUCTURES/INSTABILITY WAVES

One of the most important physical entities in the flow of a supersonic jet which is responsible for noise generation is the large turbulence structures/instability waves. Pictures (see sketch below) of these instability waves are provided in ref. [3]. They are usually called the Kelvin-Helmholtz instability waves. They generally appear in a form with either axisymmetric or helical (flapping) geometry. These instability waves derive their energy from the mean flow. They are also responsible for the mixing and entrainment of ambient gas into the jet flow.

LARGE TURBULENCE STRUCTURES/INSTABILITY WAVES

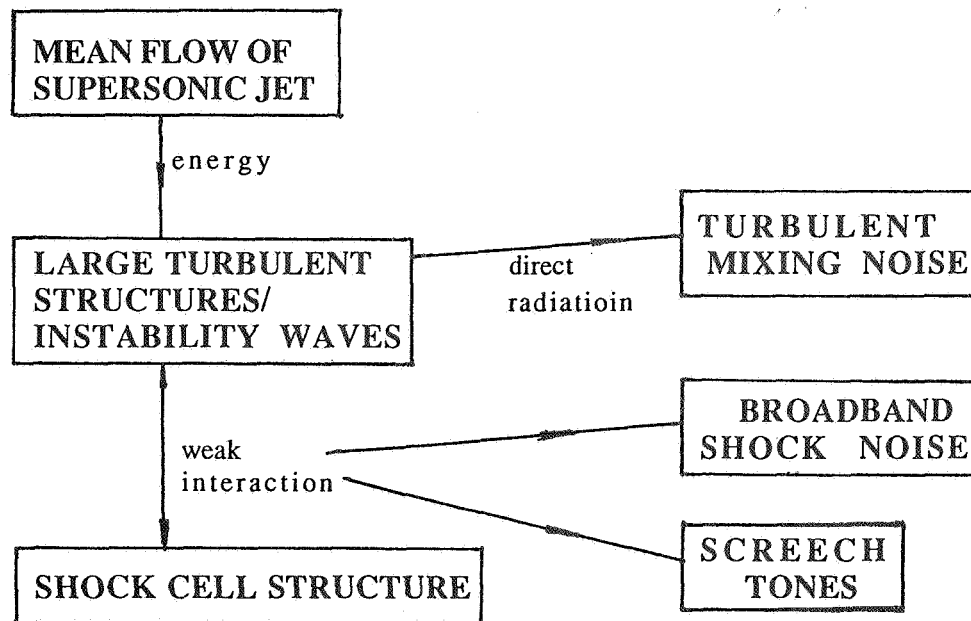


Large scale instability waves in the mixing layer of a supersonic jet excited by upstream sound waves

SUPERSONIC JET NOISE THEORY

There exists now a fairly good understanding of how the three principal components of supersonic jet noise are generated. The crucial element is the large turbulent structures/instability waves of the jet flow. These instability waves extract energy from the mean flow as they propagate downstream along the jet column. The turbulent mixing noise is generated directly by the supersonic components (relative to the ambient speed of sound) of these instability waves. The screech tones and the broadband shock associated noise are generated by the weak interaction of these instability waves and the shock cell structure as the former propagate through the latter.

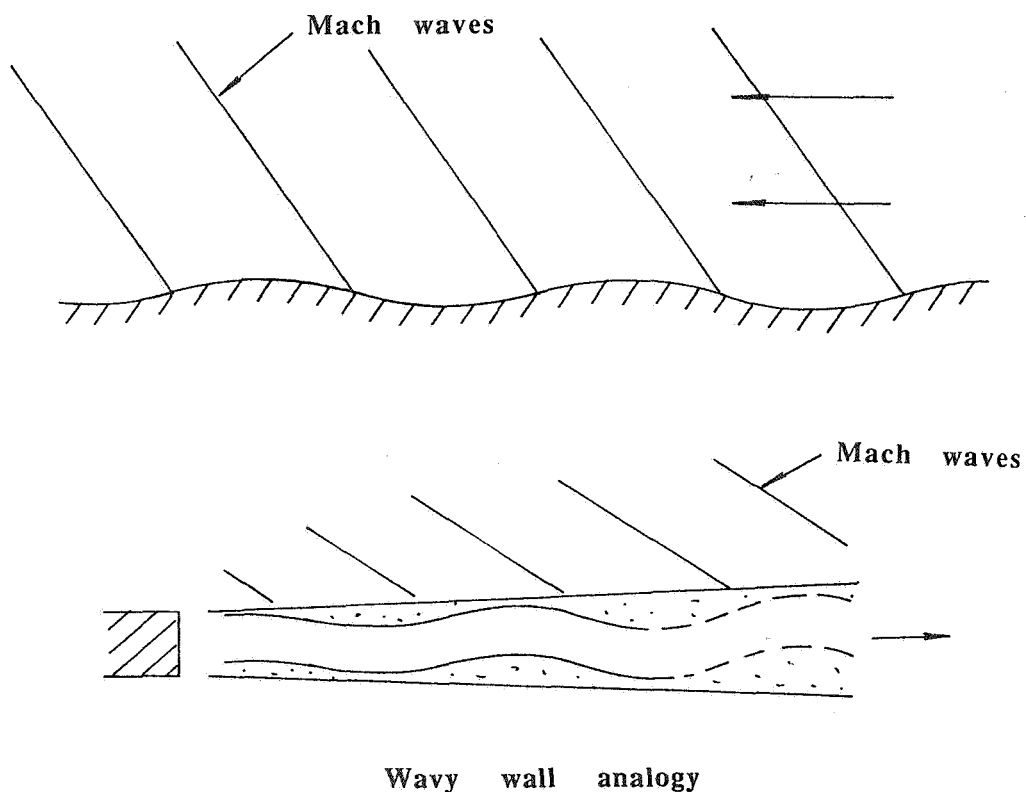
SUPERSONIC JET NOISE THEORY



GENERATION OF TURBULENT MIXING NOISE

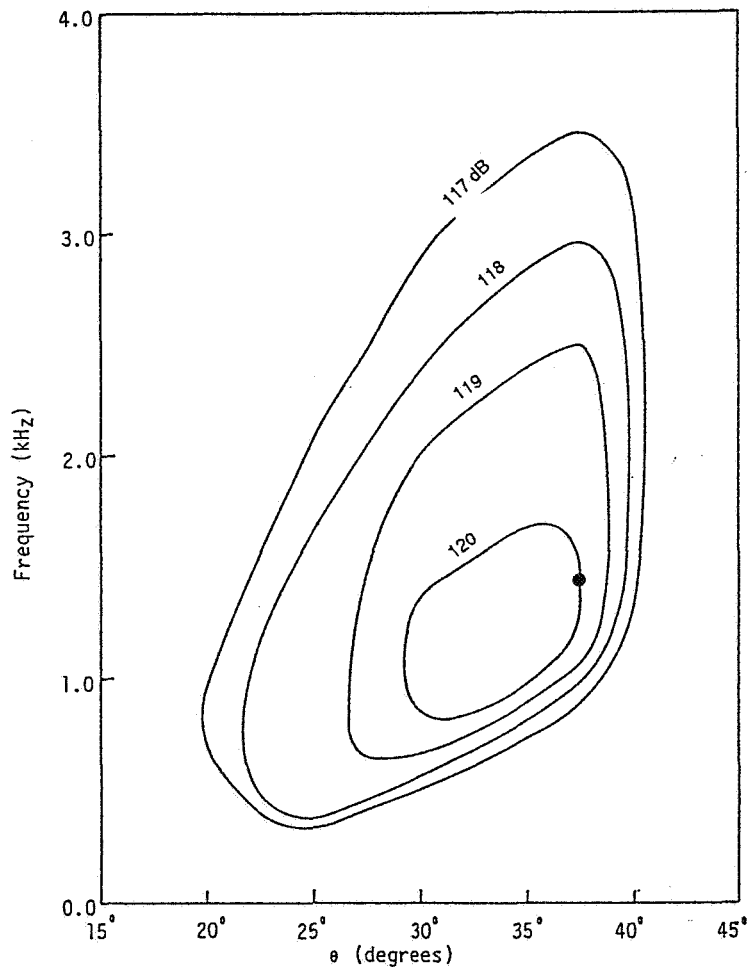
To understand how instability waves generate turbulent mixing noise let us remind ourselves the problem of supersonic flow past a solid wavy wall. The solution of this problem suggests that Mach waves are formed. These Mach waves extend to infinity away from the wall indicating that acoustic disturbances are radiated to the far field. Now an instability wave travelling with supersonic velocity relative to the ambient speed of sound is analogous to the problem of supersonic flow past a wavy wall [4]. Mach waves are radiated. The principal direction of radiation is normal to the Mach wave front. The frequency of the radiated sound is equal to the frequency of the instability wave.

TURBULENT MIXING NOISE



COMPARISONS BETWEEN PREDICTED PEAK NOISE FREQUENCY AND DIRECTION OF RADIATION WITH MEASUREMENTS

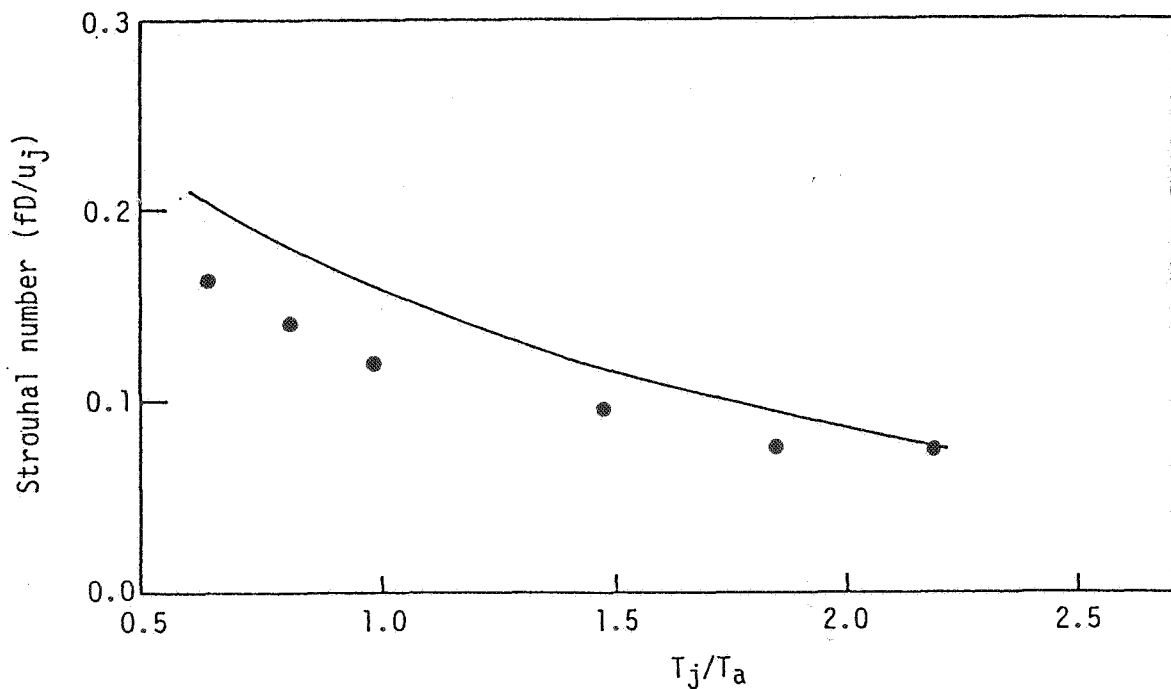
If indeed the dominant part of turbulent mixing noise is generated by Mach wave radiation associated with the instability waves then the dominant noise frequency of a perfectly expanded supersonic jet must be nearly equal to that of the most amplified instability waves. Further the direction of peak noise radiation must be equal to the Mach wave radiation angle of the most amplified instability wave. Extensive comparisons between the calculated (theoretical) and measured peak frequencies and directions of radiation for jets of different Mach number and total temperature have been carried out in ref. [5]. Good agreements are found (see figure below).



Comparison of the frequency and direction of Mach wave radiation of the most amplified instability wave of a Mach 2 jet at a total temperature of 855°F. Shown are contours of equal sound-pressure-level in the θ -frequency plane. ● theoretical value.

STROUHAL NUMBER OF MAXIMUM SPL OF HOT SUPERSONIC JETS

For slightly supersonic cold jets the instability waves would propagate downstream with subsonic velocity relative to the ambient speed of sound. In this case a direct wavy wall analogy would produce no sound. In order to determine the noise generated by the large scale subsonic instability waves their spatial growth and decay in the flow direction must be taken into account. It can be easily shown that with wave amplitude variation even a subsonic instability wave would have some supersonic wave components [4]. These components will radiate noise. However, the radiation efficiency is not high and decreases rapidly with a decrease in wave propagation speed. A comparison between the calculated frequency of the most amplified instability wave and that of peak noise radiation (see figure below) shows good agreement at high jet temperature or high jet velocity. The good agreement deteriorates as the jet temperature and velocity decrease (the wave speed becomes subsonic) consistent with the above reasoning.

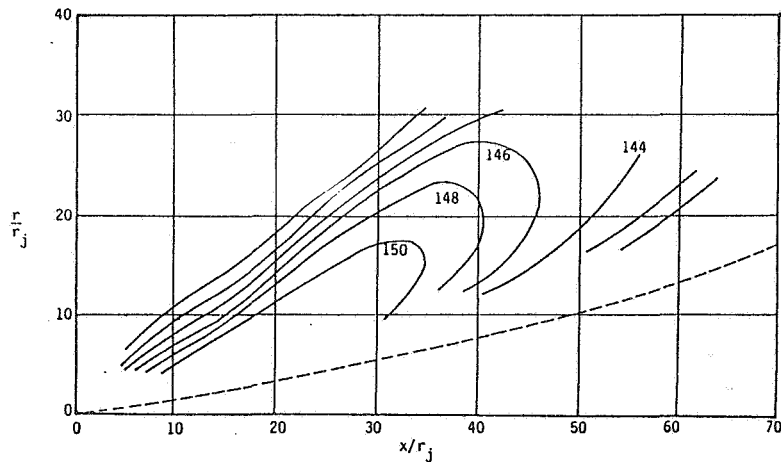
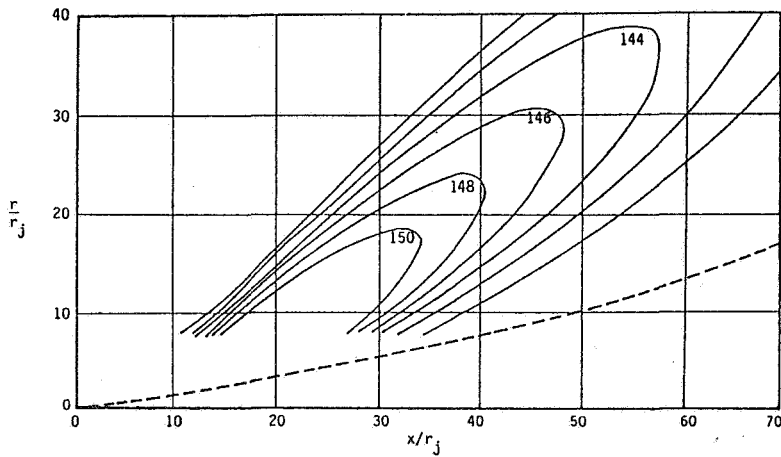


The Strouhal number at maximum sound-pressure-level of a Mach 1.7 jet as a function of jet to ambient temperature ratio.

— theory; ● experiment.

NEAR FIELD SOUND PRESSURE LEVEL CONTOURS

The instability wave theory for a single frequency wave is well established [4]. The theory can calculate the near field pressure contour (relative) distribution as well as the far field directivity at a given Strouhal number. A typical calculated near field pressure contour distribution is given below. It compares very favorably with measurements. A comprehensive turbulent mixing noise theory capable of predicting the entire noise spectrum is still unavailable at the present time.

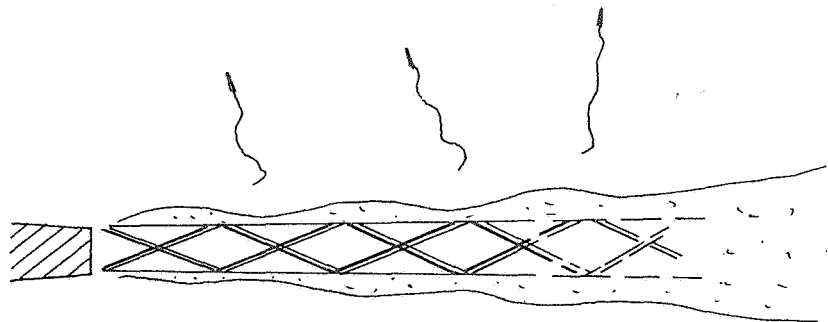


Near field sound-pressure-level contours ; $M_j = 2$, $St = 0.38$
Calculated (top) , measured (bottom)

GENERATION OF BROADBAND SHOCK ASSOCIATED NOISE

Broadband shock associated noise is generated by the weak interaction between the large turbulence structures/instability waves and the quasi-periodic shock cell structure as the former propagate through the latter. One simple way to see this is to consider a single instability wave. As this instability wave passes through the shock cells scattering takes place resulting in acoustic radiation. A very comprehensive stochastic model theory [6], [7] has been developed which can predict the spectra and directivities of this noise component. The theory can also predict the near field noise pattern as well. Recently the theory has been extended to include the effects of forward flight [8]. The predicted results compare very favorably with measurements.

BROADBAND SHOCK ASSOCIATED NOISE



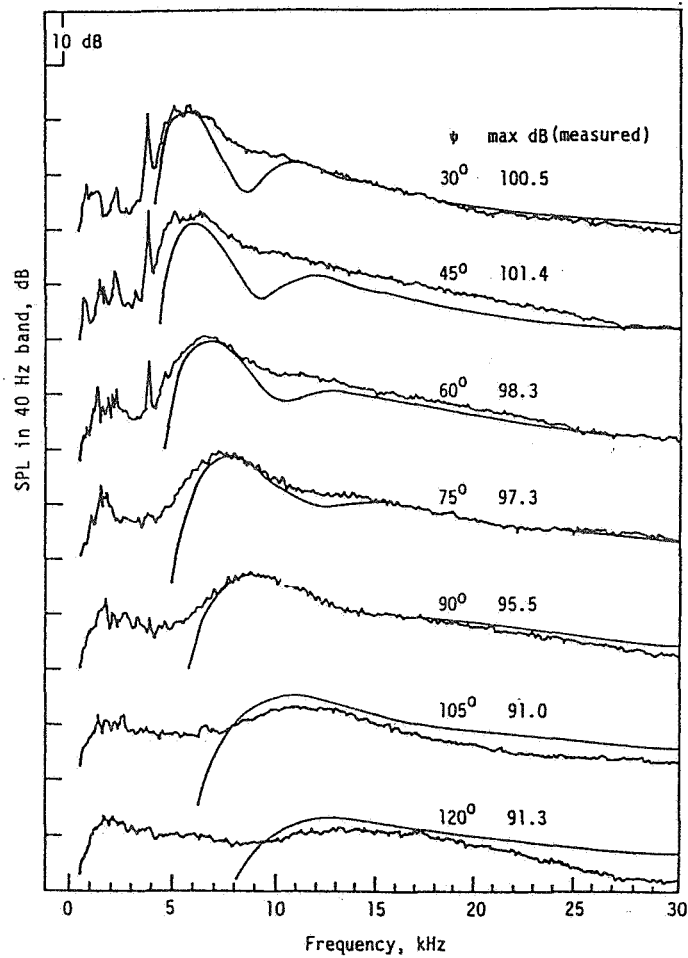
LARGE TURBULENCE
STRUCTURES/INSTABILITY WAVES

SHOCK CELL STRUCTURE

BROAD BAND
SHOCK NOISE

CALCULATED AND MEASURED FAR FIELD SHOCK NOISE SPECTRA

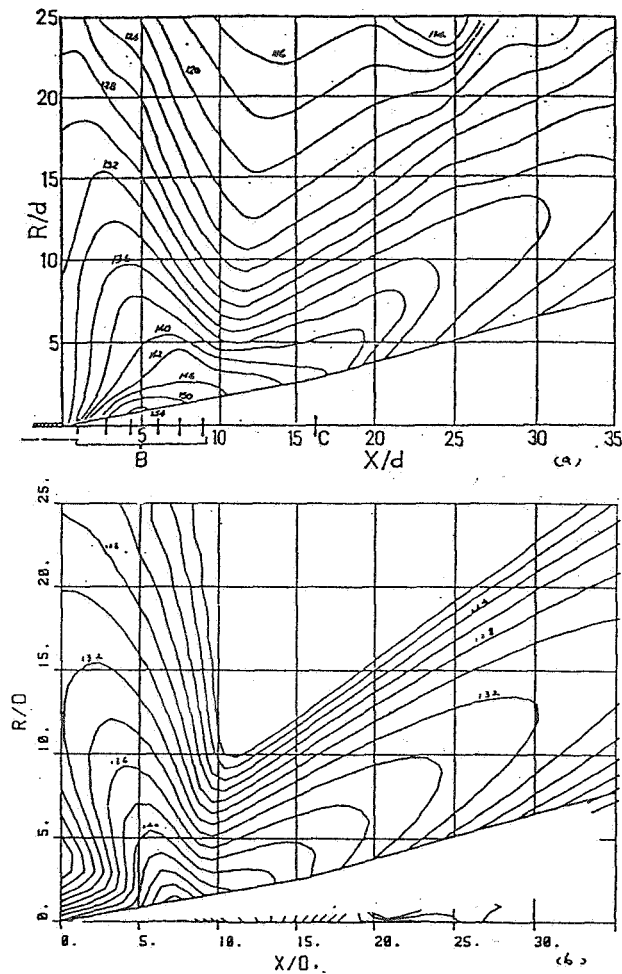
Extensive comparisons between theoretical and measured far field broadband shock associated noise have been carried out [7]. Below is a typical case. The peak frequency of broadband shock associated noise varies with the direction of radiation. The half-width of the spectral peak decreases in the forward direction. These features appear to be quite well predicted by the theory.



Far field noise spectra. $M_d=1.5$, $M_j=1.28$. \sim , measured
—, calculated

CALCULATED AND MEASURED NEAR FIELD SHOCK NOISE SPL CONTOURS

This is a comparison between the calculated and measured near field noise pressure contours on a plane passing through the jet axis according to the stochastic model theory [6] at a 1/3 octave band center frequency of 16 KHz. A 1.4 dB has been added to the calculated noise contour to give a better comparison with measurements. (The error is of the order of 1.4 dB). The broadband shock noise is represented by the lobe radiating to the left. The dominant direction of noise radiation and the location of the contours appear to be reasonably well predicted.



Near-field sound-pressure-level contours.

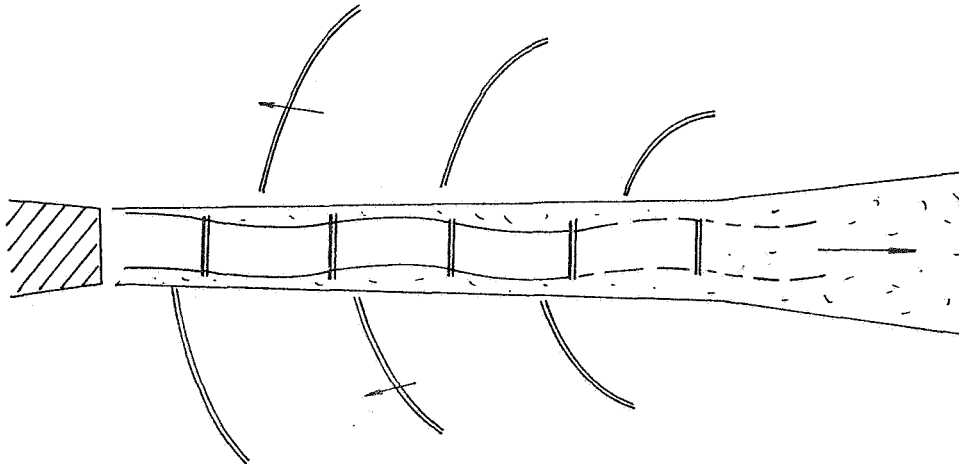
$M_j = 1.67$, $M_d = 1.5$ (a) Measured,

(b) Calculated + 1.4 dB. $f = 16$ KHz

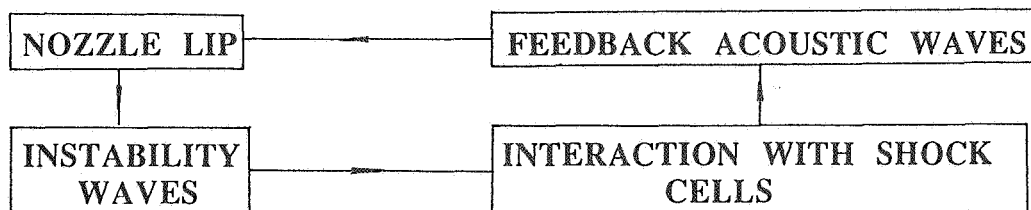
GENERATION OF SCREECH TONES

Screech tones are generated by a feedback loop [9], [10]. Near the nozzle lip the pressure and velocity fluctuations associated with acoustic disturbances outside the jet can excite the Kelvin-Helmholtz instability of the jet. The instability wave extracts energy from the mean flow and grows as it propagates downstream. At about four or five shock cells downstream the amplitude of the instability wave becomes sufficiently large to interact strongly with the shock cell structure. This interaction produces very strong acoustic radiation. A part of the acoustic waves created radiates upstream. Upon reaching the nozzle lip the acoustic waves excite the shear layer of the jet creating new instability waves. In this way the feedback loop is closed.

GENERATION MECHANISM OF SCREECH TONES

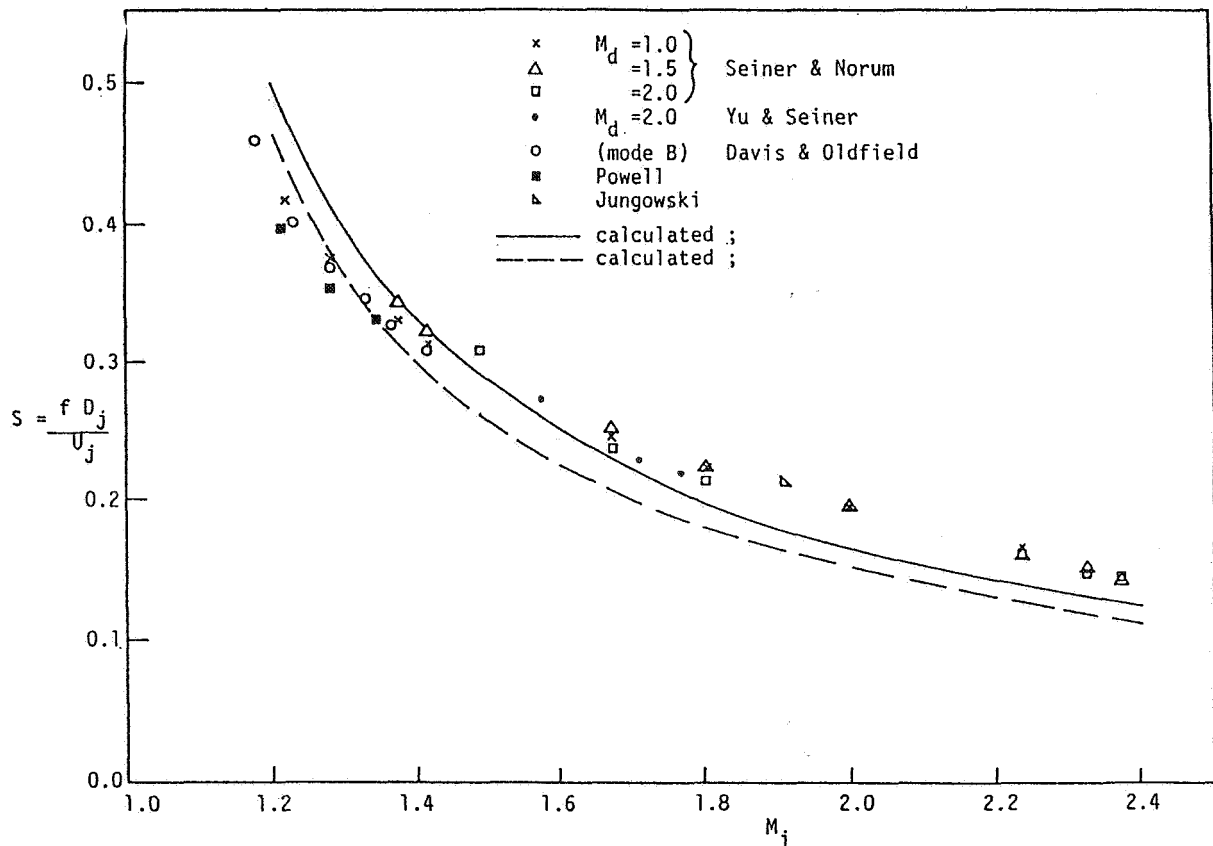


FEEDBACK LOOP



CALCULATED AND MEASURED STROUHAL NUMBER OF SCREECH TONES

By using the feedback loop model it is possible to calculate the Strouhal number of the fundamental screech tone. In this figure the solid curve represents the calculated frequency [10] as a function of jet Mach number. The dotted curve represents a simplified prediction using a simple empirical formula for the propagation speed of the instability wave. Screech tone amplitudes are very sensitive to the presence or absence of reflecting surfaces in the near environment. Sometimes it is difficult to reproduce the same screech amplitude even in the same experimental facility. Perhaps because of this variability there is no screech tone intensity prediction formula at the present time; even a totally empirical one.



The Strouhal number of fundamental stable screech tones versus fully expanded jet Mach number (cold jets).

SUMMARY AND FURUTE WORK

At the present time the generation mechanisms of the three principal noise components of supersonic jets, namely, the turbulent mixing noise, the broadband shock associated noise and the screech tones are quite well understood. A very comprehensive broadband shock associated noise prediction theory for round jets is now available. The theory can predict the far field noise spectra and directivity. A similar comprehensive turbulent mixing noise theory applicable to hot as well as cold jets is still needed. However, the noise directivity at a single frequency can be calculated within the framework of current theory. Work on developing a noise prediction theory for non-axisymmetric jets, such as jets from rectangular nozzles, is under way. A shock noise prediction scheme for non-axisymmetric jets may become available soon. The frequencies of screech tones can be predicted with reasonable accuracy. Because of its sensitivity to the surrounding environment, currently there is no theory capable of predicting the intensity of screech tones.

SUMMARY AND FUTURE WORK

- NOISE GENERATION MECHANISMS UNDERSTOOD
- GENERAL FRAMEWORK OF NOISE PREDICTION THEORY
AVAILABLE
- COMPREHENSIVE TURBULENT MIXING NOISE THEORY
(HOT JETS) NEEDED
- NON-AXISYMMERTRIC JET NOISE THEORY NEEDED
- SCREECH TONE (INTENSITY) THEORY NEEDED

REFERENCES

1. Tam, C.K.W.; Jackson, J.A.; and Seiner, J.M.: A Multiple-Scales Model of the Shock Cell Structure of Imperfectly Expanded Supersonic Jets. *J. Fluid Mech.*, Vol. 153, 1985, pp. 123-149.
2. Dash, S.M.; Wolf, D.E.; and Seiner, J.M.: Analysis of Turbulent Underexpanded Jets, Part I: Parabolized Navier-Stokes Model, SCIPVIS. *AIAA Journal*, Vol. 23, 1985, pp. 505-513.
3. Lepicovsky, J.; Ahuja, K.K.; Brown, W.H.; and Burrin, R.H.: Coherent Large-Scale Structures in High Reynolds Number Supersonic Jets. NASA CR-3952, 1985.
4. Tam, C.K.W.; and Burton, D.E.: Sound Generated by Instability Waves of Supersonic Flows. Part 2. Axisymmetric Jets. *J. Fluid Mech.*, Vol. 138, 1984, pp. 273-295.
5. Tam, C.K.W.; Chen, P.; and Seiner, J.M.: Relationship Between the Instability Waves and Noise of High-Speed Jets. AIAA paper 91-0492, 1991.
6. Tam, C.K.W.: Stochastic Model Theory of Broadband Shock Associated Noise from Supersonic Jets. *J. Sound and Vibration*, Vol. 116, 1987, pp. 265-302.
7. Tam, C.K.W.: Broadband Shock-Associated Noise of Moderately Imperfectly Expanded Supersonic Jets. *J. Sound and Vibration*, Vol. 140, 1990, pp. 55-71.
8. Tam, C.K.W.: Forward Flight Effects on Broadband Shock Associated Noise of Supersonic Jets. AIAA paper 89-1088. (to appear in *J. Sound and Vibration*.)
9. Powell, A.: On the Mechanism of Choked Jet Noise. *Proc. Phys. Soc.*, Vol. 66, 1953, pp. 1039-1056.
10. Tam, C.K.W.; Seiner, J.M.; and Yu, J.C.: Proposed Relationship Between Broadband Shock Associated Noise and Screech Tones. *J. Sound and Vibration*, Vol. 110, 1986, pp. 309-321.

Session V. Sonic Boon (Aerodynamic Performance)

THIS PAGE INTENTIONALLY BLANK

Session V. Sonic Boom (Aerodynamic Performance)

MIT
Complexity

Sonic Boom Program Overview and Sonic Boom Source Design/Prediction/Performance Overview
Dr. Christine M. Darden, NASA Langley Research Center



PRECEDING PAGE BLANK NOT FILMED

THIS PAGE INTENTIONALLY BLANK



Sonic Boom Program

Overview

Christine M. Darden

NASA Langley Research Center

Figure 1

Sonic Boom Research Plan

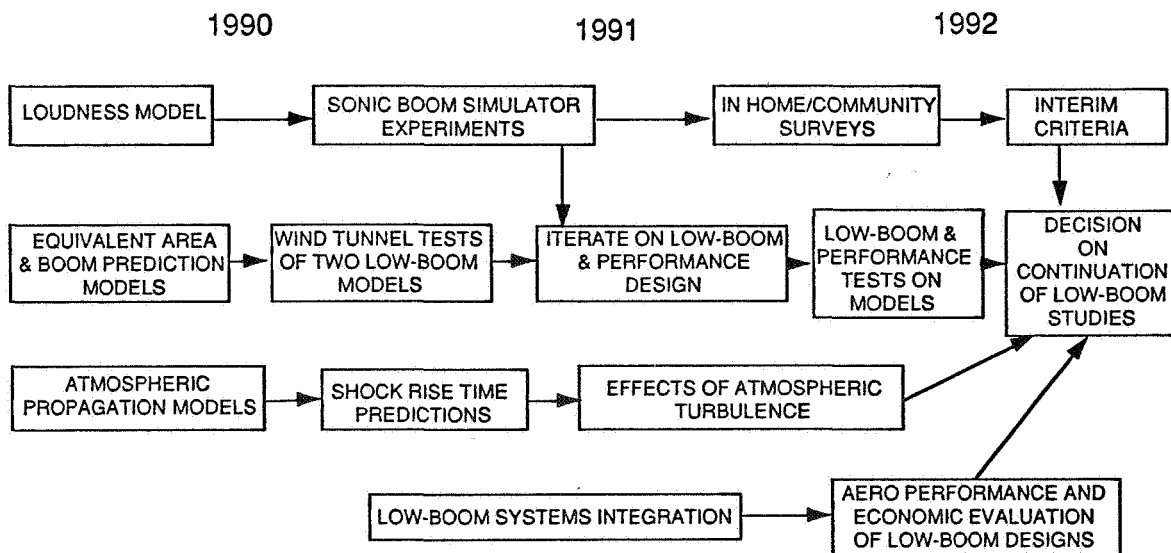


Figure 2

Sonic Boom Decision Criteria

- A low-boom configuration design comparable to an unconstrained design in terms of economic viability
 - system studies to determine trade-off between performance penalties and economic benefit of overland supersonic flight
- Low-boom design methodology validated by wind tunnel tests
 - configuration designs and models by LaRC, ARC, Boeing and DAC
- Estimate of acceptable sonic boom exposure
 - Dose-response relationship from laboratory and in-home studies
- Estimate of sonic boom levels from a low-boom configuration in a realistic atmosphere
 - Analytical modelling to include atmospheric turbulence

Figure 2

Sonic Boom Plan Beyond Decision

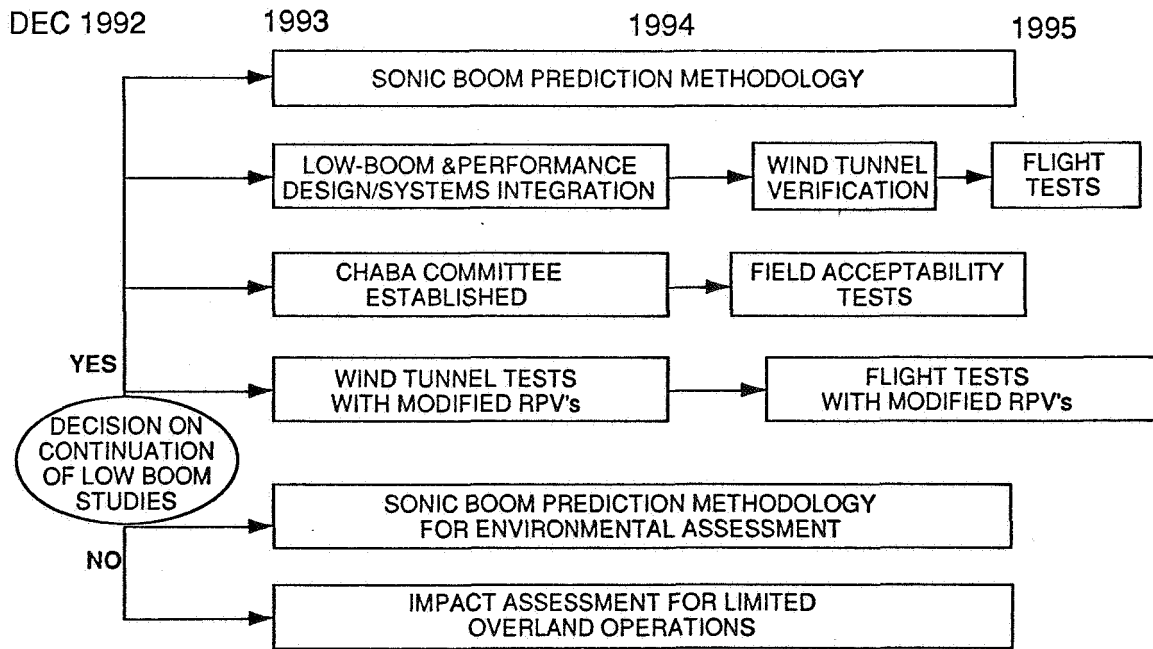


Figure 3

Sonic Boom Issues for Overwater Operations

- Supersonic operations near coastlines
 - during acceleration and deceleration (focused and secondary booms)
 - during cruise (primary boom carpet width, secondary booms)
 - requires prediction of boom levels and location, and audibility criteria
- Incidental overland supersonic operations or restricted corridors
 - environmental impact assessment
 - requires prediction of boom levels and location
 - estimated community reaction, damage probability, etc.

Figure 4

THIS PAGE INTENTIONALLY BLANK

Sonic Boom Source Design / Prediction / Performance

Overview

Christine M. Darden
NASA Langley Research Center

Figure 1

Program Elements

Configuration Design
Sonic Boom Analysis - Modified Linear Theory
Performance Analysis
Wind Tunnel Evaluation
Sonic Boom Analysis - Higher Order Methods

Figure 2

Program Participants

NASA LANGLEY

Vehicle Integration Branch

Computational Aerodynamics Branch

NASA AMES

Advanced Aerodynamics Concepts Branch

Applied Computational Fluids Branch

BOEING COMMERCIAL AIRPLANES

DOUGLAS AIRPLANE COMPANY

GRUMMAN CORPORATION

EAGLE ENGINEERING

Figure 3

Session V. Sonic Boom (Aerodynamic Performance)

Design and Analysis of Low Boom Concepts at Langley Research Center

Dr. Christine M. Darden, Robert J. Mack, Kathy E. Needleman, Daniel G. Baize, Peter G. Coen, Raymond L. Barger, N. Duane Melson, Mary S. Adams, Elwood W. Shields and Marvin E. McGraw, Jr., NASA Langley Research Center

THIS PAGE INTENTIONALLY BLANK

Design and Analysis of Low Boom Concepts at Langley Research Center

58-71
11998

By

Christine M. Darden, Robert J. Mack, Kathy E. Needleman, Daniel G. Baize, Peter
G. Coen, Raymond L. Barger, N. Duane Melson, Mary S. Adams, Elwood W.
Shields, and Marvin E. McGraw

Presented at the
First Annual High-Speed Research Workshop
May 14-16, 1991
Williamsburg, VA

Outline of Presentation

The objective of the sonic boom research in the current High Speed Research Program is to ultimately make possible overland supersonic flight by a high speed civil transport. To accomplish this objective, it is felt that results in four areas must demonstrate that such a vehicle would be acceptable by the general public, by the airframers, and by the airlines. It should be demonstrated: (1) that some waveform shape has the possibility of being acceptable by the general public; (2) that the atmosphere would not totally destroy such a waveform during propagation; (3) that a viable airplane could be built which produces such a waveform; and (4) that any performance penalty suffered by a low boom aircraft would be counteracted by the economic benefit of overland supersonic flight.

This paper addresses the work being done at Langley Research Center in support of the third element listed above --the area of configuration design. The initial part of the paper will give a review of the theory being used for configuration designs and discuss two theory validation models which were built and tested within the past two years. Discussion of the wind tunnel and theoretical results (linear theory and higher order methods) and their implications for future designs will be included.

DESIGN PROCEDURE

THEORY VALIDATION DESIGNS

WIND TUNNEL TESTS

FUTURE DESIGNS

L/D ESTIMATES

PLUME EFFECTS

SIGNATURES ON FLIGHT PROFILE

Figure 1

Design Approach for Low Boom Aircraft Concept

Two design approaches, both based on the Seebass and George^{1,2} sonic boom minimization theory, are being used in the design of low boom concepts at Langley. The first approach is illustrated in Figure 1. The design parameters of aircraft weight, length, Mach number and flight altitude, along with signature parameters which define the type of signature and the bluntness parameter of the signature are used to define a target equivalent area distribution and pressure signature as shown in the upper right corner of the figure. Working initially with an uncambered wing, the designer describes a planform and fuselage shape and iterates on this design until the Mach-sliced equivalent area is near but everywhere below the desired equivalent area. When the equivalent area for the planform and flat plate lift are judged "near enough" to the target, a camber surface is designed to increase the lift of the configuration. Again, the equivalent areas of the design are continually compared to the target equivalent area distribution until the differences in the areas are very slight. Final adjustments to the design are made in the fuselage by use of an Inverse Fuselage Design Procedure which prescribes the fuselage necessary for a given equivalent area distribution.³ More information on this design procedure can be found in reference 4.

Once the sonic boom constraints have been met, the configuration is then analyzed for performance. If it is judged to have serious performance deficiencies, then changes must be made because of aerodynamic concerns and the configuration recycled through the sonic boom design phase.

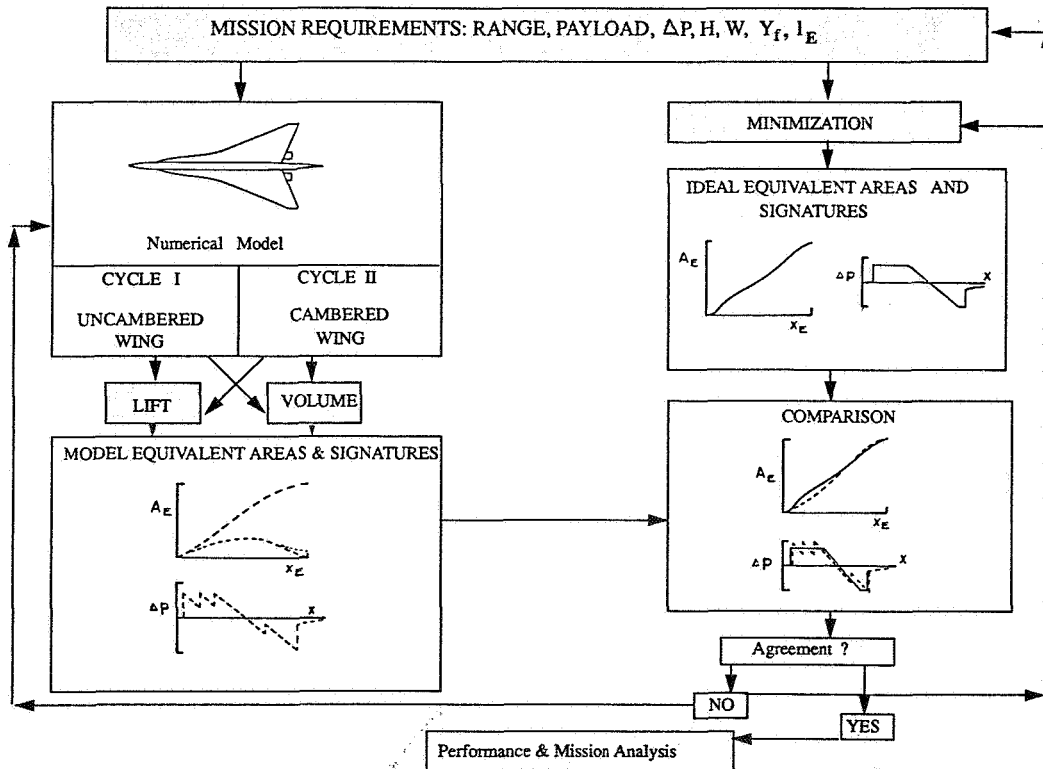


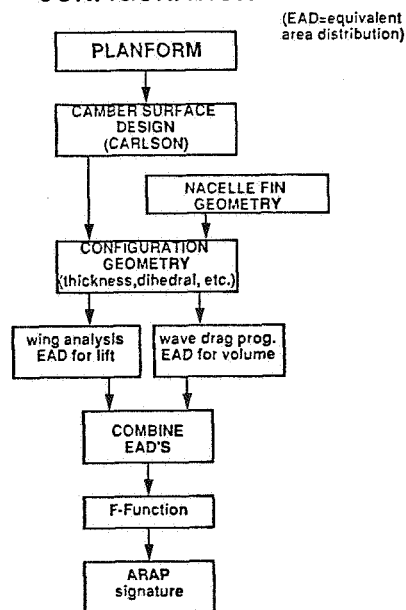
Figure 2

DESIGN APPROACH FOR BLENDED WING-BODY CONFIGURATION

A second approach for designing a blended wing-body configuration with low boom constraints is shown below. In this approach, the designer initially defines the planform of the desired wing-body and the geometry for the nacelles and fin. The camber surface is designed using the procedure of reference 5, and the thickness, twist and dihedral schedules are added. The configuration is then evaluated to determine its equivalent area distribution and its sonic boom signature is calculated using the method of reference 6.

Redesign for low boom is accomplished by a comparison between the F-function of the configuration and the target F-function. The target F-function may be derived from the method of references 1 and 2, or a related method. When the desired F-function and resulting signature have been attained, the necessary equivalent area distribution is defined. The equivalent area due to lift, pods, and fins of the original configuration is subtracted from the target equivalent area distribution so that the only area remaining is the equivalent area due to the wing-body. Final modifications to the design are made with thickness adjustments to the wing body using an inverse design procedure.⁷ All of the codes in the above approach have been automated with input and output files consistent with one another. Judgement and interface with the designer is necessary at each step of the design and analysis process.

INITIAL-CUT DESIGN AND SONIC BOOM ANALYSIS FOR BLENDED WING-BODY CONFIGURATION



REDESIGN FOR LOW-BOOM

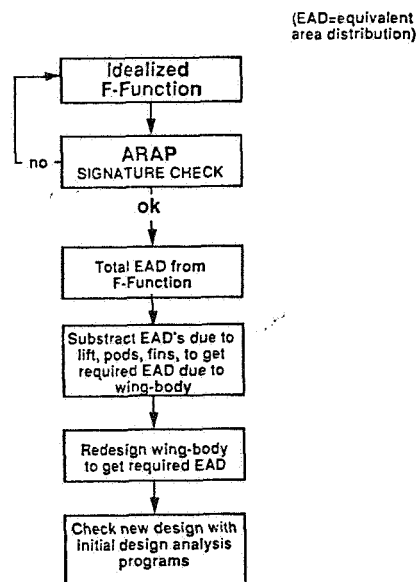


Figure 3

Sonic Boom Wind Tunnel Models

Two wind tunnel models were designed using the first approach shown in this paper⁸. To insure proper definition of the camber and twist distribution of the configuration, these models were designed to be 12 inches in length--the largest sonic boom models ever built at the Langley Research Center. Design conditions for the models are shown in the insets. One configuration was designed to cruise at Mach 2 at an altitude of 55,000 feet. The assumed weight at beginning cruise was 550,000 lbs and the full scale length was 323 feet. As shown, this configuration was designed to give a flat-top signature at design cruise conditions, with a bow shock overpressure of slightly less than 1 psf. The second model was designed for cruise at Mach 3 and an altitude of 65,000 feet. The beginning cruise weight was assumed to be 600,000 lbs and the full scale length, 313 feet. This concept was designed to give the minimum shock, or "ramp" signature at cruise conditions--again with a bow shock of slightly less than 1 psf. The models were fabricated in two pieces with an integrated sting. They both featured twist and camber and had four axisymmetric flow-through nacelles and a vertical fin.

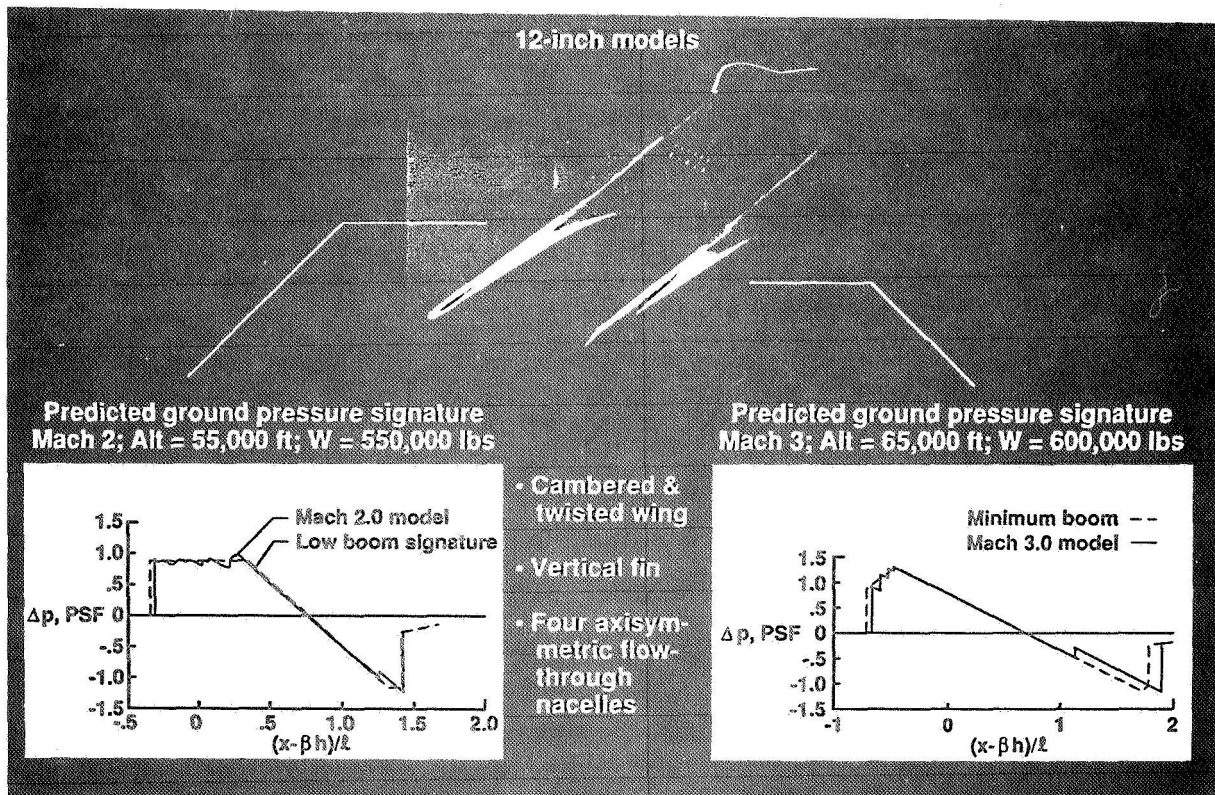


Figure 4

Wind Tunnel Tests

Existing sonic boom extrapolation methods are based on the assumption that disturbances are axisymmetric and thus 3-dimensional effects would be ignored. Because of this limitation, previous sonic boom wind tunnel signatures were measured at 3-5 body lengths away to insure that all three dimensional effects had settled. For the Langley Unitary supersonic wind tunnel which is 4X4 feet in cross section, the needed measuring distance has restricted the model size to 4 or 5 inches in length. Because an accurate representation of camber, twist and thicknesses of the current low boom configurations was felt to be essential to the validation of the theory, the decision was made to build the current wind tunnel models at 12 inches--more than twice the size of any previous sonic boom model at Langley. This size helped to alleviate the problem of fabricating an accurate representation of the concept, but aggravated the problem of accurate extrapolation. At Mach 2, measurements in the Langley tunnel would be at most 2 body lengths away with possible 3 dimensional changes still occurring. While CFD or other nonlinear 3-dimensional extrapolation methods are being developed and validated, the need to also obtain signatures at 5-6 body lengths was very important. Thus arrangements were made with the NASA Ames Research Center to test the low boom configurations in their 9 X 7' and 8 X 7' supersonic wind tunnels. These measurements would insure proper extrapolation with the larger, more accurate model. Tests on the low boom models were held at Ames in October 1990, and at Langley in December 1990 and January, 1991.

NASA AMES 9X7 UNITARY-- October, 1990

Mach 1.68, 2.00, 2.50

NASA LANGLEY 4X4 UNITARY

Test Section I-- December, 1990

Mach 2.5, 2.96

Test Section II - January, 1991

Mach 2.0, 2.5

Figure 5

Sonic Boom Test Setup

Test setup for the Mach 3 low-boom concept in test section 2 of the Langley Unitary Plan Wind Tunnel is shown in this figure. The model and a specially made angle-of-attack mechanism are mounted to the permanent tunnel strut system using a specially made sting. The model was capable of 33 inches of linear travel because of the strut mechanism, and up to 180 degrees of roll because of an additionally installed roll coupling. The model was tested at a roll angle of 90 degrees. The model and its support mechanism were also capable of lateral movement because of the permanent strut system. Measuring probes were mounted to a solid tunnel door which had replaced the usual windowed door for the sonic boom tests. The reference probe was mounted such that it was not within the disturbance field of the model at any of its anticipated locations within the tunnel. The measuring probe was located such that it would be within the field of the complete signature of the model as the model moved forward. The measuring probe was mounted to a motorized track which allowed 6 inches of linear movement and thus increased the flexibility of the body lengths at which signatures could be taken without shutting down the tunnel and manually moving the probe.

Langley Unitary Plan Wind Tunnel
Test Section 2

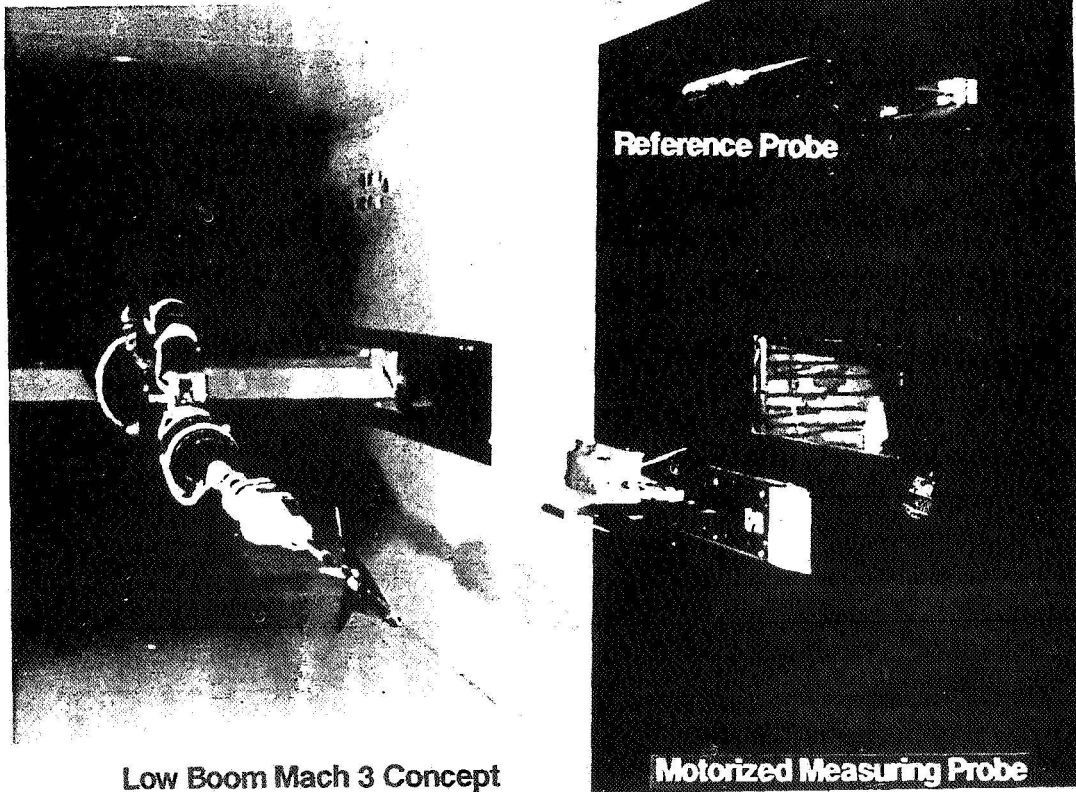
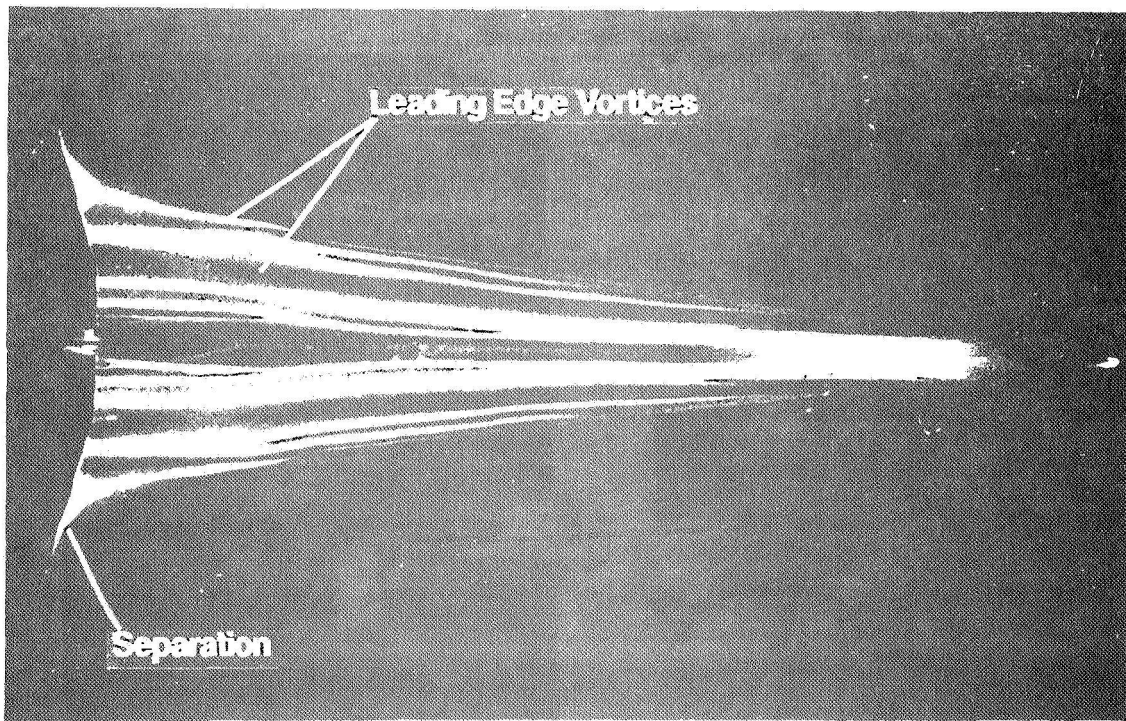


Figure 6

Oil Flow Photograph

Flow visualizations taken during the sonic boom tests included this oil flow photograph of the Mach 3 concept. Oil mixed with fluorescent dye is painted on the model and the model installed in the tunnel. When design test conditions are achieved, a vapor light is focussed on the model. Flow patterns on the surface of the model can be observed by the oil patterns which develop. For this model, at a test Mach number of 2.96 and an angle of attack of 1.96 degrees, one can see that the surface flow pattern is very complex. One would like to see very clean attached flow which is indicated by smooth patterns in a linear direction from front to back with very little puddling of the oil. Instead, there are patterns of slanted flow moving in a defined region from front to back which indicates a leading edge vortices on the surface. The puddling of the oil near the trailing edge also indicates that some separation is occurring.

Low Boom Model
Design Mach Number = 3



Mach 2.96

Angle of Attack = 1.96°

Figure 7

Wind Tunnel Results

Initial wind tunnel data indicated two unexpected results. Midway along the positive portion of the signature a large shock occurred in an area where the signature was expected to be relatively flat. Toward the end of the signature a second shock occurred before the complete resolution of the tail shock. Upon further investigation, it was decided that the final shock was the result of interference from the angle-of-attack mechanism which caused a stronger shock than anticipated. It was not clear where the first unexpected shock was originating until the nacelles were removed to provide signatures for the validation of Euler code computational calculations. The disappearance of the shock for the configuration without nacelles indicated immediately that flow was not being achieved in the small (.2 inch diameter) flow-through nacelles, and that there was a standing shock in front of the nacelles. Attempts to open the nacelles more and sharpen the front edges to try and achieve flow did not alleviate this shock. All tests at NASA Ames were done with nacelles on. The nacelles were only removed during the tests at Langley.

MACH 3 LOW BOOM CONFIGURATION
 Radial distance = 8 inches
 N = 3.1 lbs. P_{INF} = 147.3 psf

NASA Langley Unitary Wind Tunnel
 Test Section 2
 Mach number = 2.96

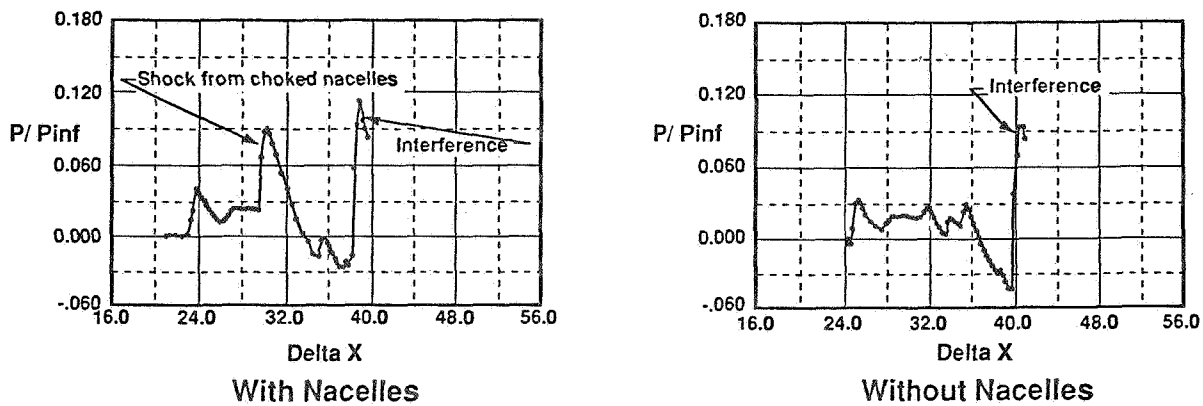


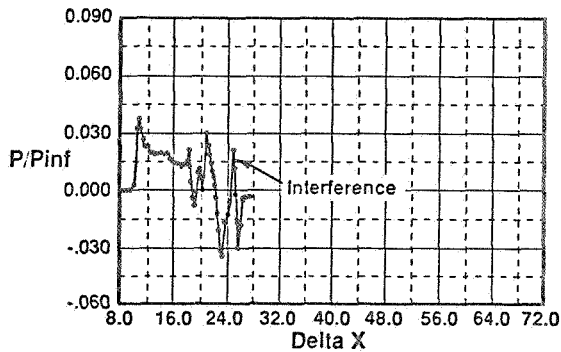
Figure 8

Wind Tunnel Results

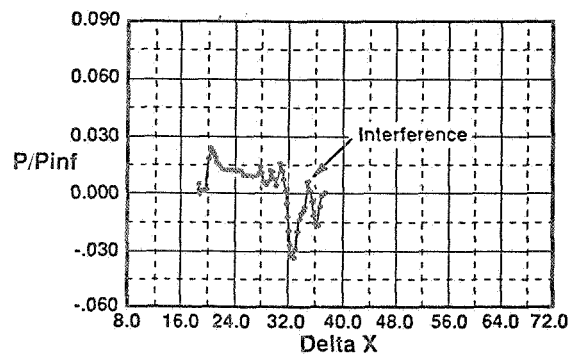
Pressure measurements at two radial distances for the Mach 2 configuration are shown in figure 9. Signatures at several distances are desirable for two reasons. With the current emphasis on sonic boom predictions using Computational Fluid Dynamics (CFD) methods, signatures at several distances are needed to validate those codes in regions where grid density and/or grid spreading could reduce accuracy. Signatures at several radial distances are also desired to observe the manner in which the signature changes as it propagates outward. The signatures shown were measured at 6 inches and 12 inches or at 1/2 and one body lengths. Attenuation of the pressure levels at the forward part of the signature are very evident as the signature propagates outward. There is damping of the compressions and expansions which occur just ahead of the major expansion, but the most negative portion of the major expansion does not attenuate. The largest changes in the character of the signature seem to be occurring in the region of the signature where 3-dimensional effects of the lifting surface would occur.

MACH 2 LOW BOOM CONFIGURATION
Without Nacelles
N = 5.1 lbs. P_{INF} = 160.2 psf

NASA Langley Unitary Wind Tunnel
Test Section 1
Mach number = 2.0



Radial Distance = 6 inches



Radial Distance = 12 inches

Figure 9

Comparison of Measured and Extrapolated Wind Tunnel Data

To investigate the accuracy of extrapolating very near-field pressure signatures, the signature measured at 1/2 body length was extrapolated⁹ to one body length and compared with the signature as measured at one body length. The results of the comparison are shown on this figure. Note that in the forward portions of the signature where volume is the major portion of the equivalent area the agreement between the measured and extrapolated data is excellent. The latter half of the signatures differ significantly, however. For the first two shocks and expansions, the extrapolated signature is less than that measured; the slopes of the expansion regions differ considerably and the measured signature has the larger expansion. These differences would indicate that an axisymmetric propagation method does not account for all of the flow field phenomena; i.e. the flow in that region is highly three-dimensional. Signatures at greater distances are needed to ascertain just how far radially one must be before there are no 3-dimensional effects.

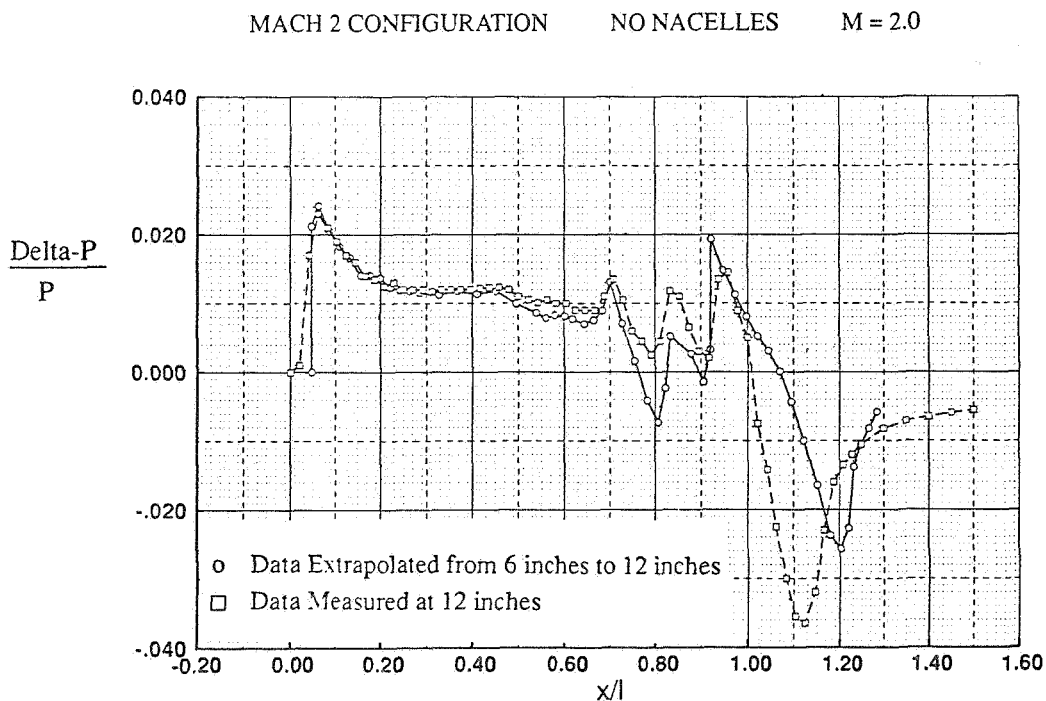


Figure 10

Comparison of Ground Signatures

An example of the differences in the ground signatures when wind tunnel data is extrapolated from two different distances is seen in figure 11. The signature on the left was extrapolated from data taken at 1/2 body length and the data on the right was extrapolated from data taken at one body length. For this Mach 2 configuration which was designed to prevent shock coalescence, the bow shock levels of the ground signatures are nearly the same. The most significant differences in the two signatures are just before the expansion where three-dimension effects are strongest in the near-field signature, and the length of the signature. Since current indications are that loudness is a better indication of sonic boom disturbance than bow shock level¹⁰, these differences in the latter portion of the signatures could lead to significant differences in their loudness.

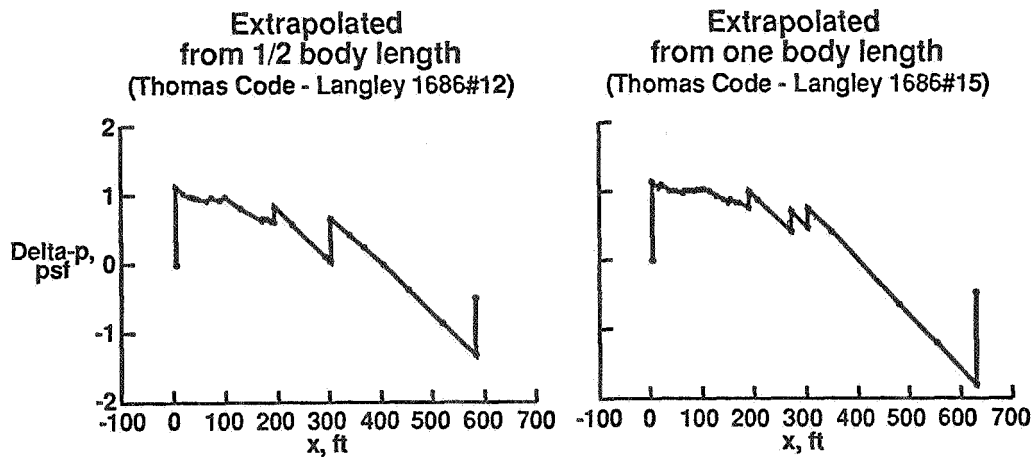


Figure 11

Flow Field Cross Sections

Perhaps an explanation of the flow field phenomena around the shaped, low-boom configurations can be explained with figure 12, which shows a flow field cross section for a low boom configuration at three axial locations as predicted by an Euler computational method¹¹. Note that at mid aircraft, the flow field is relatively clean, with only the bow shock being prominent. At the aft end of the aircraft, very strong shocks emanating from the region of the wing are evident. As one moves further downstream, the flow field immediately beneath the configuration is still very clean, but the strong shocks generated by the wing are moving toward the flight path. It is probably the strong effect of the wing that is being seen in the wind tunnel data just ahead of the expansion region. These results would indicate that for low boom configurations where the primary effort has been to reduce disturbances in the flight path, the non-zero azimuth angles can not be ignored either for ground level signatures or for the influences they have on the flight path signatures.

Low Boom Configurations

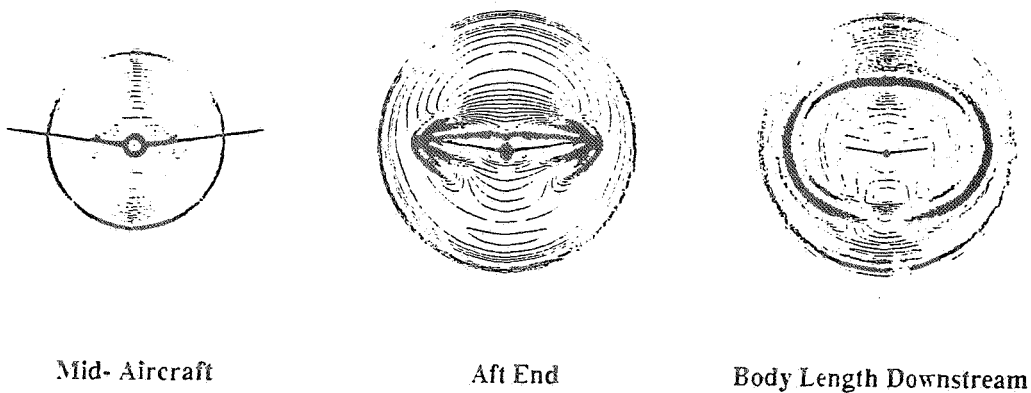


Figure 12

Comparison of Extrapolated Wind Tunnel Data and Target Signature

A comparison of extrapolated wind tunnel data taken at one body length from the Mach 3 configuration with test conditions of Mach 2.96 and normal force 3.06 lbs is compared with the target signature for the same flight conditions. As can be observed, the objective was to obtain a bow shock of 0.94 psf followed by an isentropic increase in pressure to 1.45 psf. The extrapolated data does not show this behavior. The bow shock level is 1.8 psf and a second shock increases the pressure to 1.95 psf. There could be several reasons for the discrepancy in the expected signature and the actual signature: (1) linear theory methods used in the design of the configuration become less valid at Mach numbers as high as 2.96¹²; (2) the isentropic rise in pressure is less stable and is therefore more difficult to maintain during propagation; (3) boundary effects which cannot be properly scaled on these 12-inch models may have an effect on the wind tunnel results.

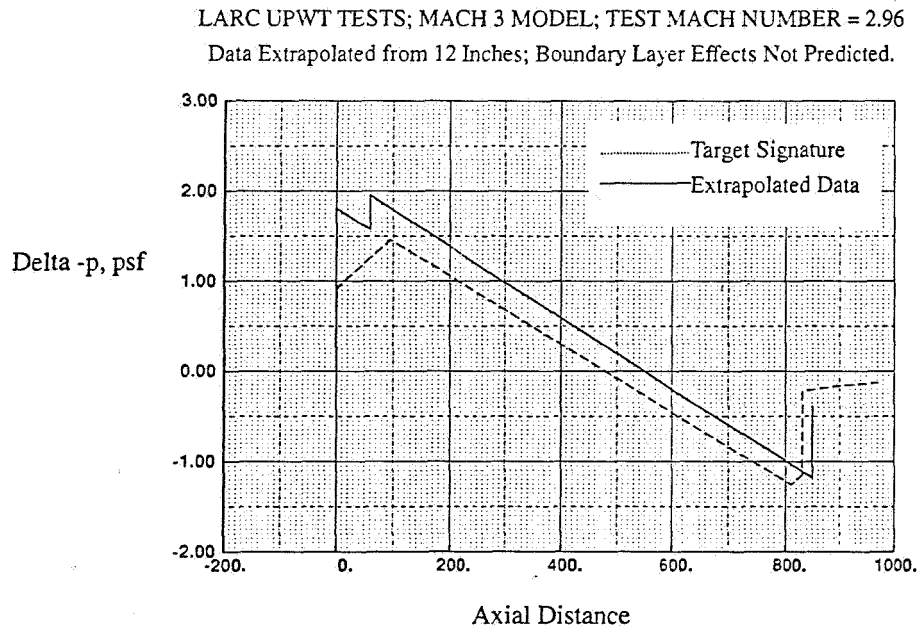


Figure 13

Comparison of Extrapolated Wind Tunnel Data and Target Signature

A comparison of the extrapolated wind tunnel data and the target signature for the Mach 2 configuration is seen in figure 14. Also shown on the signature is the signature predicted from the geometry using linear theory methods. Test conditions were Mach 2 and normal force 5.1 lbs. As can be seen, the agreement between the forward part of the extrapolated wind tunnel signature and the target signature is excellent. The largest discrepancies are in the region near the expansion where uncertainty about 3-dimensional effects still exist and in the overall length of the signatures. If significant changes do not occur in wind tunnel results taken at 3 to 4 body lengths, then these results appear to validate the minimization theory for these twisted and cambered configurations at Mach 2.

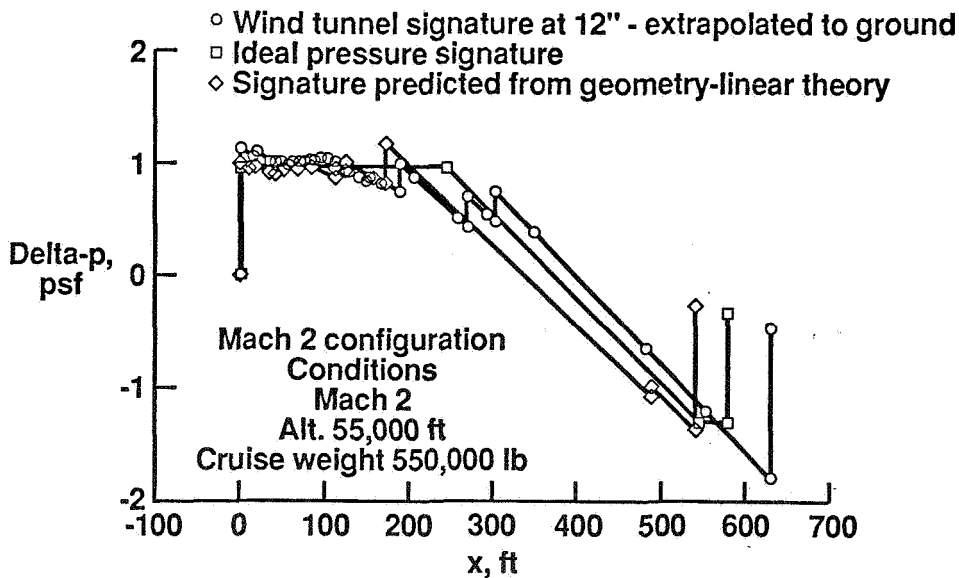


Figure 14

Theoretical Bow Shock Overpressures

Several factors have contributed to the decision for the range of Mach numbers to be considered in the next cycle of low boom designs. Included among those factors are: (1) initial indications that ozone considerations may lead to cruise altitudes of around 45,000 feet; (2) the wind tunnel results which indicated that the linear theory design methods may be invalid at higher Mach numbers; and (3) the decision in the High Speed Research (HSR) program that future designs would center around Mach 2.4. An additional factor is shown on figure 15. Shown on this figure are two carpet plots which include results of the minimization code for a minimum shock type signature. The plot on the left shows for the condition Mach 1.6, the equivalent length necessary for a given bow shock overpressure at a given altitude. This figure shows that to achieve the lowest bow shock level at the shortest length, one would cruise at the lowest altitude. An increase in altitude increases the length necessary. The second carpet plot shows that for an altitude of 44,000 feet one would cruise at the lowest Mach number to achieve the lowest bow shock level at the lowest length. Using as guidance information from this plot as well as guidance from the other factors, the choice was made to choose Mach number between 1.6 and 2 for the second cycle of low boom designs in which the emphasis will be placed on integrating performance.

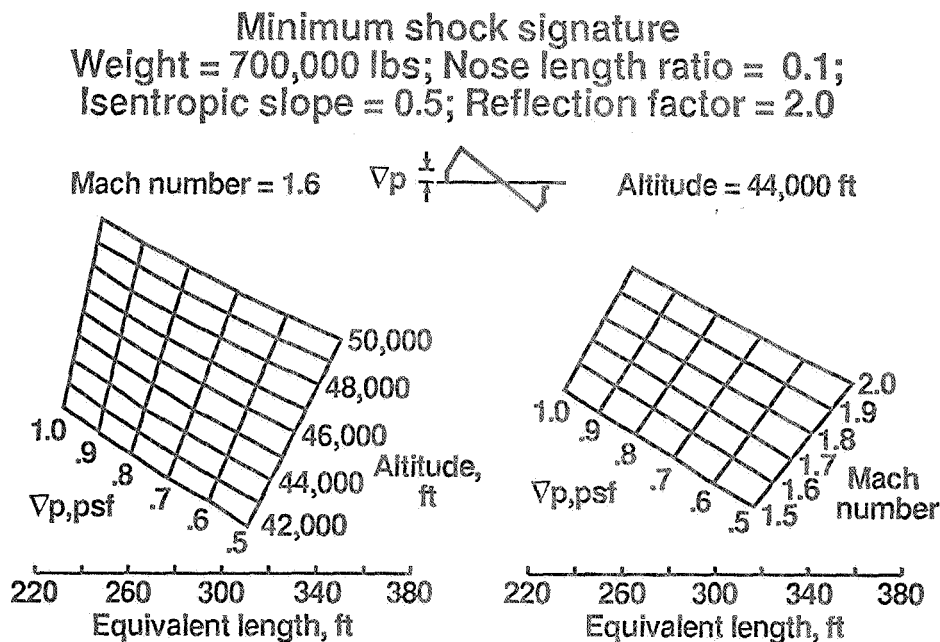


Figure 15

Sonic Boom Design Efforts

Target conditions and a preliminary planform chosen as Mach 1.6 low boom design are shown on figure 16. The target signature shown is one conceived at Boeing Airplane Company as one method of improving the stability problems of the minimum shock signature but still maintaining some of the weight advantage allowed by that signature. Target design flight conditions include Mach 1.6, 45,000 ft altitude, a beginning cruise weight of 650,000 lbs and an overall length of 323 lbs. The theoretical equivalent area distribution and its resulting pressure signature with a bow shock of approximately 0.85 psf are shown. Signature conditions listed are input parameters which define some of the variable parameters in the minimization code. The configuration planform shown is still in its developmental stage.

Second Generation

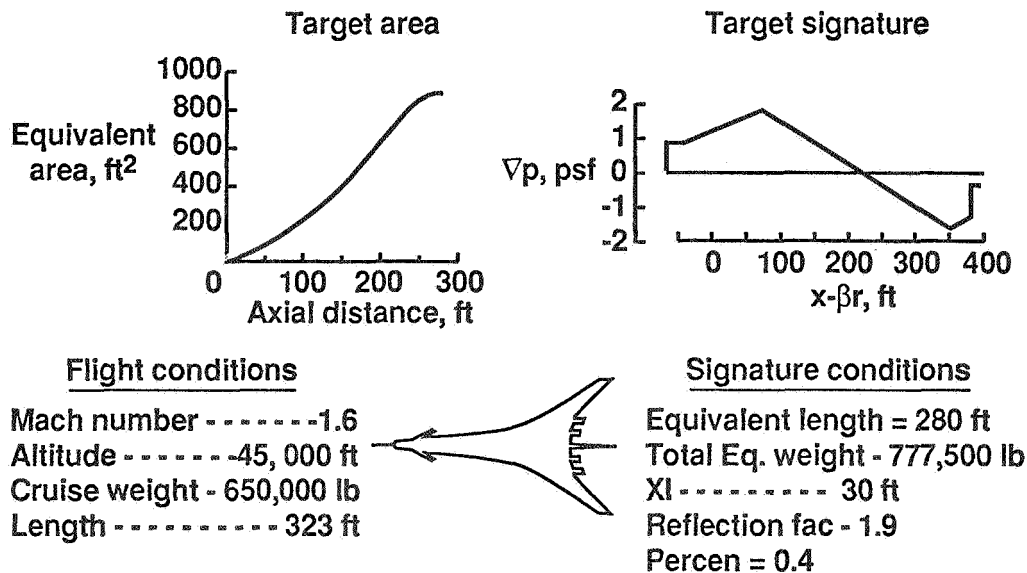


Figure 16

Performance Comparisons

The ultimate goal of the configuration minimization portion of the sonic boom program, is to develop a low-boom configuration which would be competitive with a baseline configuration which has no low boom constraints but which would have to cruise subsonically overland. Shown in figure 17 is an L/D comparison of a baseline Mach 2 concept with no low-boom constraints, but which has been optimized aerodynamically and three low boom configurations. The Low Boom I concept was designed as a theory validation model and very little effort was placed on the performance. Low Boom II represents an intermediate design effort which was subsequently dropped because of performance estimates and Low Boom III is the current 1.6 design being worked. This figure does not separate Mach numbers effects from these results but does give an indication of improved performance for the low boom designs. Also these results are for a trimmed aerodynamic concept but for untrimmed low boom configurations. L/D estimates for Low Boom I are quite poor when compared to the Aerodynamic baseline. Design efforts on the Low Boom II concept improved the subsonic characteristics significantly but the supersonic performance estimates were still quite low. Very preliminary estimates of L/D for the current Mach 1.6 design show significant L/D improvements--subsonically better than the baseline and nearly equal to the baseline at its design Mach number of 1.6. Recall that the results for the Mach 1.6 design are very preliminary and are subject to change. They are shown only to indicate that with effort toward systems integration, the performance of the low boom designs should improve.

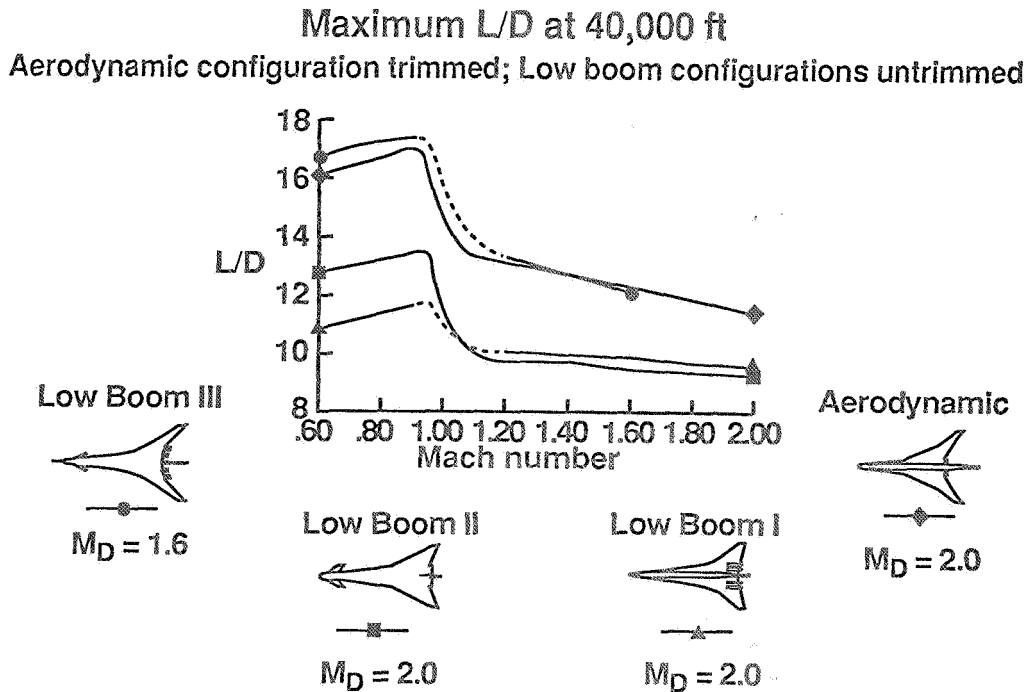


Figure 17

Effect of Engine Plume on Sonic Boom Signatures

Concern has been expressed about the effect of the engine plume on the sonic boom signature of shaped configurations. To get an estimate of its effects, an Euler code was used to calculate the plume of the low boom Mach 3 concept based on the pressure ratios defined for the in-house Mach 3 engine¹³. In normal sonic boom calculations, the plume is approximated by a cylindrical extension. Shown on figure 18 are comparisons of the sonic boom signature for the Mach 3 configuration cruising at Mach 3 at 60,000 ft initially with the cylindrical plume and beside it with the calculated plume. It can be seen that for the nozzle defined, the plume at 60,000 feet completely obscures any benefit of shaping. The pressure signature for the same Mach 3 configuration cruising at Mach 2 and 55,000 feet is shown on the second line. Although some effect of the plume is still evident, it is much less than the effect at 60,000 feet. Initially these results were used to conclude that the effect at Mach 1.6 and 45,000 feet would be not be noticeable. It was found however, that a different engine was necessary for those conditions and when actual calculations were made, the effect of the plume at 45,000 feet was comparable to that shown at 55,000 feet. Clearly plume effects cannot be ignored during the design process.

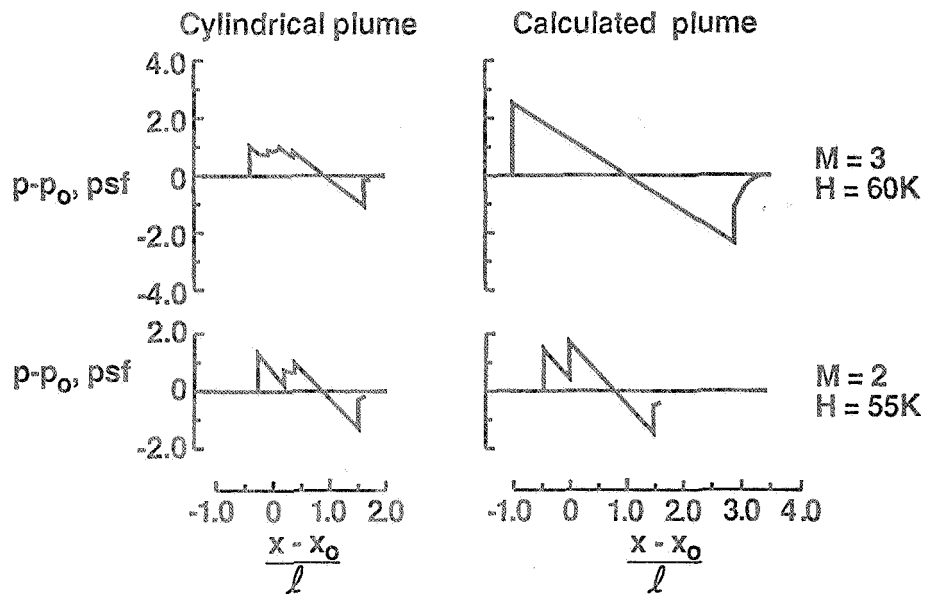


Figure 18

Sonic Boom Contours as a Function of Mach Number and Altitude

The sonic boom prediction method using modified linearized theory methods has been automated and integrated into an in-house performance code¹⁴. Results of sonic booms at various altitudes for the Low Boom I configuration are shown as contours on figure 19. These boom levels were calculated for steady state conditions but it was found that acceleration and climb rates typical for a transport configuration did not significantly change the results. Climb profiles for optimum performance and with boom constraints are shown on this figure.

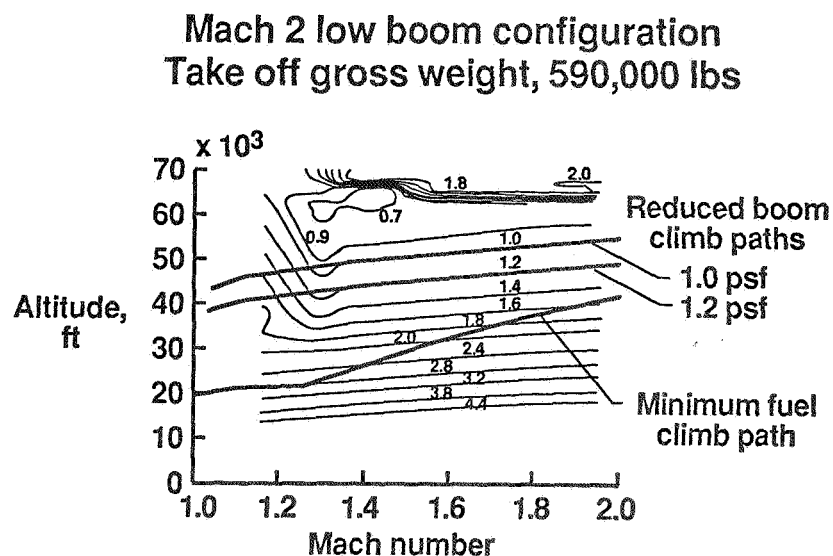


Figure 19

Ground Pressure Signatures for Optimum Performance Flight Profile

Shown in figure 20 are the ground level signatures for the low boom Mach 2 configuration as it climbed to cruise along the optimum performance flight path. All signatures are plotted to the same scale for comparison. Note that during the cruise portion of the flight the signature achieves its flat top shape as predicted, but during climb, bow shock levels as high as 2.8 psf are generated.

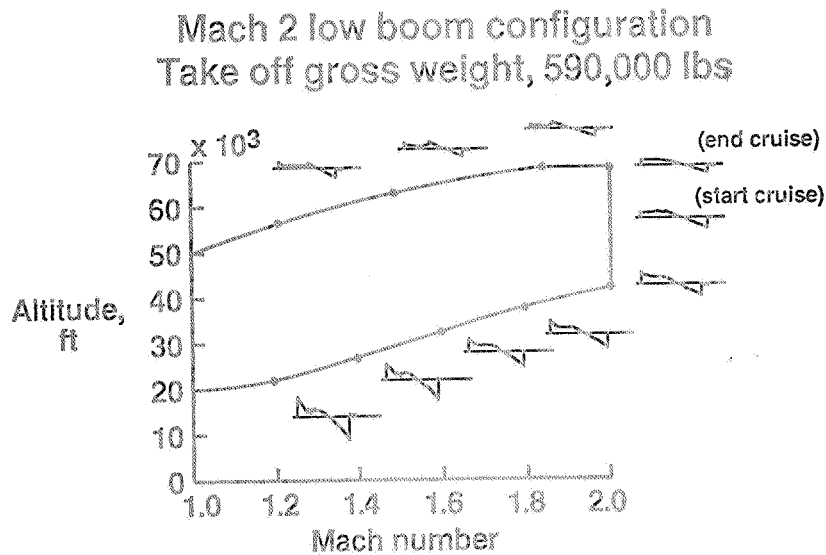


Figure 20

Ground Sonic Boom Signatures for Restricted Flight Profiles

Shown in figure 21 is the flight path necessary and sonic boom generated when the sonic boom bow shock level is restricted to 1.2 psf. As can be seen, to limit the boom to 1.2 psf, supersonic speeds must not be achieved until 35,000 feet. For this flight profile, there is a 2% penalty in total range when compared to the performance profile.

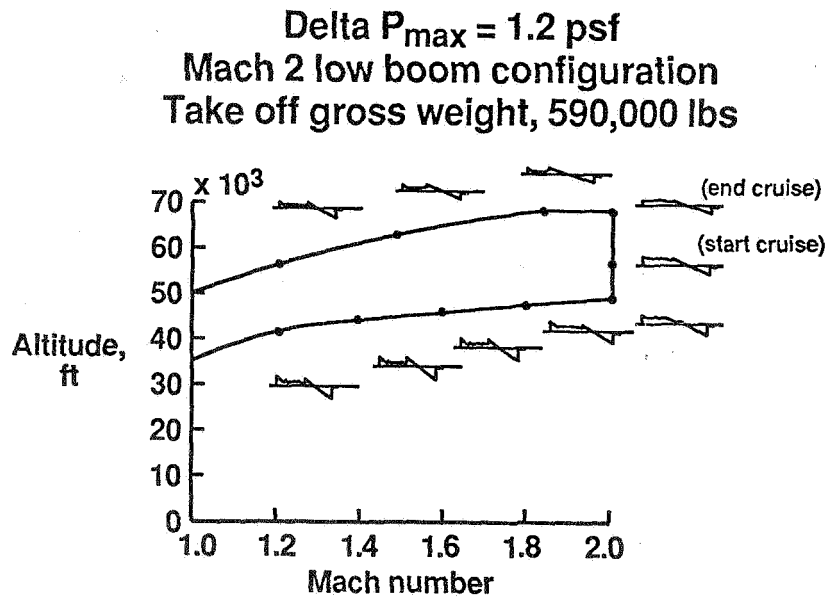


Figure 21

~~C3~~

Ground Sonic Boom Signatures for Restricted Flight Profile

To limit the boom to 1.0 psf., figure 22 shows that the configuration must be at approximately 43,000 feet before going supersonic. This profile results in a 5% range penalty when compared to the optimum performance path. It is evident from these results that the entire flight profile of the low boom configuration must be considered when evaluating its economic performance.

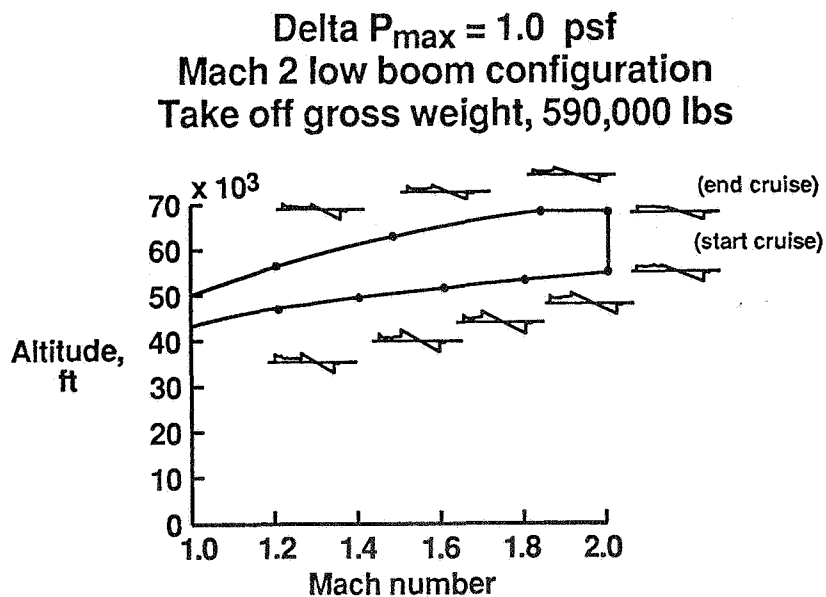


Figure 22

C-3.

Concluding Remarks

Wind Tunnel results indicate theory validation, especially at Mach 2, but signatures at greater distances needed.

Next designs will target lower Mach numbers and will stress integration of performance and low boom characteristics.

Next designs will be tested for low boom and performance.

Plume effects and entire mission profile must be considered in the design and evaluation of configurations.

Figure 23

References

1. Seebass, R. and George, A.R., "Sonic Boom Minimization." *Journal of the Acoustical Society of America*. Vol. 51, Pt. 3, Feb. 1972, pp. 686-694.
2. Darden, Christine M.: *Sonic-Boom Minimization with Nose-Bluntness Relaxation*. NASA TP-1348, 1979.
3. Mack, Robert J. and Needleman, Kathy E.: *A Semi-empirical Method for Obtaining Fuselage Normal Areas from Fuselage Mach Sliced Areas*. NASA TM-4228, December, 1990.
4. Mack, Robert J and Needleman, Kathy E.: *A Methodology for Designing Aircraft to Low Boom Constraints*. NASA TM 4246, February, 1991.
5. Carlson, Harry; and Walkley, Kenneth B.: *Numerical Methods and a Computer Program for Subsonic and Supersonic Aerodynamic Design and Analysis of Wings with Attainable Thrust Considerations* NASA CR-3808, 1984.
6. Hayes, Wallace D.; Haefeli, Rudolph C.; and Kulsrud, H.E.: *Sonic Boom Propagation in a Stratified Atmosphere, With Computer Program*. NASA CR-1299, 1969.
7. Barger, Raymond L. and Adams, Mary S.: *Fuselage Design for a Specified Mach-Sliced Area Distribution*. NASA TP-2975, February 1990.
8. Mack, R. and Needleman, K.: *The Design of Two Sonic Boom Wind Tunnel Models from Conceptual Aircraft Which Cruise at Mach Numbers of 2.0 and 3.0*. AIAA Paper #90-4026. Presented at 13th Aeroacoustics Conference, October 22-24, 1990, Tallahassee, FL.
9. Thomas, Charles L., "Extrapolation of Sonic Boom Pressure Signatures by the Waveform Parameter Method." NASA TN D-6832, 1972.
10. Needleman, Kathy E.; Darden, Christine M.; and Mack, Robert J.: *A Study of Loudness as a Metric for Sonic Boom Acceptability*. AIAA Paper #91-0496. Presented at the 29th Aerospace Sciences Meeting, January 7-10, 1991, Reno, NV.
11. Siclari, M. and Darden, C.: *An Euler Code Prediction of Near to Mid-field Sonic Boom Pressure Signatures*. AIAA paper #90-4000. Presented at the 13th Aeroacoustics Conference, October 22-24, 1990, Tallahassee, FL.
12. Darden, Christine M.: *Study of the Limitations of Linear Theory Methods as Applied to Sonic Boom Calculations*. AIAA Paper #90-0368. Presented at the 28th Aerospace Sciences Meeting, January 8-11, 1990, Reno, NV.
13. Barger, Raymond L. and Melson, N. Duane: *Comparison of Jet Plume Shape Predictions, and Plume Influence on Sonic-Boom Signatures*. Proposed NASA TP, May 1991.
14. Coen, Peter G.: *Development of a Computer Technique for the Prediction of Transport Aircraft Flight Profile Sonic Boom Signatures*. Master's Thesis. George Washington University, May, 1991.

THIS PAGE INTENTIONALLY BLANK

Session V. Sonic Boom (Aerodynamic Performance)

omit

HSCT Design for Reduced Sonic Boom
George T. Haglund, Boeing Commercial Airplane Group

PRECEDING PAGE BLANK NOT FILMED

THIS PAGE INTENTIONALLY BLANK

N94-33471

59-05
11999

HSCT DESIGN FOR REDUCED SONIC BOOM

George T. Haglund
Boeing Commercial Airplane Group
P. O. Box 3707 M/S 3T-CJ
Seattle, WA 98124-2207

High-Speed Research Workshop
First Annual Technical Review
May 14 - 16, 1991
Williamsburg, Virginia

PRECEDING PAGE BLANK NOT FILMED

LOW-SONIC-BOOM DESIGN PERSPECTIVE

CURRENT GOAL: No perceptible boom over populated areas

ASSUMPTION IN HSCT VIABILITY STUDIES:
No supersonic flight over land
Optimized over water routing

HSCT ENVIRONMENTAL IMPACT STUDIES WITH "ACCEPTABLE" BOOM

OBJECTIVES:

Evaluate the impact of applying innovative sonic boom technology to practical HSCT configurations, for possible overland supersonic cruise.

Identify design issues, performance and noise characteristics, and economic benefits relative to a baseline configuration.

RESULTS:

Three low-boom configurations developed, one in each HSCT Phase III, IIIA, and IIIB.

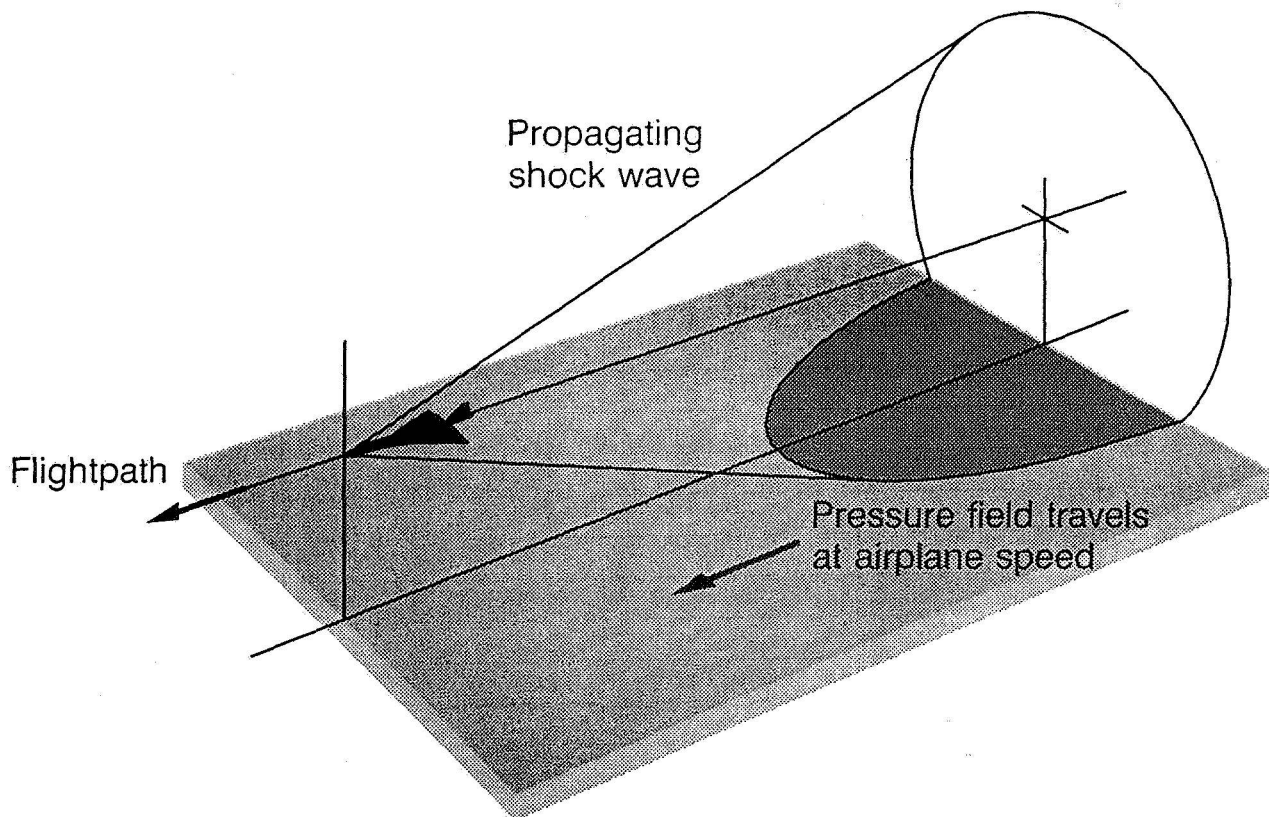


Figure 1. Sonic boom pressure field.

DESIGN APPROACH FOR REDUCED SONIC BOOM

Unfortunately, the sonic boom design goal is not yet firmly established, because we do not know enough to precisely define sonic boom waveforms that are psycho-acoustically acceptable to humans. However, for this study, the sonic boom design goal was to obtain a sonic boom waveform at the ground with loudness of 72 dBA or less. The 72 dBA loudness criterion was developed from an analysis of available human response test data acquired during the 1970s (ref. 2). This reduced loudness is obtained by reducing the magnitude of the pressure jump across each shock wave in the sonic boom waveform to a value of about 0.75 lb/ft².

The sonic boom constraint defined above has a profound effect on the airplane design. In particular, the airplane lifting surfaces must be highly swept, lightly loaded, and spread along the horizontal length of the airplane. In addition, the distribution of volume must be closely dove-tailed to the lift distribution. An appropriate flight condition (Mach, altitude, and gross weight) must also be selected to achieve a realistic configuration.

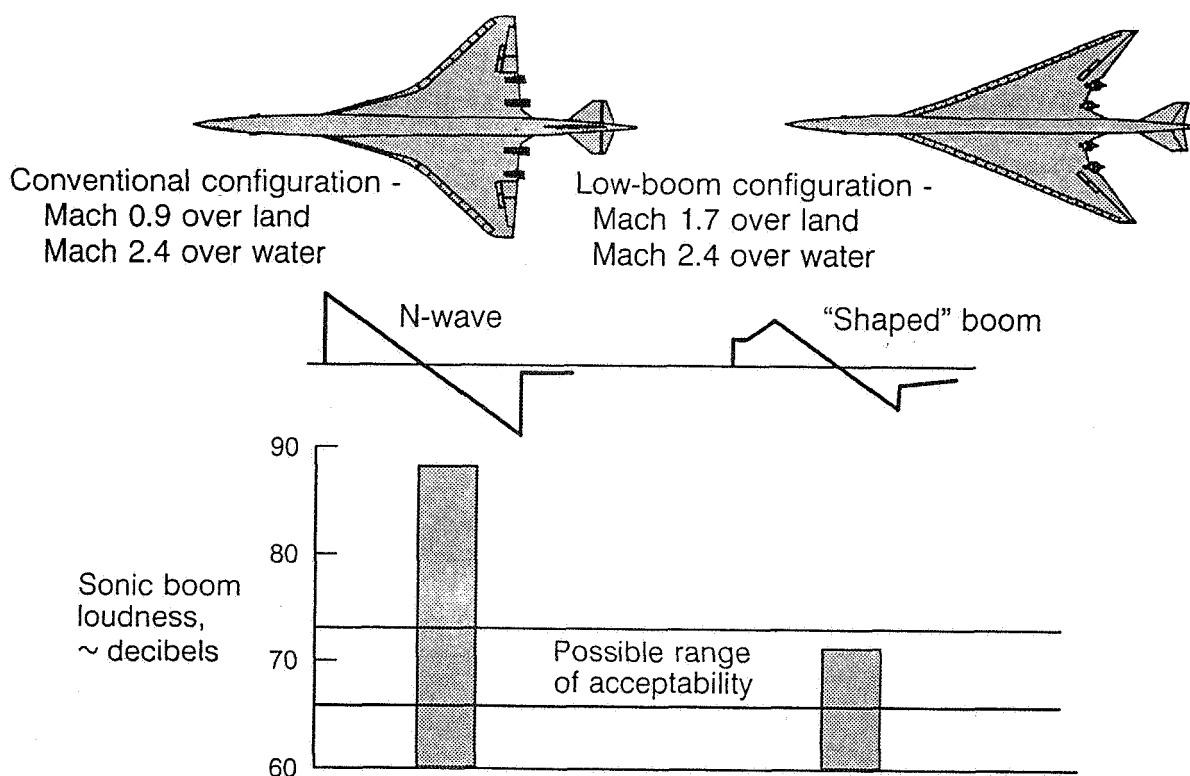


Figure 2. Conventional and low-boom concepts compared.

TARGET SONIC BOOM WAVEFORMS , PHASE III

In HSCT Phase III, configuration III was designed with the objective of meeting the 72 dBA target with 1.0 lb/ft² shocks at Mach 1.5 cruise with a "ramp" waveform, shown below (refs. 2 through 5). The design loudness of 72 dBA was not met, however, due to the stronger-than-desired tail shock and intermediate shocks. In Phase IIIA, the target waveform for Mach 1.7 cruise was revised to be a "delayed ramp" waveform with 0.90 lb/ft² shocks, resulting in configuration IIIB. Again, however, the calculated loudness of 77 dBA did not meet the loudness goal, primarily because of an update to the shock-wave rise-time effect.

In Phase IIIB, the target shock strengths were reduced to 0.75 lb/ft² to achieve the 72 dBA target loudness. In addition, the target waveform was revised slightly, as shown below.

Predicted Sonic-Boom Waveform at the Ground (Sea Level),
 $K_R = 1.9$, standard day temperature, no wind

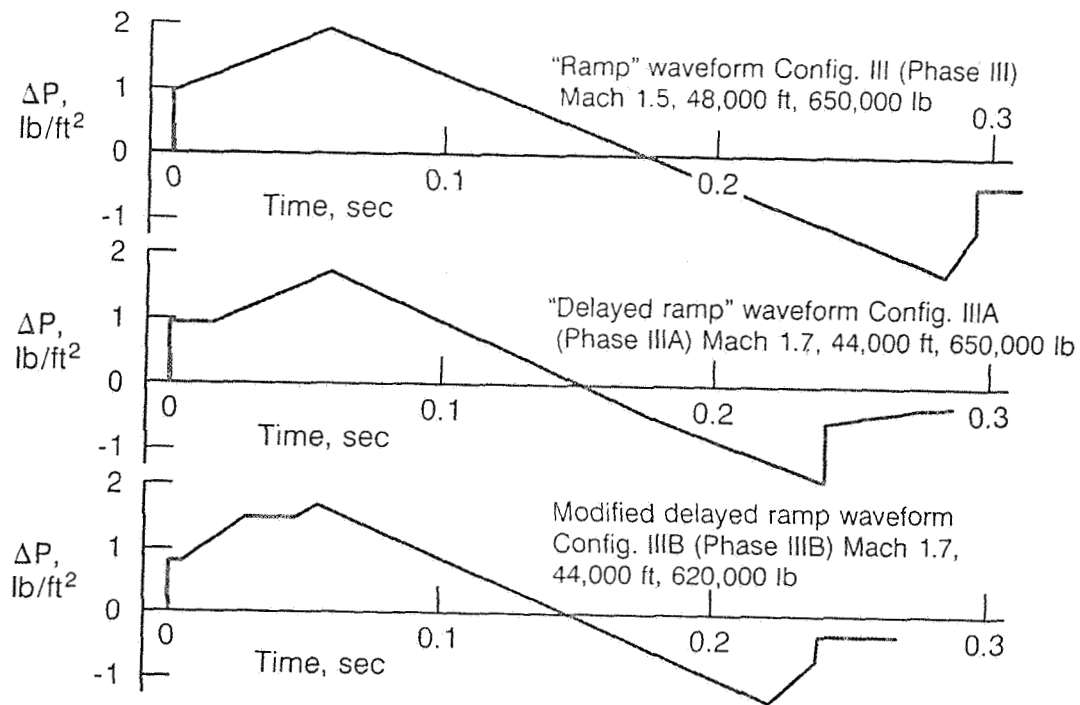


Figure 3. Target sonic boom waveforms.

AIRPLANE DESIGN FOR REDUCED SONIC BOOM LOUDNESS

The sonic boom design constraint was imposed in the form of an overall target distribution of the Whitham F-function, which is directly related to the target sonic boom waveform at the ground. The target F-function fundamentally defines the airplane lift and volume aerodynamic characteristics close to the airplane (Ref. 6). The sonic boom disturbance at the ground includes the effects of atmospheric propagation (Refs. 6 and 7). Figure 4 shows the overall target F-function and the associated sonic boom waveform at the ground.

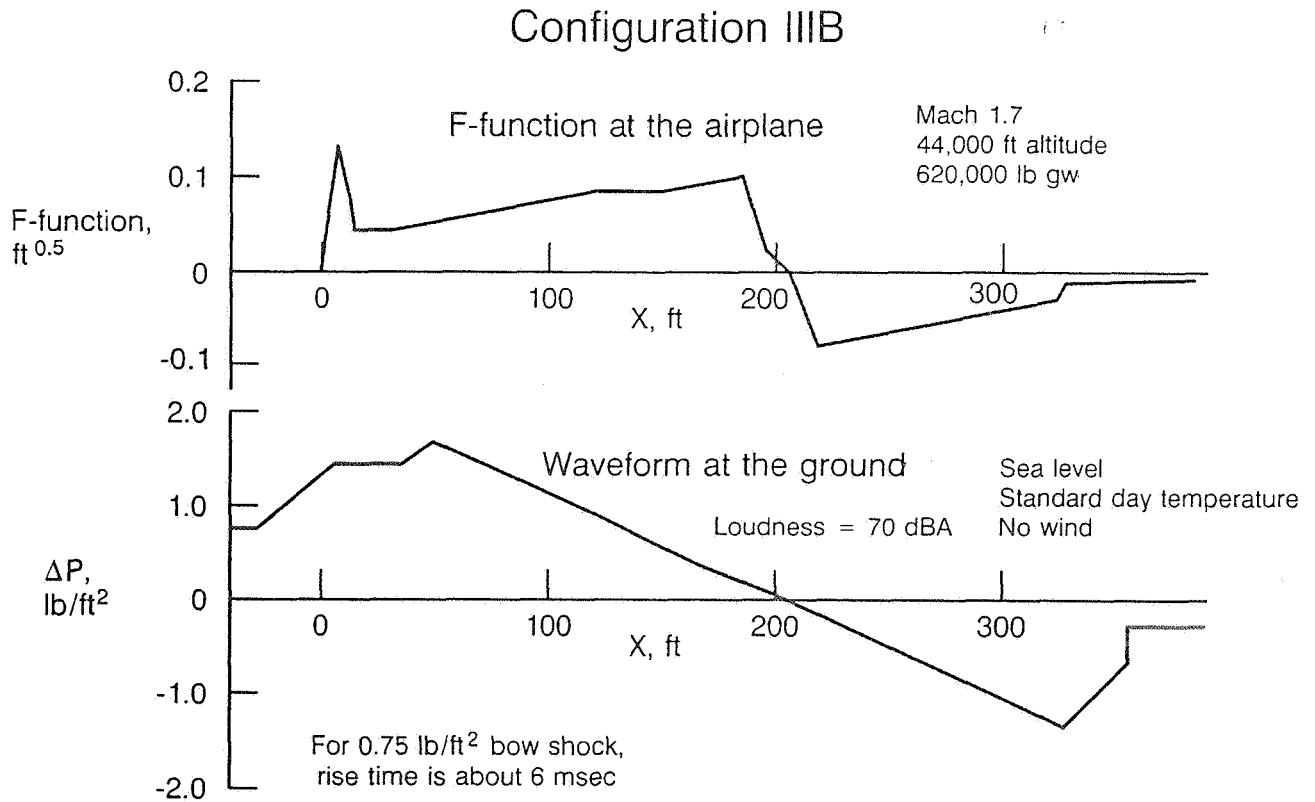


Figure 4. Target F-function and waveform.

DESIGN PROCEDURE FOR LOW SONIC BOOM

Figure 5 outlines the design process that was used in Phase IIIB to define configuration IIIB. Many iterations in geometry were required to approach the desired overall airplane F-function. The lift and volume contributions of each airplane component (wing, body, nacelles, horizontal tail, and vertical tail) must be located and shaped appropriately, while considering any mutual interference effects. Each design iteration led to a correction in the actual airplane F-function and a directly-related correction to the geometry.

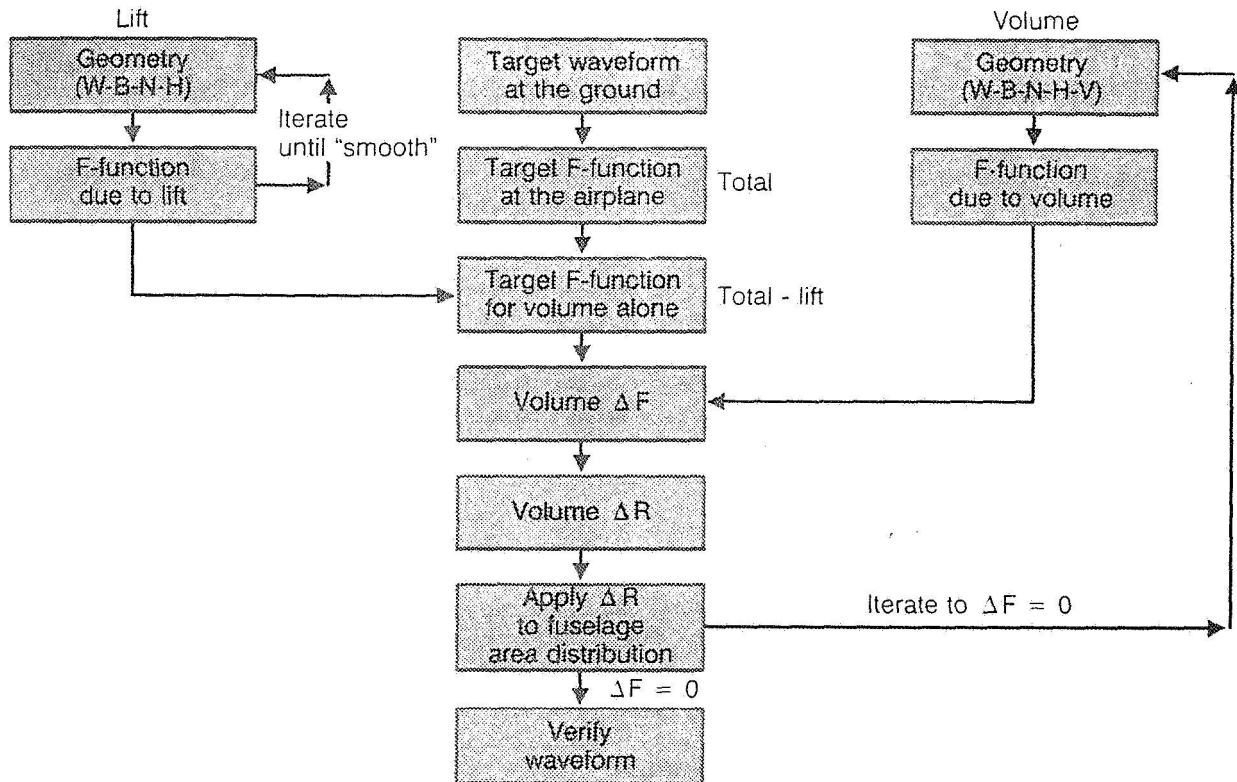


Figure 5. Design procedure for low sonic boom.

WING DESIGN AND NACELLE LIFT EFFECTS

Because the sonic boom from large, heavy cruise vehicles is lift-dominated, the most important airplane component is the wing planform and the lift distribution that it produces. Accordingly, previous Phase III studies have focused on arrow-wing planforms, wing leading-edge strakelets, and appropriate wing camber and twist designs. However, another aspect of the lift distribution is the lift produced by the nacelles, mounted aft on the wing lower surface. The positive pressures from the nacelle forebodies pressurize the wing lower surface, producing a beneficial lift force of up to 10% of the total lift. Because the effect is strong and localized, it should be considered early in the design phase. The Phase IIIA configuration required a rather severe fuselage area-ruling to counteract the non-smooth lift distribution in the vicinity of the nacelles.

Therefore, one of the major goals of Phase IIIB was to achieve a smooth overall lift distribution, considering the nacelle lift-interference effects. This was accomplished as follows: 1), use of new baseline nacelles, having a smaller area growth, and 2) revised wing camber and twist design, with a reflex in the camber surface near the nacelles.

Figure 6 shows the improvement in the F-function due to lift, by comparing the F-functions of the IIIA configuration and the new IIIB design. These F-functions were calculated by converting the lift distributions into the equivalent bodies of revolution for the start-of-cruise condition, according to the standard sonic boom methods (Refs. 7 and 8).

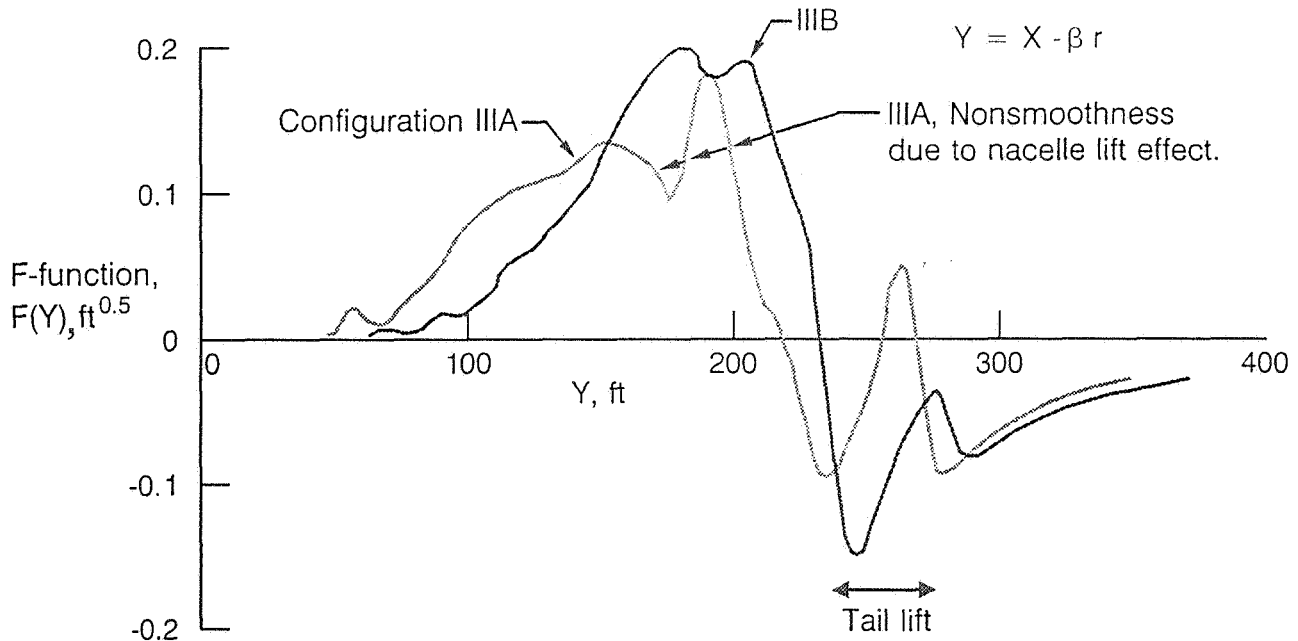


Figure 6. Calculated F-functions due to lift.

AREA DISTRIBUTIONS AND F-FUNCTION DUE TO VOLUME

The details of the volumetric components were defined next, beginning with the fuselage forebody. The forebody shape is important because it produces the initial 0.75 lb/ft^2 shock wave and the constant-pressure region of the target sonic boom waveform. It was defined by the method of Reference 9, with a slight reduction of forebody cross-sectional area to account for forebody lift. Figure 7 shows the area distribution and F-function produced by all of the volumetric components.

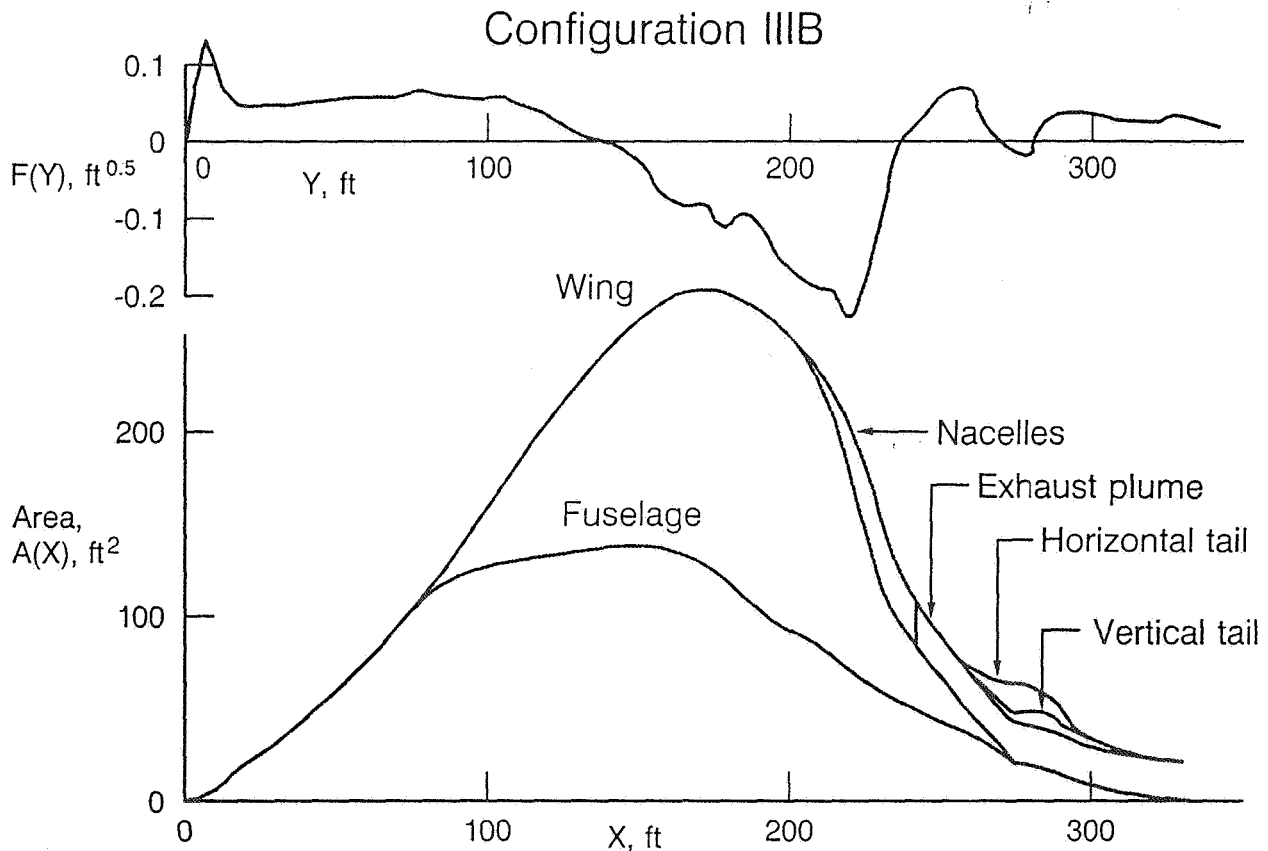


Figure 7. Area distributions and F-functions due to volume.

FUSELAGE AREA DISTRIBUTIONS

The fuselage area distribution shown in Figure 8 is quite different from previous low-boom configurations, because of the 0.75 lb/ft^2 constraint and the smoother lift distribution. The aft-body shape in particular is impacted by the more severe sonic boom constraint, resulting in reduced seating capacity (only 237 mixed-class or 252 all-tourist passengers). This fuselage shape could be improved, in terms of seating capacity and also wave drag, by modifying the wing planform and lift distribution. In addition, the aft-body design needs more investigation.

Figure 8 shows the severe area-ruling of the IIIA configuration in the vicinity of the nacelles, due to the non-smooth lift distribution. This effect was reduced considerably for configuration IIIB.

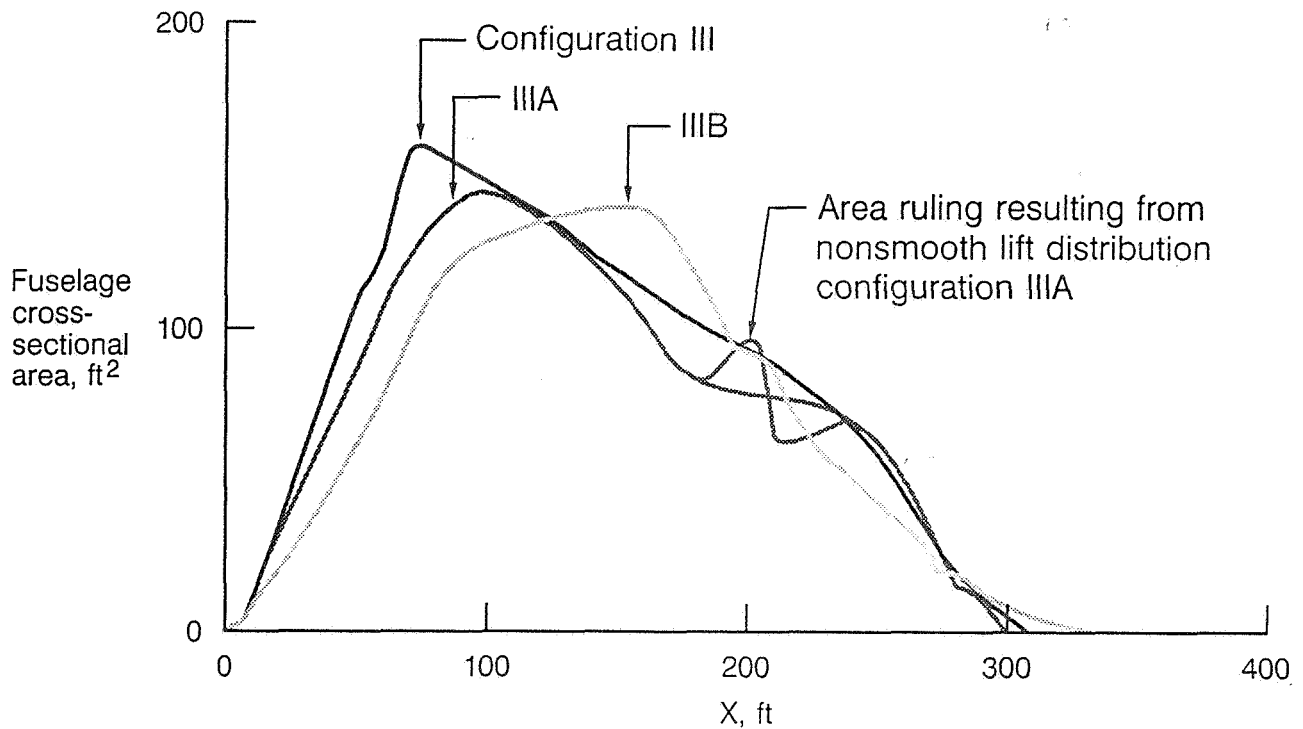


Figure 8. Fuselage area distributions.

LOW SONIC BOOM DESIGN, CONFIGURATION IIIB

The drawing of the uncycled configuration, the Model IIIB, is shown in Figure 9. This drawing was used as the basis for developing the sonic boom characteristics, as well as the inputs and scalars for the performance sizing program.

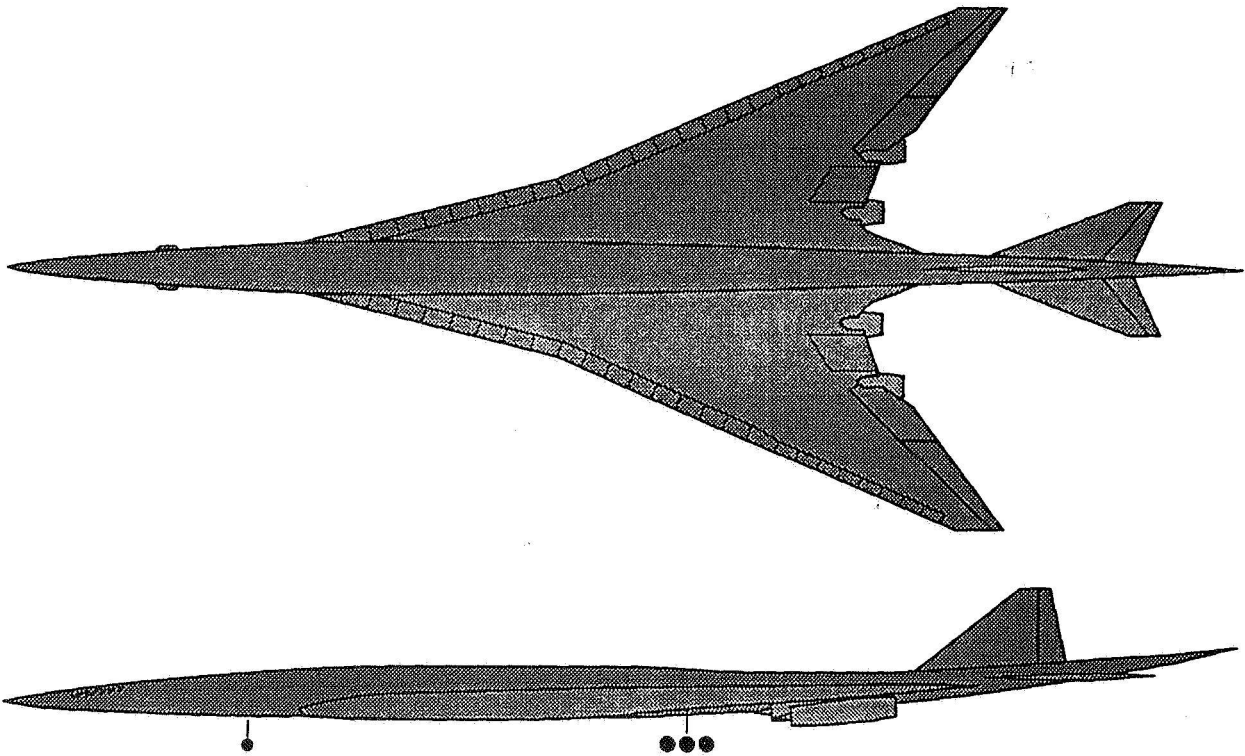


Figure 9. Model IIIB, General Arrangement.

SONIC BOOM CHARACTERISTICS

The Mach 1.7 overland cruise sonic boom waveform at the ground was calculated for the start-of-cruise condition and is shown in Figure 10. The bow and tail shocks meet the 0.75 lb/ft^2 design goal. Although the waveform exhibits smaller pressure jumps and isentropic pressure increases, the calculated sonic boom loudness is 71 dBA, which is less than the design goal of 72 dBA. The small pressure jumps are not significant for sonic boom loudness.

The calculated loudness is sensitive to the shock-wave rise time. For this study, rise-time values were determined from an empirical analysis of N-wave sonic booms produced by Air Force fighter and SR-71 aircraft. The rise time of the 0.75 lb/ft^2 bow shock is about 6 msec; the smaller shocks have an appropriately longer rise time.

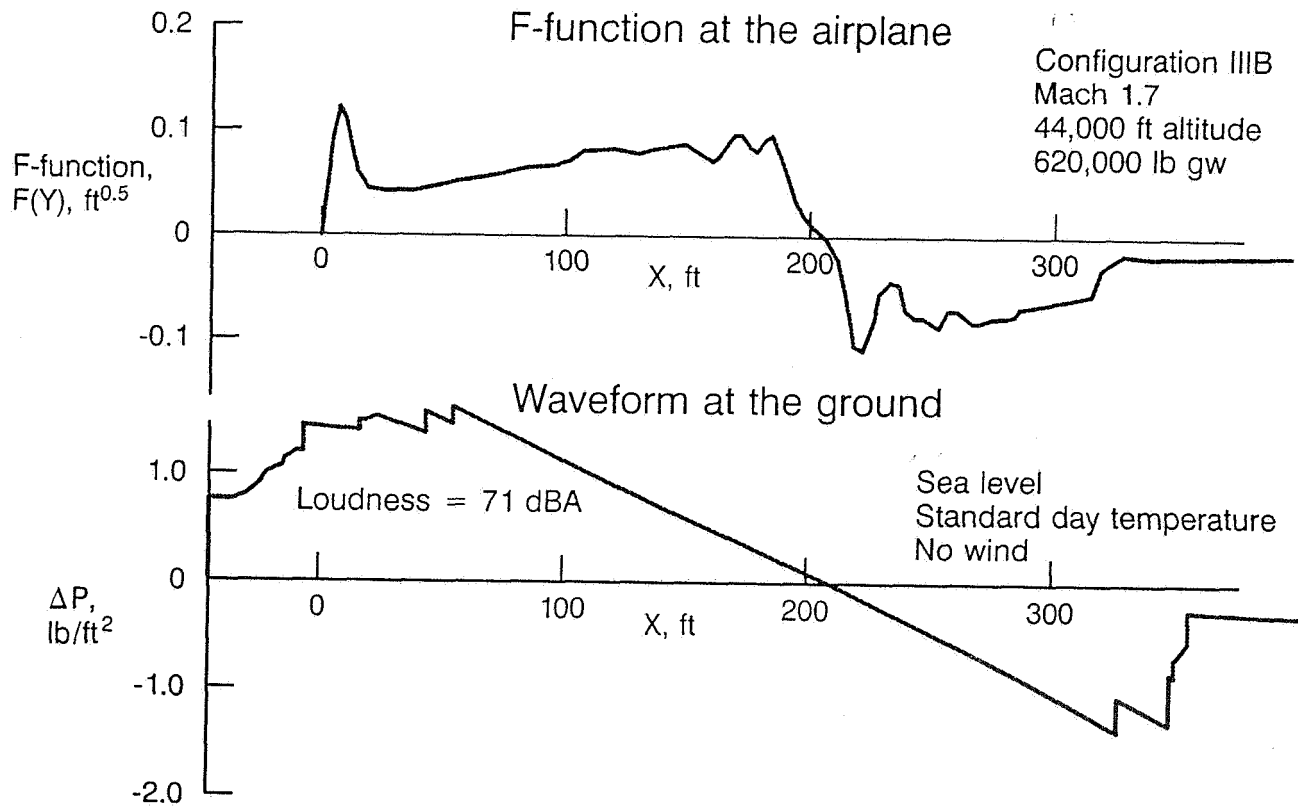


Figure 10. Actual F-function and waveform.

SIZING, PERFORMANCE, AND NOISE CHARACTERISTICS

The airplane is sized for a 5000 n. mi. mission by fuel volume (wing area) and minimum takeoff weight (engine size). Figure 11 compares Model IIIB to its baseline airplane. Despite the large 15% loss in payload from 279 to 237 passengers required to achieve the target 0.75 lb/ft^2 waveform, the takeoff gross weight increased 2%, OEW increased 8%, engine size increased 6%, while block fuel was essentially unchanged. On the other hand, takeoff and landing performance of Model IIIB was substantially improved relative to the baseline due to the low wing loading dictated by the fuel volume requirement. This in turn lead to lower takeoff noise levels for the Model IIIB, -2.7 EPNdB and -1.3 EPNdB at the sideline and community points, respectively.

The performance assessment of the Model IIIB relative to the baseline was done at the average fleet mission of about 3450 n.m., of which about 25% is flown over land. The baseline flies the overland portion of the flight at Mach 0.9, while Model IIIB flies it at Mach 1.7, which reduces the block time by about 0.5 hour.

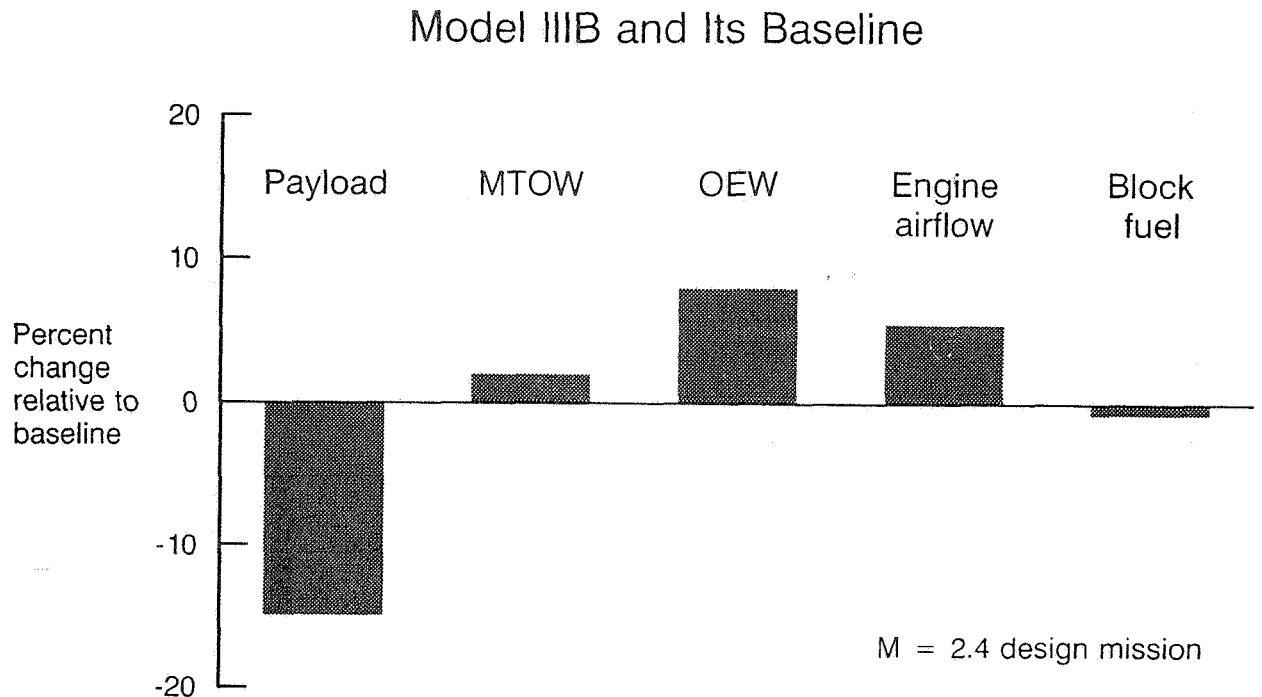


Figure 11. Performance comparison, Model IIIB and its baseline.

SUMMARY OF PHASE III CONFIGURATIONS

During the Phase III low sonic boom studies, several configurations have been designed, with different sonic boom and configuration constraints. Figure 12 gives a comparison of their respective design conditions and constraints. The early studies illustrated the advantages of lower altitude and reduced supersonic Mach number. Higher Mach number, as well as higher altitude, make the low-boom design problem inherently more difficult because far-field propagation pushes the waveform toward the form of the far-field N-wave, rather than the "shaped" low-boom waveforms. Therefore, at higher Mach or altitude, severe configuration changes are required to achieve the shaped near-field waveforms with reduced shock strength. For example, the Mach 2.4 low-boom configuration 2B had significant drag and weight penalties, and a balance problem due to a wing location far back on the fuselage. The Mach 2.4 configuration was not pursued further, because of these formidable design problems.

In Phase IIIA, a new sonic boom target waveform was developed, the "delayed ramp" waveform, and the cruise Mach number was increased from Mach 1.5 to 1.7. The delayed ramp waveform has several desirable features from the standpoints of configuration design, sonic boom propagation, and loudness.

Overwater Cruise is at Mach 2.4 in all Cases

Phase	Configuration	Sonic boom constraint (target)	Overland start-of-cruise design condition			
			Mach	Altitude, ft	GW, lb	
III	1B	Ramp waveform, $\Delta P_{SH} = 1.0 \text{ lb/ft}^2$ 72 dBA loudness	1.5	48,000	650,000	Special forebody shape, arrow-wing planform with strake, staggered nacelles, etc.
	2B	Same as 1B	2.4	53,000	650,000	Much longer forebody, bigger strake, aft wing location, drag penalty, 20% increase in TOGW.
	III	Same as 1B	1.5	48,000	650,000	Two-post landing gear, 268 PAX. Actual boom loudness 78 dBA.
IIIA	IIIA	Delayed ramp waveform $\Delta P_{SH} = 0.9 \text{ lb/ft}^2$ 72 dBA loudness	1.7	44,000	650,000	Minor configuration changes from III, 253 PAX, 77 dBA loudness.
IIIB	IIIB	Modified delayed ramp $\Delta P_{SH} = 0.75 \text{ lb/ft}^2$ 72 dBA loudness	1.7	44,000	620,000	Smoother lift distribution, new nacelles, modified fuselage with aft-body extension, four-post landing gear, 237 PAX, 71 dBA loudness.

Figure 12. Summary of low-sonic-boom design constraints.

IMPACT OF SONIC BOOM DESIGN CONSTRAINT

For the 5000 n.m. mission, relative to a baseline configuration, the low-boom designs typically have the following characteristics: heavier TOGW, higher L/D, and similar block fuel. These characteristics are compared in Figure 13 for the three low-boom configurations and their respective baseline configurations. The 0.75 lb/ft² design (IIIB), however, suffers from reduced L/D and passenger count, as a direct result of the severe sonic boom design constraint. Accordingly, its block fuel per passenger is 17% greater than the baseline.

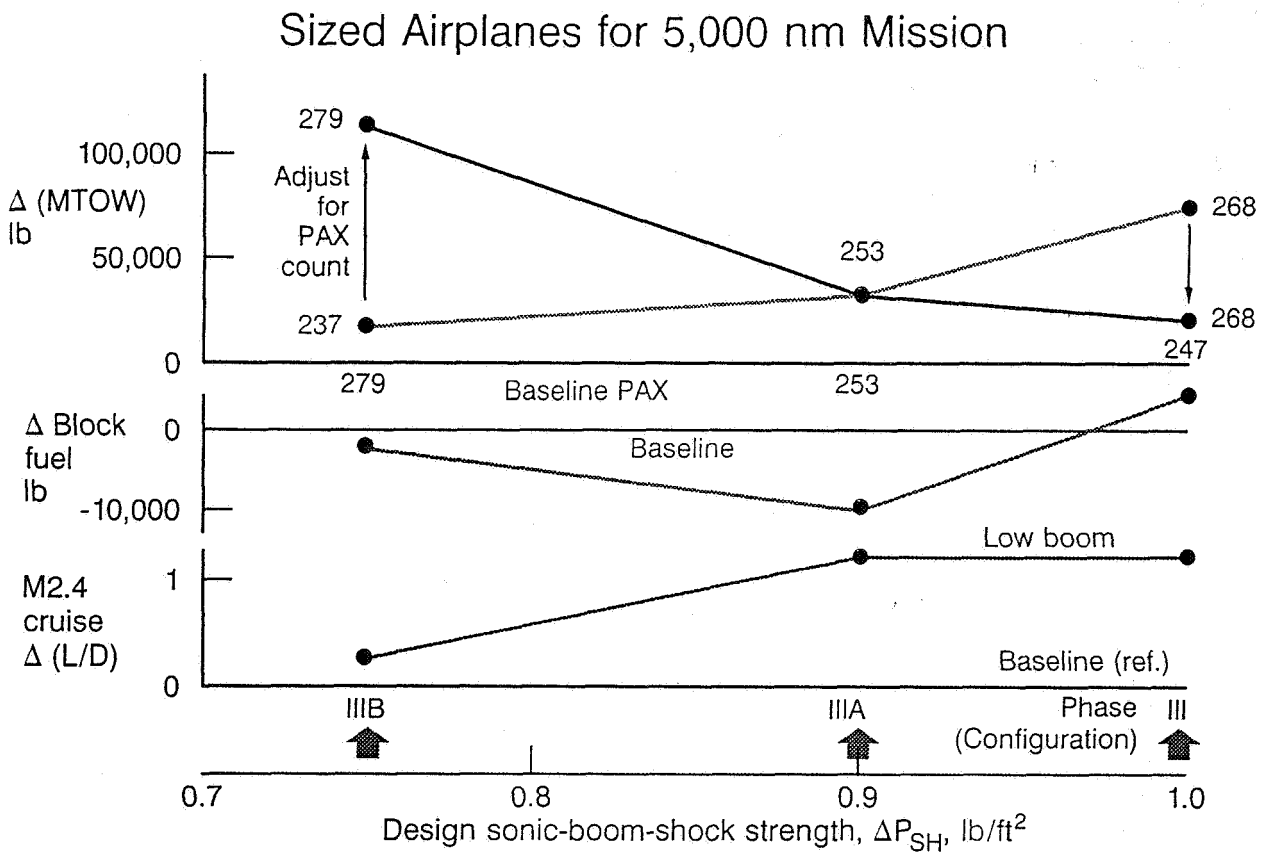


Figure 13. Effect of the level of the sonic boom constraint.

WING LOADING CONSIDERATIONS

In designing for reduced sonic boom, the wing loading, W/S_{REF} , is a particularly important design variable. For conventional configurations, the lift is concentrated over only about 50% of the total airplane length. Such wings have obvious advantages in terms of weight and skin friction drag. For the low-boom configurations, however, the lift must be distributed over a larger fraction of the airplane length and over a larger wing area. For example, the design wing loading of the low-boom configuration IIIB is about 63 lb/ft^2 , whereas the wing loading of the baseline configuration is close to 100 lb/ft^2 .

The effect of airplane sizing for optimum cruise performance is illustrated for configuration IIIB when it is sized for the 5000n.m. mission. As shown in the table below, the wing area was reduced from 9870 to 8632 ft^2 , which increased the wing loading from 63 to 73 lb/ft^2 ; optimum cruise performance is obtained with the higher wing loading. The increase in wing loading, however, means that the wing lift may then be too concentrated and the low-boom design requirement may no longer be satisfied. This result indicates that there may be an inherent penalty for low-boom configurations because of the sonic boom requirement for a relatively large, lightly-loaded wing. Obviously, another cycle in the design procedure is needed, to develop the best compromise between the low-boom requirements and optimum cruise performance. In all of the Phase III studies, only a single pass was made through the sizing exercise.

	Gross Weight, W, lb At Start-of-Cruise	Effective Wing Area, S_{REF} , ft^2	Wing Loading, W/S_{REF} , lb/ft^2
Design Pt., Config. IIIB	620,000	9870	63
Sized Apl., (5000n.m.), Config. IIIB	628,000	8632	73

CONCLUSIONS

Configuration IIIB was designed for reduced sonic boom loudness at the ground and was compared to a baseline configuration in terms of size, performance, and noise. The following statements summarize the major conclusions:

1) In designing for reduced sonic boom loudness, many design variables must be considered, including flight condition variables and configuration design constraints that conflict with the sonic boom constraints.

2) In the "shaped boom" concept, shock coalescence and waveform aging must be retarded to avoid the N-wave form. Minimum aging occurs at the lower altitudes and lower supersonic Mach numbers.

3) The sonic boom loudness goal of 72 dBA was achieved by keeping the shock waves to less than 0.75 lb/ft^2 , based on an empirically-derived rise time of six msec.

4) Compared to previous Phase III sonic boom constraints of 1.0 and 0.9 lb/ft^2 , the 0.75 lb/ft^2 constraint produced additional penalties in gross weight, drag, passenger count, and performance.

5) A long, slender aft body was required for the 0.75 lb/ft^2 constraint, which resulted in a 15% reduction in seating capacity to only 237 mixed-class passengers (or 252 all-tourist), and a 2% increase in maximum takeoff gross weight relative to the baseline airplane.

6) Takeoff noise was decreased by about 2 EPNdB, due to the low wing loading dictated by the fuel volume requirement.

7) A performance benefit for operating at Mach 1.7 over land, rather than at Mach 0.9, did not materialize because of the large decrease in the ratio of payload to takeoff gross weight.

8) The deficiencies of configuration IIIB in terms of drag, weight, and passenger count can be improved somewhat by additional design work and a better compromise between the low-boom requirements and optimum cruise performance; the more severe design constraint of 0.75 lb/ft^2 makes the design process more difficult.

REFERENCES

1. "High-Speed Civil Transport Studies, Task 3.2 -- Special Factors Assessment, Sonic Booms." Boeing Document D6-53322-3, August 1987, Contract NAS1-18377.
2. Brown, J. G., and Haglund, G. T., "Sonic Boom Loudness Study and Airplane Configuration Development." AIAA Paper 88-4467, presented at the AIAA/ASEE Aircraft Design, Systems, and Operations Conference, September 7-9, 1988, Atlanta, Georgia.
3. "High-Speed Civil Transport Study, Airframe Technology," NASA CR 181879, 1989.
4. "High-Speed Civil Transport Study, Special Factors," NASA CR 181880, 1989.
5. "High-Speed Civil Transport Study," NASA CR 4233, September 1989.
6. Hayes, W. D., Haefeli, R. C., and Kulsrud, H.E., "Sonic Boom Propagation in a Stratified Atmosphere, with Computer Program," NASA CR 1299, 1969.
7. Haglund, G. T., and Kane, E. J., "Study Covering Calculations and Analysis of Sonic Boom During Operational Maneuvers, Vol. III, Description of Computer Program and Estimation of Limitation Near Caustics," FAA Report EQ 71-2, Feb. 1971.
8. Middleton, W. D., and Lundry, J. L., "A System for Aerodynamic Design and Analysis of Supersonic Aircraft. Part 1, General Description and Theoretical Development," NASA CR 3351, December 1980.
9. Darden, Christine M., "Sonic-Boom Minimization with Nose-Bluntness Relaxation," NASA TP 1348, 1979.

THIS PAGE INTENTIONALLY BLANK

Session V. Sonic Boom (Aerodynamic Performance)

omit

Sonic Boom Prediction and Minimization Using Computational Fluid Dynamics
*Dr. Thomas A. Edwards and Raymond Hicks, NASA Ames Research Center; Samson Cheung, MCAT Institute;
and Susan Cliff-Hovey, Mike Madson and Joel Mendoza, NASA Ames Research Center*

PRECEDING PAGE BLANK NOT FILMED

THIS PAGE INTENTIONALLY BLANK

510-71
12000

**SONIC BOOM PREDICTION AND
MINIMIZATION USING
COMPUTATIONAL FLUID DYNAMICS**

T. Edwards
R. Hicks
S. Cheung*
S. Cliff
M. Madson
J. Mendoza

NASA Ames Research Center
Moffett Field, California

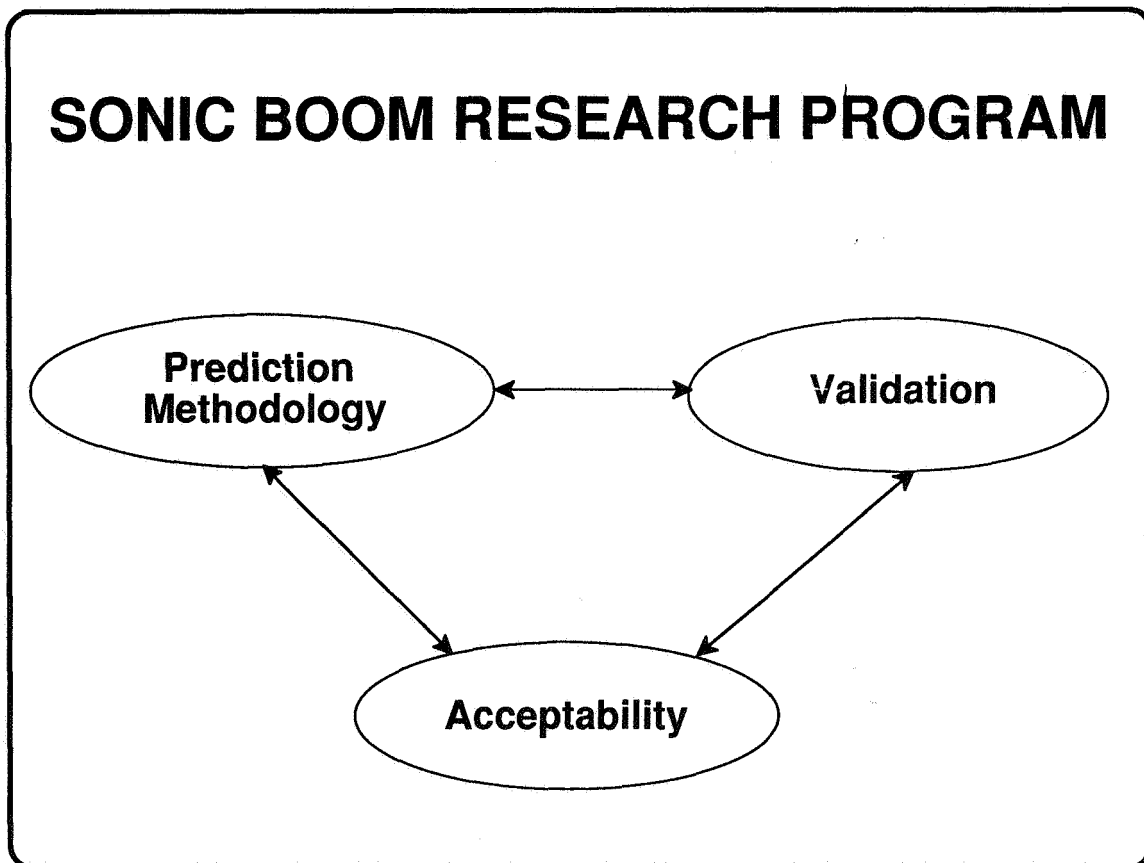
*MCAT Institute
San Jose, California

First Annual High Speed Research Workshop
May 14-16, 1991
Williamsburg, Virginia

INTRODUCTION

This paper describes the NASA Ames Research Center program in sonic boom prediction methodologies. This activity supports NASA's High Speed Research Program (HSRP). An overview of the program, recent results, conclusions, and current effort will be given. This effort complements research in sonic boom acceptability and validation being conducted at Langley and Ames Research Centers.

The goals of the sonic boom element are: to establish a predictive capability for sonic booms generated by High-Speed Civil Transport (HSCT) concepts; to establish guidelines of acceptability for supersonic overland flight; and to validate these findings with wind tunnel and flight tests. The cumulative result of these efforts will be an assessment of economic viability for supersonic transportation. This determination will ultimately be made by the aerospace industry.



CFD SONIC BOOM PROGRAM

Established approaches to sonic boom prediction and minimization utilize linear supersonic aerodynamics and quasi-linear acoustic propagation theory. However, the accuracy of these methods deteriorates as the Mach number or angle of attack increases, and they have difficulty modeling complex geometries and propulsion system effects. The new generation of proposed HSCTs will be highly optimized in all respects, and hence will require improved accuracy in optimizing the sonic boom.

It has been proposed to utilize computational fluid dynamics (CFD) to provide the near-field pressure distribution. This approach has several advantages: nonlinear effects and geometric complexities can be fully accounted for, including propulsion system effects; the pressure field can be propagated to a distance sufficiently far from the vehicle that linear propagation theory is valid; a complete aerodynamic description of the vehicle is generated, facilitating simultaneous analysis of the complete system; and a common database can be used for low speed analysis and off-design performance.

The first element of this project was to validate CFD codes for sonic boom prediction. Three test cases of increasing complexity were selected for this purpose, and results of this study will be given later. Other aspects of the CFD activity include predictions of sonic boom for proposed configurations, pre-test analysis of wind tunnel models and post-test diagnostics, and numerical minimization of sonic boom loudness using CFD and optimizer technology.

AMES SONIC BOOM PROGRAM (COMPUTATIONAL)

- **Code validation**
- **CFD near-field prediction**
- **Experiment support**
- **Loudness reduction**

EXPERIMENTAL SONIC BOOM PROGRAM

Wind tunnel testing is another important aspect of the sonic boom effort. The 9x7-foot tunnel at Ames accesses the Mach 1.5 to 2.5 range and allows large models to be tested with measurements at sufficiently large altitudes for code validation and linear extrapolation. This facility was used extensively in the 1970's to test SST concepts. However, "tailored" waveforms are a relatively new concept and a sonic boom database needs to be developed for these configurations. Thus, as low-boom models are produced, the 9x7 will be used to measure sonic boom performance, providing code validation data and benchmarking progress of low-boom designs.

AMES SONIC BOOM PROGRAM (EXPERIMENTAL)

- **Update data base**
- **Verify design methods**
- **Demonstrate performance**

AMES COOPERATIVE RESEARCH

At NASA Ames, the Applied Computational Fluids Branch (RFA) and the Advanced Aerodynamic Concepts Branch (RAC) are contributing to the sonic boom prediction methodology. The Applied Computational Fluids Branch is emphasizing code validation and coupled aerodynamic optimization/sonic boom minimization, while the Advanced Aerodynamic Concepts Branch is performing aerodynamic optimization and complex configuration analysis, and conducting wind tunnel tests with CFD correlation.

Care has been taken to integrate the effort in sonic boom prediction described here with the other elements of sonic boom analysis. Langley-developed low-boom models have been tested in the Ames 9x7 tunnel, and CFD correlation with these tests is in progress. Preliminary results will be presented later. Future models developed by Langley, Ames, and industry will be tested as well.

The acceptability criteria and atmospheric effects will play heavily into the determination of a successful supersonic overland design. Results from this research will be factored into the analysis as they become available. Complementary efforts in sonic boom minimization are also integrated between the centers. Validated CFD codes will be used as numerical wind tunnels to assess sonic-boom-minimized designs. Comprehensive systems analysis using linear methods will, in turn, provide a baseline for subsequent nonlinear analysis using CFD.

AMES SONIC BOOM RESEARCH ORGANIZATIONS

- **Applied Computational Fluids (RFA)**
CFD validation, sonic boom prediction and minimization, aerodynamic optimization
- **Advanced Aerodynamic Concepts (RAC)**
CFD validation, sonic boom prediction, aerodynamic optimization, wind tunnel tests

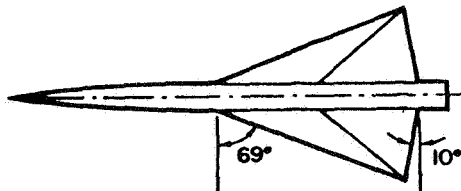
CFD VALIDATION STUDIES

As mentioned earlier, three test cases were chosen to validate CFD codes for sonic boom prediction and to gain experience in the modeling requirements. These configurations were tested in the Ames 9x7-foot tunnel in the 1970's and have experimental data available at a variety of operating conditions and altitudes (see Ref. 1). These geometries represent a progression of geometrical and physical complexity, from a cone-cylinder to a low aspect-ratio wing to a delta-wing body.

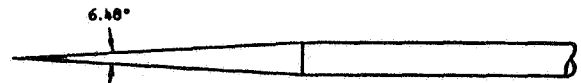
In addition, a succession of CFD codes was applied to these test cases. These include TRANAIR, a full-potential code with local mesh refinement capability; TEAM, an Euler/Navier-Stokes code with versatile zonal grid capability; AIRPLANE, an unstructured-grid Euler solver; and UPS, a parabolized Euler/Navier-Stokes code.

Initially, the CFD codes were used to generate a solution in the near-field, about one-quarter to one body length vertically below the vehicle. The pressure on the centerline was then extracted from the solution and used to initialize a quasi-linear extrapolation code to propagate the signal to the desired altitude. Other methods of incorporating CFD into the sonic boom analysis were subsequently investigated have been reported in Ref. 2.

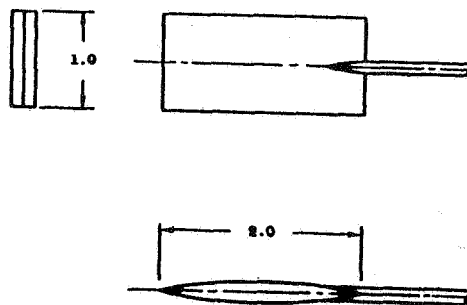
CFD VALIDATION MODELS



Delta Wing/Body



Cone Cylinder

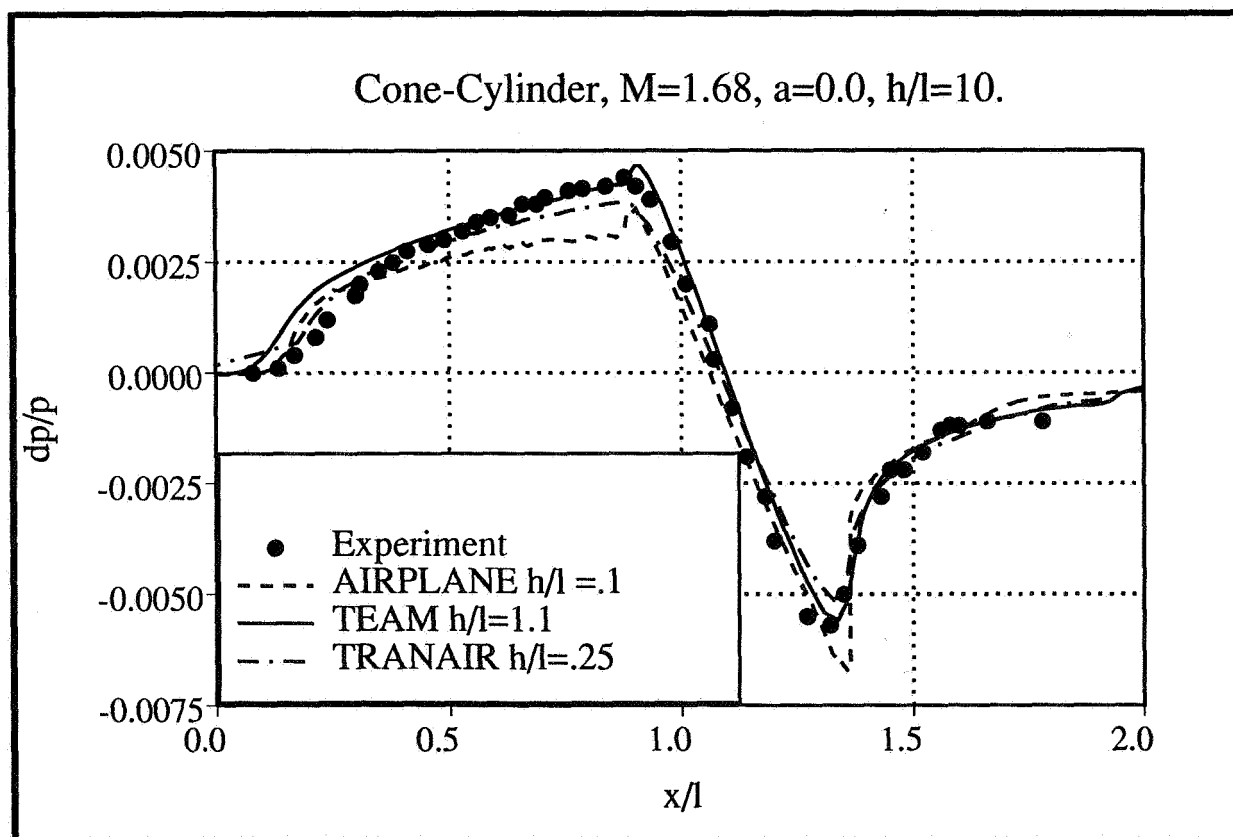


Low-Aspect-Ratio Wing

CONE-CYLINDER VALIDATION

A cone-cylinder geometry was the first test case, where the cone angle is 6.48 deg. and the test Mach number was 1.68. The overpressure signature for this model was measured at altitudes of 10 and 20 cone lengths. Because of the large altitude and very weak shock generated by the geometry, this case was a good test of dissipative errors present in the computations.

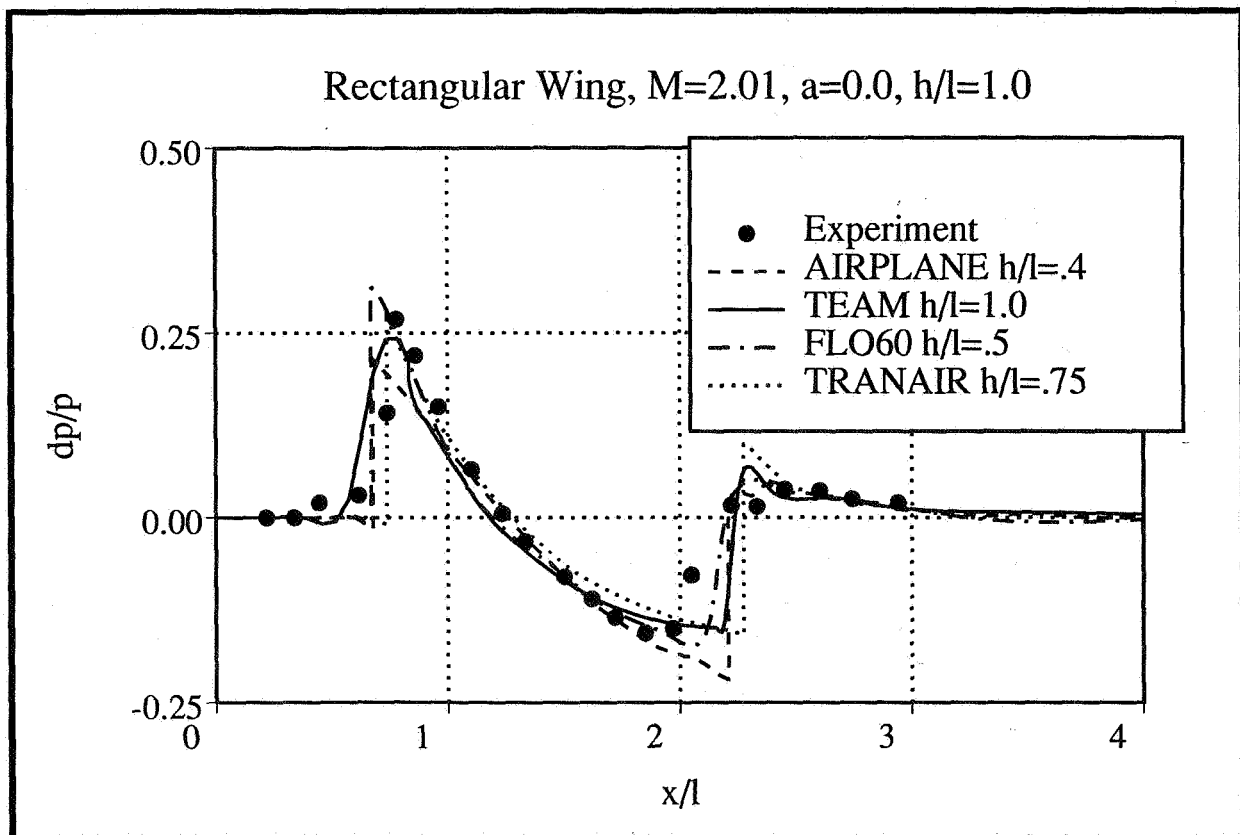
Results for this case using the UPS code have been reported previously in Ref. 2, and further results will be reported in Refs. 3 and 4. The figure below shows the results for the AIRPLANE, TEAM, and TRANAIR codes at an altitude of ten cone lengths. All three codes show very good correlation with the data. Previous studies with the UPS code indicated that grid resolution at the expansion was critical to capture the weak disturbance generated by this shape. Note that the correlation with the data improves as the altitude at which the linear extrapolation commences is increased, as indicated in the legend.



LOW ASPECT-RATIO WING VALIDATION

The second test case was a low aspect-ratio ($AR=0.5$) rectangular-planform wing. The airfoil was a 12.5%-thick biconvex section. The test Mach number was 2.01 and overpressure data were taken at altitudes of 1 and 8 chord-lengths. This geometry generated a non-axisymmetric flow field near the body, requiring a 3-D calculation for the near-field. Also, the sting was large relative to the body, and contributed significantly to the strength and location of the tail shock.

Again, the computational results show good correlation with the data taken at one body length. The error in tail shock location arises mainly from sting interference not modeled in the computations.



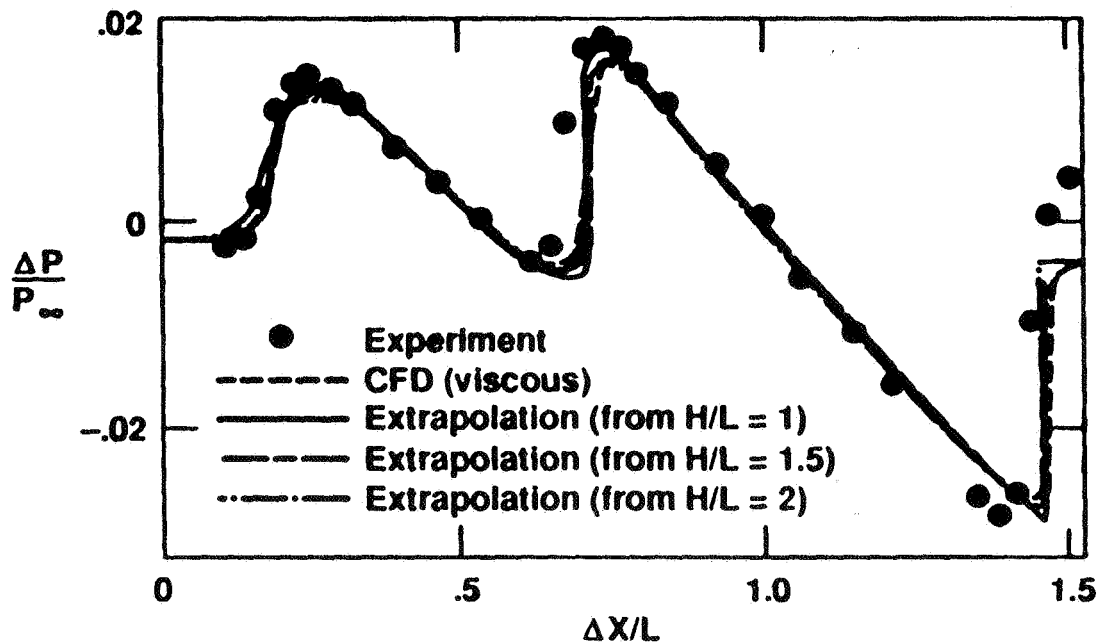
DELTA-WING BODY VALIDATION

The final test case was a delta wing mounted on an ogive-cylinder fuselage. The airfoil section was a 5%-thick double-wedge; the wing leading edge sweep was 69 deg. and the trailing edge was swept forward 10 deg. This model was tested at Mach numbers of 1.68 and 2.7, and at lift coefficients of 0, 0.08, and 0.15. The higher Mach number swept the Mach lines further back and substantially increased the size of the domain required to propagate the shock structure to a given altitude from the body. Furthermore, the higher angles of attack generated strong shocks that necessitated good grid resolution in the far field. Also, the sting on this model ramped down from the fuselage diameter to about half its thickness, and this effect required accurate modeling in the computations to match the expansion and tail shock correctly.

The figure shows correlations at an altitude of 3.1 body lengths. The extrapolation interface was varied to determine if near-field effects were still present, and it is clear that at one body length, the flow is sufficiently linear and axisymmetric for sonic boom extrapolation purposes. Subsequent studies have shown this to be valid as close as one-half body length altitude. The wing span may be a better metric for sensitivity to non-axisymmetric features, and so it is worth noting that for this case, the altitude of one-half body length corresponds to one full wing span.

SENSITIVITY TO EXTRAPOLATION ALTITUDE

Pressure signal at $H/L = 3.1$



CONCLUSIONS FROM PRIOR RESEARCH

The code calibration studies to date have provided great insight into the applicability of CFD to sonic boom prediction. At this point, it can be said without reservation that CFD can be used in conjunction with quasi-linear extrapolation methods to predict sonic booms in the near and far flow field accurately. In many ways, CFD paves the way to much more rapid progress in sonic boom minimization. Errors in wind tunnel data may arise from flow quality, intrusive probes, and model geometry, none of which are present in a good computational discretization. Furthermore, CFD offers fast turnaround and low cost, so high-risk concepts and perturbations to existing geometries can be investigated quickly. It is clear that at this time, the role of the wind tunnel in low-boom model design is to benchmark progress at significant intermediate stages and at the final design point of numerical model development.

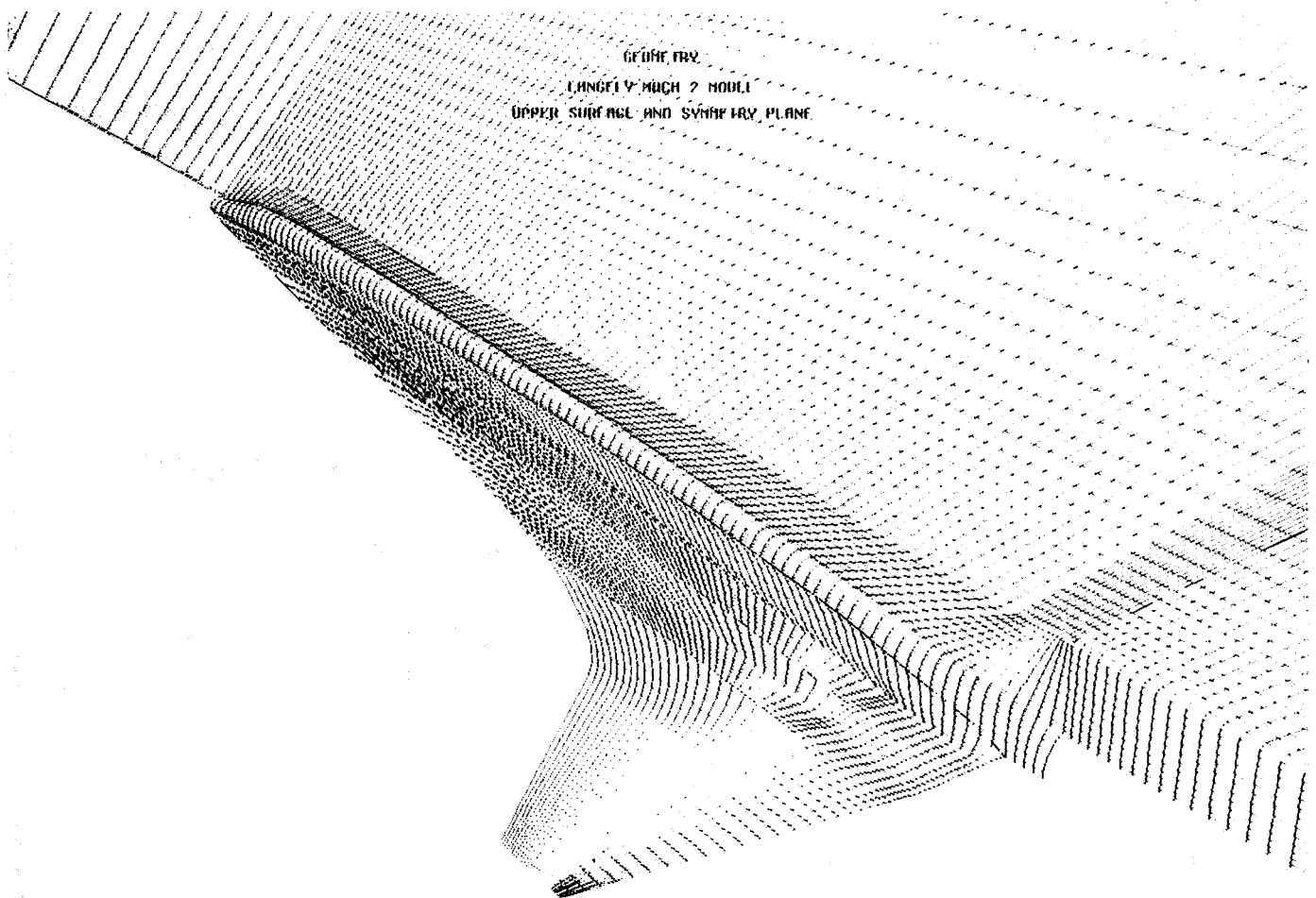
Our studies have demonstrated that for HSCT concepts, Euler (inviscid) flow analysis is sufficient for accurate sonic boom predictions. The most critical aspect is resolving the geometry and flow field. This requires fine surface grids and solution-adaptive grid procedures to keep the computational expense down. The computational domain needs to extend beyond the range of nonlinearities and non-axisymmetric (at least in a local sense) flow; as rules of thumb, an overpressure ratio (dp/p) of less than one-half and an altitude of at least on wing span are required to employ linear methods to propagate the pressure to the far-field.

CONCLUSIONS FROM PRIOR RESEARCH

- Euler equations simplest sufficient flow model
- Geometry and grid resolution are critical
- Solution domain must extend beyond nonlinear and nonaxisymmetric range of flow ($dp/p < .5$, $z > L/2, b$)

LOW-BOOM MODEL INVESTIGATION

The next phase of developing sonic boom prediction methodologies focuses on low-boom vehicle concepts. NASA Langley-developed low-boom models for cruise Mach numbers of 2 and 3 were tested in the 9x7-foot tunnel. The geometry of the Mach 2 model included flow-through nacelles, which increased the complexity of the computational model significantly. A multi-block grid, shown below, was generated for this body and solutions are being run to correlate with the wind tunnel data.



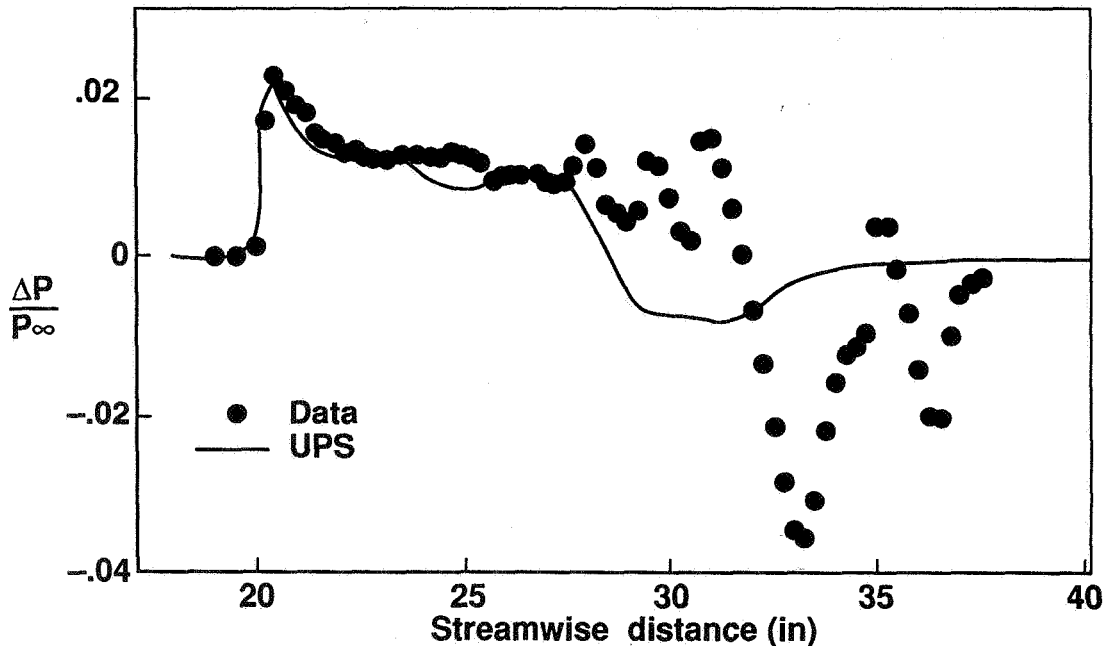
LOW-BOOM MODEL INVESTIGATION

A preliminary result has been obtained for the Mach 2 cruise condition on a geometry that included only the wing and fuselage. The front half of the signature is seen to correlate fairly well with the data, but significant discrepancies are apparent on the rear half. The large expansion and trailing shocks in the data are thought to be due to the sting and strain gauge disturbances, which were not modeled computationally. Further investigations are in progress to understand this result fully. Solutions will be obtained with blocked, flow-through, and power-on nacelles also.

MACH 2 LOW-BOOM MODEL

Sonic Boom at $H/L = 1$

$M = 2$ $\alpha = 0.69$

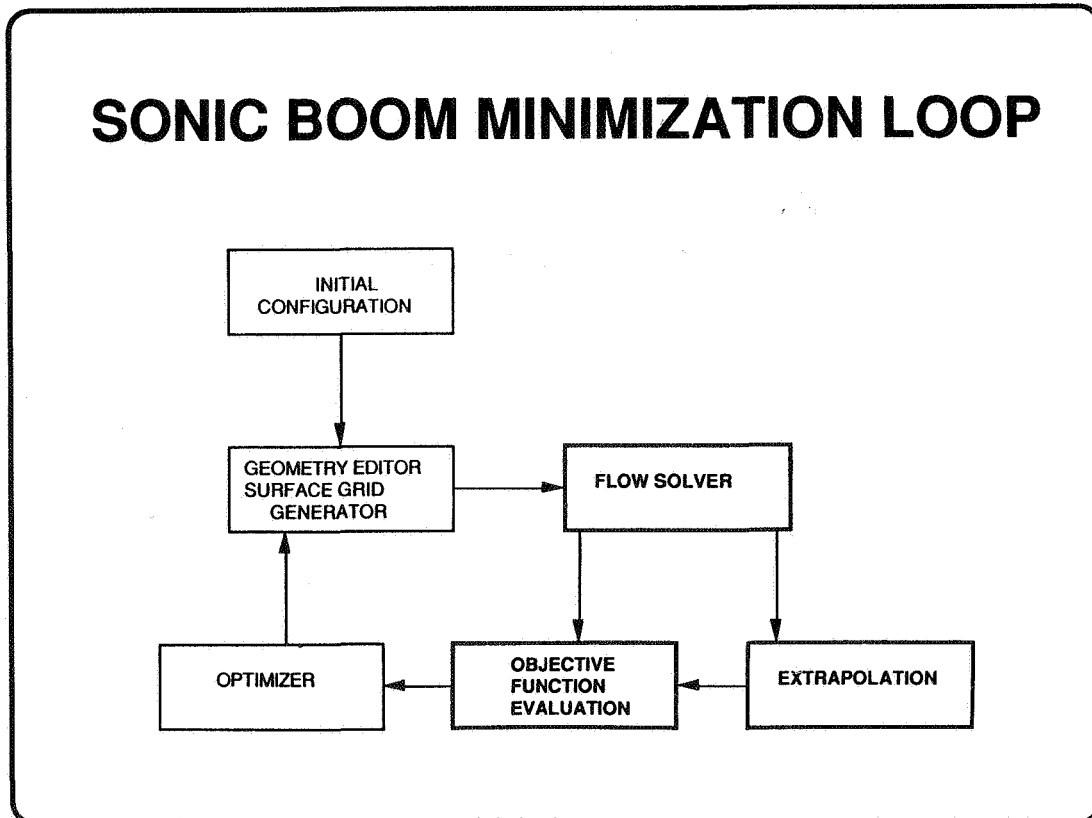


CURRENT RESEARCH OBJECTIVES

As mentioned earlier, attention is now being turned to higher-order effects on sonic boom. This research includes the effect of the propulsion system, which impacts the sonic boom through flow blockage from the pylons and nacelles, inlet spillage, and the exhaust plume. The SA-1150 model will be used to investigate the effect of nacelle placement, while computational studies are underway at NASA Langley to assess the plume effects.

Economic viability is another major thrust now being addressed. This is being pursued through simultaneous aerodynamic optimization and sonic boom minimization. Recognizing that supersonic flight over land is useful only if the resulting vehicle is efficient, these two disciplines need to be linked during the design. The flow chart below demonstrates conceptually how to proceed toward a design that derives the highest aerodynamic efficiency from a vehicle that also achieves desired sonic boom levels. The CFD solution is used both to predict the aerodynamics and sonic boom. Then, a gradient-type optimizer perturbs a parameter space defining the vehicle geometry to reduce the objective function (for example, a combination of sonic boom loudness and drag-to-lift ratio). The new geometry is generated and the iteration loop continues. A good baseline configuration is desirable because of the computational expense involved in this procedure.

The successful conclusion of this effort will yield several valuable products. First, a proof-of-concept configuration will be obtained which demonstrates good aerodynamic efficiency and achieves target sonic boom levels. Also, a base of knowledge about propulsion system effects and integration will be developed. Finally, validated codes will be produced that will be available to impact the HSCT design.



SUMMARY

To summarize the sonic boom prediction effort thus far, we can state that code validation studies are complete and the numerical/physical modeling requirements are well understood. Currently, efforts are being focused on low-boom model development and verification, along with an investigation of propulsion system effects on optimized models. A major milestone in the upcoming year will review progress toward a low-boom design that has good aerodynamic efficiency.

It should also be noted that both NASA Ames and NASA Langley Research Centers will be using the HSCT as a demonstration problem for multidisciplinary numerical analysis on massively parallel computers under the High Performance Computing and Communications Program (HPCCP). The advances in design methodology sought in this program will be of significant and direct benefit to the HSRP effort.

SUMMARY

- **CFD validation complete**
- **Follow-on research In progress:**
 - Complex geometry**
 - Propulsion effects**
 - Optimization**
- **Major milestone to meet in early CY92**
- **HPCCP to contribute**

FUTURE RESEARCH

Several avenues merit further exploration. Regardless of low-boom designs, many operational issues for supersonic aircraft must be addressed. Some of these are the prediction of off-track booms, which generally receive little attention but may be significant. Also, superbooms generated during acceleration and climbout may endanger structures in their path, and atmospheric focusing and refraction may affect the availability of supersonic corridors. Nonlinear analysis can be brought to bear upon these phenomena.

Looking beyond the current HSCT development cycle opens up the possibility of advanced concepts in supersonic vehicles that are best investigated computationally until a promising design emerges. The use of oblique wings, canards, and unconventional nacelle installations may offer improved sonic boom performance with superior aerodynamics as well.

POTENTIAL FUTURE RESEARCH

- **Off-track boom prediction**
- **Maneuvering booms**
- **Caustics**
- **Advanced concepts**

REFERENCES

1. Mendoza, J., and Hicks, R., "Further Studies of the Extrapolation of Near-Field Overpressure Data," NASA TM-X-2219, 1971.
2. Cheung, S., Edwards, T., and Lawrence, S., "Application of CFD to Sonic Boom Near- and Mid-Field Prediction," AIAA paper 90-3999.
3. Cliff, S., and Thomas, S., "Euler/Experiment Correlation of Sonic Boom Pressure Signatures," paper to be presented at AIAA 9th Applied Aerodynamics Conference, Baltimore, MD, Sept. 23-26, 1991.
4. Madson, M., "Sonic Boom Predictions for Three Generic Models Using a Solution-Adaptive Full Potential Code," paper to be presented at AIAA 9th Applied Aerodynamics Conference, Baltimore, MD, Sept. 23-26, 1991.

omit

Session V. Sonic Boom (Aerodynamic Performance)

Sonic Boom Configuration Minimization
Robert A. Sohn, Douglas Aircraft Company

THIS PAGE INTENTIONALLY BLANK

Sonic Boom Configuration Minimization

511-05
12001

by

R. A. Sohn
Douglas Aircraft Co.

May 15, 1991
Williamsburg, Virginia

The pressure pulse on the ground accompanying supersonic overflights is popularly known as a "sonic boom." It differs significantly from the pressure pulse accompanying subsonic overflights in that it typically contains two shocks (front and rear). These shocks are audible, and, due to their impulsive nature and rapid onset, can often times be startling and annoying. To a first approximation, the annoyance caused by these shocks constitutes the current sonic boom "problem" for supersonic commercial transports.

Theoretically, it is not necessary to have shocks reach the ground for supersonic overflight. Techniques that carefully control the growth of aircraft volume and lift can be employed to eliminate the shocks. The primary drawback to these techniques is the fact that they typically require long, slender bodies outside the range of feasible structures for today's technology. The audible sonic boom, then, is a fallout of current technology, and not a necessity of supersonic flight.

Technology will eventually advance to the point where shockless booms are feasible for commercial supersonic aircraft, opening up large portions of the commercial air transport market that are currently landlocked to supersonic aircraft, and creating a significant business opportunity for those who are poised to exploit the new technology. For this reason it is important to continue sonic boom minimization research, even in the face of considerable skepticism.

THE SONIC BOOM "BIG PICTURE"

- AUDIBLE SONIC BOOM IS A FALLOUT OF CURRENT TECHNOLOGY - NOT A NECESSITY OF SUPERSONIC FLIGHT

- TECHNOLOGY WILL EVENTUALLY ENABLE SHOCKLESS BOOMS

- INCORPORATION OF LOW-BOOM TECHNOLOGY INTO 2ND GENERATION SST:
 - DESIRABLE....YES
 - FEASIBLE.....???

- LOW-BOOM TECHNOLOGY EVENTUALLY = \$\$\$

The current low-boom technology is focussed on shaping the pressure pulse so as to minimize those aspects that most contribute to the loudness of the boom, primarily the shock strengths. Pioneering work by Seebass and George in the early 1970's¹ showed that a body of revolution could be defined to generate a specified sonic boom shape that minimized the shock strength, maximum overpressure, or the impulse of the waveform. This body of revolution can then be approximated with wing/body configurations by matching the equivalent area distribution with the proper control of aircraft volume and lift. This process has been formalized into a computer program by Darden called SEEB.²

The SEEB code is the most widely used tool for sonic boom minimization today. It has proven to be a powerful tool for designing low-boom configurations and has led to the design of several sonic boom wind tunnel models. Some of the limitations of the SEEB code include a restriction to two basic waveform types (front shock and overpressure minimized), and a lack of adequate treatment of off-track waveforms (SEEB only addresses the undertrack waveform).

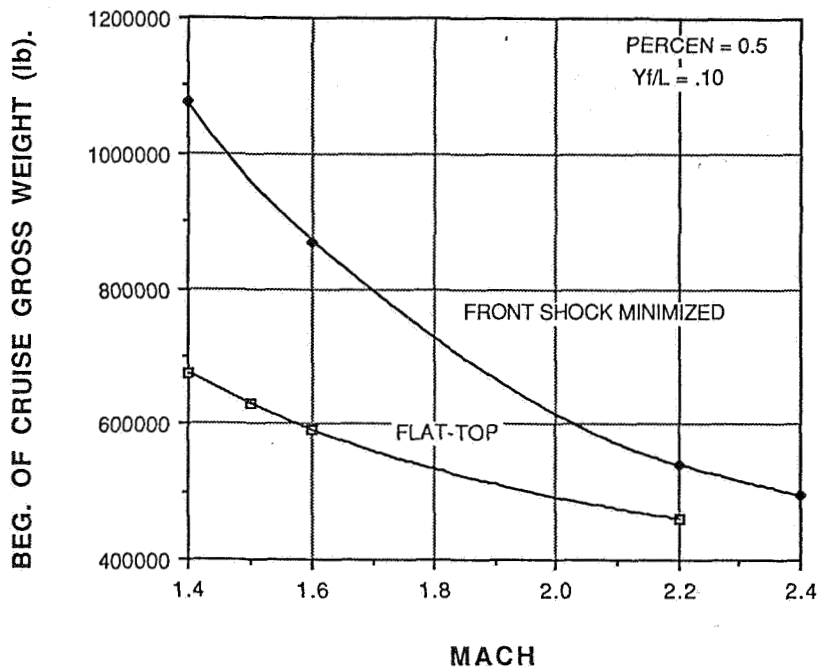
CURRENT LOW-BOOM TECHNOLOGY

WAVEFORM SHAPING

- **CURRENT ACTIVITY CENTERS ON AREA DISTRIBUTIONS FROM SEEB COMPUTER CODE (SEEBASS/GEORGE SCHEME)**
 - **GOOD STARTING POINT (IT WORKS)**
 - **LIMITED IN PARAMETER SPACE**
 - **LIMITED TO UNDERTRACK WAVEFORM**

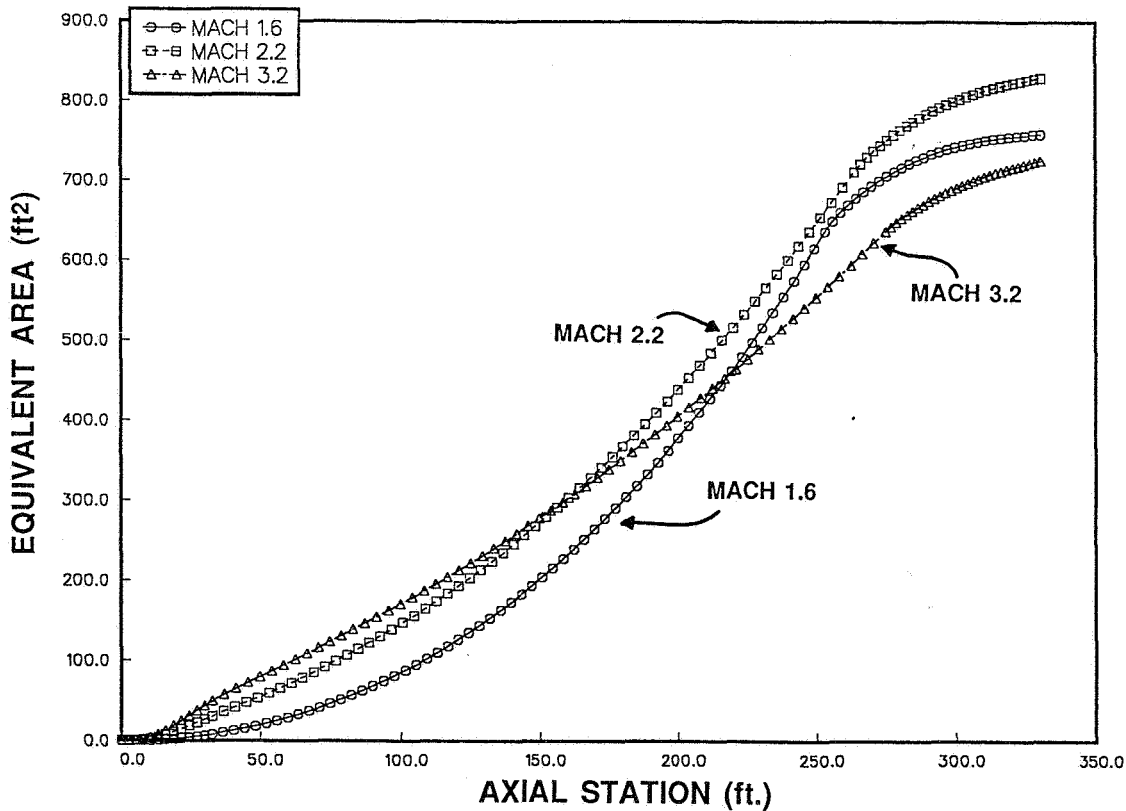
The choice of Mach number for a low-boom aircraft is crucial to the success of the resultant design. The physics of waveform shaping require vastly different combinations of shapes and weights to achieve similar loudness levels on the ground. The figure below shows the theoretical beginning of cruise weight allowable for low-boom configurations vs. design Mach number for the two classes of waveforms to achieve equal loudness levels. Two things are immediately evident; higher Mach numbers severely limit the weight of low-boom aircraft, and the flat-top (overpressure minimized) waveform is much more restrictive than the front shock minimized waveform, particularly at lower Mach numbers.

MACH NUMBER IMPACT ON GROSS WEIGHT EQUAL LOUDNESS CURVES



The choice of Mach number strongly impacts the shape of the low-boom aircraft as well as the weight. Shown below are equivalent areas of equal loudness for three Mach numbers; 1.6, 2.2, and 3.2. Whereas the previous figure showed a clear advantage to designing for lower Mach numbers, in this figure it can be seen that the equivalent area distribution required at Mach 1.6 is much more slender than that required at Mach 2.2 or 3.2. This can cause problems in several areas including structures, payload capability, and balance. This figure, coupled with the previous one, illustrates some of the trade-offs involved in choosing a design Mach number for low-boom aircraft. The best low-boom design is one that represents the optimum compromise between all of the various parameters.

EQUAL LOUDNESS EQUIVALENT AREAS



Based on some of the data shown previously, Douglas Aircraft conducted low-boom configuration studies under the 1990 NASA contract with a mixed Mach number configuration flying at Mach 1.6 overland and Mach 3.2 overwater. Mach 1.6 was chosen overland based on sonic boom criteria (primarily weight considerations) for a front shock minimized waveform, and Mach 3.2 was chosen overwater to maintain the maximum level of productivity possible. The initial cruise weight and altitude were set at 669,000 lb. and 42,000 ft. respectively. Internal SEEB parameters include a nose bluntness ratio of 0.1, secondary pressure rise ratio of 0.7, and front/rear shock ratio of 1.0.

The sonic boom goal for 1990 is to achieve a Stevens' MkVII perceived loudness³ level of 90 PLdB undertrack at the beginning of cruise. The MkVII loudness metric is appropriate for high-energy, impulsive sounds and has been proven accurate for estimating and tracking human subjective response to sonic booms, including shaped booms.⁴

DAC 1990 CRAD DESIGN

- MACH 1.6 OVERLAND / MACH 3.2 OVERWATER. (30 % OVERLAND MISSION)
- 669,000 lb. BEGINNING OF CRUISE WEIGHT
- 42,000 ft. BEGINNING OF CRUISE ALTITUDE
- SEEB PARAMETERS:
 - NOSE BLUNTNESS (Y_f/L) = 0.1
 - SECONDARY PRESSURE RISE = 0.7
 - FRONT/REAR SHOCK RATIO = 1.0
- SONIC BOOM DESIGN GOAL - STEVENS MkVII LOUDNESS < 90 PLdB

By the end of the contract work period a low-boom configuration was defined to meet the desired sonic boom goals. The configuration, shown below, is 355 ft. long, and carries 286 passengers mixed class. The beginning of cruise, undertrack sonic boom (also shown) has a perceived loudness of 89 PLdB, 1 dB under the design goal. The desired front shock minimized shape was achieved in the front portion of the waveform with a 0.6 psf. front shock. Some weak shocks persisted in the middle of the waveform. These shocks slightly increase the loudness of the boom.

Salient characteristics of the low-boom aircraft, named the SB14, include a high sweep wing to generate the desired lift distribution, two aft mounted engines to smooth the volume distribution, and wing tips extending beyond the aft fuselage to smooth the transition back to free stream flow. It is also worthy to note that the SB14 has no horizontal tail.

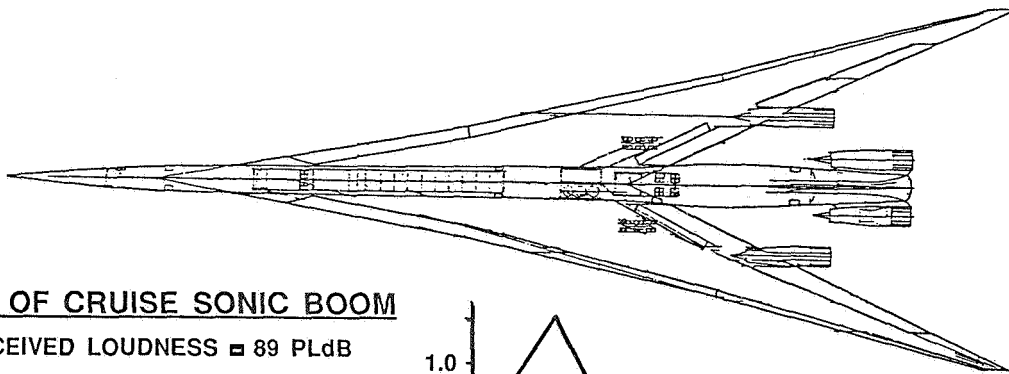
SONIC BOOM STATUS

SEPT. 1990

MACH 3.2 OVERWATER/ MACH 1.6 OVERLAND

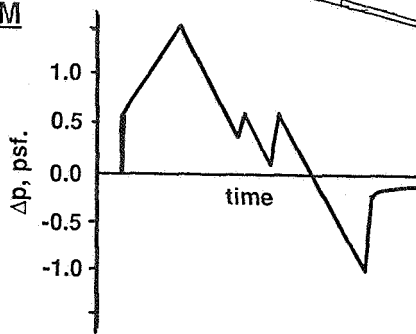
286 PASSENGERS

355 FT. LENGTH



BEG. OF CRUISE SONIC BOOM

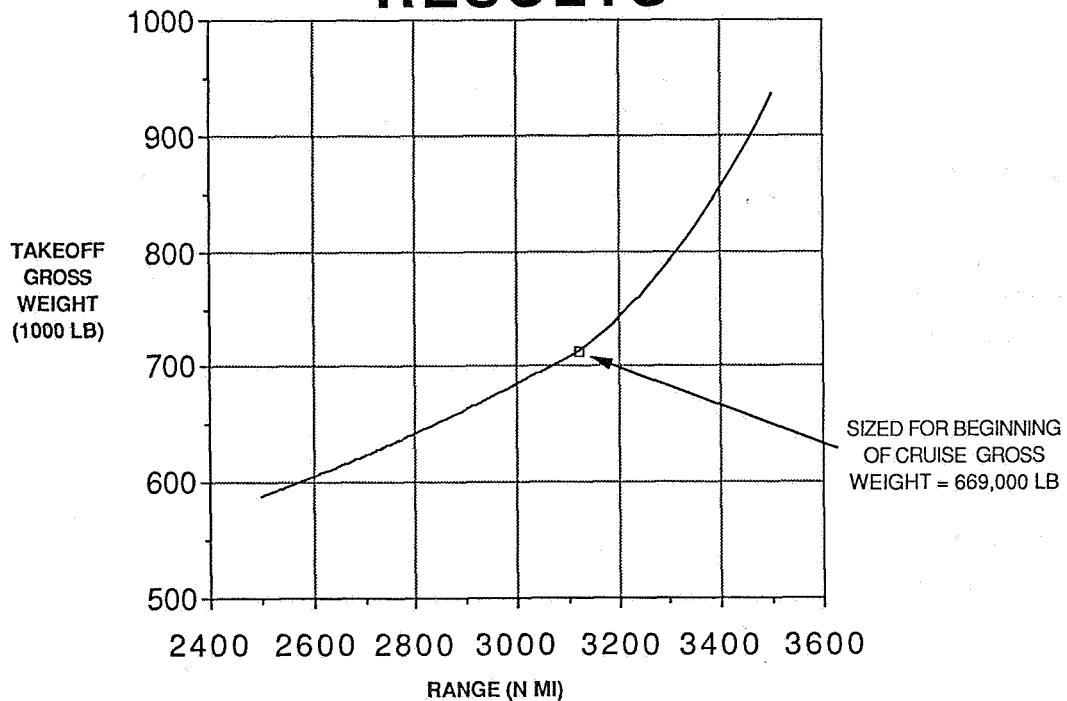
- PERCEIVED LOUDNESS = 89 PLdB
- SHOCK STRENGTH = 0.6 psf.
- MAX. OVERPRESSURE = 1.5 psf.



MCDONNELL DOUGLAS CORPORATION PROPRIETARY RIGHTS ARE INCLUDED IN THE INFORMATION DISCLOSED HEREIN. RECIPENT BY ACCEPTING THIS DOCUMENT AGREES THAT NEITHER THIS DOCUMENT NOR THE INFORMATION DISCLOSED HEREIN NOR ANY PART THEREOF SHALL BE REPRODUCED OR TRANSMITTED TO OTHER DOCUMENTS OR USED OR DISCLOSED TO OTHERS FOR MANUFACTURING OR ANY OTHER PURPOSE EXCEPT AS SPECIFICALLY AUTHORIZED IN WRITING BY MCDONNELL DOUGLAS CORPORATION.
UNPUBLISHED - CREATED ON PREPARATION DATE OF THIS DOCUMENT. ALL RIGHTS RESERVED UNDER THE COPYRIGHT LAWS BY MCDONNELL DOUGLAS CORPORATION.

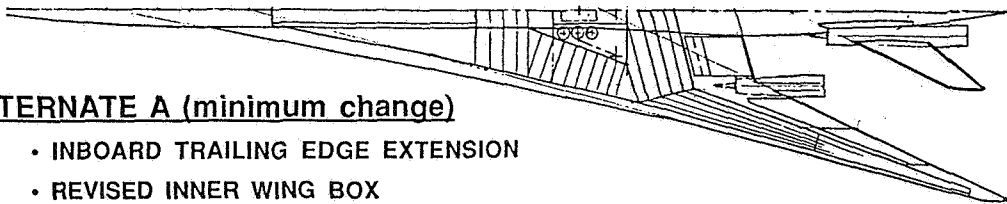
The overall performance of the SB14 suffers from poor low-speed aerodynamic characteristics, poor wing structural qualities, and balance (high speed trim) problems. The figure below shows that the mission range is 3150 n.mi. for a beginning of cruise weight of 669,000 lb., roughly half of the 6500 n.mi. baseline design goal. Unlike most aircraft, the SB14 cannot be sized up to increase the range because the sonic boom design point must be strictly adhered to.

PERFORMANCE AND SIZING RESULTS



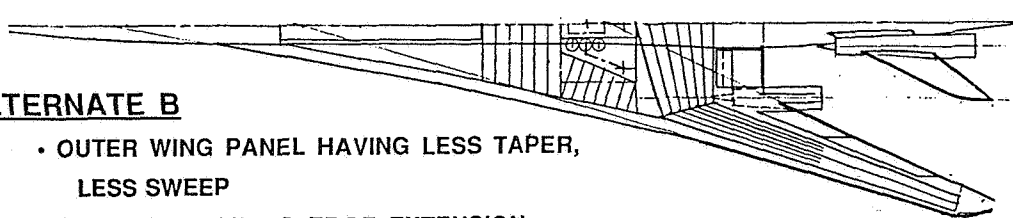
Several configuration modifications have been identified for the SB14 to improve its overall performance. These modifications focus on bringing down the weight of the wing and improving the low speed aerodynamics and high speed trim characteristics. Two of the potential modifications are shown below. Alternate A represents a minimum planform change approach where the inner wing box is modified and the inboard trailing edge is extended in conjunction with mounting the two aft engines on a vee-tail. Alternate B represents a more drastic modification where the outer wing panel is unswept, the outboard wing chord is increased, and a large chord inboard wing box is incorporated along with the modifications of Alternate A. It is believed that these modifications can bring the performance of the low-boom aircraft back up to par with the baseline standard.

POTENTIAL CONFIGURATION MODS



ALTERNATE A (minimum change)

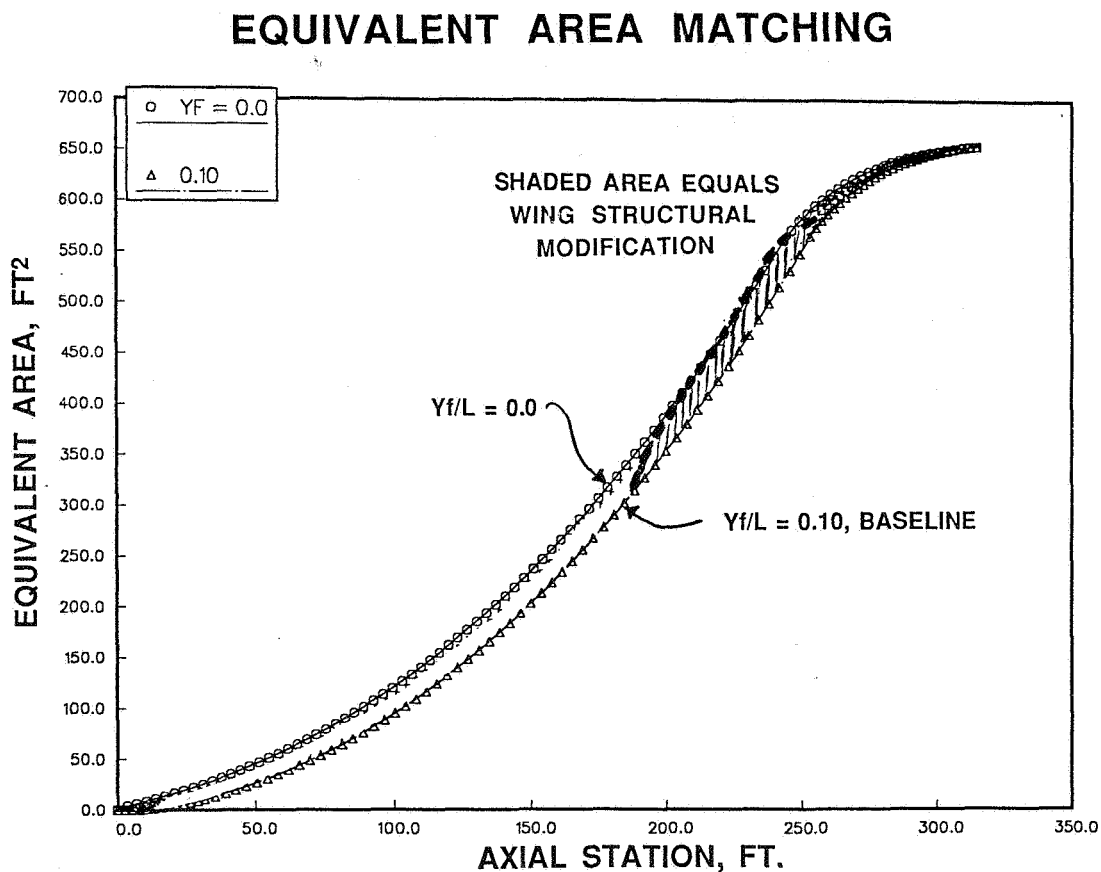
- INBOARD TRAILING EDGE EXTENSION
- REVISED INNER WING BOX
- INBOARD AFT ENGINES ELEVATED ON AFT VEE TAIL



ALTERNATE B

- OUTER WING PANEL HAVING LESS TAPER, LESS SWEEP
- INBOARD TRAILING EDGE EXTENSION
- LARGE CHORD INBOARD WING BOX
- INBOARD AFT ENGINES ELEVATED ON AFT VEE TAIL

The configuration modifications shown in the previous figure can be incorporated with little to no impact on the sonic boom if they are implemented carefully. In the figure below two equivalent area distributions are shown. Both represent ground waveforms less than or equal to the 90 PLdB goal. One of the area distributions was generated for a nose bluntness factor of 0.10 corresponding to the 1990 design point. The other area distribution was generated with a nose bluntness factor of 0.0. The shaded area between the two curves represents the estimated area increase from the modifications shown previously for Alternate A. By increasing the nose bluntness (decreasing the factor) it is possible to incorporate the desired configuration modifications with little to no sonic boom penalty.



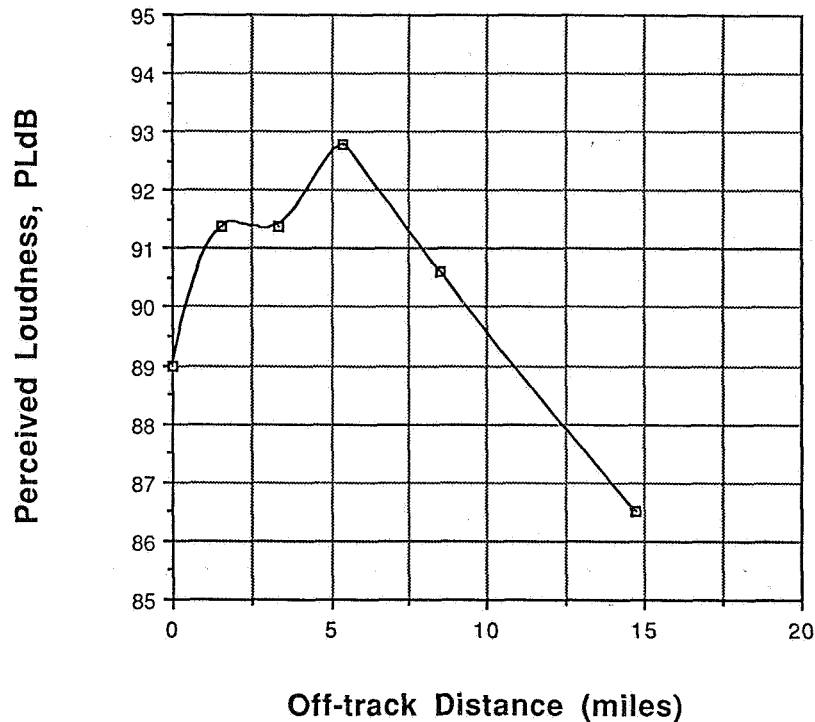
The previous figure showed that it is possible to incorporate the desired modifications to the SB14 wing by increasing the nose bluntness of the configuration. The corresponding increase in wave drag from such an increase is shown in the table below. By changing the nose bluntness parameter (Y_f) from 0.10 to 0.0 the wave drag is increased by 13.7% which in turn decreases the L/D_{max} from 8.576 to 8.446 (1.52%). This represents a minimal aerodynamic impact and is not significant compared to the potential weight savings that can be achieved through implementing the planform changes mentioned previously. These studies indicate that the performance of the SB14 can be brought up to the baseline standard with minimal changes to the sonic boom levels and the aerodynamic drag.

IMPACT OF NOSE BLUNTNES ON AERODYNAMIC CHARACTERISTICS

Y_f	C_{dwave}	ΔC_{dwave} (%)	$C_{dmin(tot)}$	L/D_{max}	$\Delta L/D_{max}$ (%)
0.10	.001373	0.0	.00707	8.576	0.0
0.05	.001430	4.2	.00712	8.555	-0.24
0.00	.001561	13.7	.00723	8.446	-1.52

It was mentioned earlier that the SEEB code is limited to undertrack waveforms. This is not usually considered to be a serious limitation because for most aircraft the sonic boom levels decrease off-track, primarily because of the increased attenuation realized over greater propagation distances. The plot shown below of loudness level vs. off-track distance at the beginning of cruise indicates that this is not the case for the SB14. The off-track boom reaches a peak level of 92.7 PLdB before attenuating out to the cutoff value of 86.5 PLdB on the edge of the carpet. This atypical increase in off-track levels is the result of a lack of attention to off-track area growth during the initial design stage for the SB14. Currently no methodology exists for minimizing off-track booms, though it is clearly prescribed by results such as these.

Loudness Level vs. Off-Track Distance



SUMMARY

- **CURRENT EFFORTS LIMITED TO SEEB CODE, EXTENSIONS OF PARAMETER SPACE MAY BE USEFUL**
- **SEEB F-FUNCTION AND DESIGN PARAMETERS EXERT CONSIDERABLE INFLUENCE ON AIRCRAFT GEOMETRY**
- **1990 STUDY AIRCRAFT MEETS LOW BOOM CRITERIA UNDERTRACK BUT HAS UNACCEPTABLE PERFORMANCE**
- **PLANFORM AND STRUCTURAL MODS APPEAR FEASIBLE TO ENHANCE PERFORMANCE**
- **OFF-TRACK LEVELS MUST BE MONITORED AND CONTROLLED**

FINAL THOUGHT

QUESTION IS NOT IF LOW-BOOM AIRCRAFT CAN BE DESIGNED,

BUT RATHER WHEN IT WILL BE DESIGNED,

AND WHEN WILL THE TECHNOLOGY BE AVAILABLE.

TRUE FINAL THOUGHT (I PROMISE)

**" IF YOU THINK ABOUT ANYTHING LONG ENOUGH
SOMETHING IS BOUND TO POP INSIDE YOUR HEAD
BESIDES A COLD"**

- VIN SCULLY

REFERENCES

1. George, A.R., and Seebass, R., "Sonic Boom Minimization Including Both Front and Rear Shocks", AIAA Journal, 9 (10), 2091-2093, October 1971.
2. Darden, C.M., "Sonic Boom Minimization With Nose Bluntness Relaxation", NASA TP 1348, 1979.
3. Stevens, S.S., "Perceived Level of Noise by Mark VII and Decibels (E)," JASA, 51 (2) (Part 2), pp. 575-601, 1972.
4. Niedzwiecki, A., and Ribner, H.S., "Subjective Loudness of Sonic Boom: N-Wave and Minimized ('Low Boom') Signatures," UTIAS TN-215, 1977.

Session V. Sonic Boom (Aerodynamic Performance)

omit

Sonic Boom Predictions Using a Modified Euler Code
Dr. Michael J. Siclari, Grumman Corporate Research Center

THIS PAGE INTENTIONALLY BLANK

N94-33474

SONIC BOOM PREDICTIONS USING A MODIFIED EULER CODE⁺

512-71
12002

M.J.Siclari
Grumman Corporate Research Center
Bethpage, New York

First Annual
HIGH-SPEED RESEARCH WORKSHOP
May 14-16, 1991
Williamsburg, Virginia

+ This work was sponsored by NASA Langley Research Center, Advanced Vehicle Division,
Dr. Christine Darden

PRECEDING PAGE BLANK NOT FILMED

INTRODUCTION

The environmental impact of a next generation fleet of high-speed civil transports (HSCT) is a great concern in the evaluation of the commercial development of such a transport. One of the potential environmental impacts of a high speed civilian transport is the sonic boom generated by the aircraft and its effects on the population, wildlife, and structures in the vicinity of its flight path. If an HSCT aircraft is restricted from flying overland routes due to excessive booms, the commercial feasibility of such a venture may be questionable.

NASA has taken the lead in evaluating and resolving the issues surrounding the development of a high speed civilian transport through its High-Speed Research Program (HSRP).

The present paper discusses the usage of a Computational Fluid Dynamics (CFD) nonlinear code in predicting the pressure signature and ultimately the sonic boom generated by a high speed civilian transport.

NASA has designed, built, and wind tunnel tested two low boom configurations for flight at Mach 2 and Mach 3 (see Ref. 1). Experimental data was taken at several distances from these models up to a body length from the axis of the aircraft. The near field experimental data serves as a test bed for computational fluid dynamic codes in evaluating their accuracy and reliability for predicting the behavior of future HSCT designs.

Sonic boom prediction methodology exists which is based on modified linear theory. These methods can be used reliably if near field signatures are available at distances from the aircraft where nonlinear and three dimensional effects have diminished in importance. Up to the present time, the only reliable method to obtain this data was via the wind tunnel with costly model construction and testing.

It is the intent of the present paper to apply a modified three dimensional Euler code to predict the near field signatures of the two low boom configurations recently tested by NASA.

APPROACH

In order to compute the supersonic flow field about a configuration, a three dimensional Euler code called MIM3D (Multigrid-Implicit-Marching) was modified to accommodate the unique prediction of sonic boom signatures below and aft of an aircraft configuration. The numerical scheme is based on a Jameson type finite volume vertex Runge-Kutta scheme (Ref.2). Further documentation of the present method as applied to high speed flows can be found in Refs. 3 and 4.

The three dimensional unsteady Euler equations are solved using an implicit marching technique. Stability and smooth shocks are maintained with the addition of second and fourth order dissipation. The steady state solution at each marching plane is obtained using an explicit multi-stage Runge-Kutta time integration scheme with local time stepping and implicit residual smoothing to accelerate convergence. To further accelerate convergence to a steady state solution in each marching plane, a multigrid scheme can also be applied in the crossflow plane.

The solution is started at the apex of the configuration by assuming a small conical nose cap based on the geometry of the configuration at the first step. The unique aspects of this technique is that it is very fast and requires very little memory for large grids.

The sonic boom version of this code called MIM3DSB has been modified to retain accuracy for sonic boom computations. Unlike aerodynamic computations, where only accurate surface data needs to be predicted, sonic boom computations require accuracy in the field below and aft of the aircraft. For example, to predict a pressure signature just one body length below an HSCT flying at Mach 3, the computation must be carried out with sufficient accuracy to 3 body lengths aft of the end of the configuration. Since the same number of grid points normal to the body are available, a loss in resolution occurs as the computation proceeds aft of the end of the vehicle.

Some of the key modifications incorporated into the present method to retain accuracy are as follows:

- adaptive outer grid boundary that automatically senses the bow shock wave and adapts the grid
- downstream boundary that corresponds to the freestream Mach cone
- multiblock grid that allows for a switch from a wing-body type grid with a slit for wake matching to a simple polar grid aft of the configuration
- sonic boom pressure signature output at user specified distances below the aircraft. These signatures can then be extrapolated to the ground using sonic boom extrapolation methods.

The present sonic boom Euler code has been applied to axisymmetric projectiles and wing-body configurations in Ref. 5.

Figure 1 shows a side view of a typical grid topology used in the present Euler code for the Mach 3 low boom configuration. The aircraft is extended with a sting. In this case, the sting represents the actual sting used to support the model in the wind tunnel. The sting then terminates in a Mach cone surface where freestream boundary conditions are applied. The grid is then restricted to lie between the outer boundary just outside the bow wave and a downstream Mach surface. The outer boundary is progressively adapted to the shape of the bow wave by the computation. Essentially, the outer boundary is part of the solution. To compute a pressure signature at just one body length normal to the axis of the Mach 3 aircraft, the computation must be carried out 3 to 4 body lengths aft of the aircraft. As illustrated by Figure 1, if the grid topology was extended to the axis of the aircraft, a loss of accuracy of the solution would occur due to the increase in distance from the aircraft axis to the outer grid boundary as the computation proceeded downstream.

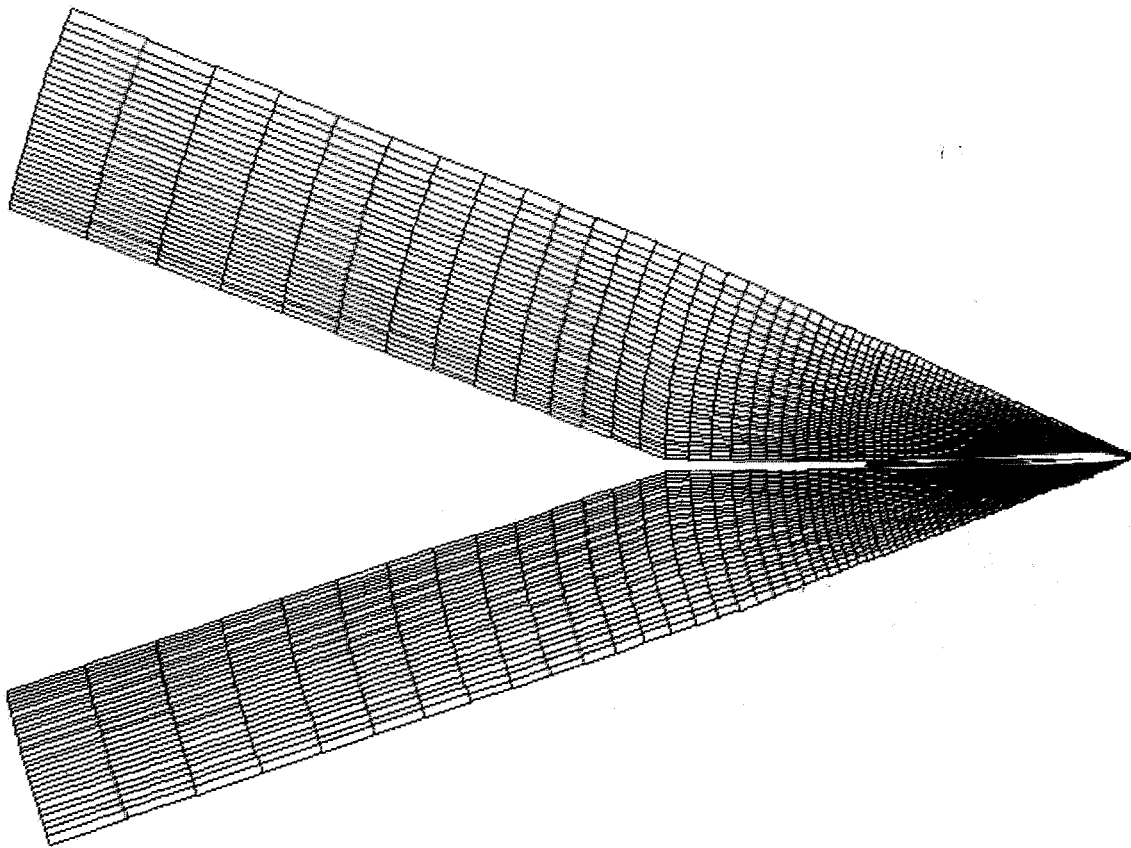


Figure 1 Side View of Grid Topology Used For Sonic Boom Computations

Figure 2 shows the overall grid topology for the Mach 3 low bow configuration. A typical stacked crossflow plane grid topology is used over the aircraft. At the end of the wing, the grid is switched to a new block with a polar grid containing the sting. Hence, the computation is performed using two grid blocks. One contains the aircraft, and the second block, the sting and Mach surface. The furthest distance downstream at which the computation remains valid is determined by the length of the sting extension. This occurs because the sting effects the strength of the tail shock. If the sting is too short, the Mach surface, where artificial freestream boundary conditions are imposed, will effect the formation of the tail shock. Typically, the length of the sting varied by a half to one aircraft length. This allowed for computations of pressure signatures from one to three body lengths normal to the aircraft axis. The length of the sting also effects accuracy for a given grid resolution. As the sting is made longer, and distance between outer boundary and Mach surface increases causing a loss in accuracy given the same number of mesh points.

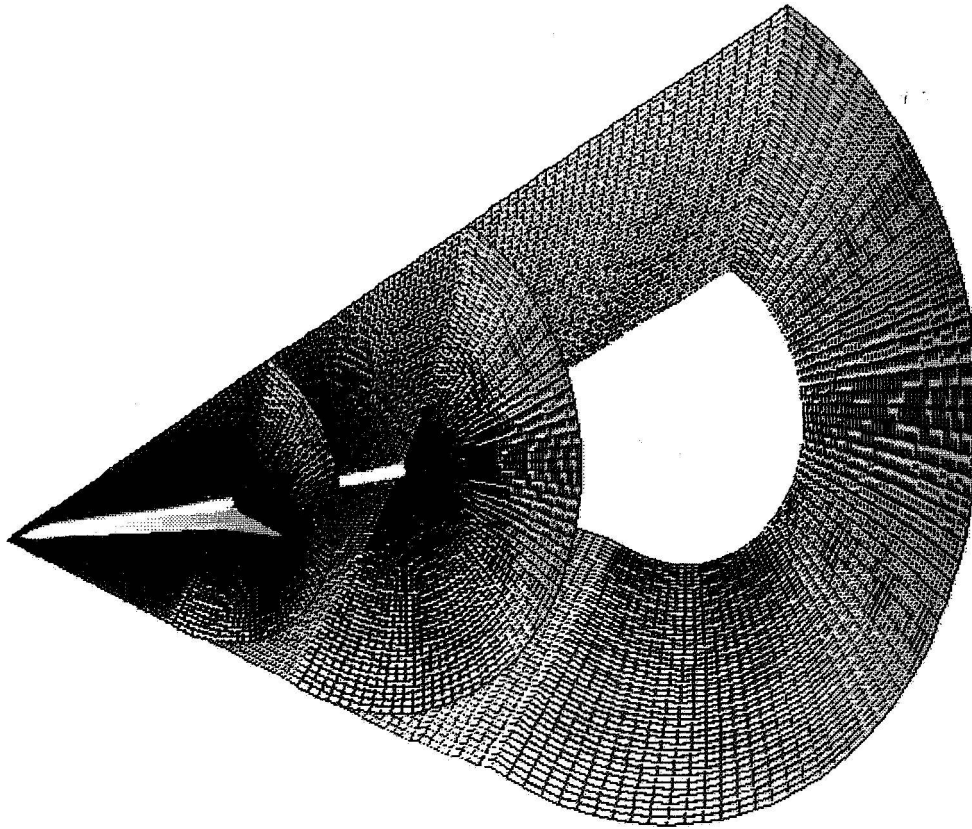


Figure 2 Three Dimensional View of Sonic Boom Grid Topology

Figure 3 shows the geometry and computed aft pressure contours at $M_\infty = 3.0$, $\alpha = 1.97^\circ$ for NASA's Mach 3 low boom configuration. The Mach 3 model has a needle nose and a highly swept wing which cranks to a supersonic leading edge. The cranked wing generates a strong shock as indicated by the isobars. The fuselage is also fitted to a sting where a shock at the attachment point to the sting is also indicated by the isobars. As mentioned earlier, the solution is carried out on two mesh blocks. The resolution of the mesh block containing the aircraft was (89×91) in the crossflow plane with 106 marching steps. The resolution of the second block was (95×95) by 127 marching steps for a computation carried out to three body lengths normal to the aircraft axis or 12 body lengths downstream of the aircraft. The second block does not use a fixed axial step size but a stretching function that gradually increases the step size. The axial step size far downstream can be as much as one-half the aircraft body length. Hence, approximately 850,000 points were used to compute the flow in the vicinity of the aircraft and approximately 1.1 million points were used to compute the flow to 15 body lengths downstream of the aircraft.

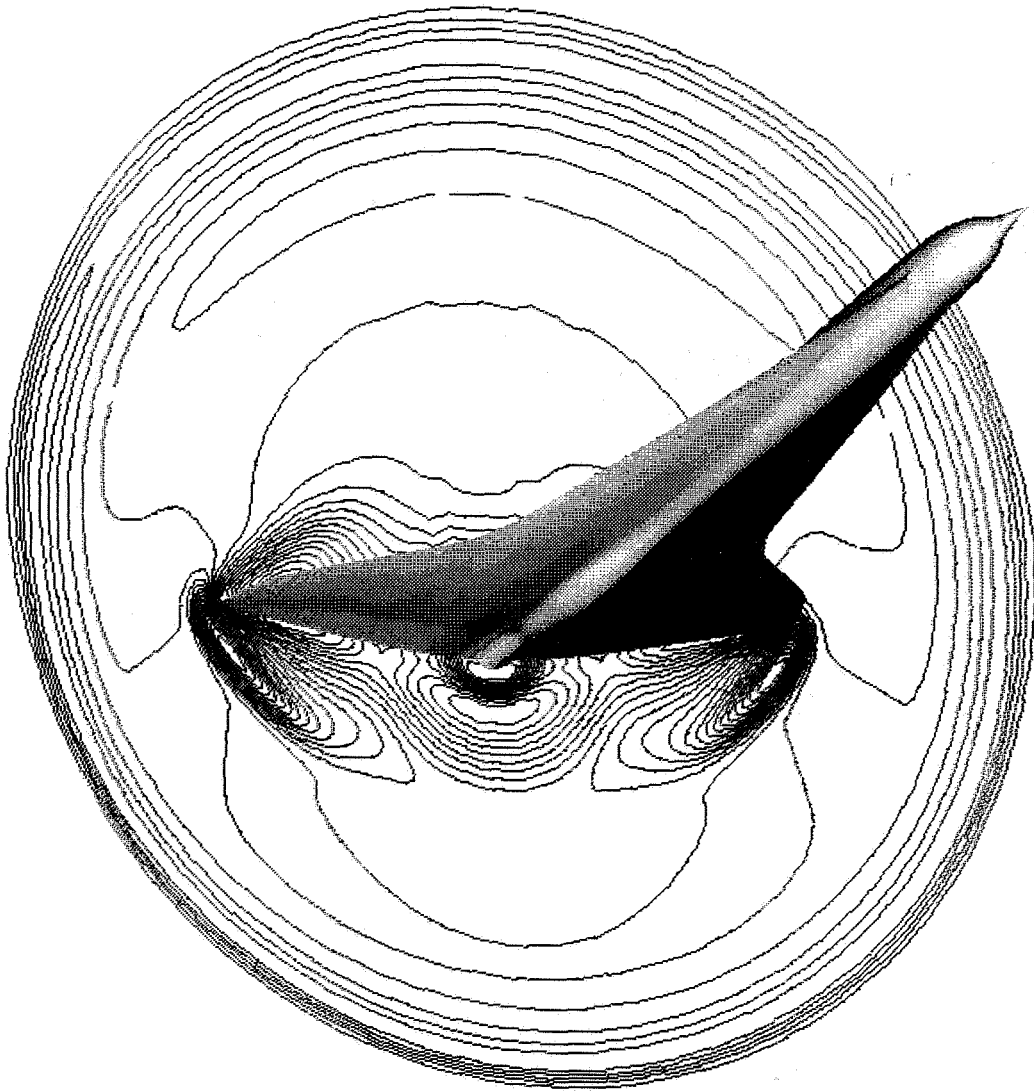


Figure 3 NASA's Mach 3 Low Boom Configuration

Figure 4 shows the near field computed pressure contours for the Mach 3 configuration at $M_\infty = 3.0$, $\alpha = 1.97^\circ$. The symmetry plane and back plane contours are both illustrated. The bow shock is clearly evident. The contours are relatively clean in the symmetry plane up to the aft end of the aircraft. In this region, several shocks begin to appear. The sting attachment shock and a strong shock around the leading edge of the wing due to the wing crank.

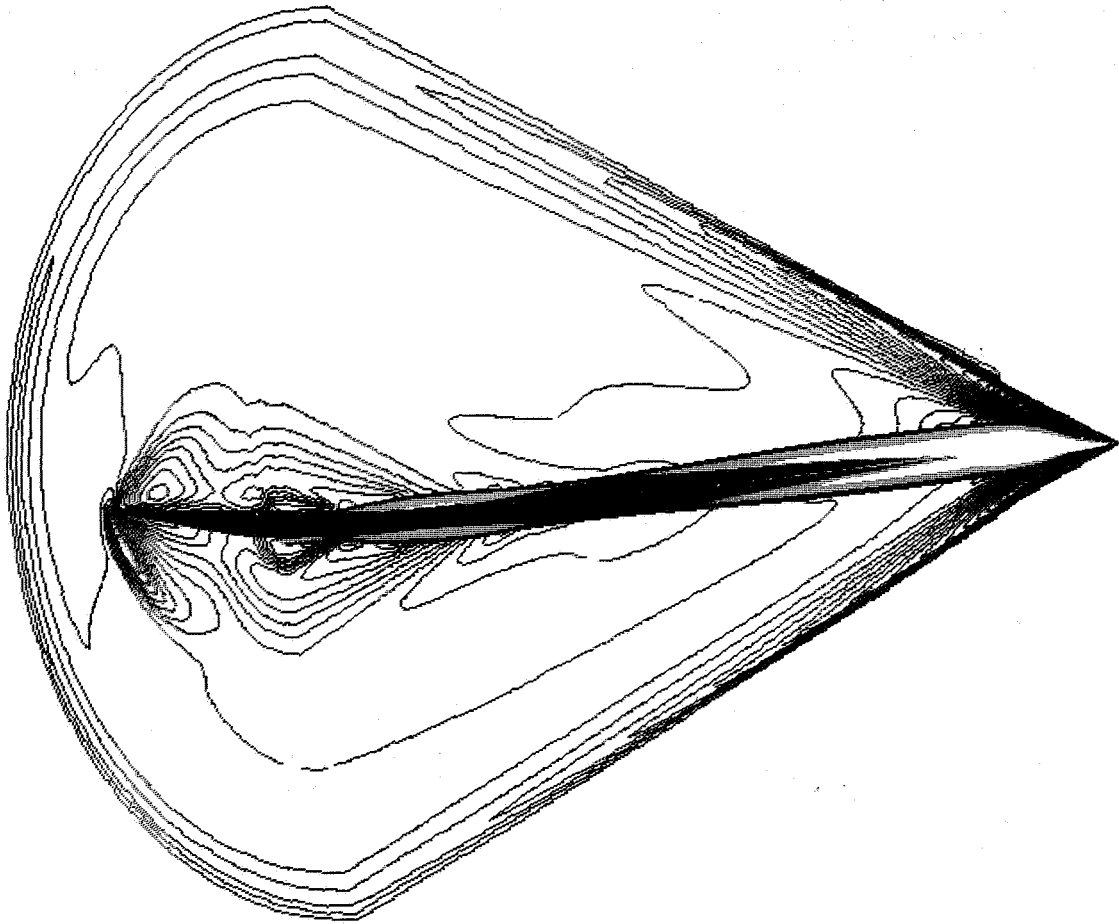


Figure 4 Near Field Pressure Contours for the Mach 3 Configuration

Figure 5 shows the computed symmetry plane pressure contours for the Mach 3 configuration at $M_\infty = 3.0$, $\alpha = 1.97^\circ$. In this figure, the sting is shown which is almost an aircraft length in size. Towards the aft end of the aircraft, the contour of the fuselage produces a large expansion terminated in a shock at the sting attachment point. A wing trailing edge shock may also occur but is not evident in the isobars.

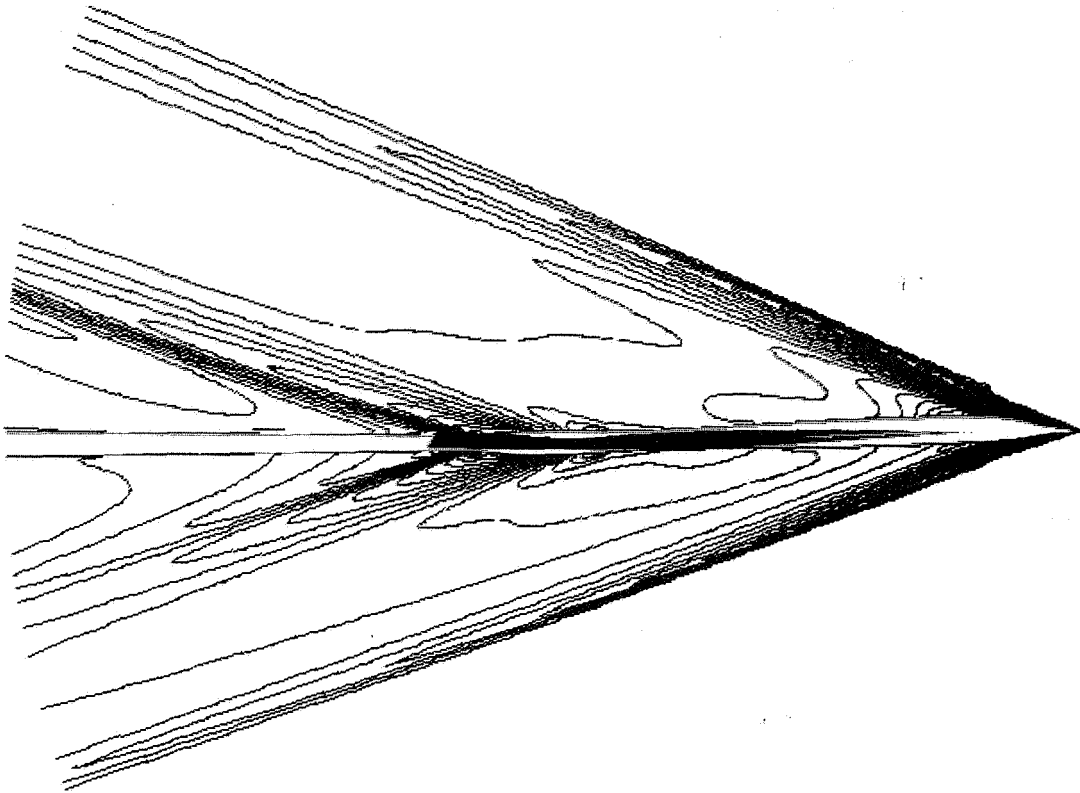


Figure 5 Symmetry Plane Pressure Contours for the Mach 3 Configuration

Figure 6 dramatically displays the sonic boom computation and the complexity of the flow field downstream of the aircraft. The computed isobars are shown in a plane at the end of the sting. In the leeward part of this plane, a strong shock is shown. This is probably the coalescence of the wing trailing edge shock and sting attachment shock. On the windward side, the situation is less clear and clearly more complex. A strong shock occurs due to the wing crank and expansion due to the wing tip. It is interesting to note that the circular isobars just to the right and left of the sting are vortices generated by the wing tips.

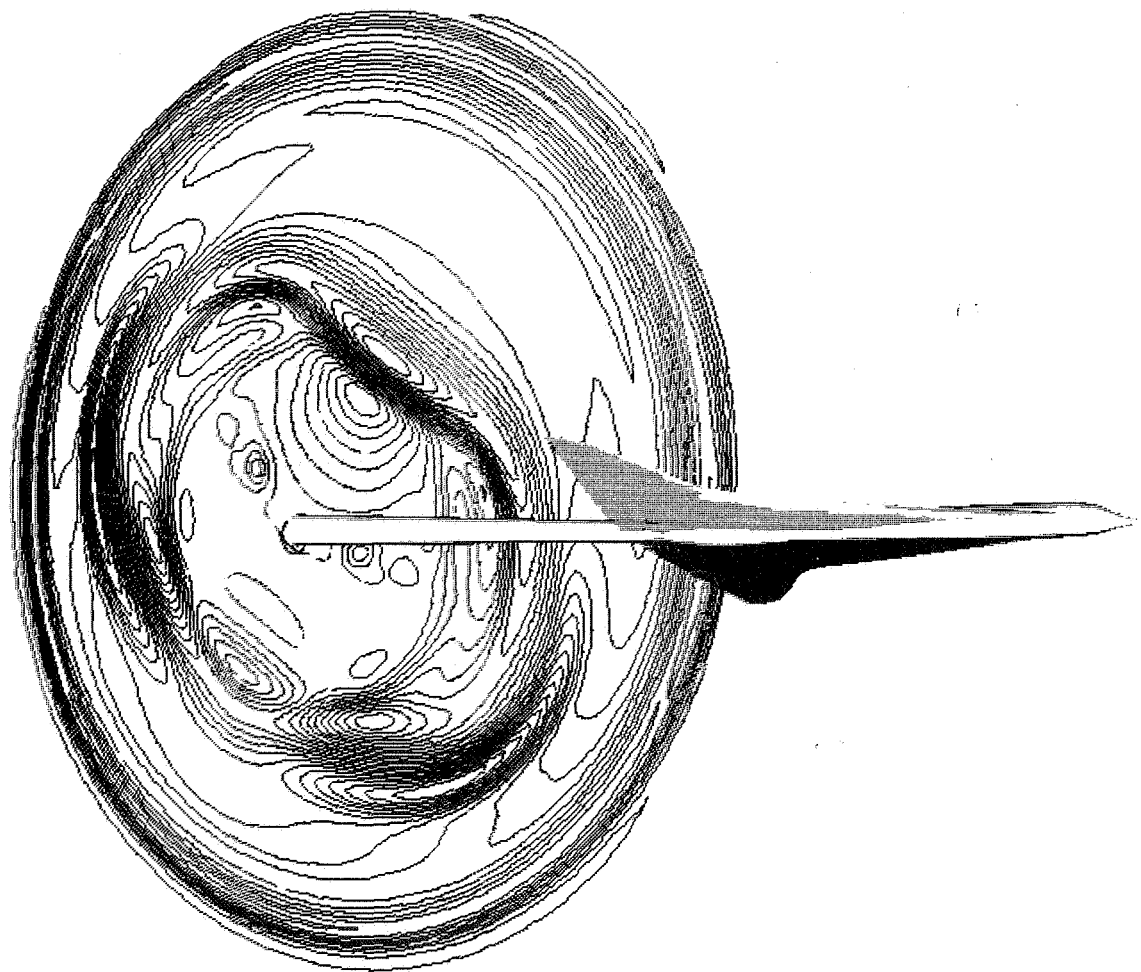


Figure 6 Near-Field Downstream Pressure Pattern of the Mach 3 Configuration

Figure 7 further illustrates the sonic boom computation for the Mach 3 configuration flying at $M_\infty = 3.0$, $\alpha = 1.97^\circ$. In this figure, three downstream planes are shown with their computed isobar pressure patterns.

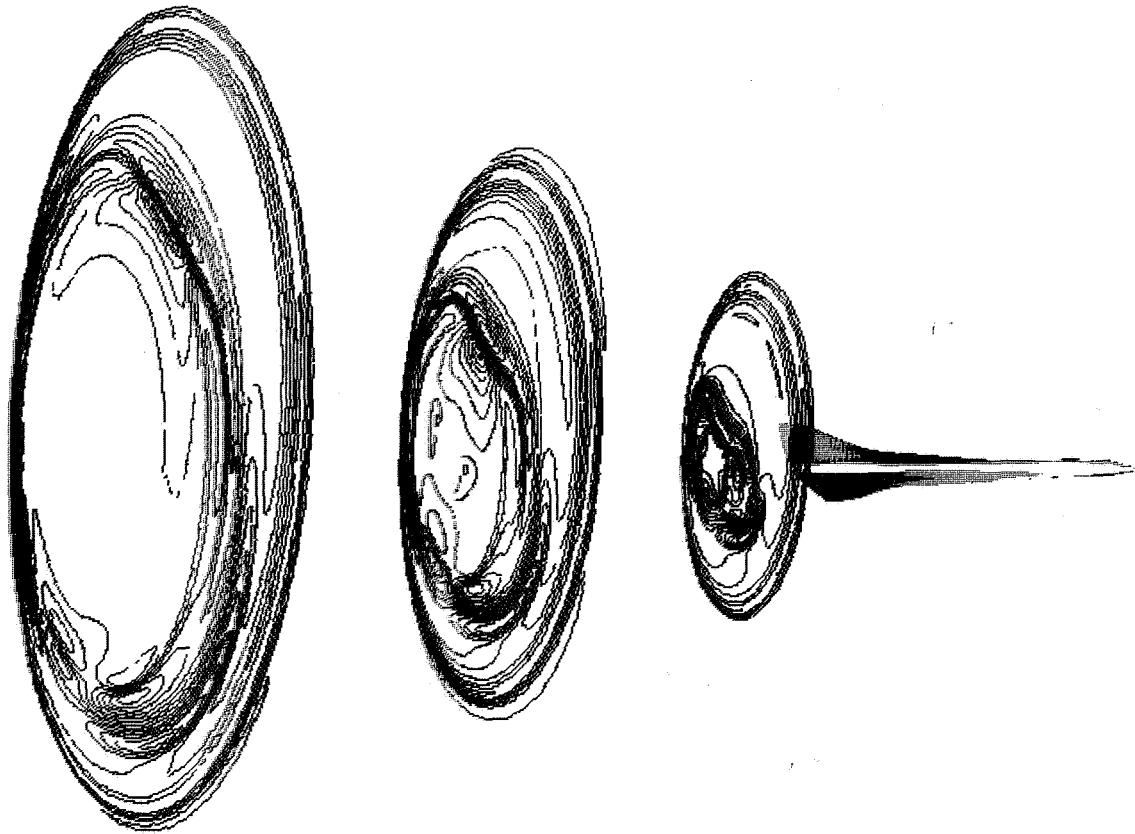


Figure 7 Propagation of Midfield Downstream Pressure Patterns for the Mach 3 Configuration

Figure 8 shows the geometry and computed back plane isobars at $M_\infty = 2.0$, $\alpha = 0.67^\circ$ for the NASA Mach 2 low boom configuration. This configuration has a flat platypus nose which is blunt in planeform. Several shocks are illustrated in the back plane isobar pattern including wing trailing edge and wing crank shocks. The computation was performed on a 89×91 crossflow plane grid by 104 steps for the aircraft. The resolution of the second grid block was 95×95 with 116 marching steps to carry the computation out to 10 body lengths downstream of the aircraft. Hence, both the Mach 2 and Mach 3 configurations required about 2 million points to achieve signatures three body lengths normal to the aircraft axis.

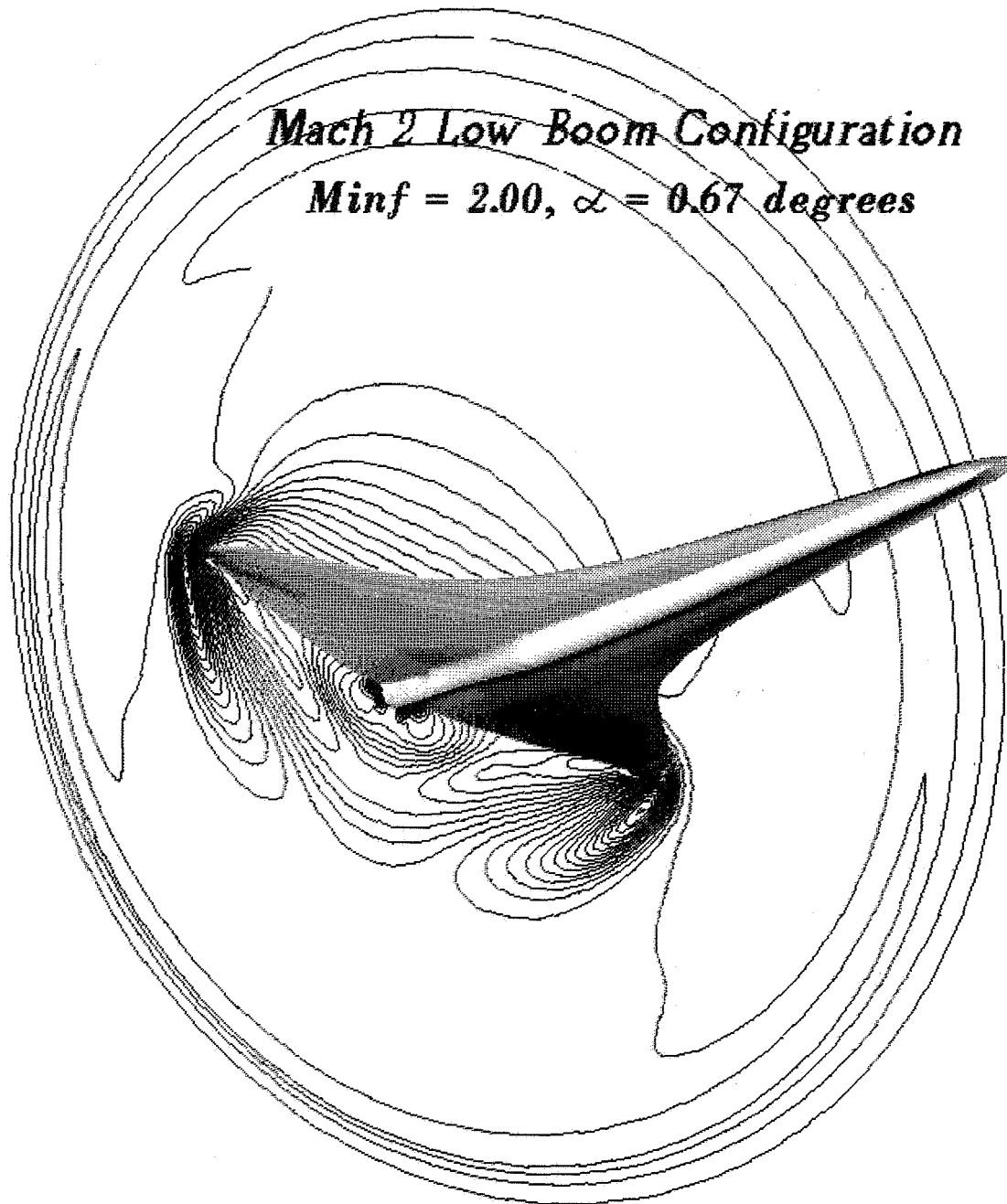


Figure 8 NASA's Mach 2 Low Boom Configuration

Figure 9 shows the computed isobars for the Mach 2 configuration at $M_\infty = 2.0$, $\alpha = 0.67^\circ$. The symmetry plane and back crossflow plane pressure patterns are illustrated. The strong attached shock generated by the supersonic leading edge crank of the wing is clearly shown. The leeward isobars in the back plane clearly shows the trailing edge shock of the wing.

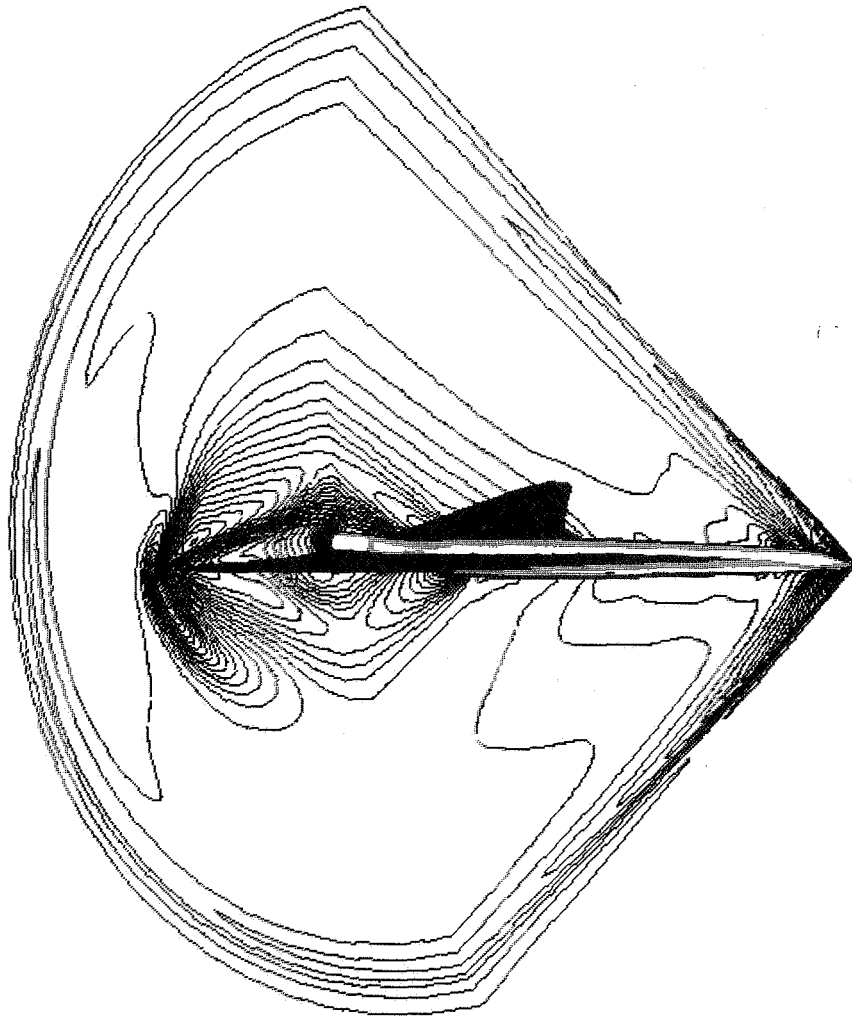


Figure 9 Near Field Pressure Contours for the Mach 2 Configuration

Figure 10 shows the symmetry plane contours for the Mach 2 configuration extending about one aircraft length behind. A strong trailing edge shock is shown in the leeward plane. There are possibly two shocks shown in the windward plane, neither of which extend very far into the field below the aircraft in comparison to the leeward plane.

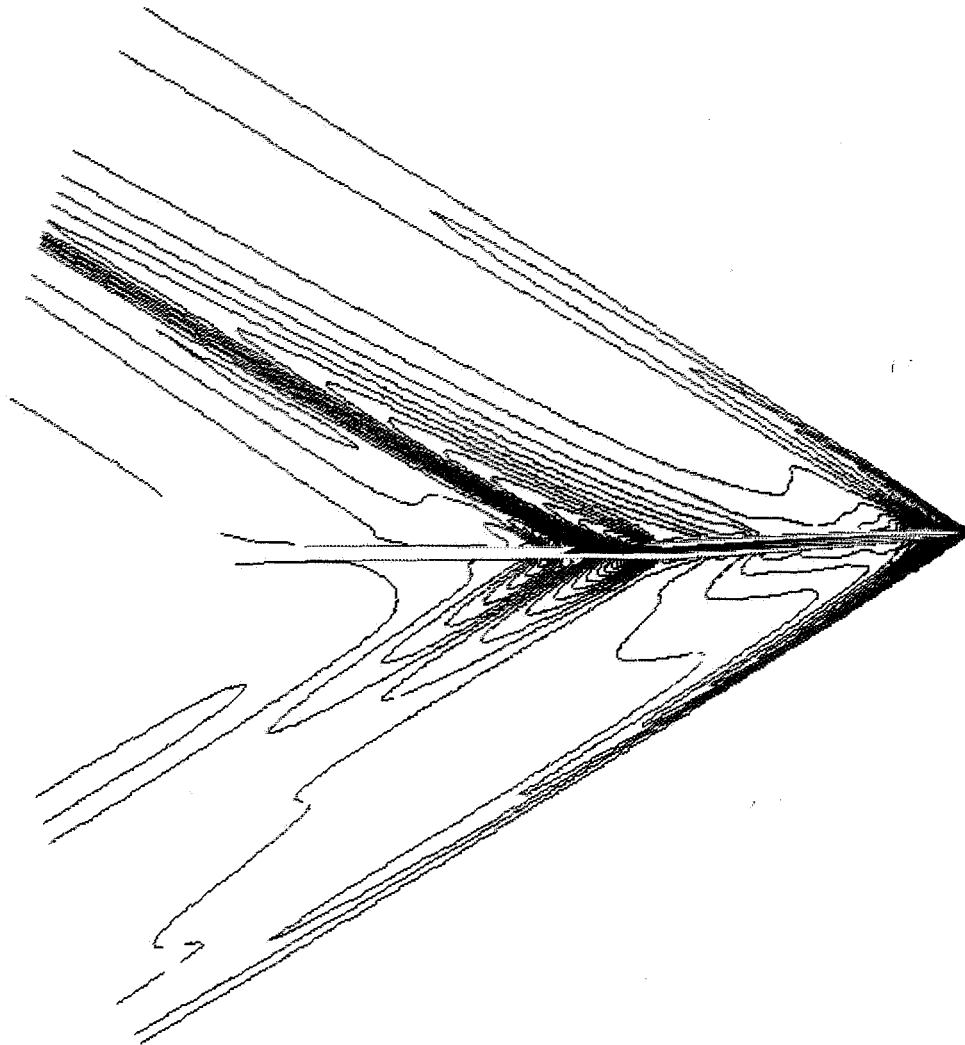


Figure 10 Symmetry Plane Pressure Contours for the Mach 2 Configuration

Figure 11 shows the computed isobars in two planes aft of the Mach 2 configuration indicating the complex flow pattern generated by the aircraft. The leeward trailing edge shock is shown and the wing crank leading edge shock. The wing crank shock does not appear to extend to the windward symmetry plane.

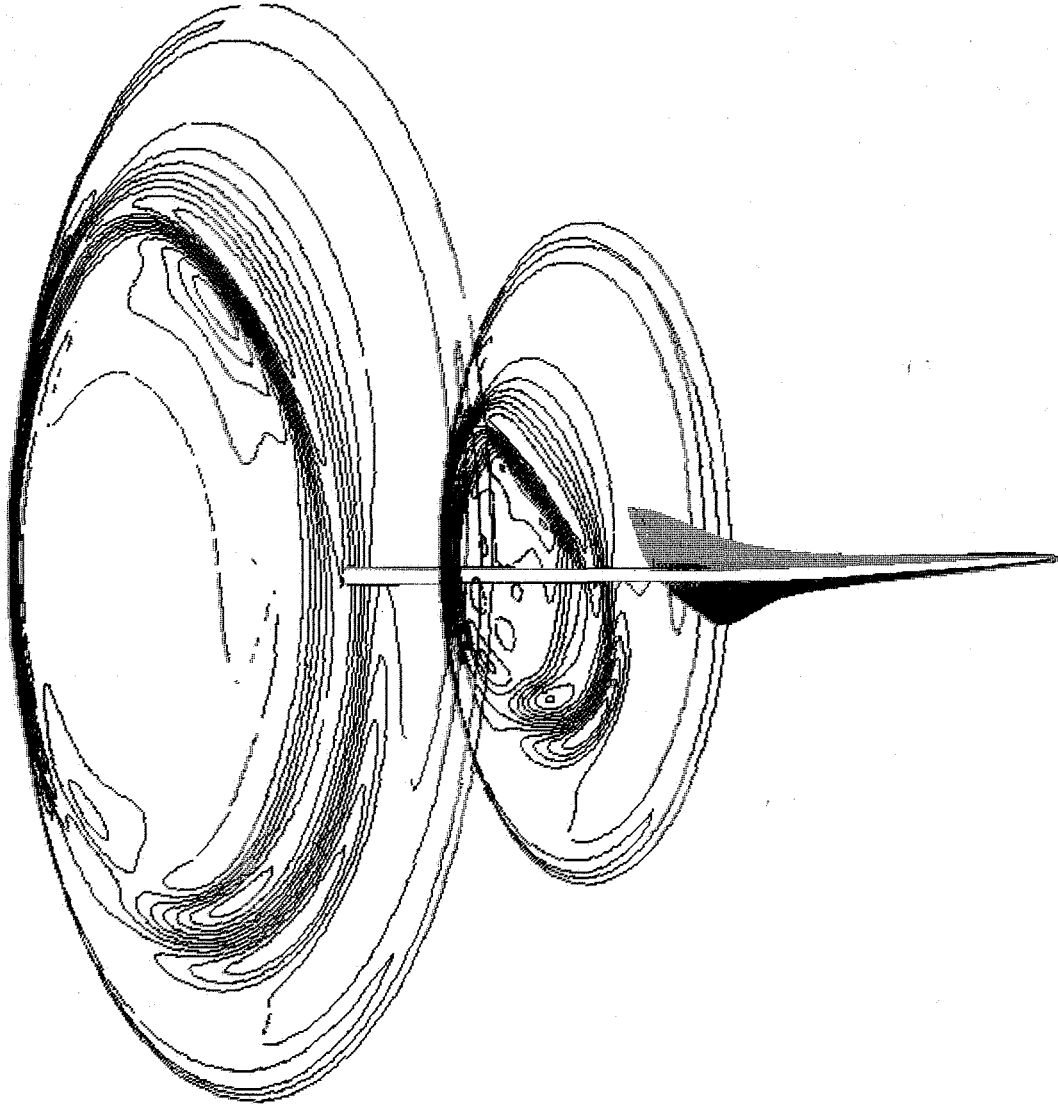


Figure 11 Propagation of Downstream Pressure Pattern of Mach 2 Configuration

Two sets of computations for each configuration were carried out with the same grid density except with different length stings. One set of computations had a sting one half of the aircraft length and the other with .8 of an aircraft length. The longer sting reduced the resolution somewhat because it increases the spatial distance between the outer boundary and downstream Mach cone boundary given a fixed number of grid points. The longer sting allowed for obtaining solutions for pressure signatures up to three body lengths normal to the aircraft axis. The shorter sting gave valid solutions for one body length.

Figure 12a shows the computed pressure signatures very close to the body at $h/\ell = 0.17$ and 0.50 where the nondimensionalizing length ℓ was taken to be 300 feet for both Mach 2 and Mach 3 configurations. At $h/\ell = 0.17$, a strong bow shock overpressure occurs followed by a relatively flat signature until the back end of the aircraft. An expansion occurs due to the shape of the fuselage followed by a single shock due to the sting attachment or wing trailing edge or both. The signature decays very rapidly to $h/\ell = 0.50$. Figure 12b shows the effect of the sting length on the computed pressure signatures below the two configurations at one body length. The pressures are plotted versus full scale coordinates in feet. In both cases the first half of the signature agrees well. The strength of the shock just prior to the rear expansion is slightly stronger in both cases for the shorter sting with effectively higher resolution. It is interesting to note that the length of the signature up to the expansion is about one body length. The overall length of the signatures is about 1.5 to 2 aircraft lengths. The expansion and recompression occurs aft of the configuration. In the Mach 3 signature, the Mach cone boundary is beginning to interfere with the solution as indicated by the very rapid recompression of the tail shock.

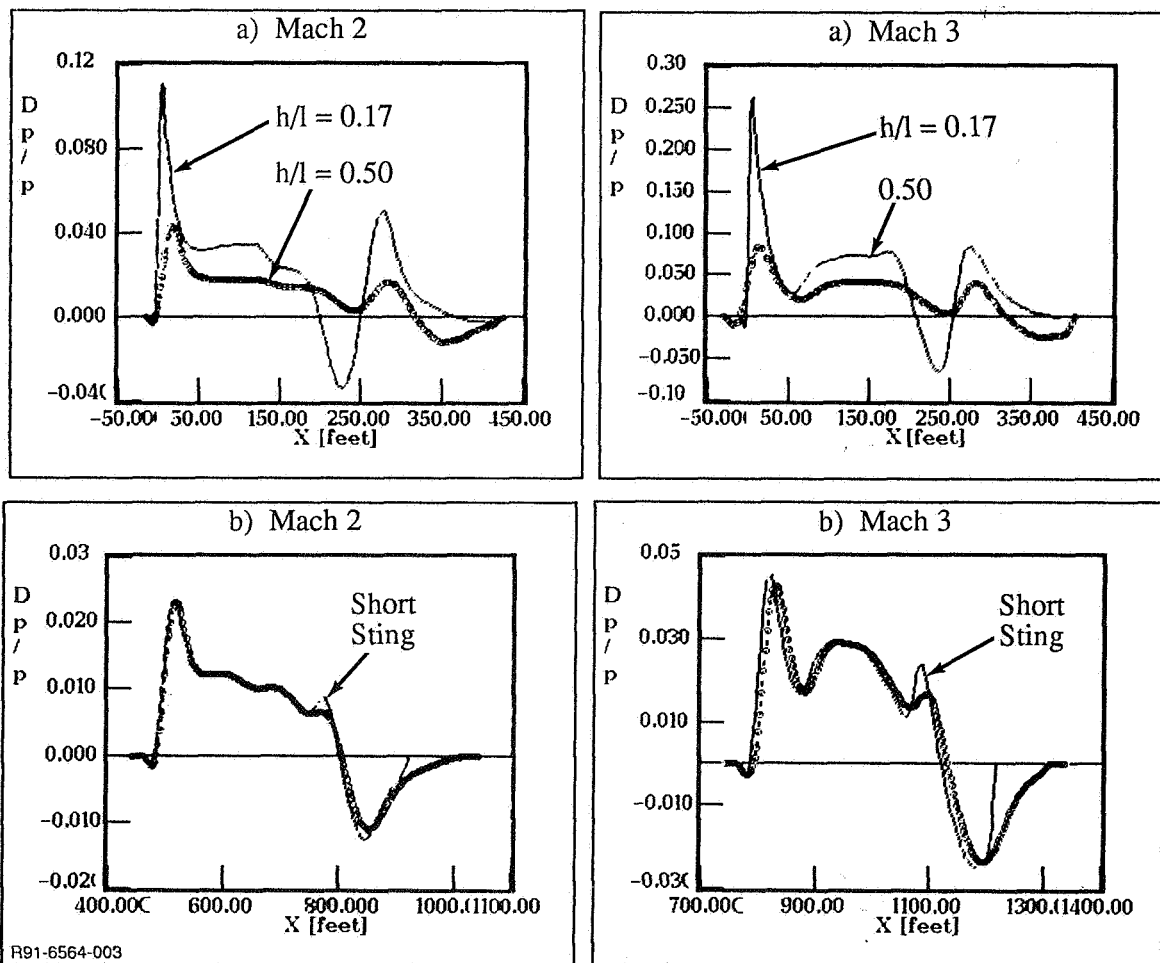


Figure 12 Computed Near Field Pressure Signatures for the Mach 2 and Mach 3 Configurations

Figure 13 shows the computed pressure signatures compared to recent wind tunnel model data (see Ref. 1) for both the Mach 2 and Mach 3 configurations. Both models were 1/300 scale or about 12 inches in length. The wind tunnel model data was converted to full scale in feet to compare to the computations. The wind tunnel data was taken at two different distances below the aircraft for each configuration. For both configurations, good correlation with the data is shown for both distances for the forward half of the signature. At $h/\ell = 0.5$, the Mach 2 data shows a series of shocks and expansions in the last half of the signature. The computation shows a single shock and expansion. At $h/\ell = 1.0$, slightly better correlation is achieved. The data still show a series of shocks and expansions with a final very large expansion twice that of the computation. Virtually the same type of correlation is shown for the Mach 3 configuration. At the present time, the origin of these multiple shocks and large expansion shown on the latter half of the signature is unknown.

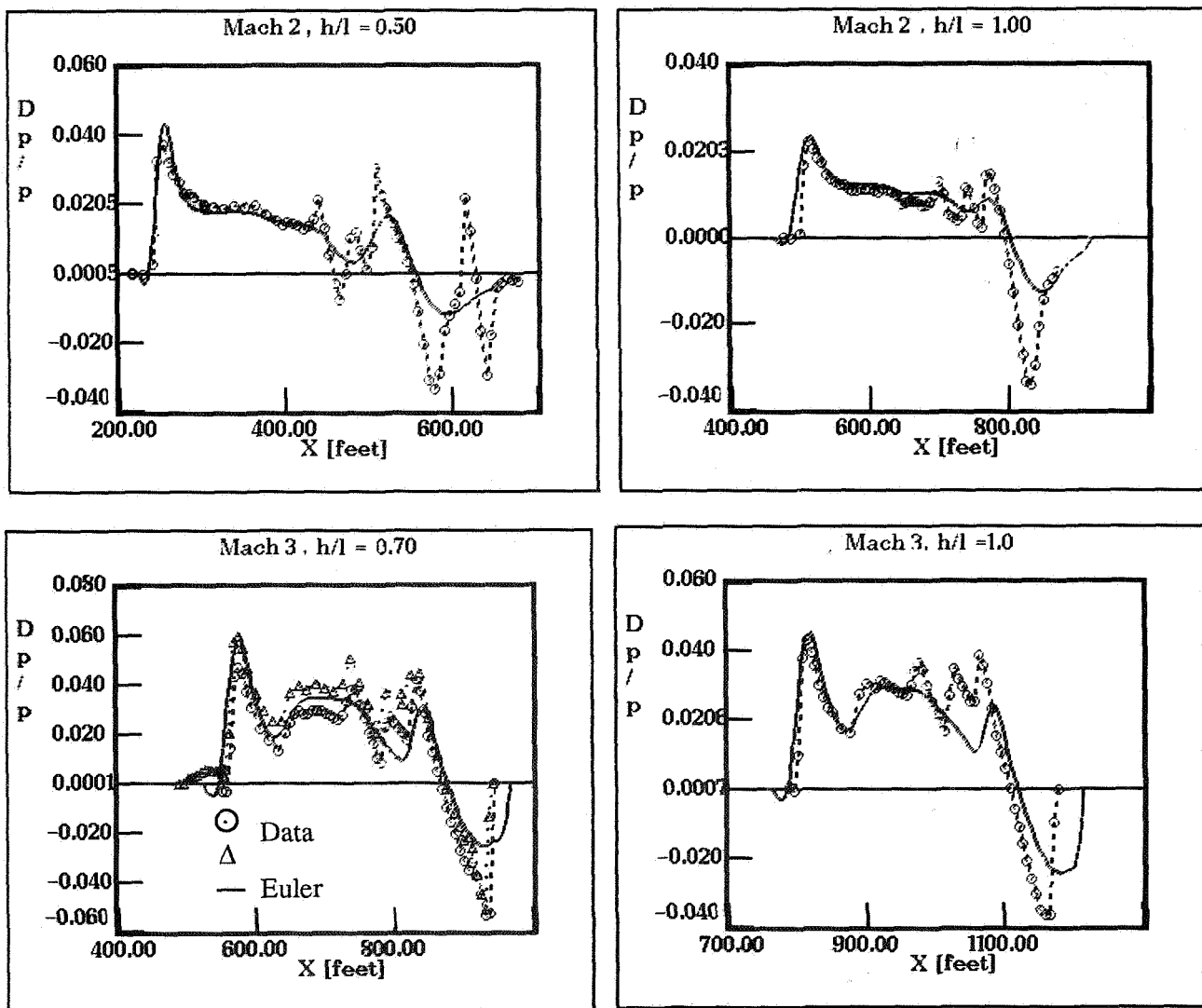


Figure 13 Comparison of Computed Near Field Pressure Signatures to Wind Tunnel Data

To obtain information on the ground signature of these two configurations, the method and computer code of Thomas (Ref. 6) was used to extrapolate both near field wind tunnel model data and computations. The computer code of Thomas uses the waveform parameter method for sonic boom extrapolation which is shown to be equivalent to the F-function method and is based on the same fundamental concepts from geometric acoustics and isentropic wave theory. It is ideal for this application because it accepts as input any height pressure signature data below or to the side of the aircraft and accounts for atmospheric effects. Figure 14 shows the extrapolated ground signatures for both the computed and wind tunnel data for the Mach 2 configuration flying at 55,000 feet. A reflection factor of 1.9 was used at the ground in the Thomas code. The wind tunnel data measured at distances of one half and one body length and computed results at $h/\ell = 0.50, 1.0$ and 3.0 were extrapolated to see the effect of nonlinearities and three-dimensional effects on the ground signatures. The initial overpressure from the extrapolated wind tunnel data (Fig. 14b) varies between 1.1 and 1.2 lbs/ft². The extrapolated computed signatures shown in Fig. 14a show a variation in the initial overpressure of 1.15 to 1.25 in good agreement with the wind tunnel data. The computed signatures extrapolated from $h/\ell = 0.50$ and 1.0 correspond to the shorter sting and slightly higher resolution. These signatures show a secondary shock at about 300 feet aft of the initial overpressure. The extrapolated signature from $h/\ell = 3$ does not have this secondary shock but shows a steeper compression prior to 200 feet. Figure 14c shows two extrapolated computations from $h/\ell = 1.0$ and 3.0 compared to the wind tunnel data extrapolated from $h/\ell = 1.0$. Overall good agreement with the wind tunnel data is achieved. The secondary shocks and the strengths of the tail shock is not predicted well.

Figure 15 shows both the wind tunnel data and computed results extrapolated to the ground using the method of Thomas for the Mach 3 configuration flying at 65,000 feet. The wind tunnel data at both measured distances below the aircraft are extrapolated and are shown in Fig. 15b. At $h/\ell = .7$, the data extrapolation indicates an initial bow shock rise of about 1.8 lbs/ft² and a secondary shock rise to 2.4 lbs/ft². The extrapolated ground signature from data at $h/\ell = 1.0$ indicates some coalescence with an initial shock rise to about 1.6 and a secondary shock rise to about 1.8 lbs/ft². Hence, for the Mach 3 configuration, the extrapolated ground signature is sensitive to the distance below the aircraft where data has been taken. Figure 15a shows the ground signatures extrapolated from the computed results at several locations below the aircraft corresponding to $h/\ell = 0.5, 1.0$ and 3.0 . The computed results at $h/\ell = 0.5$ and 1.0 come from the model with the shorter sting and slightly higher resolution. The $h/\ell = 3.0$ extrapolation was for the model with the long sting. The initial shock rise is in agreement for all these extrapolated signatures. A small secondary shock occurs near the end of the aircraft or at about 300 feet in the signature. This shock is only predicted for the highly resolution signatures. The tail shock occurs further aft and grows in strength as the distance for extrapolation increases. Figure 15c also shows a comparison of the extrapolated signatures from wind tunnel data and computations at $h/\ell = 1.0$. The comparison is in good agreement except that the wind tunnel data shows a stronger secondary shock in a different location than the computation. Both indicate an initial shock rise of about 1.6 lbs/ft². The wind tunnel data shows a secondary rise to about 1.8 lbs/ft².

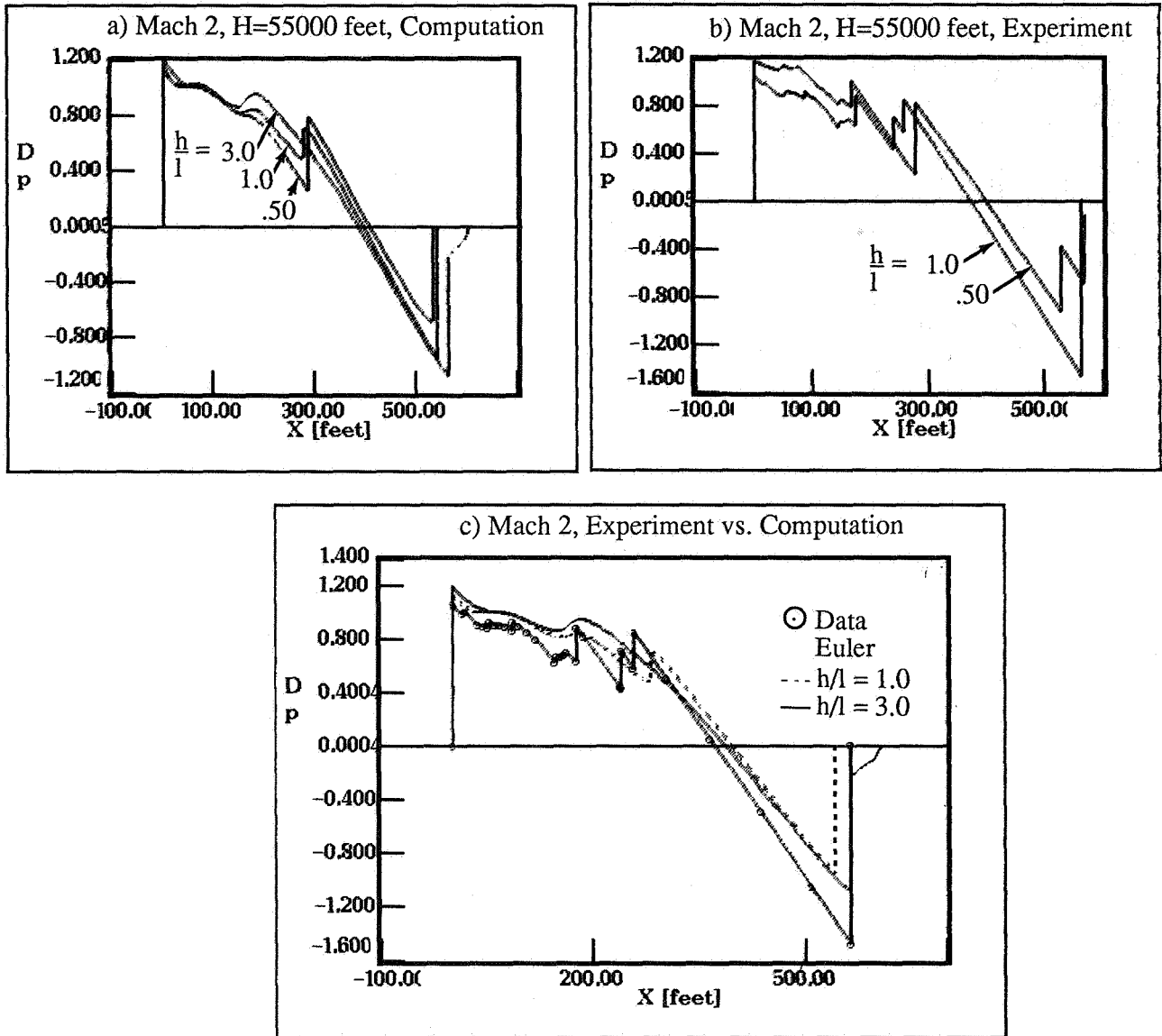


Figure 14 Comparison of Extrapolated Ground Signatures to Extrapolated Wind Tunnel Data for the Mach 2 Configuration

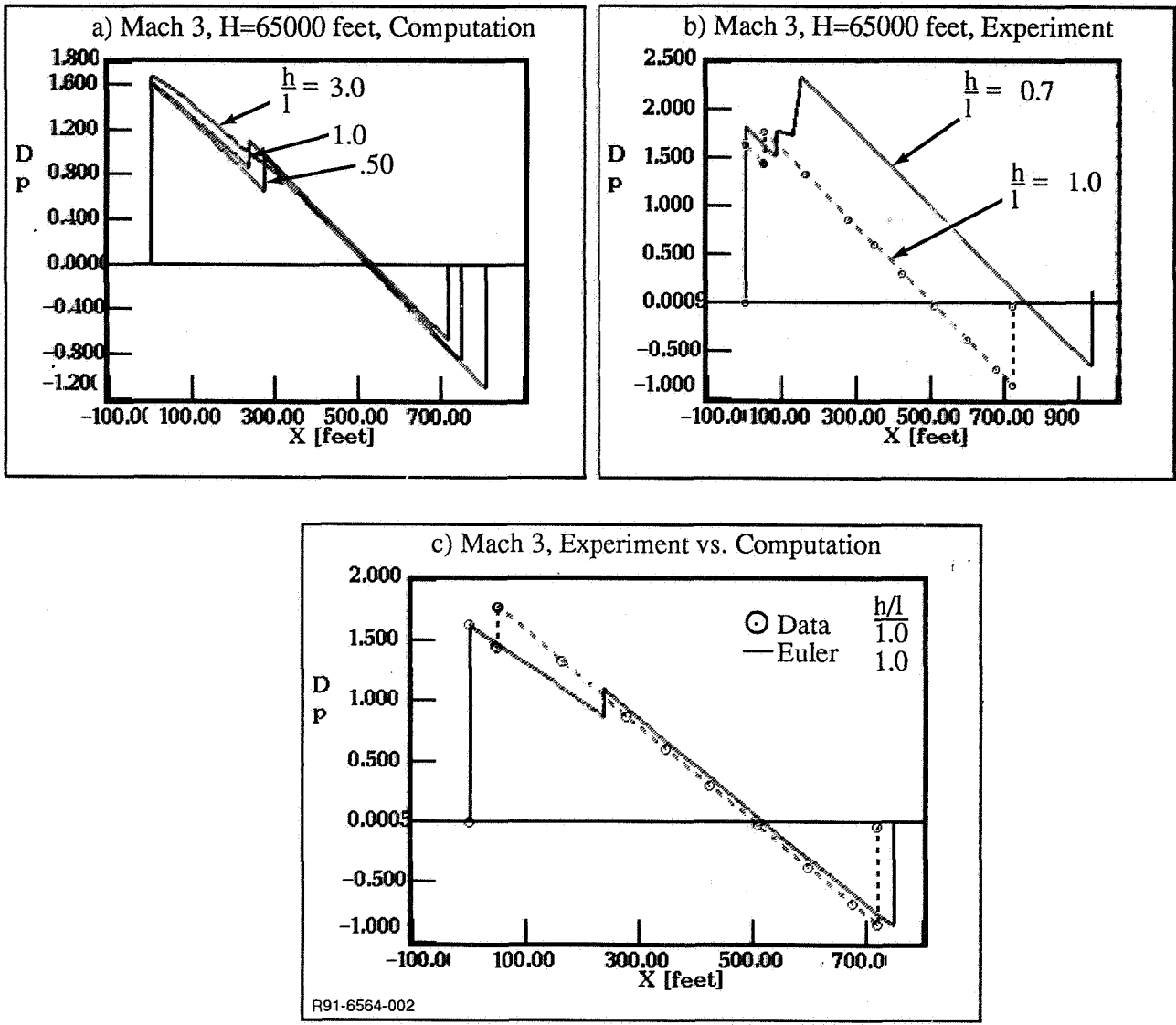


Figure 15 Comparison of Extrapolated Ground Signatures to Extrapolated Wind Tunnel Data for the Mach 3 Configuration

Figure 16 shows the three-dimensional computed pressure footprint generated by the Mach 2 configuration at $h/\ell = 1.0$ below the aircraft. The computed results are from the model using the slightly longer sting. The pressure footprint is plotted laterally out to two aircraft lengths. Plotted to the left of the three dimensional footprint are pressure signatures at constant lateral distances or azimuthal angles from the centerline of the aircraft. At the first signature off the axis ($\phi = 14^\circ$), the effect of the strong wing crank shock begins to become prominent in the form of a second shock. In the third ($\phi = 26.6^\circ$) and fourth ($\phi = 36.9^\circ$) signatures, the first overpressure begins to diminish and the second overpressure due to the wing crank shock increases to an overpressure value greater than the value of the bow shock overpressure at the centerline. In addition, the large expansion due to the wing tips also becomes prominent on the off centerline signatures.

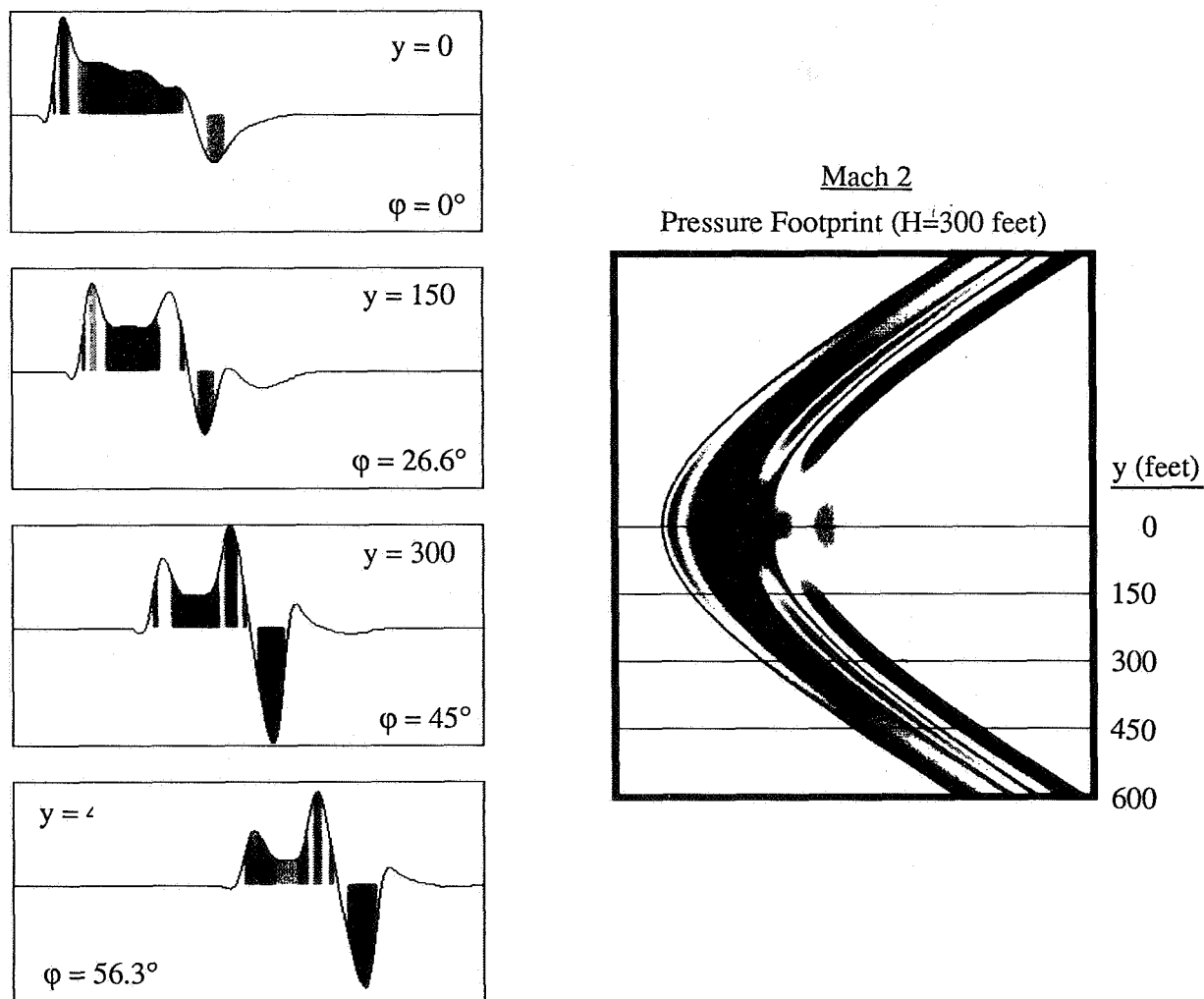


Figure 16 Three-Dimensional Pressure Footprint of the Mach 2 Aircraft at $h/\ell = 1.0$

Figure 17 shows the same type of plot for the Mach 2 configuration except that the three-dimensional footprint corresponds to an $h/\ell = 3.0$ below the aircraft. In this figure, the footprint is plotted out to a lateral distance of three aircraft lengths. A similar behavior of the off axis pressure signatures is indicated. The signature at $\phi = 26.6^\circ$ are plotted in both Figure 16 and 17 and occur along the same azimuthal ray and look very similar. Hence, the three-dimensional or off centerline behavior of the sonic boom footprint does not seem to vary significantly from an $h/\ell = 1.0$ to an $h/\ell = 3.0$ below the aircraft.

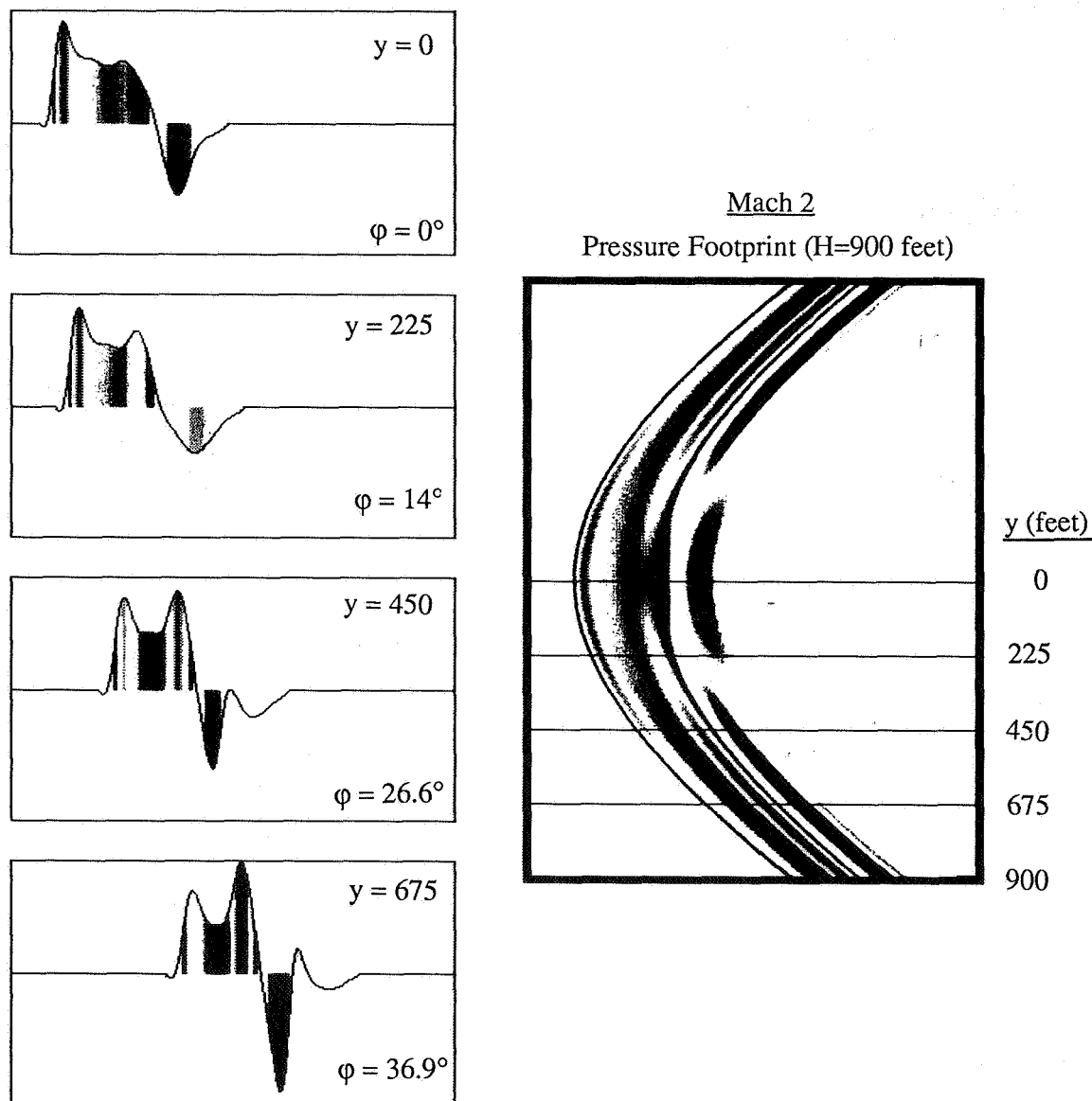


Figure 17 Three-Dimensional Pressure Footprint of the Mach 2 Aircraft at $h/\ell = 3.0$

To determine the three-dimensional behavior of the ground sonic boom for the Mach 2 configuration footprint, the signatures of Figures 16 and 17 were input to the Thomas sonic boom extrapolation code. Figure 18 shows the resulting ground signatures for the Mach 2 configuration flying at an altitude of 55,000 feet. $\phi = 0^\circ$ corresponds to the flight path ground axis. If two azimuthal angles were the same from Figures 16 and 17, both signatures were extrapolated. At 5.72 miles from flight path centerline, the initial bow shock rise decays slightly but a second stronger overpressure occurs due to the wing crank shock at about 1.45 lbs/ft². Further off the centerline at 8.73 miles, the second overpressure rises to almost 1.5 lbs/sq ft. At 12.44 miles from flight path centerline, the second overpressure begins to diminish. The Thomas extrapolation method also indicates that these two shocks begin to coalesce into a single larger initial boom in comparison to the signature along the centerline. The three-dimensional results also indicate that boom overpressures up to 25% greater in magnitude can be felt to the side of the aircraft flight path axis due to the aircraft's supersonic leading edge wing crank.

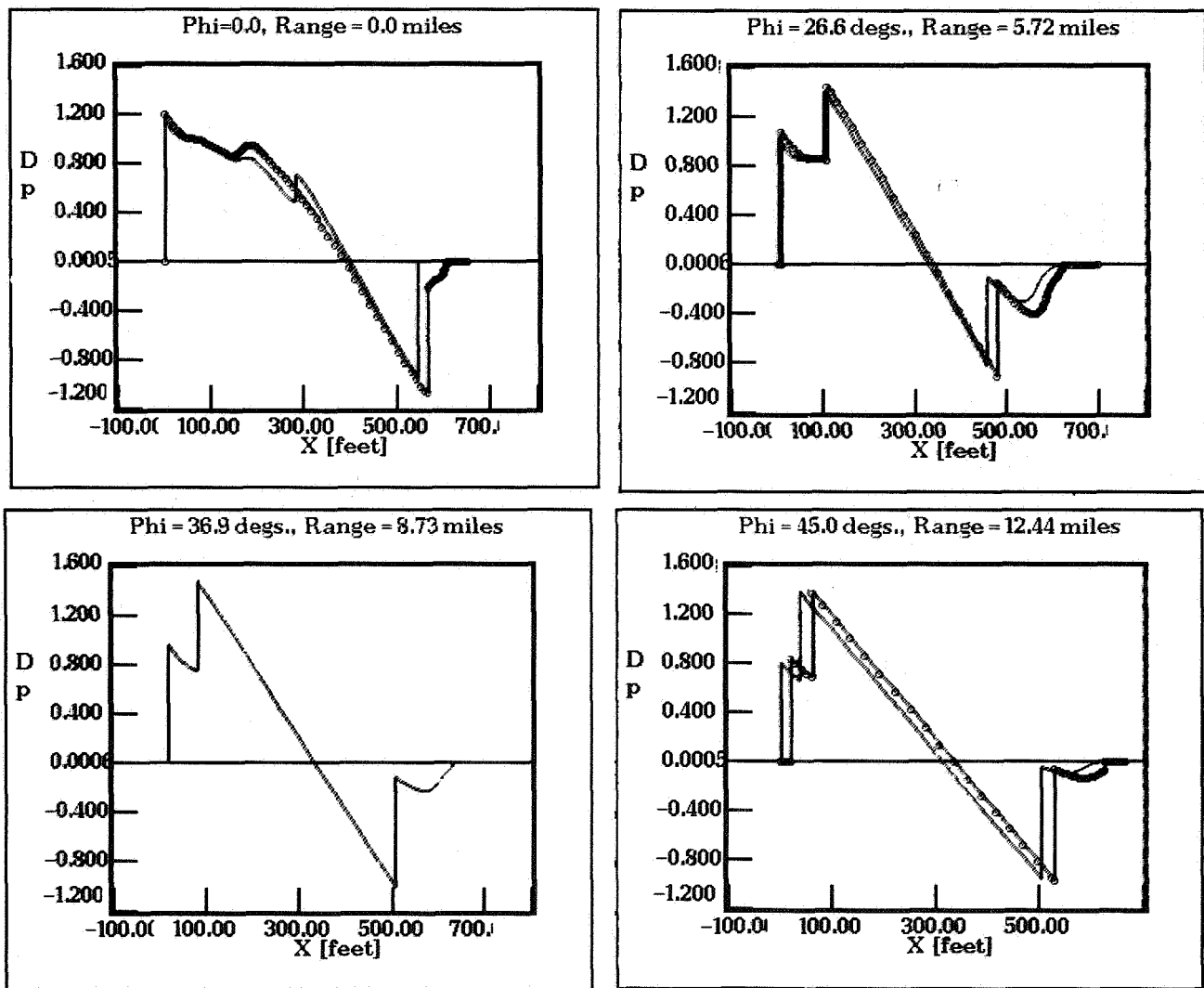


Figure 18 Off Flight Path Axis Ground Extrapolations for the Mach 2 Configuration

Figure 19 shows the three-dimensional footprint computed for the Mach 3 configuration at $h/\ell = 1.0$ below the aircraft. A similar pattern of behavior occurs for the Mach 3 configuration as was indicated for the Mach 2 model. A strong second shock occurs off the centerline due to the wing crank shock whose magnitude is equal or slightly greater than the centerline overpressure.

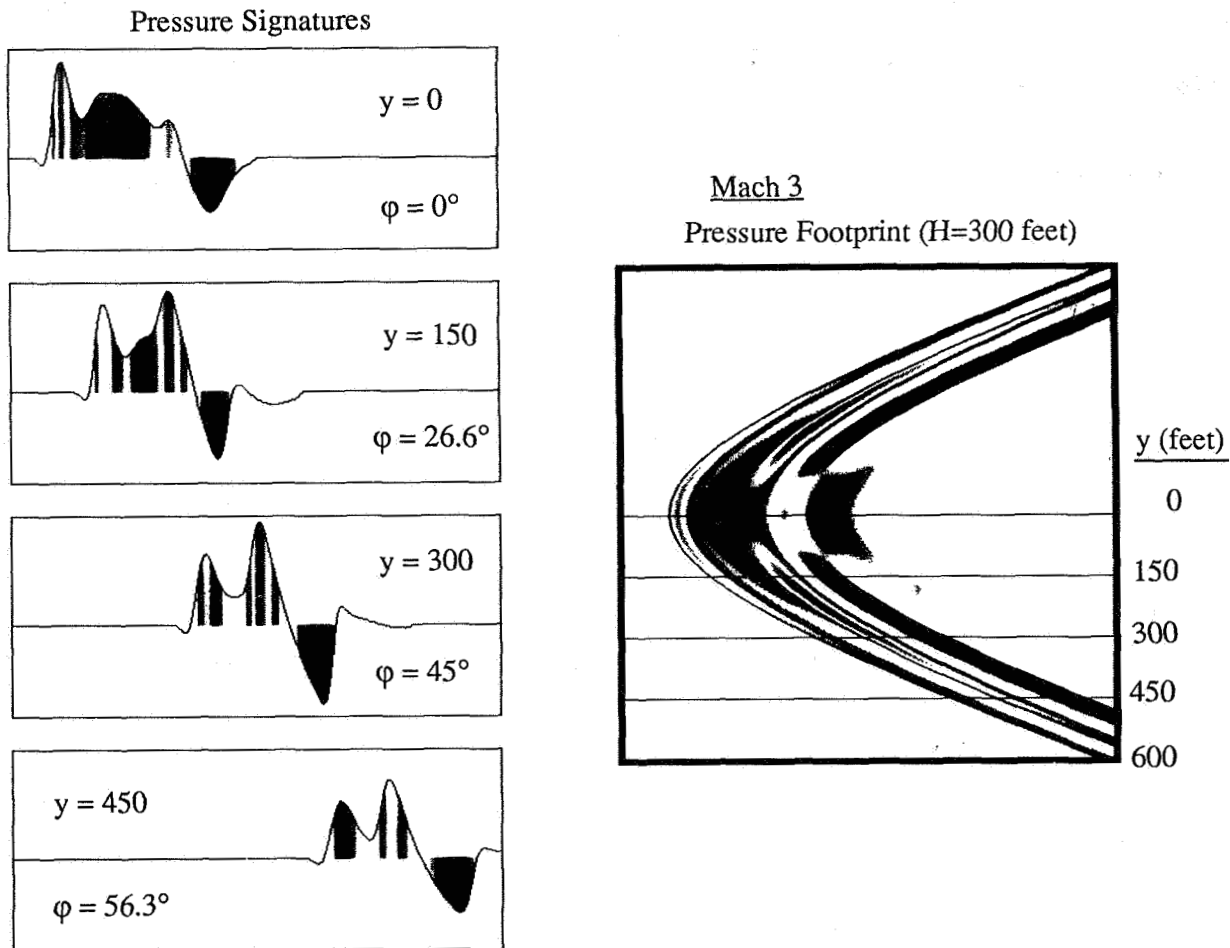


Figure 19 Three-Dimensional Pressure Footprint of the Mach 3 Aircraft at $h/\ell = 1.0$

Figure 20 shows a similar set of plots for the three-dimensional pressure footprint of the Mach 3 configuration but at $h/\ell = 3.0$ below the aircraft. This footprint extends to three aircraft lengths off the axis. Comparing the signatures in Figures 19 and 20 at $\phi = 26.6^\circ$, the second overpressure is rising well above the initial bow shock rise.

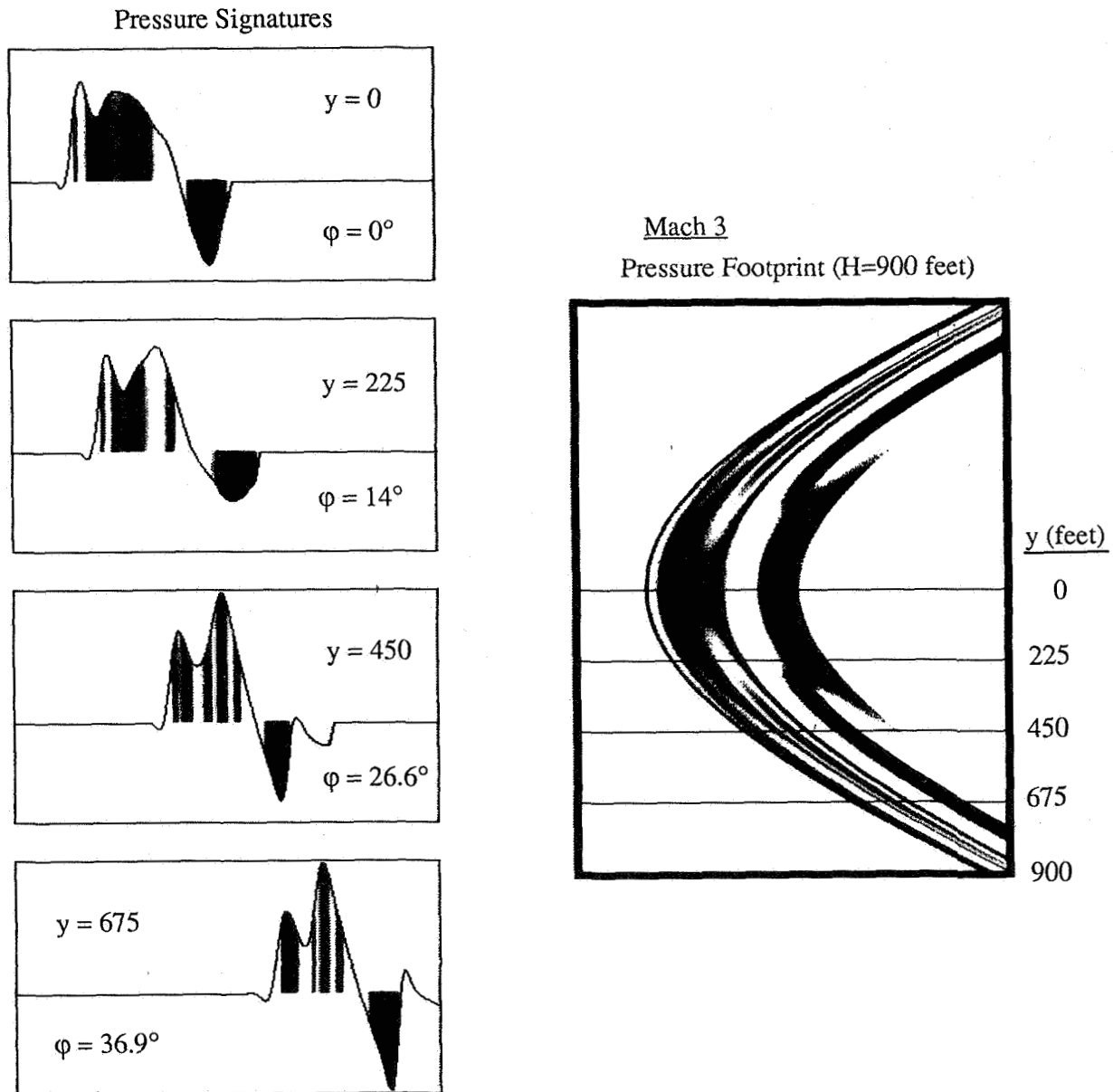


Figure 20 Three-Dimensional Pressure Footprint of the Mach 3 Aircraft at $h/\ell = 3.0$

Figure 21 shows the corresponding ground signatures extrapolated using the Thomas code for the Mach 3 configuration flying at 65,000 feet. In contrast to the ground behavior of the Mach 2 configuration, the Thomas code essentially predicts the coalescence of the bow shock with the second overpressure into a typical N wave. The off aircraft axis signatures only show a 10% rise in comparison to the centerline. The strength of the signature or boom remains relatively constant due to the second shock up to 10 miles from the flight path centerline, at which point, the boom begins to decay due to the long ray path to reach the ground.

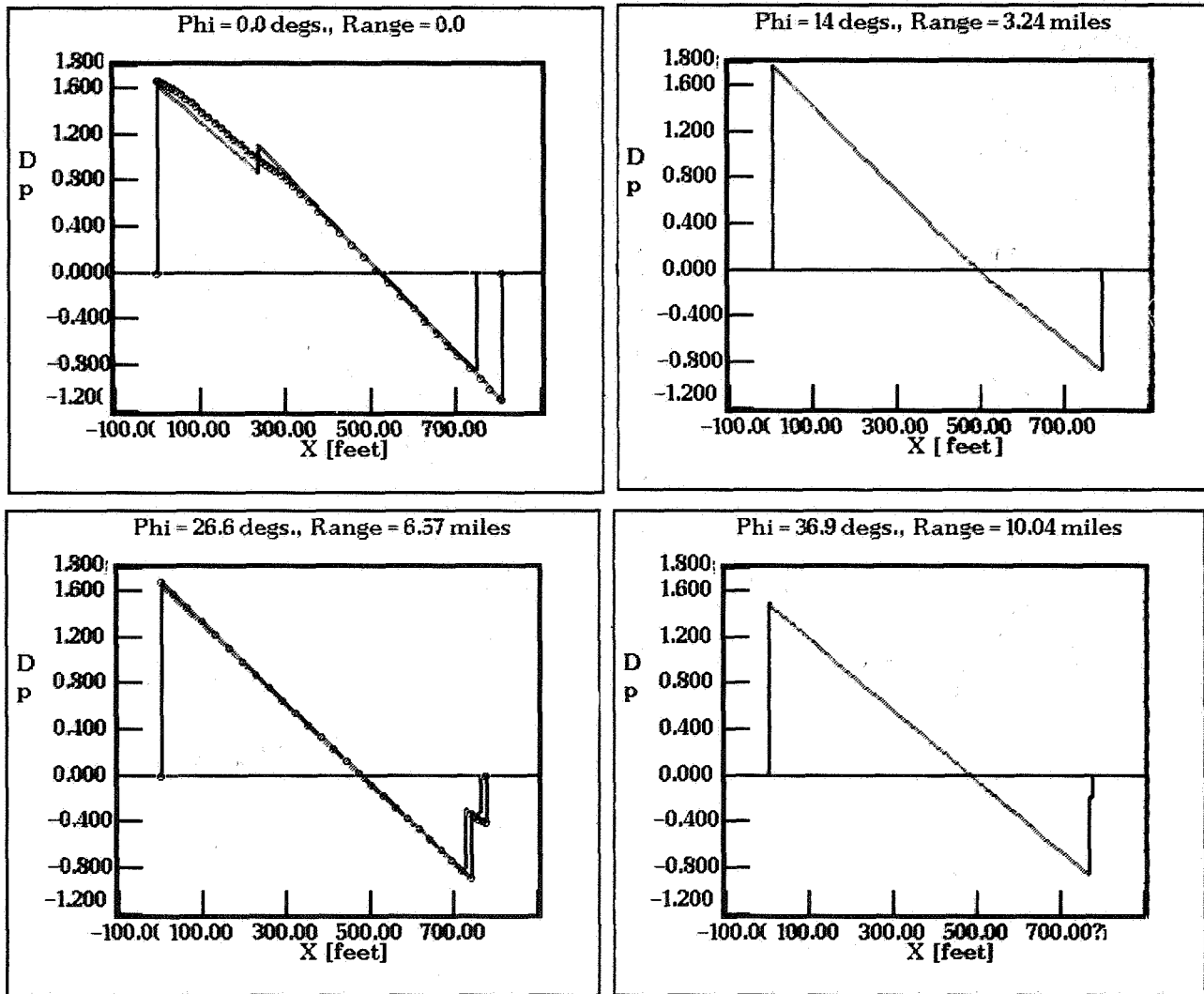


Figure 21 Off Flight Path Axis Ground Extrapolations for the Mach 3 Configuration

REFERENCES

1. Mack, R.J. and Darden, C.M., private communication, April, 1991, data to be published.
2. Jameson, A., "A Vertex Based Multigrid Algorithm for Three-Dimensional Compressible Flow Calculations," ASME Symposium on Numerical Methods for Compressible Flow, Anaheim, CA, Dec. 1986.
3. Siclari, M.J., "Hybrid Finite Volume Approach to Euler Solutions for Supersonic Flows," AIAA J., Vol. 28, No. 1, Jan. 1990, pp. 66-74.
4. Siclari, J., "Three-Dimensional Hybrid Finite Volume Solutions to the Euler Equations for Supersonic/Hypersonic Aircraft," AIAA Paper No. 89-0281, presented at the 27th Aerospace Sciences Meeting, Reno, NV, Jan. 1989.
5. Siclari, M and Darden, C., "An Euler Code Prediction of Near to Mid-Field Sonic Boom Pressure Signatures," AIAA Paper No. 90-4000, presented at the AIAA 13th Aeroacoustics Conference, Tallahassee, FL, Oct., 1990.
6. Thomas, C.L., "Extrapolation of Sonic Boom Pressure Signatures by the Waveform Parameter Method," NASA TN D-6832, June 1972.

Session V. Sonic Boom (Aerodynamic Performance)

omit

Overview of Feasibility Study on Conducting Overflight Measurements of Shaped Sonic Boom Signatures Using RPV's

Domenic J. Maglieri, Victor E. Sothcott, Thomas N. Keefer and Percy J. Bobbitt, Eagle Engineering, Inc. - Hampton Division

THIS PAGE INTENTIONALLY BLANK

N94- 33475

**OVERVIEW OF FEASIBILITY STUDY ON CONDUCTING
OVERFLIGHT MEASUREMENTS OF SHAPED
SONIC BOOM SIGNATURES USING RPV'S**

5/3-71
1200.3

**D.J. Maglieri, V.E. Sothcott, T.N. Keefer Jr., P.J. Bobbitt
Eagle Engineering, Inc. - Hampton Division
Hampton, Virginia**

**First Annual High-Speed Research Workshop
Williamsburg, Virginia
May 14-16, 1991**

PRECEDING PAGE BLANK NOT FILMED

787

OUTLINE OF PRESENTATION

Before beginning this presentation, it is appropriate to acknowledge the sincere interest and financial support provided by the NASA Langley Research Center under contract NAS9-17900.

An outline of the material to be used in the present paper is given in figure 1. It begins with a indication of the origin and objectives of the feasibility study. This is followed by a discussion of various simulation methods of establishing the persistence of shaped sonic boom signatures to large distances including the use of recoverable RPV/drones. The desirable features to be sought after in an RPV along with a rationale for the selection of a "shaped" sonic boom signature will be addressed. Three candidate vehicles are examined as to their suitability with respect to a number of factors, in particular, modifiability. Area distributions and associated sonic boom signatures of the basic and modified Firebee vehicle will also be shown.

An indication of the scope of the proposed wind tunnel and flight test programs will be presented including measurement technologies and predicted waveforms.

Finally, some remarks will be made summarizing the study and highlighting the key findings. Finally, some remarks will be made summarizing the study and highlighting the key findings.

- Origin / objectives of feasibility study
- Simulation methods
- Desirable features for RPV
- Selection of shaped sonic boom signature
- Candidate vehicles
- Basic / modified Firebee characteristics
- Wind-tunnel and flight programs
- Summary remarks

Figure 1

MAJOR THRUSTS IN SOLUTION TO HSCT OVERLAND SONIC BOOM

The future success of commercial high-speed overland flight will depend, in large part, on providing a solution to the sonic boom problem. Without some unforeseen technological breakthroughs that may eliminate the sonic boom, current efforts are aimed at modifying the boom signature in order to make it more acceptable. The term "more acceptable" infers modifications to the signature that includes not only reducing the peak overpressure (or intensity of the boom), but shaping the signature to look something other than the typical N-wave. Variations include so-called "flat-top" waveforms, "ramp-type," and variations of each (that increase shock rise times and change frequency spectra) have all been shown to reduce loudness and noisiness¹ at least to observers out-of-doors. Sonic boom waveform (signature) modifications must also benefit "indoor" listeners and also reduce structural response.

Three major thrusts are required in the solution of the sonic boom problem associated with overland flights of a High-Speed Civil Transport (HSCT), as indicated by the three outer circles shown in figure 2. These three major thrusts include the establishment of criteria for an acceptable waveform, being able to design a viable aircraft to an existing shaped (or acceptable) waveform, and quantifying the effects of the atmosphere through which this shaped waveform will propagate. These three major thrusts are, in fact, the three major research priorities that were recognized by a panel of experts from industry, government, and universities as the key areas to be addressed.² A reasonable data base from small model wind tunnel tests^{3,4} and theory^{5,6} exists indicating that vehicles can be designed to produce modified sonic boom signatures (non N-wave types) of the type that may be more acceptable from a people and structural response aspect.

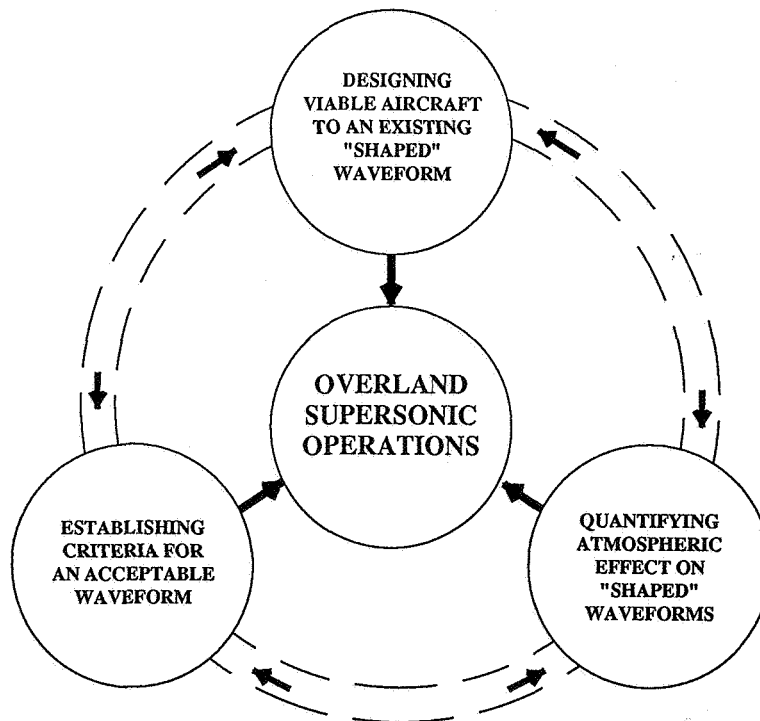


Figure 2

**MEASURED SONIC BOOM SIGNATURES OF A BASIC AND MODIFIED
MODEL IN THE WIND TUNNEL**

An indication of the status of sonic boom signature modifications as established by wind tunnel model tests and theory is given in figure 3. Measured sonic boom signatures are shown for various distances from the models for two vehicle configurations, one designated a basic body which is to produce an N-wave signature in the far field, and the other designated a modified body which is to produce a flat-top signature in the far field.

Signature measurements at 2.5, 5, and 10 body lengths (h/l) from the model illustrate the development of the waveforms for the two models. Note that the basic configuration signature sketches to the left side of figure 3, which is to result in an N-wave on the far field, still retains the multiple saw-tooth shock characteristic out to 10 body lengths. However, the signatures on the right side of the figure relating to the model designed to produce a flat-top signature in the far field show flat-top waveforms at all three measurement positions. In this case, tunnel test section length and model size constraints limit the furthest measurement to 10 body lengths from the model.

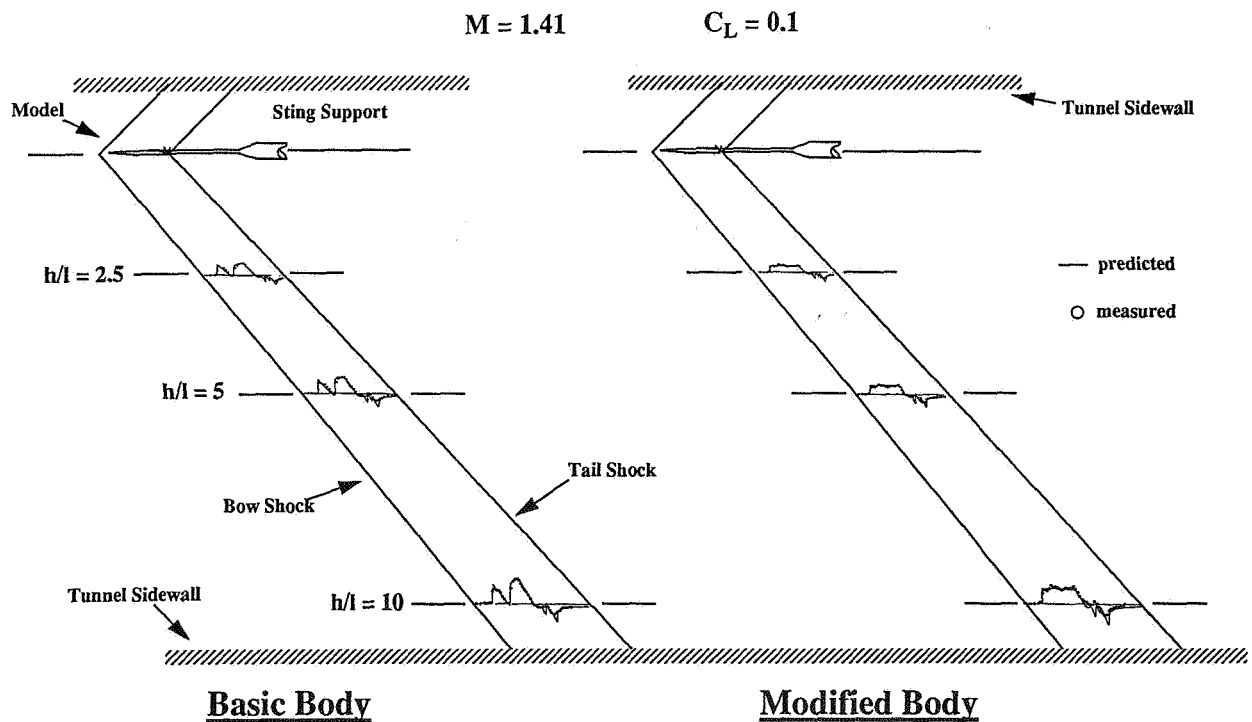


Figure 3

SCHEMATICS OF SONIC BOOM SIGNATURE DEVELOPMENT

Wind tunnel model near-field signatures of the type shown in figure 3 are then inserted into the sonic boom prediction program and propagated to distances/body lengths equivalent to full-scale aircraft flying at cruise altitudes ($h/l \sim 300$) and the resulting sonic boom signatures are established as illustrated by the shock-field signature schematics given in figure 4. Although the original intent of figure 4 was to highlight the so-called low-boom high-drag paradox,² the figure is used herein to illustrate the rapid coalescence of the near- and mid-shock field of the basic saw-tooth signature into an N-wave at the ground. The modified flat-top signature appears to propagate as a flat-top waveform from near- and mid-field to the far-field at ground level. Experimental verification of the coalescence of the basic saw-tooth signature into an N-wave, as predicted by theory and wind tunnel model tests, has been established from in-flight measurements in the near- and far-field and at a ground level for large aircraft flying at high altitudes.^{7,8,9,10} A corresponding full-scale/large-scale experimental verification for configurations designed to produce "shaped" (non N-wave signatures) waveforms has not yet been demonstrated. In fact, of the more than 13,000 sonic boom signatures that have been measured to date involving some 18 different size, shape, and weight aircraft and even space vehicles operating at a range of Mach numbers to 23 and heights to 250,000 feet, all have had typical saw-tooth/N-wave shapes. Thus there is the need for experimentally establishing whether a "shaped" waveform, shown to be "do-able" on wind tunnel models out to about 10 body lengths, will persist out to representative full-scale flight conditions of about 200 to 300 body lengths.

N-WAVE DESIGN

FLATTOP WAVE DESIGN

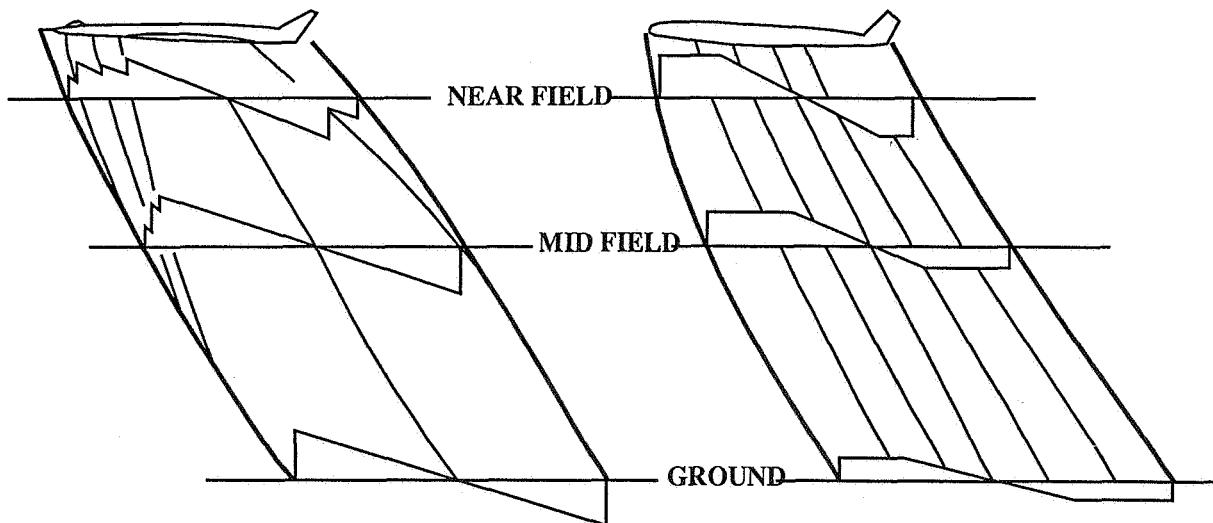


Figure 4

OBJECTIVES OF FEASIBILITY STUDY

As indicated in figure 5, there are two objectives to be addressed in the present study. The primary objective is to assess the feasibility of utilizing relatively large remotely piloted vehicles (RPV's) or drones to experimentally establish the persistence of "shaped" sonic boom signatures out to representative cruise flight distances (200 to 300 body lengths) in a real atmosphere. A secondary objective would be to provide an early indication of the influence of the atmosphere on "shaped" waveforms as they propagate from the vehicle to the ground. This would be especially informative since the present data base on atmospheric influences on sonic boom signatures is based entirely on saw-tooth/N-wave type sonic boom shapes.

- ① Experimentally establishing whether a "shaped" waveform, shown to be "do-able" on wind-tunnel models out to about 10 body lengths, will persist out to representative flight conditions of about 200-300 body lengths.
- ② Obtain early indication of influence of atmosphere on "shaped" waveform.

Figure 5

METHODS OF ESTABLISHING PERSISTENCE OF MODIFIED SONIC BOOM SIGNATURES

In addition to the preferred use of recoverable RPV targets/drones to accomplish the objectives of this feasibility study that is, in fact, the primary thrust of the current study, six other approaches to establishing the persistence of modified sonic boom signatures were identified and are listed in figure 6. An examination was made of the pros and cons of each technique. The six techniques consist of the use of very large supersonic wind tunnels and very small models, the use of large ballistic range firing equivalent bodies of revolution, the use of a whirling-arm technique and complete vehicle geometries (winged bodies) in a large anechoic wind tunnel or enclosure, the use of a full-scale rocket sled track, the adapting of a model shape nose probe attached to a current supersonic aircraft and, finally, the use of lower cost nonrecoverable RPV targets/missiles.

Study findings regarding these alternate approaches to experimentally establishing the persistence of shaped sonic boom signatures to very large distances were, for the most part, not suitable. Only two of the six techniques addressed are considered promising. The following remarks highlight the study findings regarding the six alternate schemes. The use of nonrecoverable vehicles and missiles were deemed inappropriate since the required sonic boom shape modifications would have a significant influence on the basic flight characteristics and stability and control. Costs are also a significant factor since each flight would require a vehicle and its associated geometric modifications. Very large wind tunnels, supersonic sled tracks, and aircraft nose probes are also considered not applicable; large wind tunnels because they are nonexistent, sled tracks because of the presence of the ground surface, and nose probes because of the overwhelming influence of the airplane shock flow field. The ballistic range and whirling-arm techniques are, however, considered applicable, especially the former.¹¹ Each of these latter two simulation techniques may be used to generate a substantial data base on sonic boom signatures relative to vehicle geometries and atmospheric influences; the ballistics range using equivalent bodies of revolution and the whirling-arm technique using complete airplane geometries (winged vehicles).

- Large supersonic tunnels / small models / uniform "atmosphere"
- Ballistics range / bodies of revolution / variable "atmosphere"
- Whirling arm / winged model / anechoic tunnel / variable "atmosphere"
- Supersonic rocket sled track
- Nose probe on supersonic aircraft
- Lower cost non-recoverable RPV vehicles / missiles
- ✓ • Controllable / recoverable RPV targets / drones

Figure 6

COMPARISON OF REAL AND SCALED SIMULATION

A fundamental question that needs to be addressed regarding the present feasibility study is whether or not the proposed scheme to utilize relatively large RPV's will more firmly establish the credibility of "modified" waveforms. Some of the concerns being expressed can be illustrated with the use of figure 7. Shown in the figure are two schematics of the shock-signature patterns representing the full-scale real airplane case of a 200-foot long vehicle flying supersonically at 60,000-foot altitude (300 body lengths) as shown on the left side of the figure, and the situation for a 30-foot RPV flying supersonically at about 9,000-foot altitude (also 300 body lengths) shown on the right side of the figure. Although the requirement to simulate the 300 body length equivalency is duplicated for both full-scale and RPV cases, the consistency of the atmosphere in terms of the influence of atmospheric pressure, temperature, sound speed, density, oxygen-nitrogen, and relative humidity at the vehicle altitudes is not duplicated. In addition, the so-called "scaled height" as it relates to signature freezing" must be addressed. The questions, therefore, are twofold: first, do atmospheric parameters play a significant role in the persistence of "modified" signatures; second, is "scale height" required to establish "frozen" modified signatures? Discussions relative to these two issues suggest that confirmation of the persistence of "modified" sonic boom signatures will be established based upon the simulation of equivalent body lengths, especially since atmospheric density is increasing with decreasing altitude.

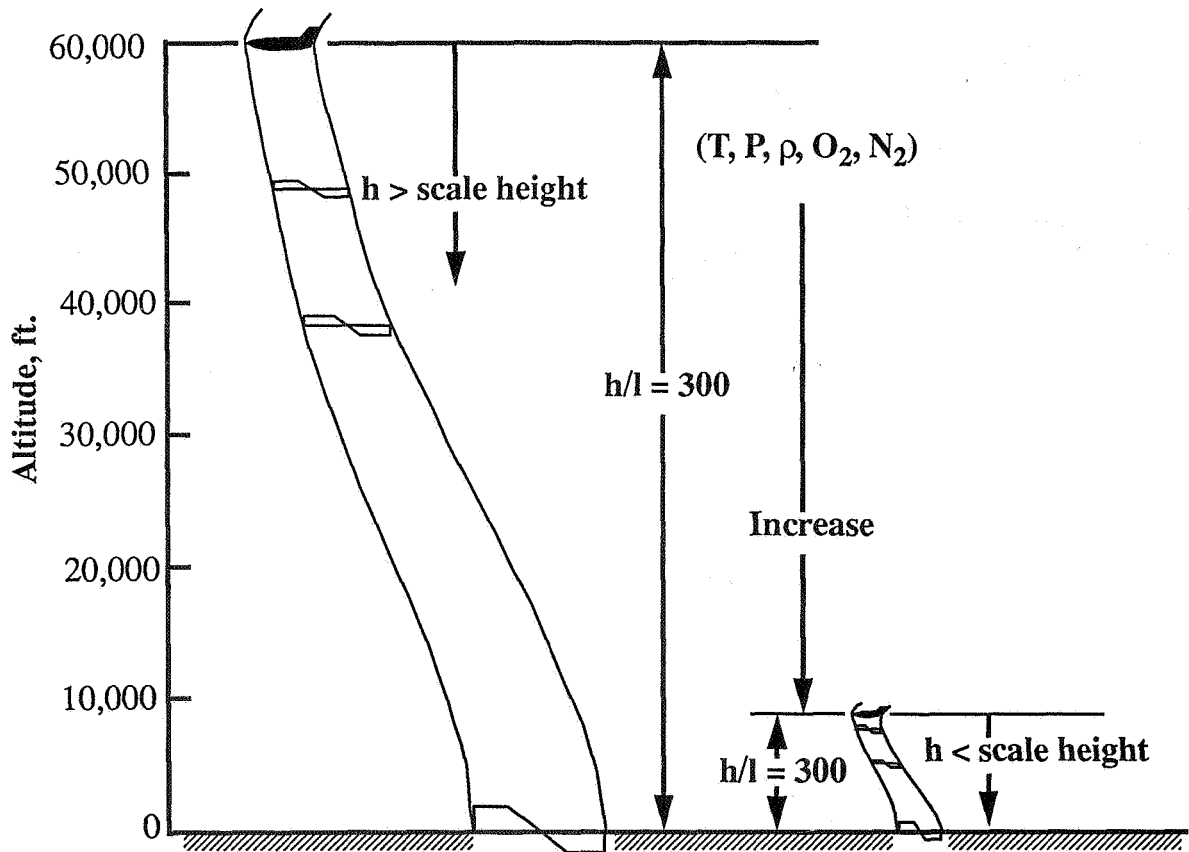


Figure 7

DESIRABLE RPV FEATURES

In selecting a recoverable RPV, a number of requirements were addressed along with such factors as availability, suitability, costs, and operational/launch capability. Seven features were identified as being desirable, if not required, in the RPV selection and these are listed in figure 8. The vehicle should be relatively large (20 to 30 feet in length), capable of Mach 1.2 to 2.5 ranges at altitudes of about 5,000 to 10,000 feet, be controllable, able to hold steady-level Mach altitude for about 5 miles, be ground launched, recoverable, and modifiable.

Vehicle length is critical in establishing its operating altitude as established by the 200 to 300 body length simulation. Since the secondary objective of this effort is to acquire an early look at the effects of atmospheric turbulence in the first 1,000 to 3,000 feet or so of the Earth's boundary layer, vehicle flight altitudes greater than 3,000 are desirable. Thus, a minimum vehicle length of about 13 feet is established. Sonic boom minimization studies have focussed on the Mach range 2.0 to 3.0 but have also been conducted at Mach numbers as low as 1.5.¹² The minimization concept and signature persistence should be demonstrable at even lower Mach numbers. The only real concern is that the vehicle be able to operate a speed sufficiently greater than the cutoff Mach number (Mach number below which boom will not reach the ground). For altitudes from 5,000 to 10,000 feet, the highest cutoff Mach number is the order of 1.1 or less.¹³ Thus, flights at Mach 1.2 and greater are appropriate.

Since the vehicle is to be modified in the sense of changing its equivalent area distribution, it is preferred to make the area additions to the nonlifting portions of the vehicle which will, hopefully, have little effect on the basic vehicle loads and stability and control. The drag of the modified vehicle will differ from the basic configuration.

Finally, a ground-launched recoverable vehicle will not only be very cost effective, it will eliminate a number of activities that could complicate the program and degrade the safety aspect of the flight operations.

- Relatively large size (20 - 30 ft.)
- $M = 1.2 - 2.5$ at 5,000 - 10,000 ft.
- Controllable flight
- Hold steady-level Mach-altitude for 5 miles
- Ground-launched
- Recoverable
- Modifiable

Figure 8

~~e.4~~

SIGNIFICANT FEATURES OF MODIFIED SONIC BOOM SIGNATURE

In order to establish the persistence of modified sonic boom signatures to long distances, a number of concerns must be addressed relative to the signature characteristics and these are indicated in figure 9. First of all, the shape of the signature is of paramount importance. That is to say that the overpressure level of the "shaped" signature is of secondary importance in the sense that "modified" or "shaped" RPV/drone may have Δp 's larger than the "basic" unmodified vehicle. Also, the "shaped" signature need not have similar bow and tail shocks. It is known from laboratory subjective response studies that any modifications to sonic boom signatures should be equally applied to both bow and tail shocks; that is, if a flat-top signature is developed, it should be symmetrical in regards to bow and tail shocks. Waveform symmetry places a significant constraint on vehicle modifications. On the other hand, designing a vehicle to produce a nonsymmetrical "modified" waveform is more easily acquired. Finally, the "modified" signature must be distinguishable from an N-wave as measured at ground level (200 to 300 body lengths).

- Shape of signature is of paramount importance
- Δp level of "shaped" signature is of secondary importance
- "Shaped" signature not required to be symmetrical
- "Shaped" signature must be distinguishable from an N-wave

Figure 9

RELATIONSHIP OF SIGNATURE SHAPES TO
VEHICLE AREA DEVELOPMENT

In order to design a vehicle to have a “modified” or “shaped” sonic boom waveform, it must combine its equivalent area due to both volume and lift to produce a reasonably smooth total area development along its longitudinal axis similar to the ones shown in the lower portion of figure 10.² Note that very little change in area development is required to the vehicle in order to produce either a flat-top waveform, shown to the left of the figure, or a ramp-type waveform shown to the right of the figure. However, each of these equivalent area distributions are considerably altered from that associated with a basic/standard vehicle design that produces an N-waveform (as illustrated in the upper center portion of the figure). Since the required modifications to any RPV/drone must be made in terms of “adding to” rather than “taking away” area, the subject test vehicle will most likely require a nose extension along with area additions mid-ship on the vehicle.

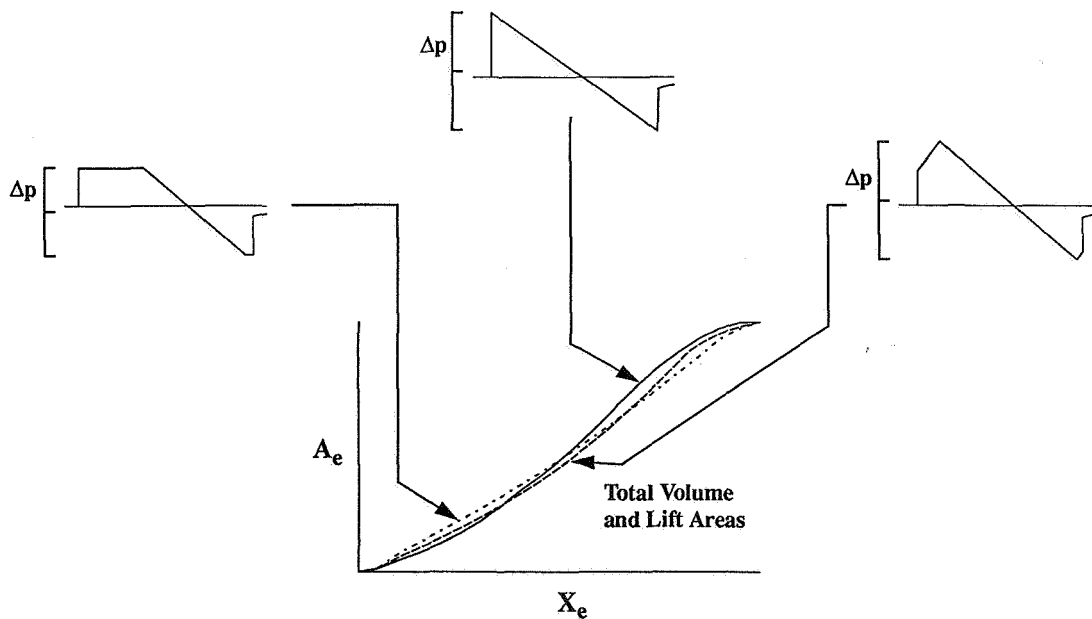


Figure 10

SPECTRAL CHARACTERISTICS OF BASIC AND MODIFIED SIGNATURES

Since the present study is aimed at developing "modified" signatures of the flat-top and ramp-type waveforms that are nonsymmetrical, that is, changing the positive portion of the signature but not the negative phase, it is of importance to examine the signature spectra of each of these types of waveforms as compared to the basic symmetrical N-wave to see if any significant changes are evident. A comparison of the spectra for an N-wave, a flat-top positive phase waveform, and a ramp-type positive phase waveform is given in figure 11. Little if any difference is noted to exist between the three waveform spectra. This suggests that from the standpoint of signature identification due to atmospheric influences, there are no driving reasons to select a ramp-type "modified" signature over one having a flat-top waveform shape. This allows for some latitude in the selection of and modification to a particular RPV/drone configuration.

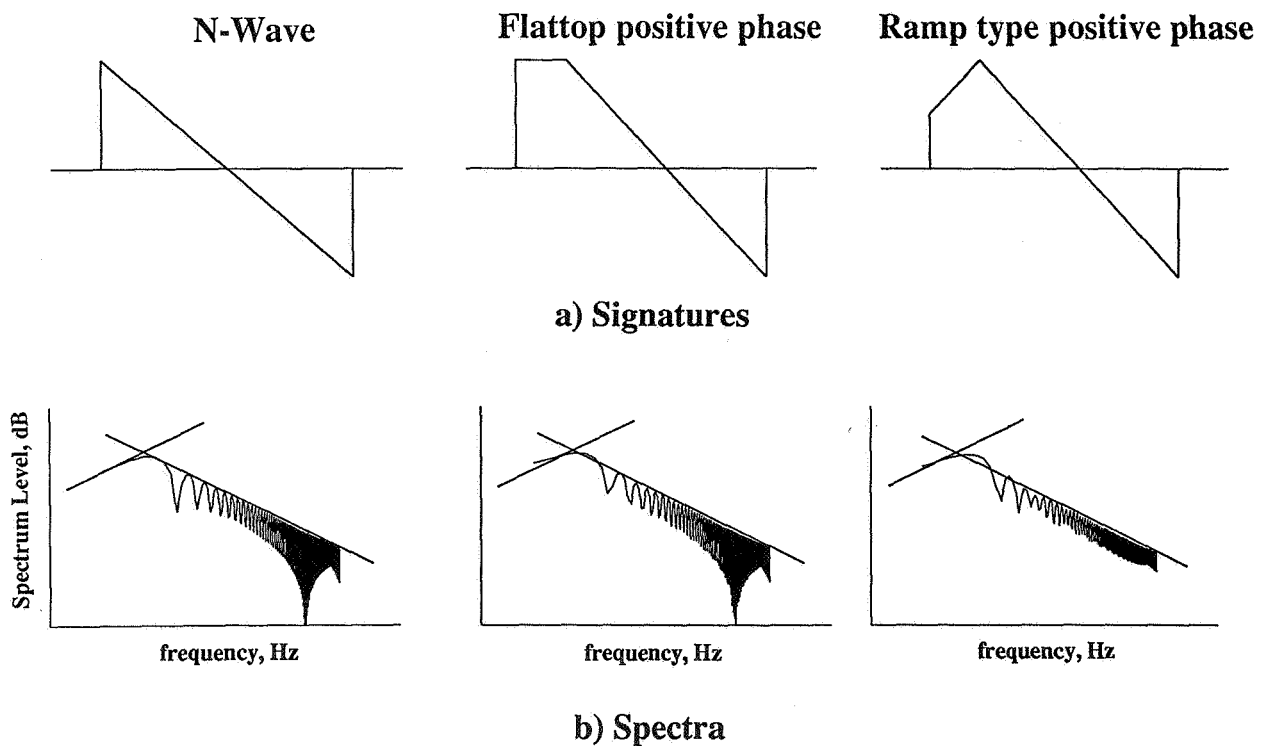


Figure 11

CANDIDATE TEST VEHICLES CONSIDERED IN STUDY

There are three candidates in the class of recoverable vehicles that were considered in this study and these are shown in figure 12. The first of these recoverable vehicles is the Teledyne Ryan Firebee (BQM-34 E) shown in the top portion of the figure. The Firebee is a wing-tailed aircraft type controllable-recoverable supersonic RPV target of about 28 feet in length, weighs about 1,900 pounds, is powered by a J-69 turbojet, and is of 1970 vintage. It can be either air- or ground-launched and has a Mach capability of about 1.3 at about 8,000 feet increasing to Mach 1.5 at 20,000 feet. Only about eight of these vehicles are in existence since they have been phased out of operation by the Navy and Air Force. Two complete vehicles with spares (except engines) are currently retained by NASA Langley Research Center. These vehicles were routinely launched at Pt. Mugu, Puerto Rico, and Tyndall and have experienced reuse rates of about 10 sorties. Currently, the vehicle is being phased out of DoD operations.

A QF-4 drone aircraft was the second recoverable vehicle to be considered in this study and is shown in the center portion of figure 12. The QF-4 is a drone version of the F-4 fighter and is about 58 feet in length, has an average weight of about 45,000 pounds, is powered by two J-79 turbojet engines, and is of 1960 vintage. As a drone, it is remotely operated as a normal aircraft in terms of performing takeoff-landings and landings and supersonic flights. It has a Mach capability of about 1.3 to 1.4 at about 18,000 feet. It is understood that the QF-4 drones will probably be in use at Pt. Mugu for the next decade or so.

The third recoverable vehicle considered is the Martin Marietta SLAT shown in the lower portion of the figure. It is a finned-missile type controllable-recoverable supersonic RPV target of about 18 feet in length, weighs about 2,500 pounds, is powered by an airbreathing ramjet and is of 1990 vintage. It is air-launched and has a Mach capability of 2.5 at 8,000 feet. The "SLAT" is still in the development stage and is being launch-tested at Pt. Mugu.

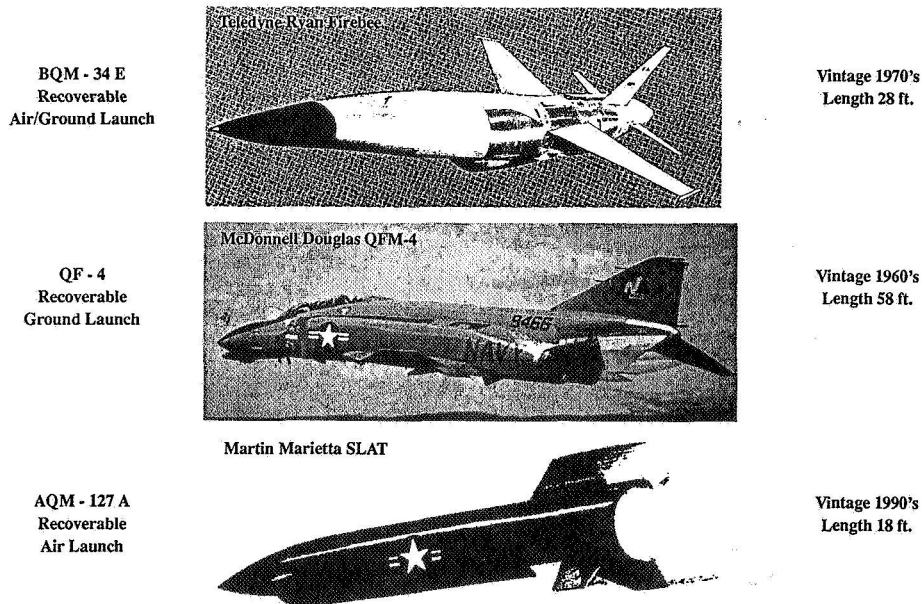


Figure 12

AREA DISTRIBUTIONS AND SONIC BOOM SIGNATURES OF
CANDIDATE VEHICLES

The most significant feature in the selection of an appropriate test vehicle, regardless of cost and availability, is the "modifiability" of the vehicle. The area developments of the Firebee, QF-4, and SLAT are given in figure 13 along with the associated sonic boom signature that would be observed at the 300 body length and corresponding Mach-altitude combinations. Note that all three signatures are of the "saw-tooth" character and are rapidly approaching an N-wave shape. In addition, the equivalent area distributions for the "airplane type" Firebee BQM-34 E and the QF-4 drone airplane are similar since they are both winged-tailed configurations and, thus, more gradual in their area buildup than for the finned-missile SLAT which displayed a very rapid area buildup from the nose to a flatter more constant area development along the mid-aft constant diameter portion of this vehicle. Thus, in order to generate a "shaped" signature (flat or ramp type) out of any of the three vehicles, extensions to the forward portion of the vehicles will be required in order to generate the typical area buildups indicated previously on figure 10. Extension of the nose section of the SLAT to provide for the required more gradual area buildup to produce a ramp or flat-top sonic boom waveform could seriously alter the existing matched nose-inlet design of the basic SLAT vehicle. Area must also be added to the mid-aft sections in order to maintain a smoothly increasing area development.

Both the Firebee RPV and the QF-4 drone have equivalent area developments that are more amenable to modification in terms of providing for a ramp or flat top type sonic boom signature. Because the Firebee RPV has a higher fineness ratio than the QF-4, it also has a more gradual equivalent area development as noted in figure 13. Extension of the nose section on the smaller, more slender, Firebee would appear to present less of a problem than to do the same procedure on the full-scale QF-4 drone airplane. In addition, the two inlets on each side of the QF-4 could present more difficulties than the single "belly" type inlet on the Firebee in terms of uniformity of flow and boundary layer buildup. Finally, the necessary area additions required on the mid-sections of each vehicle suggest that the Firebee would be least difficult to alter.

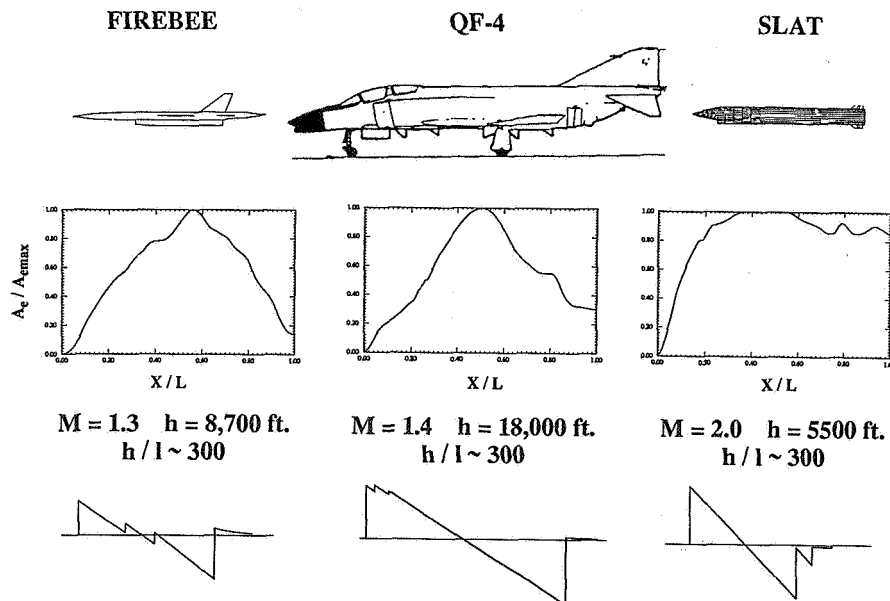


Figure 13

AREA DISTRIBUTIONS AND SIGNATURE CHARACTERISTICS OF FIREBEE CONFIGURATIONS

Selection of the 28-foot long Firebee vehicle as a primary candidate sets the flight altitude-Mach combination of 8,700 feet (300 body lengths) and 1.3, respectively. At these given Mach-altitude conditions, calculations were made of the equivalent area distributions for the basic vehicle and the equivalent area developments required to produce a boom signature having a flat top positive phase and one having a ramp-positive phase signature at ground level. These results are presented in figure 14. At the top of the figure are schematic illustrations of the profile view of the basic Firebee and profiles of the two altered vehicles that are designed to give a flat-top and ramp-type signature. Note that the nose and midsection portions (beneath the inlet) of the latter two vehicles required modification in the form of a nose extension and added area to the midsection. The basic (unmodified) vehicle area distribution shown on the left part of the figure has been carried over to the other two area plots as dashed lines in order to give a visual feel for where area (or volume) had to be added in order to end up with the area developments that produce the flat-top and ramp-type positive phase of the boom signature.

On examining the two modified signatures in terms of their "distinguishability" from the basic Firebee signature (almost an N-wave) it would appear that the flat top positive phase waveform would be preferred over that of the ramp type since the latter appears not too far from becoming an N-wave. In either case, it would be highly desirable to have a flat-top waveform with as long a "flat" duration as possible or a ramp-type with a "large" ramp (i.e., very little initial vertical bow-shock rise) as possible. Increasing the boom signature emphasis of the flat top and ramp characteristics required, primarily, greater extensions to the vehicle nose than the present 3.0 feet for the two cases shown.

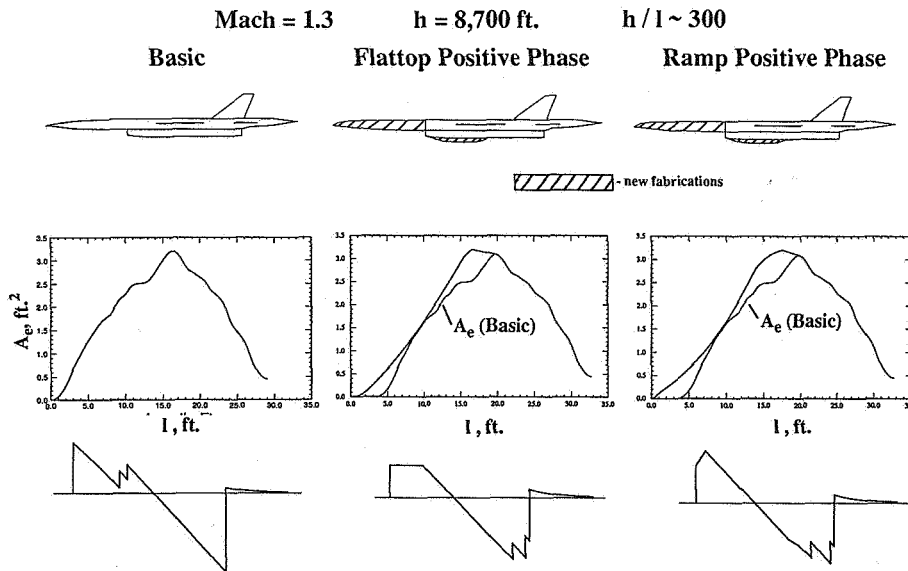


Figure 14

SCOPE OF WIND TUNNEL AND FLIGHT TEST

The scope of the Firebee wind tunnel and flight test program may be illustrated with the aid of figure 15. As indicated by the upper portion of the figure, sonic boom and force models of the basic and modified configurations would be tested at Mach 1.25 and 1.5 in the NASA LaRC 8-foot transonic tunnel (8-ft. TT) and Unitary Plan Wind Tunnel (UPWT), respectively. One model 1-foot length, considered large enough to provide geometric fidelity and also to house a six-component internally mounted strain-gage balance, would suffice for both sonic boom and force tests in each facility and permit boom signature measurements of from 1 to 4 body lengths from the model. A single model with interchangeable nose and belly sections would be utilized for the basic and modified vehicles.

Force tests will establish whether the sonic boom modifications significantly alter the vehicle flight characteristics. Boom tests will provide confirmation of and guidance to the flight test program with respect to the sonic boom signatures expected for the baseline and modified vehicles. Pressure signatures in the near-field from 1 to 4 body lengths would be made for zero-lift and at angles of attack associated with cruise. The flight test program would begin upon completion of the wind tunnel tests. As noted in the lower portion of figure 15, the primary tests, (those required to accomplishing the primary objective) are indicated by the solid lines. A set of desirable tests (designed to accomplish the secondary objective) are indicated by the dashed lines. Note that the primary flight tests (four blocks to the left of the figure) are conducted under minimal atmospheric influences and involve a minimum of two passes each of the baseline and modified vehicles at the design Mach-altitude conditions of 1.3 and 8,500 feet, respectively (300 body lengths), followed by a similar set of runs at Mach 1.5 and 20,000 feet (700 body lengths).

Depending on the Firebee flight recovery success rate, the basic and modified vehicles could be flown at repeat conditions of the Mach-altitude for highly active lower-layer atmospheric conditions (represented by the four boxes to the right of figure 13). Thus, an early indication of the influence of the lower turbulent layers of the atmosphere on modified signatures will be observed.

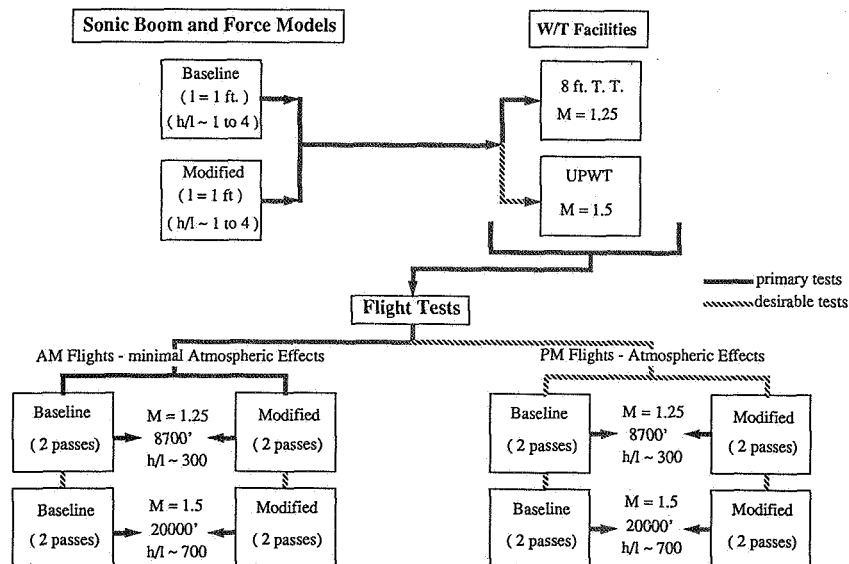


Figure 15

**PREDICTED SONIC BOOM SIGNATURES FOR WIND TUNNEL TESTS OF
FIREBEE MODELS**

The predicted sonic boom signatures for the wind tunnel tests of the one-foot model representing the baseline Firebee configuration and one modified to produce a flat top or ramp positive phase signatures operating at Mach 1.25 in the 8-foot transonic tunnel and at distances of 1, 2, 3, and 4 body lengths (h/l) from the model are illustrated in figure 16. The signatures are drawn approximately to scale in terms of the pressure and time scale in order to provide a better feel for how much change is taking place in the signature characteristics as distance from the model is increased and, also, to provide a view of the difference between the basic and modified signatures. Such comparisons will provide insights into the final selection of a modified waveform relative to the final vehicle design. Note that the signatures are fairly complex in terms of number of shocks and that both the flat top positive phase and the ramp type positive phase signatures persist at all distances from the model.

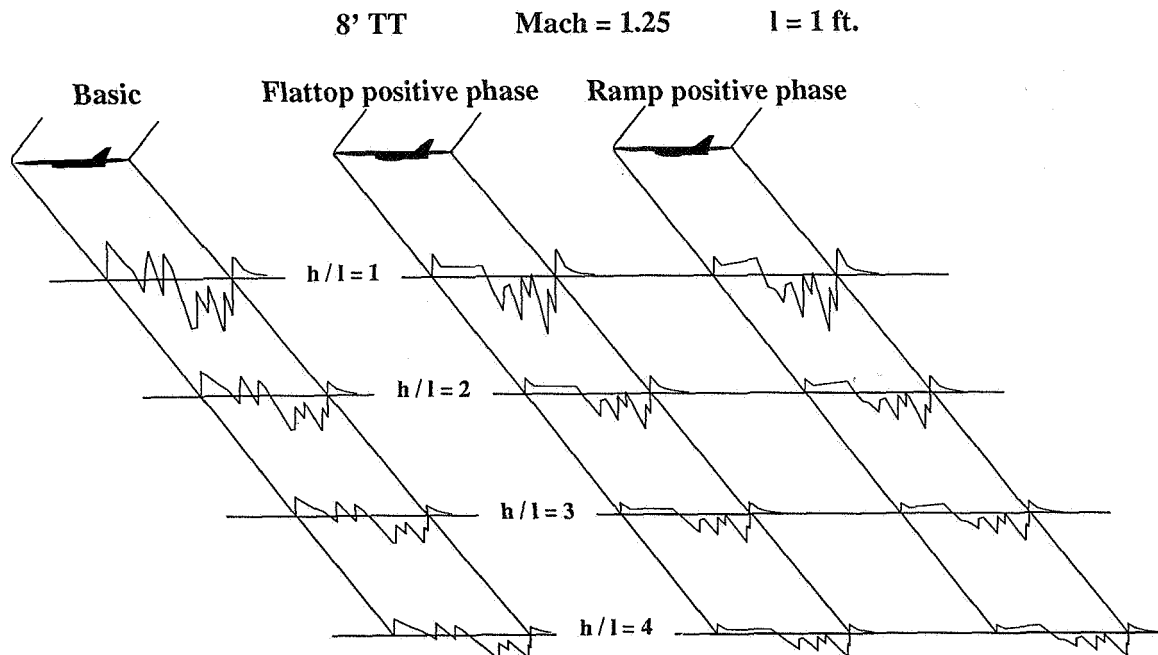


Figure 16

**PREDICTED SONIC BOOM SIGNATURES FOR FLIGHTS OF FULL-SCALE
FIREBEE VEHICLES**

The predicted sonic boom signatures for flights of the full-scale 28-foot Firebee and one modified to produce the flat top or ramp positive phase signatures, operating at Mach 1.25 and at 8,700-foot altitude are shown for distances of 50, 100, 200, and 300 body lengths from the vehicle in figure 17. Once again, as for the wind tunnel case, the signatures are plotted to scale in terms of pressure and time so that a visual display of what would be observed if measurements could be made at each of the distances that the calculated signatures are shown. Note that the basic Firebee (unmodified) signature develops from a fairly complex "sawtooth" waveform in the near-field to a near N-wave at ground level. The two modified signatures retain their pronounced flat top and ramp character out to 100 or so body lengths. As distance increases to 300 body lengths, the ramp type waveform is beginning to steepen into a near N-wave. The flat top waveform, however, is still quite distinguishable.

In addition to the planned sonic boom measurements at ground level (300 body lengths), it also appears feasible to acquire measurements at 100 and 200 body lengths from the vehicle using an airborne measurement platform. Such near- and mid-field signature measurements will greatly enhance the program findings and add significant insight and confidence in sonic boom signature minimization as it relates to vehicle design.

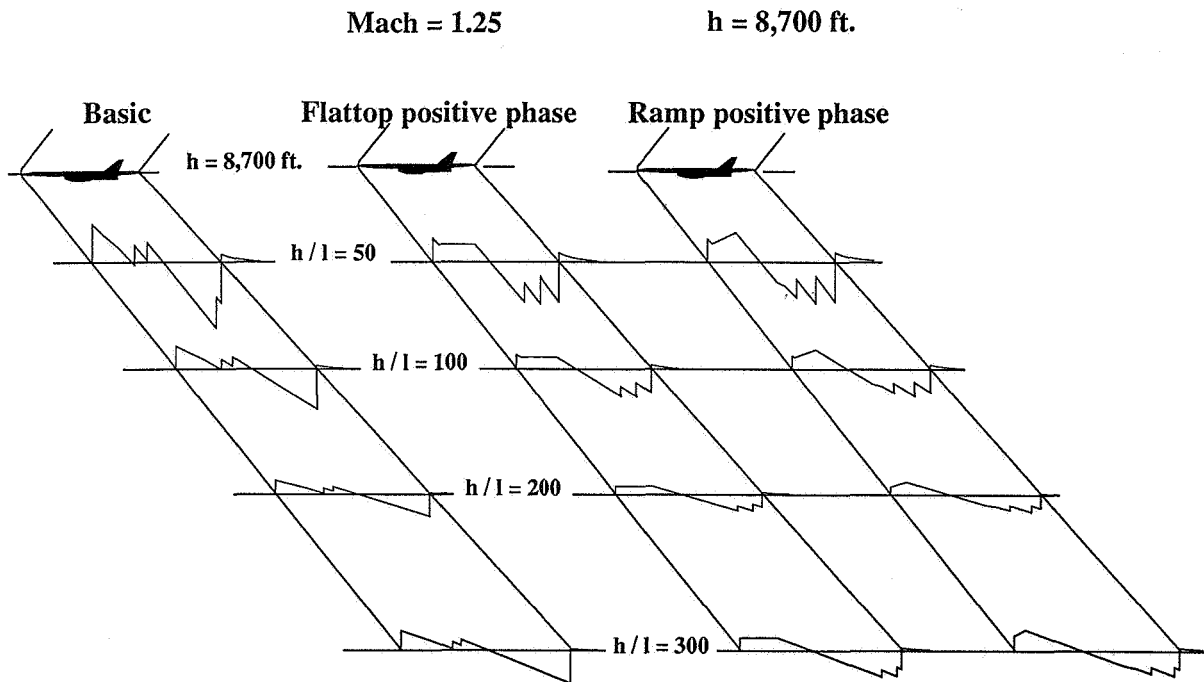
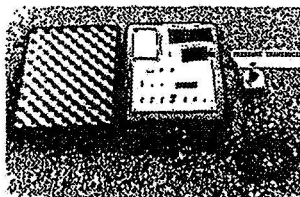
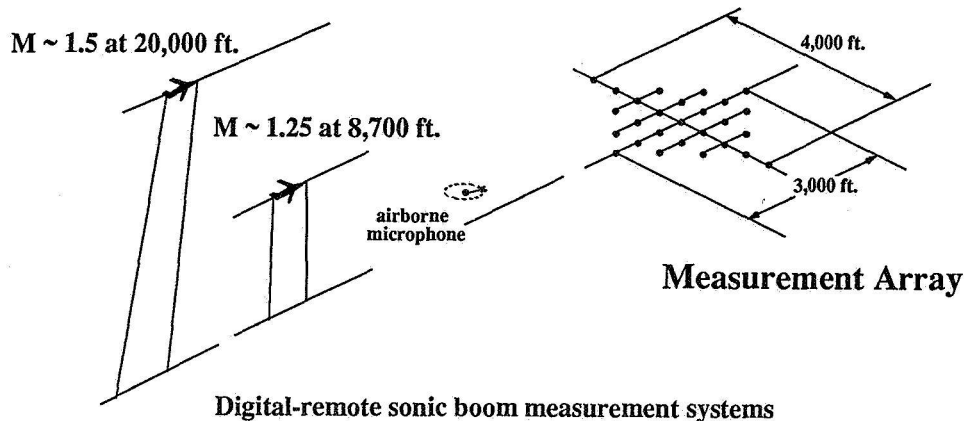


Figure 17

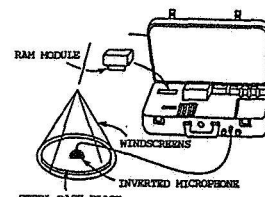
FIREBEE SONIC BOOM FLIGHT TEST SETUP

An indication of the manner in which sonic boom measurements will be acquired during the Firebee flight tests is presented in figure 18. Shown in the figure are schematic illustrations of the Firebee flying at the design conditions (relative to boom signature modifications) of Mach 1.25 and an altitude of 8,700 feet and also an off-design condition of Mach 1.5 and an altitude of 20,000 feet above ground level over a large array of microphones spaced along the ground track for a total of 3,000 feet and at various distance to each side of the track out to about 2,000 feet. Having such an arrangement eases the constraints of having the vehicle fly exactly along the desired ground track centerline both in terms of its lateral displacement and heading. The microphone separation will also provide an indication of the stability of the atmosphere through which the shock waves propagate and also provide information on character of the signatures at lateral locations. It is planned to make use of the digital-remote self-triggering measurement systems, PATS, developed by NASA-Johnson Space Center (Portable Automated Systems¹⁴) and USAF BEAR System (Boom Event Analyzer Recorder¹⁵) shown in the lower portion of the figure. The equivalence of these systems as compared to the previously employed NASA analog sonic boom measurement systems has been demonstrated.¹⁶

Also shown on the figure is a schematic of an orbiting airborne measurement platform carrying one of the remote-digital boom measurement units aloft to altitudes of 3,000, 6,000 and even 10,000 feet aboard an RPV surveillance vehicle such as the USMC Pioneer. The combination of the relatively slow speed of the vehicle, about 40 miles per hour, and the high signal-to-noise ratio associated with the sonic boom signature (in reference to airflow noise over the microphone) should permit quantitative boom signature measurements. The weight of the digital-remote boom measurement unit is well within the current payload capability of the Pioneer vehicle. However, an initial flight test using the Pioneer airborne sonic boom arrangement would be required to assure that the concept is valid.



NASA JSC - "PATS"



USAF - "BEAR"

Figure 18

SUMMARY REMARKS

A study has been made to determine the feasibility of experimentally establishing whether a “shaped” sonic boom signature, shown to be “do-able” on wind tunnel models out to about 10 body lengths, will persist out to representative flight conditions of about 200 to 300 body lengths. The study focuses on the use of relatively large supersonic remotely-piloted and recoverable vehicle. Other simulation methods that may accomplish the objectives were also addressed and include the use of nonrecoverable target drones, missiles, full-scale drones, very large wind tunnels, ballistic facilities, whirling-arm techniques, rocket sled tracks, and airplane nose probes.

The feasibility of experimentally establishing the persistence of modified sonic boom signatures to representative flight conditions using a relatively large supersonic remotely-piloted and recoverable vehicle has been established. It has been determined that the Firebee BQM-34 E vehicle is a suitable test vehicle in terms of its adaptability to geometric modifications, operational capabilities regarding Mach-altitude, availability, and costs.

A key ingredient addressed within the study include selection of a modified (shaped) and identifiable sonic boom signature that differs from the normally observed saw-tooth N-wave signatures, is one that is compatible with vehicle geometric alterations. It was determined that nonsymmetric “shaped” signatures would be utilized and include both a flat-top positive phase waveform and a ramp-type positive phase waveform.

The experimental program involved wind tunnel tests on models and full-scale flight tests. Wind tunnel tests would be conducted in the Langley 8-foot Transonic Tunnel at Mach 1.25. It is also highly desirable to conduct tests in the Langley Unitary Plan Wind tunnel at Mach 1.5 for correlation with past sonic boom experience. Flight tests would be conducted at Pt. Mugu, California, with the WSMR, New Mexico, as an alternate site.

- Study has been conducted to examine the feasibility of experimentally demonstrating the persistence of “shaped” boom signatures to very large distances in a real atmosphere
- Study focussed on use of relatively large supersonic recoverable RPV
- Findings confirm feasibility of conducting overflight measurements of sonic boom signatures using Firebee RPV
- Nonsymmetric “shaped” boom signatures will be utilized
- Experimental program involves both W/T test on models and full scale flight tests
- W/T test would be conducted in LaRC 8' TT at Mach 1.25
- Highly desirable to conduct tests in LaRC UPWT at Mach 1.5 for correlation with past sonic boom experience
- Flight tests would be conducted at Pt. Mugu or WSMR

REFERENCES

1. Niedzwiecki, A.; and Ribner, H. S.: Subjective Loudness and Annoyance of Filtered N-Wave Sonic Booms. *J. Acoustic Soc. America*, vol. 6, no. 3, 1974, pp 705-707.
2. Darden, Christine; et al: Status of the Sonic Boom Methodology and Understanding. NASA CP-3027, 1988.
3. Carlson, Harry W.; McLean, F. Edward; and Shrout, Barrett L.: A Wind Tunnel Study of Sonic Boom Characteristics for Basic and Modified Models of a Supersonic Transport Configuration. NASA TM X-1236, 1966.
4. Carlson, Harry W.; Barger, Raymond L.; and Mack, Robert J.: Application of Sonic Boom Minimization Concepts in Supersonic Transport Design. NASA TN D-7218, 1973.
5. Seebass, R.; and George, A.R.: Sonic Boom Minimization. *J. Acoustic Soc. America*, vol. 51, 1972, pp. 686-694.
6. Darden, Christine M.: Minimization of Sonic Boom Parameters in Real and Isothermal Atmospheres. NASA TN D-7842, 1975.
7. Maglieri, Domenic J.; Ritchie, Virgil S.; and Bryant, John F.: In-Flight Shock-Wave Pressure Measurements Above and Below a Bomber Airplane at Mach Numbers 1.42 to 1.69. NASA TN D-1968, 1963.
8. Carlson, Harry W.: Correlation of Sonic Boom Theory With Wind Tunnel and Flight Measurements. NASA TR R-213, 1964.
9. Garrick, I. E.; and Maglieri, D. J.: A Summary of Results on Sonic Boom Pressure-Signature Variations Associated With Atmospheric Conditions. NASA TN D-4588, 1968.
10. Morris, Odell, A.; Lamb, Milton; and Carlson, Harry W.: Sonic Boom Characteristics in the Extreme Near Field of a Complex Airplane Model at Mach Numbers of 1.5, 1.8, and 2.5. NASA TN D-5755, 1970.
11. Bauer, A. B.; and Bagley, C. J.: Sonic Boom Modeling Investigation of Topographical and Atmospheric Effects. Report No. FAA-NO-70-10, 1970.
12. Mack, Robert J.; and Darden, Christine M.: Wind-Tunnel Investigation of the Validity of a Sonic-Boom-Minimization Concept. NASA TP-1421, 1979.
13. Randall, D. G.: Methods for Estimating Distributions and Intensities of Sonic Bangs. R&M no. 3113, British A.R.C., 1959.
14. Stansbery, E. G.; and Stanley, J. F.: Descent Sonic Boom Measurements for STS-26 Including a Mach 23 Measurement. NASA JSC-23579, 1989.
15. Lee, Robert A., et al: Boom Event Analyzer Recorder (BEAR): System Description. USAF AAMRL-TR-89-035, 1989.
16. Lee, Robert A.: Air Force Boom Event Analyzer Records (BEAR): Comparison With NASA Boom Measurement System. USAF AAMRL-TR-88-039, 1988.

THIS PAGE INTENTIONALLY BLANK

Session VI. Propulsion Systems Studies

PRECEDING PAGE BLANK NOT FILMED

THIS PAGE INTENTIONALLY BLANK

omit

Session VI. Propulsion Systems Studies

The NASA Sponsored HSCT Propulsion Studies
William C. Strack, NASA Lewis Research Center

PRECEDING PAGE BLANK NOT FILMED

THIS PAGE INTENTIONALLY BLANK

THE NASA SPONSORED HSCT PROPULSION STUDIES

First Annual High Speed Research Workshop

Williamsburg, Virginia

May 14-16, 1991

William C. Strack
NASA Lewis Research Center

N94-33476

514-07
12004

Objectives

One objective of the NASA-sponsored HSCT propulsion studies is to determine the potential benefits of alternative advanced technologies. These benefits should be explicitly expressed in terms of meeting either environmental acceptability or economic viability. The potential benefit information is used to screen alternative technology candidates to the most promising technologies that, if successfully developed, will enable the propulsion system to achieve high performance and low weight without unduly sacrificing favorable emissions and noise characteristics.

A second objective is the provision of key information to high-level decision makers--enabling them to make rational decisions concerning the technology program content. It will be necessary to pursue more than one concept/technology until experimental validity is convincingly demonstrated. Some technologies will likely fail to achieve their stated goals and timely program redirection depends upon far-sighted system studies to provide such information.

HSCT Propulsion Systems Studies

Objectives

1. *Determine potential benefits of alternative advanced technologies*
 - *Environmental acceptability*
 - *Economic viability*

2. *Provide key information enabling rational decisions concerning technology program content*

Major Propulsion Issues

The issues identified here reflect a global perspective that is important to keep in mind in our quest to identify the enabling technologies. The first issue, "What level of HSC technology is required to attain competitiveness with anticipated subsonic technology," cannot be answered solely from a propulsion viewpoint. We need to forecast potential improvements in both subsonic and supersonic technology to properly assess the merits of HSR expenditures.

It would be very desirable to obtain a quantitative answer to issue 2. The price we pay for environmental acceptability should be expressed in economic terms.

While much of the needed propulsion technology can be unequivocally identified now, there remains a significant uncertainty about which engine cycle is preferable and, therefore, the required engine-specific technology.

Similarly, the preferable noise suppression strategy is presently uncertain. The noise suppression approach is intimately related to the engine cycle selection in this highly complex system.

HST Propulsion Systems Studies

Major Propulsion Issues

1. *What level of HST technology is required to attain competitiveness with anticipated subsonic technology ?*
2. *What price do we pay to achieve various levels of environmental acceptability ?*
3. *Which engine cycle is preferable ?*
 - *Determines engine-specific technology*
4. *Which noise suppression strategy is preferable ?*
 - *Front end approach (Tandem-fan, VCE, Flade, ...)*
 - *Rear end approach (mixer-ejector nozzle, acoustic liners, TAS, ...)*
 - *Hybrid*

Approach

There are a great multitude of propulsion system alternatives that need to be considered. Complicating a comprehensive evaluation of the many choices is the frequent lack of a credible database from which to formulate analytical models. Examples include the emission models for both the LPP and RQL type combustors. Until an experimental database is established, NO_x vs. performance tradeoffs will remain speculative.

Regardless of these shortcomings, the comparative evaluations need to be conducted on a system basis (a mission simulation) to avoid misleading analyzes. The general approach is to conduct complete mission analysis evaluations at the engine companies and NASA utilizing representative airframe and mission definitions supplied by the airframe manufacturers. Upon completion of the screening studies performed by the engine community, a recommended subset of propulsion systems are transmitted to the airframe manufacturers for a final selection that includes installation effects.

Since the emphasis should be on resolving first order issues, highly sophisticated analysis is neither needed nor appropriate except in cases where reliable simple models do not yet exist.

HST Propulsion Systems Studies

Approach

- 1. Identify propulsion system alternatives**
 - *Components (inlets, nozzles, combustors, ...)*
 - *Engine types (TBE, VCE, MFTF, Flade, Tandem-fan, ...)*
 - *Technology levels (2000 EIS, 2005 EIS, 2010 EIS, ...)*
- 2. Perform comparative evaluations on a system basis**
 - *Propulsion system performance and weight*
 - *Installation on a representative airframe*
 - *Mission simulation and evaluation criteria*
- 3. *Involve engine companies, airframe manufacturers, and NASA***

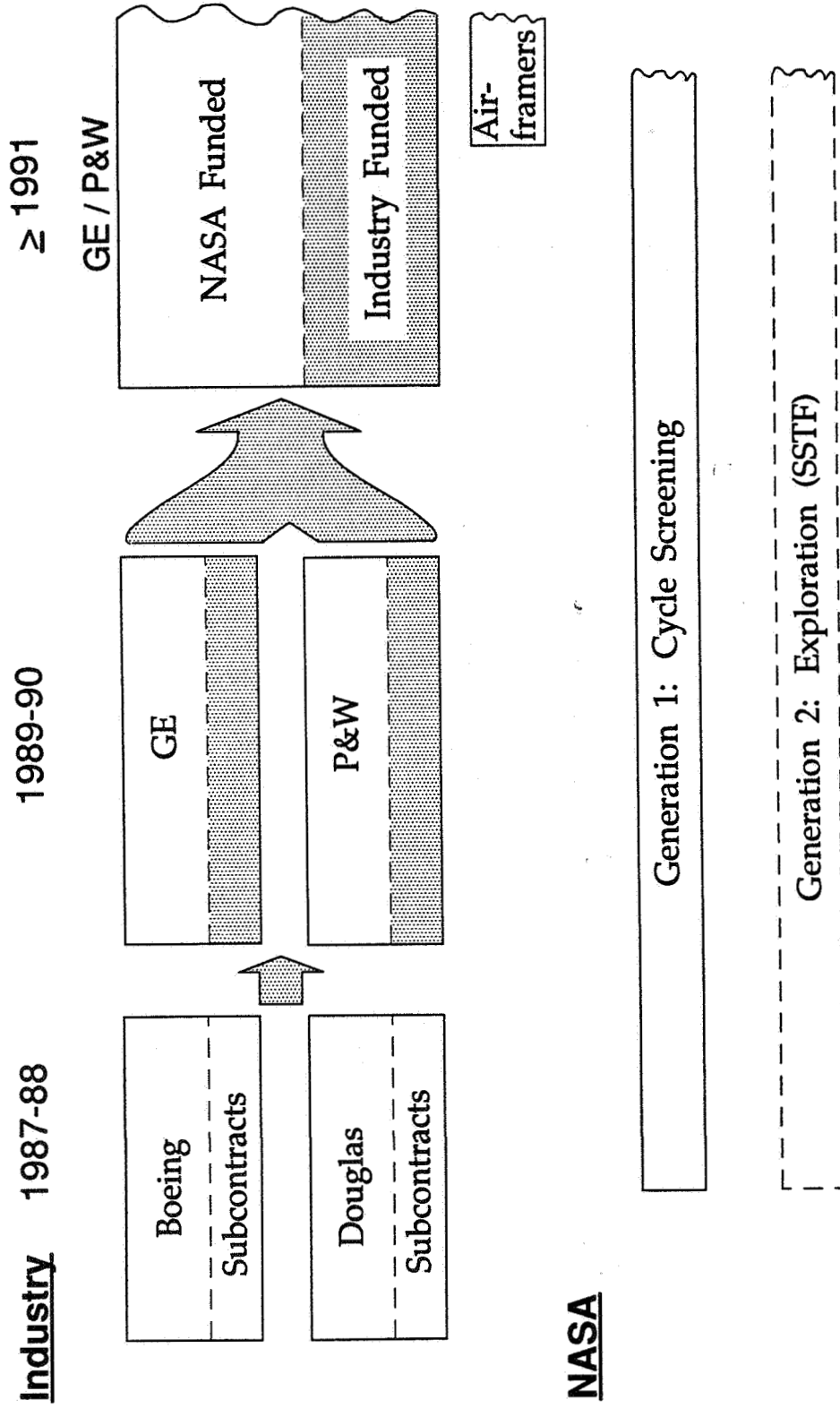
Studies Arrangement

The HSR industry propulsion studies have undergone a radical change in administration. They began life as subcontracts to the two airframe manufacturers. The arrangement was strengthened in 1989 when prime contracts were issued to both engine companies and they initiated IR&D and company funded internal support. Further strengthening occurred late in 1990 when General Electric and Pratt & Whitney initiated an unprecedented collaborative effort in recognition of the fact that a single combined approach is more effective than a parallel, but fragmented approach. In addition, airframe manufacturers are being funded to investigate propulsion-airframe installation options including inlet and nozzle concept screening.

NASA is also conducting in-house engine cycle screening studies to augment the industry studies. This effort is used mainly to help guide the industry effort by providing rapid first-order analyses that identify major drivers and sensitivities. Although not part of the HSR program, related studies are underway of potential second-generation HST powerplants such as the supersonic throughflow fan engine (SSTF).

HSR Propulsion System Studies

Studies Arrangement



HSR Propulsion System Studies Elements

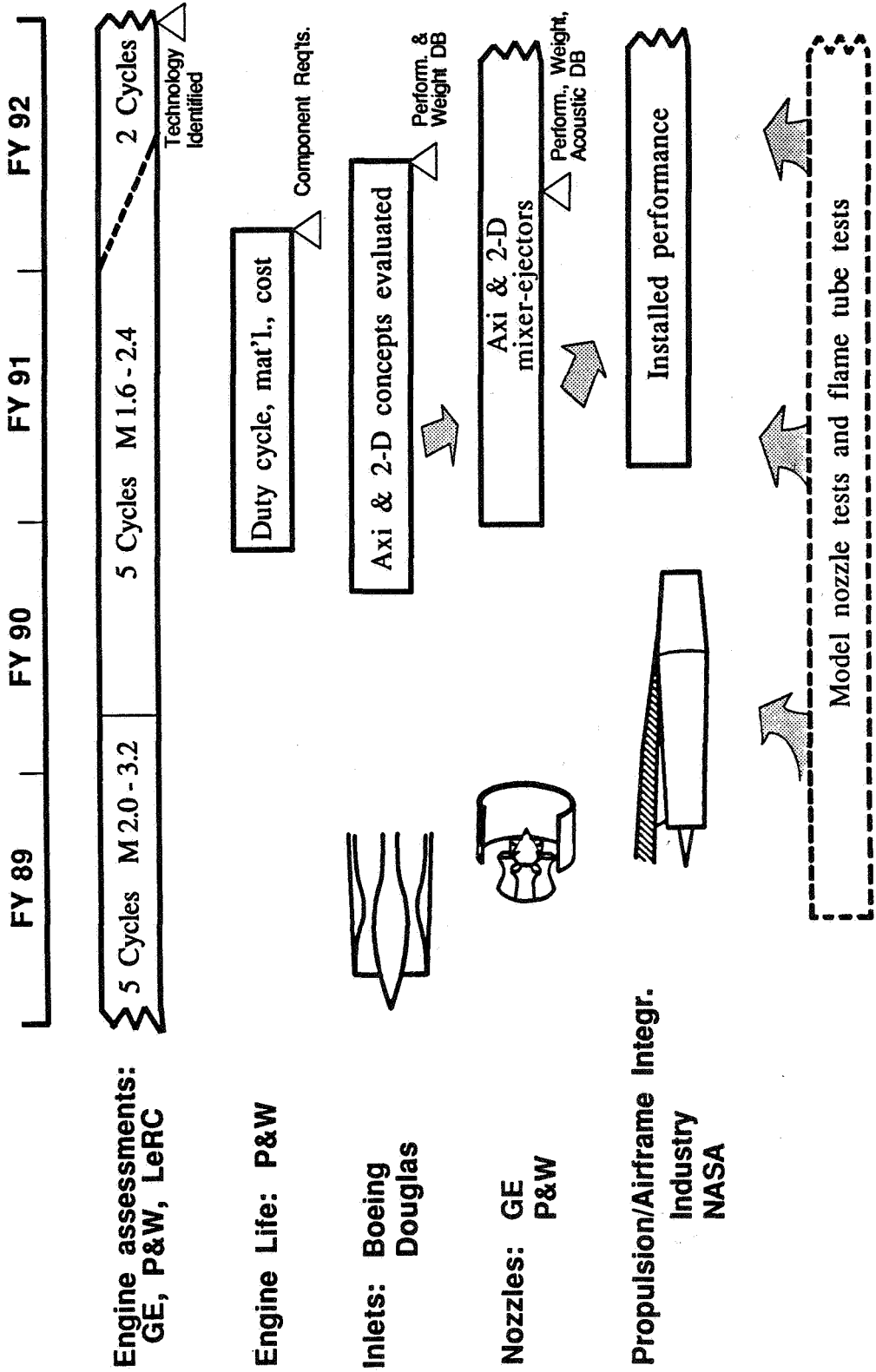
Until recently the propulsion studies effort was essentially addressing the issue of which engine cycle is most attractive. This investigation began over a broad range of flight speeds. Now it is focused almost exclusively at Mach 2.4 and there are five candidate cycles (engine types). Since a propulsion technology program cannot support a large multiplicity of engine types, the goal is to identify the two most promising cycles sometime in 1992. This selection will identify the engine-specific portion of the enabling technology program.

However, since the relative attractiveness of a given engine cycle also depends in large measure upon the inlet, nozzle, and airframe installation, a significant effort was begun in 1991 to establish an analytical database that characterizes the performance, weight, and acoustics of these important elements.

Since much of the effort to date relied on fighter engine design databases, a separate effort has been devoted to determine the impact of converting these designs to yield commercial engine life where the duty cycle is substantially different and leads to creep rather than cyclic fatigue failure.

All of this analytical information, together with ongoing experimental model nozzle and combustion flame tube tests, will be integrated into the propulsion system technology decision process that occurs during 1992.

HSR PROPULSION SYSTEM STUDIES ELEMENTS



Propulsion Concept Status

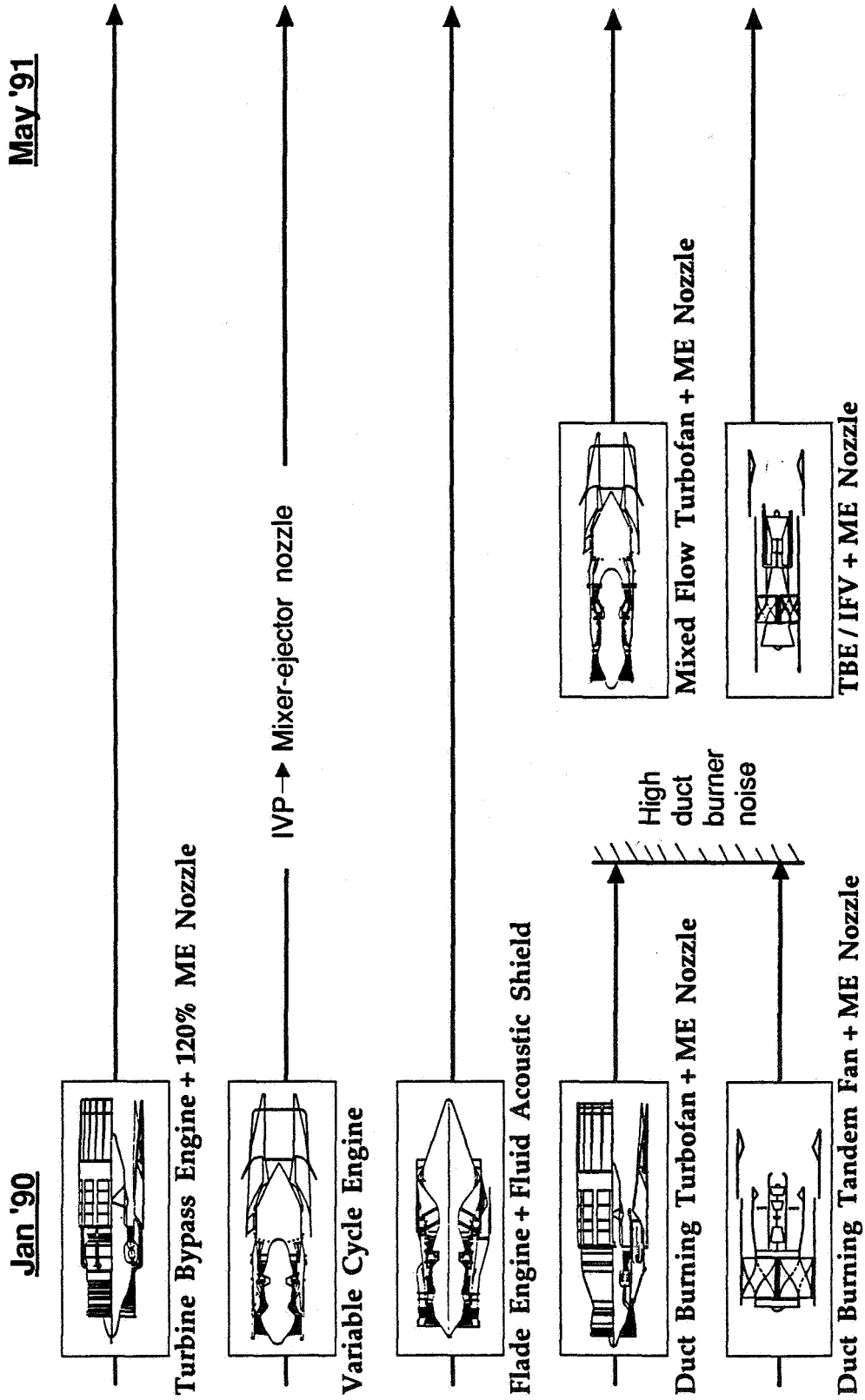
In early 1990, there were five candidate propulsion concepts being evaluated as depicted in the lefthand column. Only two of these concepts are being considered today unaltered--the turbine bypass engine (TBE) with a 120 percent airflow-augmented mixer-ejector (ME) nozzle and the "flade" engine with a fluid acoustic shield. The variable cycle engine survives but with a mixer-ejector nozzle instead of an inverted velocity profile (IVP) exhaust nozzle.

Both the duct burning turbofan (also known as the Variable Stream Control Engine) and the duct burning tandem fan have been dropped due to their excessively high burner noise. Replacing them are the mixed flow turbofan and the turbine bypass engine with an inlet flow valve (a tandem fan variant)--both with mixer-ejector nozzles.

Of the five current alternatives, only the TBE depends solely on an aft-end approach to achieve FAR36-3 noise compliance. All of the others use some form of the front-end, high-flow approach (variable cycle) together with a more modest aft-end acoustic suppression requirement.

HSR Propulsion System Studies

Propulsion Concept Status



HSR Propulsion System Technologies

To illustrate the importance of identifying the most promising propulsion concept, this table summarizes some of the concept-specific technologies associated with each of the current contenders as well as generic technologies required by all of them.

Due to the rather high risk associated with many of these technologies, it may well be wise to pursue more than one concept in the technology development program to provide a reasonable level of confidence.

The following presentations provide a status review of the propulsion studies.

HSR PROPULSION SYSTEM TECHNOLOGIES

	TBE	VCE	TF	Flade
Generic { Low NOx Combustor CMC Materials IMC Nozzle Materials Commerical Life TM Inlet/Engine/Nozzle System incl. controls	✓	✓	✓	✓
	✓	✓	✓	✓
	✓	✓	✓	✓
	✓	✓	✓	✓
	✓	✓	✓	✓
Concept Specific { Mixer-Ejector Nozzle Bypass Valving Inlet Flow Valve Var. Bypass Injectors High-Flow Fan (Quiet ?) Flade Fan Fluid Acoustic Shield	✓	✓	✓	✓
	✓	✓	✓	✓
	✓ (IFV version)	✓	✓	✓
	✓	✓	✓	✓
	✓	✓	✓	✓
	✓	✓	✓	✓

THIS PAGE INTENTIONALLY BLANK

Session VI. Propulsion Systems Studies

omit

A NASA Lewis Comparative Propulsion System Assessment for the High-Speed Civil Transport
Jeffrey J. Berton, William J. Haller, Jonathon A. Seidel and Paul F. Senick, NASA Lewis Research Center

PRECEDING PAGE BLANK NOT FILMED

THIS PAGE INTENTIONALLY BLANK

A NASA Lewis Comparative Propulsion System Assessment for the High-Speed Civil Transport

**First Annual High-Speed Research Workshop
May 15, 1991
Williamsburg, Virginia**

**Jeffrey J. Berton
William J. Haller
Jonathan A. Seidel
Paul F. Senick**

**Aeropropulsion Analysis Office
NASA Lewis Research Center**

N94-33477

315-07
12005

HSR Propulsion System Studies

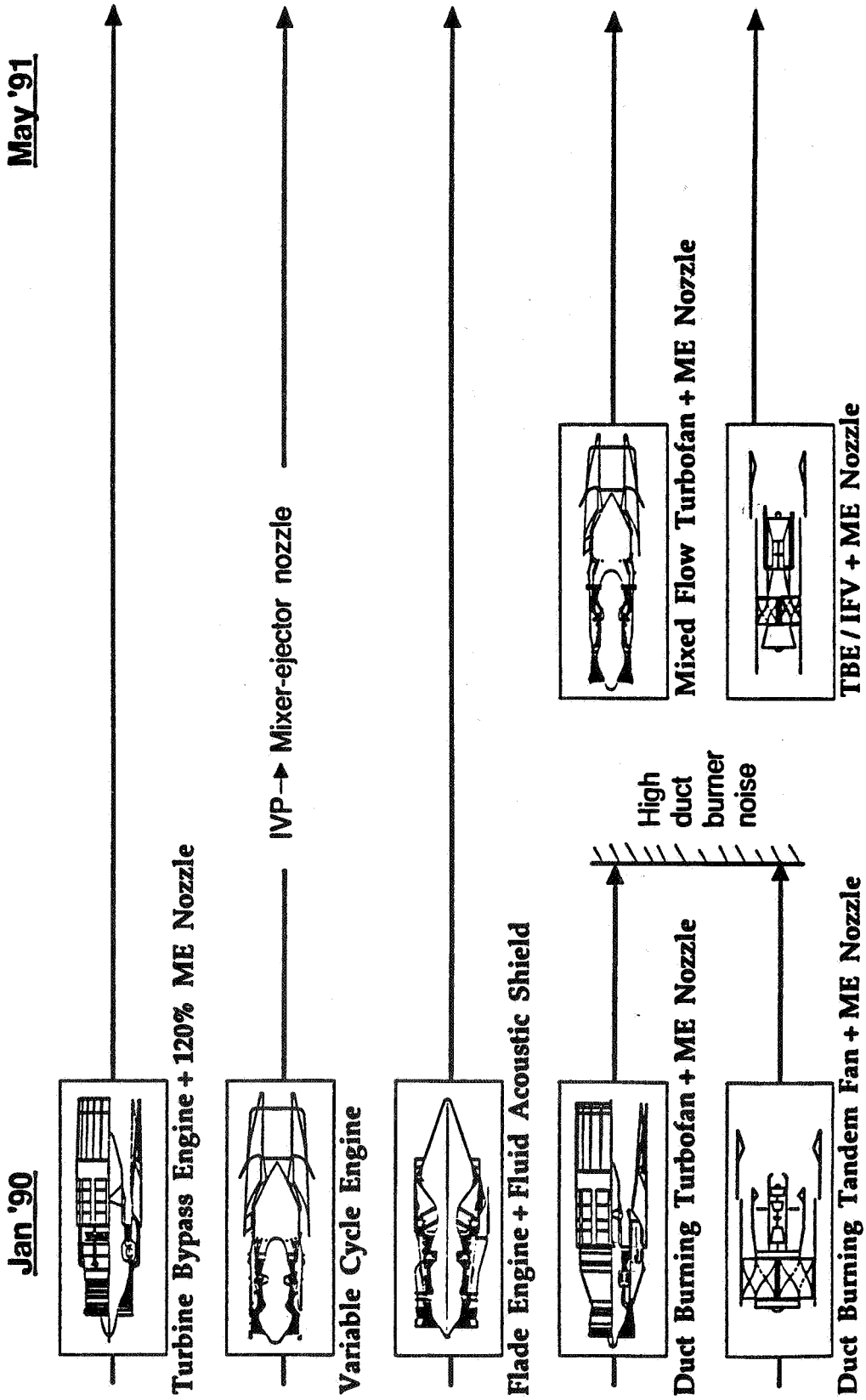
Concept Status

At the beginning of 1990, five engine concepts were under consideration for the HSCT propulsion system. The turbine bypass engine (TBE) was originated by Boeing during The Supersonic Cruise Research (SCR) studies of the 1970s. The variable cycle engine (VCE) with an inverted velocity profile (IVP) was General Electric's best engine during the same study. The IVP took the hot core stream and moved it to the outside and the fan flow was ducted to the center of the nozzle exhaust. This had been shown to give up to 6 dB noise suppression relative to a conic nozzle. The Flade engine is a VCE with an additional bypass stream added for use during takeoff. The variable stream control engine (VSCE) was Pratt & Whitney's best candidate engine during SCR. It used a duct burner to generate the IVP exhaust. The tandem fan approach was a means of greatly increasing airflow during takeoff to reduce the jet velocity and hence the noise.

The TBE concept with a suppressor nozzle (mixer-ejector (M-E)) is still attractive. The IVP nozzle on the VCE was attractive during SCR which had a noise goal of FAR36 Stage 2. The IVP alone, however, could not reduce the noise level to Stage 3, which is about 6 dB quieter. Therefore, it became necessary to also add a suppressor type nozzle which destroyed the IVP. This resulted in eliminating the crossover ducts in the VCE and adding a mixer-ejector nozzle for the current concept. The VSCE was dropped from consideration due to high duct burner noise and the inability for the IVP to meet Stage 3 requirements. The mixed flow turbofan with the M-E nozzle was added because of its inherently low exhaust velocity. The Flade engine also has low jet velocities and requires much less suppression in the nozzle. The tandem fan was only studied at Mach 3.2 and used heavy materials in the valve because of the high temperature at this cruise speed, and still may require a M-E nozzle. It also had excessive noise due to a duct burner placed in the bypass stream. This combination together with the higher weight and added nacelle length made it unattractive. However, at the lower temperatures of M2.0 to M2.4, lighter materials can be used and a valved version of the TBE is now being studied both at P&W and I-H at LeRC.

HSR Propulsion System Studies

Propulsion Concept Status



HSR Propulsion System Studies

Candidate Propulsion Concepts: LeRC Assessment

The Turbine Bypass Engine is a turbojet engine where compressor discharge air is bypassed around the combustor and the turbine at maximum power. As the turbine inlet temperature is reduced, the amount of air bypassed is reduced to maintain constant corrected flow (W/P) through the turbine. This keeps the airflow through the engine high and reduces both spillage and boattail drag at part power. Of the four engines shown here it is the only one that does not necessarily require an afterburner.

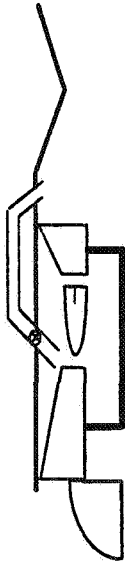
The mixed flow turbofan and variable cycle engine are very similar. The major difference is the addition of a valve in the front of the VCE which allows the bypass ratio to increase during takeoff. The Flade engine is a derivative of the VCE where an additional tip fan is added to the VCE front fan. This can be used to "high flow" the engine during takeoff to reduce the core velocity and lower the jet noise. In addition, this Flade flow can be collected and used to create a fluid acoustic shield on the bottom half of the engine. During supersonic cruise, the tip fan is unloaded by changing the angle of its inlet guide vanes.

Due to its recent inclusion in our studies, the tandem fan has not yet been investigated in great detail and is not presented in this analysis.

HSR Propulsion System Studies

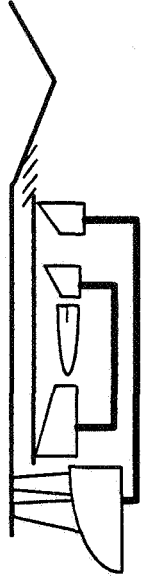
Candidate Propulsion Concepts: LeRC Assessment

Turbine bypass engine



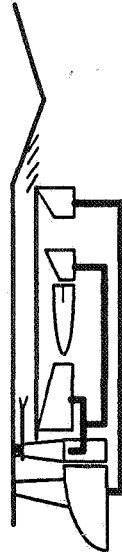
- Simple cycle
- Low cruise temperature

Mixed flow turbofan



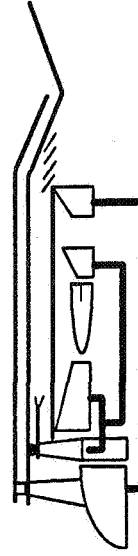
- Low jet velocity
- Good subsonic SFC

Variable cycle engine



- Variable bypass
- Good subsonic SFC

Flade engine



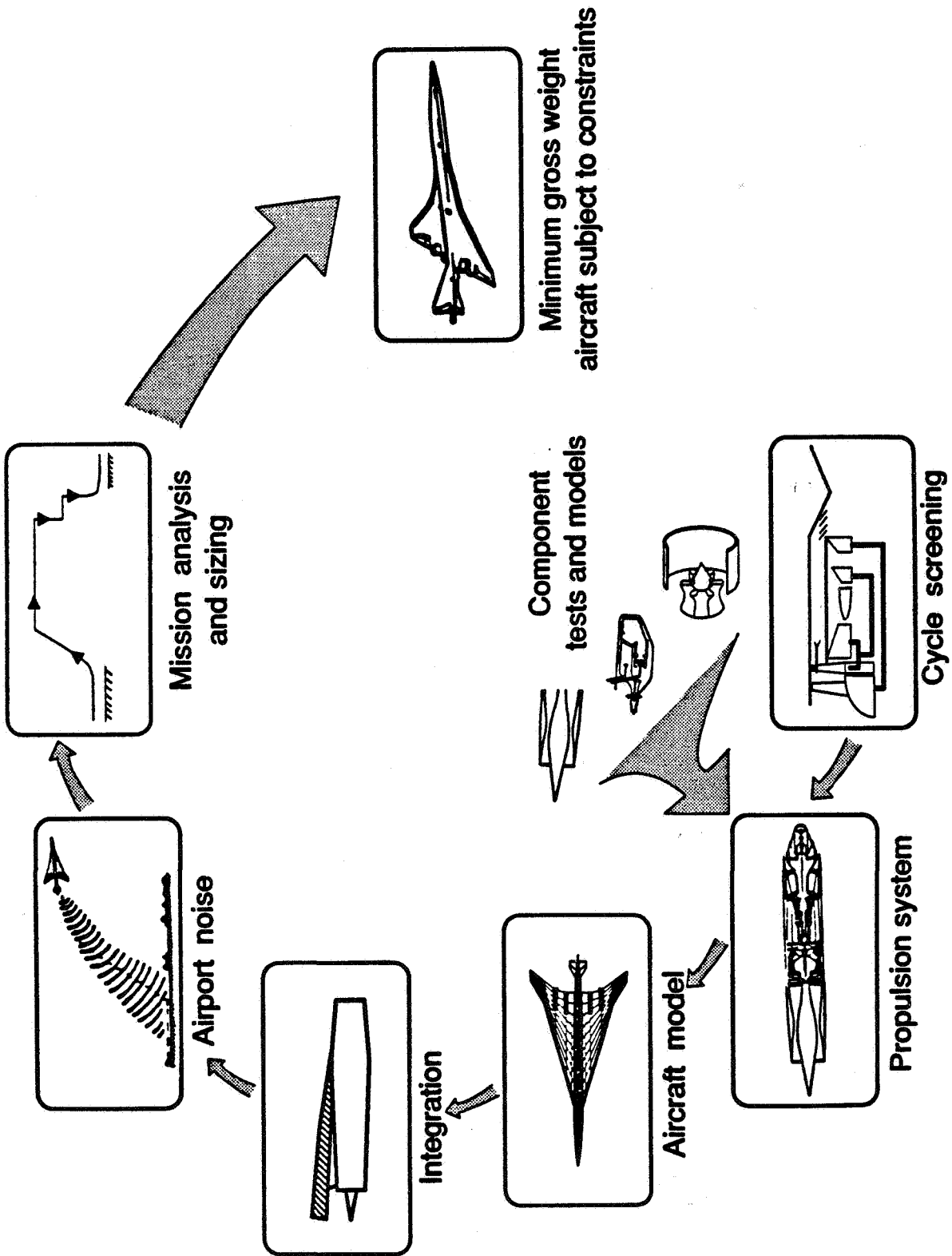
- Low jet noise
- Variable bypass
- Good subsonic SFC

HSR System Study Flowpath

A wide variety of engine cycle concepts of interest are modeled in the Navy/NASA Engine Program. The installation code uses component maps for the inlet and nozzle to generate installed (isolated nacelle) engine data. These data are supplied to a mission code along with an aircraft model (currently the Boeing Mach 2.4 model 1080-834). The propulsion system is installed on the wing (currently assuming no interference drag penalty based on results from other studies). The mission code is used to fly the aircraft over the mission and a noise code used to calculate the airport noise. A fuel balanced aircraft takeoff gross weight is then calculated which satisfies any constraints.

As better component data becomes available from tests and/or analytical studies by NASA and the contractors, the models in the computer codes are refined and the mission performance recalculated.

HSR System Study Flowpath



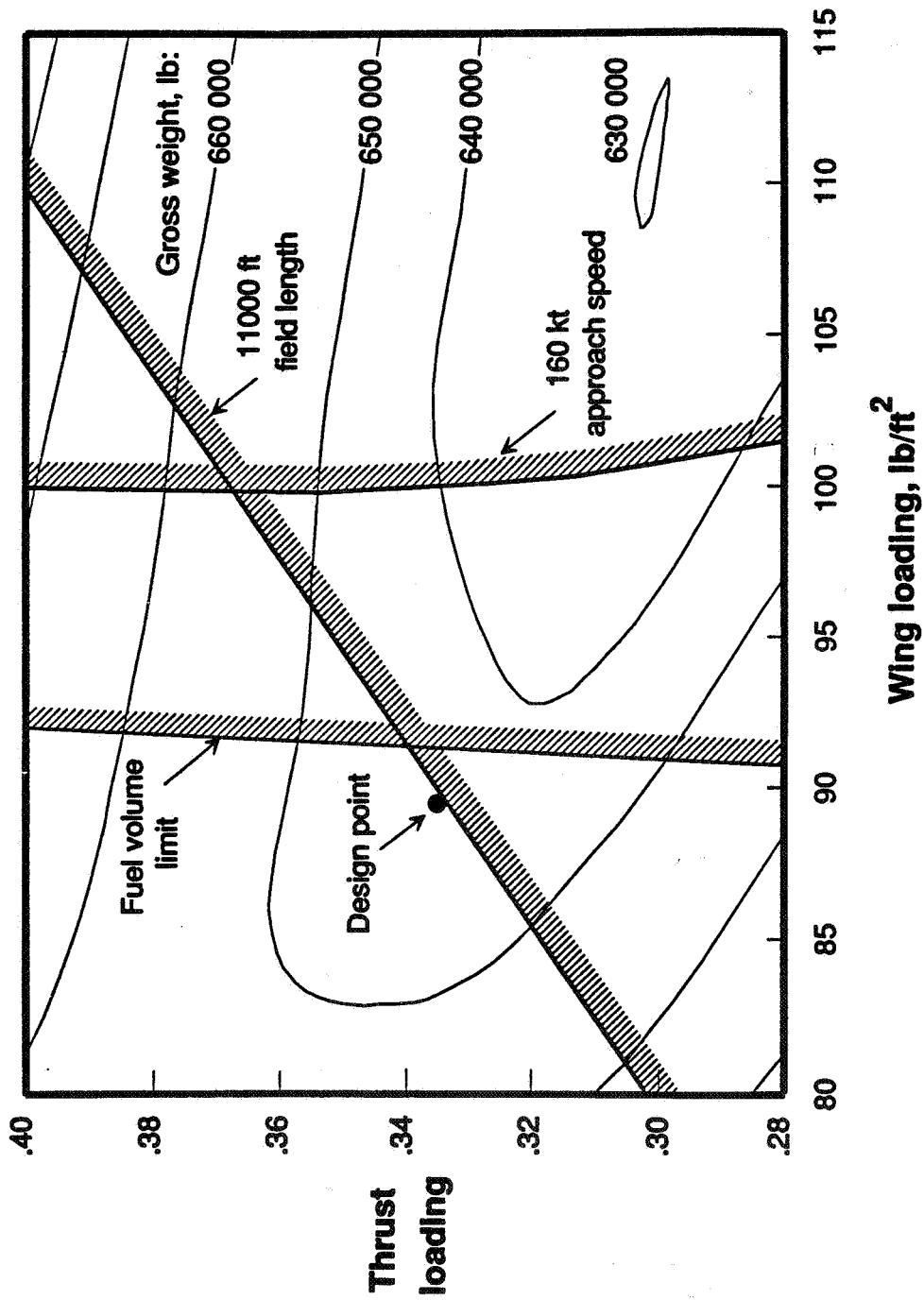
Design Point Aircraft Sizing - No Noise Constraint

Thumbprints of aircraft takeoff gross weight (TOGW) as a function of wing loading and thrust loading were generated. A low wing loading implies a larger wing and high thrust loading implies a larger engine. TOGW contours are shown on this thumbprint. Also shown are three of the constraints: the wing must be large enough to allow a 160 KT approach speed upper limit, the wing volume must be large enough to contain the mission fuel, and the wing must be large enough and the thrust high enough to takeoff in a field length less than 11,000 feet. The latter constraint is the only one that is active in constraining the gross weight on this figure.

Design Point Aircraft Sizing - No Noise Constraint

Mach 2.4 Cruise; 5000 n mi Range

Mixed Flow Turbofan



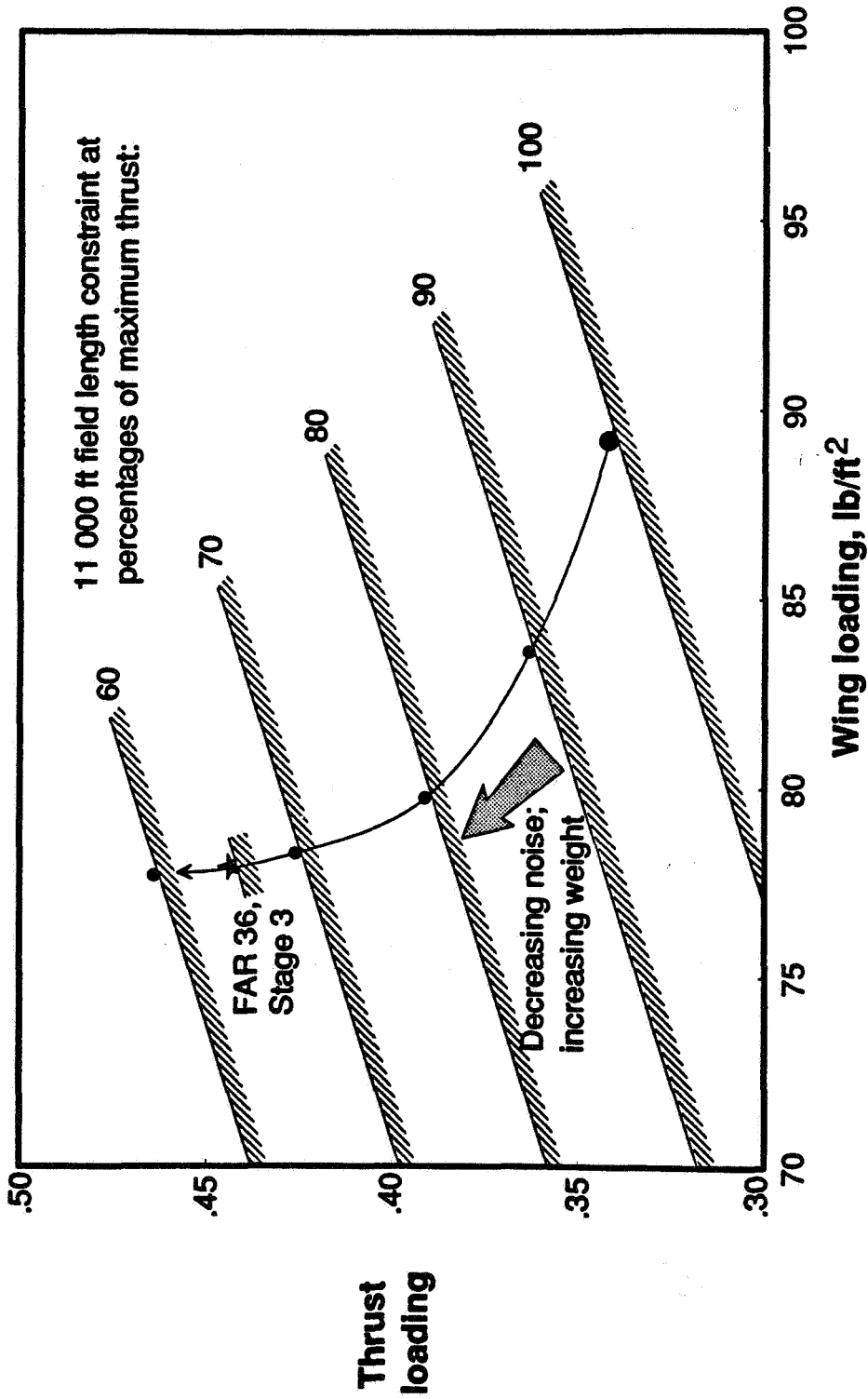
Impact of Noise Constraint

On the previous figure, all takeoffs were at 100% power. The field length constraint at this power is repeated here. The engines can be oversized (higher thrust loading) and then throttled back during takeoff to reduce the jet velocity, and hence, the noise. Larger degrees of oversizing results in lower noise but higher TOGW. Here it can be seen that at a 65% power takeoff, the FAR36 Stage 3 noise limit can be achieved.

Impact of Noise Constraint

Engine Oversizing With Part-Power Takeoff and Programmed Throttle

Mixed Flow Turbofan



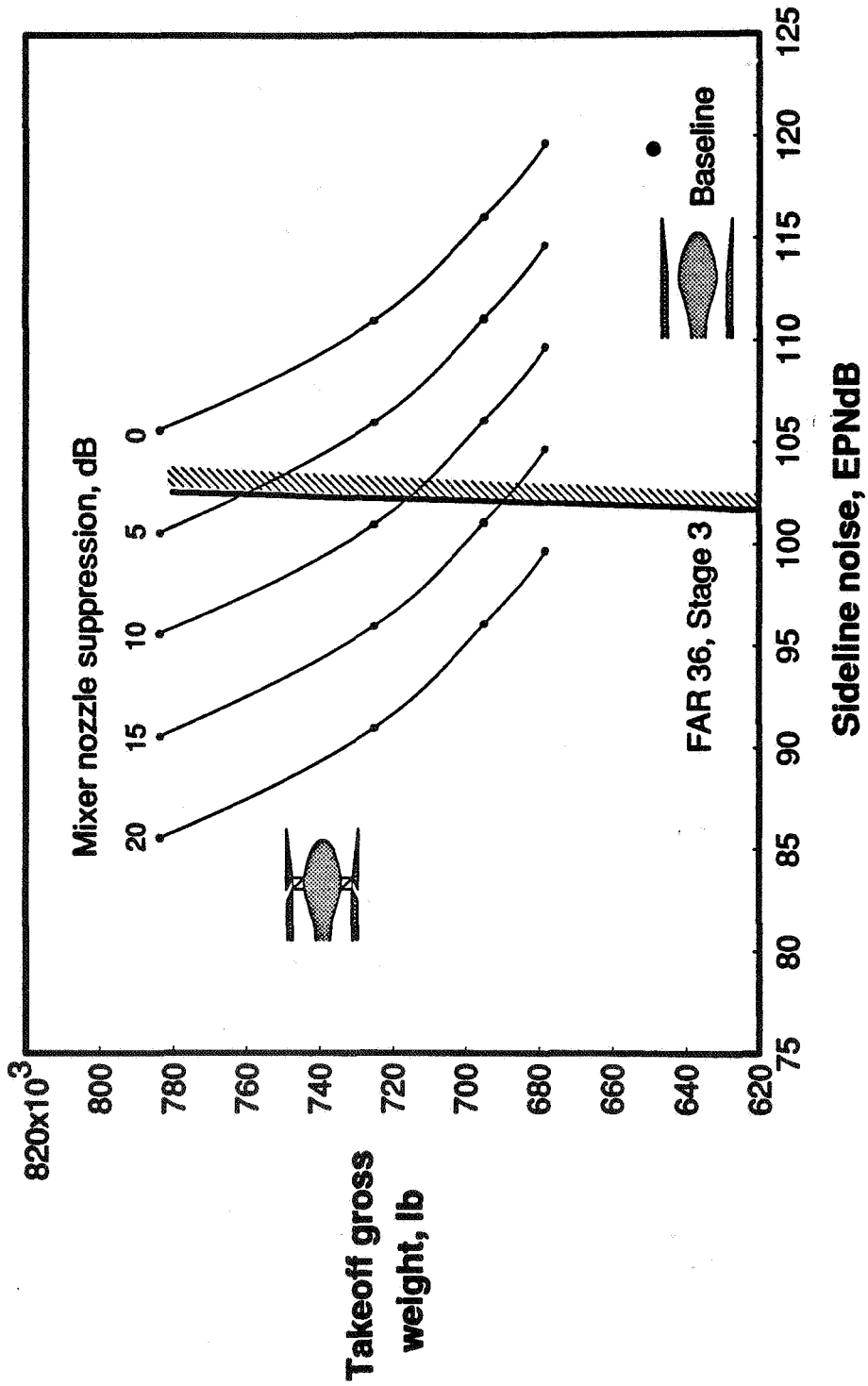
Noise Impact on Aircraft Size

GE, P&W and Boeing are all investigating at mixer-ejector (M-E) nozzles for quieting the HSCT engines. If one calculates the fully-mixed jet velocity and corresponding jet noise for these nozzles using the Clark-Stone noise code, this resulting noise would be far below FAR36-Stage 3. Non-uniform mixing and mixing noise, however, has shown noise levels far above the ideal level in initial acoustic tests of these nozzles. Until a better database is available for developing noise models for the M-E nozzles, we are treating their performance parametrically.

The baseline point shown is the TOGW without a noise constraint. If the additional weight and thrust loss of a M-E nozzle is considered, the TOGW rises and the noise rises slightly. If it is assumed that no noise suppression is provided by the nozzle, then the TOGW increases as the noise level is reduced by oversizing the engine and taking off at part power as shown on the previous figure. This "0 dB" line is then translated to the left for 5, 10, 15, and 20 dB levels of assumed M-E nozzle noise suppression. Thus, if the suppression level is about 17 dB or more, no oversize is necessary. Anything less than this will require some amount of engine oversizing to meet the noise requirement.

Noise Impact on Aircraft Size

Clark-Stone Jet Noise Model
Mach 2.4 Turbine Bypass Engine



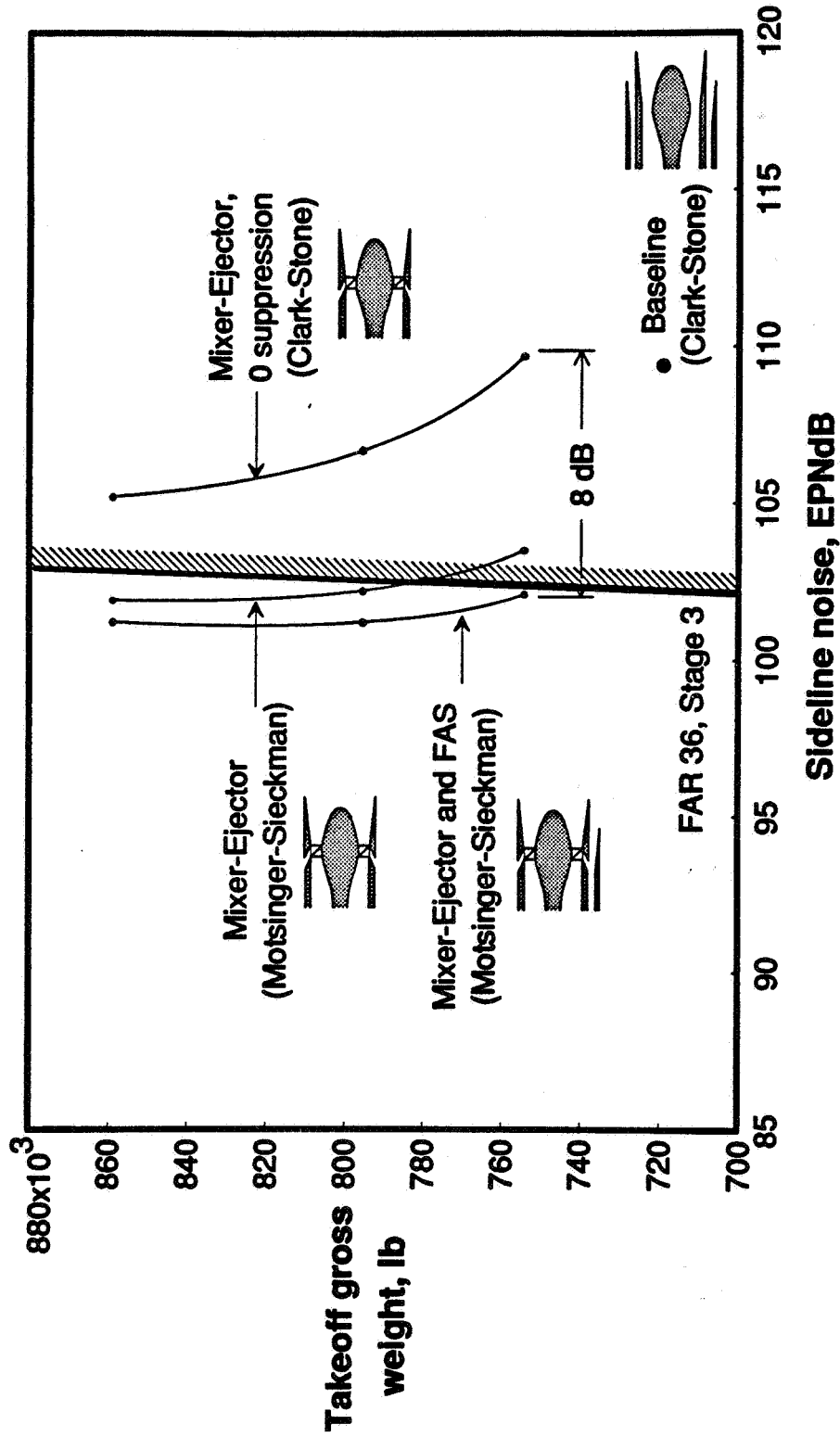
Noise Impact on Aircraft Size - Flade

For the Flade engine, an extensive noise database exists covering the range of exhaust conditions of the M-E nozzle. This database and the Motsinger-Sieckman (M-S) noise prediction code were a result of the previous SCR studies.

Again, a "0 dB" suppression curve is shown as well as the noise predicted by the M-S code. Only a small amount of engine oversize is necessary to meet Stage 3. If the Flade flow is collected into a fluid acoustic shield, the additional suppression (~1.5 dB) may enable the aircraft to meet Stage 3 with no engine oversizing based on this preliminary analysis.

Noise Impact on Aircraft Size

Mach 2.4 Flare Engine



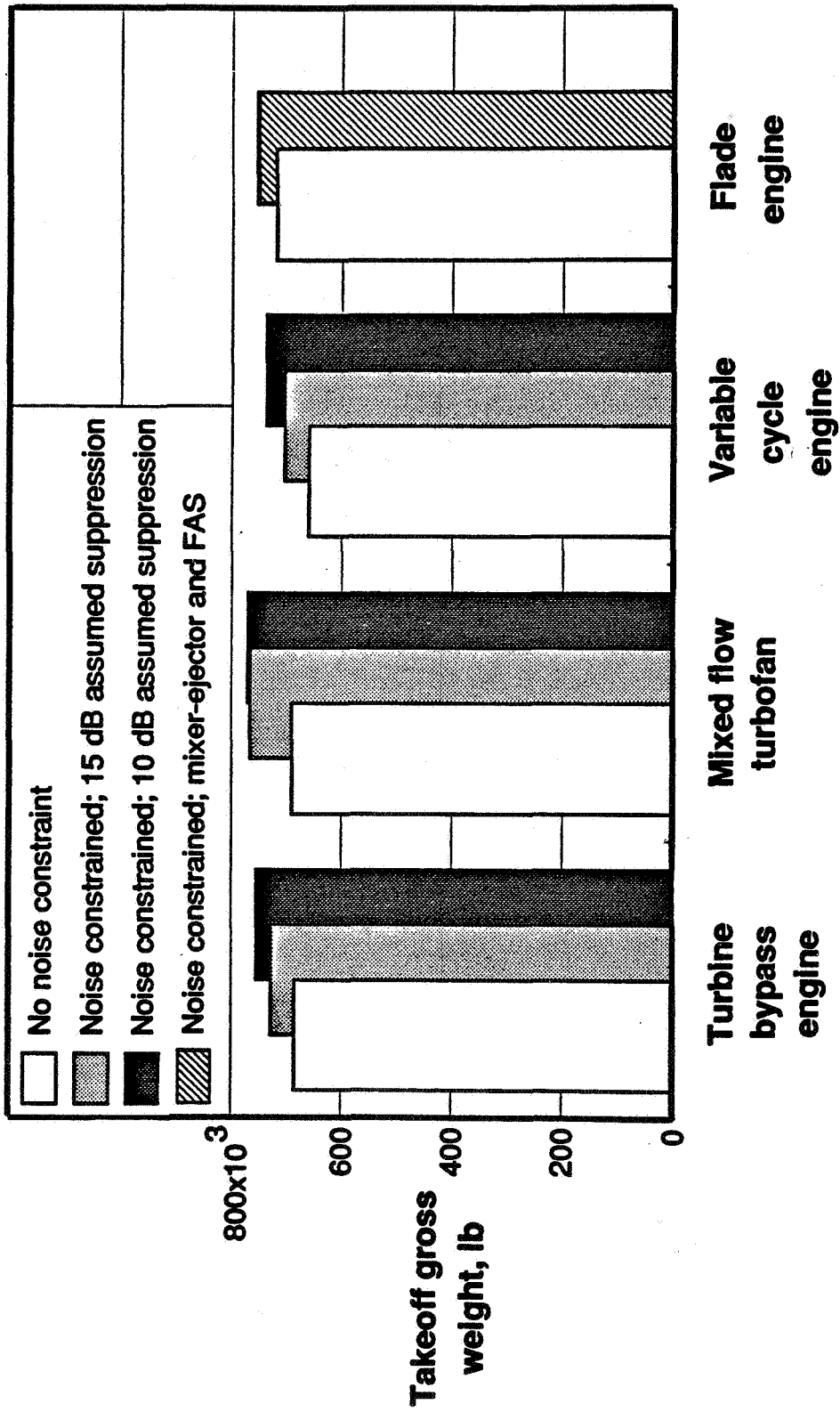
Takeoff Gross Weight Assessment

The takeoff gross weights (TOGW) for the four engine types are shown. The open bars represent the weights when there is no imposed noise constraint. The difference in weights is less than 5% between all the engines and is considered to be insignificant at this time. They are all, however, about 50,000 pounds higher than the previous comparison shown at the Aero Propulsion Conference held at NASA Lewis in March. The new ground rules agreed to by P&W and GE in terms of T3 and T4 limits, cooling requirements, AN², etc. have been incorporated into our in-house studies. This has resulted in about a 20% increase in base engine weight which is reflected in this TOGW growth.

For the TBE, MFTF and VCE, the method previously shown for calculating TOGW with various amounts of assumed mixer performance has been used. The MFTF only needs about 10 dB so there is essentially no difference in TOGW at 15 dB suppression. The TBE and VCE both require oversizing at both 10 and 15 dB. The Flade TOGW was calculated using the M-S code and the Fluid acoustic shield noise reduction procedure. Again, noise constrained TOGW varies less than 5% between the candidate cycles. As previously mentioned, we have not yet reached the point in the analysis of the TBE with an inlet flow valve to include its performance in this status report.

Takeoff Gross Weight Assessment

All Supersonic 5000 n mi Mission

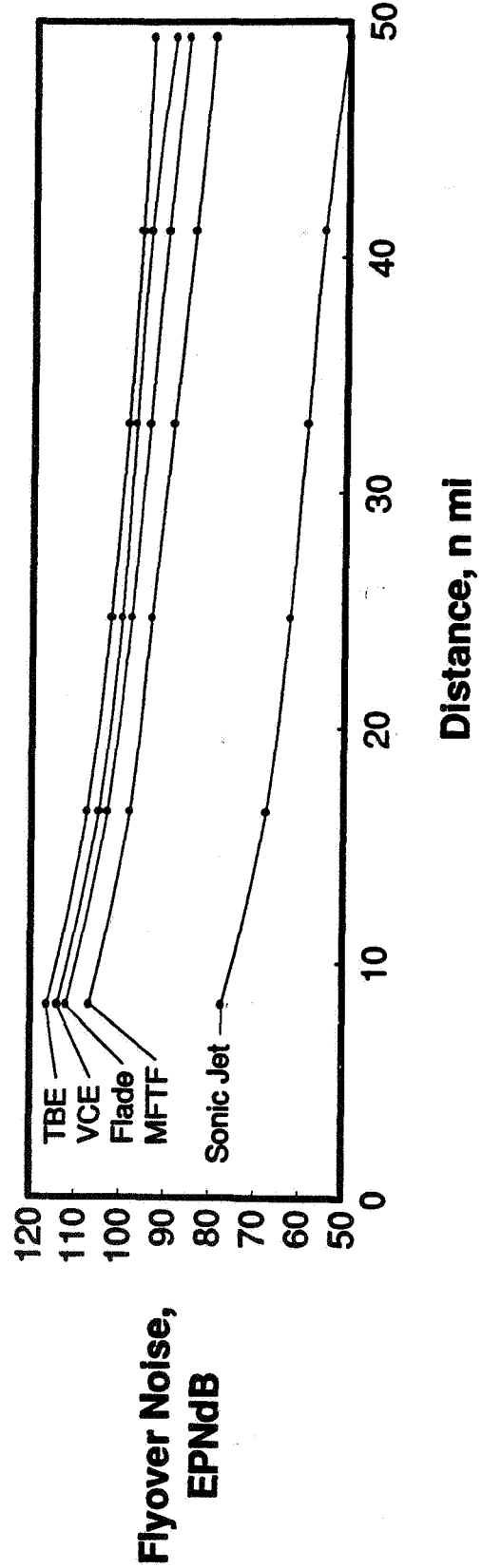
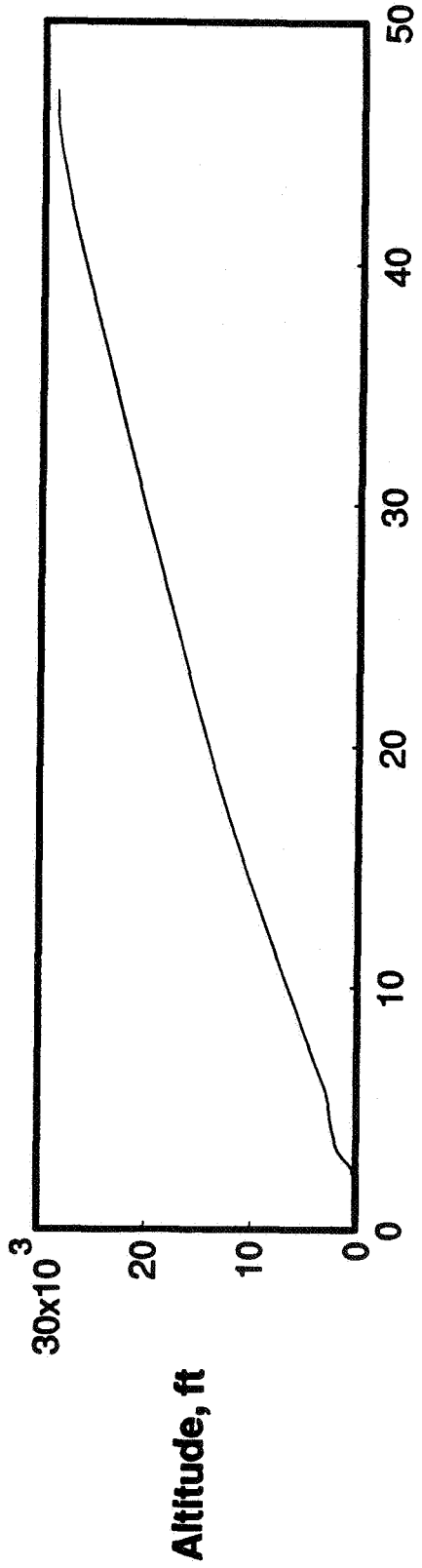


Impact of HSCT Flyover Noise

A possible problem with the HSCT is that high-altitude flyover noise along the flight path is significantly higher than that of subsonic aircraft.

In the airport vicinity, the HSCT engine operates with the mixer-suppressor nozzle deployed, a throttle cutback, and possibly a programmed throttle lapse rate. As the vehicle climbs to cruise, the suppressors are stowed and the engine power raised. Shown here is a band of flyover noise for all of the study engines as a function of distance from the airport and the corresponding altitude of the aircraft. Noise levels of 100 dB are reached at an altitude of 20,000 feet compared to 60 dB for a sonic jet representing subsonic aircraft. It therefore may be necessary to employ part power climbs to very high altitudes and/or noise suppression during the climbout based on this very preliminary assessment. In addition, it should be pointed out that the model used for calculating noise propagation may be deficient. More refined models of atmospheric attenuation and high aircraft velocity may significantly change the absolute level of these results.

Impact of HST High-Altitude Flyover Noise



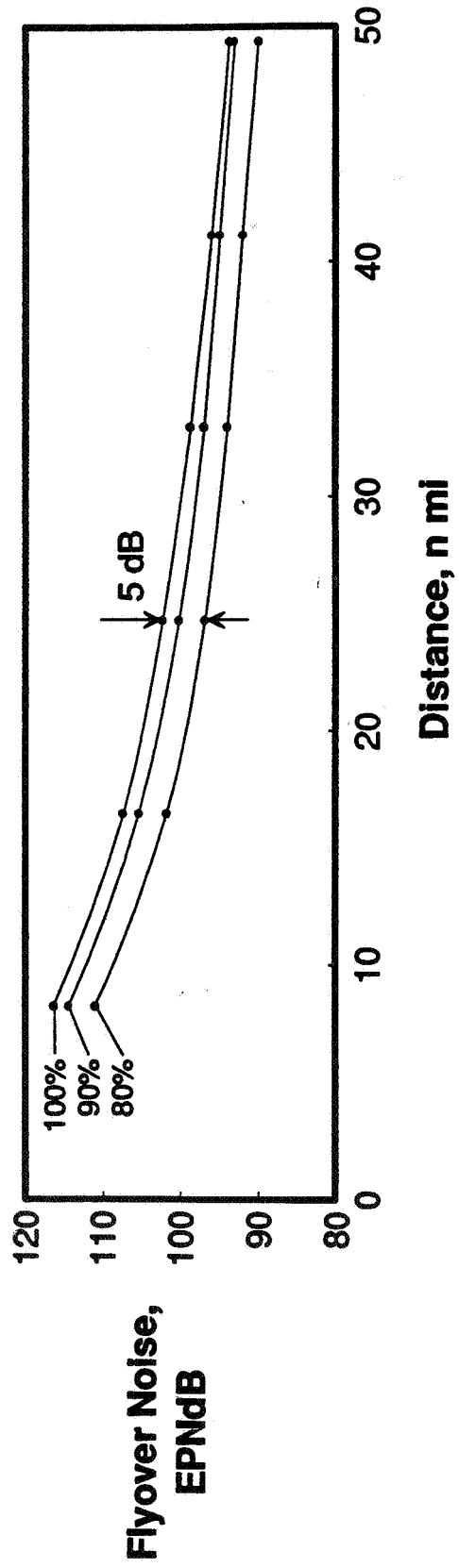
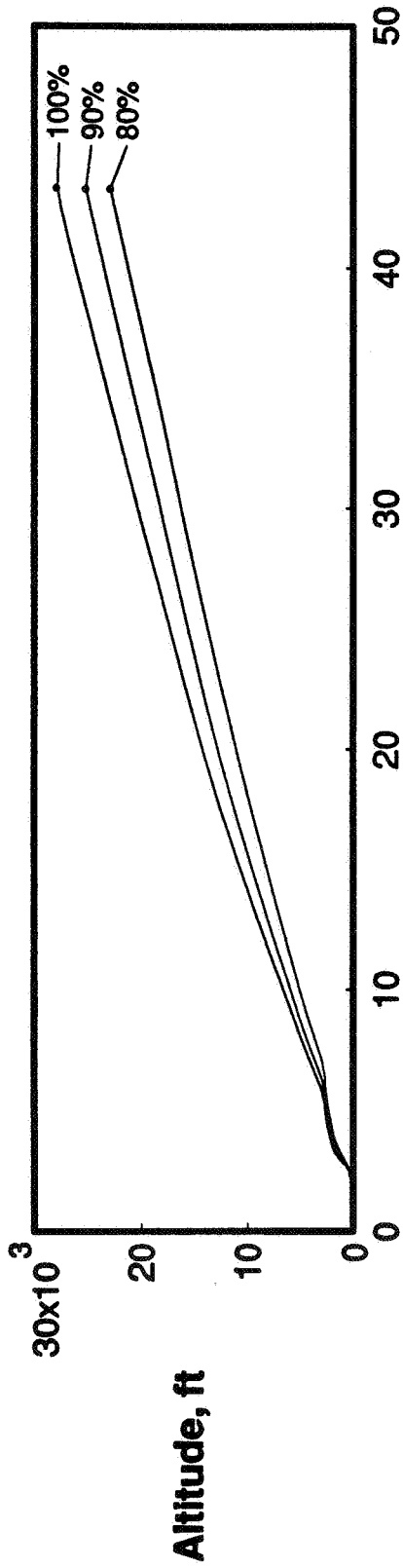
Impact of HSCT Flyover Noise - Throttled Climb

A throttled climb can potentially reduce the flyover noise along the climbout flight path by approximately 5 dB as shown. Further reductions may be possible, but this needs to be studied.

Impact of H SCT High-Altitude Flyover Noise

Throttled Climb - Turbine Bypass Engine

Throttle Settings: 100, 90, 80 Percent



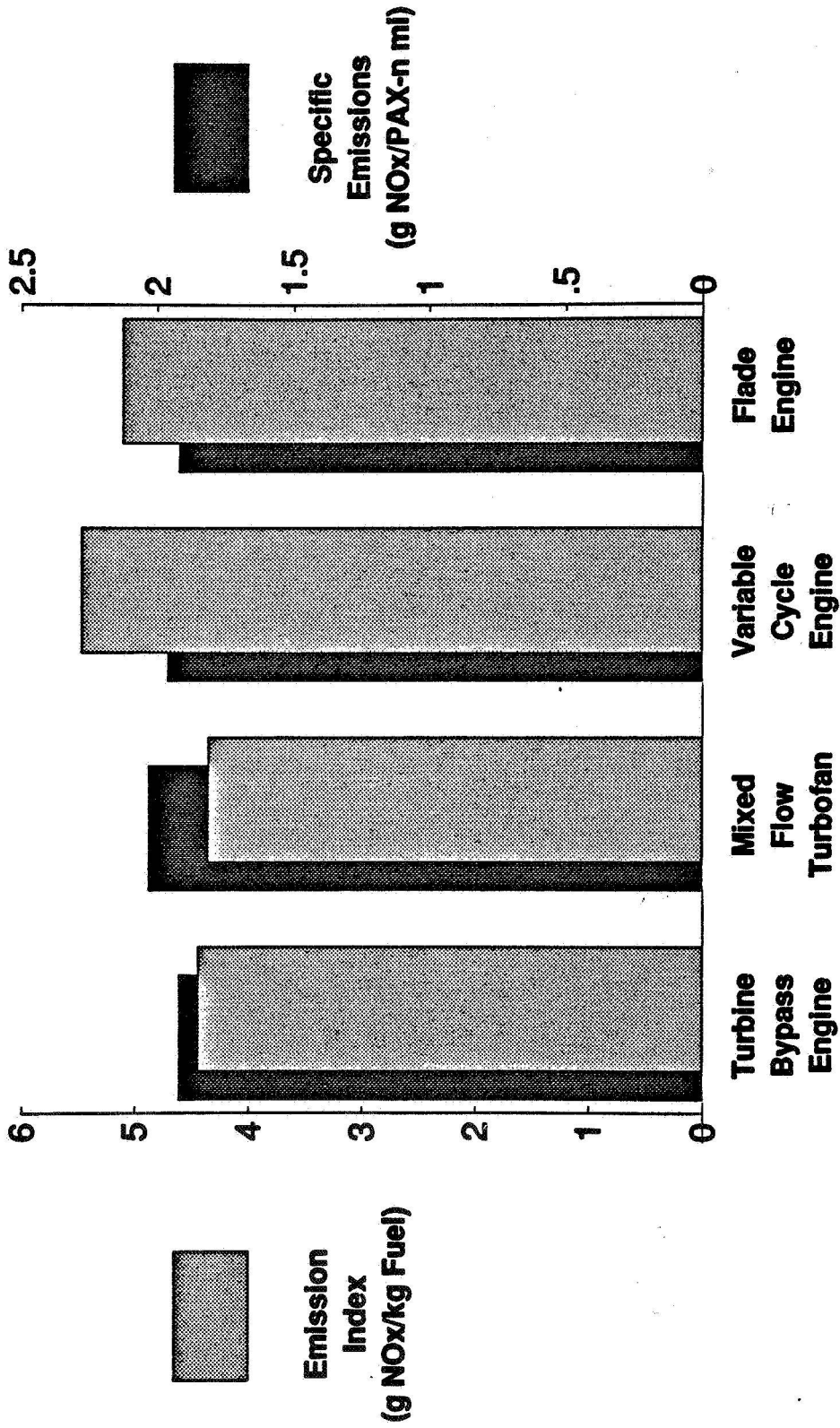
HSR NO_x Reduction Status

The emission index for the four engines are all approximately at the goal value of 5. This is a result of the engines meeting the P&W/GE agreed upon T₃ and T₄ limits. There has not yet been a correlation developed for the LPP and RQL combustor emissions because of the very limited Flametube database. The correlation used to predict EI is based on clean combustor data from the 1970s adjusted to pass through the EI goal value of 5 at typical HSCT conditions.

Specific emission is also shown which is based on both the emissions index and fuel burned during cruise in terms of grams of NO_x per passenger nautical mile. This parameter would reflect any changes in engine fuel efficiency. None of the engines thus far show any significant advantage.

HSR NO_x Reduction Status

Based on HSR Goal for Emission Index Dependency



Current Assessment of HSCT Ozone Depletion

Ozone damage due to NO_x is a function of both the amount of NO_x produced and the altitude at which the NO_x is released.

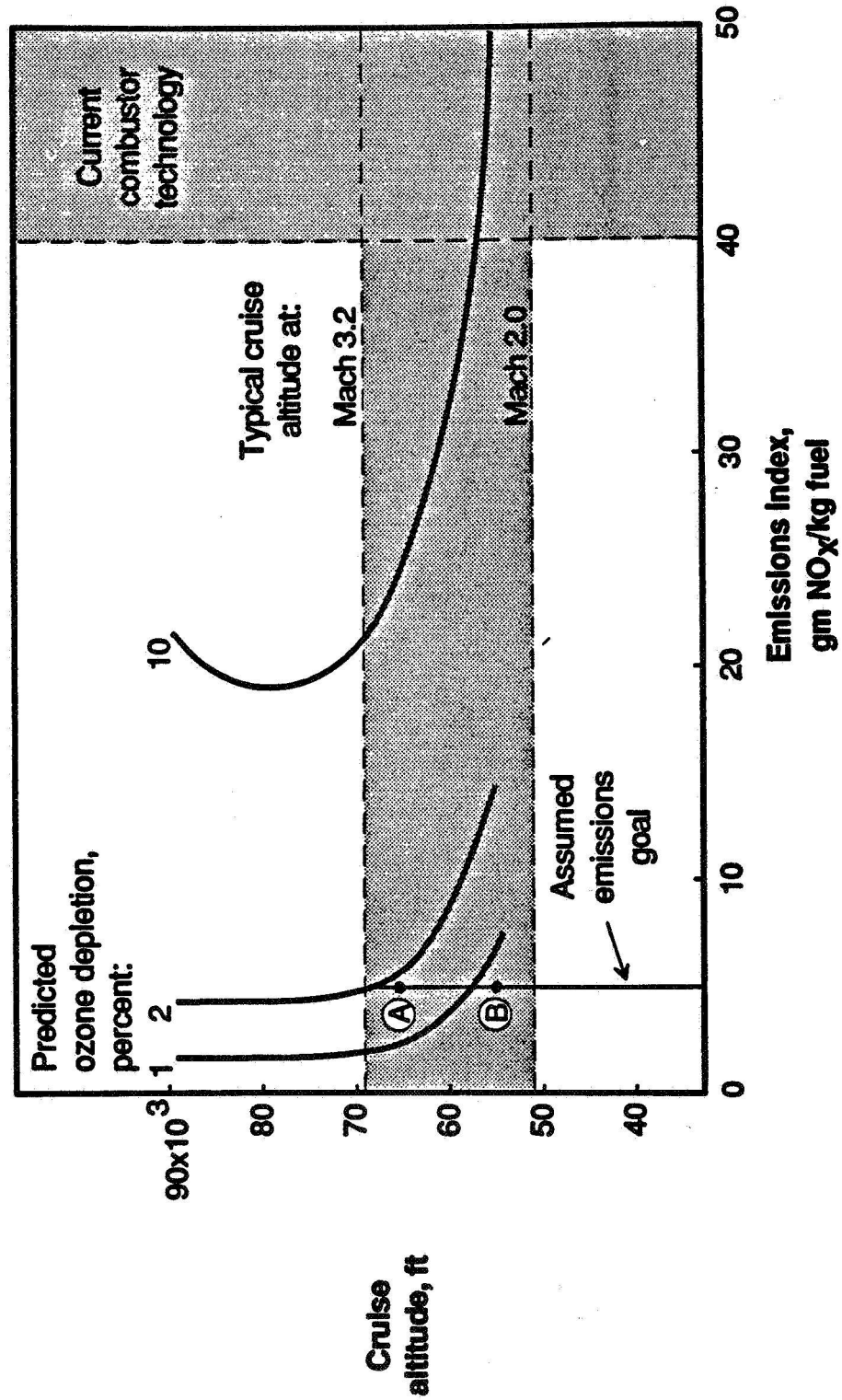
Shown here is a plot of emission index (EI) vs. cruise altitude and the levels of steady-state ozone depletion for a fleet of 600 HSCTs.

A typical cruise altitude for an HSCT would be about 50,000 feet at M2.0 and 70,000 feet at Mach 3.2. Current technology clean combustors have an EI of 40+.

At the assumed goal of the low NO_x combustor program of an EI of 5, the steady state depletion of the ozone layer is about 2 percent at 65,000 feet (point A). This damage can be reduced approximately in half by flying at 55,000 feet. It is not NASA's position to advocate a lower, non-optimal, cruise altitude to combat ozone depletion. It is much more preferable to design low NO_x combustors. Reduction of cruise altitude is a rather simplistic method of reducing ozone depletion. This lower cruise altitude could be used by either reducing the cruise design Mach number or by flying at a non-optimum altitude and suffering a range penalty.

Current Assessment of High Speed Civil Transport Ozone Depletion

NO_x Effect Alone

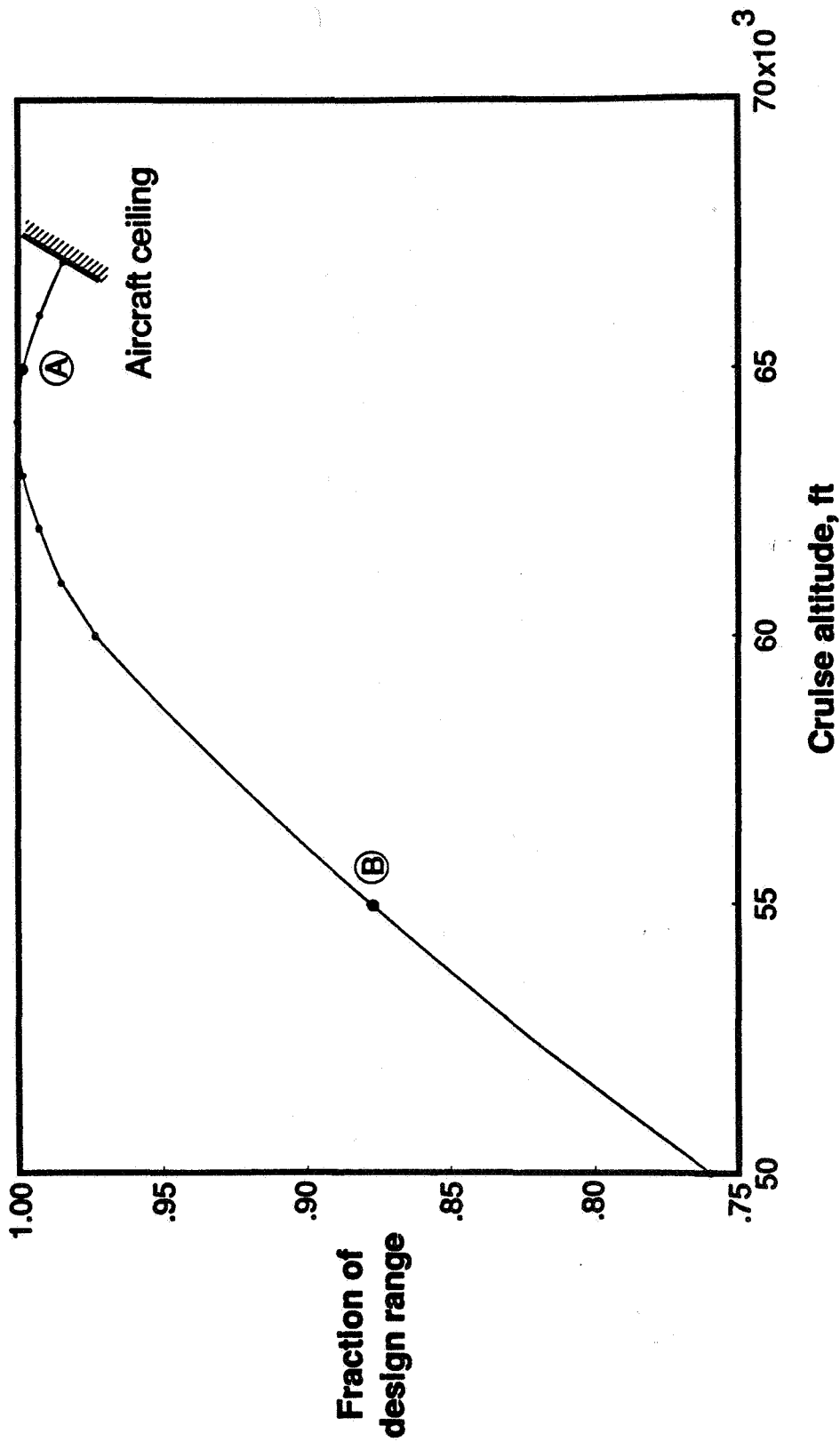


Influence of Non-Optimum Cruise Altitude on Range

The range penalty for flying an aircraft designed for M2.4 cruise at 65,000 feet at the non-optimum cruise altitude of 55,000 feet is shown here to be about 12%. This is a worse case scenario where the wing size and engine size have been fixed based on the higher altitude. If it were known in advance that the cruise altitude would be 10,000 feet lower, the aircraft and engine parameters would have taken on different optimum values and the range penalty would have been less than 12%.

Influence of Non-Optimum Cruise Altitude on Range

Mach 2.4 Turbine Bypass Engine Designed at 65 000 ft

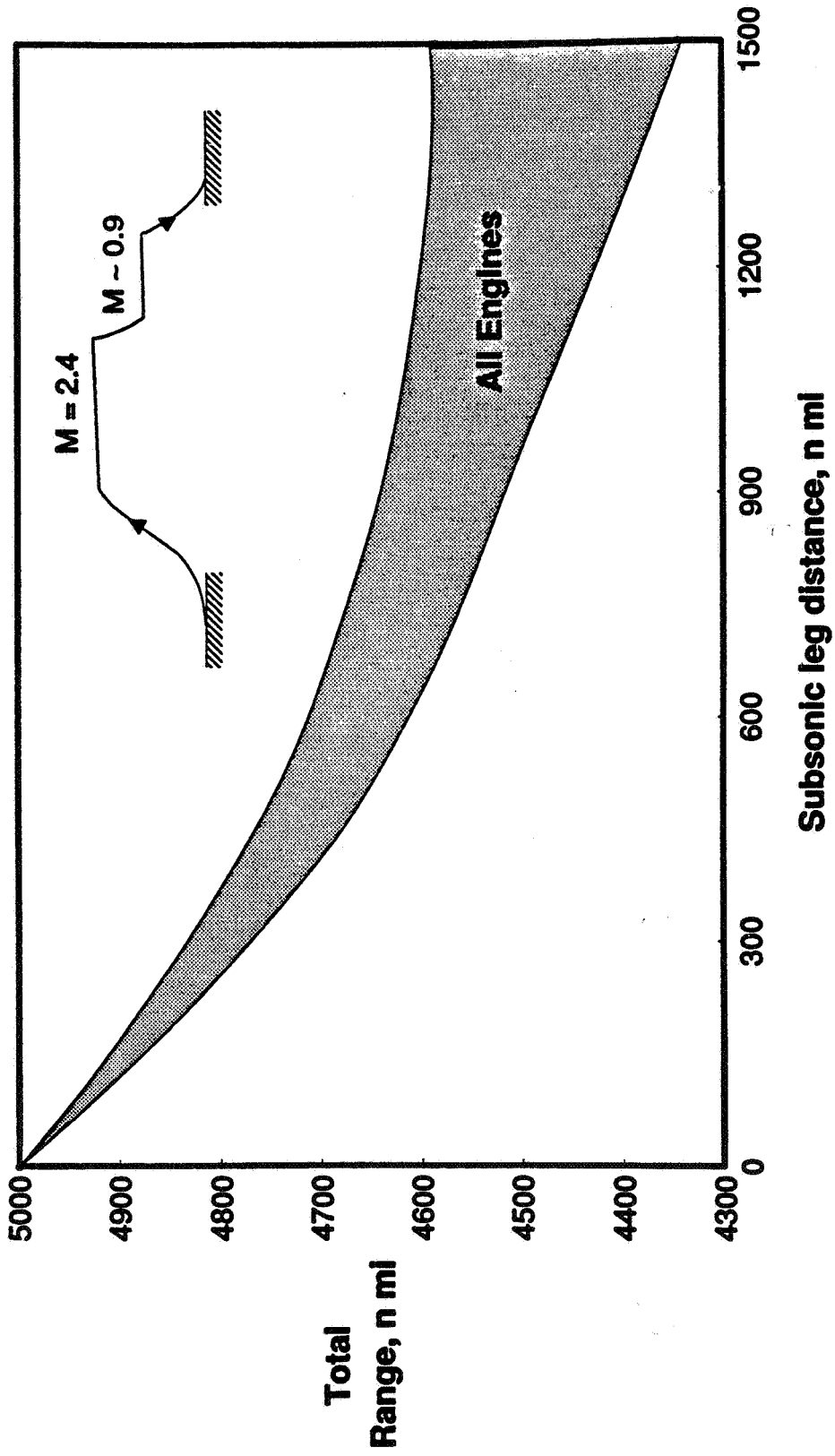


Influence of Subsonic Leg on Range

Here too, a worse case scenario has been assumed. For all four engine candidates, the penalty of flying 1/3 of the mission subsonically is about 500 nmi or 10% of the initial design range. The difference between the engine types is less than 5%. If a large subsonic range is to be included in the design mission, a different value of wing loading, engine size, and engine cycle parameters would be chosen.

Influence of Subsonic Leg on Range

Design Range: 5000 n mi



Study Conclusions

At the present time, there appears to be less than 5% difference in TOGW between the candidate engine cycles. TOGW may not be the sole determiner as to best engine. Cost, reliability, maintainability, complexity and other considerations will also enter into the selection process.

The aero/acoustic performance of mixer-ejector nozzles will be critical in the selection process. The two relatively low exhaust velocity engines, the MFTF and Flade, require the least nozzle noise suppression.

This study has been done only at M2.4. Emissions and the impact on the protective ozone shield could possibly force the lowering of cruise altitudes and Mach number.

Study Conclusions

- **All four candidate propulsion systems are viable contenders.**
- **Mixer-ejector nozzle aeroacoustic performance is critical in meeting FAR 36, Stage 3, noise requirements and may influence propulsion cycle selection.**
- **Allowable emissions may dictate cruise altitude and Mach number.**

Areas Requiring More In-Depth Analysis

Before a more definitive answer as to the best engine type can be ascertained, the analytical models used in conducting the mission analysis need improvement.

The mixer-ejector nozzle noise/performance requirements will vary with the engine type. Aircraft redesign/sizing models must be improved to account for the various effects of engine oversizing that reflects the accompanying changes in aircraft Cg, structure, flutter, landing gear etc. Better models for the propulsion/airframe integration must be developed to accurately reflect the different nacelle shapes and lengths between the engine types. Detailed flowpath calculations and experimental data must be generated to accurately predict engine weight and performance. Also, the accuracy of present noise prediction methods for flyover noise propagation must be verified or improved.

Areas Requiring More In-Depth Analysis

- **Mixer-ejector nozzle noise/performance**
- **Aircraft redesign/sizing**
- **Propulsion/airframe integration**
- **Propulsion system weight/performance**
- **Takeoff noise modeling/techniques**
- **Other Mach numbers**
- **Other cycles**
- **High-altitude flyover noise propagation**

Key Contracted Efforts

The major contracted studies in place to help improve the database were previously shown in the overview for this session. They address some of the key concerns, namely, the best type of inlet, the mixer ejector nozzle performance, 2D vs. Axi configurations for both, and the differences between military and commercial life requirements and duty cycle for supersonic engines.

Key Contracted Efforts

- **Boeing inlet study**
 - 2-D vs. axisymmetric
 - Amounts of internal/external compression
- **Douglas inlet study for Flade engine**
- **Lockheed nozzle study**
 - 2-D vs. axisymmetric
 - Amount of ejector augmentation
- **General Electric and Pratt & Whitney nozzle study**
- **Pratt & Whitney engine life study**

THIS PAGE INTENTIONALLY BLANK

Session VI. Propulsion Systems Studies

omit

Pratt & Whitney/General Electric Propulsion Systems Studies Introduction
Samuel C. Gilkey, GE Aircraft Engines; and Richard W. Hines, Pratt & Whitney Aircraft

PRECEDING PAGE BLANK NOT FILMED

THIS PAGE INTENTIONALLY BLANK

N94-33478

516-07
12006

**P&W / GE PROPULSION SYSTEMS STUDIES
INTRODUCTION**

**SAMUAL C. GILKEY
RICHARD W. HINES**

**NATIONAL AERONAUTICS AND SPACE ADMINISTRATION
FIRST ANNUAL HIGH SPEED RESEARCH WORKSHOP
MAY 14-16, 1991**

PRECEDING PAGE BLANK NOT FILMED

**P&W / GE HSCT COLLABORATION
JOINT PROPULSION STUDIES**

Before P&W and GE present the results of our NASA engine study tasks, we will present a brief introduction covering our joint study organizations; the engine concepts we are studying; the groundrules we have defined for our studies; our engine evaluation criteria; our study plans; and the range of NASA study tasks.

- **ORGANIZATIONS**
- **ENGINE CONCEPTS**
- **GROUND RULES**
- **ENGINE EVALUATION CRITERIA**
- **STUDY PLANS/MILESTONES**
- **NASA STUDY TASKS**

Figure 1

**P&W / GE HSCT COLLABORATION
PARALLEL TECHNICAL ORGANIZATION**

The P&W/GE joint venture is a cooperative program organization made up of various functional organizations from both companies. These technical organizations have defined joint plans and common groundrules, and are now undertaking the technical tasks required in each technical discipline associated with the engine studies.

- **TECHNICAL DISCIPLINES WORKING TOGETHER ON:**
 - **JOINT PLANS**
 - **COMMON GROUND RULES**
 - **TECHNICAL TASKS**

Figure 2

HSCT ENGINE CONCEPTS

In an effort to maximize the benefits of our joint efforts, and minimize duplication, P&W and GE decided to pursue those engine concepts that we each had the most knowledge about, and choosing just one common engine concept, the mixed flow turbofan, to be pursued by each company.

P&W

- TURBINE BYPASS ENGINE
- MIXED FLOW TURBOFAN
- TURBINE BYPASS ENGINE WITH INLET FLOW VALVE

GE

- MIXED FLOW TURBOFAN
- VARIABLE CYCLE ENGINE
- FLADE

Figure 3

ENGINE CYCLE / DESIGN GROUND RULES

2005 ENTRY INTO SERVICE

P&W and GE have defined a common set of groundrules to be used in the engine studies. These groundrules are based on 2005 entry into service. These groundrules will be used to perform our joint engine studies leading to engine concept selection. The groundrules will be periodically reviewed and adjusted based on airframe company requirements and technology development.

AIRFLOW SIZE	650 LB/SEC
THRUST CLASS	50-60,000 LB
MACH NUMBER	2.4
CYCLE TEMPERATURES	2900°F MAX T₄₁ 1250°F MAX T₃
COMPONENT EFFICIENCY	LATE '90's TECHNOLOGY AVAIL.
MATERIALS	LATE '90's TECHNOLOGY AVAIL.
COMMERCIAL LIFE	18,000 HRS/9,000 CYCLES COLD SECTION 9,000 HRS/4,500 CYCLES HOT SECTION

Figure 4

ENGINE EVALUATION CRITERIA

As we perform our engine studies leading to engine concept selection, it is important to define the evaluation criteria to be used to select an engine concept. P&W and GE are in the process of defining the criteria and then making sure we are addressing the critical areas to meet the criteria identified.

- **PERFORMANCE**
- **WEIGHT**
- **PRICE**
- **MAINTENANCE COST**
- **RELIABILITY**
- **EMISSIONS**
- **NOISE**
- **AIRCRAFT MANUFACTURER ASSESSMENT**
- **IN-HOUSE MISSION EVALUATION**
- **COMPLEXITY / RISK ASSESSMENT**

Figure 5

1991 HSCT SYSTEM STUDIES PLAN

The 1991 HSCT systems studies plan covers the total P&W and GE planned IR&D and NASA contract engine studies. We will be reviewing our NASA contract studies which are presently being performed as well as the results from recently completed NASA studies.

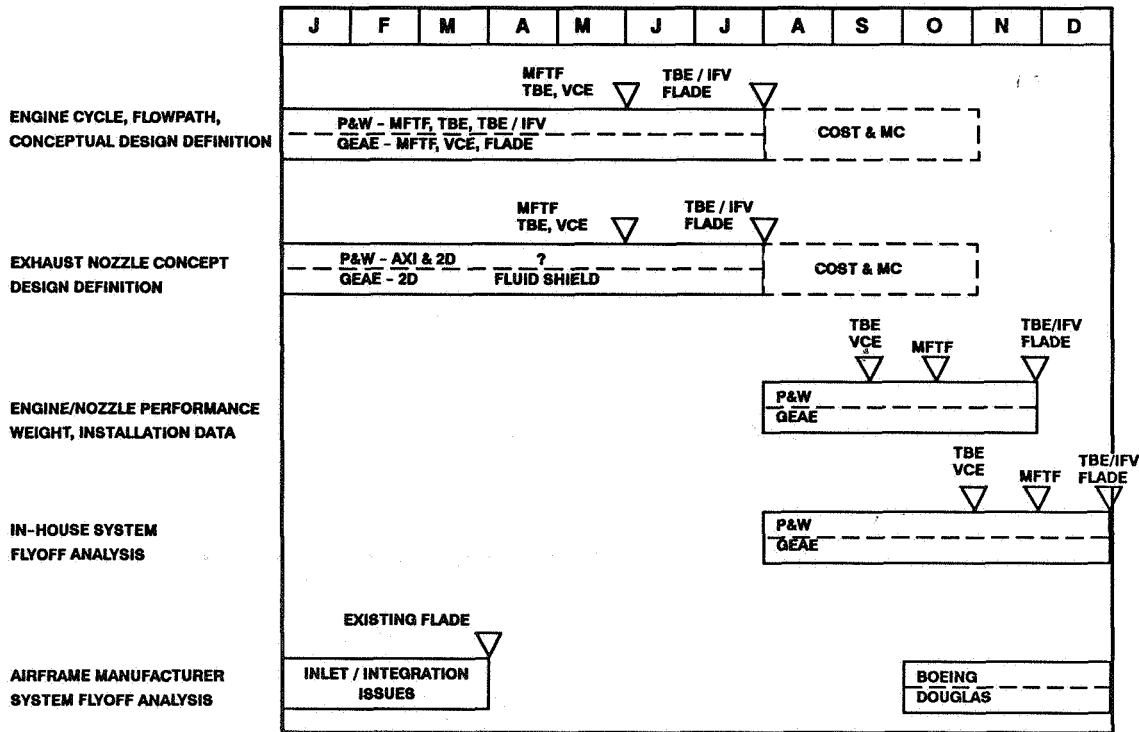


Figure 6

P&W NASA STUDY TASKS

There are three NASA study engine tasks presently being performed by P&W. They are:

1. An engine life study evaluating the impact of the severe engine environment associated with the HSCT mission.
2. Definition of a mixed flow turbofan engine.
3. Conceptual design and evaluation of an axisymmetric exhaust nozzle vs. a 2D exhaust nozzle.

- **MACH 2.4 TURBINE BYPASS ENGINE (TBE) LIFE STUDY**
- **MACH 2.4 MIXED FLOW TURBOFAN (MFTF) STUDY**
- **AXISYMMETRIC VERSUS 2D NOZZLE CONCEPTUAL DESIGN**

Figure 7

GE NASA STUDY TASKS

Present NASA engine studies being performed by GE cover a wide range of tasks from engine definitions; engine cycles and flowpaths; to exhaust nozzle mechanical design; and combustion efficiency trades.

- **UPDATE M2.4 VCE CYCLE & FLOWPATH**
- **M2.4 FLADE CYCLE & FLOWPATH**
- **M2.4 TURBOJETS CYCLE & FLOWPATH**
- **EXHAUST NOZZLE TRADES**
- **MIXED FLOW TURBOFAN**
- **M2.4 FLADE NOZZLE MECHANICAL DESIGN**
- **COMBUSTOR EFFICIENCY TRADE**
- **M1.6 VCE CYCLE & FLOWPATH**

Figure 8

THIS PAGE INTENTIONALLY BLANK

Session VI. Propulsion Systems Studies

omit

Results of GEAE HSCT Propulsion System Studies
Fred H. Krause, GE Aircraft Engines

PRECEDING PAGE BLANK NOT FILMED

THIS PAGE INTENTIONALLY BLANK

Results of GEAE HSCT Propulsion System Studies

First Annual High Speed Research Workshop

May 15, 1991

Williamsburg, Virginia

Fred H. Krause
HSCT Project
GE Aircraft Engines

N94-33479

317-07
12007



THIS PAGE INTENTIONALLY BLANK

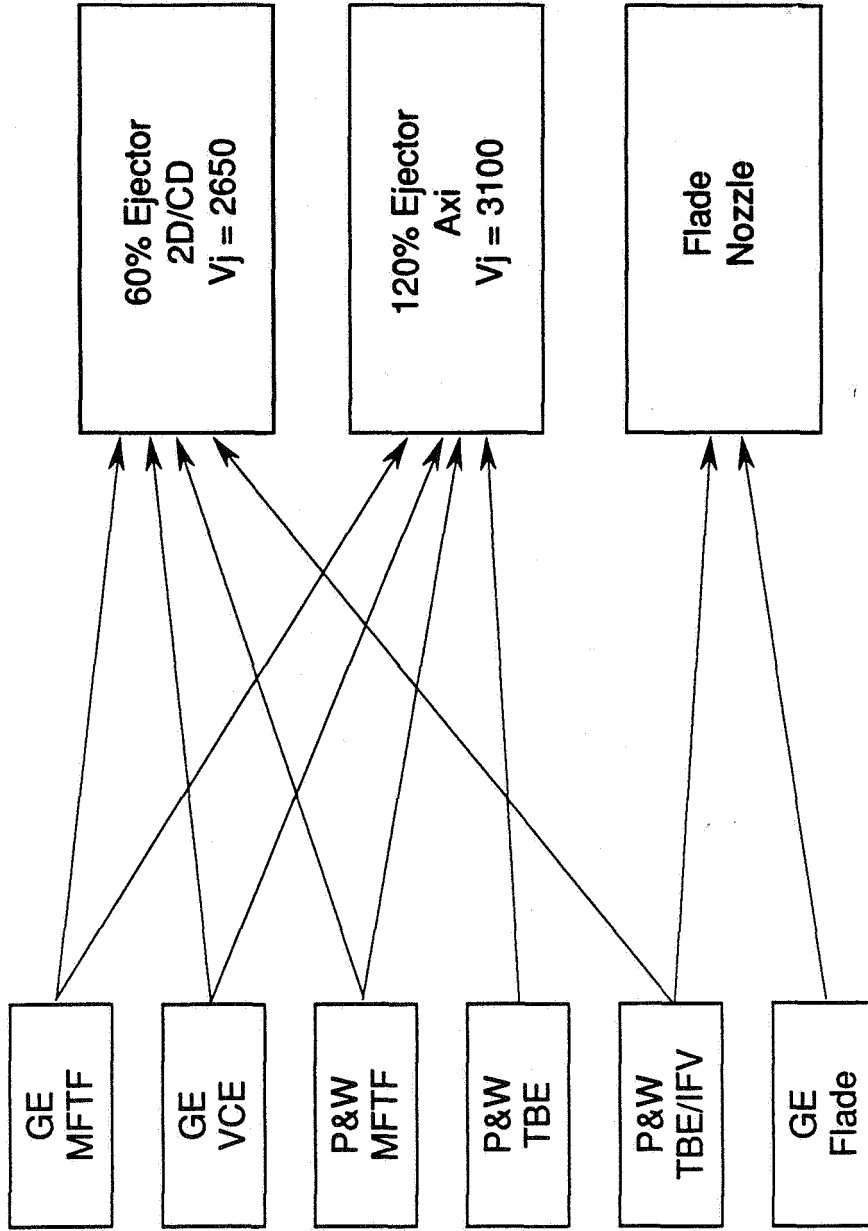
Good Afternoon. I've got good news and bad news. First the good news; I am not going to talk about emissions or sonic boom. The bad news is, that I will talk about acoustics.

This afternoon I am going to give you a very brief overview of the results of GE's HSCT propulsion system design studies. I will also cover our plans for the remainder of this year. A large part of my presentation revolves around the acoustic nozzle design and its impact on the propulsion system performance. Our studies have shown that this component is a key driver on the HSCT propulsion and aircraft system designs. Cruise Cfg, acoustic performance, nozzle weight, and takeoff Cfg are all critical nozzle design features.

HSCT Engine and Nozzle Options - Being Evaluated

P&W and GEAE are evaluating a number of engine concepts, the mixed flow turbofan (MFTF), the variable cycle engine (VCE) (double bypass engine), the turbine bypass engine (TBE), the turbine bypass engine with inverted flow valve (TBE/IFV), and the fan on blade (FLADE). Three different exhaust nozzle concepts, one with 60% ejector flow, one with 120% ejector flow, and a fluid shield type nozzle for the FLADE, are being evaluated. Engine cycle studies are being conducted at Mach 2.4 and Mach 2.0 with both NASA and company funding.

HSCT Engine and Nozzle Options – Being Evaluated



Between GE and P&W We are Covering All Options

This is just a quick look at the systems studies GEAE is performing this year both under IR&D and NASA contract. The first three items are an example of the way our IR&D and contract studies complement one another. The first line represents our Flade Cycle and flowpath studies for 1991. We have selected a baseline cycle and flowpath for the Flade concept under NASA contract this year. We will continue to look at Flade performance with alternate airflow schedules for the next 5-6 months. Mean while, under our IR&D studies we will conduct a mechanical preliminary design of this engine. Starting in July, we plan Flade nozzle design studies under NASA contract. During the first three months of this year we did some MFTF precursor studies under overhead funding. Now we are on contract for the cycle/flowpath and mechanical design of a Mixed Flow turbofan for HSCT.

Again, with the VCE we will do cycle/flowpath trade studies under NASA contract and the preliminary mechanical design under IR&D.

Under our UPS contract we are conducting an axisymmetric exhaust nozzle trade study for high specific thrust engines. This morning Muni Majjigi talked about our 2-D suppressor ejector nozzle design. Under this task order we are trying to apply what we learned in the design of the 2-D nozzle to axisymmetric nozzle designs. I will briefly show some of the results of that task and I think Marty Smith of Pratt will have a few words to say about 2-D vs. Axi acoustic nozzle designs.

GE HSCT – Systems Studies

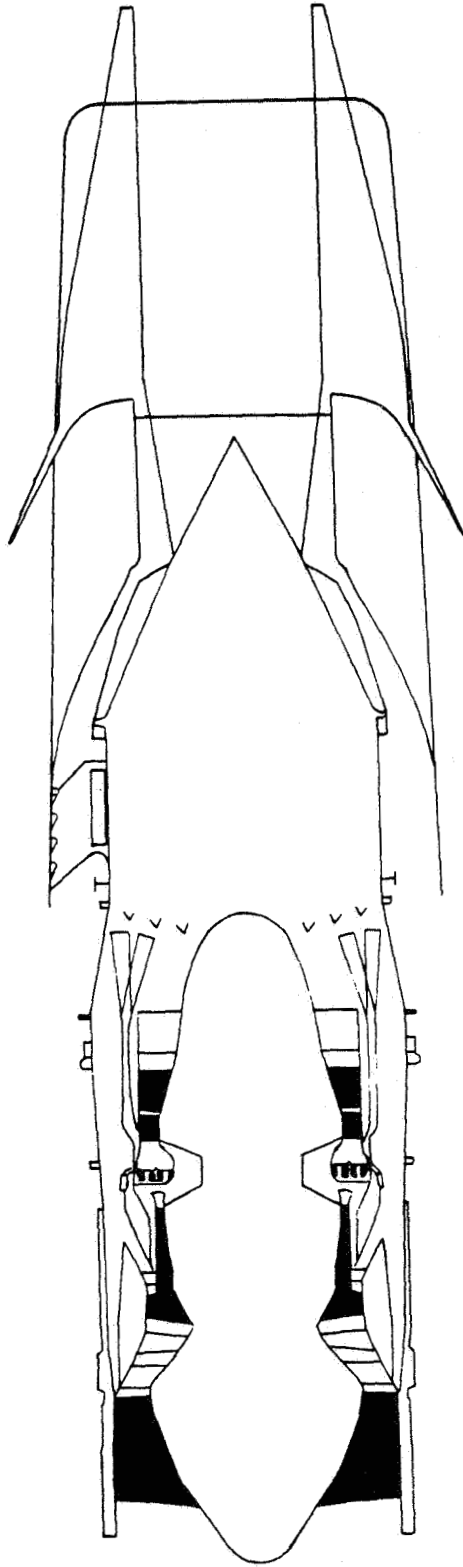
	Jan	Feb	Mar	Apr	May	Jun	Jul	Aug	Sep	Oct	Nov	Dec
• Flade cycle/flowpath												
• Flade mechanical design												
• Flade nozzle PD												
• Mixed flow turbofan												
• Update VCE												
• VCE mechanical design												
• Axi-exhaust nozzle trades												
• GE/NASA nozzle installation												
• Inlet studies												
• Control system payoff studies												
• Control system definition												

Between NASA Contract and IR&D GEAE Will Generate the Data Needed for Downselect

GE Variable Cycle Engine

The GE variable cycle engine is a double bypass engine with an overall pressure ratio of 25 and a bypass ratio of 0.65. The data shown is based on earlier design groundrules. We are in the process of updating this design to reflect the common design groundrules. This engine is shown with a 2D-CD ejector nozzle with 60% secondary flow entrainment.

GE Variable Cycle Engine



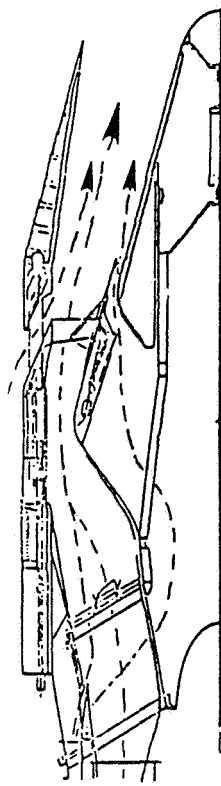
FPR	4.8
PROA	25
BPR	0.65
Weight	- Core 5951
	- Exhaust nozzle 4979
	- Total 10,930

SFC subsonic	.90
SFC supersonic	1.24
T41 cruise	2750°F
T3 cruise	1200°F
Cfg cruise	.986
Cfg takeoff	.93

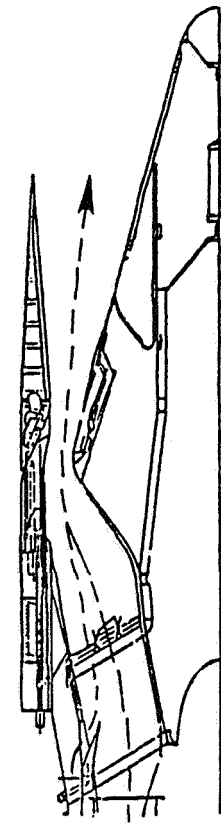
This data is based on GE design ground rules. Engine design is being updated in 1991 to common design groundrules

This chart shows our basic axisymmetric acoustic nozzle design. It represents the final nozzle design from our AST studies and the starting point for HSCT work. The four primary operating modes are shown. In the take off mode, the ejector flap is slid aft to open the ejector inlet. Some flow from the fan duct is brought down through the struts and into the plug where it exists tangentially to the core flow in the divergent section of the nozzle. All of the core flow and the rest of the fan flow mix and exit the main nozzle between the chutes which are hopefully filled with ambient air. Our goal for this nozzle is 60% flow entrainment. In the AST days the A8 of this nozzle was limited such that during acceleration some of the fan flow had to exit through the plug. This could give us on Inverted Velocity Profile type noise reduction 3-5dB during the climb out/acceleration flight regimes without opening the ejector. In the supersonic cruise mode the nozzle operates like a standard plug nozzle. A8 is varied by sliding the ejector flap fore and aft and A9 internal can also be varied by changing the ejector flap angle. In the reverse mode, the ejector flap moves all the way aft exposing the reverser guide vanes and a blocker door drops down to close off the primary nozzle.

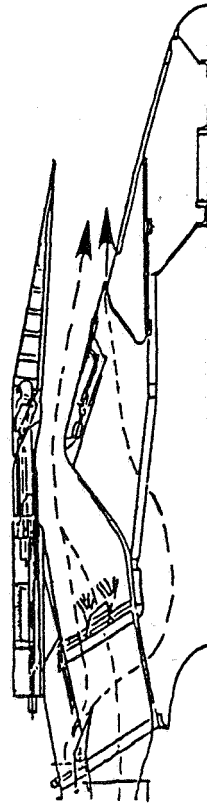
Coannular Nozzle With 20 Chute Suppressor and Ejector Operating Modes



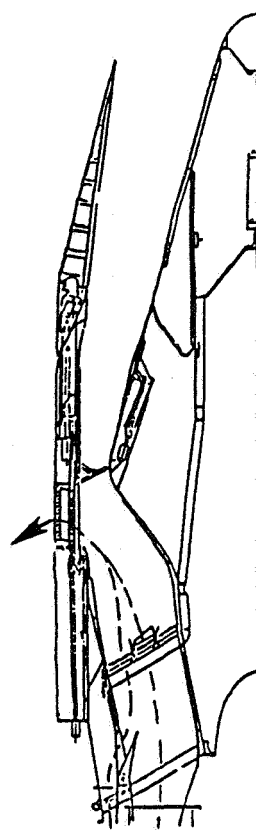
Takeoff



Supersonic Cruise



Acceleration



Reverse

The Final AST Nozzle is the Starting Point for Current HSCT Work

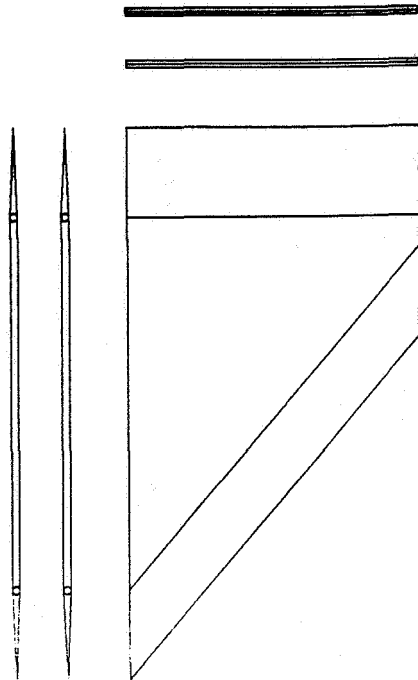
One of the areas that we are exploring under our axi exhaust nozzle trade studies is innovative chute design. A key to getting 60% flow entrainment is suppressor area ratio, which is the ratio of the total area at A8 to the core flow area at A8. We would like the chute exit area to be twice that of the core flow. It is impossible to stow such large chutes in a plug like I showed on the last viewgraph unless they have variable geometry. The collapsing chutes on the right hand side of this chart might be stowable out of the core stream during the other operating modes, but they are obviously complex and heavy.

The chute design on the left hand side of the screen would always be in the stream, but the leading edge would close during suppressed operation. For the other flight conditions it would be open with flow going through it. It would obviously want to be located in a low mach number flow region of the nozzle.

Both of these approaches are complex and heavy and hopefully won't be required.

Innovative Chute Design

Opening chutes



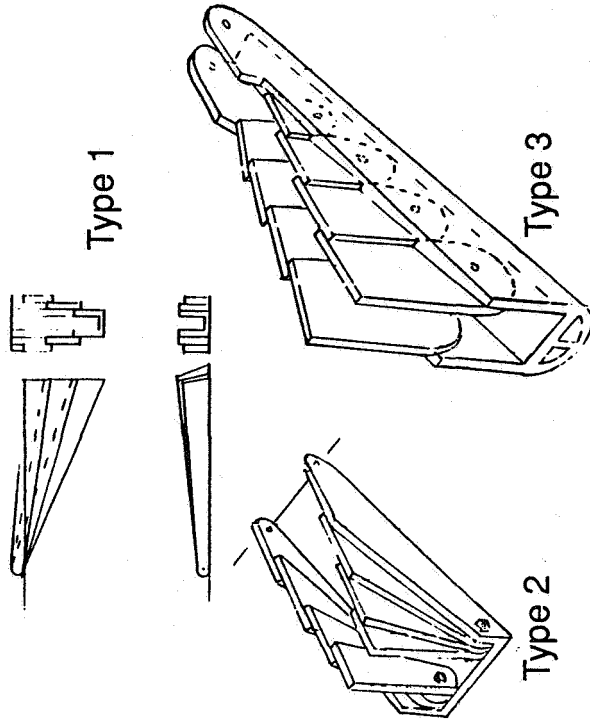
Advantages

- Stowage area
- Blockage ratio
- Complex shapes

Disadvantages

- Weight
- Actuation
- Performance

Collapsing chutes



Advantages

- Stowage area
- Chutes out of stream
- Blockage ratio

Disadvantages

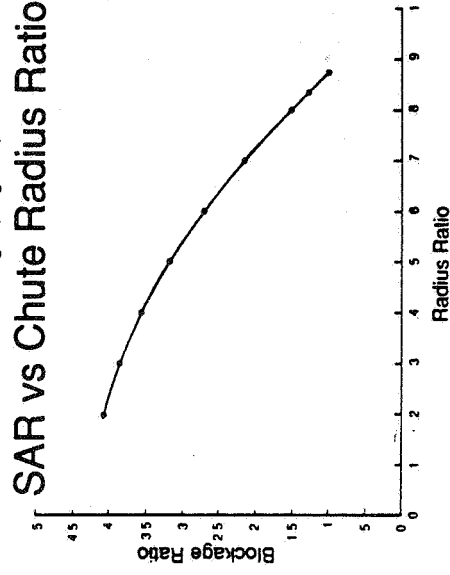
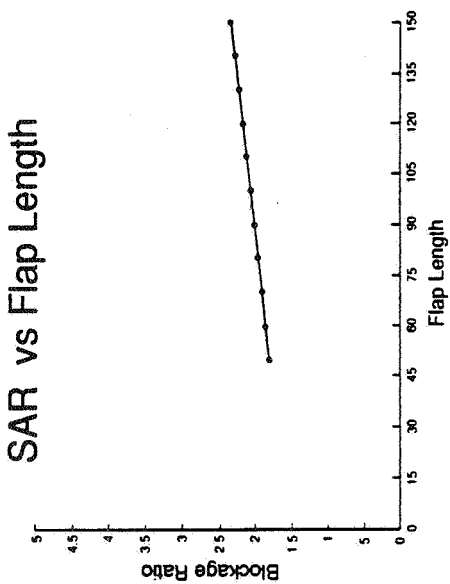
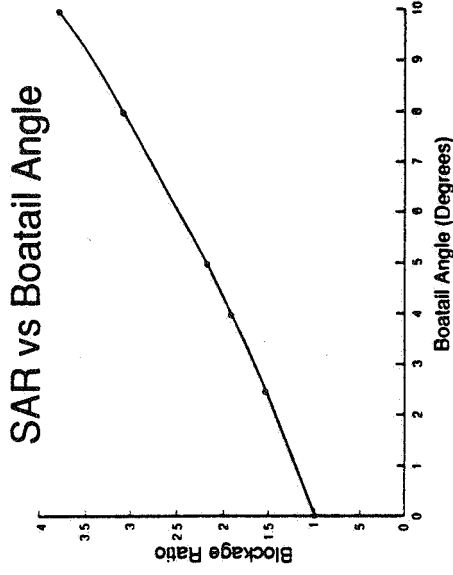
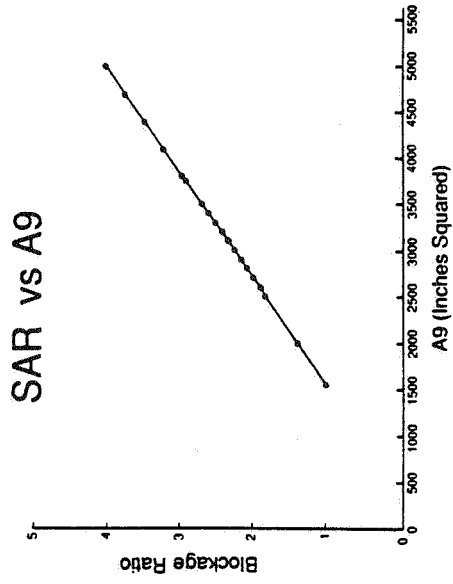
- Weight
- Actuation
- Performance
- Simple shapes

Complicated and Heavy . . . Hopefully They Won't be Necessary

This chart shows some very early results from our trade studies on a baseline nozzle which is similar to the AST type nozzle I showed a couple of charts ago. The first plot shows supersonic area ratio versus A9. A9 is obviously limited by what is required for reasonable supersonic cruise performance. We will generally accept a small cruise perf penalty for a slightly larger SAR. Ejector flap length has a small but positive influence on stowable suppressor size. But again flap length is limited by weight and performance considerations. Fixing all the nozzle design parameters except boattail angle we see that boattail angle has a significant impact on SAR but boattail angle is limited to 2.5 to 4.0 degrees for reasonable supersonic nozzle performance. The final plot is really a plot of chute radius ratio vs SAR. Chute radius ratio is the chute radius to the top of the chute divided by the radius to the bottom of the chute. A practical limit is out here about 0.6 - 0.7.

We will be doing sensitivities for aero performance, acoustics and weight for these same geometric design parameters.

Axi Acoustic Design Trade Studies



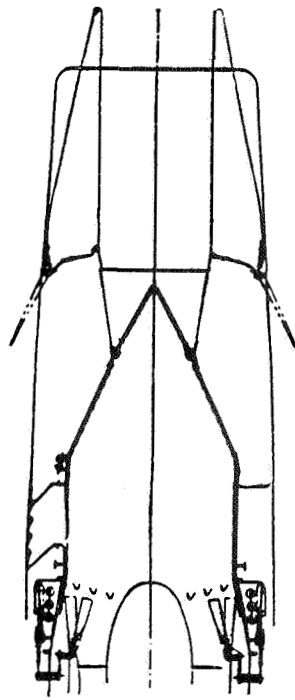
GEAE is Bounding the Geometric Problem

This chart is a look at our current 2-D suppressor ejector nozzle. Mr. Majjigi described this nozzle and its anticipated aero/acoustic performance in some detail during this morning's source noise session. The nozzle as designed has a suppressor area ratio over 2.5 with convergent divergent chutes. We anticipate that it would pump an additional 60% (of the engine flow) through the ejectors and into the exhaust nozzle. In the upper left hand corner of the figure the nozzle is shown in its take off position with the chutes deployed fully. The chutes may be retracted partially for conditions where A8 required is larger. In all other modes the chutes are retracted. In the supersonic mode the boattail angle is $\sim 4^\circ$ and the nozzle is slightly expanded beyond the optimum area ratio for internal performance.

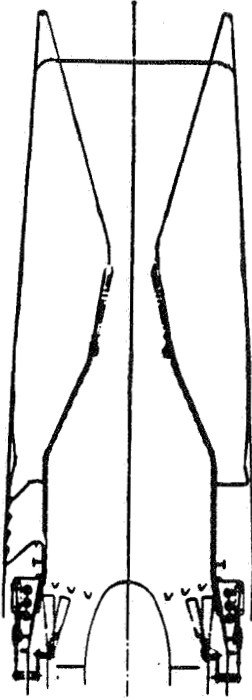
In the subsonic mode the boattail angle approaches 15° . I should point out that the secondary flaps shown here are 80 inches long.

In the thrust reversing mode the nozzle closes at the throat and the reverser doors are opened exposing the reverser vanes. With all of these operating modes and control variables accurate geometry control will be critical to maximizing performance at cruise and noise suppression at take off.

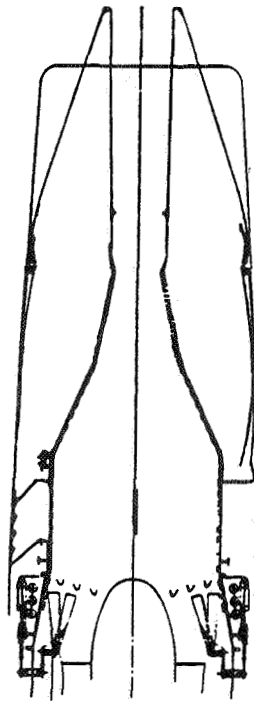
2DCD Nozzle Operating Modes



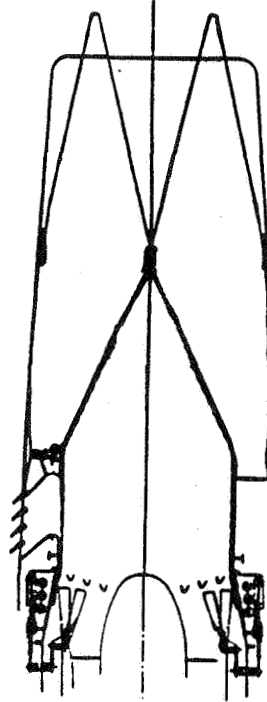
Takeoff



Supersonic



Subsonic



Thrust Reversal

Accurate Geometry Control Critical to Maximizing Performance at Cruise and Maximizing Noise Suppression at Takeoff

GE is still trying to evaluate both axi and 2-D nozzle concepts. There are advantages and disadvantages to both types. This chart highlights some of the advantages/disadvantages of 2-D nozzles as compared to axi nozzles.

~~8/11~~

Unfortunately at this point we have not had an airframe manufacturer evaluate the installation benefits on one type versus the other.

2D vs Axi

Advantages

- Increased perimeter
- Suppressor area ratio
- Variable A8
- Acoustic treatment surface area
- Manufacturability

Disadvantages

- Structure weight
- Ejector inlet area
- Leakage/performance loss

Installation?

Both Concepts Will Continue to be Evaluated

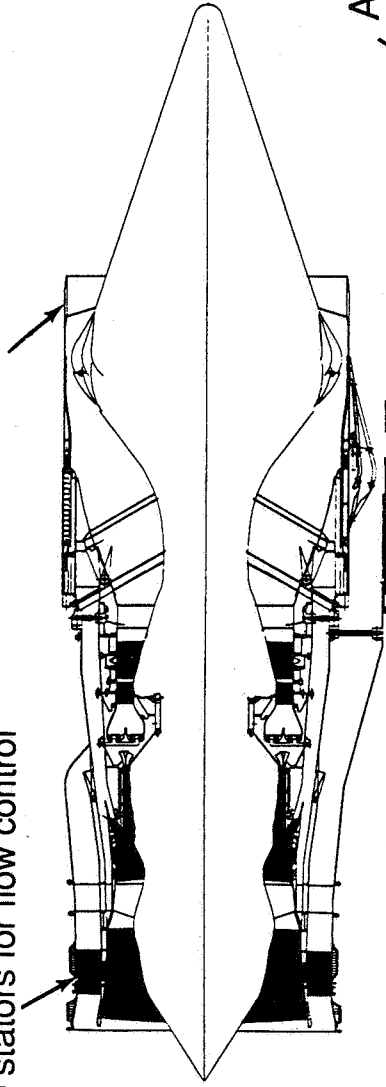
Several speakers over the past two days have talked about multiple approaches to the noise reduction problem. The first being complex high flow entrainment suppressor ejector nozzles that entrain 60-120% additional ambient air into the nozzle, thus reducing the mean jet velocity in a high specific thrust engine. The high flow engine is another approach. Most of you are familiar with the Rolls Royce Tandem Fan concept. This is GE's approach. The Flade or Fan on Blade engine augments flow during take off and subsonic flight regimes (climb, acceleration and cruise) resulting in a higher bypass engine. The Flade is attached to the second fan stage and is driven by the LP turbine. Variable inlet guide vanes regulate the flow into this stage ala the convertible engine concept which GE developed and tested for the DARPA X-Wing program.

Some minimum amount of flow must go through the Flade stage even in supersonic flight regimes but inlet boundary layer bleed air would probably be used resulting in an installed engine performance improvement.

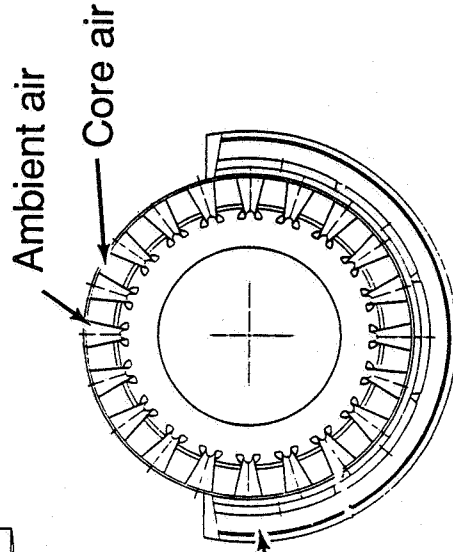
Another feature of the Flade propulsion system is the fluid shield nozzle concept. The Flade flow is collected in an annular duct which wraps around the bottom 200° of the engine to form an acoustic shield. The shield provides additional noise reduction, beyond the noise reduction which results from the much lower mixed jet velocity required to make the thrust with the larger mass flow of the Flade engine.

GEAE "Flade" HSC T Propulsion Concept Low Noise Geometry Setting Shown

- High flow Fladed fan concept
 - Variable stators for flow control
- Simple suppressor



- Minimum Flade flow during supercruise
 - Inlet boundary layer air could be used
 - C/D nozzle shape for best supercruise performance
- For low noise takeoff
 - Flade flow used to form an acoustic shield for additional noise reduction

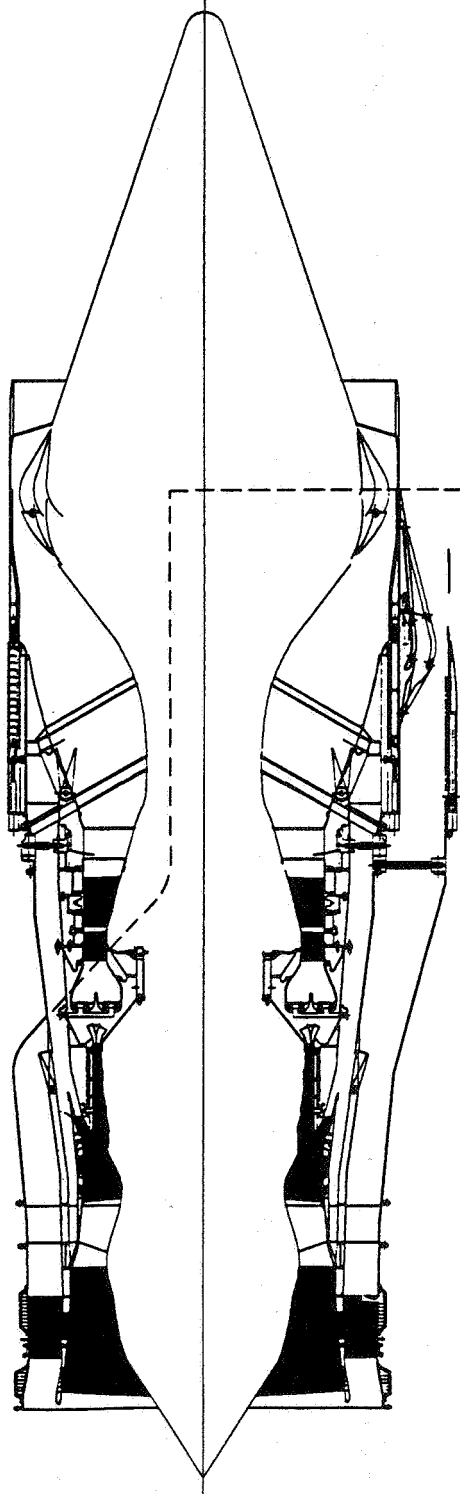


GEAE's High Flow Concept Beats the Noise Problem

GE Fan on Blade (Flade)

The data shown on this page reflects the latest GE Flade designs based on the joint GE/P&W HSCT propulsion system design groundrules. The air flow of the basic core VCE engine is 650 pps. While the Flade pumps an additional 250 pps. A unique feature of the Flade concept is that the core engine is sized/ designed for supersonic cruise while the flade is sized/ designed for takeoff conditions. An axisymmetric exhaust nozzle with variable exit areas and minimum suppression on the core flow is being used.

GE Fan on Blade Engine (Flade)



FPR	4.95	SFC subsonic	0.92
PROA	21.7	SFC supersonic	1.31
BPR	0.33	T41 cruise	2600°F
Flade PR	1.8	T3 cruise	1180°F
Weight	- Core	Cfg cruise	.982
	- Exhaust nozzle	Cfg takeoff	.95
	- Total		11,985

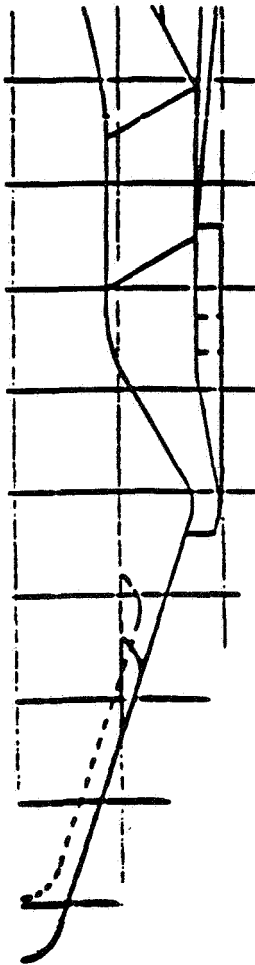
This chart depicts 3 nozzle concepts which we studied for the Flade. The first concept we studied was a two stream exhaust where all of the Flade flow was ducted through the struts into the plug and out parallel to the core flow. This results in an inverted velocity profile which could be worth 4 dB of suppression. This amount of suppression could be enough if you had a modest take off thrust requirement and a large flade flow. The problem is that this nozzle is large and heavy.

The second approach which we tried was a 3 stream nozzle without a suppressor but with the fluid shield. The fluid shield is shown on the bottom and it would wrap around the bottom 200-230 degrees of the nozzle. The fan flow is ducted through the plug. This concept is the simplest and lightest, but it was still not quite good enough from an acoustics perspective.

The final concept is a fluid shield with suppressor chutes but no ejector flaps as Sam mentioned in the GE/P&W summary talk yesterday. This nozzle weigh about 15% more than the second concept, but it does meet the Stage III noise goals.

Acoustic Nozzle Options Studied

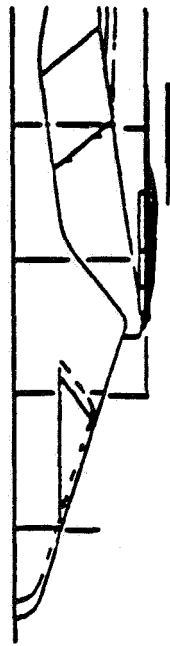
Two stream



Weight = 6,620 lb

- Flare through plug
- Simplest/largest
- ≈ 4 dB

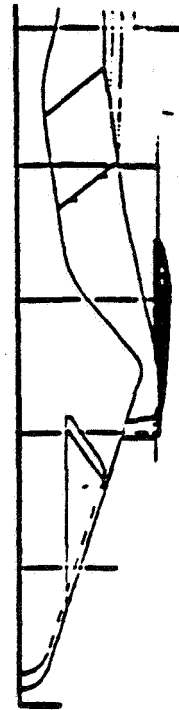
Three stream without suppressor



Weight = 3,980 lb

- Fan flow through plug
- Fluid shield ≈ 3 dB
- IVP ≈ 3 dB

Three stream with suppressor



Weight = 4,565 lb

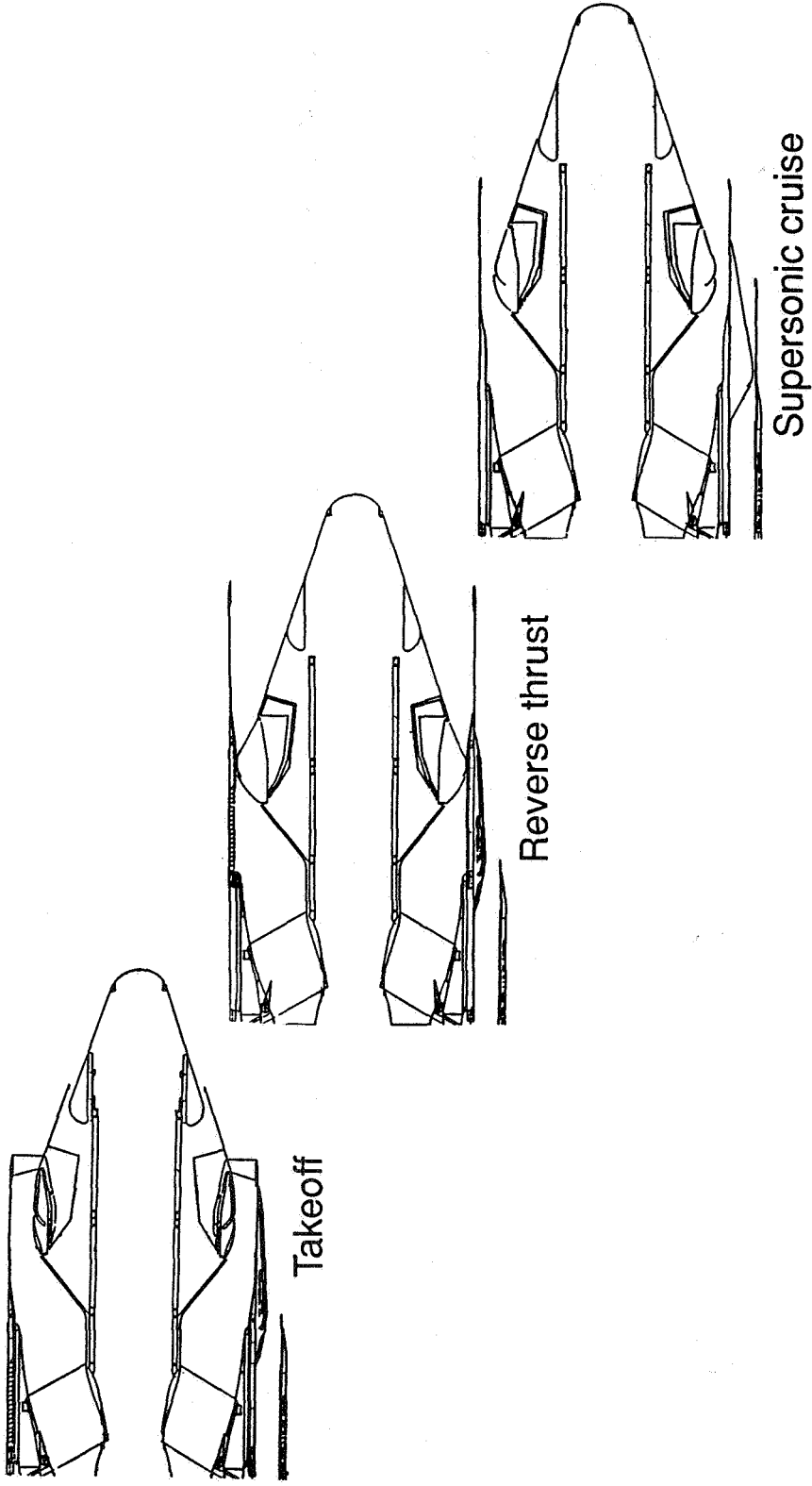
- Fan flow through plug
- Fluid shield ≈ 3 dB
- IVP ≈ 3 dB
- Suppressor chutes ≈ 5 dB

All Flare Nozzles Capize on Low V_{javg}

Three Flade operating modes are depicted here. The first - takeoff I have described previously. The second is reverse thrust. In this mode the plug expands to seal the aft nozzle exit at the throat and the outer duct slides aft to expose the reverser cascades. Note that the reverser uses only the 120-140° circular arc around the top of the nozzle so that the reversed thrust does not have to go through the Flade duct.

In the supersonic cruise mode the outer duct fore/aft position controls A9 internal for maximum nozzle performance.

Flade Nozzle Operating Modes



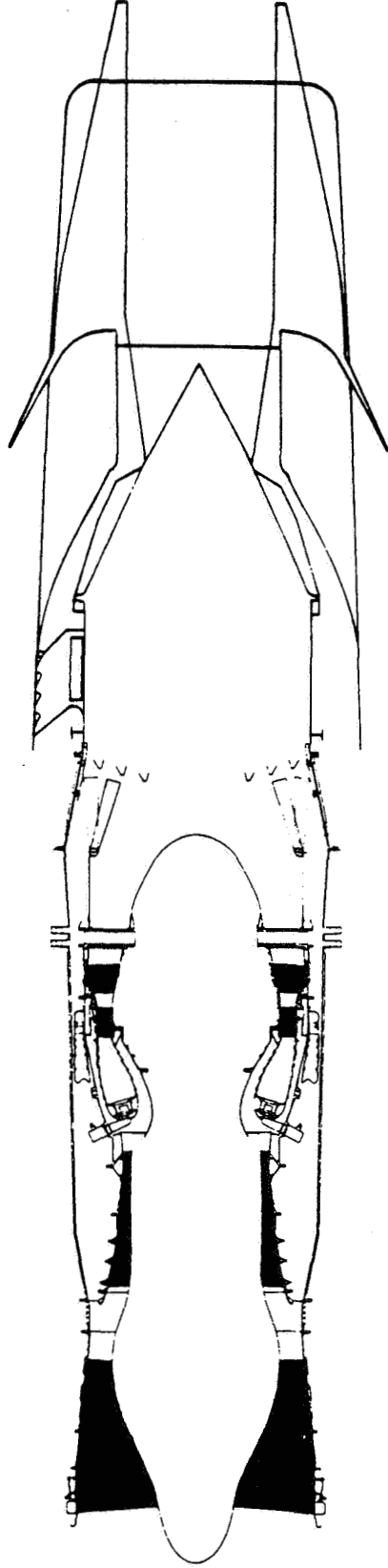
*The Lack of Ejector Flaps on the Flade Nozzle
Reduces Weight and Complexity*

GE Mixed Flow Turbofan

Recently GE has agreed with Pratt to study mixed flow turbofans. We have selected this engine type to be a test case for comparing our design methodologies and will eventually agree on a cycle to be designed by both companies. We can then compare flowpath and mechanical design results.

The current GE mixed flow turbofan engine is a low bypass ratio turbofan with an overall pressure ratio of 21.5. This engine is shown with a 2D-CD ejector nozzle with 60% secondary flow entrainment. Nozzle thrust coefficients are based on this exhaust nozzle. The cycle and preliminary design activity on this engine is due to be completed in the next few months.

GE Mixed Flow Turbofan



FPR	4.75			SFC subsonic	TBD
PROA	21.5			SFC supersonic	TBD
BPR	0.15			T41 cruise	TBD
Weight	- Core	TBD		T3 cruise	TBD
	- Exhaust nozzle	TBD		Cfg cruise	.982
	- Total	TBD		Cfg takeoff	.95

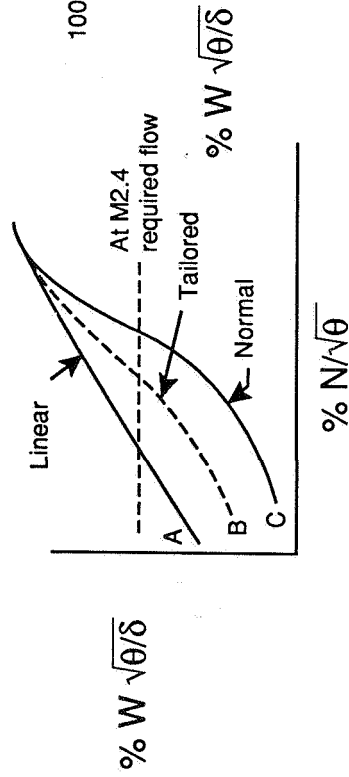
SUMMARY CHART UNAVAILABLE AT TIME OF PUBLICATION

Compression System Characteristics

- Will set max percent rpm (105-110-115+)
- Will impact no. stages, turbine radius, weight, etc.

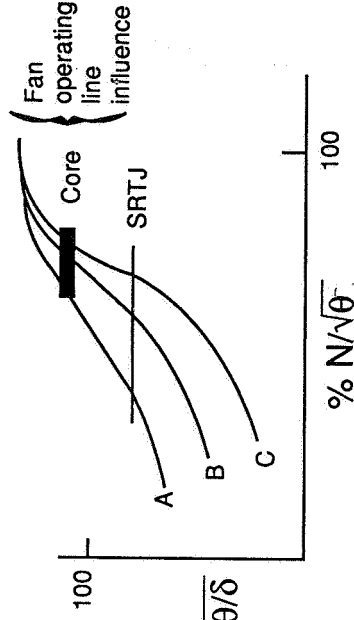
Fan

- A – Without IGV
- B & C – With IGV



Compressor core or SRTJ

- A – Minimum variable stators
- B – Additional variable stators
- C – Full/rear variable stators



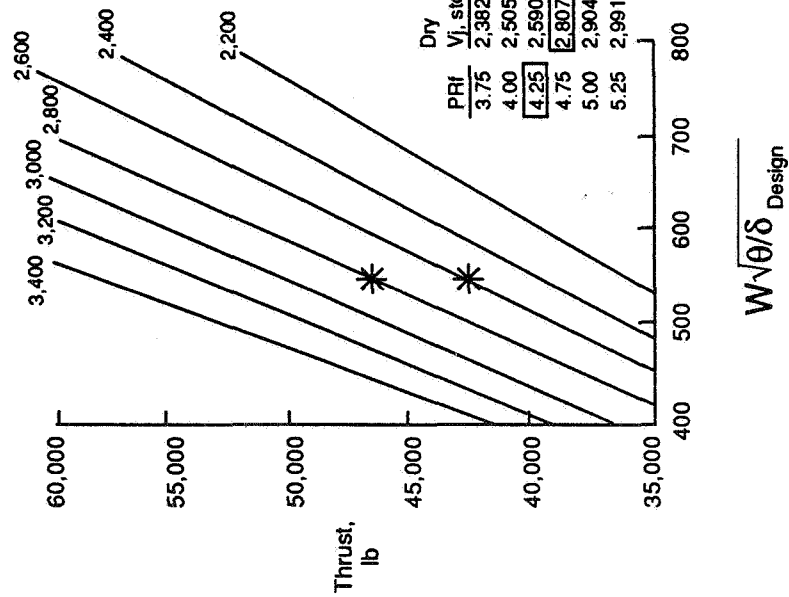
*Compression System Characteristics Are
A Key to the MFTF Design*

Our preliminary turbofan cycle studies are looking at the impact of take off acoustics and thrust requirements at the sideline measuring point and top of climb on the design fan pressure ratio, bypass ratio and airflow size. The right hand plot shows thrust versus airflow for lines of constant jet velocity. If we enter this plot with a jet velocity limit at which we think that we can meet Stage III noise requirements, we can pick off a minimum airflow size. In this case, let's assume we feel comfortable that with our suppressor nozzle we can meet Stage III with a V_j of 2700 fps and that the thrust required is 38,000 lbs. We would determine that a 530 pps engine with a fan pressure ratio of 4.25 would meet the requirements. With this engine we would have no dry thrust margin so we would pick a FPR of say 4.75. This gives us the capability to push the throttle to a V_j of 2921 fps which could give up another 4,000 lbs of thrust.

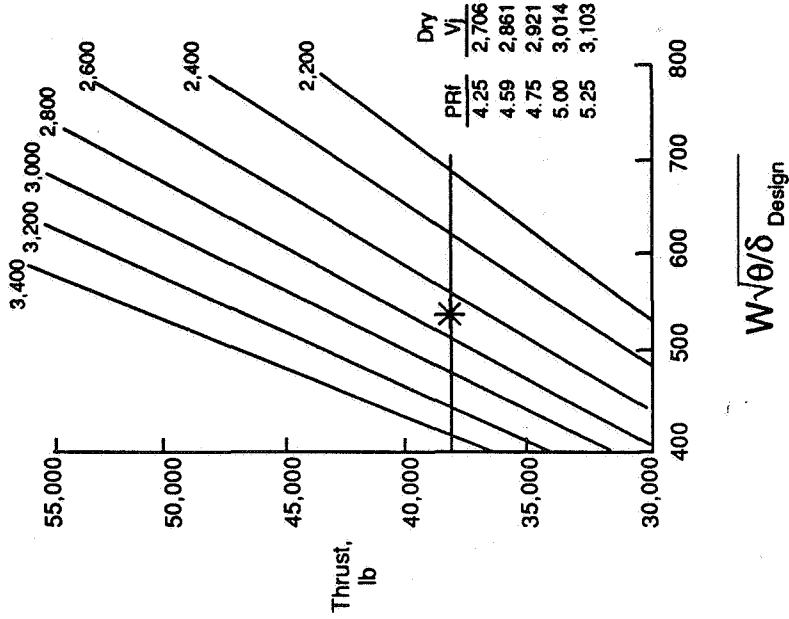
Preliminary Turbofan Studies

At SLS - standard day
Vj - comp. exp

Cfg = 0.95



At 0.322/689' + 18°
Vj - comp. exp



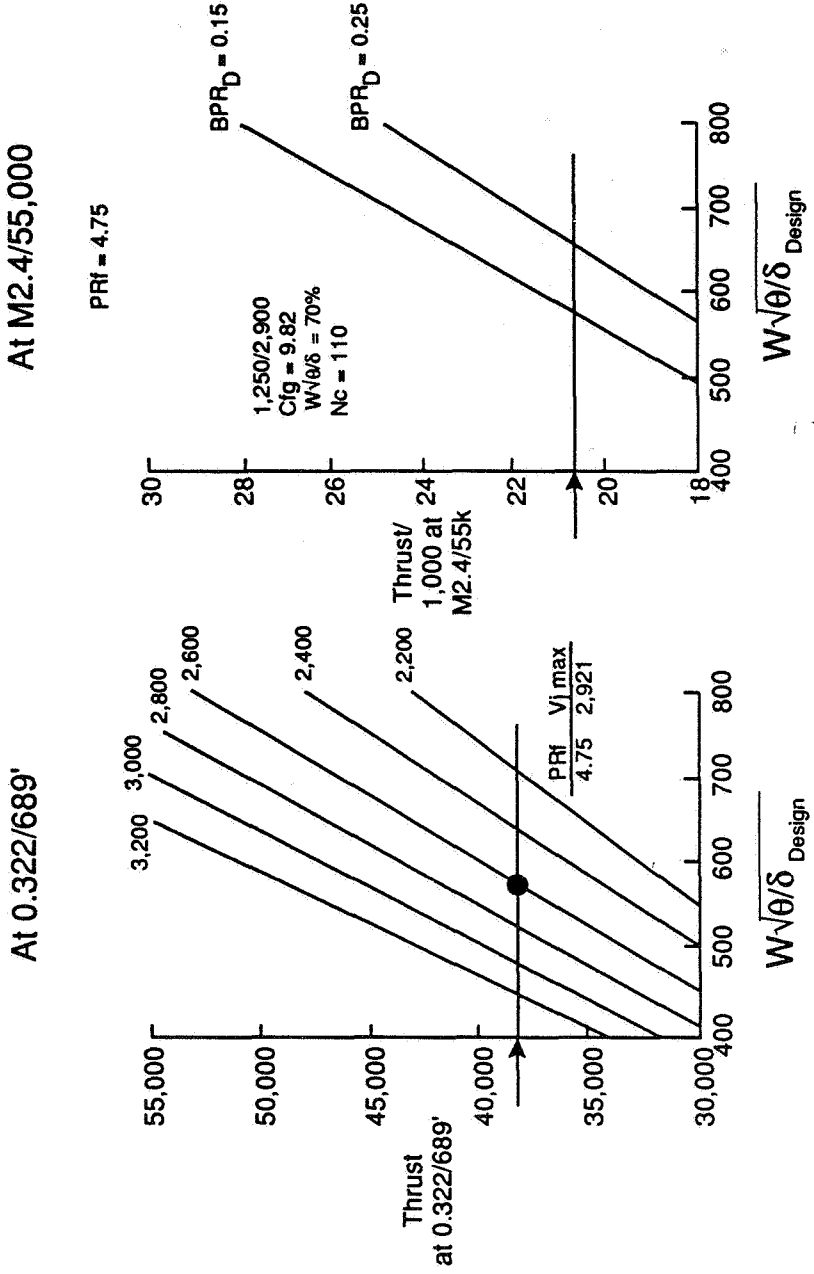
Acoustic Requirements Drive the Design at Takeoff

The plot on the right shows how the Design Bypass Ratio along with the top of climb thrust requirement size the engine for a given fan pressure ratio. Assuming that the top of climb thrust requirement is 20,750 lbs for a $BPR_D = 0.15$ the engine needs to be about 550 pps. Slightly larger than the take off requirement from the previous chart but a good match. For a design BPR of 0.25 the required engine size grows to 650 pps and the takeoff thrust available would be substantially more than the requirement.

Our studies to date on this type of engine have been limited, but we are working with P&W and NASA to find the best MFTF design and compare it to the other candidate propulsion systems.

Preliminary TF Studies

PRf = 4.75, BPR



Top of Climb Thrust and Design Bypass Ratio Size the Engine

I think that the conclusions chart is reasonable self explanatory. The bottom line is. We are not ready to select an engine concept yet, but within the next year and one half, our propulsion system studies and acoustics tests should put us in a position to eliminate several concepts.

Summary

- GE/P&W have agreed on a reasonable set of design ground rules
- GE/P&W exploring wide range of propulsion system and nozzle options
- Cycle and flowpath trade studies are key to evaluating concepts
- Mechanical design trade studies are oriented towards meeting subsonic commercial engine life with a supersonic engine
- By this time next year the results of the design trade studies, the acoustic tests, the emission testing and aircraft sizing studies should help answer the three challenges
 - Noise
 - Emissions
 - Economics

THIS PAGE INTENTIONALLY BLANK

Session VI. Propulsion Systems Studies

omit

Pratt & Whitney Propulsion Systems Studies Results/Status
Martin G. Smith, Jr. and George A. Champagne, Pratt & Whitney Aircraft

PRECEDING PAGE BLANK NOT FILMED

THIS PAGE INTENTIONALLY BLANK

N94- 33480

518-07
12008

**P&W PROPULSION SYSTEMS STUDIES
RESULTS / STATUS**

**MARTIN G. SMITH, JR.
GEORGE A. CHAMPAGNE
ADVANCED ENGINE PROGRAMS
PRATT & WHITNEY**

**NATIONAL AERONAUTICS AND SPACE ADMINISTRATION
FIRST ANNUAL HIGH SPEED RESEARCH WORKSHOP
MAY 14-16, 1991**

PRECEDING PAGE BLANK NOT FILMED

921

P&W PROPULSION SYSTEMS STUDIES

NASA FUNDED EFFORTS TO DATE

Propulsion systems studies for the High Speed Civil Transport (HSCT) were resumed in 1987 after a hiatus of 6 or 7 years. The initial NASA-sponsored efforts were funded through subcontracts under the Boeing (NAS1-18377) and Douglas (NAS1-18378) primary contracts from the Langley Research Center. The very early studies covered a wide range of cruise Mach numbers and provided performance, installation and weight information for both existing and newly-defined study engines, with the primary goal of narrowing the Mach number range to the region of interest. Later studies under these subcontracts included tasks devoted to the environmental issues of noise and stratospheric cruise emissions.

The NASA Lewis Research Center contracted directly with Pratt & Whitney for a series of studies over a three year period beginning in late 1987. These studies included evaluation of various engine cycles with a major emphasis on the airport noise reduction challenge. The current NASA-Lewis funded studies include investigation of the design trades available to achieve satisfactory life in a commercial supersonic transport application, mixed flow turbofan cycle and conceptual design studies and an axisymmetric vs two dimensional nozzle conceptual design and evaluation study.

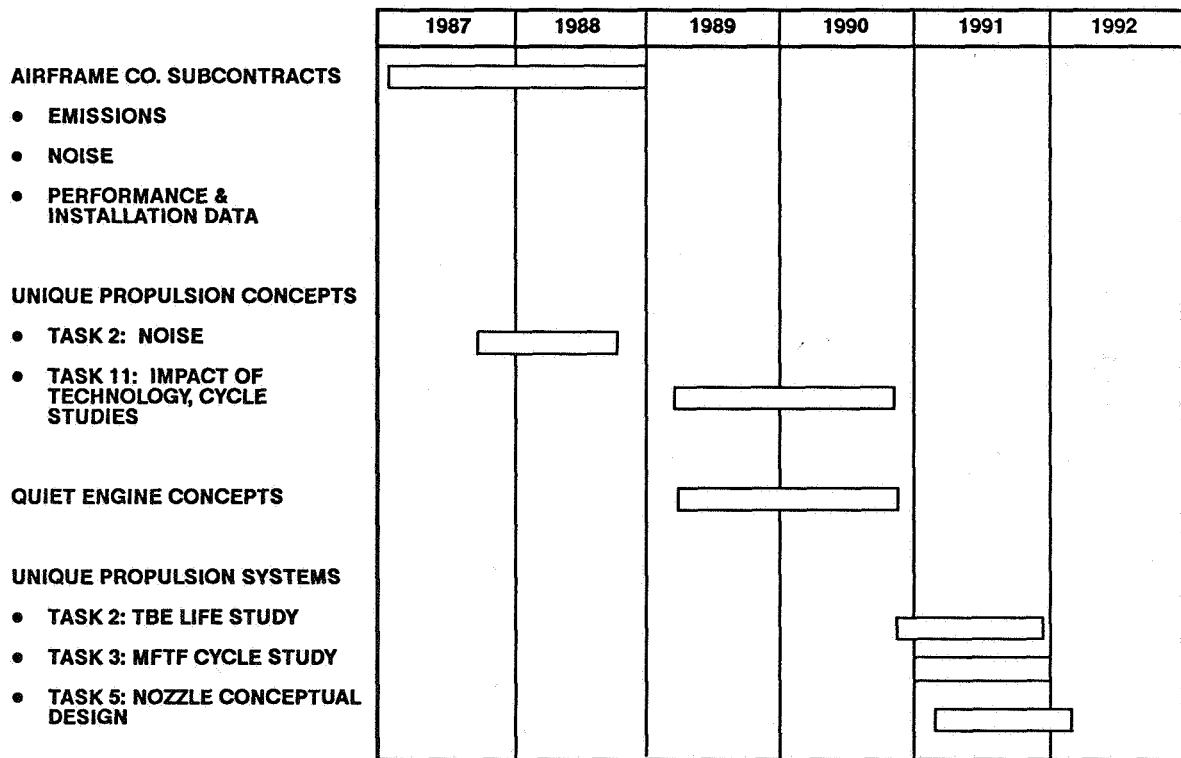


Figure 1

P&W ENGINE CONCEPTS

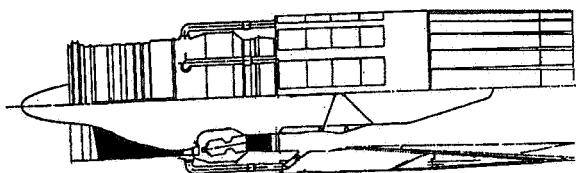
Shown in Figure 2 are four engine concepts which have been, or are being, investigated for potential future application to a High Speed Civil Transport. The turbine bypass engine (TBE) is a single spool turbojet with an oversized compressor and a compressor bleed system that bypasses flow around the turbine. This feature enables the TBE to operate at maximum turbine inlet temperature over the entire flight envelope. It also provides higher compressor pressure ratio and more thrust variation at constant airflow than a comparable turbojet during part throttle operation. It has an inherently high exhaust jet velocity and must rely on a very effective suppressor nozzle to achieve the FAR 36 Stage III noise goal.

The turbine bypass engine equipped with an inlet flow valve is intended to provide lower exhaust jet velocity through increased inlet total airflow at takeoff, while maintaining the turbojet cycle for climb and supersonic cruise operation.

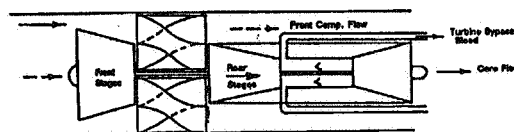
The variable stream control engine (VSCE) is a moderate bypass ratio twin spool turbofan which uses fan duct augmentation for takeoff, transonic/supersonic acceleration and supersonic cruise. The VSCE derives its name from the ability to independently control the primary and fan duct exhaust streams via its two burners and two exhaust throat areas.

The mixed flow turbofan (MFTF) is the type of engine being widely used for many current and planned military aircraft. It is typically a low bypass ratio twin spool configuration and may be equipped with an afterburner for thrust augmentation. For the HSC T application, the use of an afterburner is being considered for use at thrust critical transient conditions, such as transonic acceleration, but may not be necessary. The MFTF has an inherently lower exhaust jet velocity than the TBE and would not require as much noise suppression in the nozzle to meet the FAR36 Stage III goal.

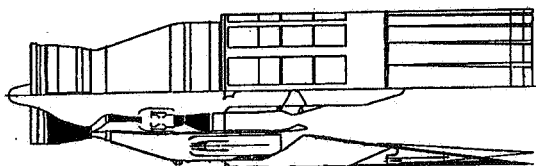
TURBINE BYPASS ENGINE



TURBINE BYPASS ENGINE WITH INLET FLOW VALVE



VARIABLE STREAM CONTROL ENGINE



MIXED FLOW TURBOFAN

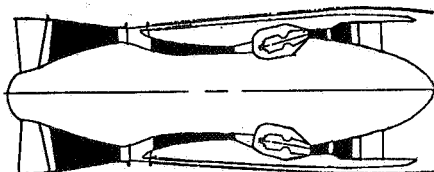


Figure 2

P&W COMBUSTOR FOCUS
RICH BURN-QUICK QUENCH CONCEPT

Pratt & Whitney is focusing its High Speed Research (HSR) combustor technology development on the rich burn quick quench (RBQQ) concept, which is illustrated in Figure 3, to achieve very low levels of oxides of nitrogen (NO_x) emissions. Combustion takes place in three distinct zones: the fuel rich zone, rapid quench zone and fuel-lean zones.

All of the fuel is injected and reacted in the fuel rich zone. Because of the lack of enough oxygen for complete combustion, the rate of formation of NO_x is low. To complete the combustion process, which consists of carbon monoxide to carbon dioxide conversion and smoke oxidation, the rich zone combustion products pass through a second reaction zone in which the mixture strength is lean and temperature sufficiently high to carry out the reactions, but avoiding the higher levels at which formation of NO_x can be accelerated. The rich-to-lean mixture transition must be accomplished in the quick quench section of the combustor located between the rich and lean zones. Large quantities of air are introduced in this section to mix rapidly without accumulating time at elevated temperatures.

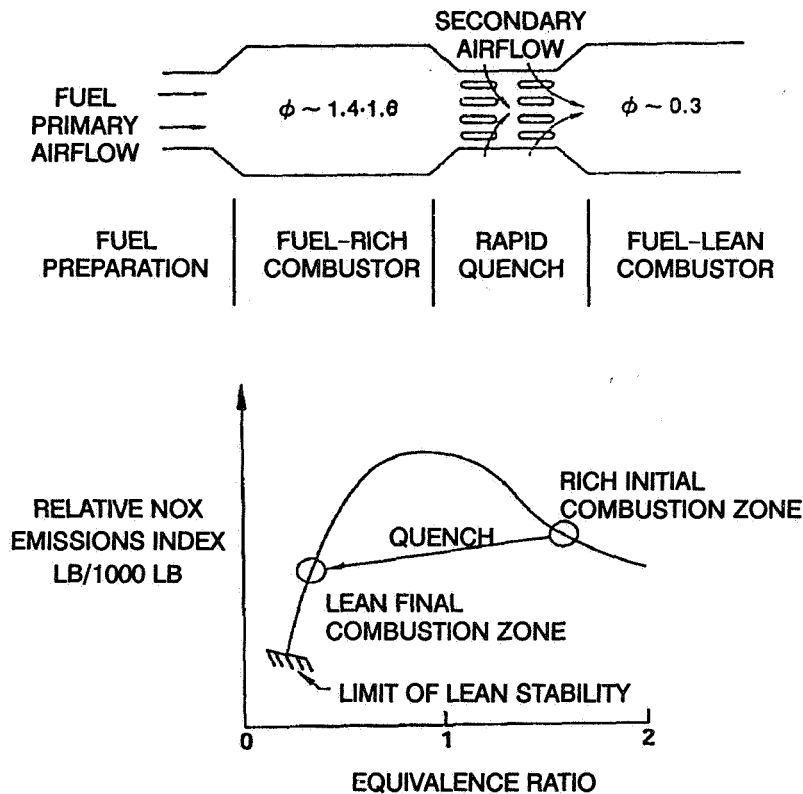


Figure 3

MIXER EJECTOR NOZZLE CONCEPT
LARGE FLOW ENTRAINMENT REDUCES JET NOISE

The mixer/ejector suppressor nozzle concept illustrated in Figure 4 is currently being investigated under the HSR low noise nozzle technology development program. The nozzle concept relies on a large amount of ambient airflow entrainment to rapidly mix with the high temperature exhaust flow, thereby lowering the jet velocity and the associated jet noise. It has a retractable mixer which is deployed at takeoff and stowed for cruise.

Also shown in Figure 4 is the theoretical reduction in noise as a function of the amount of entrained flow. The Pratt & Whitney goal is to achieve over 100% flow entrainment and approximately 20 db noise reduction in the nozzle.

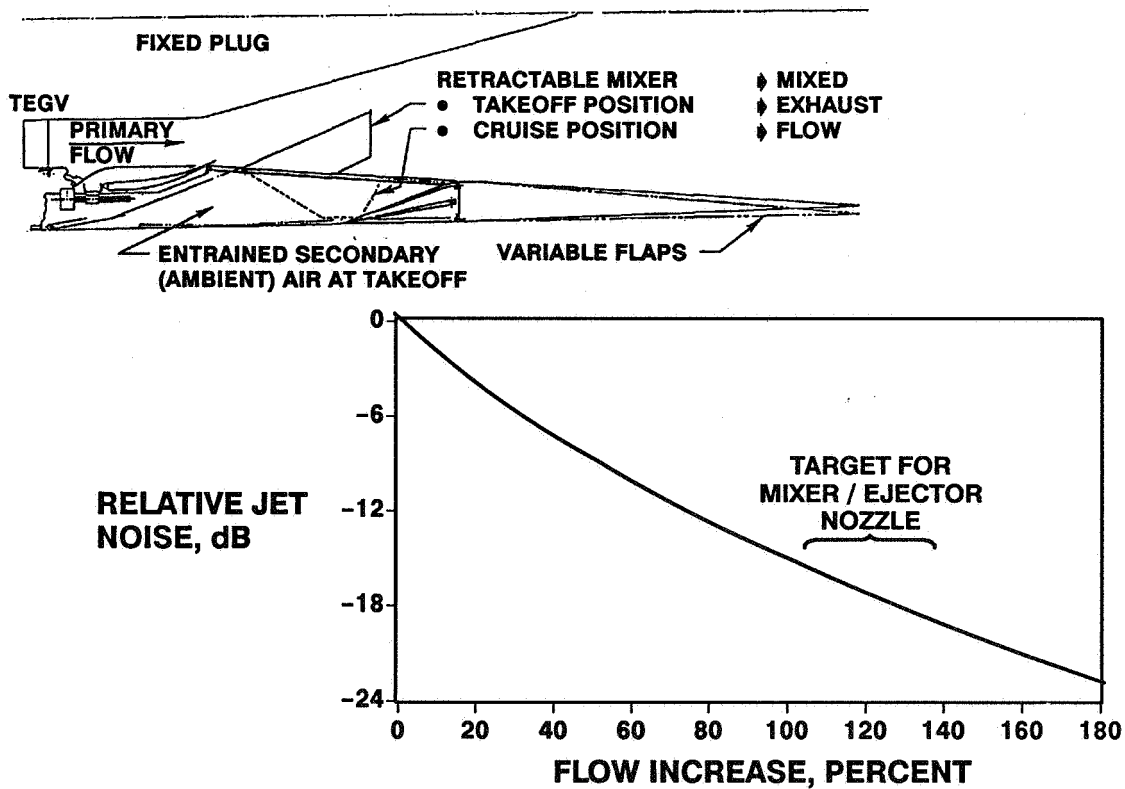


Figure 4

TECHNOLOGY IMPACT ON NO_x EMISSIONS
MATURE RBQQ COMBUSTOR REDUCES NO_x UP TO 85%

The projected impact of propulsion technology advances on NO_x emissions, takeoff noise and integrated propulsion/airframe system performance will now be described. Figure 5 presents the supersonic cruise NO_x emissions trend for three technology time period TBE's from current technology with entry into service (EIS) in 1995 to year 2005 EIS. If current technology combustors were utilized, NO_x would more than double for the year 2005 EIS engine due to its 200°F increase in combustor inlet and exit temperatures and over 50% increase in combustor pressure level. The mature RBQQ combustor is projected to reduce NO_x emissions up to 85% for this engine or 70% relative to the current technology cycle and combustor.

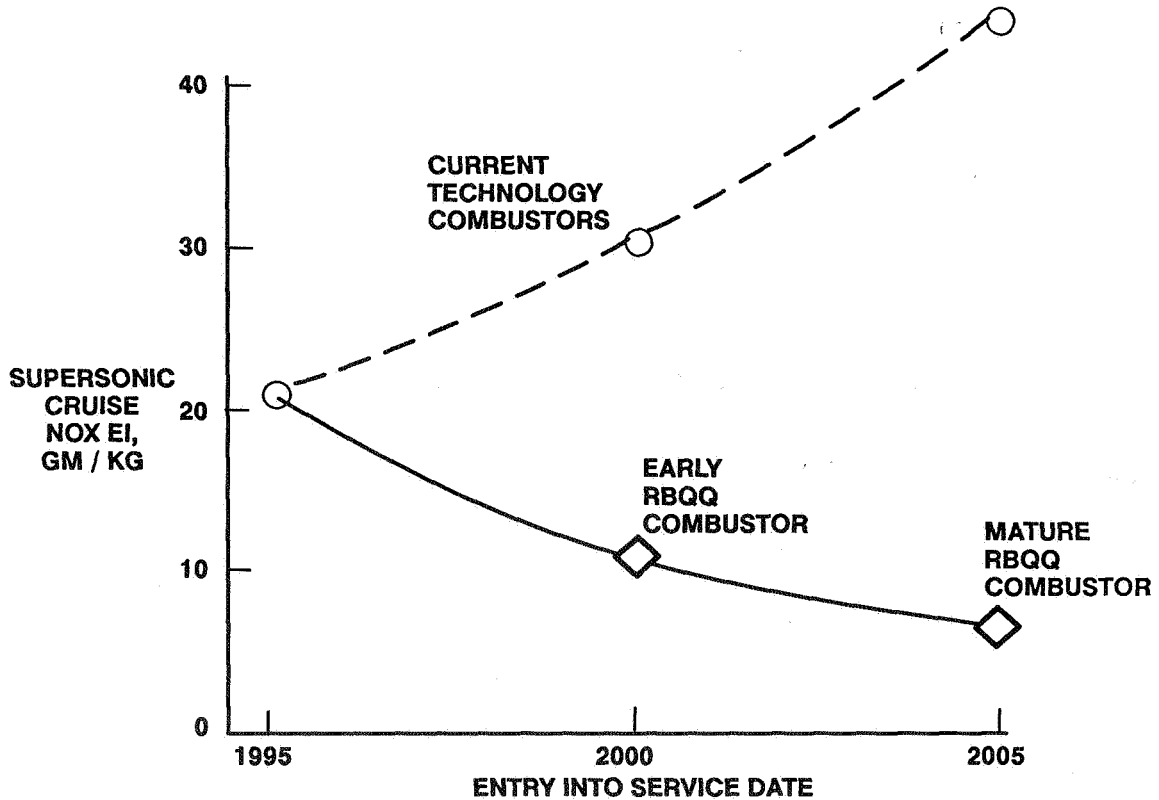


Figure 5

TECHNOLOGY IMPACT ON SIDELINE NOISE CHARACTERISTICS
MACH 2.4 TURBINE BYPASS ENGINES – 600 LB/SEC AIRFLOW SIZE

The jet noise comparison for the same 1995, 2000 and 2005 EIS TBE's is presented in Figure 6. The unsuppressed jet noise increases with increased thrust (and attendant jet velocity) for the later time period engines due to the higher combustor temperatures. For the 1995 EIS engine a conventional tube/chute mechanical noise suppressor is estimated to provide about 12 db noise reduction, but is still 8 db above the FAR36 Stage III rule. The mixer/ejector suppressor nozzle concept utilized for the later time frame engines is projected to provide on the order of 20 db suppression (based on 120% flow entrainment), but still is 2 to 3 db above Stage III at maximum power. However, the noise goal can be met throttling the engines while still providing more thrust than the 1995 EIS engine.

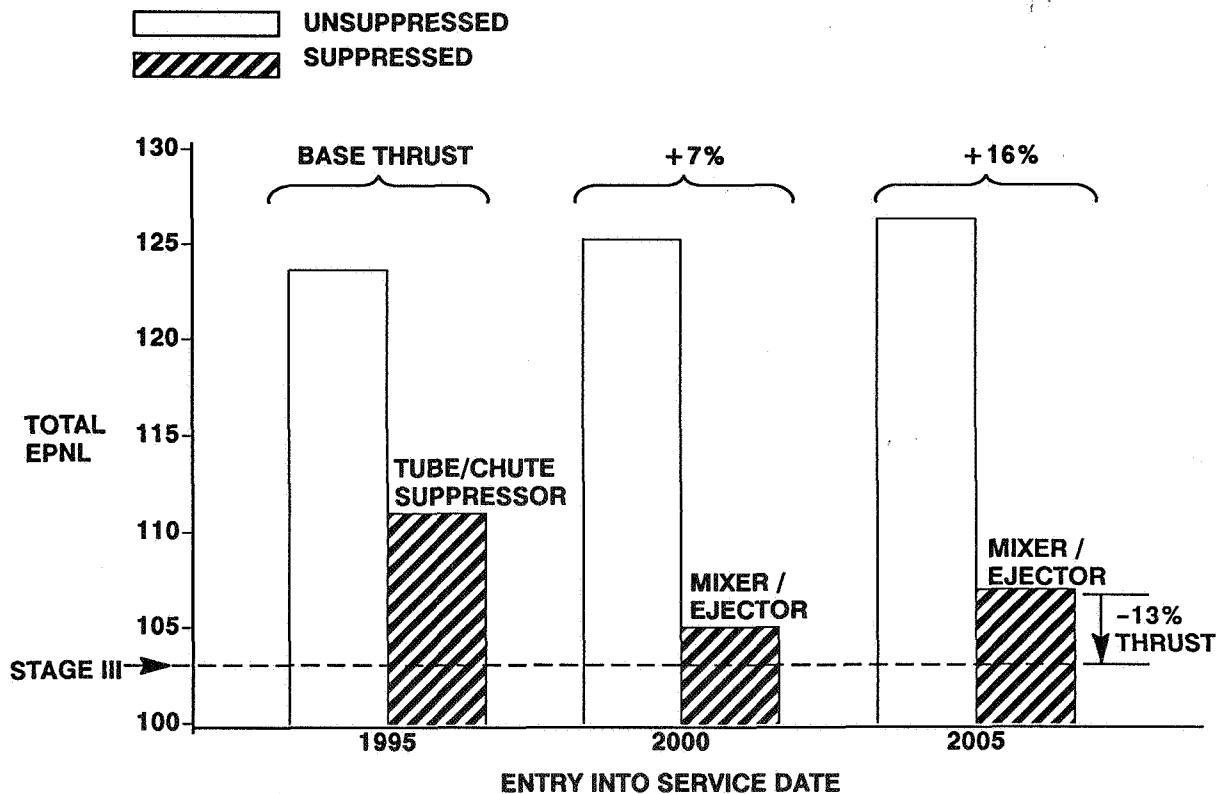


Figure 6

TECHNOLOGY IMPACT ON TAKEOFF GROSS WEIGHT
PROVIDES UP TO 12% TOGW REDUCTION

The results of the integrated propulsion/airframe system evaluation of the 1995, 2000 and 2005 EIS Mach 2.4 TBE's are illustrated in Figure 7. The figure shows aircraft takeoff gross weight (TOGW) required for 5000 nm design range as a function of engine corrected airflow (WAT2) divided by TOGW. Noted on each of the curves are the WAT2/TOGW values needed to satisfy the various engine sizing constraints. The solid symbols on the year 2000 and 2005 curves represent the points sized for the required takeoff field length while meeting the Stage III sideline noise goal. The 1995 and 2000 TBE critical engine sizes are set by the time to climb criteria. The 1995 TBE produces a sideline noise level of 110 db at the time-to-climb sized point as noted on the curve. A point is also noted on the 1995 TBE curve that reduces the noise by just one db via throttling back and oversizing the engine at takeoff, and is obviously an unacceptable penalty to pay for noise reduction. The time to climb sizing criteria for the year 2000 engine provides a larger engine than required to meet the noise goal. The year 2005 TBE engine size is set almost simultaneously by the time-to-climb and takeoff field length/Stage III noise criteria. The payoff for the year 2005 engine relative to the current technology year 1995 engine is a 12% takeoff gross weight reduction and 7 1/2 EPNdb reduction in sideline noise.

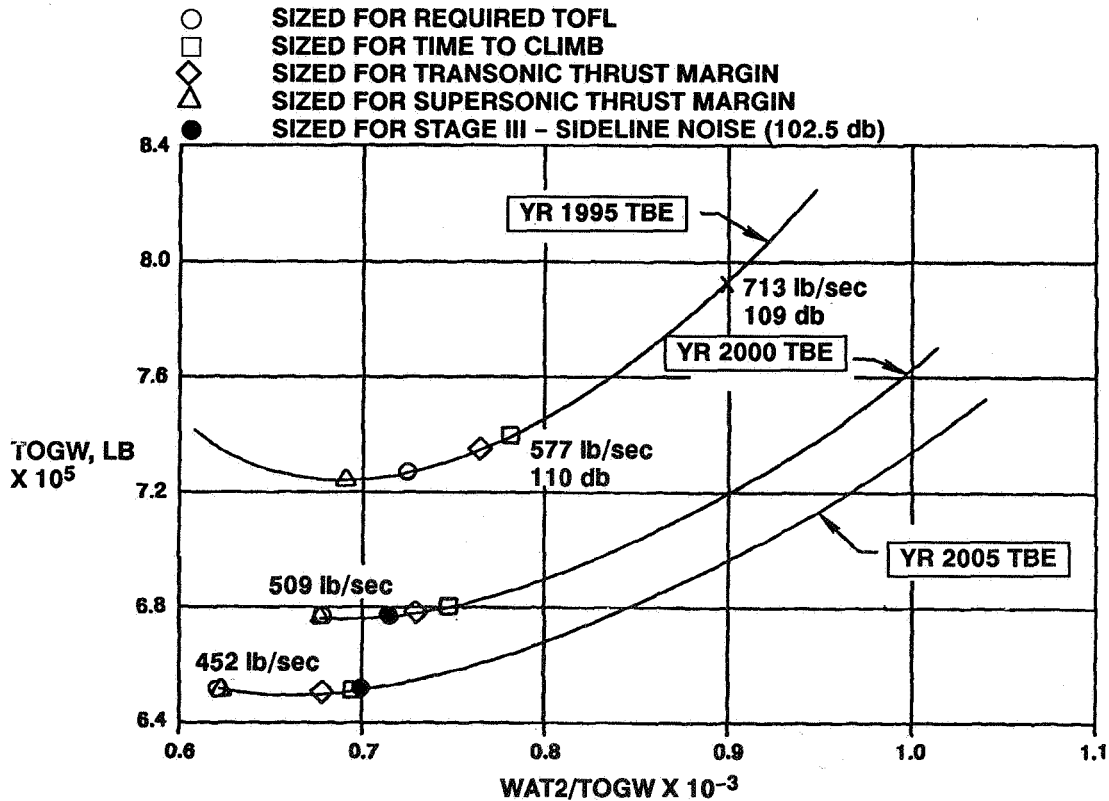


Figure 7

MACH 2.4 TBE VERSUS VSCE FLYOFFS
TBE PROVIDES 12% TOGW OR 19% RANGE IMPROVEMENT

Shown in Figure 8 is a comparison between the year 2005 EIS TBE and VSCE designed for Mach 2.4 cruise. The comparison is shown both on the basis of takeoff gross weight for a design range of 5000 nm and range for a fixed TOGW. The figure shows a 12% TOGW or 19% range advantage for the TBE. The contributions to the TBE's range advantage are depicted and are shown to be due primarily to improved fuel consumption during climb and cruise. These results are for an all-supersonic mission profile. A mixed subsonic/supersonic mission with a 1000 nm subsonic cruise leg was also considered. For the mixed mission the TBE range advantage is reduced to about 15% relative to the VSCE. In summary, the system evaluation results show the TBE is clearly superior to the VSCE for a Mach 2.4 cruise application. As will be shown later, studies at Mach 3.2 produced similar results.

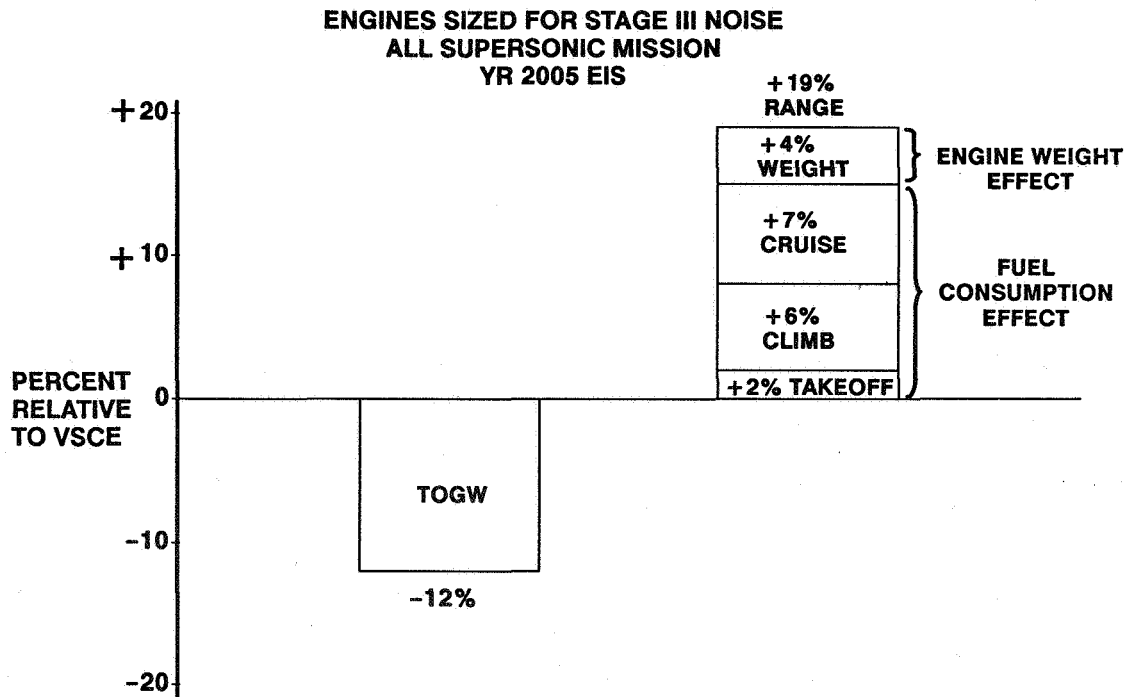


Figure 8

**HSCT QUIET ENGINE CONCEPTS (QEC)
MACH 3.2 NOISE REDUCTION CONCEPTS**

Two major challenges in the design of propulsion systems for High Speed Civil Transports (HSCT) are complying with noise and emissions environmental standards while providing economically acceptable aircraft. These issues create a dilemma in engine design because low exhaust jet velocities are required to meet takeoff noise regulations while high exhaust jet velocities are required for economical supersonic cruise operation. Previous studies have shown that engines incorporating mechanical suppression concepts to meet FAR Stage III noise regulations must be oversized by 50 to 70% relative to the sizes that will provide the most attractive aircraft economics.

The objective of the Quiet Engine Concept (QEC) study was to examine propulsion concepts that can achieve a large increase in airflow during takeoff operation to reduce the average exhaust velocity to acceptable levels. Two methods of accomplishing large flow increases were examined.

The first method utilizes a flow inverter valve between compression system stages to transport flow from the front compression stage around the rear stages while simultaneously ducting additional ambient air into the rear compression stages. This concept can increase engine total airflow by 30 to 70%.

The second method utilizes a mixer/ejector nozzle to increase the engine exhaust flow by up to 120% during takeoff and landing operation.

As shown in Figure 9 these two methods of increasing engine airflow were evaluated for various propulsion concepts to identify their applicability and effectiveness in reducing takeoff noise. Propulsion concepts studied for a Mach 3.2 HSCT included non-augmented turbine bypass engines (TBE), variable stream control engines (VSCE) and non-augmented mixed flow turbofans (MFTF).

- **TURBINE BYPASS ENGINE (TBE) WITH:**
 - **INLET FLOW VALVE AND MIXER EJECTOR NOZZLE**
 - **MIXER EJECTOR NOZZLE**

- **VARIABLE STREAM CONTROL ENGINE (VSCE) WITH:**
 - **INLET FLOW VALVE AND MIXER EJECTOR NOZZLE**
 - **MIXER EJECTOR NOZZLE**

- **NON AUGMENTED MIXED FLOW TURBOFAN WITH:**
 - **MIXER EJECTOR NOZZLE**

Figure 9

TBE INLET VALVE/EJECTOR NOZZLE CONCEPT SCHEMATIC

In this concept, illustrated in Figure 10, the 120% exhaust flow increase is achieved through the use of an inlet flow valve and an ejector nozzle. The inlet valve is positioned between the first and second stage of the compressor, and is used during takeoff to divert the front stage exhaust flow around the rear stages and bring in 500 lb/sec ambient air to supply the rear stages. During climb/acceleration and cruise operation, the inlet valve is repositioned so that all the flow entering the front stage passes through the rear stages and the auxiliary inlet air doors are closed.

The ejector nozzle is used to entrain 281 lb/sec flow during takeoff to increase the total exhaust flow to 1450 lb/sec. and reduce the jet velocity to the required 1450 ft/sec. A mixer is used to achieve a flat velocity profile exiting the nozzle.

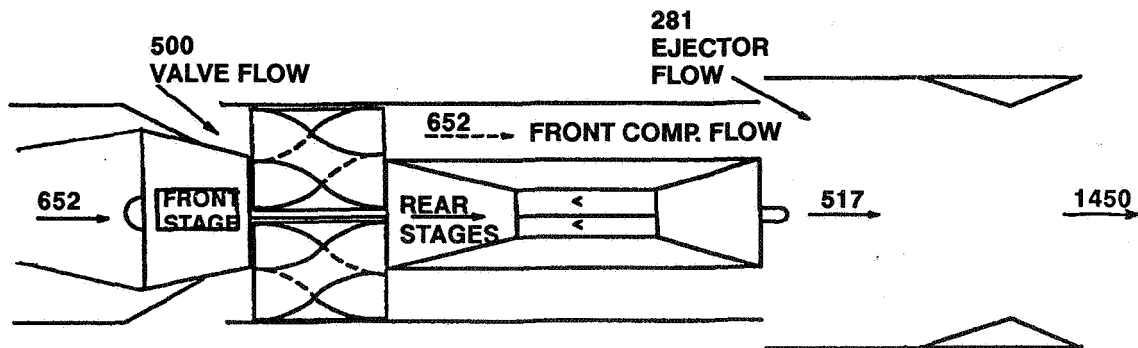


Figure 10

IMPACT OF INLET FLOW VALVE ENGINE LENGTH INCREASED BY 60 INCHES

As shown in Figure 11, incorporation of the inlet flow valve into the flowpath requires significant flowpath changes to the high pressure compressor. When a valve is incorporated into the engine, the corrected airflow entering the rear stages will vary significantly between high mode and low mode operation. To insure that the rear stages would be compatible with the specific flow variations, the area at the rotor inlet was increased relative to the conventional engine. At the sea level takeoff design point the specific flow into rear aft stages during high mode operation is 40.6 compared to 36.1 during low mode operation. Analysis indicated that this range of specific flows produced good efficiency during both high and low mode operation.

An additional item of concern is the pressure distortion which will occur when the valve transitions from high to low mode operation. The front and rear stages of the compressor must be designed with sufficient stall margin to allow stable transient operation. Accordingly, the compressor rear flowpath was modified from a Constant Mean Diameter (CMD) to a Constant Outer Diameter (COD) configuration and the entire flowpath was moved radially outward. This process increased the average mean wheel speed through each airfoil row, improving the stage work capability at the expense of additional weight. Since the inverter valve was designed to accept axial inlet and deliver axial exit flow, vanes incorporating variable trailing edge flaps were positioned at the inlet and exit of the inverter valve. The vane geometry is set as required to achieve compatibility with the change in flow ratios between high and low mode operation.

Incorporation of an inlet flow inverter valve in the TBE increases the engine length by 60 inches and the weight by 2740 lb or 22%. The inlet valve weighs 1280 lb, and the modifications to the basic engine weight 1460 lb.

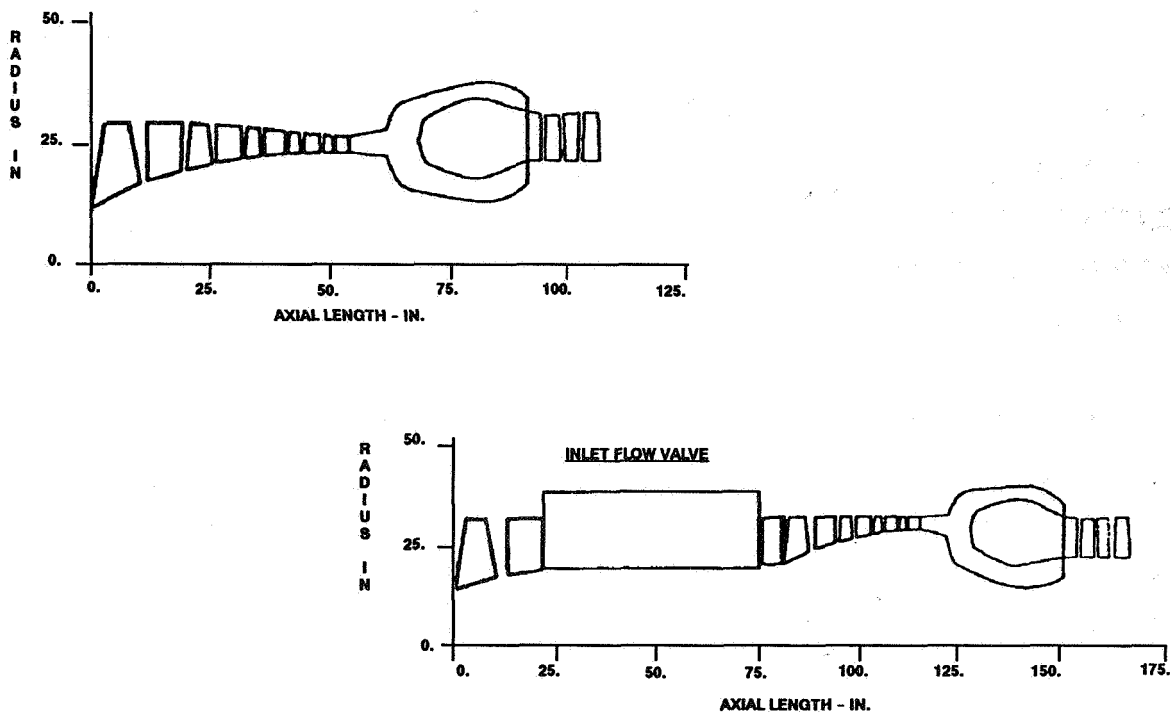


Figure 11

MACH 3.2 QUIET ENGINE CONCEPTS

IMPACT OF NOISE REDUCTION CONCEPTS ON TBE POWERED MACH 3.2 HSCT

Mission analyses were conducted for a TBE powered Mach 3.2 HSCT which carries a passenger load of 61,500 lb for a distance of 5000 n. mi. In order to achieve a takeoff field length (TOFL) of 12,000 feet, a total net thrust (FNTOT) to takeoff gross weight (TOGW) ratio of 0.287 is required.

In the 1970s, engines with mechanical noise suppressors (MNS) and acoustically treated nozzles were examined. Figure 12, Column 1 shows that such an engine, sized for the TOFL requirement, achieves a sideline jet noise level of 111, which is 9 EPNdB above the Stage 3 requirement of 102 EPNdB for a 675,000 lb TOGW aircraft.

If a mixer/ejector nozzle (MEN) can entrain 770 lb/sec flow and mix it fully with the 660 lb/sec exhaust flow of the TBE to achieve an effective exhaust velocity of 1450 ft/sec, column 2 shows that the FAR Stage 3 noise requirement can be met with a 687,000 lb TOGW aircraft.

Column 3 shows that if an inlet flow valve (IFV) with 74% flow and a mixer ejector nozzle (MEN) with 43% flow entrainment are used, the aircraft TOGW increases to 768,000 lb because the inlet flow valve increases the propulsion system weight by 22%.

	MNS <u>NOZZLE</u>	M/E <u>NOZZLE</u>	IFV + <u>M/E NOZZLE</u>
TOGW, LB	674,800	686,700	767,800
ENGINE FLOW SIZE, LB/SEC	630	641	717
ENGINE WEIGHT, LB	11490	12220	16675
SIDELINE EXHAUST FLOW, LB/SEC	650	1430	1600
• MAIN INLET + FUEL	650	660	740
• INLET VALVE	---	---	550
• EJECTOR NOZZLE	---	770	310
SIDELINE EXHAUST VELOCITY, FT/SEC	2760	1450	1450
UNSUPPRESSED NOISE, EBNdB	123	101	102
SUPPRESSED NOISE, EPNdB	111	---	---
STAGE III RULE, EPNdB	102	102	102.5

Figure 12

MACH 3.2 QUIET ENGINE CONCEPTS

IMPACT OF NOISE REDUCTION CONCEPTS ON VSCE POWERED MACH 3.2 HSCT

In the 1970's variable stream control engines with mechanical noise suppressors (MNS) were examined. During takeoff operation, the duct burner is on and produces a duct stream exhaust velocity that is 70% higher than that of the core stream. The Inverted Velocity Profile (IVP) produces an unsuppressed jet velocity of 119 EPNdB. Mechanical noise suppressors for this concept provide an additional 2 EPNdB reduction in noise, as shown in Figure 13, Column 1. If the engines are sized to achieve the 12,000 ft. takeoff field length, a sideline jet noise of 117 EPNdB is produced.

In order to achieve the Stage 3 noise regulation, a mixer/ejector nozzle (MEN) with 120% flow entrainment is required. Column 2 shows that a VSCE with a MEN produces an aircraft TOGW of 800,000 lb.

	BASELINE <u>IVP, MNS</u>	MIXER EJECTOR <u>NOZZLE</u>
TOGW, LB	744,300	799,800
ENGINE FLOW SIZE, LB/SEC	682	733
ENGINE WEIGHT, LB	11710	14110
SIDELINE EXHAUST FLOW, LB/SEC	705	1635
• MAIN INLET + FUEL	705	755
• EJECTOR NOZZLE	---	880
SIDELINE EXHAUST VELOCITY, FT/SEC	2730	1450
UNSUPPRESSED NOISE, EBNdB	119	103
SUPPRESSED NOISE, EPNdB	117	---
STAGE III RULE, EPNdB	102	103

Figure 13

MACH 3.2 QUIET ENGINE CONCEPTS

TBE AND MFTF PROVIDE TOGW REDUCTION OF 14 TO 16% OVER VSCE

Mixer/ejector nozzles have been evaluated for a non-augmented turbine bypass engine (TBE), a non-augmented mixed turbofan (MFTF) and duct burning variable stream control engine (VSCE). The results are summarized in Figure 14. The TBE concept provides the best supersonic cruise fuel consumption, while the MFTF provides the lightest weight propulsion system. The VSCE, which operates with the duct burner on during supersonic cruise, has the highest Mach 3.2 cruise TSFC and requires the largest aircraft to satisfy the mission. The TBE and MFTF powered aircraft are 14 and 16% lighter than the VSCE powered aircraft, respectively.

	<u>VSCE/MEN</u>	<u>TBE/MEN</u>	<u>MFTF/MEN</u>
TAKEOFF GROSS WEIGHT, LB	799,800	686,700	675,300
ΔTOGW, %	BASE	-14	-16
ENGINE FLOW SIZE, LB/SEC	733	641	631
ENGINE WEIGHT, LB	14,110	12,220	10,960
MACH 3.2 CRUISE TSFC, LB/HR/LB	1.72	1.63	1.65
SIDELINE NOISE, EPNdB	103	101	101
STAGE III RULE, EPNdB	103	102	102

Figure 14

TURBINE BYPASS ENGINE LIFE STUDY

OBJECTIVES

A wide variety of propulsion system concepts have been considered for application in a 2nd generation supersonic transport. Based upon these studies, the Turbine Bypass Engine (TBE) has emerged as one of the promising candidates. Selection of the best propulsion system requires more in-depth studies to identify the optimum cycle and configuration for each engine. The objectives of the Turbine Bypass Engine Life Study are: (1) to update the conceptual definition of a Mach 2.4 TBE to include commercial life requirements and the latest material and structural technology projections and (2) to define critical component technology programs which must be carried out prior to initiation of engine full-scale development. (See Figure 15). The engine incorporates aerodynamic, material, and structural technologies projected to have technical readiness in the year 2000, with a corresponding Entry Into Service in 2005.

- **UPDATE THE CONCEPTUAL DESIGN DEFINITION OF MACH 2.4 TBE TO INCLUDE COMMERCIAL LIFE REQUIREMENTS FOR A YEAR 2005 ENTRY INTO SERVICE DATE**
- **DEFINE CRITICAL COMPONENT TECHNOLOGY PROGRAMS WHICH MUST BE CARRIED OUT PRIOR TO INITIATION OF FULL SCALE DEVELOPMENT**

Figure 15

HIGH SPEED CIVIL TRANSPORT ENGINES

SUPERSONIC CRUISE MISSION REQUIRES MAXIMUM TEMPERATURE OPERATION FOR MUCH HIGHER PERCENTAGE OF TIME

Achieving commercial life in an HSCT propulsion system poses a substantial challenge to the engine designer. An HSCT engine operates at near maximum cycle temperatures and rotational speeds from transonic acceleration through the end of supersonic cruise, resulting in the majority of the mission spent at the most severe combination of stress levels and temperature conditions. In contrast, current subsonic transports operate at the most severe engine conditions only during takeoff, generally less than 1% of the total flight time. A comparison of typical turbine temperature histories for a future HSCT versus a current subsonic transport is shown in Figure 16.

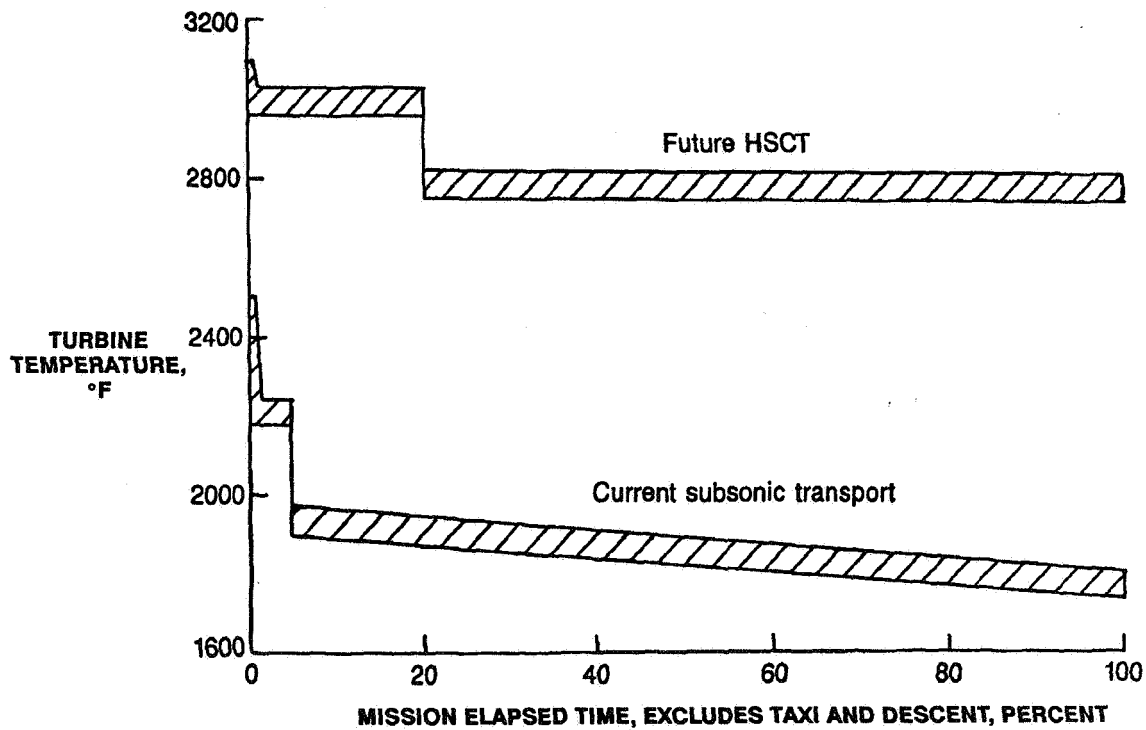


Figure 16

**TURBINE BYPASS ENGINE LIFE STUDY
CYCLE & CONFIGURATION GROUND RULES**

The primary TBE cycle parameters for the life study were defined to be consistent with the groundrules established by the P&W/GEAE HSCT Propulsion Team. These groundrules, shown in Figure 17, resulted from previous studies conducted under HSR Phase I coupled with updated estimates of projected material capabilities, structural concepts and cooling technologies. The maximum compressor discharge temperature was limited by material constraints in the aft compressor stage airfoil and disk rim. Additional constraints on the compressor discharge temperature were cooling requirements for the low NO_x combustor liner and the turbine blade attachments. The maximum combustor exit temperature was limited based upon achieving acceptable turbine airfoil cooling with the specified compressor discharge temperature. Although these temperatures may not seem aggressive when compared to military engines, consideration of the HSCT duty cycle makes them highly aggressive.

The primary parameter varied in the flowpath study is turbine maximum AN², which establishes the rotational speed of the engine. High AN² designs have heavier, more complicated disks and attachments but may achieve weight and drag reductions by reducing the number of airfoils, reducing the engine diameter, and/or reducing the engine length. However, at some level, engine life will be reduced or the weight/performance benefits will be offset by other considerations. For each configuration, iterations are performed between the performance and flowpath to account for any required changes in secondary flows and/or component efficiencies. Selected compressor and turbine attachments and disks are then designed to insure structural feasibility and aid in establishing engine weight trends. A mission analysis is then performed for each engine to identify the optimum set of component aero/mechanical design groundrules.

CYCLE	INLET CORRECTED AIRFLOW SIZE, LB/SEC	650
	PRESSURE RATIO	19
	T41 HOT DAY TAKEOFF, °F	2900
	T41 STD DAY MACH 2.4 CLIMB, °F	2800
	T3 MAX, °F	1250
	TAKEOFF THRUST, LB	58000
TURBINE AN² (SETS RPM), IN² - RPM²		400 - 500 X 10⁸

Figure 17

TURBINE BYPASS ENGINE LIFE STUDY

DUTY CYCLE - ALL SUPERSONIC AND AVERAGE MISSIONS

The HSCT will be sized for an all-supersonic mission with an assumed design range of 5000 nautical miles. However, a typical mission will result in a mixture of subsonic/supersonic flight with an average range on the order of 3500 nautical miles. The TBE engine will be designed to meet commercial life requirements based upon the typical flight profile. Lower life will result from utilization in an all-supersonic mission environment. The TBE life study will determine the difference in engine life between an all supersonic and a typical mixed mission.

Figure 18 depicts the variation in rotor speed, compressor exit temperature and turbine inlet temperature as a function of time for the all-supersonic and mixed missions. Note the large reduction in all three parameters for subsonic cruise operation. This serves to further illustrate the severity of supersonic cruise operation relative to subsonic.

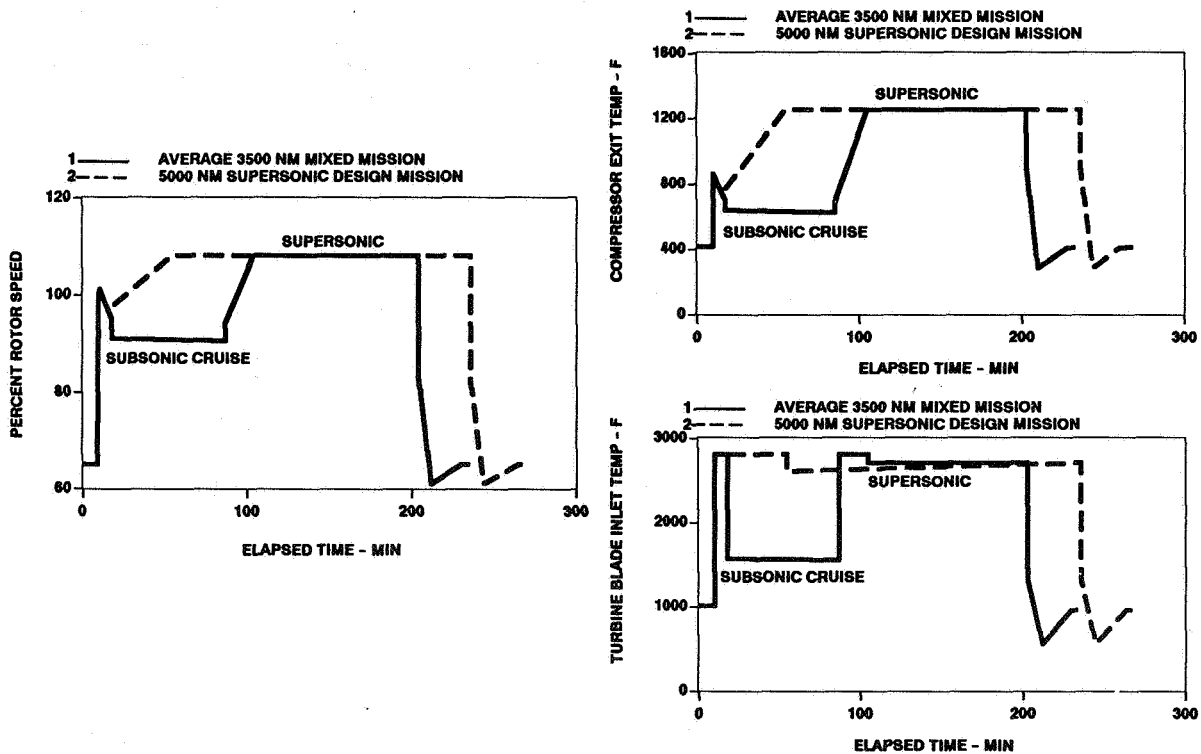


Figure 18

TURBINE BYPASS ENGINE LIFE STUDY FLOWPATH COMPARISON

Some parametric flowpaths considered during this study are shown in the Figure 19, compared against the baseline engine configured with a turbine maximum $AN^2 = 450 \times 10^8 \text{ in}^2\text{-rpm}^2$. The compressor and turbine configurations for each engine were optimized to achieve the best combination of airfoil count, flowpath shape, and flowpath elevation to achieve efficiency and stall margin goals. All of the compression systems feature advanced low aspect ratio 3-D swept aerodynamics to reduce shock losses. The stators feature a "hyperbow" design to control endwall boundary layers, reducing secondary flow losses and improving stability. The combustor is representative of the low NO_x Rich-Burn Quick-Quench concept. The turbine features advanced 3-D aerodynamics for improved efficiency.

Going from maximum $AN^2 = 400$ to $450 \times 10^8 \text{ in}^2 \text{ rpm}^2$ results in lower compressor and turbine elevations due to increased rpm capability and shorter length. Progressing from 450 to $500 \times 10^8 \text{ in}^2 \text{ rpm}^2$ still provides a reduction in compressor and turbine elevations, but a 2 inch length increase. A 6 stage compressor flowpath has also been defined which reduces engine length about 10 inches, but results in compressor evaluations comparable to the maximum $AN^2 = 400 \times 10^8 \text{ in}^2 \text{ rpm}^2$ case.

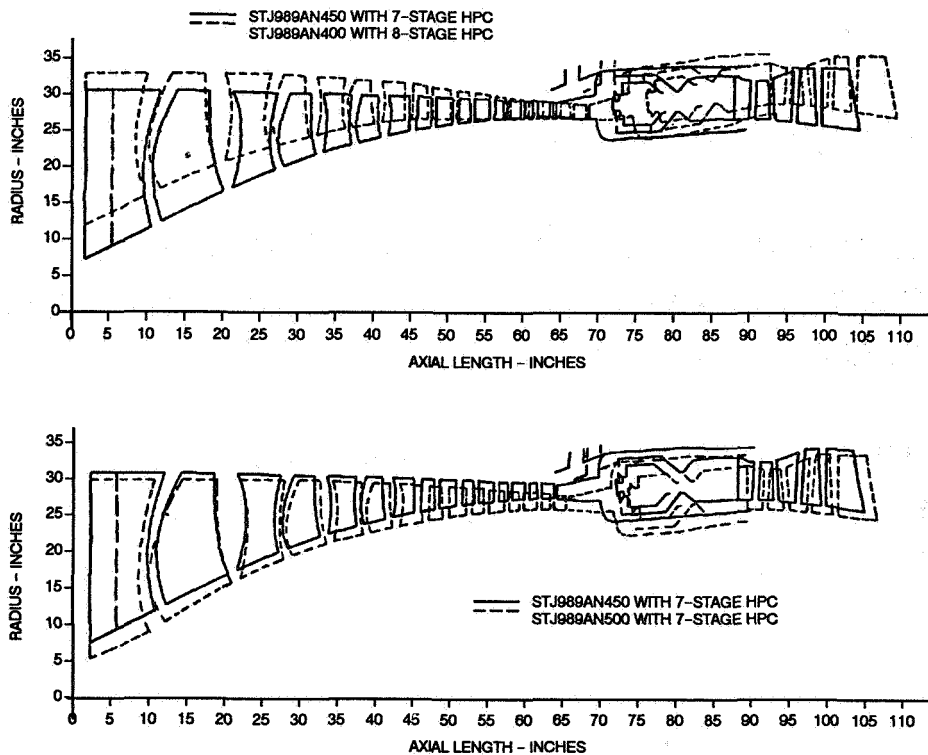


Figure 19

MIXED FLOW TURBOFAN STUDY

OBJECTIVES

The objectives of the mixed flow turbofan study are shown in Figure 20. This study will investigate the potential of low bypass ratio, mixed exhaust cycles and configurations, including augmented and non-augmented systems, for a Mach 2.4 application.

Economically attractive candidates from the cycle matrix will be carried through flowpath and mechanical design evaluation to provide weight, price, and maintenance cost estimates. Resulting engines will be "flown" on a reference aircraft model to establish relative merits on the basis of integrated propulsion/airframe system performance and economics. Performance and installation characteristics for the most promising engine will be provided to NASA and two airframe contractors in the form of data packs. Updates to the technology plan will be made based on any new requirements arising from this task.

- **CONDUCT EVALUATION OF MACH 2.4 MFTF CYCLES**
- **SELECT CYCLE(S) FOR CONCEPTUAL DEFINITION TO INCLUDE COMMERCIAL LIFE REQUIREMENTS FOR A YEAR 2005 ENTRY INTO SERVICE DATE**
- **DEFINE THE CRITICAL COMPONENT TECHNOLOGY PROGRAMS WHICH MUST BE CARRIED OUT PRIOR TO INITIATION OF FULL SCALE DEVELOPMENT**

Figure 20

MIXED FLOW TURBOFAN STUDY
CYCLE MATRIX (20 CYCLE COMBINATIONS)

The cycle matrix shown in Figure 21 covered fan pressure ratios (FPR) from 3.8 (maximum for a two stage fan) up to 5.0 for a three stage fan. Each cycle was defined with a maximum turbine blade inlet temperature (T41) of 2900°F and a cycle overall pressure ratio (OPR) at sea level takeoff determined by a maximum compressor exit temperature of 1250°F. Varying the sea level takeoff turbine temperature while holding climb maximum T41 fixed introduced variations in "throttle ratio", which determined sea level reference bypass ratio (BPR) as well as BPR excursion from sea level to top of climb. The takeoff T41 - FPR combinations resulted in exhaust velocities from 2100 to 2800 feet per second. This matrix offers trades in subsonic and supersonic thrust specific fuel consumption versus thrust capability (engine sizing).

FAN PRESSURE RATIO	3.8 TO 5.0
THROTTLE RATIO (T41 CLIMB / T41 SLS)	1.05 TO 1.25
MAX COMPRESSOR EXIT TEMP, °F	1250
MAX TURBINE BLADE INLET TEMP, °F	2900
BYPASS RATIO	.04 TO .59
TAKEOFF JET VELOCITY, FPS	2113 TO 2818

Figure 21

MIXED FLOW TURBOFAN STUDY

CYCLES COVER WIDE RANGE OF TRANSONIC AND SUPERSONIC THRUST

Maximum climb thrust (FNT) at both transonic ($M = 1.1$) and supersonic ($M = 2.4$) conditions covers a wide range across the cycle matrix at the base flow size of 650 lb/sec. The trends shown in Figure 22 indicate increasing thrust when lowering design BPR by increasing FPR at constant throttle ratio or when lowering design BPR by increasing throttle ratio (reduced takeoff T41) at constant FPR. The major effect with the latter approach is the steeper supersonic thrust increase relative to transonic, which is a result of the reduced BPR excursion from sea level to altitude by relatively "upmatching" the high spool and higher fan pressure ratio relative to design (flatter operating line).

The 5.0 FPR cycles are limited to low throttle ratios to maintain takeoff T41's sufficient to support a BPR of 0.1 or greater at desirable mixing conditions.

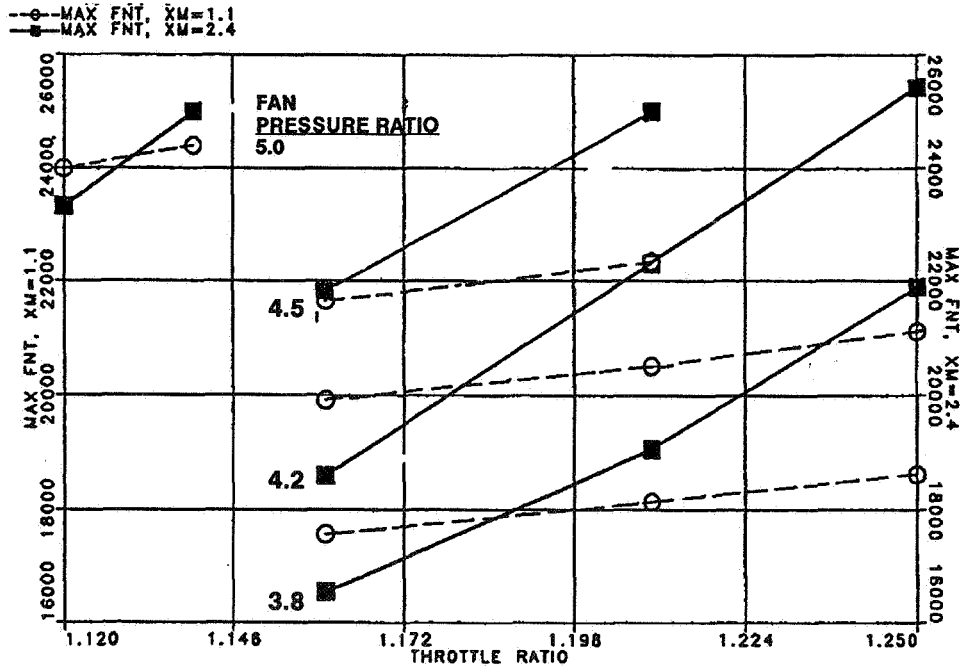


Figure 22

MIXED FLOW TURBOFAN STUDY
REQUIRED ENGINE SIZES (NON AUGMENTED)

By calculating scaled flow sizes required for each cycle to meet typical airplane thrust requirements at takeoff, transonic climb, and supersonic climb, the critical sizing condition can be determined. All of the cycles shown in Figure 23 are transonic thrust sized. At high throttle ratios, the supersonic sizing criteria approaches the take-off requirement, both of which are well below the transonic sizes; this indicates that a significant engine size reduction could be achieved with the addition of thrust augmentation during transonic climb, which is being considered.

In general, the higher FPR, higher specific thrust cycles result in smaller engine size, approaching the "zero BPR" turbine bypass engine (TBE). However, this size reduction is achieved with higher jet velocity cycles which tend to make achievement of the Stage III noise goal more difficult.

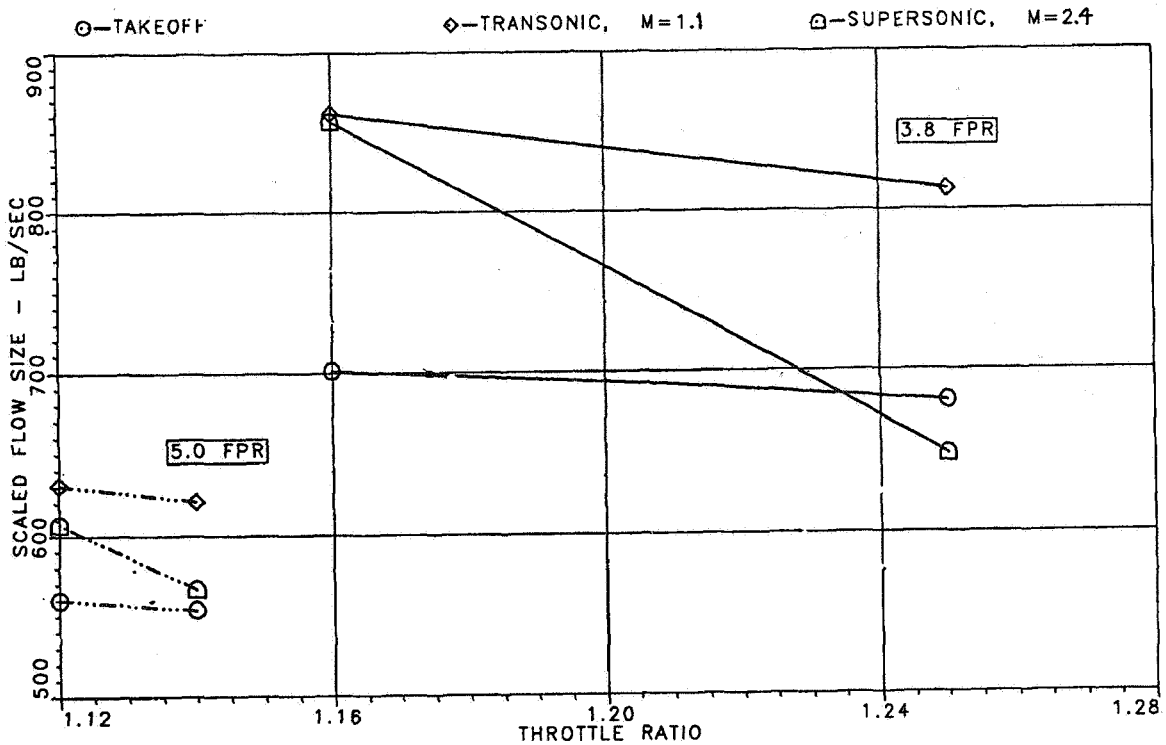


Figure 23

EXHAUST NOZZLE CONCEPTUAL DESIGN

OBJECTIVES

The goal of the nozzle design task is to develop conceptual mechanical designs of both an axisymmetric and a two dimensional mixer ejector nozzle around a Mach 2.4 Turbine Bypass Engine (TBE). The designs will include aerodynamic, acoustic, mechanical, and structural analyses to obtain realistic estimates of dimensions, weight, and performance potential. Critical materials and structural technologies will be identified to achieve a balance between nozzle weight, aerodynamic and acoustic performance, and life. Results will be provided to airframe manufacturers for overall propulsion/airframe system integration and evaluation. (See Figure 24).

- **DEVELOP CONCEPTUAL DESIGNS OF MACH 2.4 AXISYMMETRIC AND TWO DIMENSIONAL (2D) MIXER EJECTOR NOZZLES TO IDENTIFY CRITICAL MATERIALS AND STRUCTURAL TECHNOLOGIES FOR A YEAR 2005 ENTRY INTO SERVICE DATE**
- **COMPARE RESULTING PERFORMANCE, WEIGHT, ACOUSTIC AND DIMENSIONAL CHARACTERISTICS AND PROVIDE TO AIRFRAME MANUFACTURER FOR EVALUATION**

Figure 24

EXHAUST NOZZLE CONCEPTUAL DESIGN
AREA AND OPERATING TEMPERATURE REQUIREMENTS

Operating characteristics for the TBE were evaluated across both a 5000 nm all supersonic mission and a 3500 nm mixed subsonic – supersonic cruise mission. As shown in Figure 25, a wide range of variable throat and nozzle exit areas are required to maintain optimum engine matching and maximum nozzle performance characteristics. The nozzle inlet temperature history during these missions shows extended operation at nearly maximum nozzle temperatures of 1800-1900°F. Other design requirements established include: (1) reverse thrust capability similar to current high BPR turbofans, (2) acoustically treatable nozzle surface area equal to $L/D = 2$, (3) FAR36 Stage III noise rules with 120% ejector flow pumping, and (4) thrust coefficient goals of .982 at cruise and .95 at takeoff, including leakage.

NOZZLE AREA VARIATION REQUIREMENTS - 2005 EIS TBE

A_{THROAT} (A8): 800 - 1180 IN²

TAKEOFF - 855 IN²
SUPERSONIC CRUISE - 1000 IN²

A_{EXIT} (A9): 1400 - 4200 IN²

1400 @ SUBSONIC CRUISE
2120 @ TRANSONIC CRUISE
3940 @ MIXER/EJECTOR DEPLOYED TAKEOFF
4200 @ TOP OF CLIMB

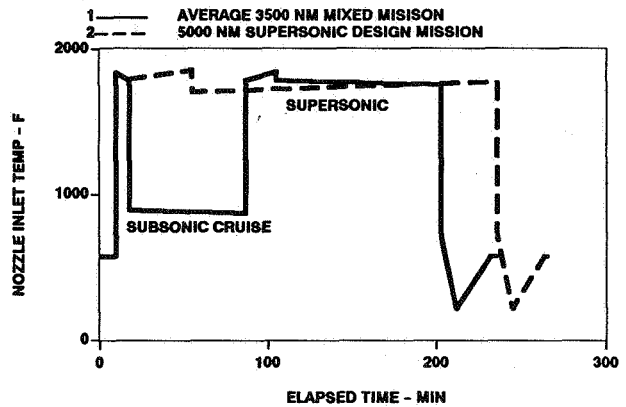


Figure 25

PROPULSION SYSTEMS STUDIES
SUMMARY OF RESULTS / STATUS

A summary of propulsion systems studies results and status is given in Figure 26.

Pratt & Whitney propulsion systems studies during the last several years have quantified the potential payoffs for technology advancements in emissions, noise and overall system performance (as measured by aircraft TOGW or range). The payoffs relative to current technology are 8 db lower airport sideline noise, 85% lower NO_x emissions index and 12% reduction in aircraft TOGW.

Several types of engines have been shown to have the potential to meet the FAR36 Stage III noise goal when equipped with the mixer/ejector nozzle. The VSCE has been shown to be not competitive in terms of TOGW for both Mach 2.4 and 3.2 applications. Therefore, this cycle has not been included in our current study plans.

The TBE and MFTF have been shown to be competitive for Mach 3.2 and therefore, are included in the current Mach 2.4 joint GEAE/P&W study activity.

The mixer/ejector nozzle concept has been identified as the most attractive approach to meeting the FAR36 Stage III noise goal. Consequently, a conceptual design study of axisymmetric and two-dimensional mixer ejector nozzle configurations is underway.

- **PROJECTED TECHNOLOGY ADVANCEMENTS PROVIDE SIGNIFICANT IMPROVEMENTS IN NOISE, EMISSIONS AND AIRCRAFT TOGW**
- **TBE, VSCE AND MFTF WITH 120% FLOW ENTRAINMENT MIXER EJECTOR NOZZLES ACHIEVE SIDELINE NOISE GOAL**
- **TBE WITH INLET FLOW VALVE AND 43% NOZZLE FLOW ENTRAINMENT ACHIEVES SIDELINE NOISE GOAL**
- **TBE PROVIDES LOWER TOGW THAN VSCE (12% FOR M 2.4, 14% FOR M 3.2)**
- **TBE TOGW IS COMPETITIVE WITH MFTF FOR MACH 3.2**
- **MACH 2.4 TBE, MFTF ENGINES AND MIXER/EJECTOR NOZZLES ARE CURRENTLY BEING DEFINED AND EVALUATED USING COMMON GEAE/P&W GROUND RULES**

Figure 26

THIS PAGE INTENTIONALLY BLANK

omit

Session VII. Emission Reduction

THIS PAGE INTENTIONALLY BLANK

Session VII. Emission Reduction

omit

Low Emissions Combustor Technology for High-Speed Civil Transport Engines
Richard W. Niedzwiecki, NASA Lewis Research Center

THIS PAGE INTENTIONALLY BLANK

N94-33481

5,9-07

12009

Low Emissions Combustor Technology for High-Speed Civil Transport Engines

Richard W. Niedzwiecki

NASA Lewis Research Center

HIGH SPEED RESEARCH WORKSHOP

SESSION #7 - EMISSION REDUCTION



NASA HSR OZONE RESEARCH OBJECTIVES

The engine emissions of primary concern are nitrogen oxides (NO_x) which, through a series of known catalytic reactions, could adversely impact the earth's protective ozone layer. Although continuing atmospheric studies are needed to fully understand and quantify the levels that would yield no damage, it is clear that technology development focused on reducing NO_x emissions is paramount before U.S. industry could commit to a high-speed transport development program. Fortunately, prior emissions reduction programs such as the Department of Energy sponsored research for stationary gas-turbine powerplants indicate that reduction to levels in the range of 3 to 8 grams of NO_x per kilogram of fuel burned is possible with advanced combustor design approaches. Further NO_x reduction and potential elimination may also be achievable through secondary means such as downstream (post-combustion) injection of chemical reactants.

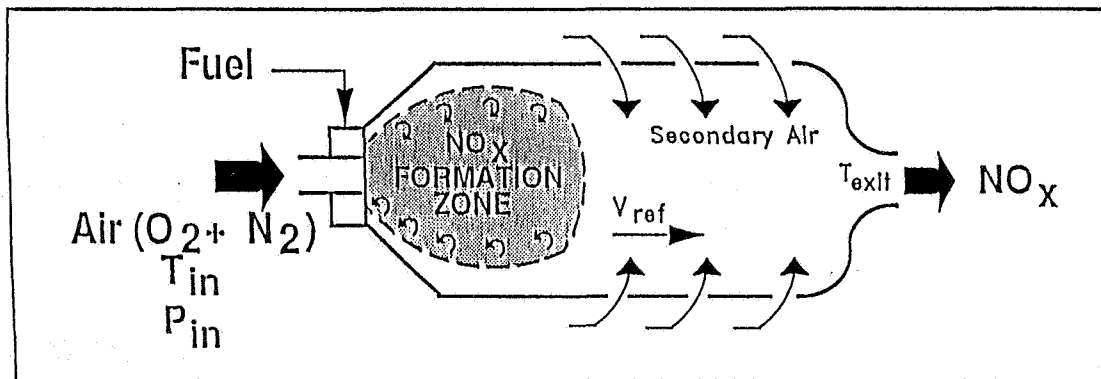
NASA HSR Ozone Research Objectives

- **Determine potential impact of HSCT aircraft fleet on protective ozone layer.**
- • **Establish technologies and operational procedures that insure no significant ozone depletion.**

NO_x FORMATION

Oxides of nitrogen are formed in combustion systems of engines. In operation, fuel and air are supplied to the combustor and ignited. The subsequent heat produced causes the nitrogen and oxygen in the air to combine to form nitric oxide (NO), lesser amounts of nitrogen dioxide (NO₂) and trace amounts of other nitrogen/oxygen compounds. All of these are commonly referred to as oxides of nitrogen or NO_x. Two NO_x formation mechanisms have been identified; Prompt NO_x and Thermal NO_x. Prompt NO_x results when the combustion process initiates. Fuel hydrocarbon fragments react with air nearly instantaneously to form small amounts of NO_x. Due to the speed of the reactions, these processes are essentially uncontrollable. Thermal NO_x formation occurs more slowly and is the major production source of this emittant. Formation of thermal NO_x is very dependant on temperature levels in the combustor and the length of time that high temperatures persist. Controlling thermal NO_x through temperature/residence time management is the major thrust of the emissions program.

NO_x Formation



Prompt NO_x

- Fast reactions
- Hydrocarbon fragments
- 0–1 gm/kg fuel (E.I.)
- Uncontrollable

Thermal NO_x

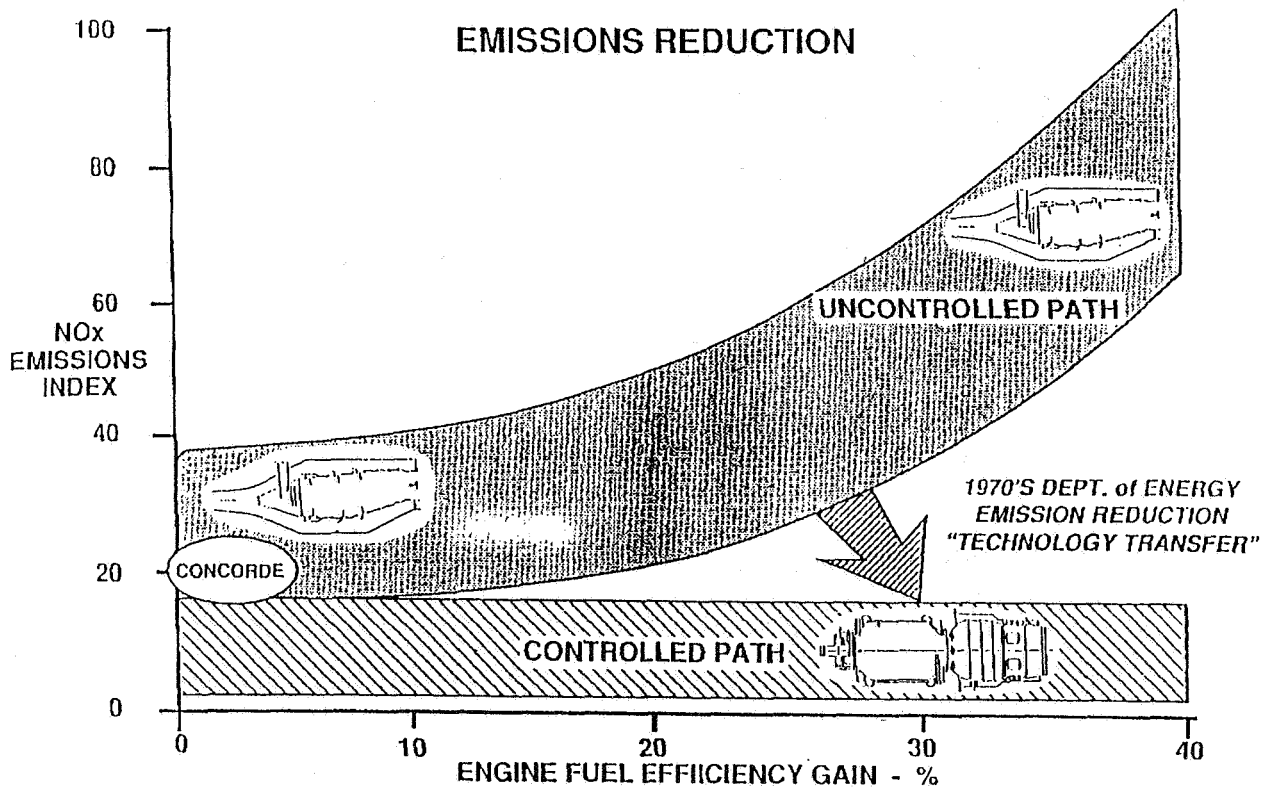
- Slow reactions
- $N + O_2 \longleftrightarrow NO + O$
- $N_2 + 3O \longleftrightarrow 2NO + O$
- Controllable

Correlation: $NO_x \propto \frac{e^{T_{in}/k} P_{in}^{1/2} T_{exit}}{V_{ref}}$

EMISSIONS REDUCTION

Shown is a plot of NOx emissions against engine fuel efficiency gain. To increase engine efficiency, operation at higher temperatures and pressures is required. These higher temperature and pressure conditions also increase NOx formation. As an example, the Concorde produces a NOx emission index value of 16-20. If energy efficient cycles are employed, NOx values could increase to the large levels indicated by the top band. The objective of this program is to employ very advanced NOx reduction methods to reduce NOx levels to theoretically low levels shown in the bottom band. The technology base for these reductions lie in 1970's emission research and in department of energy research conducted in the late 1970's and early 1980's.

High Speed Research Program



HSCT SUPERSONIC CRUISE COMBUSTION OPERATING CONDITIONS

These conditions are representative of those anticipated to be required for future commercial supersonic aircraft. Future presentations in this session use these conditions as a baseline for data comparison. The operating conditions are much more severe, thus making NO_x control more difficult than those projected for prior 1970's supersonic aircraft; in fact, they represent a severity increase of from three to six.

HSCT Supersonic Cruise Combustion Operating Conditions

T_{in}, °F1000 - 1350

P_{in}, atm12 - 14

T_{exit}, °F.....3000 - 3400

**FuelJET-A TSJF
(Thermally stabilized jet fuel)**

NO_x CORRELATIONS

The severity of combustor operating conditions and their impact on NO_x formation can be determined by correlating parameters such as those shown below. Three correlating parameters are listed. Although different in form, they all produce similar results. The (3) subscript refers to combustor inlet conditions; the (4) subscript refers to combustor exit conditions, (V_{ref}) is a measure of velocity in the combustor; (HO) is the relative humidity.

NO_x CORRELATIONS

$$\begin{aligned}
 \text{GE;} \quad \text{NO}_x \text{ EI} &= 23.8 \left(\frac{P_3}{432.7; \text{psia}} \right)^{0.4} e^{\frac{T_3 - 1027.6; \text{F}}{349.9; \text{F}} + \frac{6.29 - \text{Ho}}{53.2}} \\
 &= 0.0986 (P_3; \text{atm})^{0.4} e^{\frac{T_3; \text{K}}{194.4; \text{K}} - \frac{\text{Ho}}{53.2}}
 \end{aligned}$$

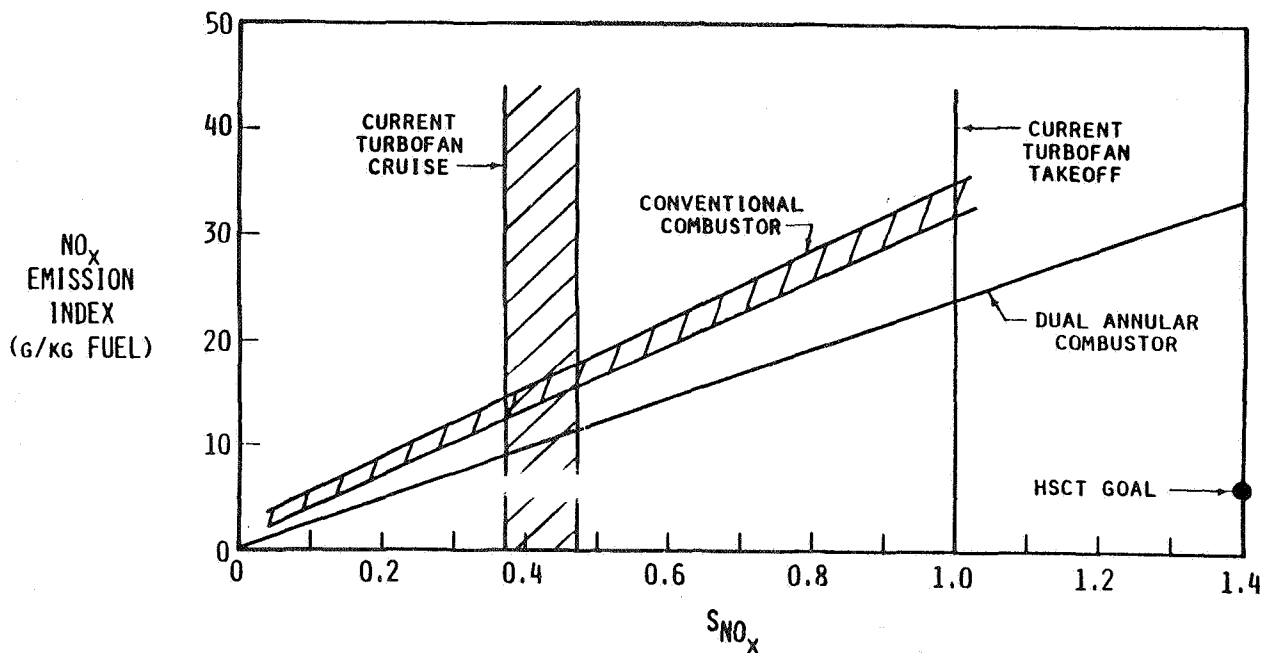
$$\text{P\&W;} \quad \text{NO}_x \text{ EI} \sim \frac{P_3^5 T_4}{V_{\text{ref}}} e^{\frac{T_3; \text{K}}{288; \text{K}} - \frac{\text{Ho}}{53.2}}$$

$$\text{NASA;} \quad \text{NO}_x \text{ EI} \sim \frac{P_3^5 T_4}{V_{\text{ref}}} e^{\frac{T_3; \text{K}}{288; \text{K}}}$$

TYPICAL NO_x CHARACTERISTICS OF A CURRENT TECHNOLOGY AND LOW NO_x COMBUSTORS

This chart illustrates application of one of the NO_x correlating parameters, the GE parameter. The plot is NO_x E.I. vs. severity of combustor operating conditions. The top, cross-hatched band indicates NO_x characteristics of current, conventional combustors now in use for aeronautical missions. The lower line indicates NO_x levels achievable employing the NO_x reduction technology evolved in the 1970's for aircraft combustors. As can be seen, considerable additional NO_x reduction is required to achieve program goals.

Typical NO_x Characteristics of a Current Technology and Low NO_x Combustors



$$S_{NO_x} = \left(\frac{P_3}{432.7} \right)^{0.4} \left(\frac{T_3 - 1027.6}{349.9} + \frac{6.29 \cdot H_0}{53.2} \right)$$

HSCT EMISSION REDUCTION STRATEGIES

This chart lists available NO_x reduction strategies. Nearly all have merit and should be pursued. However, only low emission combustors offer the potential for NO_x reductions approaching the 90 percent level and, thus represents the major thrust of the program. Second stage clean-up consists of the introduction of compounds into the combustor exhaust stream to react with the NO_x to produce benign elemental nitrogen. This approach, while being employed for terrestrial emission control, will be very difficult- possibly impossible- to employ on flight systems. However, its applicability, because of its very low NO_x potential, is currently being studied.

HSCT EMISSION REDUCTION STRATEGIES

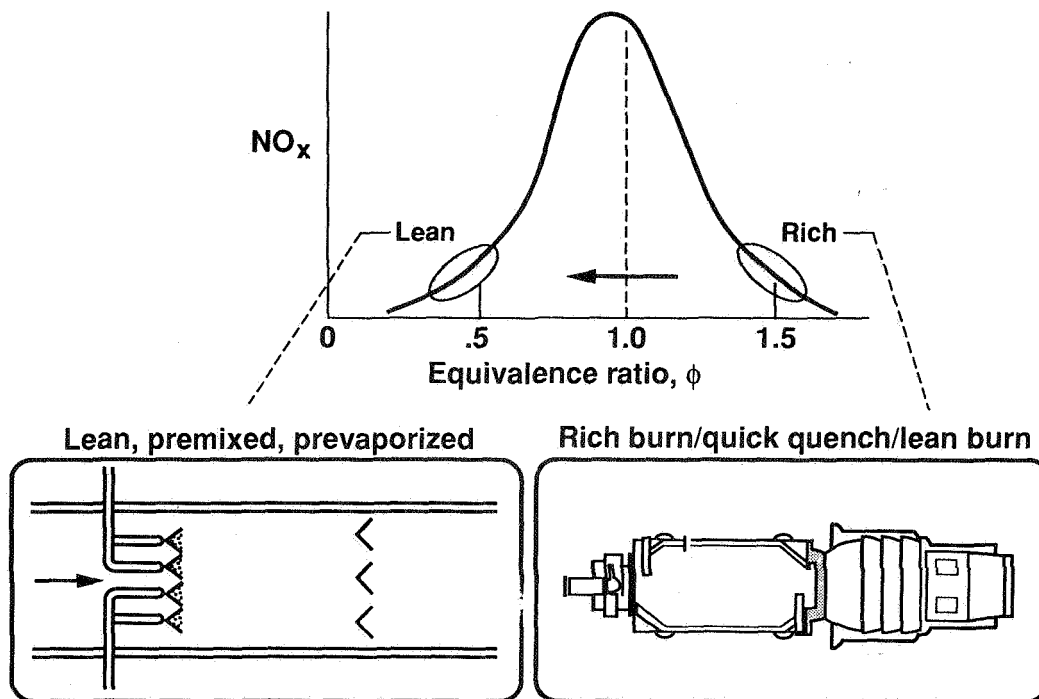
STRATEGY	EXAMPLE APPROACH	NO _x ASSESSMENT STATUS
Advanced Airframe	High L/D & Low W _{Structure}	~ 20 to 30% Reduction
High Efficiency Engine	Supersonic Throughflow Fan Advanced Core	~ 20 to 40% Reduction
Modified Engine Cycle	Combustor Pre-Cooling Reduced Cycle T & P	Excessive HX Size Excessive Efficiency Loss
Low Emission Combustors	Lean Pre-Mixed / Pre-Vaporization Rich Burn / Quick Quench / Lean Burn	~ 80 to 90% Reduction (EI ~ 5) *
Second Stage Cleanup	NO _x Destruction Additives	EI → 0 Potential * - Very High Risk

* Extrapolation of Terrestrial Data Base

Variation of NO_x with Equivalence Ratio

The figure below illustrates the principle that NO_x production is a maximum near a stoichiometric equivalence ratio (1.0) where there is a "perfect" mixture of fuel and air such that all of the fuel is burned with all of the air to produce combustion products. If combustion occurs in a lean mixture (excess combustion air), or in a rich mixture (excess fuel), lower flame temperatures occur and lower NO_x emissions are produced. This is the basis for the two major concepts shown schematically in the figure. The Lean-Premixed-Prevaporized (LPP) concept continually burns a lean mixture to produce low NO_x. The Rich Burn Quick Quench/Lean Burn (RQL) concept burns rich in the first stage of combustion, quickly quenches the mixture to minimize the time spent near stoichiometric, then burns lean in the final stage of combustion. These two concepts are the main contenders for the future low NO_x combustor for the HSCT.

Variation of NO_x with Equivalence Ratio



EMISSION REDUCTION PROGRAM

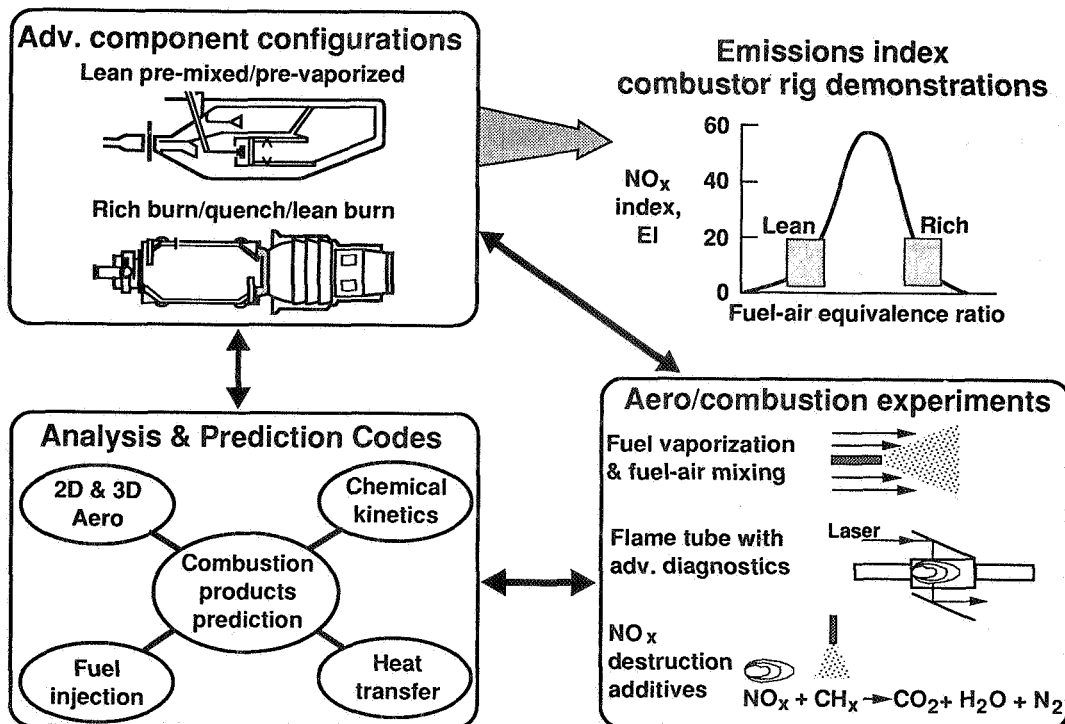
The approach to emissions reduction technology development couples both analytical and experimental capabilities which first build a strong fundamentals foundation, and then integrates and applies that knowledge base to engine-level combustor hardware for verification.

Analysis codes are used to assess proposed concepts for screening and to also identify areas of concerns requiring lab experiments for resolution. Enhancements to the codes will occur throughout the program.

Lab experiments are the primary source of the knowledge base. Results define key design factors, foster formulations of alternate concepts, and demonstrate achievable NO_x reduction levels.

Development of low-emission combustors will be accomplished by; evolving key sub-components such as the fuel injectors, and mixing devices; integrating them in selected combustor designs; and, development tests at simulated operating conditions.

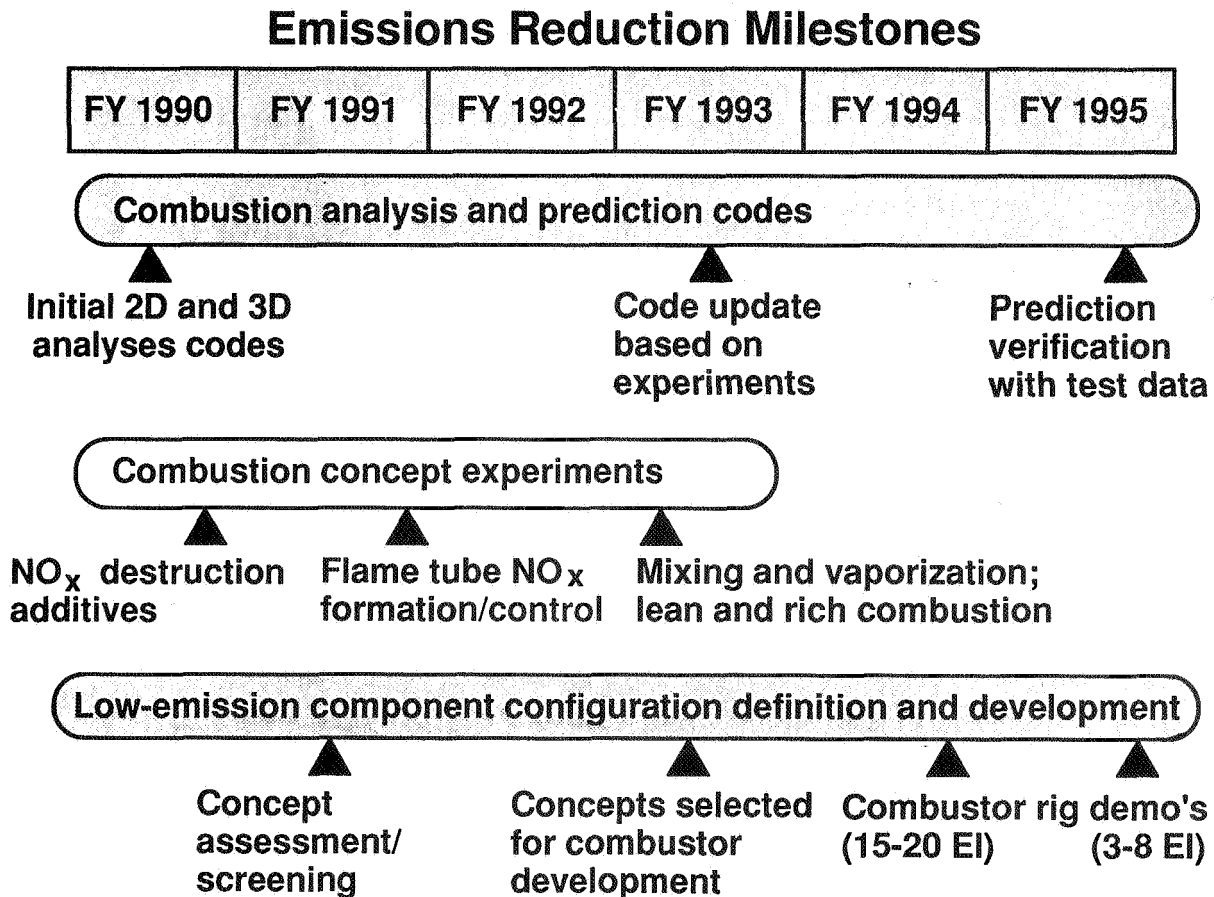
Emissions Reduction Program



EMISSION REDUCTION MILESTONES

This chart illustrates the program elements and key milestones. Program success depends on achievement of all milestones. However, the most critical are the following:

- o FY91: Demonstrate ultra-low NO_x levels in flame tube experiments conducted at simulated supersonic cruise conditions.
- o FY92: Select the prime combustion approach for combustor development.
- o FY95: Demonstrate ultra-low NO_x levels in combustor test rigs.



SUMMARY

This chart briefly describes current program status.

Summary

- **Flame tube experiments have been initiated to demonstrate ultra low NO_x emission levels for LPP; to be evaluated in 1991 RQL combustion approaches.**
- **Stable of existing computer codes being evaluated/upgraded/validated to analyze low emissions combustor concepts**
- **Efforts with engine companies are in process to evaluate combustor concepts leading to selection of prime approach at end of FY 1992.**

Session VII. Emission Reduction

omit

Theoretical Study of Thermodynamic Properties and Reaction Rates of Importance in the High-Speed Research Program
Stephen Langhoff, Dr. Charles W. Bauschlicher, Jr. and Richard Jaffe, NASA Ames Research Center

THIS PAGE INTENTIONALLY BLANK

**Theoretical study of thermodynamic properties
and reaction rates of importance in the
high-speed research program**

**Stephen Langhoff, Charles Bauschlicher, and Richard Jaffe
Computational Chemistry Branch
NASA Ames Research Center
Moffett Field, CA 94035**

S20-77
12010

presented at

The First Annual High-Speed Research Workshop

Introduction

One of the primary goals of NASA's high-speed research program is to determine the feasibility of designing an environmentally safe commercial supersonic transport airplane. The largest environmental concern is focused on the amount of ozone destroying nitrogen oxides (NO_x) that would be injected into the lower stratosphere during the cruise portion of the flight. The limitations placed on NO_x emission require more than an order of magnitude reduction over current engine designs. To develop strategies to meet this goal requires first gaining a fundamental understanding of the combustion chemistry.

To accurately model the combustor requires a computational fluid dynamics approach that includes both turbulence and chemistry. Since many of the important chemical processes in this regime involve highly reactive radicals, an experimental determination of the required thermodynamic data and rate constants is often very difficult. Unlike experimental approaches, theoretical methods are as applicable to highly reactive species as stable ones. Also our approximation of treating the dynamics classically becomes more accurate with increasing temperature. In this article we review recent progress in generating thermodynamic properties and rate constants that are required to understand NO_x formation in the combustion process. We also describe our one-dimensional modeling efforts to validate an NH_3 combustion reaction mechanism. We have been working in collaboration with Marty Rabinowitz at Lewis research center, to ensure that our theoretical work is focused on the most important thermodynamic quantities and rate constants required in the chemical data base.

Outline

- Thermodynamic properties
 1. C-H bond dissociation energies of CH₄
 2. Resolution of the controversy concerning the C-H bond energy of acetylene
- Reaction rate constants
 1. Lifetime of HN₂ to unimolecular decay
 2. C₂H₂ + C₂H₂ → ?
 3. propane + O → propyl + OH
- Modeling
 1. 1D modeling to validate an NH₃ combustion mechanism (H-N-O)
 2. 1D modeling of turbine combustors with CH₄ fuel to identify important H-C-N-O reactions.

Calculation of heats of formation

Although the heat of formation is well known for many molecules, individual bond energies are often very uncertain. We have developed an inexpensive computational approach for predicting accurate (1 to 2 kcal/mole) C-C and C-H bond energies [1-2]. Currently we are attempting to assess the accuracy with which we can compute N-H, N-N, O-H and O-O bond energies [3]. An accurate knowledge of bond energies is required to model the chemistry occurring in jet engines. For purposes of calibration, we have studied the successive bond energies of methane [1]. These are compared with experiment in the following table. At a modest level of theory, our directly calculated values are about 2 kcal/mole too small after the inclusion of the vibrational zero-point energy (ZPT). However, 0.5 kcal/mole accuracy is achievable with very large calculations. When we add 2 kcal/mole to correct for deficiencies in the theoretical bond energies (column labeled estimate), excellent agreement is obtained with experiment. This gives us considerable confidence that our results for hydrocarbons and other systems, such as ketene [2] and methanol [4] are also very accurate.

C-H dissociation energy in C₂H₂

There is currently considerable controversy regarding the C-H dissociation energy of acetylene, $D_0^0(\text{HCC-H})$. This is in large part due to the low and presumably very accurate value determined by Green, Kinsey and Field (GKF) [5] using Stark anticrossing spectroscopy. Their result, 126.647(2) kcal/mole, is claimed to be an *upper bound*, and is consistent with the 127 ± 1.5 kcal/mole estimate of Segall *et al.* [6] obtained by measuring the kinetic energy (K.E.) of the hydrogen atom fragment using Doppler multiphoton ionization spectroscopy. However, these values are substantially smaller than previous theoretical estimates [7,8] and other recent experimental results, such as the D_0 value of 131.3 ± 0.7 kcal/mole measured by Ervin *et al.* [9] using the techniques of negative ion photoelectron spectroscopy and gas phase proton transfer kinetics.

We undertook a systematic study of the C-H bond dissociation energy in acetylene with respect to improvements in the level of theoretical treatment [10]. Our best estimate for the D_0 value of 130.1 ± 1.0 kcal/mole is in good agreement with the recent experiment of Ervin *et al.* [9] and previous theoretical calculations [7,8]. We believe our error bars to have a better than 90% probability of bracketing the correct D_0 value, and we therefore seriously question the recent upper bound inferred from Stark anticrossing spectroscopy [5]. Detailed theoretical studies of the C₂H₂ and C₂H vibrational frequencies have also led us to revise upward the D_0^0 values determined from kinetic data.

Experimental

$\leq 126.647 \pm 0.002$	Stark anti-crossing spectroscopy
$127. \pm 1.5$	$\text{HCCH} + h\nu \rightarrow \text{C}_2\text{H} + \text{H(K.E.)}$
124-127	Kinetic data
131.3 ± 0.7	$\Delta H_{acid}(\text{HCCH}) + \text{EA}(\text{C}_2\text{H}) - \text{IP}(\text{H})$
$132. \pm 2$	$\text{HCCH} + h\nu \rightarrow \text{C}_2\text{H(K.E.)} + \text{H}$
132.6 ± 1.2	photoionization of HCCH

Theoretical

130.1 ± 1.0	MRCI
-----------------	------

Reaction Rate Constants

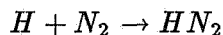
The first step in determining an accurate rate constant is to compute the potential energy surface – that is, for “all” possible arrangements of the atoms, solve for the electronic energy. The surface must then be fit to an analytic form in order to solve for the nuclear motion on this surface using either classical or quantum mechanical scattering methods. We are currently exploring the use of variational transition state approaches with tunneling corrections for determining qualitative (factor of 2-3) reaction rate constants and product branching ratios. One of the advantages of this method is that it requires only a small portion of the complete potential energy surface. This approach has been applied to determining the rate constant of the reaction of propane with atomic oxygen— see later discussion.

Several reactions are currently under study in our laboratory. For example, the reaction



is being studied, since this reaction consumes most of the O_2 in typical hydrocarbon combustion. However, the rate constant for this reaction is uncertain by a factor of six at flame temperatures. A global potential energy surface (PES) has been developed and fitting is in progress [11-14].

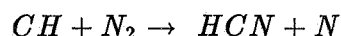
Another molecule that we have studied extensively is HN_2 , since it has been postulated as an important species in thermal De- NO_x processes. A global PES has been developed for



and an accurate lifetime has been computed for the HN_2 molecule [15-18].

The reaction of C_2H_2 with itself is postulated to be important in the final steps of hydrocarbon combustion. We believe that acetylene must first be converted to the vinylidene isomer (CCH_2) before reaction can occur— see later discussion.

The reaction

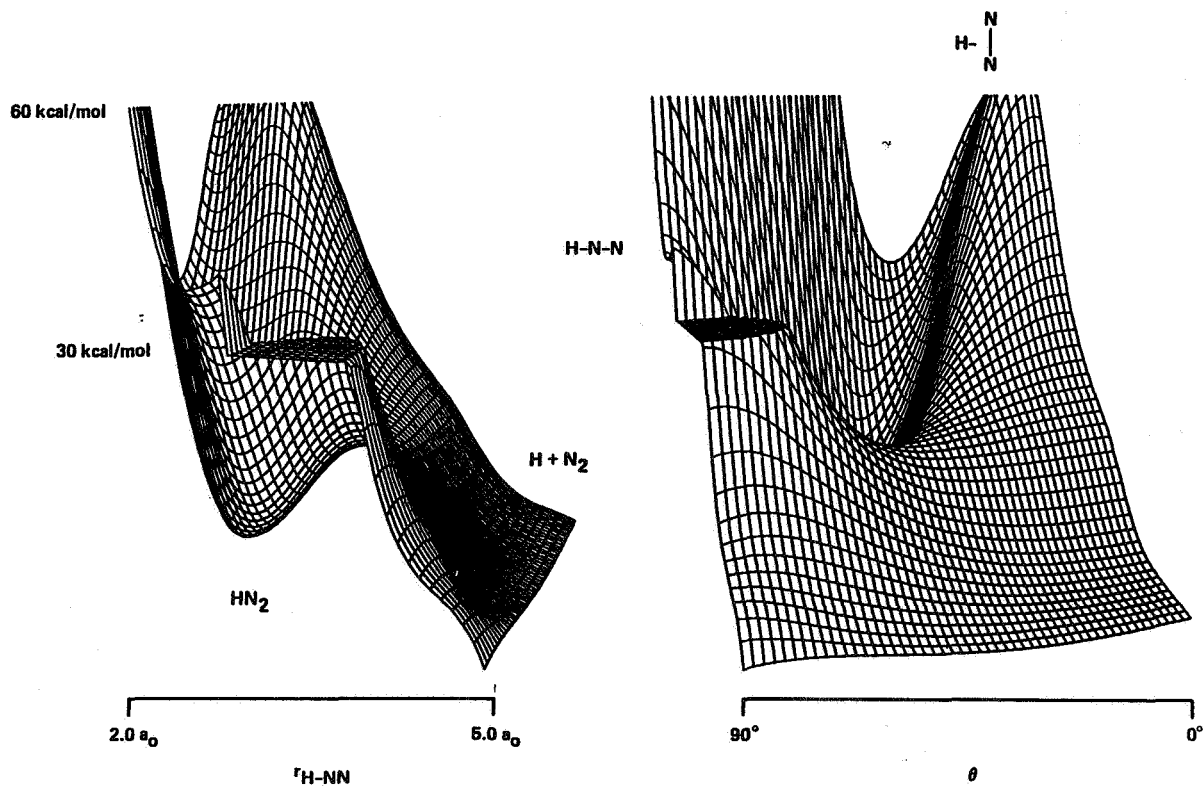


is believed to be the rate determining step in “prompt NO_x ” formation. A large number of stationary points have been located on this potential energy surface. Large-scale investigations of the surfaces are in progress. Finally, work is beginning on the $CH_3 + O_2$ and $CH_3 + OH$ reactions to determine product branching ratios. Model studies have shown these to be important in the combustion of jet fuel.

Global potential energy surface for $\text{H} + \text{N}_2 \rightarrow \text{HN}_2$

The HN_2 species has been postulated as an important intermediate in the thermal De- NO_x process. The HN_2 species was found to be unstable with respect to $\text{H} + \text{N}_2$ by 3.0 kcal/mol, but quasibound by 12.2 kcal/mol due to a barrier to dissociation—see figure below. The computed $\text{N}_2\text{-H}$ lifetime [17] (based on 1-D tunneling through an Eckart barrier) was five orders of magnitude smaller than the value assumed in the experimental analysis. Koizumi and Schatz (Northwestern) have fit this surface and carried out coupled channel calculations to determine the lifetime. These rigorous calculations confirm those based on a Wigner model of tunneling that indicate this radical has a very short lifetime to unimolecular decomposition [18].

This suggests that commonly used reaction mechanisms for NO_x chemistry such as the Sandia reaction set [19] are incorrect.





The reaction of C_2H_2 with itself is postulated to be important in the final steps of hydrocarbon combustion. It is exceedingly unlikely that any reaction takes place between two acetylene molecules at the temperatures of interest, but the vinylidene (CCH_2) isomer is only about 30 kcal/mol above acetylene, and a number of products can result from reaction of vinylidene with acetylene.

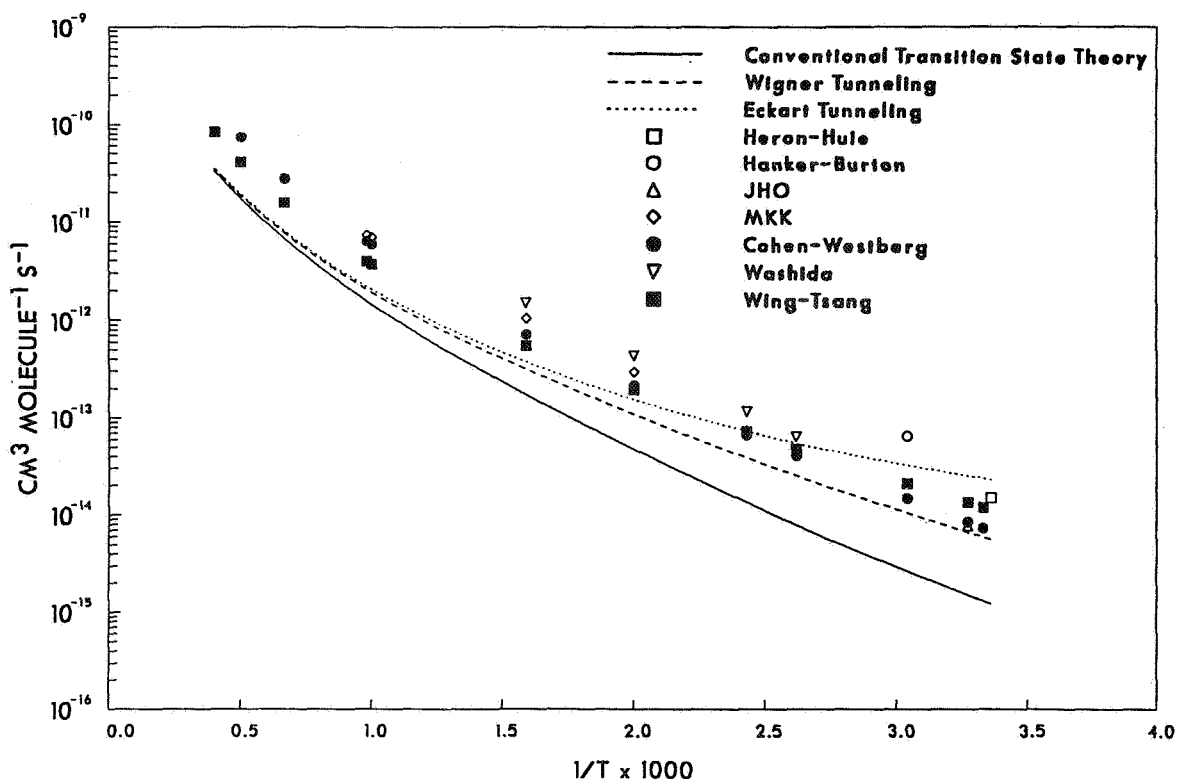
So far, seven stable isomers of C_4H_4 have been found using self-consistent-field (SCF) and multiconfigurational self-consistent-field (MCSCF) wave functions, as well as several stationary points that are not minima or are not stable with respect to symmetry-breaking nuclear distortions. The lowest energy C_4H_4 isomer is vinylacetylene, which is about 45 kcal/mol more stable than two acetylenes. Butatriene is about 10 kcal/mol higher in energy, and methylenecyclopropene is about 14 kcal/mol higher still. Another isomer, cyclobutadiene, is only a little more stable than two acetylenes. The other stationary points are much higher in energy. The energetics here are not fully refined at the correlated level, but correlation does not seem to have a significant effect on the thermochemistry.

Several pathways have been followed on this surface using large MCSCF configurational spaces, in preliminary attempts to find transition states for the first reaction steps of vinylidene with acetylene, but while these have yielded another fairly stable isomer, carbenecyclopropane, and transition states for some rearrangements have been found, the initial transition states have not yet been located. However, the investigation is at an early stage and there should not be a problem determining the reaction pathways.

The Reaction of Propane with Atomic Oxygen

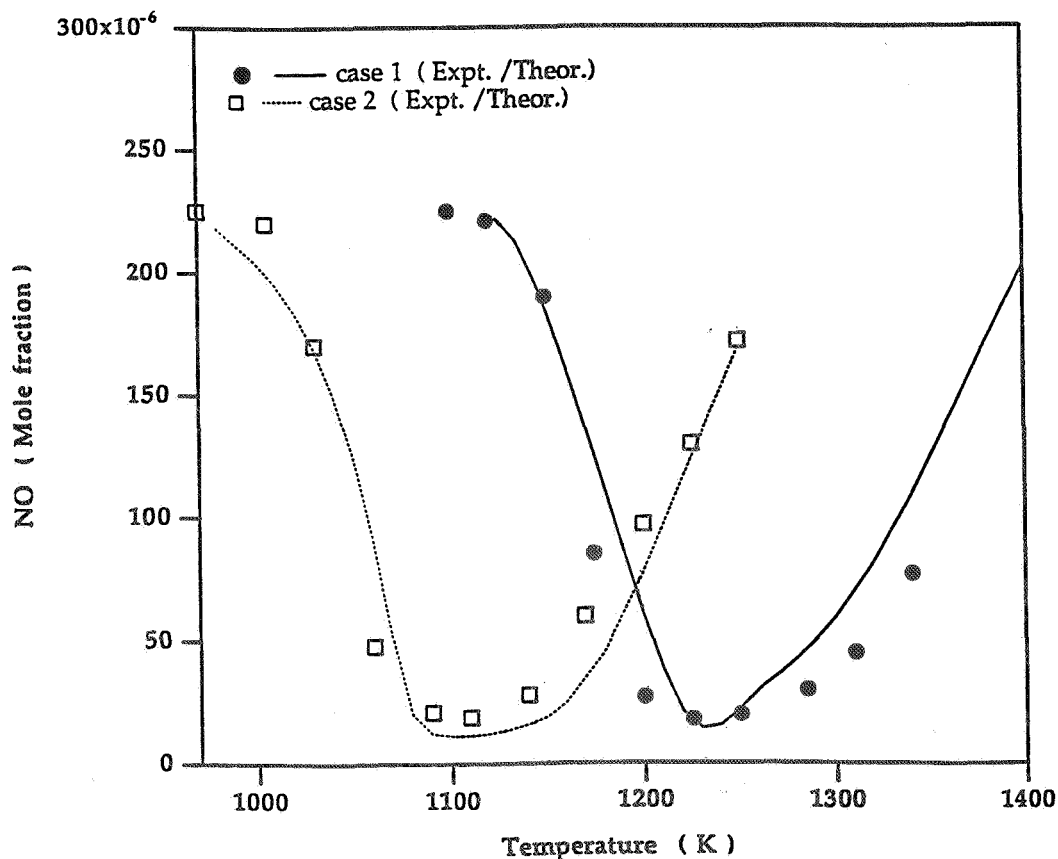
We have studied the hydrogen abstraction from the central carbon of propane by ground state oxygen [20]. The energy barrier on the potential energy surface was determined using SCF gradient methods. A more accurate barrier and exoergicity were determined using correlated methods. Furthermore, a correction factor to account for deficiencies in the basis set and electron correlation treatment was determined by carrying out large scale calculations for the analogous reaction $\text{H}_2 + \text{O} \rightarrow \text{H} + \text{OH}$. This correction lowers the saddle point and product energies by 4.66 kcal/mol relative to the reactants. The final computed energies are 4.36 kcal/mol for the barrier and 7.00 for the exoergicity. These compare favorably with the experimentally determined values of 5.0 and 7.0 kcal/mol.

The potential energy profile, molecular geometries and vibrational frequencies were used for a transition state theory calculation of the rate constant for the hydrogen abstraction reaction. Two approximate treatments of tunneling were carried out. The Wigner model assumes that the energy barrier is an inverted parabola truncated at the reactant and product energy limits. The Eckart model uses a potential energy function based on a modified hyperbolic secant. It can be seen from the figure that the transition state theory calculations with either tunneling model agree with the experimental data to within a factor of two over the entire temperature range (300-2000K). Greater than a factor of two accuracy in the rate would require a global surface, which is exceedingly difficult for a system with this many atoms.



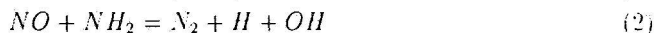
Thermal de-NO_x

Experiment of Lyon and Hardy [21] showing NO removal by ammonia injection. The process works in a narrow temperature range, and oxygen must be present for NH₂ formation. Initial conditions of experiment are: NO=225 ppm, NH₃=450 ppm, O₂=1.23%, remainder He. The pressure is 1.1 atm and the observations are made at 0.1 sec. Case two is similar to case one except for 225 ppm H₂ displacing an equal amount of He. Modeling shown here uses the reaction mechanism of Miller and Bowman [19], with a long lifetime for N₂H ($\tau=10^{-4}$ sec). Calculations assume a plug flow reactor, and are similar to Miller and Bowman [19]. The same calculations done with a shorter N₂H lifetime, in an attempt to match the theoretical value of the lifetime ($< 10^{-9}$ sec), are unable to reproduce the experimental results.



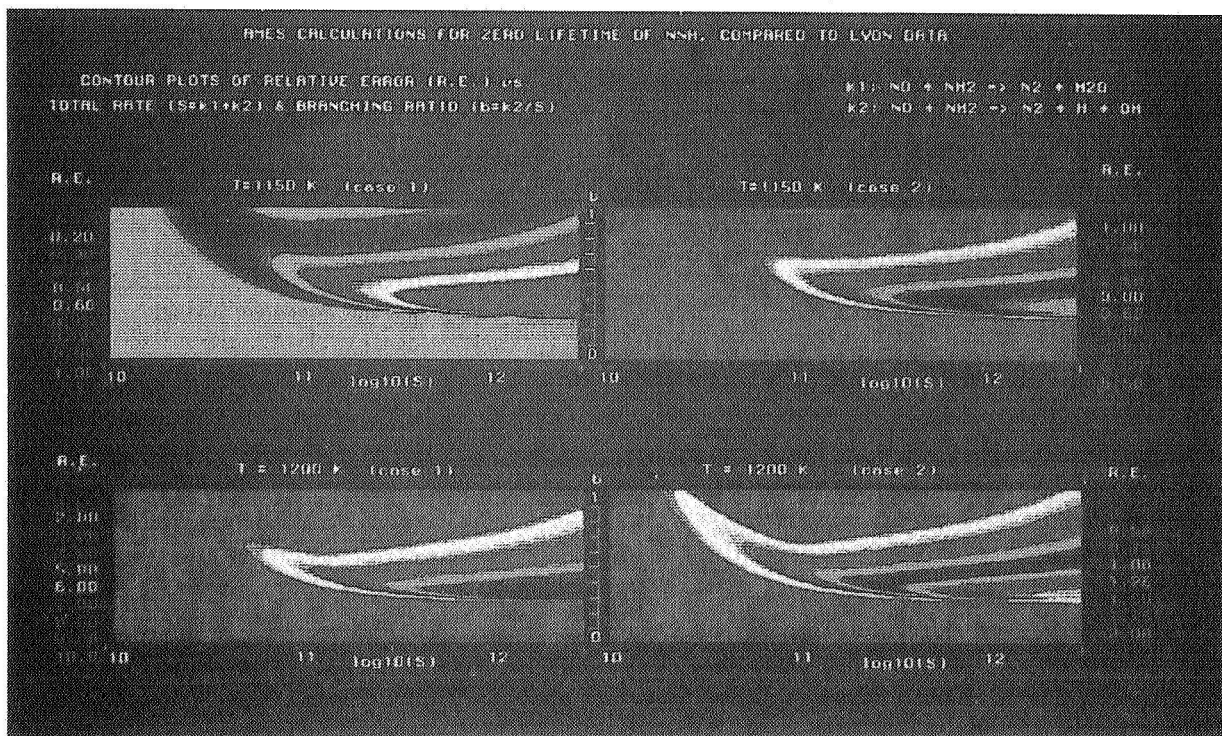
Thermal de-NOx: no N_2H .

In the limit of very short N_2H lifetime ($< 10^{-9}$ sec), we can assume a spontaneous decay of N_2H into N_2 and H . The NO removal mechanism then hinges on two important reactions:



where the second reaction replaces $NO + NH_2 = N_2H + OH$. The first equation has a chain-terminating character, while the second is chain branching and will be important at low temperatures (combined with $NH_3 + OH = NH_2 + H_2O$). A systematic study is performed in an attempt to find a consistent reaction mechanism, without N_2H , that explains the data. The parametric variables are the total forward rate of reactions (1) and (2), $S = k_1 + k_2$ and the branching ratio $b = k_2/S$. At two temperatures for which there is simultaneous experimental data for cases 1 and 2, we plot the deviation from the experimental result as a function of both the total rate and the branching ratio. The contour plots are for the Relative Error, defined as $R.E. = |NO - NO^*|/NO^*$, where NO^* is the experimental value observed. The ordinates are the total rate (x-axis, in \log_{10} units, and ranging from 10 to 13), and branching ratio (y-axis, ranging from 0 to 1). Valid regions are for small R.E. (blue regions), and are mutually exclusive for $T=1150$ K. A narrow overlap may exist at $T=1200$ K, without convincing evidence. The disagreement at $T=1150$ K is due to the fact that for most values of S and b , the production of NH_2 is not sufficiently fast to start the NO removal. Calculations were performed for a plug-flow reactor.

These results indicate that the presence of reaction (2) cannot by itself explain the experimental data. Since the assumption of a plug-flow reactor may be invalid, partial recirculation zones in the reactor may be able to introduce radicals early in the stream and speed up the removal of NO at low temperatures. The same systematic series of calculations should be done also for Perfectly-Stirred and Partially-Stirred reactors.



Conclusions

Computational chemistry techniques have utility in computing accurate thermodynamic properties such as C-H bond energies. Accurate C-H bond energies have been computed for methane, ethylene, ketene, acetylene, and methanol. Reaction rates can be computed at least to within a factor of two. The reactions currently under study in our laboratory include $\text{H} + \text{O}_2 \rightarrow \text{HO} + \text{O}$, $\text{H} + \text{N}_2 \rightarrow \text{HN}_2$, C_2H_2 with itself, $\text{CH} + \text{N}_2 \rightarrow \text{HCN} + \text{N}$, $\text{CH}_3 + \text{OH}$, and $\text{CH}_3 + \text{O}_2$. Our calculations demonstrate that the HN_2 molecule has a short lifetime ($< 10^{-9}$ sec) to unimolecular decomposition. We are presently trying to incorporate this fact into model studies of the effect of NH_3 on NO removal. We have been working in close collaboration with Marty Rabinowitz at Lewis to ensure that we are addressing the key chemical issues involved in reducing NO emission in jet engines.

References

1. Bauschlicher, C. W.; and Langhoff, S. R.: Theoretical study of the C-H bond dissociation energies of CH₄, C₂H₂, C₂H₄, and H₂C₂O. *Chem. Phys. Lett.* 177, 133 (1991).
2. Bauschlicher, C. W.; and Langhoff, S. R.: Theoretical study of the C-H bond dissociation energy of C₂H. *Chem. Phys. Lett.* 173, 367 (1990).
3. Langhoff, S. R.; Bauschlicher, C. W.; and Taylor, P. R.: The computation of C-C and N-N bond dissociation energies for singly, doubly, and triply bonded systems. *Chem. Phys. Lett.*, in press.
4. Bauschlicher, C. W.; Langhoff, S. R.; and Walch, S. P.: Theoretical study of the bond dissociation energies of CH₃OH. to be submitted.
5. Green, P. G.; Kinsey, J. L.; and Field, R. W.: A new determination of the dissociation energy of acetylene. *J. Chem. Phys.* 91 (1989) 5160.
6. Segall, J.; Lavi, R.; Wen, Y.; and Wittig, C.: Acetylene C-H bond dissociation energy using 193.3-nm photolysis and sub-dopplar resolution H-atom spectroscopy: 127 ± 1.5 kcal/mol. *J. Phys. Chem.* 93, (1989) 7287.
7. Curtiss, L. A.; and Pople, J. A.: Theoretical study of the C-H bond dissociation energy of acetylene. *J. Chem. Phys.* 91, (1989) 2420.
8. Montgomery, J. A.; and Petersson, G. A.: On the C-H bond dissociation energy of acetylene. *Chem. Phys. Lett.* 168, 75 (1990).
9. Ervin, K. M.; Gronert, S.; Barlow, S. E.; Gilles, M. K.; Harrison, A. G.; Bierbaum, V. M.; DePuy, C. H.; Lineberger, W. C.; and Ellison, G.B.: Bond strengths of ethylene and acetylene. *J. Am. Chem. Soc.* 112, 5750 (1990).
10. Bauschlicher, C. W.; Langhoff, S. R.; and Taylor, P. R.: Theoretical study of the C-H bond dissociation energy of acetylene. *Chem. Phys. Lett.* 171, 42 (1990).
11. Walch, S. P.; Rohlfiing, C. M.; Melius, C. F.; and Bauschlicher, C. W.: Theoretical characterization of the minimum energy path for the reaction $H + O_2 \rightarrow HO_2^* \rightarrow HO + O$. *J. Chem. Phys.* 88, 6273 (1988).
12. Walch, S. P.; and Rohlfiing, C. W.: Theoretical characterization of the potential energy surface for $H + O_2 \rightarrow HO_2^* \rightarrow HO + O$, II. The potential for H atom exchange in HO₂. *J. Chem. Phys.* 91, 2373 (1989).
13. Walch, S. P.; Duchovic, R. J.: Theoretical characterization of the potential energy surface for $H + O_2 \rightarrow HO_2^* \rightarrow HO + O$, III. Computed points to define a global potential energy surface. *J. Chem. Phys.*, in press.

14. Walch, S. P.; and Jaffe, R. L.: Computed reaction rate for $\text{H} + \text{HO}_2 \rightarrow \text{H}_2 + \text{O}_2$. J. Chem. Phys., to be submitted.
15. Walch, S. P.: Theoretical characterization of selected regions of the ground state potential surface of N_2H_2 . J. Chem. Phys., 91, 389 (1989).
16. Walch, S. P.: Theoretical characterization of the potential energy surface for $\text{H} + \text{N}_2 \rightarrow \text{HN}_2$, II. Computed points to define a global potential. J. Chem. Phys., 93, 2384 (1990).
17. Walch, S. P.; Duchovic, R. J.; and Rohlfing, C. M.: Theoretical characterization of the minimum energy path for hydrogen atom addition to N_2 : Implications for the unimolecular lifetime of HN_2 . J. Chem. Phys., 90, 3230 (1989).
18. Koizumi, H; Schatz, G. C.; and Walch, S. P. A coupled channel study of HN_2 unimolecular decay based on a global *ab initio* potential surface. J. Chem. Phys., submitted.
19. Miller, J. A.; and Bowman, C. T.: Mechanism and modeling of nitrogen chemistry in combustion. Prog. Energy Combust. Sci. 15, 287 (1989).
20. Laskowski, B. C.; Jaffe, R. L.; and Duchovic, R. J.: Potential energy surfaces for the $\text{O}(^3\text{P}) + \text{propane}$ reaction. to be submitted.
21. Lyon, R. K.; and Hardy, J. E.: Discovery and development of the thermal DeNO_x process. Ind. Eng. Chem. Fundam. 25, 19 (1986) and references therein.

Session VII. Emission Reduction

omit

HSR Combustion Analytical Research
Dr. H. Lee Nguyen, NASA Lewis Research Center

THIS PAGE INTENTIONALLY BLANK

HSR COMBUSTION ANALYTICAL RESEARCH

521-25
12011

H. Lee Nguyen
NASA Lewis Research Center
Cleveland, Ohio

High Speed Research Workshop
First Annual Technical Review
May 14-16, 1991



THIS PAGE INTENTIONALLY BLANK

HSR COMBUSTION ANALYTICAL RESEARCH

Program Objectives and Approaches

Increasing the pressure and temperature of the engines of a new generation of supersonic airliners increases the emissions of nitrogen oxides (NO_x) to a level that would have an adverse impact on the Earth's protective ozone layer. In the process of evolving and implementing low emissions combustor technologies, NASA Lewis has pursued a combustion analysis code program to guide combustor design processes, to identify potential concepts of greatest promise, and to optimize them at low cost, with short turnaround time. The computational analyses are evaluated at actual engine operating conditions. The approach is to upgrade and apply advanced computer programs for gas turbine applications. Efforts have been made in further improving the code capabilities for modeling the physics and the numerical method of solution. Then test cases and measurements from experiments are used for code validation.

HSR Combustion Analytical Research

Objective:

- Use advanced computer models to analyze and design combustor components and subcomponents, understand the physics, and determine how to optimize the design to improve the performance

Approach:

- Emphasis on applying and upgrading existing codes –
KIVA-II, LERC3D for gas turbine combustor applications
 - Improve codes capabilities
 - Codes validation

Figure 1

HSR COMBUSTION ANALYTICAL RESEARCH

Lewis Key Milestones

Due to schedule constraints, the analytical research program is being conducted over a period of 5 years as shown in figure 2 and involves three major milestones. The first milestone was accomplished with the development and use of two-dimensional and three-dimensional codes, KIVA-II and LeRC3D, to guide low emissions combustion concept experiments. These codes will be updated based on results obtained from combustion concept experiments by the end of FY93. These codes will then be used as predictive design tools for low emissions combustors by the end of FY95.

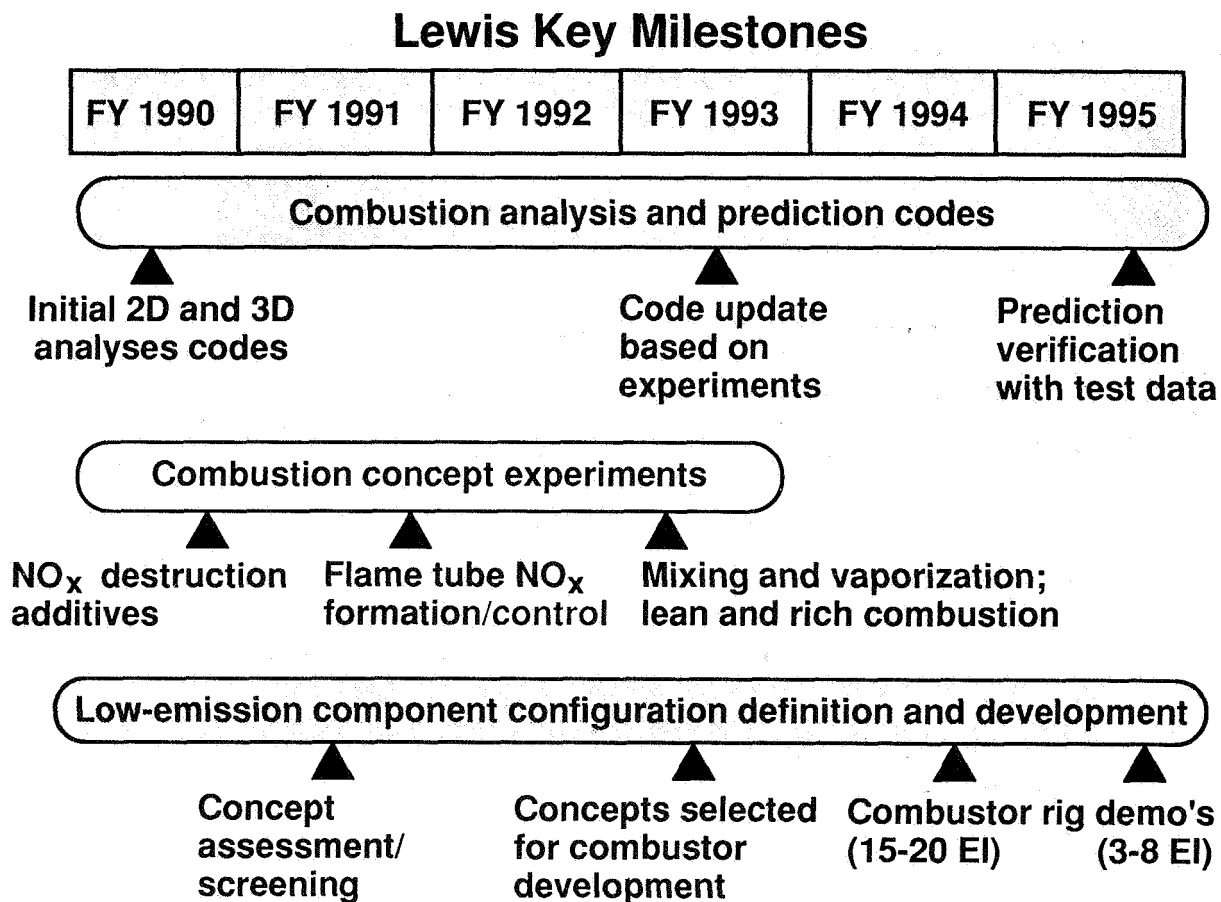


Figure 2

HSR COMBUSTION ANALYTICAL RESEARCH

Organization and Activities Listing

The overall combustion analytical codes evolution plan involves in-house research and contracts and grants; and it provides strong collaborative relationships and technology transfer between industry, universities, and government agencies. Figure 3 lists the activities for the HSR Combustion Analytical Research Program.

Organization and Activities Listing

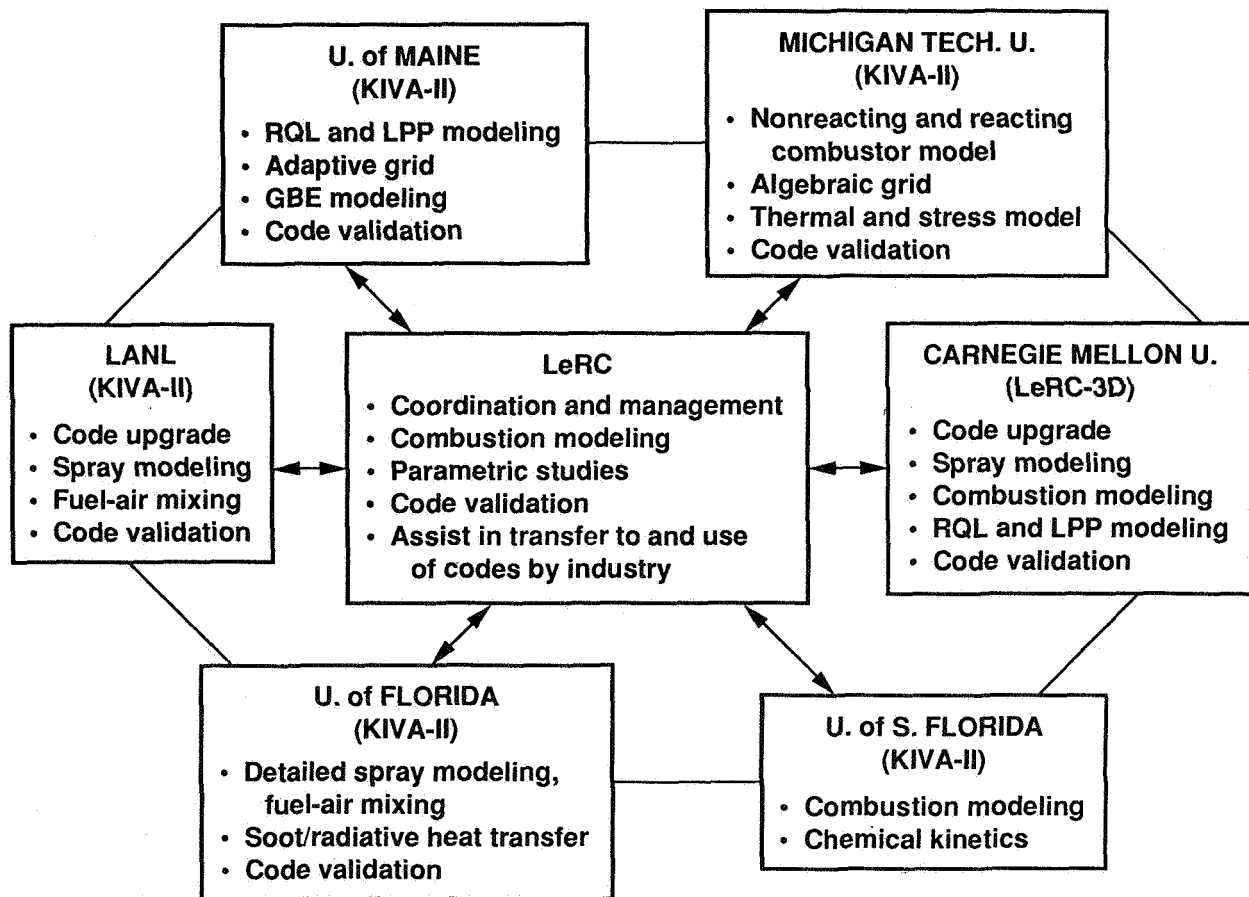


Figure 3

HSR COMBUSTION ANALYTICAL RESEARCH

Description of Computer Code KIVA-II

To provide insight into the combustion process and combustor design, KIVA-II and LeRC3D have been used. These codes are operational and calculations have been performed to guide low emissions combustion experiments. KIVA-II (ref. 1), developed by Los Alamos National Laboratory, is one of the most developed and validated codes of the available multi-dimensional computer programs for prediction of the in-cylinder combustion dynamics in internal combustion engines. There are features of KIVA-II that make it well suited for other applications, so KIVA-II has been adapted for gas turbine combustor applications.

In terms of modeling the physics, the major features of KIVA-II are as follows:

- KIVA-II is a two- and three-dimensional turbulent compressible flow solver of reacting multicomponent gas mixture with liquid spray using an Eulerian-Lagrangian approach.
- Turbulence is modeled using the $k-\epsilon$ model.
- Combustion is modeled by a chemical-kinetics-controlled model using global or detailed chemical reactions (ref. 2) or by a mixing-controlled model (ref. 3). The user can conveniently provide a chemical kinetics mechanism by making appropriate modification to the input data file (ref. 2).
- The extended Zeldovich NO_x mechanism is included.
- Stochastic particle spray model includes vaporization, coalescence, and breakup.
- A soot formation/oxidation and a radiative heat transfer model are also included.

In terms of numerics, KIVA-II is based on the following:

- Time-dependent finite-difference code with arbitrary mesh capability, using an implicit-continuous Eulerian technique with conjugate residual iteration for the flow solver.

Key Features of KIVA-II

Description of Computer Code KIVA-II

Physics

Turbulent compressible flow of reacting multicomponent gas mixture with liquid spray

κ - ϵ turbulence model with wall functions

**Combustion models:
Chemical kinetics controlled,
mixing controlled model**

**NO_x formation model:
Extended Zeldovich mechanism**

**Spray model:
Stochastic model, vaporization,
coalescence, breakup**

Soot formation/oxidation

Radiation heat transfer

Numerical method

2D or 3D time-dependent finite difference code

Arbitrary mesh

ICE method with conjugate residual iteration

Optimal quasi-second-order upwind convection

Figure 4

HSR COMBUSTION ANALYTICAL RESEARCH

Description of Computer Code LeRC3D

LeRC3D is a highly advanced code for gas turbine combustor applications. LeRC3D was developed by Carnegie Mellon University with the collaboration/sponsorship of Lewis. In terms of modeling the physics, the major capabilities of LeRC3D (ref. 4) are as follows:

- LeRC3D is a two- and three-dimensional code that solves the N-S equations for turbulent compressible flow of reacting multicomponent gas mixture with liquid spray using an Eulerian-Lagrangian approach.
- The turbulence is modeled by using a $k-\epsilon$ turbulence model with wall functions, or by using a low Reynolds number $k-\epsilon$ model of Chen and Patel, or by using a RNG-based $k-\epsilon$ model.
- Modeling of combustion is done by two different models: the chemical-kinetics-controlled model governed by global or detailed chemical kinetics mechanisms of hydrocarbon combustion, and the mixing-controlled model of Magnussen and Hjertager. The user can conveniently provide a chemical kinetics mechanism by making appropriate modification to the input data file.
- The chemical kinetics model used to study NO_x is the Zeldovich mechanism.
- The spray model includes the fuel vaporization model of Raju and Sirignano.

In terms of the numerical method of solution, LeRC3D is based on the following:

- The flow algorithm is a finite-volume, LU algorithm utilizing van Leer flux-vector splitting with the HOPE algorithm of Liou and Steffan. Source terms are treated implicitly using Shih and Chyu method, diffusion terms are treated implicitly using the procedure of Shih and Steinthorsson.
- A grid system is generated by using an algebraic grid generation method based on transfinite interpolation.

Key Features of LeRC3D

Description of Computer Code LeRC3D

Physics

Turbulent compressible flow of reacting multicomponent gas mixture with liquid spray

Turbulence models:

κ - ϵ turbulence model with wall functions

Low Reynolds no. κ - ϵ model (Chen & Patel)

RNG-based κ - ϵ model

Combustion models:

**Chemical kinetics controlled
Mixing controlled**

NO_x formation model:

Zeldovich mechanism

Spray model:

Lagrangian model of Raju & Sirignano

Numerical method

Grid generation:

Algebraic method using transfinite interpolation

Flow algorithm:

Finite-volume, LU, implicit

Code:

Efficient and robust

Figure 5

VERIFICATION OF KIVA-II CODE PREDICTIONS

Fuel Spray - Air Interaction

Figure 6 shows the prediction of a swirling fuel spray in a nonreacting airstream using the KIVA-II code and a comparison with the experimental results (ref. 5). The model air-assist atomizer embodies a nonswirl inner airstream and a swirling outer airstream which help to atomize and distribute fuel injected from a core tube. Predicted and measured air azimuthal velocity profiles are in good agreement. Fuel injection and mixing become increasingly important as more air is used for the combustion process. Detailed models of the interaction of the swirling air and the fuel spray can provide valuable insight into the effect of different variables that presently can only be evaluated experimentally on a global scale at laboratory test conditions.

Verification of KIVA-II Code Predictions Fuel Spray-Air Interaction

KIVA azimuthal velocity comparison
Calc = 070889, vte = 180,30 wte = 22,22; k-e

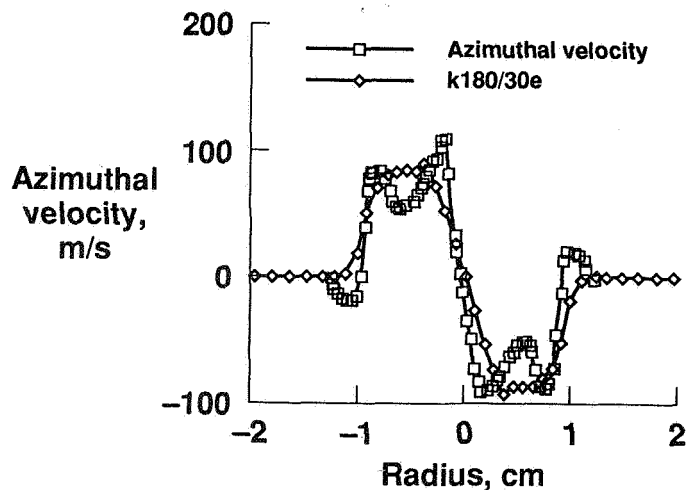
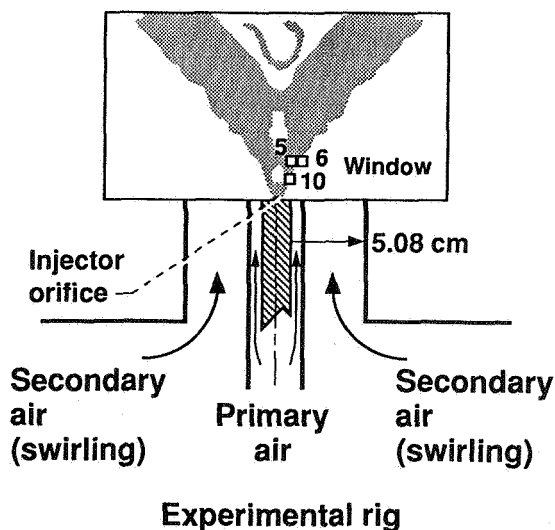


Figure 6

VERIFICATION OF KIVA-II CODE PREDICTIONS

Low NO_x Combustor Emissions

Figure 7 summarizes the comparison of experimental NO_x and CO emission index of a lean premixed prevaporized (LPP) burner (ref. 6) with KIVA-II code predictions. The simplified kinetics mechanism (ref. 2) was used. The predictions agree very well with the test data over the range of equivalence ratio and residence time reported. Calculations using KIVA-II have been performed to guide current low NO_x combustion experiments.

Verification of KIVA-II Code Predictions Low NO_x Combustor Emissions

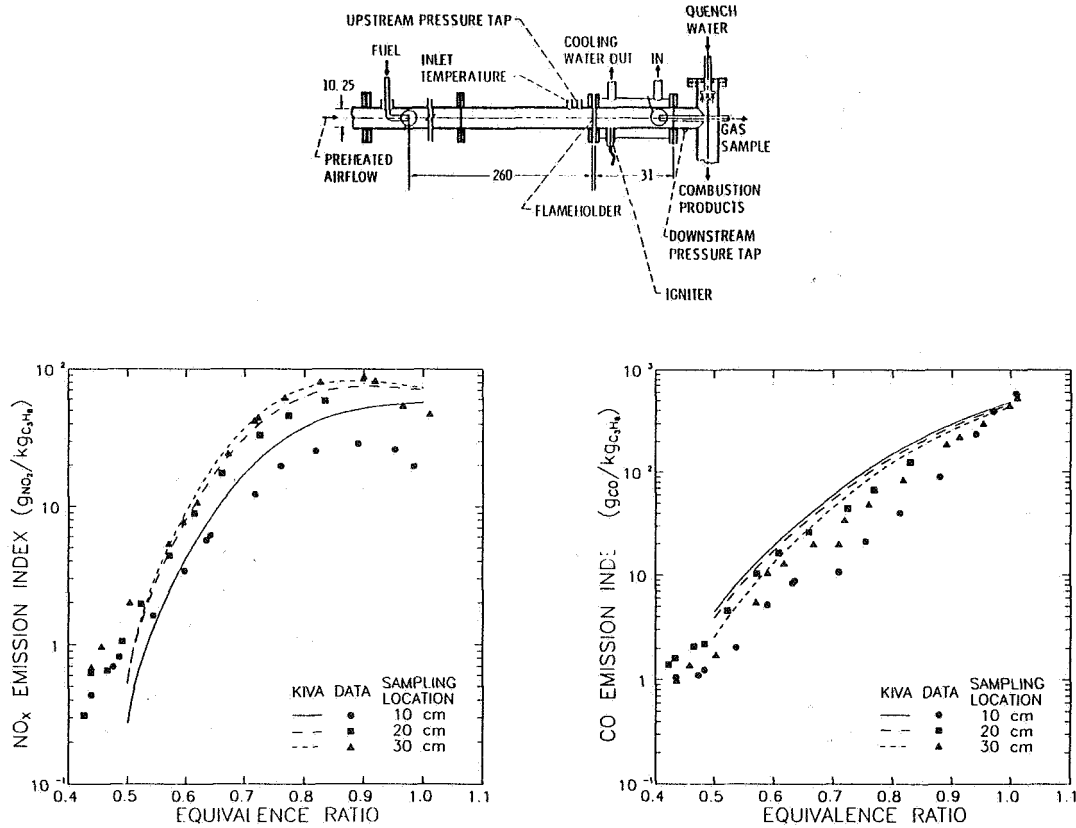


Figure 7

LOW NO_x COMBUSTOR ANALYSIS

(KIVA-II Analysis)

KIVA-II was used to perform two-dimensional analysis of the Rich Burn/Quick Quench/Lean Burn (RQL) combustor to provide detailed information on the combustor internal flow fields, fuel-air mixing, combustor emissions, gas temperature distribution, and pattern factor. A two-dimensional axisymmetric model was used with propane and primary air injected at the inlet of the rich burn section and quick quench air supplied to the two-dimensional slot in the quick quench section. The upper half above the combustor centerline showing the gas temperature profile is shown in figure 8. The rich zone and lean zone equivalence ratios were set at 1.4 and 0.65, respectively. The gas temperature contours show core hot gas regions that occur in the rich zone and lean zone flame fronts. This figure also indicates that the penetration of the two-dimensional jet reaches near the combustor centerline and that thermal quenching occurs in the quick quench section.

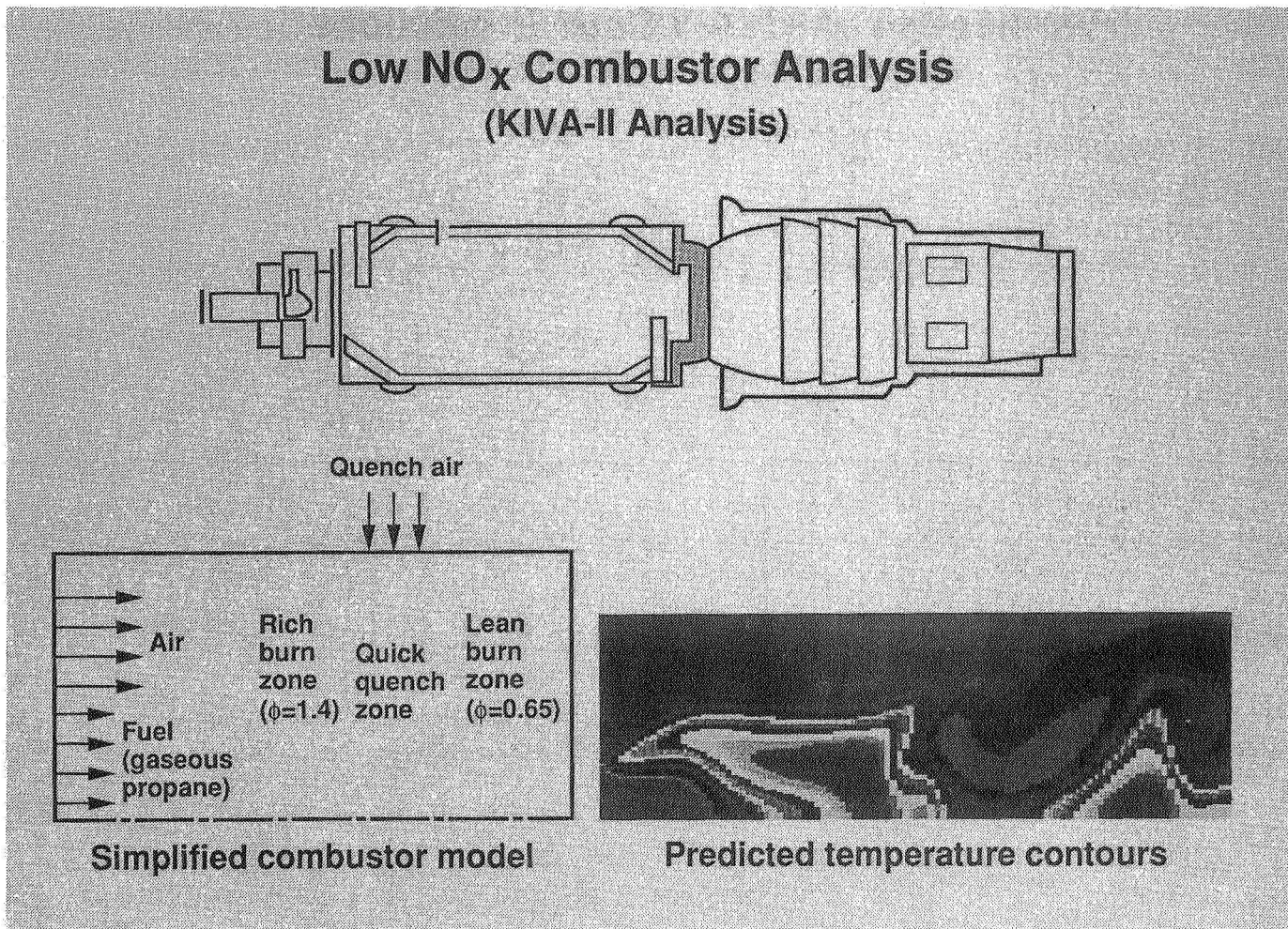


Figure 8

LOW NO_x COMBUSTOR ANALYSIS

(LeRC3D Analysis)

Figure 9 shows the flow field characteristics of the rich burn section of the RQL combustor. As an integral part of the fuel nozzle calculations, two-dimensional analyses (ref. 7) were done to provide the swirling air profiles through the swirlers of the airblast fuel nozzle. The swirlvane cascade analysis provides inlet air profiles to the rich burner analysis. The velocity vectors show a strong central recirculation zone downstream of the airblast fuel nozzle. Calculations using LeRC3D have been performed to guide current low NO_x combustion experiments.

LeRC3D Analysis

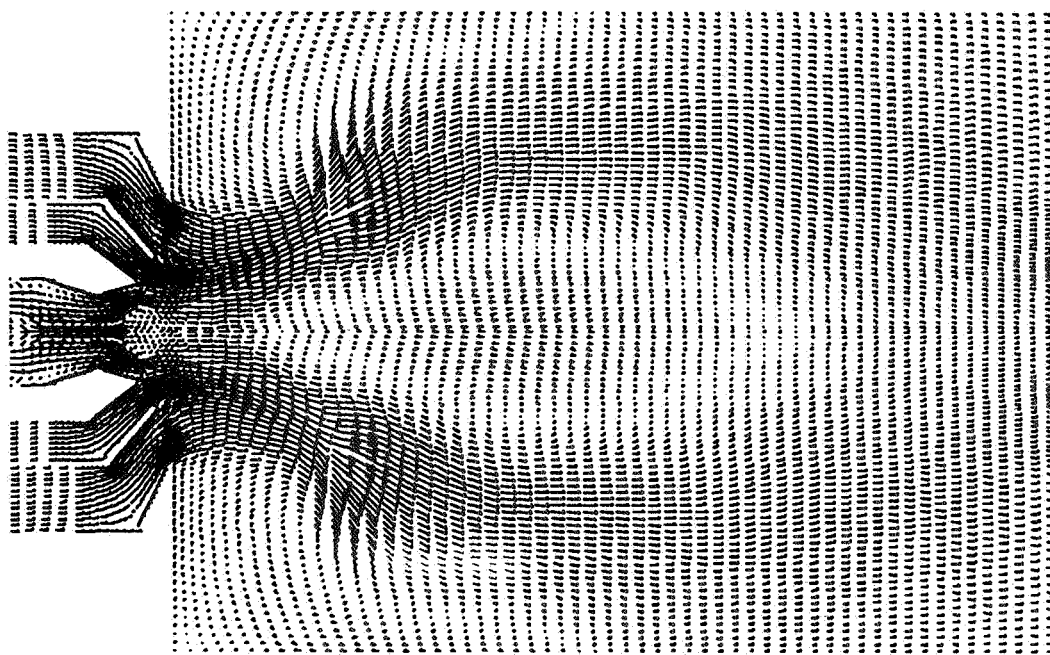


Figure 9

REFERENCES

1. Amsden, A.A., O'Rourke, P.J., and Butler, T.D., "KIVA-II: A Computer Program for Chemically Reactive Flows With Sprays," Los Alamos National Laboratory, LA-11560-MS, May 1989.
2. Nguyen, H.L., and Ying, S.J., "Critical Evaluation of Jet-A Spray Combustion Using Propane Chemical Kinetics in Gas Turbine Combustion Simulated by KIVA-II," AIAA Paper No. 90-2439, NASA TM-103173.
3. Nguyen, H.L., and Wey, M.-J., "Evaluation of a Hybrid Kinetics/Mixing-Controlled Combustion Model for Turbulent Premixed and Diffusion Combustion Using KIVA-II," AIAA Paper No. 90-2450, NASA TM-103196.
4. Nguyen, H.L., Li, Z., Howe, G.W., and Shih, T.I-P., "Calculations of the Three-Dimensional Flow and Combustion in a Staged Gas Turbine Combustor," accepted for presentation at the AIAA/SAE/ASME/ASEE 26th Joint Propulsion Conference, June 24-26, 1991.
5. Butler, T.D., "Analysis of an Air Assist Atomizer," Los Alamos National Laboratory, private communication, May 1990.
6. Anderson, D., "Effect of Equivalence Ratios and Dwell Time on Exhaust Emissions From an Experimental Premixed Prevaporizing Burner," NASA TM X-71592.
7. Micklow, G.J., and Nguyen, H.L., "Effect of Vane Twist on Performance of Dome Swirlers for Gas Turbine Airblast Atomizers," AIAA Paper No. 90-1955, NASA TM-103195.

Session VII. Emission Reduction

omit

LeRC In-House Experimental Research
Dr. Valerie J. Lyons, NASA Lewis Research Center

THIS PAGE INTENTIONALLY BLANK

N94-33484

LERC IN-HOUSE EXPERIMENTAL RESEARCH

52-25
12012

V.J. Lyons
N.A.S.A. Lewis Research Center
Cleveland, Ohio

High Speed Research Workshop
Session 7 Emission Reduction
May 14-16, 1991

PRECEDING PAGE BLANK NOT FILMED

999

At

LeRC In-House Experimental Research

The Lewis Research Center has an ambitious in-house experimental research program to conduct studies, acquire technology, and validate the capabilities and limitations of advanced low NO_x combustor concepts. This program will establish NO_x reduction technologies that will insure no significant ozone depletion in the atmosphere by future high speed civil transports (HSCT). This is critical to establishing the environmental feasibility of an HSCT. This work supports the efforts of industry and universities to determine the criteria for the HSCT combustor concept selection in 1992. The work at Lewis focuses on several flame tube combustor rigs: the Lean Premixed Prevaporized (LPP); the Rich Burn/Quick Quench/Lean Burn (RQL); the Catalytic Oxidation Rig; and the Ceramic Matrix Liner Test Rig. Advanced laser diagnostics will be applied to the flame tube rigs to provide more detailed and non-intrusive measurements of combustion flow parameters.

- **Lean Premixed Prevaporized (LPP)**
- **Rich \ Quick Quench \ Lean (RQL)**
- **Catalytic Oxidation Rig**
- **Ceramic Matrix Liner Rig**
- **Diagnostics**

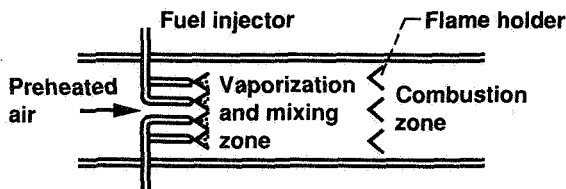
Combustion Concepts

The basic approach to thermal NO_x reduction is to reduce the flame temperature. This can be accomplished by burning lean or rich, avoiding the maximum flame temperature which occurs near the stoichiometric equivalence ratio (E.R.) of 1.0. The three concepts shown on this figure reduce NO_x emissions by burning lean (E.R. of 0.6) for the Lean Premixed Prevaporized (LPP) concept, or by burning rich (E.R. of 1.2-1.8) and then lean (E.R. of 0.6) for the Rich burn/Quick Quench/Lean Burn (RQL) concept, or by burning very rich (E.R. of 3-9) for the Catalytic Oxidation section which could be used as the rich stage for the RQL concept. These concepts are the focus of our LeRC in-house experimental efforts.

Combustion Concepts

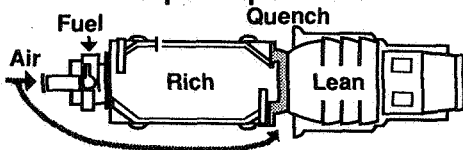
Common approach: Reduce thermal NO_x formation by reducing flame temperatures

Lean premixed/prevaporized



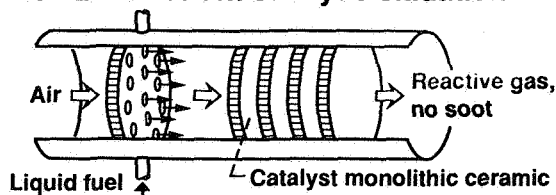
- Burning with excess air in lean zone; equivalence ratio = 0.6

Rich burn/quick quench/lean burn



- Burning with excess fuel; equivalence ratio = 1.2 - 1.8
- Burning with excess air; equivalence ratio = 0.6

Rich zone variant catalytic oxidation

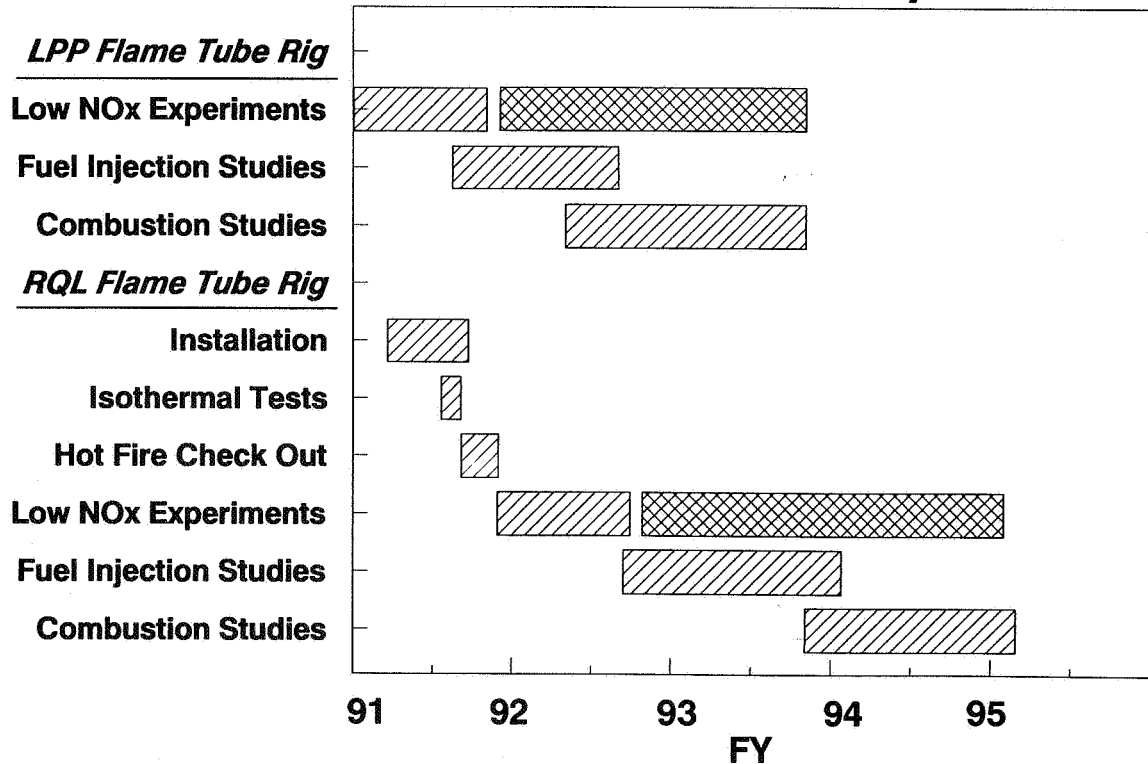


- Catalytic burning highly excess fuel; equivalence ratio = 3.0 - 9.0

Schedule for In-House Experiments

The schedule below shows the general time-frame for the major phases of the experimental work which will be performed in the LPP and RQL flame tube rigs. The term "Low NOx experiments" initially refers to the gas sampling probe measurements of gaseous emissions for various equivalence ratios and inlet pressures and temperatures. This activity is continued into a second phase which includes the use of advanced diagnostic probes through windowed sections in first the fuel/air mixing zones and then in the combustion zones of each of the flame tubes. A little more detail is given for the RQL rig which is currently in its isothermal testing phase. Within the next few weeks, the hot fire check-out will occur and the initial low NOx testing can begin.

Schedule for LPP & RQL Flame Tube Experiments



Lean Premixed Prevaporized Combustion

The objective of this portion of the LeRC in-house research program is to use a flame tube combustor to demonstrate the capability of the Lean Premixed Prevaporized (LPP) concept to reach the HSR goal of a NO_x emission index (grams of NO_x produced per kilogram of fuel burned) of between 3 and 8. Using the flame tube combustor, the effect of fuel/air distribution and degree of vaporization can be studied. Also of great interest are autoignition, flashback, turbulent mixing and lean stability. Information obtained in the flame tube about these parameters will be used to guide the design of an LPP combustor.

The approach is to use an existing NASA-designed square cross-section flame tube combustor to allow combustion testing at the high temperatures and pressures necessary for the HSR Program. This rig was designed in the late 70's to support the emissions reduction program at that time. It has a windowed section to allow laser diagnostics to probe the premixing zone. A windowed section is currently being designed to accommodate laser studies of the combustion zone.

OBJECTIVE:

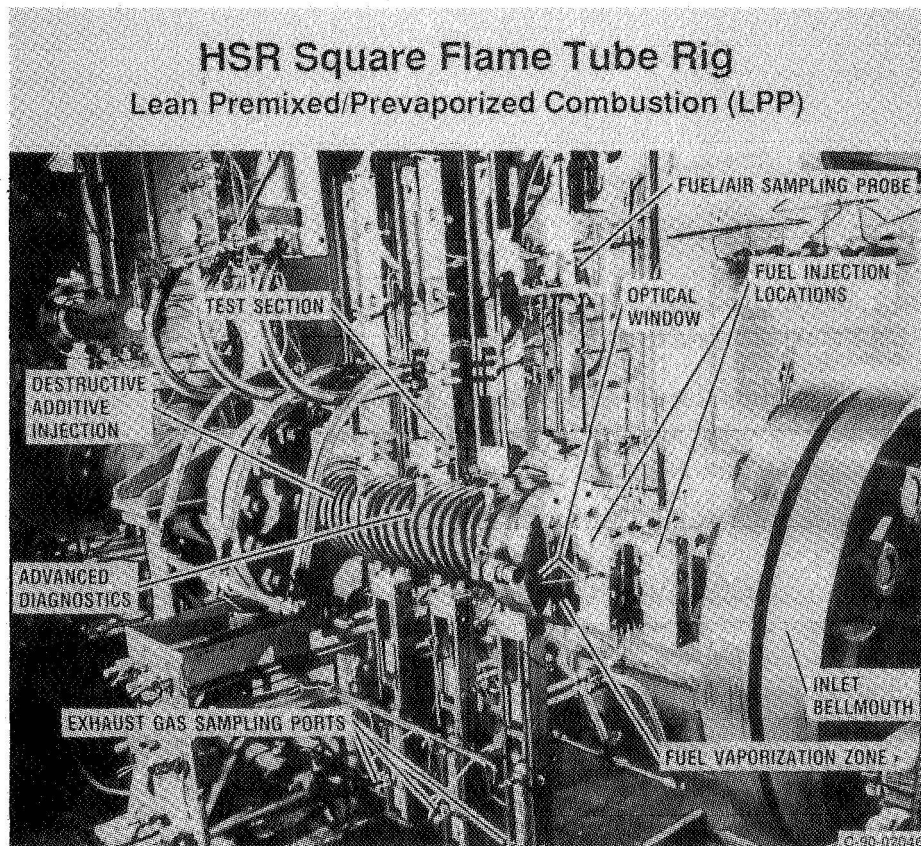
- Demonstrate the Capability of LPP to Reach the HSR Goal of NO_x E.I.'s Between 3 and 8 g/Kg**
- Experimentally Study the Effect of Fuel/Air Distribution Degree of Vaporization, and Additives on the Emission of NO_x for Advanced Low NO_x Combustors**
- Study Autoignition, Flashback, Turbulent Mixing and Lean Stability.**

APPROACH:

- Use Existing NASA Square Cross-Section Flame Tube Combustor to Reach High Temperatures and Pressures Necessary for HSR Program.**
- Use advanced laser diagnostics to obtain measurements and use in code validation.**

Lean Premixed Prevaporized Combustion LeRC Square Flame Tube Rig

The rig is shown schematically in this figure. The airflow, up to 5 lbs./second, 1100 F inlet temperature, 20 atmospheres pressure, passes from a large round-cross-sectional flow straightening plenum into a 3-inch square inlet section which leads to a multiple-conical tube fuel injector (shown later). The fuel injector can be moved by rearranging the configuration of several spool pieces so that fuel vaporization as a function of distance downstream of the fuel injector can be studied. One configuration includes the addition of a windowed section downstream of the fuel injector to allow flow visualization and laser diagnostic measurements of the degree of vaporization and droplet sizes and velocities. Just before the flame holder, a sampling probe allows sampling of the fuel/air mixture. The flameholder is an 80%-blockage, uncooled perforated plate, soon to be replaced with a water-cooled flameholder for more durability. The rig is ignited by a spark igniter, surrounded by a water-cooled jacket. The combustion section is lined with a castable silicon-carbide ceramic, which is poured around a 3-inch square wooden mold to form the test section passage and is externally water-cooled with copper cooling coils. There are 6 gas sampling probes located at 3 axial locations and 2 "radial" locations at each axial station. A windowed section for the combustion zone is planned to be ready early in 1992.

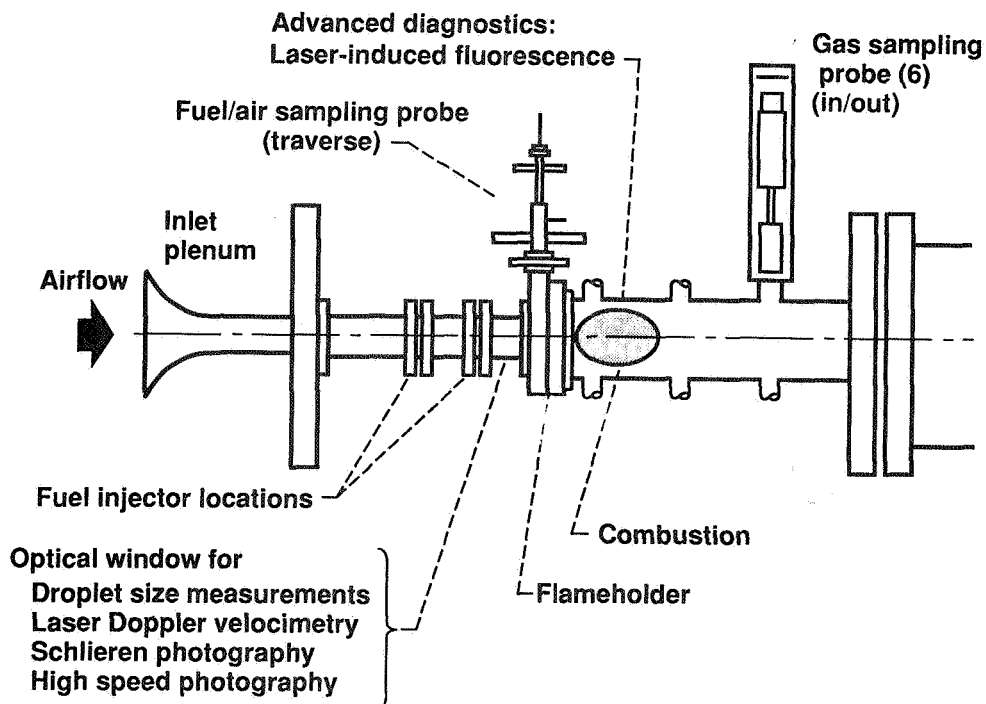


Lean Premixed Prevaporized Combustion

Photograph of LPP Rig

The LPP flame tube rig is shown in the photograph below. The non-vitiated pre-heated air passes into the rig from the right-hand side of the picture through the inlet bellmouth, where the transition from round inlet section to square test section occurs. Two possible fuel injection locations are shown and the location of the optical window section can be seen as part of the fuel vaporization zone. At the end of the fuel vaporization zone is a fuel/air sampling probe. The round flange shows the location of the flame holder, downstream of which is seen the cooling coils surrounding the combustion test section. The six exhaust gas sampling ports can be seen below and above the test section. A future windowed section will be added to allow use of advanced diagnostics in the combustion zone. The destructive additive injection called out in the photograph was an experimental program planned to verify the results of an analytical evaluation of NO_x destructive additives. However, since the analytical results showed no viable NO_x destructive additives for HSR applications, this experimental program is not expected to be carried out.

Lean Premixed/Prevaporized Combustion (LPP) LeRC Square Flame Tube Rig

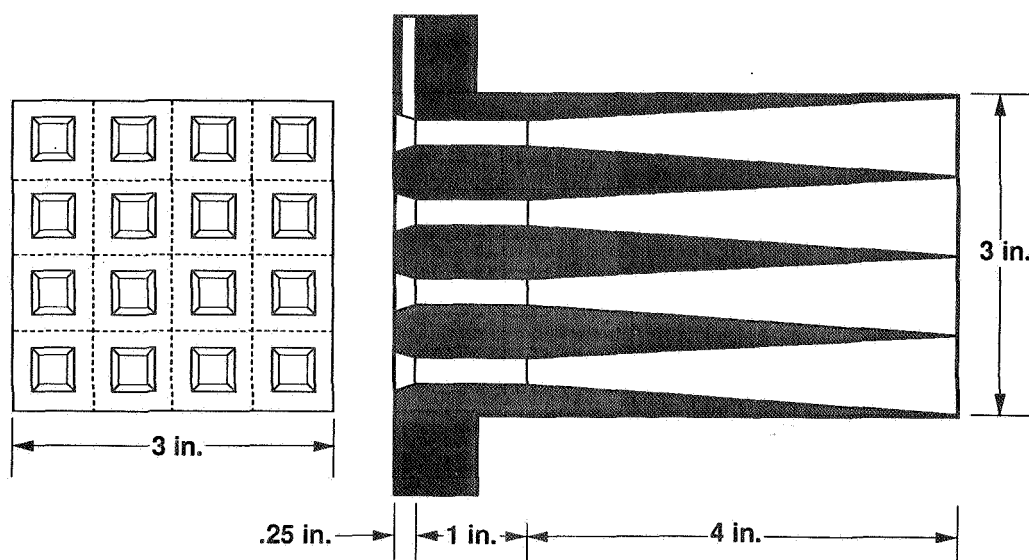


Lean Premixed Prevaporized Combustion LPP Multiple Tube Fuel Injector

A key subcomponent is the fuel injector. A unique multiple tube fuel injector is being used in the square flame tube rig at LeRC. Shown schematically below, there are 16 fuel injection passages which use the Venturi effect to provide high velocity airflow to break up the fuel into fine droplets. Very small fuel tubes enter the Venturi passage and curve around so that the fuel is injected parallel to the airflow. A small amount of air passes over these small tubes to cool them as they make their way through the fuel injector body into the Venturi passage.

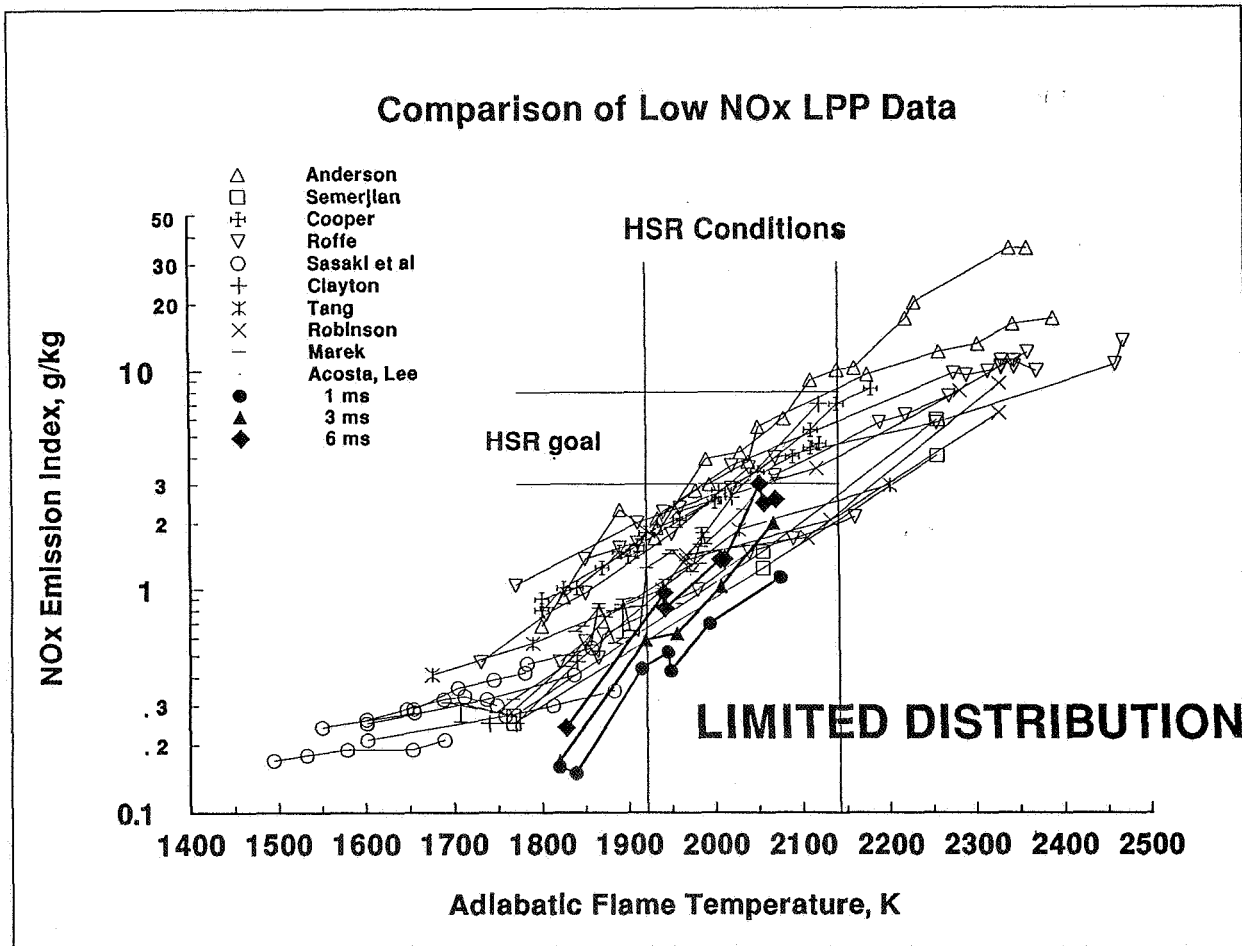
In-house water cold flow studies on one fuel passage of this fuel injector has shown that it is capable of producing extremely small droplets (on the order of 10 microns in diameter). The NO_x data obtained using this multiple tube injector was lower by an order of magnitude compared to some preliminary NO_x data obtained with a crude "spray-bar" fuel injector in the same flame tube rig.

LPP Multiple Tube Fuel Injector



Comparison of Low NO_x LPP Data

The figure below shows the emission index of NO_x (grams per kilogram fuel burned) as a function of adiabatic flame temperature in the combustion chamber. The figure is a historical representation of NO_x measurements from several research programs which studied lean premixed prevaporized combustion. The most recent results are those obtained from the LPP square flame tube rig at LeRC by Acosta and Lee. This data is shown as filled-in symbols and show encouragingly low NO_x emissions. These NO_x emissions are well within the HSR goal (less than 8 gm. NO_x/kg. fuel) at conditions representative of HSR combustor operating temperatures and pressures shown between the vertical bars.



Rich Burn/Quick Quench/Lean Burn (RQL)

The objective of this portion of the LeRC in-house research program is to use a flame tube combustor to demonstrate the capability of the Rich Burn/Quick Quench/Lean Burn (RQL) concept to reach the HSR goal of a NO_x emission index (grams of NO_x produced per kilogram of fuel burned) of between 3 and 8. Using a flame tube combustor, the effect of fuel/air distribution and degree of vaporization can be studied. Also of great interest are soot formation and burnout, CO/NO_x formation trade-off, rich zone, quench zone and lean zone residence time effects, and quick quench mixing. Information obtained in the flame tube about these parameters will be used to guide the design of an RQL combustor.

The approach is to use a NASA-designed flame tube combustor to allow combustion testing at the high temperatures and pressures necessary for the HSR Program. This rig was specially designed for the HSR program using the latest combustion codes to predict the ideal fuel and air injection schemes as well as flame tube geometry and residence times in each stage of the combustor in order to minimize NO_x formation. It will also incorporate windowed sections to allow laser diagnostics to probe the premixing and combustion zones.

OBJECTIVE:

- Demonstrate the Capability of RQL to Reach the HSR Goal of NO_x E.I.'s Between 3 and 8 g/Kg at Supersonic Cruise.**
- Study:**
 - Fuel/Air Distribution and Atomization.**
 - Soot Formation and Burnout.**
 - CO/NO_x Formation Trade-off.**
 - Rich Zone, Quench Zone and Lean Zone Residence Time Effects.**
 - Quick Quench Mixing.**

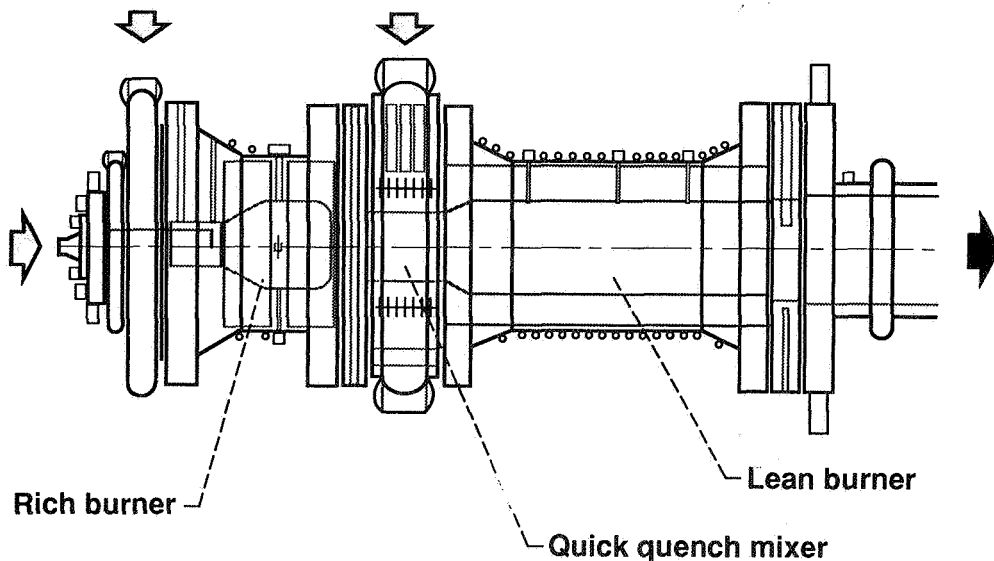
APPROACH:

- Design and Build Staged Flame Tube Combustor to Reach the High Temperatures and Pressures Necessary for HSR Program.**
- Use advanced laser diagnostics to obtain measurements and use in code validation.**

LeRC Rich Burn/Quick Quench/Lean Burn (RQL) Flame Tube Rig

The rig is shown schematically in this figure. The airflow, up to 5 lbs./second, 1100 F inlet temperature, 16 atmospheres pressure, passes through various passages entering the rich burn section. These passages supply air to various portions of the dome swirler fuel injection system (shown later). The fuel injection system can be modified by installing various fuel injectors having different airflow passages and swirler configurations. Future plans include the addition of a windowed section downstream of the fuel injector to allow flow visualization and laser diagnostic measurements of the degree of vaporization and droplet sizes and velocities in the rich burn section. The rich zone operates approximately at an equivalence ratio of 1.6. The combustion section is lined with a castable silicon-carbide ceramic and is externally water-cooled with copper cooling coils. The quick quench section supplies up to 11 lb./sec. airflow to produce a lean equivalence ratio of approximately 0.5 in the lean burn zone. Exhaust gas sampling is performed by an axially-traversing probe that takes samples in the lean burn section. A windowed section for the lean combustion zone is also planned for making laser induced fluorescence measurements of combustion species and temperatures.

Rich Burn/Quick Quench/Lean Burn Flame Tube Rig

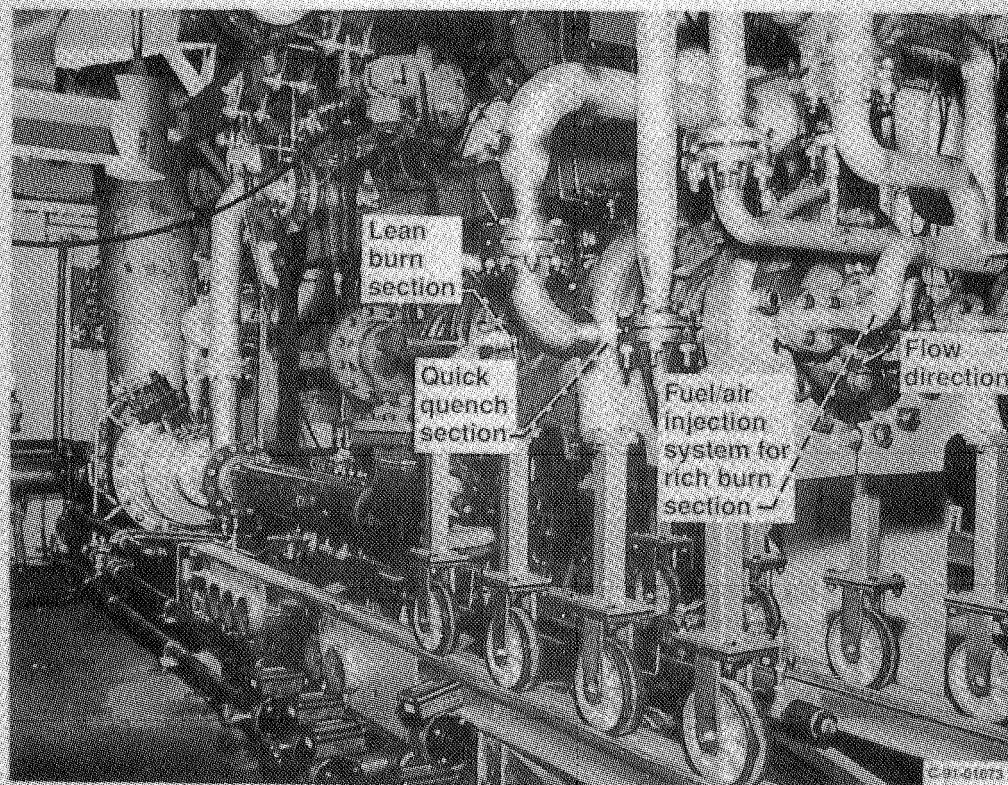


RQL Combustion

Photograph of RQL Rig

The RQL flame tube rig is shown in the photograph below. The non-vitiated pre-heated air passes into the rich burn section of the rig from the right-hand side of the picture through four air supply lines. These lines determine the air flow splits between the fuel injector inner and outer sections and the dome swirler. The large air inlet supply line for the quick quench section is shown, followed by the copper-coiled water-cooled lean burn section. The gas sampling probe will be mounted into the large flange at the end of the lean burn section. The wheels shown in the photo allow easy dismantling of the rig to allow installation of various length test sections to experimentally determine the optimum lengths for the rich and lean combustion zones.

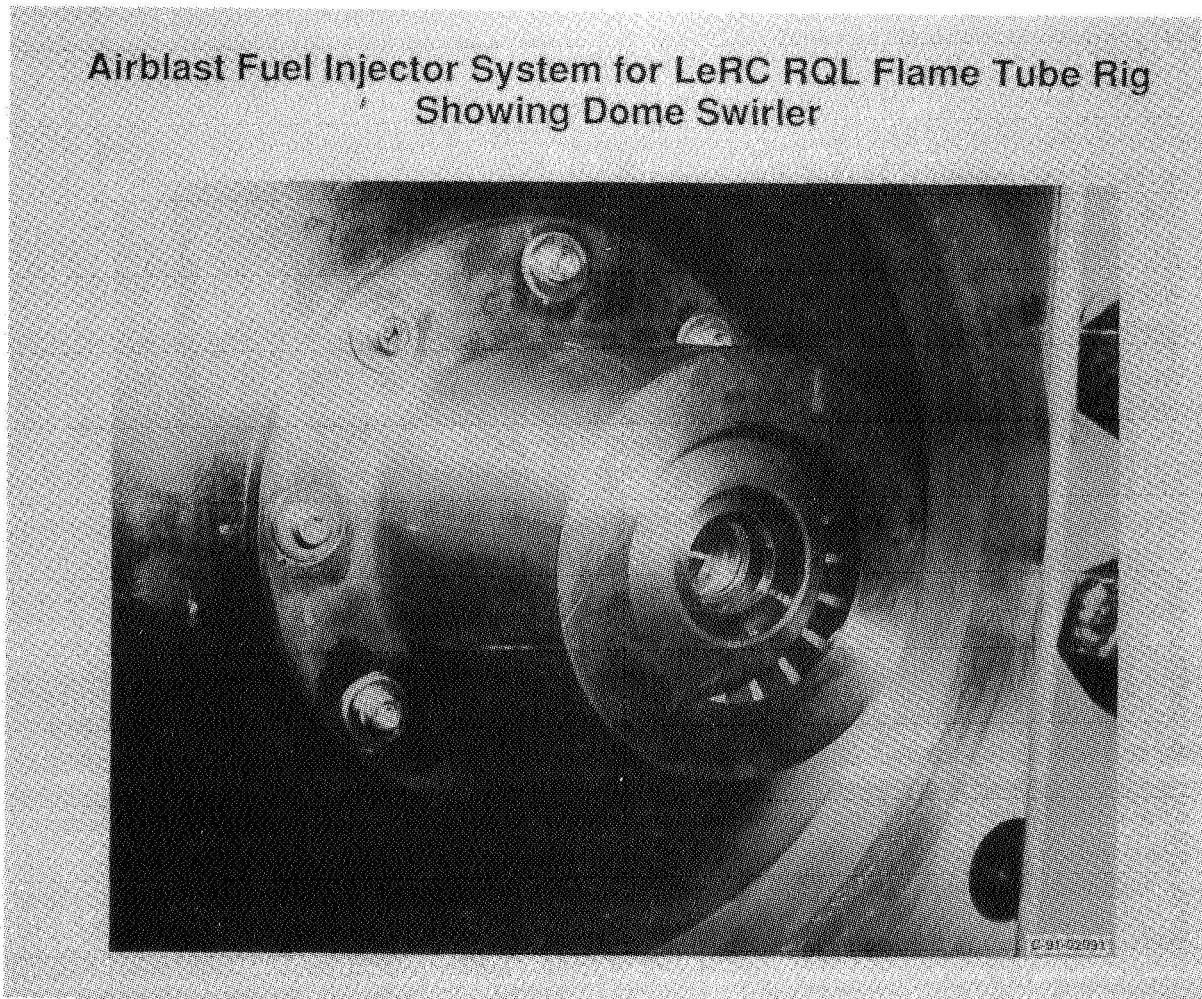
LeRC In-House Rich Burn/Quick Quench/Lean Burn (RQL)
Flame Tube Rig



RQL Combustion

Airblast Fuel Injector System

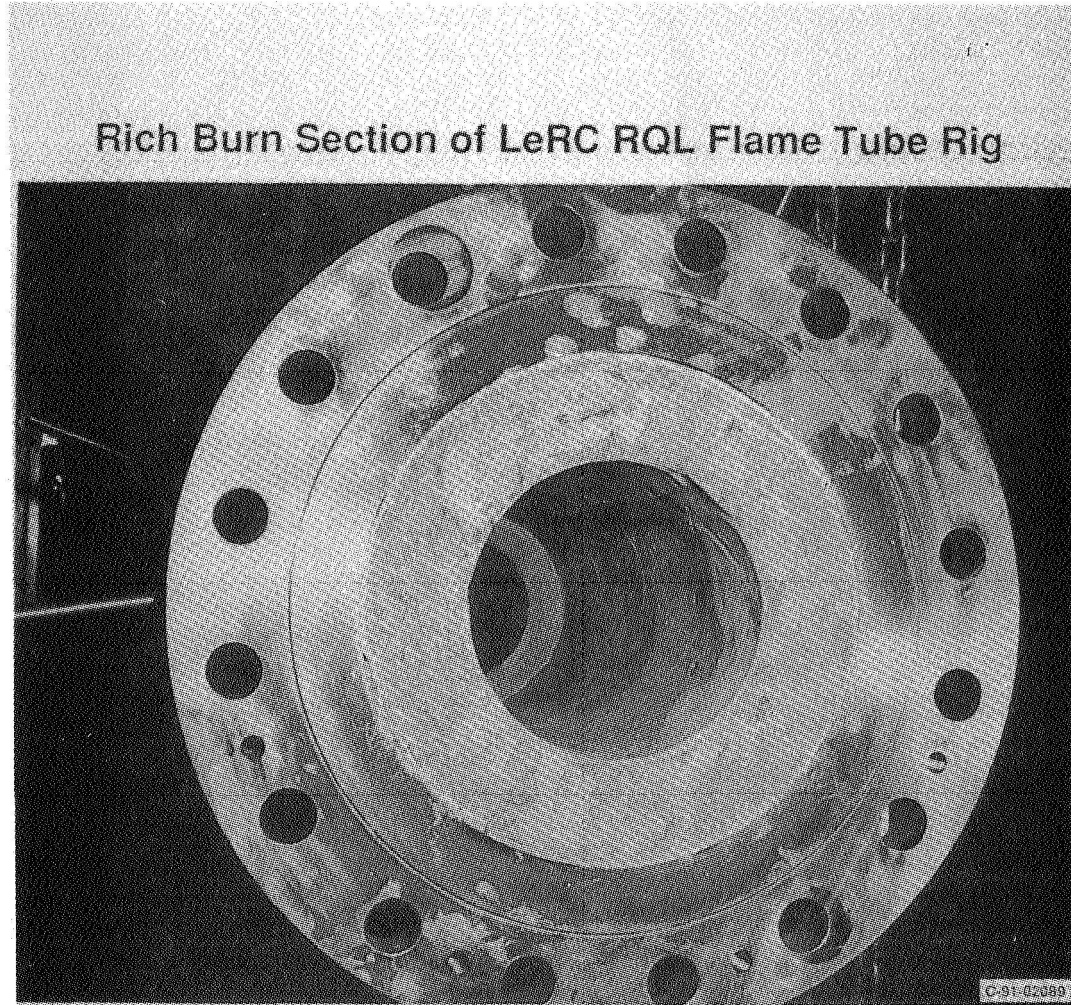
The RQL flame tube rig airblast fuel injector system with the dome swirler is shown in the photograph below. Air passes through the system both inside and outside of the fuel-flow annulus. Air also passes through the dome swirler, shown as the outer passage with the large swirl vanes in this photograph. This fuel injector has exceeded the expectations of the manufacturer in its ability to produce extremely small fuel droplets. The effect of dome air versus inner and outer annulus air on fuel atomization and soot formation will be studied with this injection system.



RQL Combustion

Rich Burn Section of RQL Flame Tube

The inside of the RQL flame tube rig rich burn section is shown in the photograph below. The entrance to the combustor as seen by the fuel injection system is shown as the foreground in this picture. The castable silicon carbide liner is shown and the transition from the 7-inch diameter combustion section to the 5-inch diameter quick quench section can be seen at the downstream end of this section. The liner is approximately 2-1/2 inches thick.

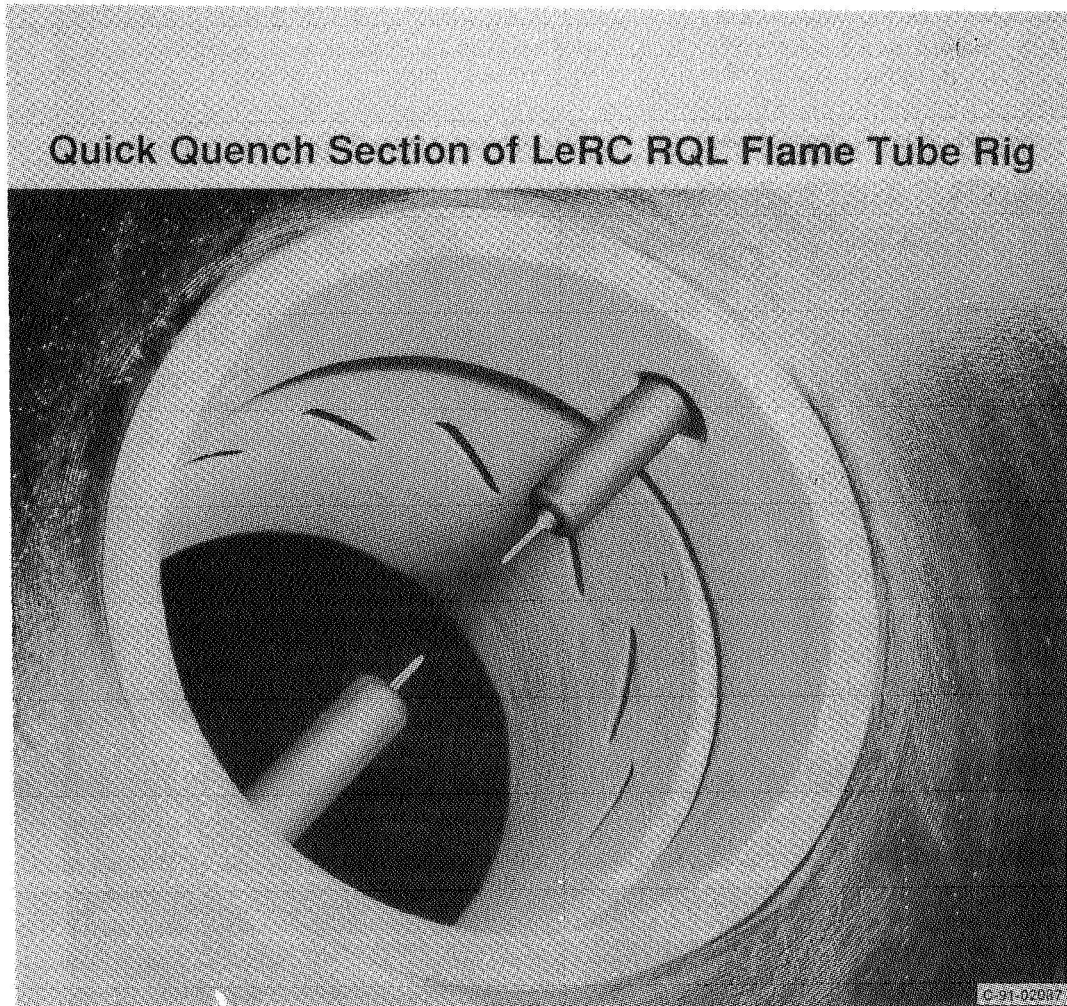


ORIGINAL PAGE
BLACK AND WHITE PHOTOGRAPH.

RQL Combustion

Quick Quench Section of RQL Flame Tube

The RQL flame tube rig quick quench section is shown in the photograph below. Air passes into the quench zone through the 45-degree slanted slots seen behind the water-cooled thermocouple probes. These thermocouples determine the exit temperature of the rich burn section. The quench section shown is 5 inches in diameter. It is made of Haynes 214 material with a thin Rockide Z coating.



Fuel-Rich Catalytic Combustion

The objective of this part of the Lewis low NO_x program is to evolve the technology for utilizing liquid kerosene fuels in high speed combustion systems and to reduce NO_x and soot emissions through very rich catalytic oxidation and staged combustion. Some phenomena of interest include fuel vaporization and distribution, catalyst activity and physical characteristics, catalyst and substrate durability, and autoignition of the very reactive gases produced. Preliminary tests will be performed in a single stage catalytic combustor. A two-stage flame tube combustor will then be designed and tested in conjunction with the rich-burn/quick quench/lean burn flame tube combustor program so that this concept can be tested at the high temperatures and pressures necessary for the HSR program goals. All of the advanced diagnostics planned for use in the RQL rig will be available for use to evaluate the catalytic combustion section's contribution to the RQL concept.

OBJECTIVE:

- Evolve the technology for utilizing liquid kerosene fuels in high speed combustion systems and reduce NO_x and soot emissions through very rich catalytic oxidation and staged combustion.
- Study:
 - Fuel Vaporization and Distribution.
 - Catalyst Activity and Physical Characteristics.
 - Catalyst and Substrate Durability.
 - Autoignition.

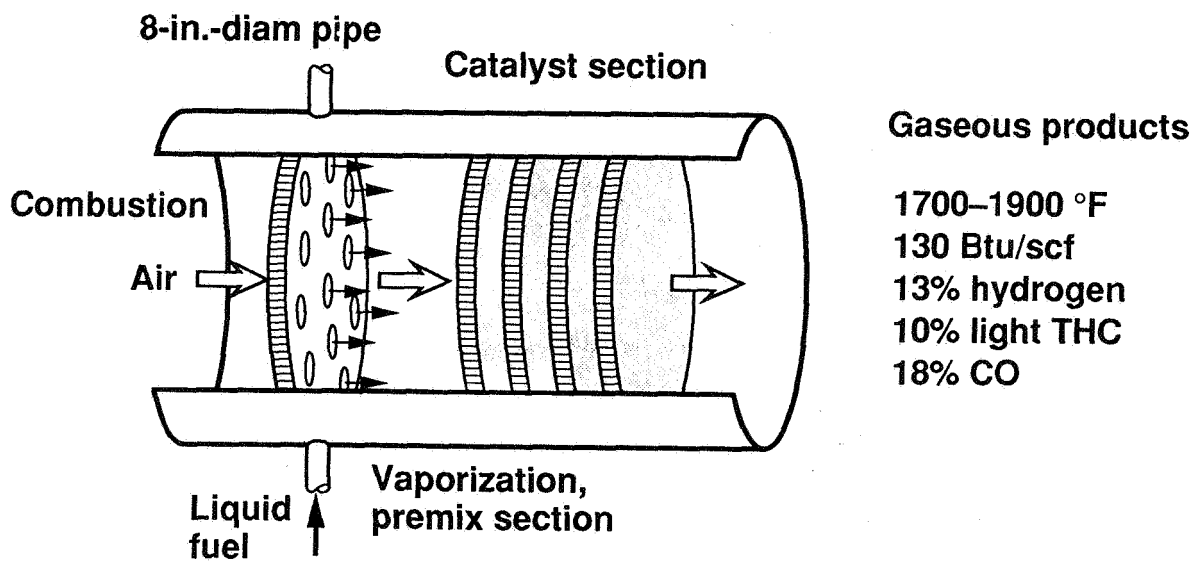
APPROACH:

- Perform preliminary tests in a single-stage catalytic combustor
- Design and build a Two-Stage Flame Tube Combustor to reach the high temperatures and pressures necessary for HSR Program.
- Use advanced laser diagnostics to obtain measurements and use in code validation.

Fuel-Rich Catalytic Combustion Test Rig

The main features of the single stage catalytic combustor are shown schematically below. In this concept, fuel greatly exceeds the available air by a factor of 3 to 9. Under these extremely fuel-rich conditions, catalytic elements are required to stabilize combustion downstream of the fuel injector and vaporization, premixing section. In the catalyst section, liquid JP fuel is transformed into a highly reactive, partially oxidized gas heated to 1700-1900 degrees F, well below the temperatures where NO_x and soot are formed. In a combustion system, this rich burn stage would be coupled with a quick quench stage and a final lean burn combustion stage. The combustion process produces large amounts of hydrogen, carbon monoxide, and partially oxidized hydrocarbons: all reactive species. Nitrogen oxide concentrations are 2.7 to 7.9 parts per million (where 100 parts per million would be required for an emission index of 1.0).

Fuel-Rich, Catalytic Oxidation Test Rig



Advanced Diagnostics

The objectives of the in-house programs in laser diagnostics is to provide non-intrusive means to measure flow characteristics in the LPP and RQL flame tube combustors. These measurements will provide data for code validation and for better understanding of both rich and lean combustion to develop design criteria for producing low NO_x combustors.

The flow characteristics of interest include the degree of fuel vaporization, flow and fuel droplet velocities, temperature profiles, chemical species and soot particle concentrations. Flow visualization techniques will also be performed which will provide information on fuel injector performance, mixing, and species concentrations.

OBJECTIVE:

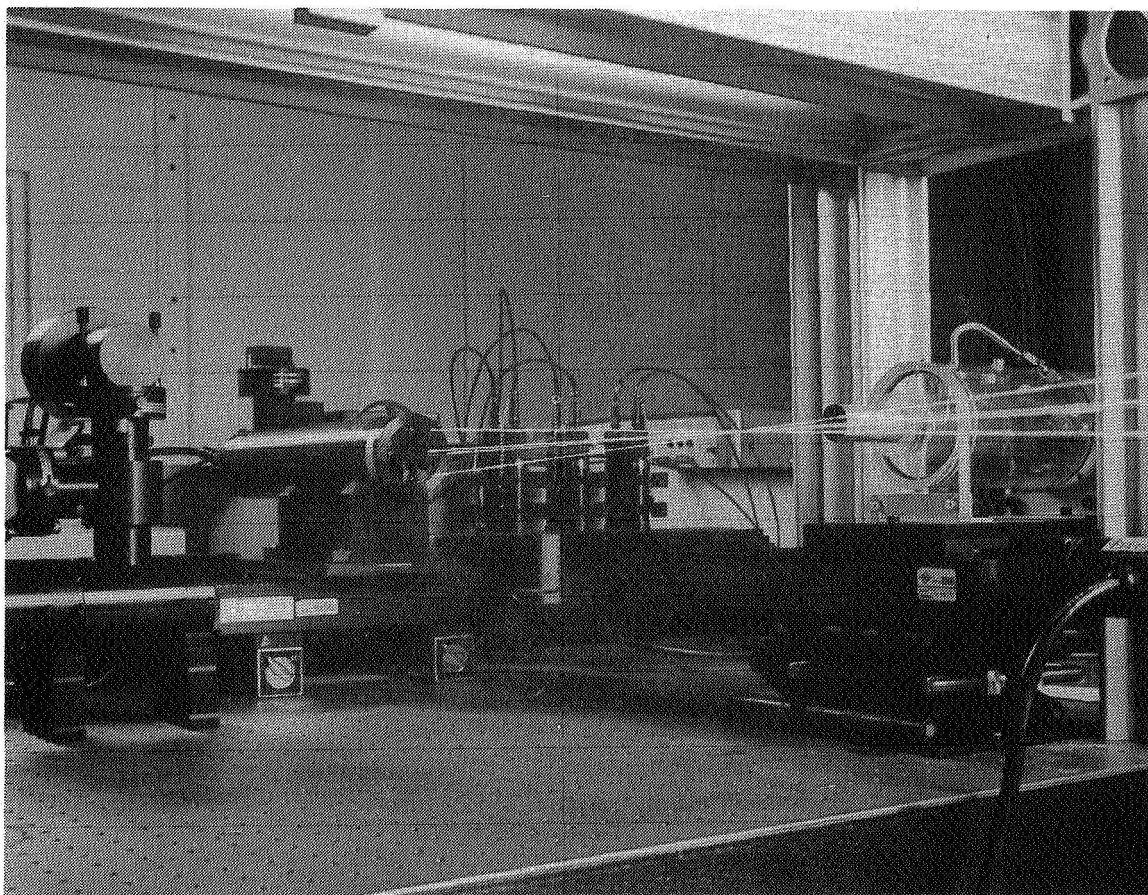
- Provide advanced laser diagnostics to measure flow characteristics in flame tube combustors to better understand the physics and chemistry of combustion for the HSR Program.
- Study:
 - Degree of Vaporization (Droplet Sizing)
 - Flow and Droplet Velocities
 - Temperature Profiles
 - Species and Soot Particle Concentrations
 - Flow Visualization (Fuel Injection, Mixing, Species)

APPROACH:

- Develop techniques both in-house and through university grants.
- Apply laser diagnostics to in-house flame tube rigs (LPP, RQL, Catalytic Oxidation).

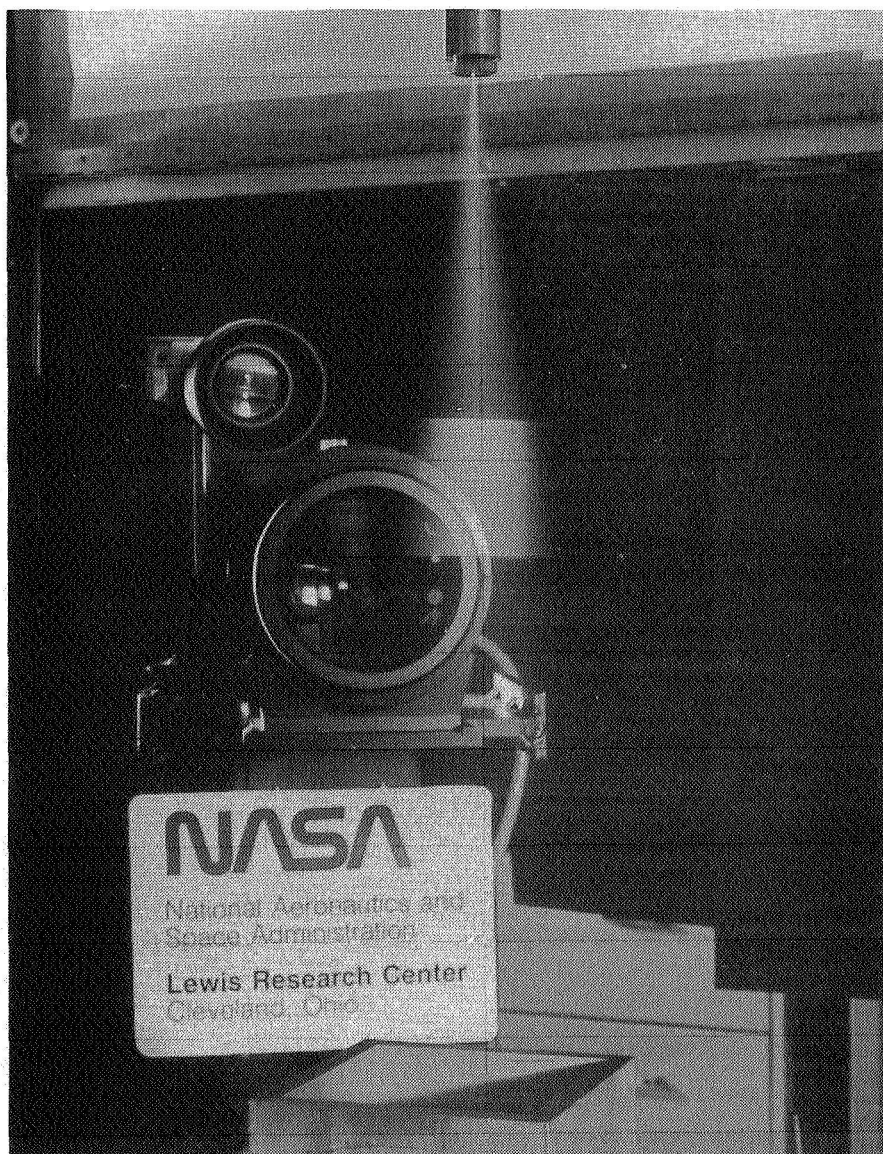
Flow Velocities

A three-component LDV system, using fiber optics, will provide flow velocity data to investigate recirculation zones within the premixing section and downstream of the flameholder, if possible. Flow velocity fields will provide information on the residence times involved in spray vaporization and flow residence times in the combustor, which will determine if local regions of high NO_x are being produced in recirculation zones in local high temperature regions. These measurements will be coupled with planned non-intrusive temperature measurements which will be provided by laser spectroscopy.



Fuel Spray Research

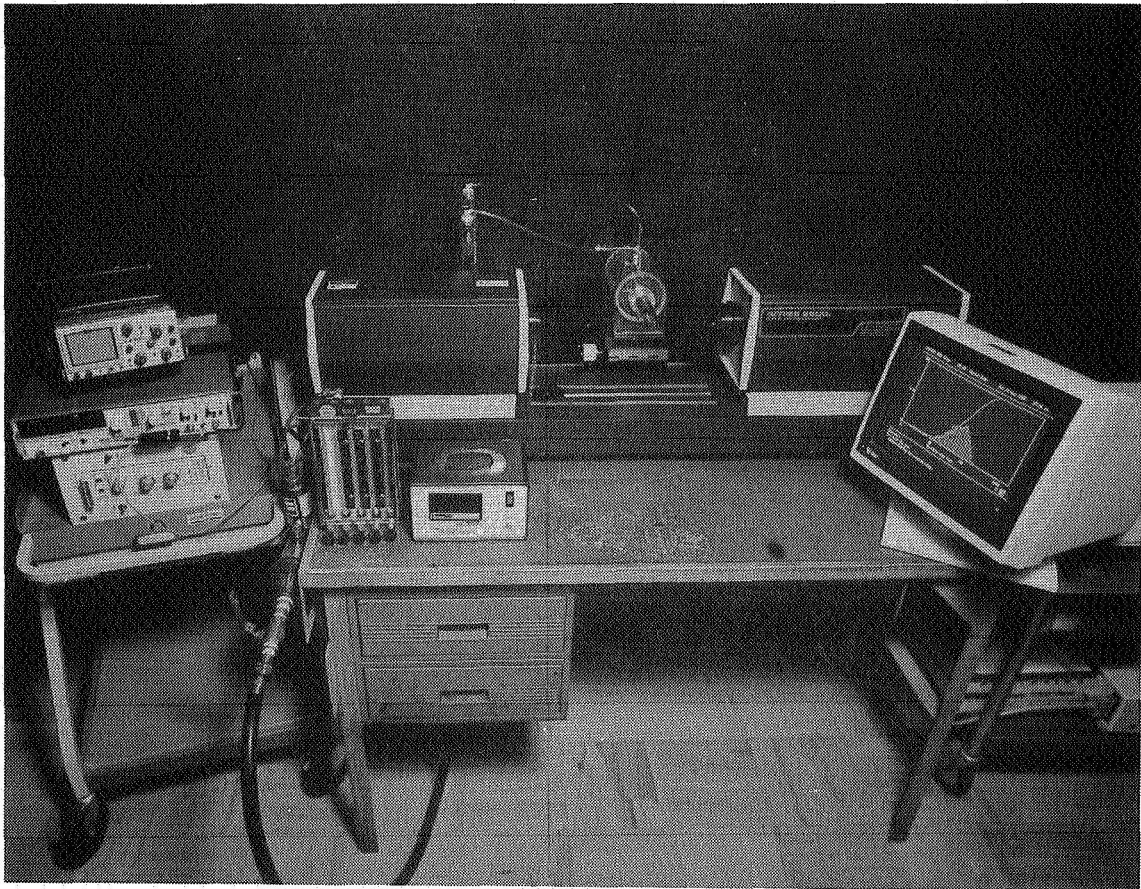
A copper vapor laser is used to illuminate and provide a strobe light source to allow flow visualization of fuel droplets in a test nozzle. In-house fundamental research on sprays, using advanced laser diagnostics will be applied to the LPP and RQL flame tubes after initial testing in simple, atmospheric bench tests such as the one seen in the photograph below. The copper vapor laser pulses at 10,000 hertz, allowing high-speed movies to be made of sprays, or allowing still photographs to be made of a spray by stopping the motion of the droplets. Phase Doppler Anemometry can be used to determine droplet velocities and sizes simultaneously in regions of interest after studying the flow visualization results. This information can be used to determine the fuel vaporization rates in a flame tube, validate codes, and be applied to future combustor designs.



ORIGINAL PAGE
BLACK AND WHITE PHOTOGRAPH

Measurement of Fuel Droplet Sizes

A Malvern particle sizer will be used to obtain fuel spray droplet sizes. This laser technique provides a line-of-sight measurement and supplies a mean droplet size to characterize the spray. This instrument will be used to study the vaporization process in the flame tube combustors (LPP and RQL) where access to the premixing sections is provided by quartz windows.

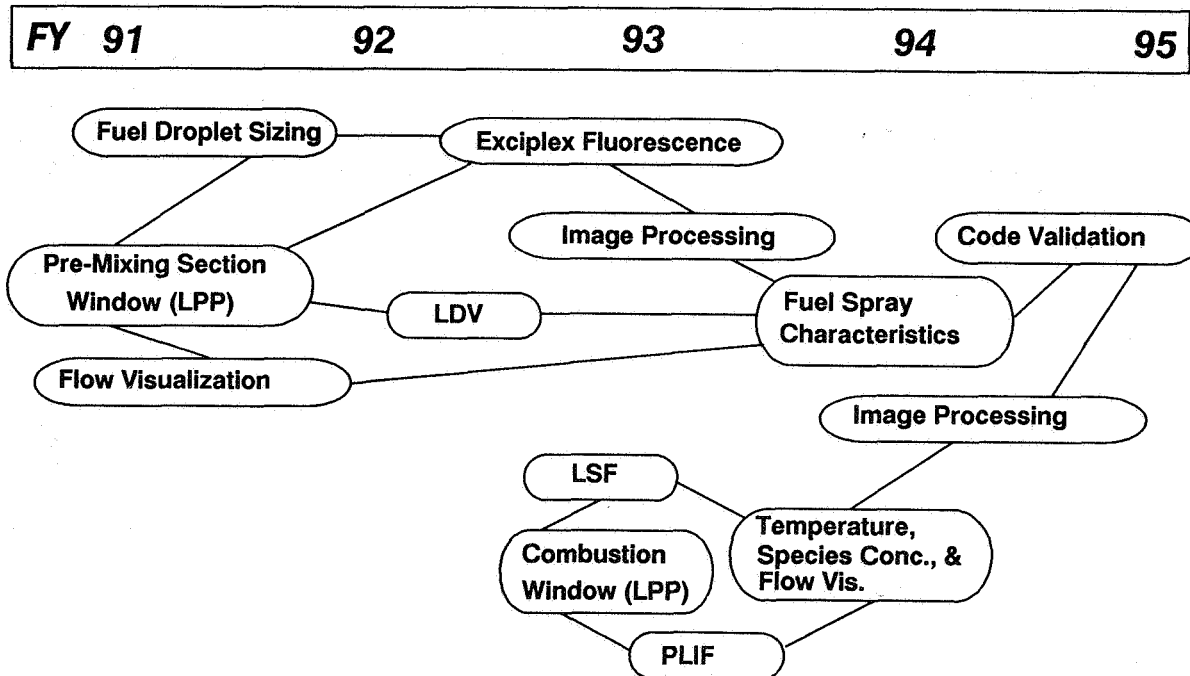


Advanced Diagnostics Schedule

The general schedule for employing various diagnostic techniques is schematically shown below. Initially, the pre-mixing section of the LPP rig will be probed with flow visualization techniques including still photography, laser-strobe photography, and schlieren photography. The Malvern particle sizer will then be used to provide fuel droplet sizes. Laser Doppler Velocimetry will be used to determine flow velocities. Later work will include application of exciplex fluorescence to determine the degree of vaporization at different positions in the premixing section. Digital image processing will be performed on the 2D images of the vapor vs. liquid concentrations to determine the extent of vaporization.

The combustion zone will be probed using laser saturated fluorescence and planar laser induced fluorescence to determine species concentrations (OH and NO) and temperature profiles. The planar measurements will be image processed to provide quantitative results. Soot measurements will be made in the RQL rig using laser scattering/extinction point measurements.

The diagnostics results from the premixing and the combustion sections from both the LPP and RQL rigs will be used to validate codes that will be used to develop low NO_x combustor designs.



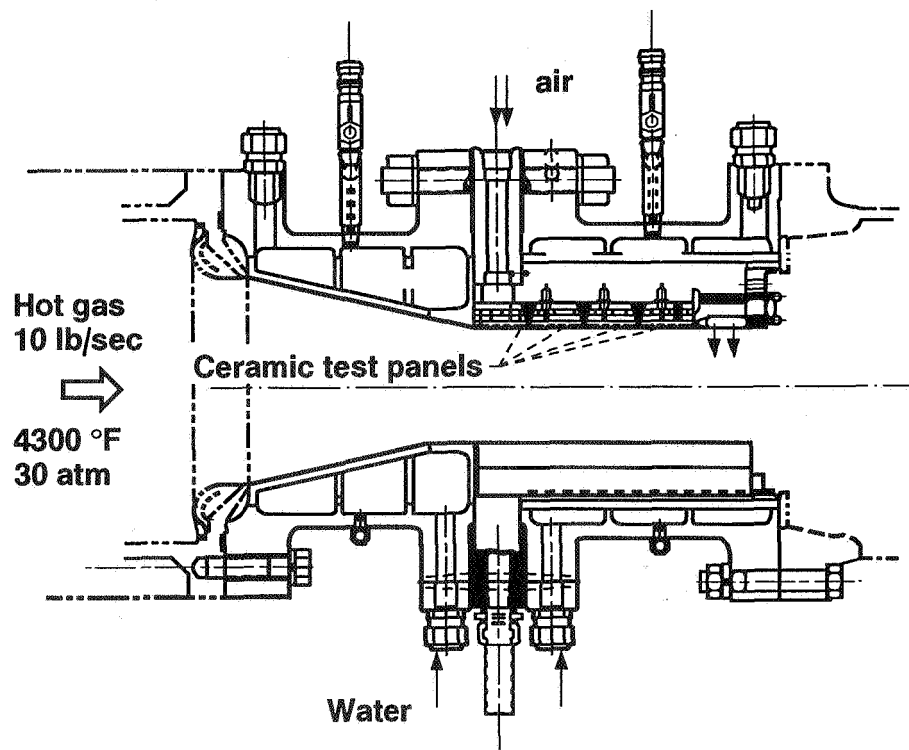
Ceramic Matrix Liner Test Rig

The ceramic matrix liner test rig was specially designed to evaluate advanced ceramic/composite materials under the extreme operating conditions which will be required by future advanced gas turbine engines. A slave combustor provides very hot (up to 4300 degrees F) high pressure (to 30 atms.), inlet gases at flow rates up to 10 lb./sec. Up to 16 separate ceramic test panels can be arranged inside the square test section such that each set of four can have different back-side cooling conditions. The rig itself is water-cooled to withstand the extreme operating conditions. This rig is nearing final installation stages and will soon be available to the materials and gas turbine engine community for use in the Enabling Propulsion Materials Program part of the HSR Program.

Ceramic Matrix Liner Test Rig

Objective:

Evaluate advanced ceramic/composite materials under advanced engine conditions.



Summary

The NASA Lewis In-House research program has produced encouraging results from the Lean Premixed Prevaporized flame tube rig, producing NO_x emission indices less than 3 gms./kg. fuel at an inlet temperatures of 930 F and pressure of 10 atm. Future plans call for increasing the inlet pressures and temperatures to encompass the whole HSR cruise condition range.

The RQL rig is well underway and will soon produce the first gas sampling probe data on NO_x levels from a flame tube designed with the latest analytical tools to produce low NO_x. Both the rich and the lean zones will have gas sampling probes installed. This rig will also provide operating conditions that will simulate the whole HSR cruise range. The operating parameters for the rich, quench and lean zones will be defined, for use in engine combustor design.

Advanced laser diagnostics are planned for fuel injection and combustion studies which will supply non-intrusive measurements of fuel vaporization, mixing, and chemical species concentrations.

The catalytic combustion program will continue to provide fundamental data that will be used to build a complete catalytic test section that will serve as the rich burn stage of the RQL combustor for two-stage experiments which will begin in FY92.

- **The LeRC LPP Rig has provided ultra-low NO_x data: E.I.'s of 1-3 gms./kg. at HSR cruise conditions.**
- **The LeRC RQL rig is in the initial check-out stages and will provide experimental NO_x data by summer, 1991.**
- **Advanced laser diagnostic systems are being set up for fuel injection and combustion studies in flame tubes.**
- **Two-stage experiments in catalytic combustion will begin in FY 92.**

THIS PAGE INTENTIONALLY BLANK

Session VII. Emission Reduction

omit

Lean Burn Combustor Technology at GE Aircraft Engines
Willard J. Dodds, GE Aircraft Engines

THIS PAGE INTENTIONALLY BLANK

LEAN BURN COMBUSTOR TECHNOLOGY
AT GE AIRCRAFT ENGINES

W.J. DODDS

523-25

12013

NASA FIRST ANNUAL
HIGH SPEED RESEARCH WORKSHOP

MAY 15, 1991

In late 1990 GE Aircraft Engines (GEAE) and Pratt & Whitney (P&W) agreed to a joint effort to conduct studies, acquire technology and validate capabilities and limitations of advanced low NOx combustor concepts with the goal of generating information necessary for concept downselect in 1992. It has been agreed that P&W will have primary responsibility for demonstration of a rich burn quick quench combustor, while GEAE will concentrate on development of a lean burn combustor. In the lean burn program, both lean premixing prevaporizing (LPP) and lean direct injection (LDI) designs will be investigated (Tacina, 1990).

One key objective of these parallel programs is, by the end of 1991, to demonstrate a NOx emissions index of 3 to 8 g/kg at HSCT cruise inlet conditions in simplified cylindrical combustors representing each of the concepts. The second objective, to be accomplished by the end of 1992, is to complete analyses and sector combustor tests necessary to assure that there are no fundamental limitations or technology barriers that would preclude successful evolution of a flightworthy combustor based on either of the basic combustor concepts.

This presentation summarizes progress to date at GE Aircraft Engines in demonstration of a lean combustion system for the HSCT. These efforts have been supported primarily by NASA contracts, with the exception of initial size and weight estimates and development of advanced diagnostics which have been conducted under GE Independent Research and Development projects. Key accomplishments to date are summarized below.

Lean Combustion Progress to Date

- **Identified combustor concepts - projected emissions, size, weight and performance impacts (3/90).**
 - **Predicted benefits of advanced materials and variable geometry (8/90).**
 - **Assessed/developed analytical capabilities for combustor design (CFD, chemical kinetics) and established design criteria (1/91).**
 - **Conducted cold flow mixing tests to identify preferred fuel injection location and verify CFD predictions (12/90).**
 - **Developed improved diagnostics (NO₂ LIF AND Laser Raman) for combustor development (3/91).**
 - **Initiated single cup rig tests to demonstrate 3-8 g/kg NOx at HSCT cruise by late 1991 (4/91).**
 - **Completed initial aero flowpaths for HSCT combustor and began mechanical design and control studies (5/91).**
-

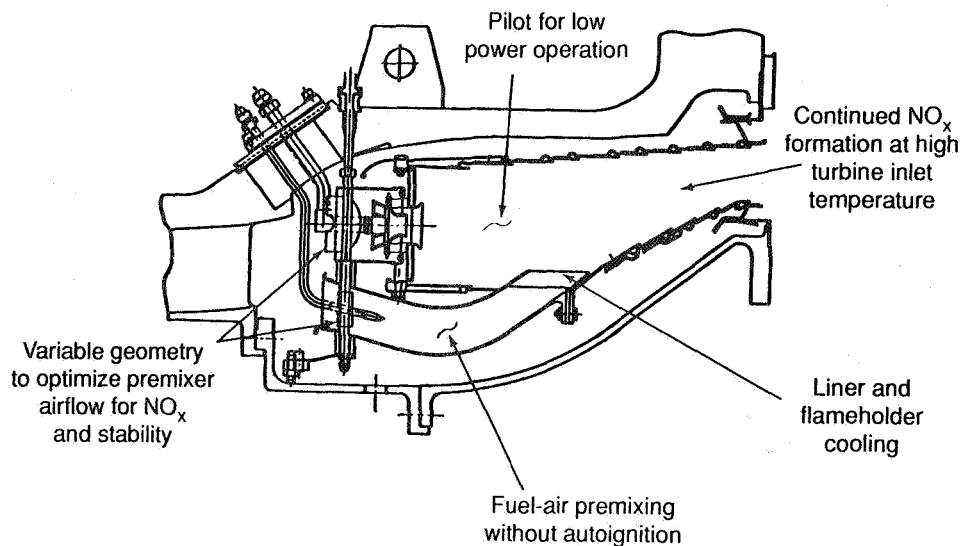
Figure 1 illustrates a parallel staged LPP combustor. A conventional pilot in the outer annulus is used for low power operation. A premixing main stage in the inner annulus is used at high power conditions.

The most challenging aspect of a LPP combustor for an HSCT engine is to obtain adequate premixing for low NO_x emissions without encountering precombustion in the mixer due to autoignition or flashback. If mixing is incomplete, NO_x will be formed in locally rich (near stoichiometric) regions of the combustion zone. Combustion within the mixer will, at best, result in increased NO_x, and could result in hardware damage to mixing ducts and flameholders.

A second major challenge is to maintain stable operation across the combustor operating range. To provide low NO_x, the premixing stage must operate very close to the lean stability limit. Local fuel-air ratio must be closely controlled with the use of fuel staging and airflow modulation to maintain stable operation.

At projected HSCT engine cruise conditions, combustor temperatures are so high that virtually all of the combustor airflow must be premixed with the fuel to achieve the NO_x goals. Thus, liner and flameholder cooling, as well as pilot stage airflow, must be minimized by using advanced materials for reduced cooling and variable geometry features to shut off pilot air at cruise conditions. Even when premixing airflow is maximized, it is critical to minimize residence time in the combustion chamber because NO_x formation rates are high even at projected combustion exit temperatures. Combustion zone residence time must be long enough to complete combustion without excessive NO_x formation.

LPP Combustor Design Issues



Roffe and Venkataramani (1978) have demonstrated that NO_x levels well below current goals can be achieved at representative HSCT cruise conditions with a well premixed system using prevaporized fuel (propane). Implementation of this technology into a liquid fueled system capable of full range operation is the present challenge.

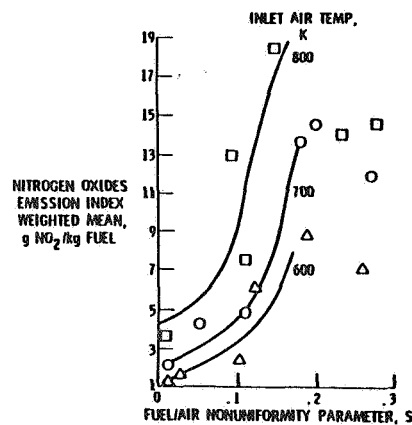
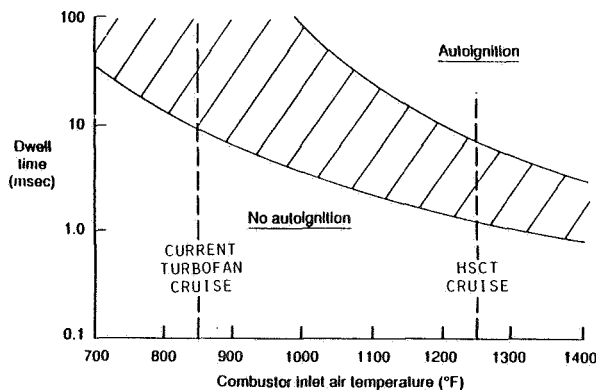
As indicated in Figure 2, at typical cruise conditions in current turbofan engines, it would take approximately 10 milliseconds for jet fuel to autoignite. This is of the same order as combustor residence times in current aircraft engine combustion systems, and is sufficient to achieve complete fuel-air mixing. However, projected HSCT cruise inlet temperatures are up to 400° F higher than those of current engines, leading to an order of magnitude reduction in available mixing time. Achieving full vaporization and thorough fuel-air premixing within 1 ms is extremely challenging.

As shown in Figure 2 (Lyons, 1979) NO_x levels are increased substantially if mixing is not complete. Thus, the major challenge of the LPP development effort is to obtain complete mixing without autoignition.

LPP Combustor Fuel-Air Mixing Issues

- Combustor inlet air pressure: 15 atmospheres liquid fuel data jet A, kerosene, etc.

- Nominal equivalence ratio of 0.6



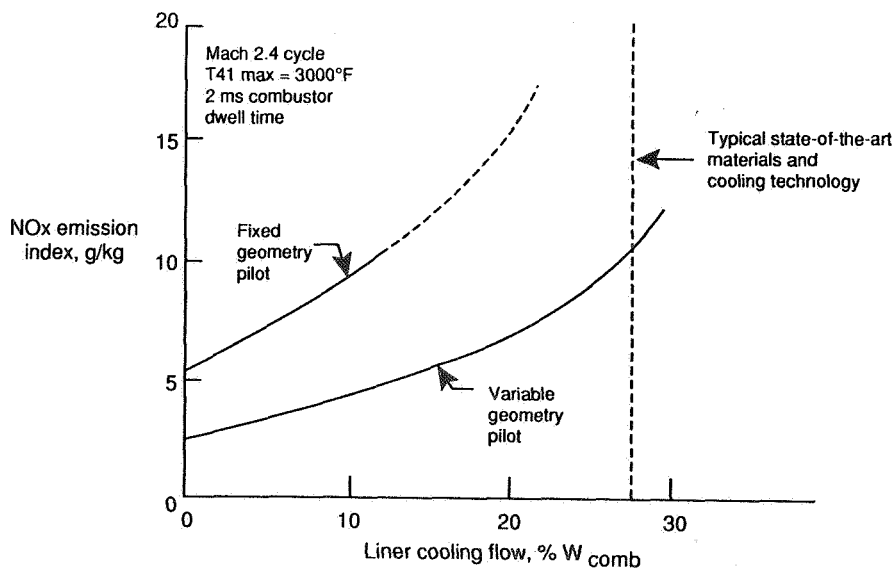
Need to Fully Mix in Less Than 1 MSEC

The importance of new technologies including advanced materials and variable geometry devices which can be used to maximize pre-mixer airflow are illustrated in Figure 3. These NO_x emission estimates were based on results of research combustor tests at representative HSCT cruise conditions with well premixed propane flames (Roffe and Venkataramani, 1978). As indicated, a premixing combustor with fixed geometry and conventional liner cooling levels would produce NO_x levels above 20 g/kg because the premixing stage would operate at relatively rich conditions with the available airflow. Use of variable geometry to force more air into the pre-mixer would reduce NO_x to about 10 g/kg, still above the goal.

With the use of variable geometry and elimination of liner film cooling, levels of about 2 g/kg are predicted. Recall, however, that NO_x levels could be somewhat higher than indicated due to the challenge of premixing at HSCT combustor inlet conditions.

Elimination of liner film cooling is also important in order to reduce quenching of CO near the combustor walls. Roffe and Venkat Raman (1981) have illustrated that wall quenching can adversely affect CO burnout.

Effects of Variable Geometry and Liner Cooling on LPP NO_x

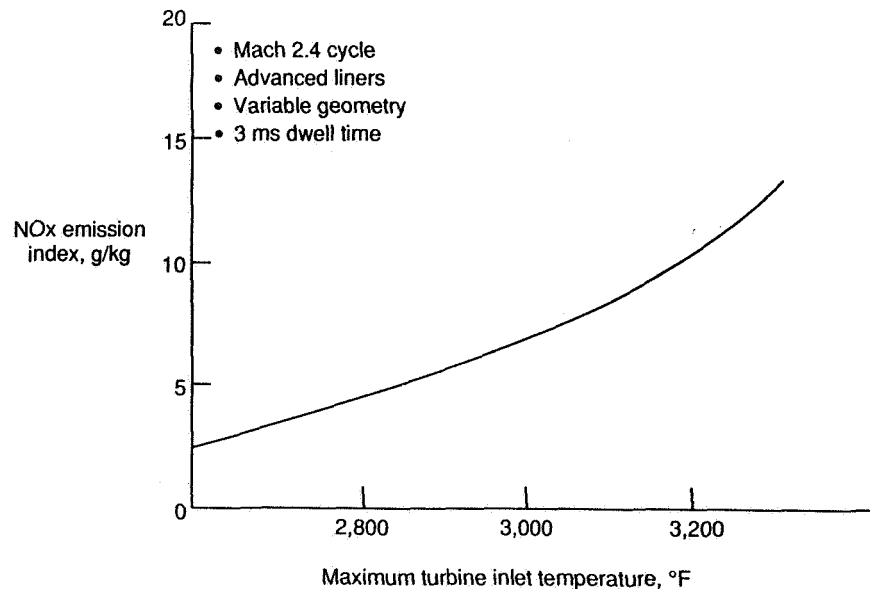


*Variable Geometry and Advanced Materials
Needed to Meet NO_x Goals*

A rule of thumb for low thermal NOx production is to keep local temperatures below 3000°F. This is in the range of steady state turbine rotor inlet temperatures at projected HSCT cruise conditions. Temperatures are even higher within the combustor, prior to addition of turbine nozzle cooling airflow. Thus, it is very important to minimize post-flame dwell time between the reaction zone and the location in the turbine nozzle where the flow is accelerated to the point that thermal NOx formation rates become negligible.

Cycle conditions are also critical to NOx production. As indicated in Figure 4, an increase of 200°F in turbine inlet temperature will nearly double NOx emissions.

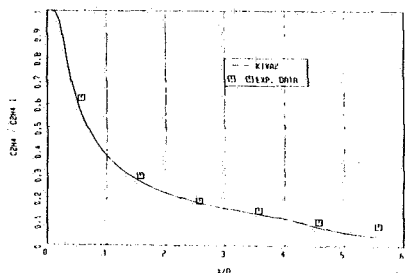
Cycle Turbine Inlet Temperature Effect on LPP NOx



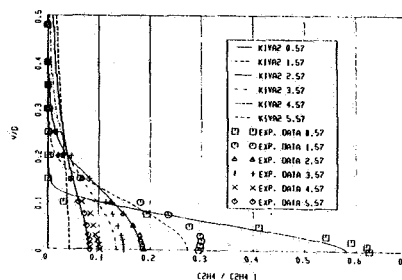
Engine Cycle Affects NOx Capability

Currently available computational fluid dynamics (CFD) codes and chemical kinetic codes have been developed and evaluated to the point where they are quite useful for LPP combustor design. Figure 5 shows a few examples that verify the usefulness of these approaches. As shown, fuel-air mixing in a duct premixer was predicted quite well with KIVA code computations. NO_x and CO chemical kinetics models also agree well with data for lean premixed systems. The example shown uses the kinetic scheme of Bittker et al. in a reactor network model to predict both prompt and thermal NO formation. Results are in good agreement with premixed combustor data. Chemical kinetic ignition delay computations based on a model developed by Jachimowski (1984) have been used to estimate the effects of inlet pressure, temperature and equivalence ratio on ignition delay. Results of these computations have been used to define and refine criteria for premixer and combustion chamber designs.

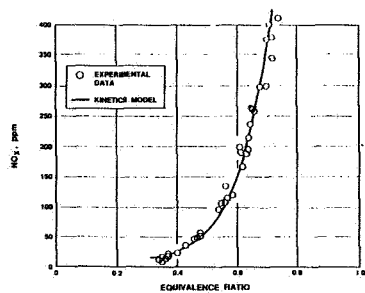
Analytical Capabilities



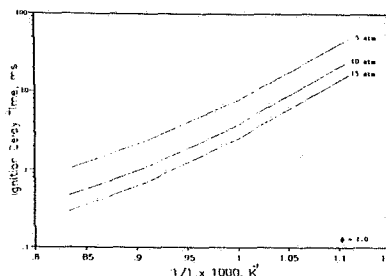
Fuel-Air Mixing in Duct
(Centerline Concentrations)



Fuel-Air Mixing
(Radial Profiles)



NO_x/CO Kinetics



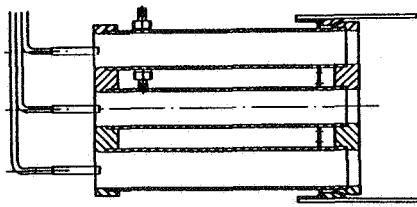
Autoignition Kinetics

The three general types of premixers shown in Figure 6 are being evaluated for use in an engine design. The duct premixer shown is a variation of the multiple tube injector that has been widely used in fundamental studies of LPP combustors. The design consists of several cylindrical air ducts. Fuel is injected near the entry of each duct, and the fuel and air mix within the duct. The flame is stabilized by a rapid expansion at the duct exit.

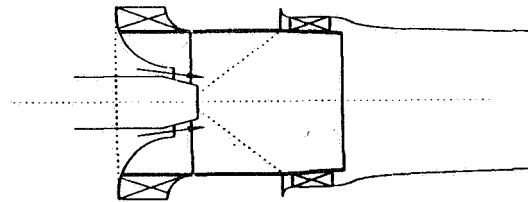
The second type of premixer uses a larger duct with a device to swirl the airflow at the inlet. Fuel is injected at the center of the vortex, and the swirling flow promotes fuel-air mixing. The duct is sized for high axial velocity, and relatively low swirl is used to prevent recirculation on the duct centerline, which could lead to flashback. The flame is stabilized at the premixer exit by the recirculation zone set up by the swirling flow.

The third fuel preparation concept is a lean direct injection device. In this device, equal portions of fuel are injected into each of many small air jets. Although the length of the air passages is not sufficient to provide complete fuel-air mixing, the design objective is to make the scale of the jets very small so that fuel-air mixing rates in the combustion zone are fast enough to provide very low NO_x levels (Hussain et al., 1981).

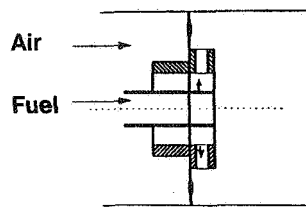
Premixer Concepts



Duct Premixer



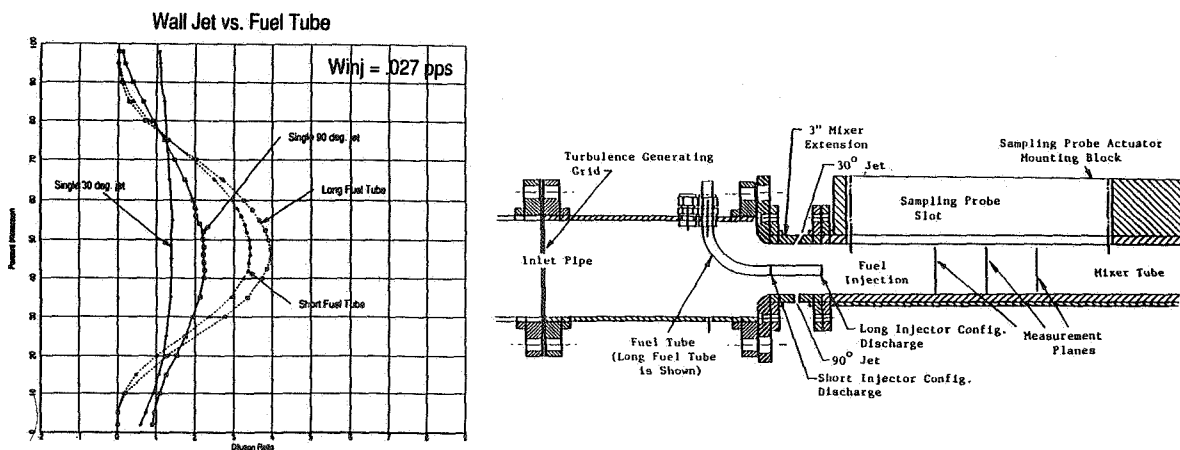
Swirl Premixer



Lean Direct Injection Flame Stabilizer

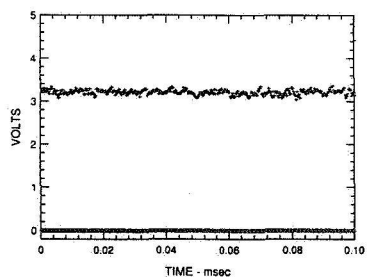
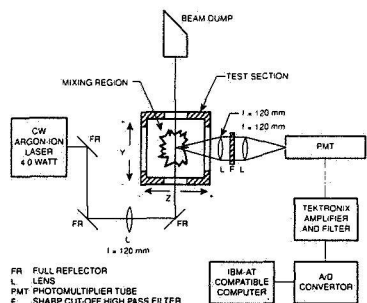
Cold flow mixing tests have been initiated to investigate different fuel injection schemes for a duct-type premixer. A large scale (approximately 5X) mixing duct has been evaluated, as shown in Figure 7. Mixing of simulated fuel and air streams has been evaluated using an ethylene tracer gas technique described by Mehta et al. (1989). These tests have been used to establish a preferred fuel injection approach for combustion tests of the duct premixer.

Cold Flow Mixing Test

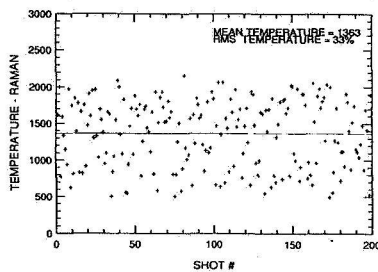
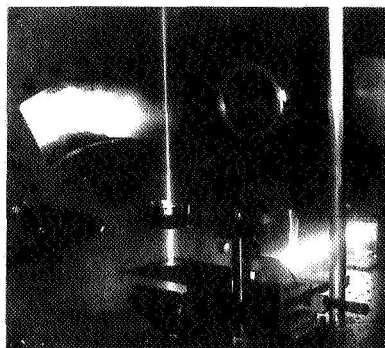


The ethylene tracer technique employed in these initial tests is useful for measuring time-averaged fuel-air mixing. However, time variations in fuel-air mixture uniformity (unsteady flow effects) can lead to increased thermal NO_x formation. In order to evaluate these unsteady effects at GEAE, NO₂ laser induced fluorescence capability has been developed for cold flow mixing tests and a spontaneous Raman system has been developed to measure average and fluctuating temperature and major species concentrations in methane flames (Figure 8). Additional work is in progress to evaluate the Raman technique in flames where distillate fuels are used.

Diagnostics Developments (GE CR&D)



NO₂ Laser Induced Fluorescence



Raman - CH₄ Flame

A cylindrical combustion test rig sized for evaluation of one full scale swirl premixer or LDI device has been built. For duct premixers, a sector or arrangement of premixers equivalent in airflow to a single swirl premixer is evaluated, as shown in Figure 9.

The objective of these single premixer combustion tests is to evaluate different premixer and fuel injector design configurations and establish effects of parametric changes in design features such as premixer length, direction of fuel injection, or combustor residence time. Fuel injector/mixers representative of engine designs are being evaluated for emissions (NO_x, CO, UHC), flame stability and lean blowout, flashback/autoignition, and ignition/flame propagation characteristics.

Typical test conditions for initial low pressure tests will be a pressure of 15-60 psia, inlet temperature of 800-1000 °F, combustor residence time of 1 to 3 ms and equivalence ratios from 0.70 to the lean limit. High pressure tests of the most promising configurations will then be conducted at pressures up to 300 psia and inlet temperatures up to 1200 °F to evaluate operation at actual HSCT engine operating conditions.

High Temperature and Pressure Duct Premixer Rig

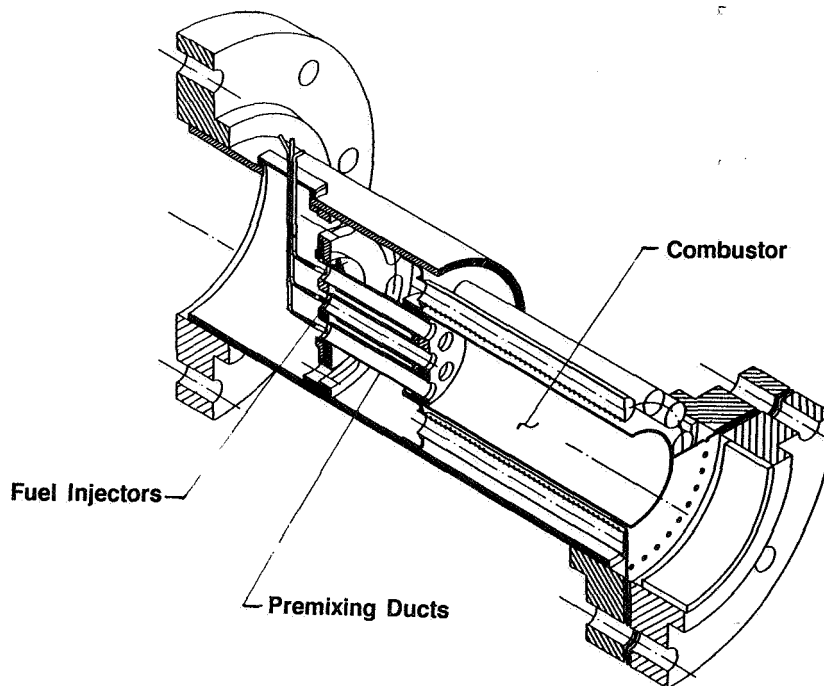
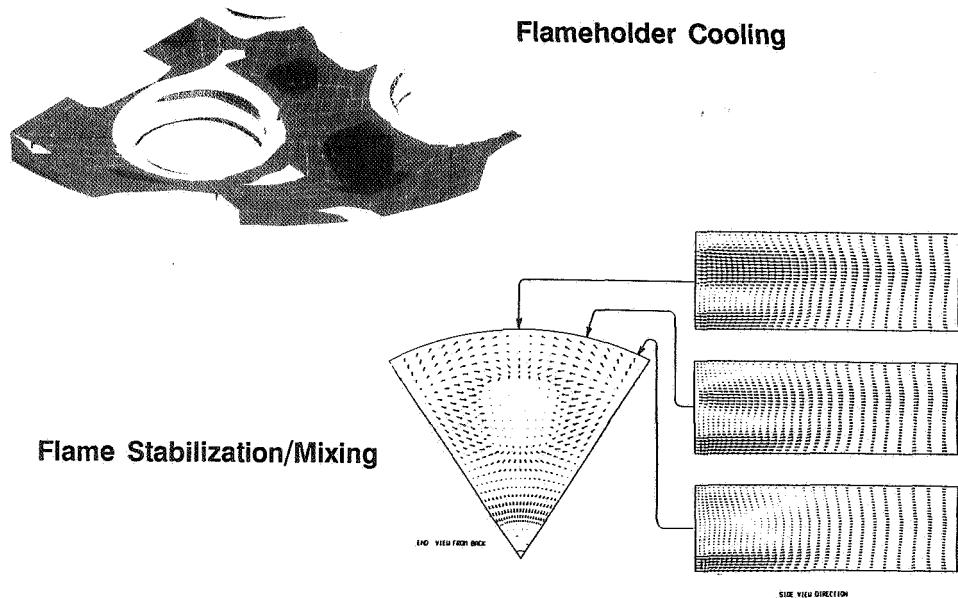


Figure 10 illustrates two of the design issues that were addressed during design of the cylindrical rig. Flameholder cooling is accomplished with backside impingement, while ceramic thermal barrier coatings are used to protect the surface that is exposed to the flame. Finite element heat transfer and stress analyses were conducted which indicate that flameholder durability will be acceptable with this design approach.

CFD analysis was used to evaluate recirculation patterns and mixing in the combustion zone downstream of the flameholder. The GE CONCERT code premixed combustion model is currently being adapted to compute NOx formation for this flameholder configuration.

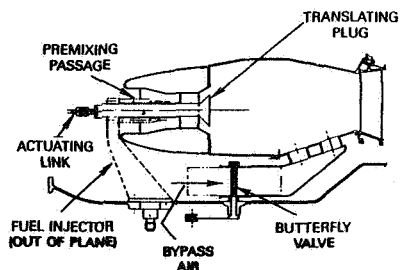
Duct Premixer Design Considerations



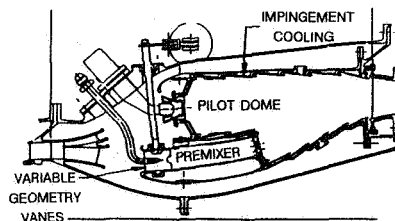
Flowpath layout studies are currently underway to define LPP and LDI systems suitable for full range operation in an HSCT engine. Combustor inlet conditions and compressor and turbine interfaces have been identified based on the most recent engine cycle studies being conducted at GEAE.

Any one of many different design concepts could potentially be used. Three options, based on previous design and development programs, are shown in Figure 11.

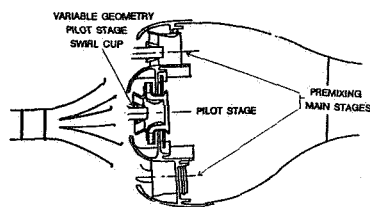
LPP/LDI Combustor Concepts



A. Single annular/wide V-G



B. Parallel staged/2-stage V-G

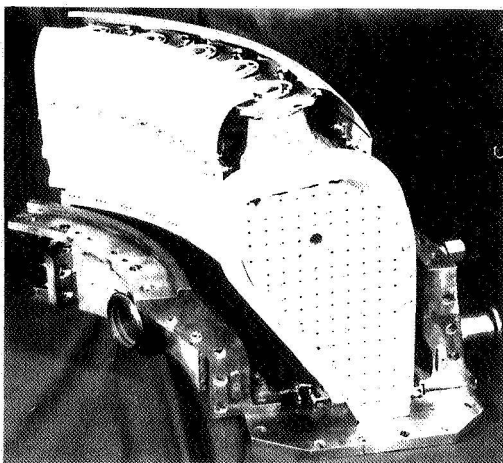


C. Three stage/pilot V-G

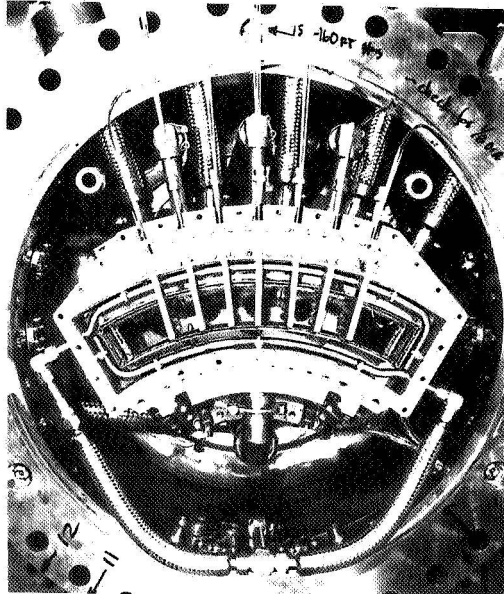
Sector combustor tests will be conducted to evaluate two selected combustor configurations and establish effects of key design and operating parameters on NO_x emissions and combustor performance. A sector combustor and test rig similar to those shown in Figure 12, incorporating all key features of an engine combustor design will be fabricated and tested to evaluate the influence of engine hardware features such as dilution holes/wall cooling, fuel-air staging and variable geometry features on emissions, exit temperature profiles, flashback/autoignition, hardware temperature and stability limits.

Two types of tests will be conducted. Initial screening will be done in low pressure tests (15-60 psia pressure and 800-1000° F inlet temperature). High pressure tests (200-300 psia maximum pressure and up to 1200° F inlet temperature) will then be conducted to evaluate emissions and autoignition of promising combustor configurations at full engine pressure.

Typical Combustor Sector Test Rig



Combustor



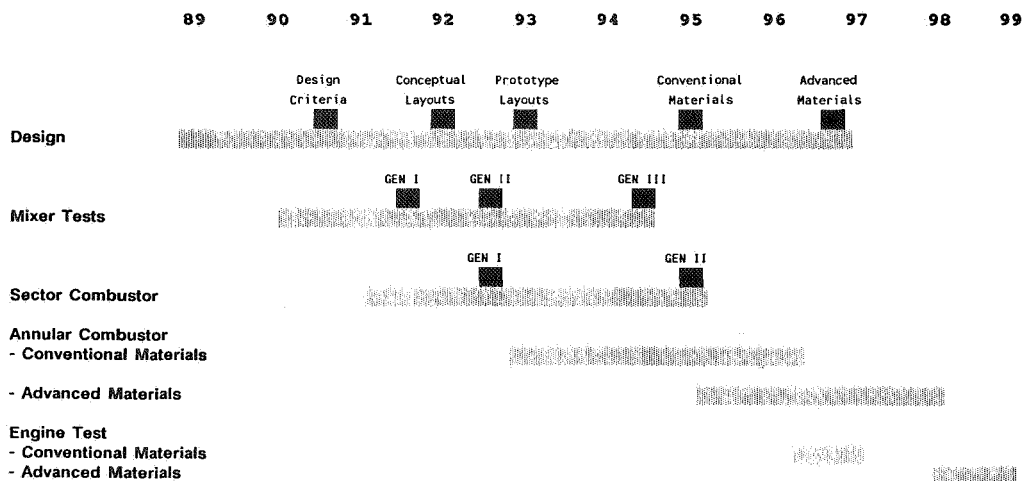
Rig

Elements of the long term HSCT combustor development plan are shown in Figure 13. The current NASA-supported work, through 1992, will include initial sector combustor tests to verify NOx emission reduction capability and identify potential technology barriers that would preclude their successful development. The next step would be to build an annular prototype of the most promising combustor design to develop and refine combustion steady state operating capability over the full range of combustor operating conditions from lightoff to maximum thrust. The objective of these annular tests would be to evolve, by the end of 1994, a combustor design capable of meeting the NOx emissions goal and providing adequate operability, performance and durability for a demonstrator engine test in an existing engine that could be operated at combustor inlet temperatures and pressures representative of the range of HSCT engine operation.

An engine quality combustor would then be built, using conventional materials, for an initial engine demonstration in 1997. The primary purpose of this engine test would be to evaluate transient response of the combustor (including fuel staging and variable geometry features) and evaluate NOx emissions in the presence of interactions with an actual engine compressor and turbine.

As indicated earlier, high temperature materials are needed to meet the HSCT NOx goals with good long-term durability. Active development of needed materials will proceed in parallel with the combustor development efforts. However, these materials will not be available for initial annular combustor rig engine tests. Combustors built with conventional materials for these early tests might rely on auxiliary cooling to permit demonstration of emissions and performance capabilities. As the advanced materials become available, a second set of rig and annular tests would be conducted to demonstrate the full potential of the evolved combustor design with combustor components which use the best of the high temperature materials.

HSCT Combustor Development Plan



REFERENCES

- Bittker, D.A. and Scullin, V.J., "GCKP84 - General Chemical Kinetics Code for Gas Phase Flow and Batch Processes Including Heat Transfer Effects," NASA-TP-2320, 1984.
- Hussain, U.S., Andrews, G.E., Cheung, W.G. and Shahabadi, A.R., "Low NOx Primary Zones Using Jet Mixing Shear Layer Combustion," ASME 81-GE-308, 1981.
- Jachimowski, C.J. "Chemical Kinetic Mechanism for the Combustion of Propane," Comb. Flame 55, 213-224, 1984.
- Tacina, R.R., "Low NOx Potential of Gas Turbine Engines," AIAA Paper No. 90-0550, 1990.
- Mehta, J.M., Shin, H., and Wisler, D. "Mean Velocity and Turbulence Measurements in an Advanced Combustor Swirl Cup, AIAA Paper No. 89-0215, 1989.
- Roffe, G. and Venkataramani, K.S., "Experimental Study of the Effect of Cycle Pressure on Lean Combustion Emissions," NASA-CR-3032, 1978.
- Roffe, G. and R.S. Venkat Raman, "Experimental Study of the Effects of Secondary Air on the Emissions and Stability of a Lean Premixed Combustor," NASA-CR-165422, 1981
- Tacina, R.R., "Low NOx Potential of Gas Turbine Engines," AIAA Paper No. 90-0550, 1990.

Session VII. Emission Reduction

emit

Rich Burn Combustor Technology at Pratt & Whitney

Robert P. Lohmann, Pratt & Whitney Aircraft; and T. J. Rosjford, United Technologies Research Center

THIS PAGE INTENTIONALLY BLANK

N94- 33486

524-07
12014

**RICH BURN COMBUSTOR
TECHNOLOGY AT PRATT & WHITNEY**

**R. P. LOHMANN
PRATT & WHITNEY**

AND

**T.J. ROSFJORD
UNITED TECHNOLOGIES RESEARCH CENTER**

**NATIONAL AERONAUTICS AND SPACE ADMINISTRATION
FIRST ANNUAL HIGH SPEED RESEARCH WORKSHOP
MAY 14-16, 1991**

NEAR TERM OBJECTIVES

The stringent NO_x emissions constraints necessary to produce an environmentally acceptable High Speed Civil Transport aircraft dictate the use of advanced combustor concepts that will require substantial technology acquisition and integration to produce a viable configuration. Under their joint HSCT Program Pratt & Whitney and General Electric have agreed to initiate this process through parallel technology acquisition and verification activities with Pratt & Whitney concentrating on rich burn combustor concepts while General Electric focuses their efforts on lean burning methods. The parallel approach permits critical evaluation of both concepts to the depth necessary to make a conclusive selection of the preferred concept after which Pratt & Whitney and General Electric will concentrate on the joint evolution of a single flightworthy and environmentally acceptable combustor based on the selected concept. This downselect between rich and lean burning approach is scheduled to occur late in CY1992 and has led to definition of the near term objectives listed on Figure 1. The intent of this presentation is to demonstrate how these timely objectives will be accomplished in a manner that is also consistent with the initiation of the larger effort that would be required to achieve technical viability of a rich burn combustor for the HSCT.

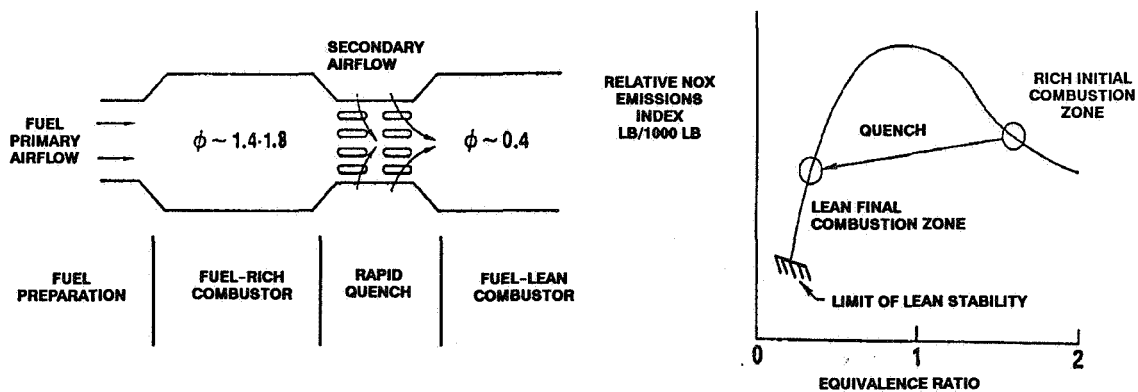
BY LATE 1992:

- **VERIFY THE EMISSIONS REDUCTION CAPABILITY OF RICH BURN COMBUSTOR CONCEPTS AT HSCT SUPERSONIC CRUISE CONDITIONS WITH GOAL OF ACHIEVING A CRUISE NO_x EMISSIONS INDEX OF 3 TO 8 GM/KG.**
- **ASSURE THAT THERE ARE NO FUNDAMENTAL LIMITATIONS OR TECHNOLOGY BARRIERS THAT WOULD PRECLUDE SUCCESSFUL EVOLUTION OF A FLIGHTWORTHY COMBUSTOR BASED ON RICH BURN CONCEPTS**

Figure 1

RICH BURN QUICK QUENCH COMBUSTOR

The Rich Burn Quick Quench (RBQQ) or Rich-Quench - Lean (RQL) combustor is the primary rich burn concept. As shown on Figure 2, all of the fuel is consumed initially in a rich combustor zone. This zone is deficient in oxygen - operating at an equivalence ratio in the range of 1.5 to 2.0. The deficiency of oxygen inhibits thermal NO_x production but the ensuing combustion products include incompletely reacted species - particularly carbon monoxide and carbonaceous particulates (smoke). Additional air is introduced into the combustor in the quench section providing the necessary oxygen to complete the combustion process. As shown in the process diagram of Figure 2 the quench air introduction must be effective to minimize NO_x production and the second phase of combustion in the lean zone occurs at temperatures dictated by combustor exit temperatures. Experience with the RBQQ combustor concept is based on potential industrial power generation engine applications which involved cylindrical or can type combustors utilizing heavier fuels from diverse feedstocks and at combustor inlet and discharge temperature levels substantially lower than those anticipated in an HSCT engine at supersonic cruise.



EXPERIENCE BASE

CONTRACTED PROGRAMS ADDRESSING CAN TYPE COMBUSTORS IN INDUSTRIAL ENGINES USING HEAVIER FUELS

Figure 2

RBQQ CRITICAL TECHNOLOGY AREAS

As enumerated in the list of Figure 3 there are five critical technology areas that must be addressed to produce a viable RBQQ combustor for the High Speed Civil Transport engine application. The experience base with experimental versions of this combustor concept is inconsistent with the HSCT application and must be extended and verified in that environment. Operation on aviation fuels and the demand for compact systems in a flight engine require definition of more relevant and aggressive design and sizing criteria. The necessity for a rapid and effective mixing process in the quench zone has been emphasized in the discussion of Figure 2. Sustaining rich oxygen deficient combustion in the rich zone dictates unique thermal/structural constraints on the liner enclosing this zone because cooling air may not be discharged into the gaspath. Fuel/air mixture preparation may have a significant role in optimizing the emissions characteristics of the rich zone because mixture uniformity could minimize smoke formation in this zone and allow more effective management of NO_x formation. Finally the operational flexibility requirements of a flight engine must be considered and is expected to lead to the need for variable geometry air admission components to provide efficient performance over the entire flight envelope.

The remainder of this presentation describes the efforts being conducted at Pratt & Whitney to address these five critical rich burn combustor technology areas. Particular emphasis is placed on technology acquisition in preparation for the downselect process and in forming the nucleus of a longer range program.

- **RBQQ VERIFICATION AND DESIGN / SIZING CRITERIA**
- **QUENCH ZONE MIXING**
- **NONEFFUSIVE COOLED RICH ZONE LINER**
- **FUEL-AIR MIXTURE PREPARATION**
- **VARIABLE GEOMETRY AIR ADMISSION**

Figure 3

CYLINDRICAL RBQQ COMBUSTOR RIG

The cylindrical Rich Burner Quick Quench Combustor rig will be the major test vehicle used in the near term effort to verify the emissions reduction potential of the rich burn concept, define relevant design criteria and establish the direction for subcomponent refinement. The rig has been designed on the basis of prior experience with experimental rich burn can type combustors for industrial engine application. The inlet air to the rig will be preheated electrically to temperatures as high as 1400°F to simulate supersonic cruise of the HSCT engine and inlet total pressures in excess of 200 psia are attainable. As shown on Figure 4, the air supply system is designed to allow variable flow split between the rich combustion zone and the quench section. Gaseous emissions and particulate concentrations are measured at the combustor exit and at the end of the rich combustion zone. Additional diagnostic instrumentation will include traversing probes to establish mixture uniformity immediately downstream of the quench air admission section, gaspath pressure measurement and heat flux sensors in the wall of the rich and lean combustion zones.

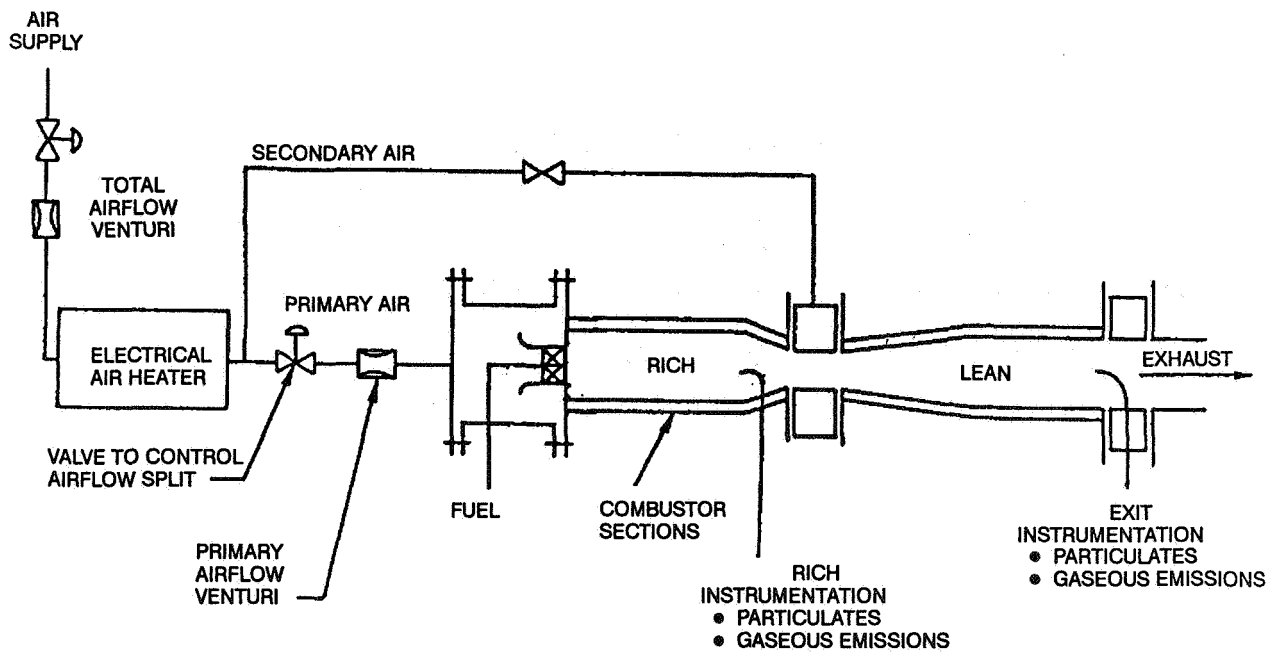


Figure 4

MODULAR RBQQ COMBUSTOR

Figure 5 shows details of the construction of the combustor section proper of the cylindrical RBQQ combustor rig. Emphasis in the design has been on flexibility of the configuration. The basic construction elements are flanged cylindrical and conical pipe sections. The noneffusive cooling requirement is achieved by externally cooling with a water jacket while casting a thick ceramic wall inside the section to permit high gaspath surface temperatures. The cylindrical sections of the rich and lean zone have been fabricated in several lengths and are interchangeable or used in series to vary residence time. The rich zone air admission and fuel injection system are installed in the inlet plenum and may be mounted on or replace the front bulkhead that separates this plenum from the combustion zone proper. The initial configuration of the rig incorporates a quench section with eight canted air inlet slots in a reduced diameter gaspath section. This quench air admission section and its adjacent conical transition pieces may be replaced with alternate components to produce different quench section configurations.

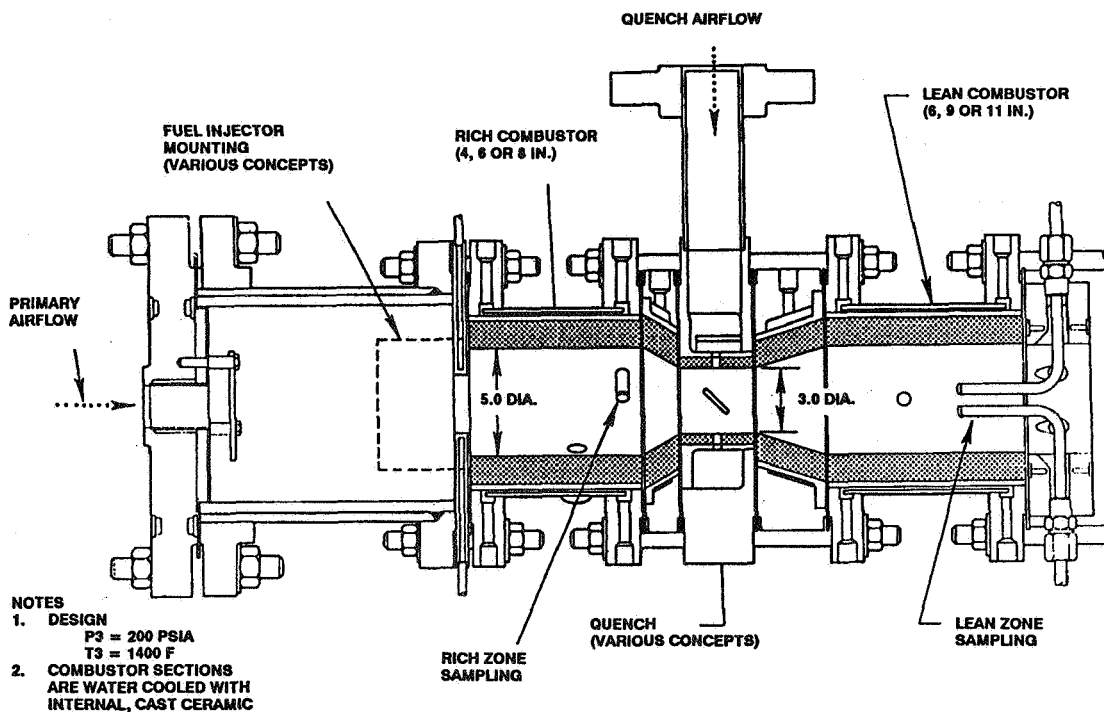


Figure 5

CYLINDRICAL RIG OBJECTIVES

The cylindrical RBQQ combustor rig is being used to accomplish several near term program objectives and to establish the direction for longer range component refinement. The table of Figure 6 lists the objectives of the activity on this rig through CY1992. The test program is being initiated with parametric evaluation of the effect of combustor inlet and operating conditions on the emissions characteristics of the RBQQ combustor concept. These will be used to verify the NO_x reduction capability of the combustor and to generate the data base for trade and optimization studies. Systematic variations of zone airloading and length will be used to optimize residence time effects and to generate corresponding stage sizing criteria. The cylindrical combustor rig will also be used for evaluating the sensitivity of the RBQQ combustor concepts to subcomponent performance. Exploiting the flexibility incorporated in its design several different rich zone fuel/air admission concepts using both single and multi-distributed sources are being designed for evaluation. Similar systematic variations in the configuration of the quench zone are also anticipated.

- **VERIFICATION OF NO_x REDUCTION CAPABILITY OF THE RBQQ AT HSCT SUPERSONIC CRUISE CONDITIONS**
- **GENERATE DATABASE FOR OPTIMIZATION AND SENSITIVITY STUDIES AT HSCT ENGINE CONDITIONS**
- **GENERATE DESIGN CRITERIA FOR ZONE SIZING AND LOADING, RICH ZONE HEAT LOADS AND LEAKAGE TOLERANCE**
- **ESTABLISH SENSITIVITY TO SUBCOMPONENT PERFORMANCE**
 - **FUEL INJECTION AND RICH ZONE MIXTURE PREPARATION**
 - **QUENCH ZONE MIXING EFFECTIVENESS**

Figure 6

QUENCH ZONE MIXING

The mixing process occurring in the quench zone is critical to the operation of the RBQQ combustor. Rapid and thorough mixing must be achieved to avoid generating excessive NO_x during the quench process. An independent task is being conducted to screen and evaluate mixing concepts for the quench zone and optimize their performance. The experimental approach involves nonintrusive measurement of the flow structure in nonreacting mixing processes. As shown on Figure 7 one of the participating streams is seeded with an oil aerosol and Mie scattering in a laser illuminated plane is measured and processed through planer digital imaging to provide instantaneous distributions of the seed concentration from which the progress of the mixing processes is evaluated quantitatively. An extensive series of cylindrical mixer configurations of the type shown on the figure have been evaluated and led to the definition of an optimum mixer geometry for the previously described cylindrical combustor rig. The quench zone mixing investigation has been subsequently redirected to an apparatus with a rectangular gaspath to explore mixing approaches that will be more compatible with the annular combustor configuration anticipated in the product engine.

OBJECTIVE

EVOLVE CONCEPTS THAT EXPLOIT FLUID DYNAMIC INSTABILITIES
AND SCALE EFFECTS TO ACHIEVE RAPID AND COMPLETE MIXING

APPROACH

USE PLANAR DIGITAL IMAGING OF MIE SCATTERING TO
QUANTITATIVELY EVALUATE MIXING PROCESSES

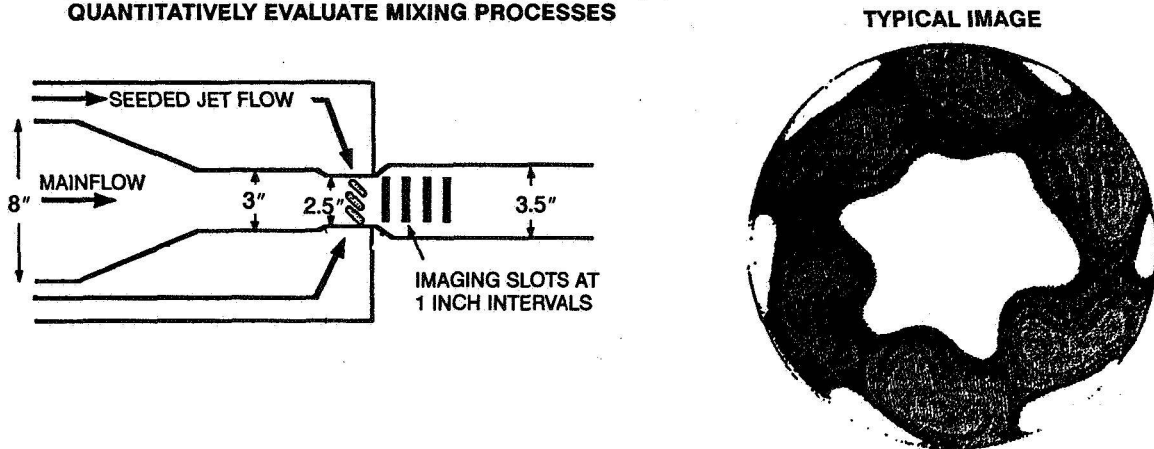


Figure 7

NONEFFUSIVE COOLED LINER

The requirements for a noneffusive cooled liner for the rich zone fo the RBQQ combustor will required a new liner material having thermal and structural properties beyond those of state of the art metallic or monolithic ceramics. The Enabling Propulsion Materials program has been established with the objective of defining and optimizing this material for use in either a rich or lean burning HSCT engine combustor. As shown by the schedule of Figure 8 this program has the milestone of producing a substantiated advanced material liner for verification testing in a demonstrator engine under the High Speed Research program in the 1998 time period.

Pratt & Whitney has also initiated studies of the requirements and constraints on the liner for the rich zone of the RBQQ combustor. As shown on Figure 8, these thermal and structural design studies are directed at three near term program objectives: providing definition of boundary conditions for the Enabling Propulsion Materials program; generating a design base for interim liner constructions for combustor rigs that will be operated under future elements fo the High Speed Research program and in conjunction with the initial output from the Enabling Propulsion Materials program provide technical data to support the combustor concept downselect process in late 1992.

1991-92 OBJECTIVES

- **DEFINE BOUNDARY CONDITIONS FOR ENABLING PROPULSION MATERIALS PROGRAM**
- **DEFINE AN INTERIM RICH ZONE LINER CONSTRUCTION FOR TEST RIGS**
- **PROVIDE TECHNICAL BASIS FOR VIABILITY POSITION FOR THE COMBUSTOR CONCEPT DOWNSELECT IN LATE 1992**

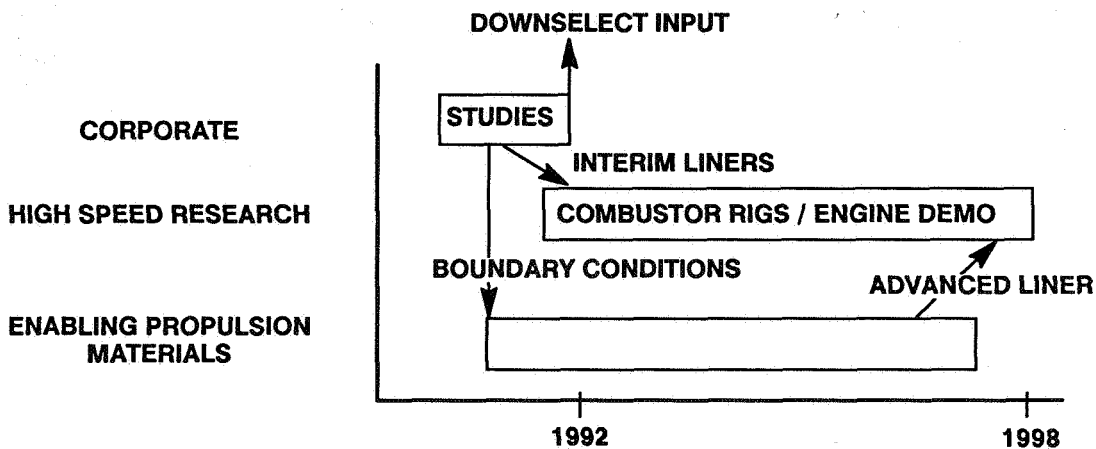


Figure 8

VARIABLE GEOMETRY REQUIREMENTS

The majority of the initial effort on the HSCT combustor concepts will concentrate on the optimization of the configuration and stoichiometry to minimize NO_x emissions at the supersonic cruise flight condition. However, acceptable performance, emissions and operability over the remainder of the flight envelope must be assured and variable geometry air admission components are expected to be required to achieve this capability. Figure 9 shows an air control mode for the RBQQ combustor that requires variable air admission on the inlet to the rich combustion zone. The rich zone equivalence ratio schedule of that figure satisfies engine cycle requirements in that the high equivalence ratios conducive to minimum NO_x production is maintained at high fuel air ratios; an equivalence ratio near unity is achieved at ground idle to minimize carbon monoxide and unburned hydrocarbon emissions and adequate lean stability is retained. This equivalence ratio schedule is shown to be achieved with only a moderate variation in rich zone airloading at high fuel air ratios.

While the definition of variable geometry airflow components and their actuation mechanisms would be deferred to a later phase of the High Speed Research program after the combustor downselect, initial evaluation of performance or emissions sensitivities to airflow shifts could be conducted in the cylindrical combustor rig. The airflow shifts would be simulated in sequential tests with interchangeable components sized to represent the extreme areas of the airflow apertures.

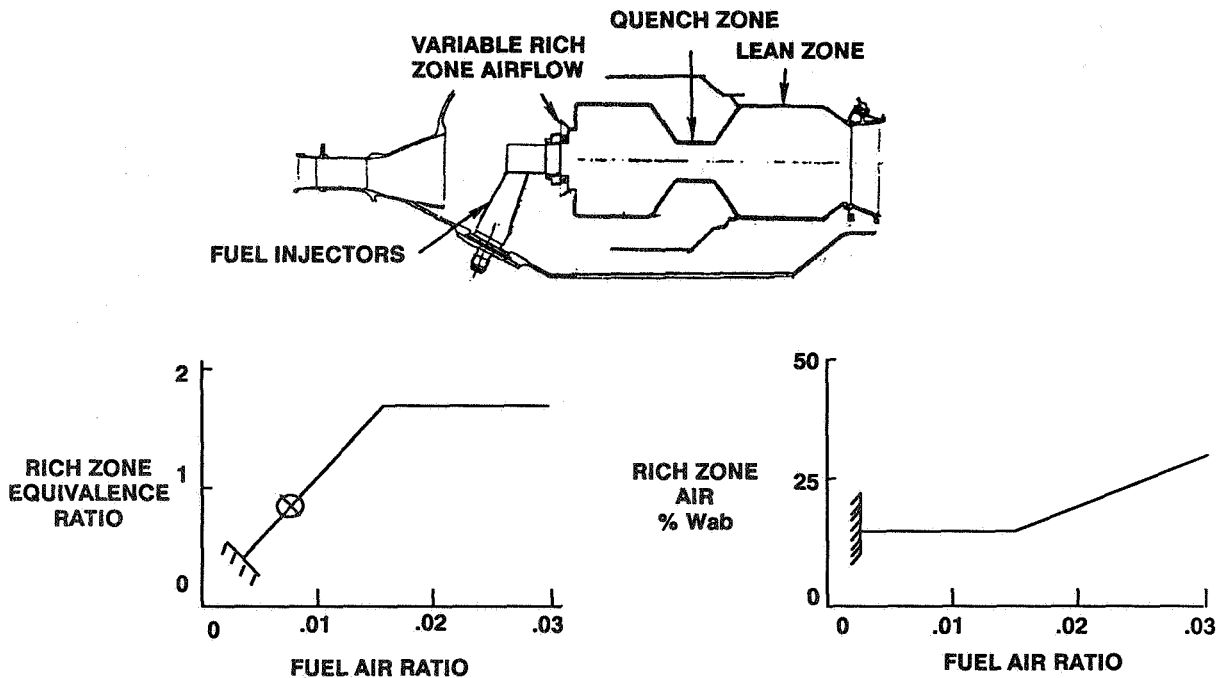


Figure 9

SECTOR COMBUSTOR RIG

While the initial evaluation and technology acquisition on the Rich Burn Quick Quench combustor concept will be conducted on the cylindrical combustor, the HSCT engine combustor is expected to be on annular configuration. To provide an assessment of the RBQQ combustor in a better simulation of an annular combustor geometry a sector combustion rig such as that shown on Figure 10 will be incorporated in the program. The design of this rig and its aerothermal details will be based on the experience derived in the previously described technology acquisition tasks. Zone sizing and rich zone fuel/air admission module configurations will be based on criteria developed from data acquired with the cylindrical combustor rig and the quench air admission system will have been optimized in the rectangular quench zone mixing evolution task. The sector combustor rig is expected to be operational in late 1992 to provide further concept verification prior to the downselect decision.

INITIAL CONFIGURATION FOR EVALUATION IN LATE 1992 BASED ON INPUT FROM THE FUNDAMENTAL TECHNOLOGY TASKS

PROVIDE DEMONSTRATION IN SIMULATED ANNULAR BURNER WITH MULTIPLE FUEL / AIR ADMISSION MODULES

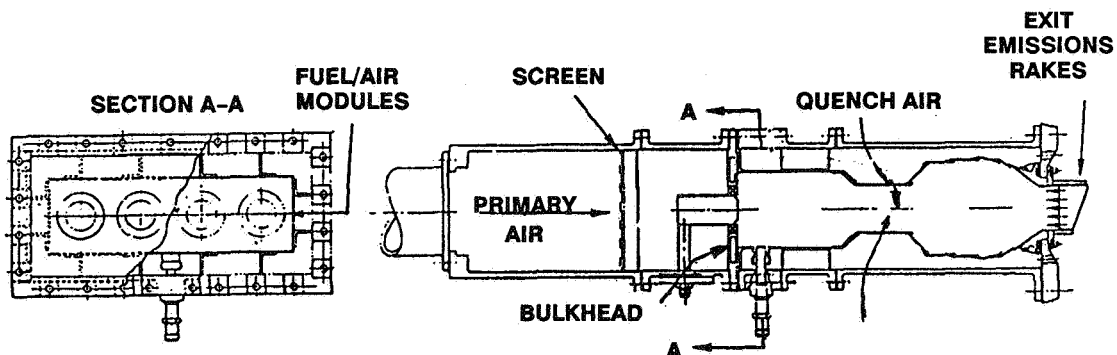


Figure 10

CONCLUSIONS

The near term program to evaluate rich burn combustor concepts for application to the High Speed Civil Transport engine will meet the intended program schedule and objectives. The fundamental technology tasks outlined will provide the necessary substantiation of the Rich Burn Quick Quench combustor concept for the downselect process. These tasks will also establish the direction for additional technology acquisition and combustor component refinement if this concept is selected. The test procedures and experimental apparatus developed and constructed under these initial tasks will be available for subsequent combustor component refinement efforts in the later phases of the High Speed Research program.

- **NEAR TERM TECHNOLOGY ACQUISITION EFFORTS WILL PROVIDE SUBSTANTIATION OF THE POTENTIAL FOR RICH BURN COMBUSTOR CONCEPTS IN THE DOWNSELECT PROCESS.**
- **DIRECTION FOR SUBSEQUENT REFINEMENT OF RICH BURN COMBUSTOR WILL BE ESTABLISHED**
- **TEST PROCEDURES AND APPARATUS FROM NEAR TERM TASKS AVAILABLE FOR SUBSEQUENT COMPONENT REFINEMENT**

Figure 11

Session VII. Emission Reduction

Low NO_x Combustor Design
Dr. Hukam Mongia, Allison

PAPER UNAVAILABLE AT TIME OF PUBLICATION

Session VII. Emission Reduction

Low NOx Mixing Research
Professor Scott Samuelson, University of California-Irvine

PAPER UNAVAILABLE AT TIME OF PUBLICATION

REPORT DOCUMENTATION PAGE

Form Approved
OMB No. 0704-0188

Public reporting burden for this collection of information is estimated to average 1 hour per response, including the time for reviewing instructions, searching existing data sources, gathering and maintaining the data needed, and completing and reviewing the collection of information. Send comments regarding this burden estimate or any other aspect of the collection of information, including suggestions for reducing this burden, to Washington Headquarters Services, Directorate for Information Operations and Reports, 1215 Jefferson Davis Highway, Suite 1204, Arlington, VA 22202-4302, and to the Office of Management and Budget, Paperwork Reduction Project (0704-0188), Washington, DC 20503.

1. AGENCY USE ONLY (Leave blank)		2. REPORT DATE April 1992	3. REPORT TYPE AND DATES COVERED Conference Publication	
4. TITLE AND SUBTITLE First Annual High-Speed Research Workshop			5. FUNDING NUMBERS WU 537-01-22-01	
6. AUTHOR(S) Allen H. Whitehead, Jr., Compiler				
7. PERFORMING ORGANIZATION NAME(S) AND ADDRESS(ES) NASA Langley Research Center Hampton, VA 23665-5225			8. PERFORMING ORGANIZATION REPORT NUMBER	
9. SPONSORING/MONITORING AGENCY NAME(S) AND ADDRESS(ES) National Aeronautics and Space Administration Washington, DC 20546-0001			10. SPONSORING/MONITORING AGENCY REPORT NUMBER NASA CP-10087, Part 2	
11. SUPPLEMENTARY NOTES				
12a. DISTRIBUTION / AVAILABILITY STATEMENT [REDACTED] until April 30, 1994 Subject Category 02			12b. DISTRIBUTION CODE	
13. ABSTRACT (Maximum 200 words) This publication is in four volumes and represents the compilation of papers presented at the First Annual High-Speed Research Workshop held in Williamsburg, Virginia, on May 14-16, 1991. This NASA-sponsored workshop provided a national forum for presenting and discussing important technology issues related to the definition of an economically viable, and environmentally compatible High-Speed Civil Transport. The Workshop and this publication are organized into 13 sessions, with Session 1 presenting NASA and Industry overviews of the High-Speed Civil Transport Program. The remaining sessions are developed around the technical components of NASA's Phase I High-Speed Research Program, which addresses the environmental issues of atmospheric emissions, community noise and sonic boom. Because of the criticality of the materials and structures technology area, and the long-term nature of the supporting research requirements, a session was added in this area to capture the ongoing work at NASA Lewis and NASA Langley and within industry.				
14. SUBJECT TERMS atmospheric science, high lift, laminar flow control, sonic boom, aeroacoustics, supersonic transport, ozone, community noise			15. NUMBER OF PAGES 565	
			16. PRICE CODE	
17. SECURITY CLASSIFICATION OF REPORT Unclassified	18. SECURITY CLASSIFICATION OF THIS PAGE Unclassified	19. SECURITY CLASSIFICATION OF ABSTRACT	20. [REDACTED]	